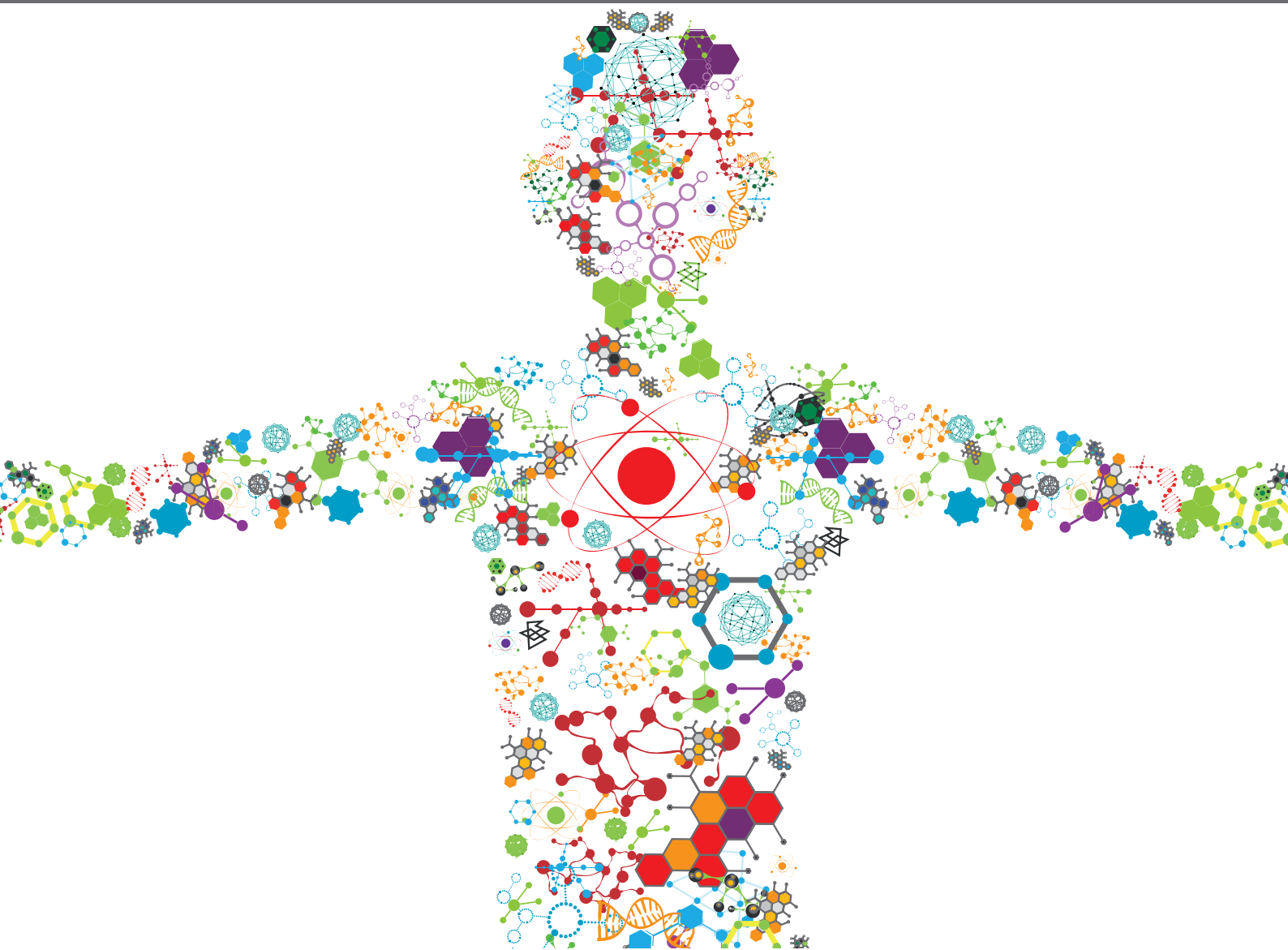


FROM BIOMASS TO BIO-ENERGY AND BIO-CHEMICALS: PRETREATMENT, THERMOCHEMICAL CONVERSION, BIOCHEMICAL CONVERSION AND ITS BIO-BASED APPLICATIONS

EDITED BY: Chao Zhao, Zhongqing Ma, Caoxing Huang, Jia-Long Wen
and Muhammad Hassan

PUBLISHED IN: Frontiers in Bioengineering and Biotechnology and
Frontiers in Chemistry





frontiers

Frontiers eBook Copyright Statement

The copyright in the text of individual articles in this eBook is the property of their respective authors or their respective institutions or funders. The copyright in graphics and images within each article may be subject to copyright of other parties. In both cases this is subject to a license granted to Frontiers.

The compilation of articles constituting this eBook is the property of Frontiers.

Each article within this eBook, and the eBook itself, are published under the most recent version of the Creative Commons CC-BY licence.

The version current at the date of publication of this eBook is CC-BY 4.0. If the CC-BY licence is updated, the licence granted by Frontiers is automatically updated to the new version.

When exercising any right under the CC-BY licence, Frontiers must be attributed as the original publisher of the article or eBook, as applicable.

Authors have the responsibility of ensuring that any graphics or other materials which are the property of others may be included in the CC-BY licence, but this should be checked before relying on the CC-BY licence to reproduce those materials. Any copyright notices relating to those materials must be complied with.

Copyright and source acknowledgement notices may not be removed and must be displayed in any copy, derivative work or partial copy which includes the elements in question.

All copyright, and all rights therein, are protected by national and international copyright laws. The above represents a summary only. For further information please read Frontiers' Conditions for Website Use and Copyright Statement, and the applicable CC-BY licence.

ISSN 1664-8714

ISBN 978-2-83250-753-7

DOI 10.3389/978-2-83250-753-7

About Frontiers

Frontiers is more than just an open-access publisher of scholarly articles: it is a pioneering approach to the world of academia, radically improving the way scholarly research is managed. The grand vision of Frontiers is a world where all people have an equal opportunity to seek, share and generate knowledge. Frontiers provides immediate and permanent online open access to all its publications, but this alone is not enough to realize our grand goals.

Frontiers Journal Series

The Frontiers Journal Series is a multi-tier and interdisciplinary set of open-access, online journals, promising a paradigm shift from the current review, selection and dissemination processes in academic publishing. All Frontiers journals are driven by researchers for researchers; therefore, they constitute a service to the scholarly community. At the same time, the Frontiers Journal Series operates on a revolutionary invention, the tiered publishing system, initially addressing specific communities of scholars, and gradually climbing up to broader public understanding, thus serving the interests of the lay society, too.

Dedication to Quality

Each Frontiers article is a landmark of the highest quality, thanks to genuinely collaborative interactions between authors and review editors, who include some of the world's best academicians. Research must be certified by peers before entering a stream of knowledge that may eventually reach the public - and shape society; therefore, Frontiers only applies the most rigorous and unbiased reviews. Frontiers revolutionizes research publishing by freely delivering the most outstanding research, evaluated with no bias from both the academic and social point of view. By applying the most advanced information technologies, Frontiers is catapulting scholarly publishing into a new generation.

What are Frontiers Research Topics?

Frontiers Research Topics are very popular trademarks of the Frontiers Journals Series: they are collections of at least ten articles, all centered on a particular subject. With their unique mix of varied contributions from Original Research to Review Articles, Frontiers Research Topics unify the most influential researchers, the latest key findings and historical advances in a hot research area! Find out more on how to host your own Frontiers Research Topic or contribute to one as an author by contacting the Frontiers Editorial Office: frontiersin.org/about/contact

FROM BIOMASS TO BIO-ENERGY AND BIO-CHEMICALS: PRETREATMENT, THERMOCHEMICAL CONVERSION, BIOCHEMICAL CONVERSION AND ITS BIO-BASED APPLICATIONS

Topic Editors:

Chao Zhao, Zhejiang A&F University, Zhejiang, China

Zhongqing Ma, Zhejiang Agriculture and Forestry University, China

Caoxing Huang, Nanjing Forestry University, China

Jia-Long Wen, Beijing Forestry University, China

Muhammad Hassan, National University of Sciences and Technology (NUST),
Pakistan

Citation: Zhao, C., Ma, Z., Huang, C., Wen, J.-L., Hassan, M., eds. (2022). From Biomass to Bio-energy and Bio-chemicals: Pretreatment, Thermochemical Conversion, Biochemical Conversion and Its Bio-Based Applications. Lausanne: Frontiers Media SA. doi: 10.3389/978-2-83250-753-7

Table of Contents

- 05 Editorial: From Biomass to Bio-energy and Bio-chemicals: Pretreatment, Thermochemical Conversion, Biochemical Conversion and Its Bio-Based Applications**
Chao Zhao, Zhongqing Ma, Caoxing Huang, Jialong Wen and Muhammad Hassan
- 09 Ultrasound-Assisted Production of Xylo-Oligosaccharides From Alkali-Solubilized Corncob Bran Using *Penicillium janthinellum* XAF01 Acidic Xylanase**
Mingchun Zhou, Guangsen Fan, Hanshuo Xia, Xiaohan Zhang, Chao Teng and Xiuting Li
- 18 Insight in the Recent Application of Polyphenols From Biomass**
Bowen Yan, Zhefan Stephen Chen, Yingying Hu and Qiang Yong
- 33 Prospects and Applications of Biomass-Based Transparent Wood: An Architectural Glass Perspective**
Jing Wang and Jian'gang Zhu
- 42 Preparation and Application in Water Treatment of Magnetic Biochar**
Qingshuang Zhao, Ting Xu, Xueping Song, Shuangxi Nie, Sun-Eun Choi and Chuanling Si
- 52 Effects of P-Coumarate 3-Hydroxylase Downregulation on the Compositional and Structural Characteristics of Lignin and Hemicelluloses in Poplar Wood (*Populus alba* × *Populus glandulosa*)**
Xiao-Peng Peng, Jing Bian, Shuang-Quan Yao, Cheng-Ye Ma and Jia-Long Wen
- 62 Research Progress on Cell Membrane-Coated Biomimetic Delivery Systems**
Mengyu Guo, Chenjie Xia, Yu Wu, Nong Zhou, Zhipeng Chen and Weidong Li
- 76 Bioprocess of Microbial Melanin Production and Isolation**
Kwon-Young Choi
- 88 The Kinetics Studies on Hydrolysis of Hemicellulose**
Qi Yuan, Shan Liu, Ming-Guo Ma, Xing-Xiang Ji, Sun-Eun Choi and Chuanling Si
- 100 Using poly(*N*-Vinylcaprolactam) to Improve the Enzymatic Hydrolysis Efficiency of Phenylsulfonic Acid-Pretreated Bamboo**
Xianqing Lv, Guangxu Yang, Zhenggang Gong, Xin Cheng, Li Shuai, Liulian Huang, Lihui Chen, Xiaolin Luo and Jing Liu
- 113 Isolation and Fractionation of the Tobacco Stalk Lignin for Customized Value-Added Utilization**
Zhi Chang Liu, Zi Wei Wang, Song Gao, Yu Xing Tong, Xi Le, Nian Wu Hu, Qun Shan Yan, Xian Gang Zhou, Yan Rong He and Lei Wang

- 122 ***Salix spp. Bark Hot Water Extracts Show Antiviral, Antibacterial, and Antioxidant Activities—The Bioactive Properties of 16 Clones***
Jenni Tienaho, Dhanik Reshamwala, Tytti Sarjala, Petri Kilpeläinen, Jaana Liimatainen, Jinze Dou, Anneli Viherä-Aarnio, Riikka Linnakoski, Varpu Marjomäki and Tuula Jyske
- 141 ***The Biodegradation of Soil Organic Matter in Soil-Dwelling Humivorous Fauna***
Xuliang Lou, Jianming Zhao, Xiangyang Lou, Xiejiang Xia, Yilu Feng and Hongjie Li
- 149 ***Lignin-Based/Polypyrrole Carbon Nanofiber Electrode With Enhanced Electrochemical Properties by Electrospun Method***
Zhou-Rui Hu, Dan-Dan Li, Tae-Hee Kim, Min-Seok Kim, Ting Xu, Ming-Guo Ma, Sun-Eun Choi and Chuanling Si
- 161 ***Pyroligneous Acids of Differently Pretreated Hybrid Aspen Biomass: Herbicide and Fungicide Performance***
Pasi Korkalo, Marleena Hagner, Janne Jänis, Marko Mäkinen, Janne Kaseva, Ulla Lassi, Kimmo Rasa and Tuula Jyske
- 175 ***Production of Hydroxymethylfurfural Derivatives From Furfural Derivatives via Hydroxymethylation***
Xianqing Lv, Xiaolin Luo, Xin Cheng, Jing Liu, Changzhi Li and Li Shuai
- 183 ***Hydrothermal Pretreatment of Lignocellulosic Feedstocks to Facilitate Biochemical Conversion***
Carlos Martín, Pooja Dixit, Forough Momayez and Leif J. Jönsson
- 200 ***Expression, Purification, and Preliminary Protection Study of Dehydrin PicW1 From the Biomass of Picea wilsonii***
Junhua Liu, Mei Dai, Jiangtao Li, Yitong Zhang, Yangjie Ren, Jichen Xu, Wei Gao and Sujuan Guo
- 209 ***Multifunctional Cellulose and Cellulose-Based (Nano) Composite Adsorbents***
Ru-Jie Shi, Tian Wang, Jia-Qi Lang, Nong Zhou and Ming-Guo Ma
- 223 ***Sustainable Production of Bioethanol Using Levulinic Acid Pretreated Sawdust***
Ali Nawaz, Rong Huang, Farah Junaid, Yiwei Feng, Ikram Ul Haq, Hamid Mukhtar and Kankan Jiang



OPEN ACCESS

EDITED AND REVIEWED BY
Manfred Zinn,
HES-SO Valais-Wallis, Switzerland

*CORRESPONDENCE
Chao Zhao,
zhaochao@zafu.edu.cn

SPECIALTY SECTION
This article was submitted to Bioprocess Engineering, a section of the journal Frontiers in Bioengineering and Biotechnology

RECEIVED 22 June 2022
ACCEPTED 17 October 2022
PUBLISHED 28 October 2022

CITATION
Zhao C, Ma Z, Huang C, Wen J and Hassan M (2022), Editorial: From biomass to bio-energy and bio-chemicals: Pretreatment, thermochemical conversion, biochemical conversion and its bio-based applications.
Front. Bioeng. Biotechnol. 10:975171.
doi: 10.3389/fbioe.2022.975171

COPYRIGHT
© 2022 Zhao, Ma, Huang, Wen and Hassan. This is an open-access article distributed under the terms of the Creative Commons Attribution License (CC BY). The use, distribution or reproduction in other forums is permitted, provided the original author(s) and the copyright owner(s) are credited and that the original publication in this journal is cited, in accordance with accepted academic practice. No use, distribution or reproduction is permitted which does not comply with these terms.

Editorial: From biomass to bio-energy and bio-chemicals: Pretreatment, thermochemical conversion, biochemical conversion and its bio-based applications

Chao Zhao^{1*}, Zhongqing Ma², Caoxing Huang³, Jialong Wen⁴ and Muhammad Hassan⁵

¹National Engineering Research Center for Wood-based Resource Utilization, College of Optical, Mechanical and Electrical Engineering, Zhejiang A&F University, Hangzhou, China, ²College of Chemistry and Materials Engineering, Zhejiang A&F University, Hangzhou, China, ³Co-Innovation Center for Efficient Processing and Utilization of Forest Resources, College of Chemical Engineering, Nanjing Forestry University, Nanjing, China, ⁴Beijing Key Laboratory of Lignocellulosic Chemistry, Beijing Forestry University, Beijing, China, ⁵U.S.-Pakistan Centre for Advanced Studies in Energy, National University of Science and Technology (NUST), Islamabad, Pakistan

KEYWORDS

pretreatment, lignocellulose fractionation, enzymatic hydrolysis, genetic engineering, bio-chemicals

Editorial on the Research Topic

From biomass to bio-energy and bio-chemicals: Pretreatment, thermochemical conversion, biochemical conversion and its bio-based applications

Lignocellulosic biomass is the most abundant renewable feedstock on the Earth, which can be used to produce bio-fuels and bio-chemicals to support the sustainable development (Chundawat et al., 2011). Owing to the dual challenges of limited resources and the impacts on the environment, research on the efficient preparation of energy and chemicals using lignocellulosic biomass has attracted considerable attention (Lin et al., 2021).

Bio-energy derived from biomass is one of the most important renewable energy sources. It includes three major types occurring in three states: solid (briquette), liquid (biodiesel, bioethanol, and bio-oil), and gaseous (biogas, syngas, and biohydrogen) (Yu et al., 2021). There are broadly two conversion platforms for biomass: thermochemical conversion and biochemical conversion (Zhao et al., 2020a). Pretreatment is a necessary procedure for obtaining homogeneous raw materials. However, there remain many challenges including biomass heterogeneity resulting from the variation in biomass components, as well as the structural variations in each constituent, complicated pretreatment processes, low conversion efficiency, the high cost of enzymatic

hydrolysis, the efficient engineering of bacteria breeding, and the application of its by-products (biochar for thermochemical conversion and lignin for biochemical conversion) (Qiao et al., 2018).

Bio-chemicals with excellent performance and high value added can be produced from biomass through physical, chemical, and biological high-tech methods. Similarly, the structure and properties of biomass limit the separation, purification, and effective utilisation of its components. There are still many challenges in the preparation of bio-chemicals from biomass, notably the selection of chemical reaction paths derived from multiscale complexity, the highly-selective depolymerisation, deoxygenation, polymerisation inhibition, and repolymerisation reactions of biomass components, especially the selective fracture of chemical bonds between cellulose, hemicellulose, and lignin (Zhao et al., 2020b).

The topic *From biomass to bio-energy and bio-chemicals: Pretreatment, thermochemical conversion, biochemical conversion and its bio-based applications* covers sustainable bio-refining processes from biomass to chemicals, sustainable pretreatment/fractionation technologies from biomass to bio-energy, genetic engineering of lignocellulosic feedstocks for bio-refinery, and sustainable bio-based applications in architecture, electrode materials, and adsorbents. We sincerely thank the 109 authors whose work we have drawn on for their excellent works on this topic. The following highlights have been drawn from their contributions to this Research Topic.

Sustainable bio-refining processes from biomass to chemicals

Zhou et al. evaluated the effects of ultrasound-assisted production of xylo-oligosaccharides (XOS) from alkali-solubilised corncob bran. The maximum yield of XOS was 20.71% at the ultrasonic parameters of 50 kHz and 0.40 W/cm². Lv et al. proposed a new reaction pathway for the synthesis of functional hydroxy-methyl-furfural (HMF) derivatives (EMFM, BHMF, and BHMF) from commercially available furfural derivatives (EMF and FA), and provided a new method to transform condensed furanics into hydrocarbon fuel through a two-step hydro-deoxygenation (HDO) process. Although such a pathway is feasible, achieving high yields of hydroxymethylated products in these reactions is challenging, owing to the parallel ring-opening reaction of furanics and condensation of the resulting ring-opening products. Therefore, future research should focus on the development of more efficient catalysts or reaction systems to suppress these side reactions and improve the selectivity of the targeted products. Korkalo et al. developed a cascade processing scheme to prepare pyrolytic acids (PAs) from the extractives of hybrid aspen bark. To obtain PAs, firstly the lipophilic and hydrophilic extracts were extracted through

pretreatment of the bark using hot water and alkaline alcohol (HWE+AAE), and then the extractives were torrefied to PAs. The PAs obtained showed excellent herbicide and fungicide performances.

As the only renewable carbon source, biomass can be converted into chemicals with great potential prospect. In recent years, many advances have been made in the preparation of chemicals from biomass; however, the majority of these are still in the laboratory research stage and cannot meet the requirements of large-scale production. Future research should focus on the following aspects: 1) strengthening the research on the reaction mechanisms and pathways of biochemical conversion; 2) further optimisation of the catalytic system and the reaction conditions to improve the yield and selectivity of target products; and 3) establishing an efficient, low-energy, low-cost and environmentally friendly product separation system. With the deepening of basic research, the large-scale production of highly value-added chemicals from biomass is becoming promising.

Sustainable pretreatment/fractionation technologies from biomass to bio-energy

Nawaz et al. explored the sustainable pretreatment of sawdust with levulinic acid-based natural deep eutectic solvents (DESs). The optimised molar ratio of levulinic acid: choline chloride was 1: 0.5, which resulted in 91% delignification and 25.87% maximum enzymatic hydrolysis of the sawdust. Fermentation produced 11.82% of bioethanol production was obtained at 30°C, and 180 rpm after 72 h. Lv et al. explored the use of poly (N-vinylcaprolactam) (PNVCL) to improve the enzymatic hydrolysis of bamboo after pretreatment with phenyl-sulfonic acid (PSA) pretreatment. A cellulosic conversion of 80% of PSA-treated-bamboo was achieved when the PNVCL loading was 1.2 g/L during enzymatic hydrolysis. Compared to the case without the addition of PNVCL, the cellulase loading of PSA-treated-bamboo was three times reduced. Mechanism research has shown that PNVCL can effectively prevent non-productive adsorption of enzymes through inter-molecular non-covalent interactions. Liu et al. isolated lignin from tobacco stalks using a hydrothermally assisted dilute alkali pretreatment. Subsequently, the isolated alkaline lignin was fractionated into five uniform lignin components using various solvents. According to the different structures of lignin fractions, Liu et al. suggested that lignin fractions with lower molecular weights were more suitable for preparing antioxidants, whereas those with high molecular weights showed great potentials for preparing carbon materials.

For biochemical conversion route, the goal of the pretreatment is to improve the enzymatic hydrolysis of

cellulose. Sustainable pretreatment technologies include green solvent-based ionic liquid and DESs. In addition, future pretreatment research should focus on the modification of traditional pretreatments, addressing aspects such as biocatalytic methods, enzyme properties and enzyme recycling, making full use of lignin valorisation, and the management of residual streams from the perspective of biorefinery.

Genetic engineering of lignocellulosic feedstocks for bio-refinery

Peng et al. studied the effects of *p*-coumarate 3-hydroxylase (C3H) down regulation on the chemical and structural characteristics of hemicelluloses and lignin, and found that the down-regulated poplar wood is beneficial for the upstream gene validation and downstream biomass conversion. Tienaho et al. studied the functional profiles of 16 northern willow clones for the use of value-added bioactive solutions. The results showed that all of the clones had antibacterial activity against *Staphylococcus aureus* and *Escherichia coli*, but no antifungal (*Aspergillus brasiliensis*) or yeastocidal (*Candida albicans*) efficacy. Additionally, *S. myrsinifolia* clone extracts showed significantly higher activities in some antioxidant tests than the commercial clone extracts and artificial clone extracts.

Both genetic modification and pretreatment are expected to reduce biomass recalcitrance, and genetic modification of plants is considered to be ultimate solution to reduce biomass recalcitrance. At present, the majority of modifications use lignin gene manipulation to reduce biomass recalcitrance, such as down-regulation of the switchgrass caffeic acid O-methyltransferase gene, or down-regulation of cinnamyl alcohol dehydrogenase which leads to incorporation of aldehyde groups in the lignin polymer. The potential for the use of atomistic molecular dynamics (MD) simulations as a predictive tool for the effect of genetic modifications on plants should be pursued in future work. This knowledge paves the way towards the development of high value-added biochemicals and other functional solutions based on genetic engineering of lignocellulosic feedstocks for biorefinery approaches.

Sustainable bio-based applications from biomass

Wang and Zhu discussed the research progress of biomass-based transparent wood (BBTW), and summarized the key technologies and potential prospects of BBTW for the replacement of architectural glass. As a green and renewable material, BBTW offers the advantages of good lighting conditions, flame retardancy, heat insulation and safety. Hu et al. designed the lignin/polypyrrole (PPy) composite

electrode films with microporous and mesoporous structures by electrostatic spinning, carbonisation, and *in-situ* polymerisation methods, which can be served as a positive material for super-capacitors. The LCNF/PPy electrode had a large specific surface area, high pore volume, and a specific capacitance of 213.7 F/g at a current density of 1 A/g. Shi et al. studied the adsorbents produced using multifunctional cellulose and cellulose-based (nano) composites. The authors believed that these biomass adsorbents will play an increasingly important role in environmental protection, particularly in wastewater treatment.

Nano-cellulose has many advantages such as high modulus, high specific surface area, special optical properties and good biocompatibility. Nano-lignin has the characteristics of a highly specific surface area, multiple chemical groups, antibacterial activity, and non-toxicity. As a green and environmental bio-based material, nano-lignocellulose has broad applications in architecture, food industry, biomedicine, environmental materials, photoelectric materials, and other fields. However, more research is needed to explore the efficient preparation of homogeneous and stable nanolignin. For nanocellulose, promoting the development of products with both cost and performance characteristics and developing green and environmentally friendly preparation methods could accelerate their industrialisation and large-scale production processes.

Author contributions

All authors listed have made a substantial, direct, and intellectual contribution to the work and the final version for publication.

Acknowledgments

We thank all the authors, reviewers, topic editors, and editorial staff at Frontiers who contributed to this Research Topic. We would like to thank Editage (www.editage.cn) for English language editing.

Conflict of interest

The authors declare that the research was conducted in the absence of any commercial or financial relationships that could be construed as a potential conflict of interest.

Publisher's note

All claims expressed in this article are solely those of the authors and do not necessarily represent those of their affiliated

organizations, or those of the publisher, the editors and the reviewers. Any product that may be evaluated in this article, or

claim that may be made by its manufacturer, is not guaranteed or endorsed by the publisher.

References

- Chundawat, S. P., Beckham, G. T., Himmel, M. E., and Dale, B. E. (2011). Deconstruction of lignocellulosic biomass to fuels and chemicals. *Annu. Rev. Chem. Biomol. Eng.* 2, 121–145. doi:10.1146/annurev-chembioeng-061010-114205
- Lin, W., Yang, J., Zheng, Y., Huang, C., and Yong, Q. (2021). Understanding the effects of different residual lignin fractions in acid-pretreated bamboo residues on its enzymatic digestibility. *Biotechnol. Biofuels* 14, 143. doi:10.1186/s13068-021-01994-y
- Qiao, X., Zhao, C., Shao, Q., and Hassan, M. (2018). Structural characterization of corn stover lignin after hydrogen peroxide presoaking prior to ammonia fiber expansion pretreatment. *Energy fuels* 32, 6022–6030. doi:10.1021/acs.energyfuels.8b00951
- Yu, Q., Wang, Y., Van Le, Q., Yang, H., Hosseinzadeh-Bandbafha, H., Yang, Y., et al. (2021). An overview on the conversion of forest biomass into bioenergy. *Front. Energy Res.* 9, 1. doi:10.3389/fenrg.2021.684234
- Zhao, C., Qiao, X., Shao, Q., Hassan, M., Ma, Z., and Yao, L. (2020a). Synergistic effect of hydrogen peroxide and ammonia on lignin. *Ind. Crops Prod.* 146, 112177. doi:10.1016/j.indcrop.2020.112177
- Zhao, C., Shao, Q., and Chundawat, S. P. S. (2020b). Recent advances on ammonia-based pretreatments of lignocellulosic biomass. *Bioresour. Technol.* 298, 122446. doi:10.1016/j.biortech.2019.122446



Ultrasound-Assisted Production of Xylo-Oligosaccharides From Alkali-Solubilized Corncob Bran Using *Penicillium janthinellum* XAF01 Acidic Xylanase

Mingchun Zhou^{1,2,3}, Guangsen Fan^{1,2,3}, Hanshuo Xia^{2,4}, Xiaohan Zhang^{2,3}, Chao Teng^{1,2,3*} and Xiuting Li^{2,3*}

¹Beijing Engineering and Technology Research Center of Food Additives, Beijing Technology and Business University, Beijing, China, ²Beijing Advanced Innovation Center for Food Nutrition and Human Health, Beijing Technology and Business University (BTBU), Beijing, China, ³School of Food and Health, Beijing Technology and Business University, Beijing, China, ⁴College of Food Science and Engineering, Jilin Agricultural University, Changchun, China

OPEN ACCESS

Edited by:

Chao Zhao,
Zhejiang A & F University, China

Reviewed by:

Junhua Zhang,
Nanjing Forestry University, China
Ruichang Gao,
Jiangsu University, China

*Correspondence:

Chao Teng
tc2076paper@163.com
Xiuting Li
lixt@btbu.edu.cn

Specialty section:

This article was submitted to
Bioprocess Engineering,
a section of the journal
Frontiers in Bioengineering and
Biotechnology

Received: 07 August 2021

Accepted: 26 August 2021

Published: 10 September 2021

Citation:

Zhou M, Fan G, Xia H, Zhang X, Teng C
and Li X (2021) Ultrasound-Assisted
Production of Xylo-Oligosaccharides
From Alkali-Solubilized Corncob Bran
Using *Penicillium janthinellum* XAF01
Acidic Xylanase.
Front. Bioeng. Biotechnol. 9:755003.
doi: 10.3389/fbioe.2021.755003

A novel treatment involving enzymatic hydrolysis using an acidic xylanase coupled with ultrasound was performed to improve the xylo-oligosaccharides (XOS) yield from corncob bran. The acidic xylanase (XynB) was purified to a most suitable pH, temperature, and operational parameters for ultrasound-assisted hydrolysis were determined. A preliminary mechanistic investigation was performed through circular dichroism (CD) spectroscopy, scanning electron microscope (SEM) and a laser particle size analyzer, and the effects of ultrasound on enzyme (XynB) and substrate (corncob bran) were assessed. The results show that the maximum XOS yield was 20.71% when the reaction pH and temperature were 4.3 and 50°C, the ultrasonic parameters were 50 kHz and 0.40 W/cm², which was 2.55 fold higher than that obtained using a non-ultrasound-assisted enzymatic preparation. Mechanism studies indicated that ultrasonic pretreatment could reduce the β -fold content and increase the random coil content. Changes in structure and size of substrate were observed. The specific surface area of the XAC molecules is easy to carry out enzymatic reaction, which is beneficial to the production of XOS.

Keywords: acidic xylanase, corncob, sonication, *Penicillium janthinellum*, xylo-oligosaccharides

INTRODUCTION

Lignocellulosic materials are the most abundant organic residues worldwide. Grains including wheat straw, rice straw, corn cobs and tobacco straw are rich in lignocellulose and are potential industrial feeds (Chapla et al., 2012). Plant biomass is an economical, available, and renewable source of biofuel, bioenergy, and a variety of value-added biomolecules (Kumar and Satyanarayana, 2015). Corncob contains about 35% xylan, which is an essential by-product of that industry. It has many functions and can be used as animal feed or return to harvested farmland (Aachary and Prapulla, 2009). It is noteworthy that the xylan, a complex five-carbon polysaccharide, is the main component in hemicellulose (Liu et al., 2021). The xylan-rich

lignocellulosic materials contain a large amount of xylan, which are composed of two to seven xylose units connected by β -1,4-glycosidic links (de Figueiredo et al., 2017; Freitas et al., 2019), selectively increase the growth of *Bifidobacteria* and *Lactobacillus* and exhibit antioxidant activities (Yamani et al., 2016; Zhang et al., 2018; Khangwal and Shukla, 2019). In addition, research on XOS has proven that it can be widely used in diet, health care industries, animal's husbandry, chemical and pharmaceutical industries (Moniz et al., 2016; Khangwal et al., 2020). The general strategies used for XOS production include pretreatments and hydrolysis (Kumar and Satyanarayana, 2015; Freitas et al., 2021). Hemicellulose extraction involves various pretreatments, which ease the subsequent XOS producing steps. At present, the main methods for pretreatment include: heat-dilute-acide hydrolysis (Liu et al., 2012), organic solvent extraction (Zhang et al., 2016), pyrohydrolysis of hemicellulose (Zhao et al., 2019) and alkaline extraction (Rashid et al., 2020). Compared to other pretreatment methods, alkaline extraction operating conditions are less demanding (lower temperature and pressure) (Badiei et al., 2014) and promote the dissolution of lignin and also protect cellulose from drastic degradation (Liu et al., 2021). It is considered an effective way to pursue high xylan extraction rates, low cost and high purity. In fact, alkaline hydrolysis causes the xylan to be subjected to endo-xylanases, resulting in high yield of XOS (Akpınar et al., 2010).

Ultrasound, a green method of extracting natural products, is a new concept that is both environment and user-friendly; at the same time, it can enhance the competitiveness of the industry and make the technology more environmentally friendly, economical and innovative (Chemat et al., 2017). This emerging technology has been used as an alternative to conventional food processing operations for inactivating or accelerating enzymatic activity and facilitating the extraction of various bioactive components (Gallego-Juárez et al., 2010). Although some studies have reported that a combination of ultrasound and pectinase (Larsen et al., 2021), cellulase (Szabo and Csiszar, 2017), lipase (Jadhav et al., 2021), α -amylase (Gaquere-Parker et al., 2018), alkaline protease (Pawar and Rathod, 2018) and saccharification enzyme (Wang et al., 2017) accelerates the enzymatic reaction. The results may be due to effects on enzyme behavior, changes in substrate structure, and effect of the reaction medium (Jian et al., 2008). Yet, reports on the hydrolysis of xylan catalyzed by ultrasound-assisted xylanase can be rarely seen. Long-term exposure to high-intensity ultrasound can restrict the enzymes' catalytic activity. However, in certain cases, enzyme activities have increased following short exposures to ultrasound (Joshi and Gogate, 2019; Farzadkia et al., 2021).

Many microorganisms are the origin of xylanase producers and there already are considerable documents on xylanase in fungi which are intensively studied (Uma et al., 2016). Studies have reported the opinion that xylanases have optimal activity at mesophilic temperatures and moderate or slightly acidic pH. Contrary to alkalophilic xylanases

(active at $\text{pH} \geq 8.0$), only few of their acidophilic counterparts (active pH between 1.0 and 5.0) have been studied so far (Kallel et al., 2016). The objective of this study was to evaluate the effect of acidic xylanase (from *Penicillium janthinellum* XAF01) on XOS production in the presence of low intensity ultrasound treatment. The circular dichroism (CD) spectra of xylanase and the scanning electron micrographs of xylan were also analyzed for determining the mechanism underlying ultrasound treatment.

MATERIALS AND METHODS

Raw Material and Preparation of Hemicellulosic From Corncob

The raw material corncob used in this work was provided by a XOS factory (Shandong Longlive Biotechnology Co.) in Shandong province, China. Dry in an oven at 60°C for 24 h, mill (60–80 mesh), and store in a closed polycarbonate container. The composition of the corncob was 45.7% cellulose, 33.3% hemicelluloses, 18.0% lignin, and 3.0% ash on a dry weight basis. Xylan was prepared according to the method of Longue Júnior with some modifications (Longue Junior et al., 2013). The optimal process conditions can be got from single factor experiment carried out by using four main factors: corncob concentration, pH, temperature and time: corncob was pretreated with 10% NaOH, with a liquid to solid ratios (L:S) (mL:g) of 10:1, at 100°C for 2 h. The liquid fraction was collected, neutralized to pH 7.0 with HCl, concentrated, and then freeze dried. The yield of the hemicellulosic fraction was 22.7% (hemicellulosic fraction/g corncob). Corncob xylan extracted using NaOH was abbreviated as XAC, which was then used as the substrate for XOS production. All other chemicals were analytical grade and commercially available unless otherwise stated.

Strain and Culture Conditions

P. janthinellum XAF01 was isolated from soil samples collected from Honghe, Yunnan province, China. For the production of xylanase, *P. janthinellum* XAF01 was cultivated in 250 ml Erlenmeyer flasks containing 60 g/L corncob as carbon source in 50 ml minimal medium (0.2% NaNO_3 , 0.6% KH_2PO_4 , 0.05% $\text{MgSO}_4 \cdot 7\text{H}_2\text{O}$, 0.15% K_2HPO_4) supplemented with 0.3% yeast extract and 1.0% beef peptone. Under a condition of pH 3.5, temperature at 25°C and lasting for 7 days, cultures grew with shaking at 125 r/min. After growth, the culture supernatant was separated from the mycelium by centrifugation at 10,000 r/min for 20 min. The supernatant solutions, hereafter called crude extracts, were stored at 4°C for subsequent use.

Enzyme Assay and Purification

Enzyme Assay

Endo- β -D-xylanase (EC3.2.1.8) activity was determined using the modified dinitrosalicylic acid (DNS) method (Bailey et al., 1992).

Briefly, 100 μ L of the culture supernatant solution and 900 μ L of a 1% (w/v) beechwood xylan (Sigma-Aldrich Pvt. Ltd., United States) suspension in 50 mM citrate buffer (pH 4.0) were mixed. The incubation of mixture was carried out at 55°C for 5 min and with the addition of 1000 μ L DNS, the reaction can be stopped. The xylanase activity unit is the needed amount of enzyme to release 1 μ mol xylose equivalent in every 60 s.

Protein concentrations were determined using Lowry's method (Lowry et al., 1951), and BSA (bovine serum albumin) used as the standard was purchased from Roche (738328).

Enzyme Purification

Each purification process was executed at 4°C. The crude enzyme was first purified with 20–50% ammonium sulfate (Sinopharm Chemical Reagent CO., Ltd.); the preliminary purified enzyme solution was subjected to dialysis for 12 h with 20 mM sodium acetate buffer, pH 3.8, and then loaded on a SP-Sepharose Fast Flow ion-exchange column equilibrated with 20 mM sodium acetate buffer, pH 3.8. The elution was carried out with a linear NaCl gradient (0–100 mm in 20 mM sodium acetate buffer, pH 3.8) at a flow rate of 1.0 ml/min.

All active fractions were concentrated to 1.0 ml and slowly loaded on a Q-Sepharose Fast Flow column, which was equilibrated with 20 mM citrate buffer (pH 5.6). At a flow rate of 1.0 ml/min, 2 ml fractions were collected after eluting protein. Fractions exhibiting xylanase activity were then collected for further use.

Sodium Dodecyl Sulfate-Polyacrylamide Gel Electrophoresis and Zymogram

Enzyme purity and molecular weight can be determined by SDS-PAGE and 12.5% (w/v) separation and 4.5% (w/v) stacked gel (Laemmli, 1970). By Coomassie Brilliant Blue G 250, the gel was stained. And the molecular weight of the enzyme is determined with a low molecular weight scale label.

The xylanase activity was detected by incubation with a zymogram gel containing 1% (w/v) birchwood xylan (Sigma-Aldrich Pvt. Ltd., United States) at 40°C for 2 h, followed by staining in Congo red solution (1 mg/ml). The dye was removed using 1 M NaCl solution till clear areas in a dark red background appeared, which is indicative of xylanase activity (Schwarz et al., 1987).

Biochemical Characterization of the Purified Xylanases

Effect of pH on Xylanase Activity and Stability

With 1% beechwood xylan as the substrate, the best pH value required in xylanase activity can be determined at 55°C in the pH range of 2.70–9.00. The highest xylanase activity was used to define 100% activity. The following buffer systems (50 mM) were used: citrate buffer, pH 2.70–5.70; acetate buffer, pH 3.20–5.80; MES buffer, pH 5.20–7.20; MOPS buffer, pH 6.20–8.20; Tris-HCl buffer, pH 7.00–9.00.

The effect of pH on the stability of xylanase was evaluated by incubating the enzyme at different pH values for 30 min at 50°C.

Samples were then cooled with ice water. Afterwards, residual activity of each sample was determined under standard conditions.

Effect of Temperature on Xylanase Activity and Stability

The optimal temperature required for enzyme activity was determined in the range of 40–60°C. In each case, samples were diluted in the optimal pH buffer solution prior to xylanase activity assay. The thermal stability of the immobilized and free xylanase were determined by incubating the enzyme in the optimal pH buffer solution for 5 h at different temperatures (40–60°C). At certain time intervals, aliquots could be extracted, and under standard conditions, residual activity can be tested. The 100% activity can be determined by the unheated enzyme.

Ultrasound-Assisted Hydrolysis of Hemicellulosic Fraction

Ultrasonic hydrolysis was carried out using a DTD5200S ultrasonic device (Beijing Hongxianglong Biotechnology Co., Ltd.) with an ultrasonic power of up to 300 W, a frequency of 135 kHz, and a microtip diameter of 10 mm. The instrument used was a US bath type reactor with five different 2.0 cm ultrasound generator probes at four different frequencies (28, 40, 50, and 128 kHz); all probes can deliver maximum power of 300 W. Prior to hydrolysis, XAC was powdered into 0.45 mm particles. Subsequently, the ground XAC were dispersed at liquid to solid ratios of 50:1 (mL:g), in 10 ml 50 mM acetate buffer (pH 3.7) and the reaction was performed using 16U/mL acidic xylanase at 40°C for 40 min. The prepared XAC was completely mixed in a beaker 3 cm shorter than the water bath, and the probe of the ultrasonic generator (about 1 cm to the liquid level) was inserted into the ultrasonic field immediately. The ultrasound intensity released from the probe was regulated to 0.04, 0.13, 0.22, 0.31, 0.40 W/cm² and the ultrasound frequencies was regulated to 28, 40, 50, and 128 kHz. Each treatment was replicated thrice.

Determination of the Kinetic Parameters of the Michaelis–Menten

The function of ultrasound (0.31 W/cm² and 50 kHz) on acidic xylanase was evaluated. The enzyme activity of xylanase at 40°C for 5 min was determined by different substrate concentrations, and the kinetic parameters of xylanase on beech xylan were determined; with the help of “GraFit” software, we calculated *K_m* and *V_{max}* values.

Test of Effect of Ultrasound on Xylanase XynB and the Substrate

CD Measurement of Acidic Xylanase XynB

Enzyme XynB (0.20 mg/ml) in 0.05 M acetate buffer (pH 3.8) was sonicated at 40°C using three categories or protocols for monitoring changes in enzyme structure under different ultrasound conditions. The first group of experiments studied the effect of ultrasound with different sound

intensity (0.04, 0.13, 0.22, 0.31, 0.40 W/cm²) at 50 kHz for 40 min. The second set of experiments was performed at different ultrasonic frequency (28, 40, 50, 128 kHz) at 0.31 W/cm² for 40 min. The third set of experiments was performed at different time points (10, 20, 30, and 40 min) at 0.31 W/cm² and 50 kHz.

After ultrasound, CD spectra were recorded by spectrometer (JASCO, Tokyo, Japan; J-815 type), and CD spectra were recorded by a quartz container with 1 mm optical path length at room temperature (20 ± 1°C). CD spectra were scanned in the far ultraviolet (260–190 nm) range with a repetition rate of 100 nm/min and a bandwidth of 0.1 nm. CD data are represented by molar ellipticity in mdeg. cm². dmol⁻¹. The α -helix in the measured molar ellipticity of xylanase was observed at 208 nm (Wang et al., 2003).

Characterization of XAC Particles

The particle sizes of xylan (XAC) and its aggregates in XAC suspension and acoustic XAC suspension were measured by TopSizer laser diffraction particle size analyzer (OMEC, Zhuhai, China). Which can provide useful information for comparing the size of non-spherical rod like xylan whiskers and their aggregates before and after sonication.

Scanning Electron Microscopy

The morphology of XAC particles as well as ultrasonic pretreated samples was observed with a VEGA\\LSU scanning electron microscope (Tescan Company, Czech Republic) at 15 kV accelerating voltage. The samples were covered with a thin layer of gold as a conductive medium under a scanning electron microscope.

Hydrolysate Analysis Using High Performance Liquid Chromatography

The degradation products in the hydrolyzate were quantitatively analyzed by effective solution chromatography (HPLC, Agilent 1260 series, Agilent Technologies, United States) equipped with a refractive index detector (Amel et al., 2016). The separation was achieved with InterWAX (KS-802) column (DM) and a RID-10 A refractive index detector. All samples were filtered through a 0.22 mm filter prior to measurement. The column was kept at 80°C and washed with high performance liquid chromatography on water at 0.6 ml/min flow rate. The concentration of oligosaccharides was determined by peak area method and compared with X2, X3 and oligosaccharides purchased from Megazyme (Ireland). The XOS yield (w/w) was worked out to be (X2 + X3)/xylan weight.

Statistical Analysis

At the significance level of $p < 0.05$, the effect of ultrasound could be comparable by variance analysis (ANOVA). OriginPro 8.0 was used for all graphs and calculations.

RESULTS AND DISCUSSION

Purification and Biochemical of Xylanase XynB

The xylanase XynB-producing strain *P. janthinellum* XAF01 was evaluated using liquid-state fermentation. Maximum xylanase activity of 1807.9 U/mL was observed in the presence of 6% corncob and 1.5% ammonium sulfate as the most appropriate inorganic nitrogen source. XynB from *P. janthinellum* XAF01 was purified using a three-step procedure described in 2.3.2. After the final step, the purification ratio of the enzyme was 1.70 times, the recovery was 2.09%, and the specific activity was 540.4 U/mg protein (Table 1). The purification of the final eluted protein was determined by SDS-PAGE and its molecular weight was estimated to be 24.1 kDa (Figure 1). The xylanase activity of purified XynB was determined by zymography.

The purified xylanase XynB was most active at pH 4.3 and 50°C (Figures 2B,C). The optimal pH and temperature required for XynB activity were mostly similar to that of purified GH11 xylanase from *Aspergillus kawachii* and *Streptomyces actuosus*, which presented highest activity at pH 4.5 and 4.0 (Dalagnol et al., 2017; Wang et al., 2017). Furthermore, XynB was stable in the pH range of 4.0–8.0, with residual activities >80% after treatment for 0.5 h (Figure 2B). In addition, Figures 2C,D show that XynB was stable at 40°C and 50°C, and the residual xylanase activity was >60% when incubated for 2 h at 45°C.

Effect of Low Intensity Ultrasonic Pretreatment on XAC Hydrolysis

Figure 3 illustrates the effect of low intensity ultrasonic treatment on XOS yield. Under the same experimental conditions, the yield of XOS without ultrasonic treatment was used as a control, the results show that extended processing time (40 min) can significantly improve XOS yield. Ultrasound intensity is listed as one of the key parameters affecting ultrasonic cavitation. In general, cavitation effect increases with ultrasonic power, and the increase continued till ultrasonic power reached 0.40 W/cm², and the XOS yield was 20.71%, which was 2.55 fold higher than that of the control (the yield of XOS without ultrasonic treatment was 5.92%). This is probably because ultrasound affects the xylan or xylanase molecular bonds directly (the deduction was confirmed by further experiments discussed later), and so does ultrasonic pretreatment frequency. Ultrasonic frequency range of 28–135 kHz corresponds to ultrasonic wavelength of 50, 35, 28, and 10.37 mm separately, which is larger than the size of xylanase and xylan molecules. The XOS yield increased considerably at all frequencies, and maximum XOS was obtained when the pretreatment frequency was 50 kHz, with an abrupt decrease at 135 kHz. This is the first study to show ultrasound-assisted xylanase-catalyzed hydrolysis of xylan and hence the presented results are novel.

Fundamentally, the main mechanisms for the increase in XOS yield are related to the micro-jet, flow field, turbulence and shear

TABLE 1 | Summary of xylanase purification from *Penicillium janthinellum* XAF01.

Purification step	Total activity(U)	Total protein (mg)	Specific activity (U/mg)	Purification factor (-fold)	Yield (%)
Crude enzyme extracts	36182.00	113.90	317.66	1.00	100.00
50–70% ammonium sulfate salt out	25564.90	10.80	2367.12	7.45	70.66
SP-Sepharose fast flow	1055.90	2.30	459.09	1.45	2.92
Q-Sepharose fast flow	756.60	1.40	540.43	1.70	2.09

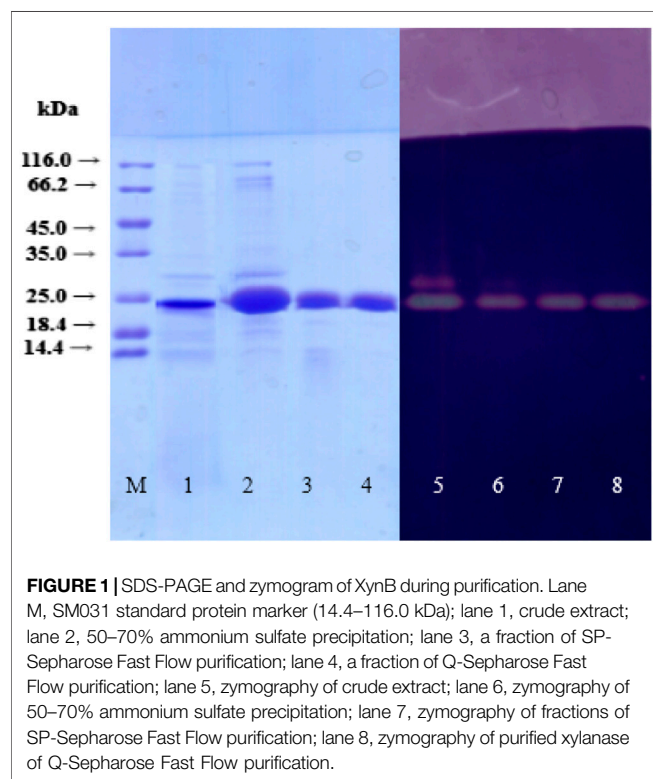


FIGURE 1 | SDS-PAGE and zymogram of XynB during purification. Lane M, SM031 standard protein marker (14.4–116.0 kDa); lane 1, crude extract; lane 2, 50–70% ammonium sulfate precipitation; lane 3, a fraction of SP-Sepharose Fast Flow purification; lane 4, a fraction of Q-Sepharose Fast Flow purification; lane 5, zymography of crude extract; lane 6, zymography of 50–70% ammonium sulfate precipitation; lane 7, zymography of fractions of SP-Sepharose Fast Flow purification; lane 8, zymography of purified xylanase of Q-Sepharose Fast Flow purification.

forces generated during the sonar process. Although several published studies showed that pretreatment of xylan was necessary prior to enzymatic hydrolysis, particle size and solubility was believed to affect hydrolysis of carbohydrates with high molecular weight (Wang et al., 2017).

Sonication pretreatment of enzyme (XynB) and substrates (XAC) was performed separately prior to enzymatic hydrolysis, which improved XOS recovery, albeit not significantly, compared to direct hydrolysis. Hence, superposition of effect enhancement may occur during ultrasound-assisted enzymatic hydrolysis. Ultrasound may be used to modify the kinetics of enzyme catalysed reactions. Mass transfer can be enhanced by strong shear and microfluidics associated with cavitation as they may alter the xylan chain, making xylanolytic enzymes more accessible to the substrate (Dalagnol et al., 2017). This is consistent with the results of ultrasound-assisted starch hydrolysis studies (Wang et al., 2017). Ultrasound-mediated improvement in enzymatic reactions can be explained using the following three parameters: substrate, enzyme, or combination of

both substrate and enzyme. The effect of any of these parameters may vary with substrate characteristics (particle size, solubility), enzyme characteristics, and reaction conditions. Studies showed that ultrasound can even strengthen the binding of enzymes to substrates and the removal of products from enzymes in reactions (Dalagnol et al., 2017).

Ultrasonic Treatment

Effect of Ultrasonic Treatment on the Kinetic Parameters

By nonlinearly fitting the kinetic data to the Michaelis-Menten equation, the kinetic parameters, maximum reaction rate (V_{max}), Michaelis constant (K_M), and catalytic efficiency (V_{max}/K_M) can be calculated. The V_{max} , K_M , and V_{max}/K_M of XynB were $189.20 \pm 6.15 \text{ mg ml}^{-1} \text{ min}^{-1}$, $23.12 \pm 0.98 \text{ mg ml}^{-1}$, and $8.18 \pm 0.35 \text{ min}^{-1}$, respectively. Sonication increased the V_{max} and V_{max}/K_M by 41.1 and 23.5%, respectively. The combination of XynB and ultrasound improved the catalytic ability. V_{max} shows the extreme rate of the enzyme reaction when the substrate is saturated, while the K_M value shows the enzyme affinity for substrate. The increase in V_{max} indicated strengthening of the xylan-xylanase complex interaction, and accelerated hydrolysis, whereas a slight decrease in K_M indicated an enhancement in the affinity between XynB and XAC, possibly because of better exposure of the xylanase active site after ultrasonication (Dalagnol et al., 2017). That is, ultrasound can increase the rate of reaction and enzyme substrate affinity, and enhance the reaction by enhancing the binding of the enzyme to the substrate. It is produced by mechanical effects of ultrasonic cavitation, and ultrasound's capability in increasing the mass transfer rate in enzymatic reactions has been reported to be supported (Sajjadi et al., 2017).

Effect of Ultrasonic Treatment on Xylanase Structure (CD Spectra Analysis)

Most enzymes are monomeric spherical proteins whose catalytic activity depends on their natural configuration. Ultrasound may alter the secondary structure of the enzyme, thereby exposing the active site of the enzyme to a better extent (Subhedhar and Gogate, 2014). The changes of secondary structure of proteins can be analyzed by CD spectroscopy, which calculates the α -helix, β -strand (β -Sheet and β -turn) and random coiling of xylanase, and the relationship between enzyme activity and secondary structure is determined (Li et al., 2015). A typical

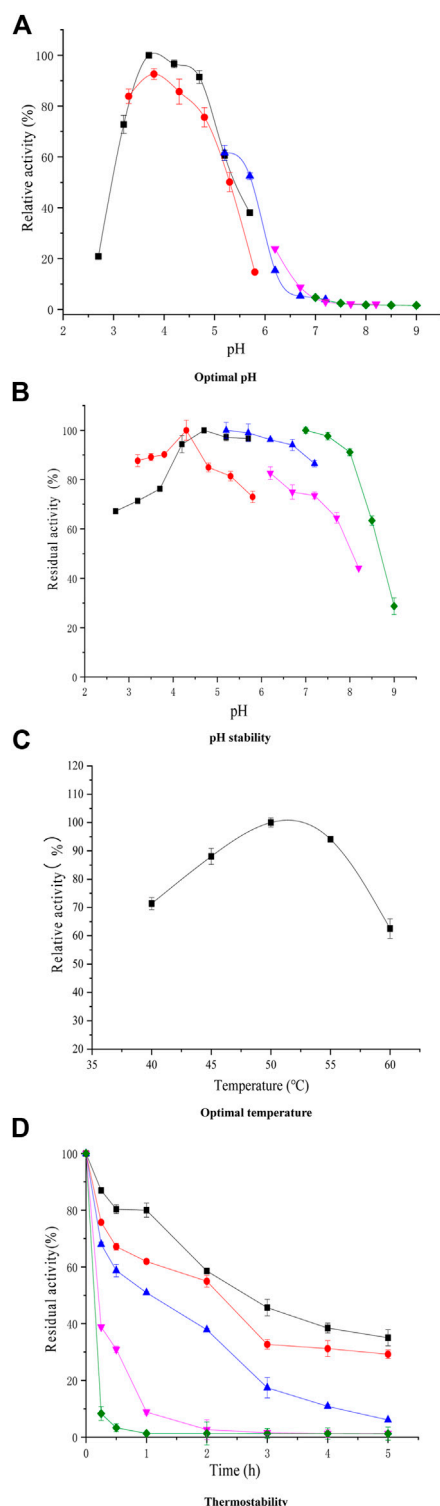


FIGURE 2 | Temperature effect [(C); pH 3.8] and pH on xylanase activity [(A); 55°C] of purified XynB and thermal stability [(D); 40–60°C] and pH stability [(B); pH 2.70–9.00] test for XynB. (■, Citric acid; ●, Acetic acid; ▲, MES; ▼, MOPS; ◆, Tris + HCL. Symbols for thermal inactivation: (■, 40°C; ●, 45°C; ▲, 50°C; ▼, 55°C; ◆, 60°C).

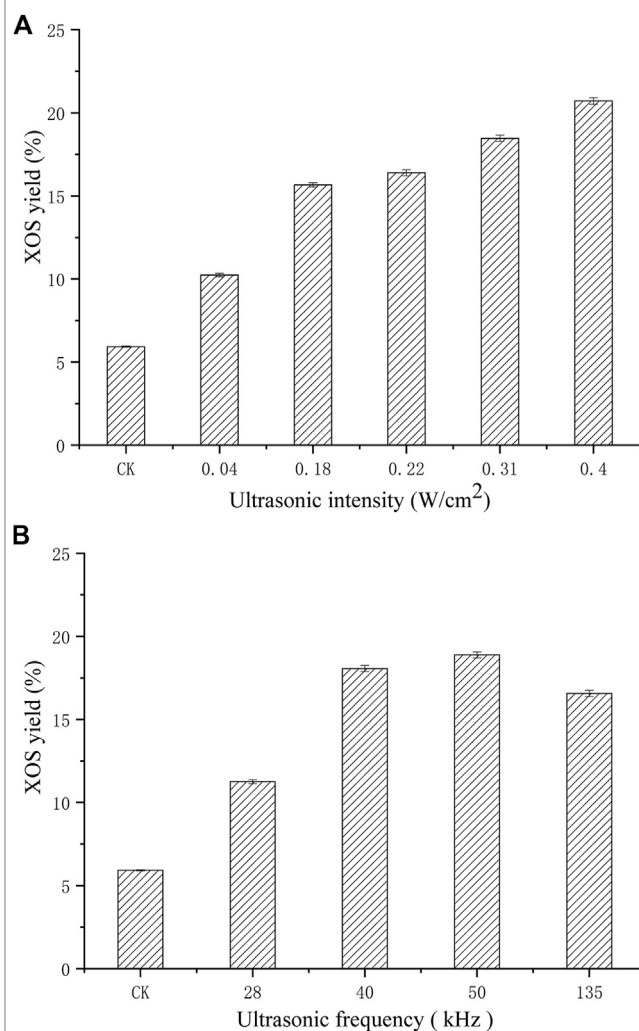
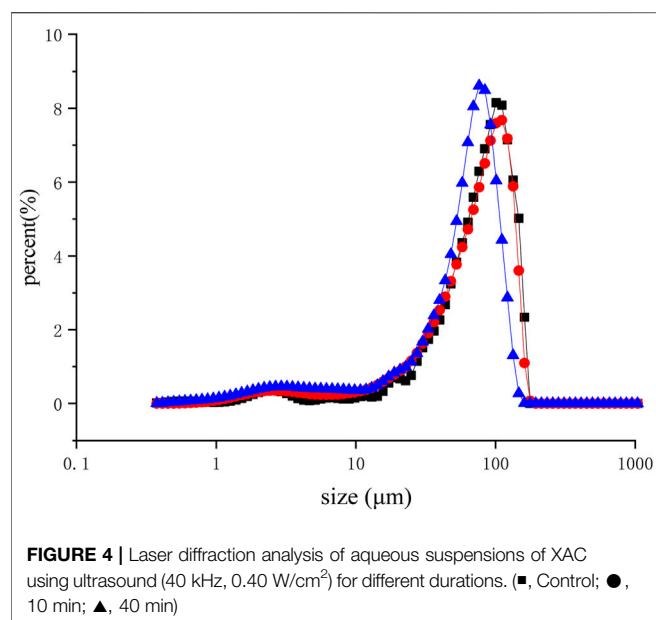


FIGURE 3 | Effects of pretreating XynB with different ultrasonic intensity (A) on xylanase hydrolysis at 50 kHz for 40 min, and ultrasonic frequency (B) on xylanase hydrolysis at 0.31 W/cm^2 for 40 min.

characteristic of all natural enzyme structure cd spectra is that the XynB spectrum has a fixed minimum peak at 209 nm and a positive peak at 195 nm, which is essentially the same as the native zymogram seen from early researches (You et al., 2010). The characteristics of proteins rich in β -chain (β -Sheet and β -turn) secondary structures can be found in these two spectra. The comparison of secondary structure content obtained using deconvolution of CD revealed an obvious difference regarding β -sheet, β -turn, and random coil. This analysis showed a slight decrease in XynB β -strand content and increase in random coil content with increase in ultrasonic intensity (from 0.04 W/cm^2 to 0.40 W/cm^2), which was believed to be related to acceleration of enzymatic hydrolysis. Similar results were obtained when ultrasonic frequency and treatment time were altered (Data was not shown). These



results indicated that ultrasonic pretreatment cast no effects on natural secondary structure of XynB, while destroying the hydrophobic interaction between protein molecules, making more internal hydrophobic groups and regions exposed to external environment.

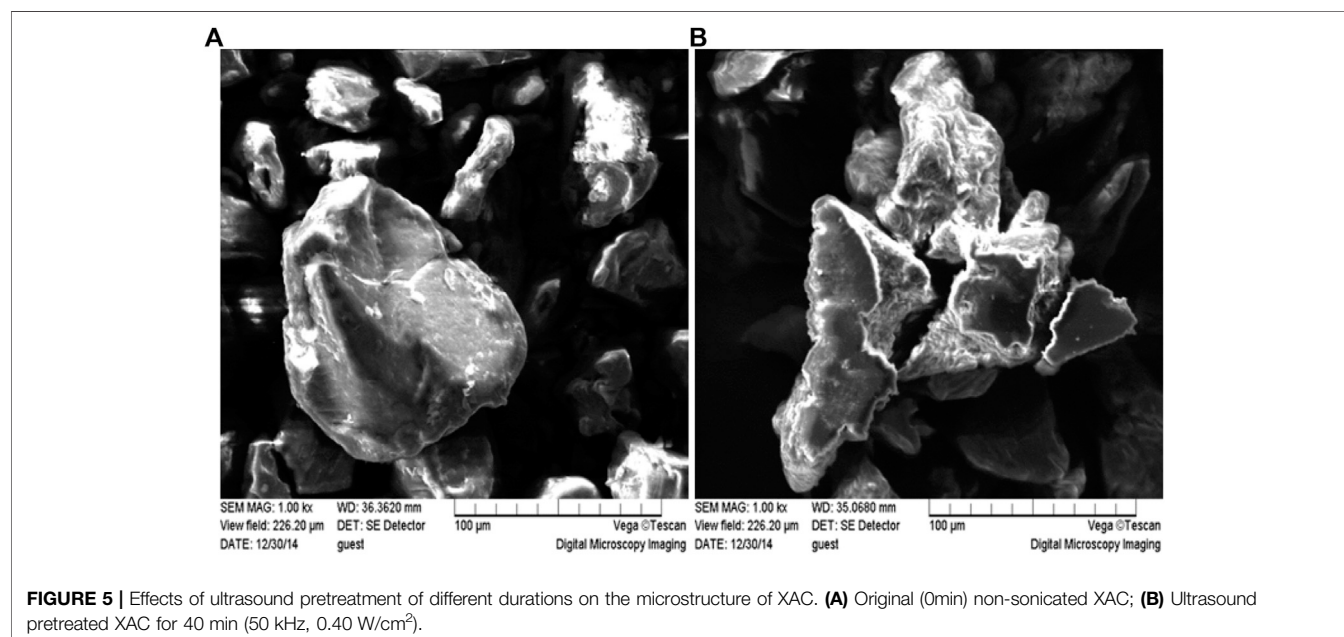
Effect of Ultrasonic Treatment on Substrate Particle Size and Microstructure (Characterization of XAC Particles and SEM Analysis)

The reduction in size is due to the high shear forces caused by ultrasonic cavitation in liquid mediums (Trujillo and

Knoerzer, 2011). After dialysis, the same volume of XAC suspension was sonicated at different times (0–40 min) and then characterized by laser diffraction. A comparison of the particle size distribution of the ultrasonic suspension (**Figure 4**) shows that the longer the ultrasonic action time, the lower the peak position of the volume distribution (76.43 μm). When the nanoparticles appeared at 40 min (from 84.79 to 65.04 μm), they expanded to smaller particles (Alvira et al., 2010).

The microstructure of XAC prior to ultrasound pretreatment was observed using scanning electron microscopy (SEM) as shown in **Figure 5**. After ultrasonic pretreatment, the XAC structure was loosened and more disordered structures and irregular fragments appeared, which changed the original (0 min) invoiced XAC suspension with large area and high density. In particular, after long-term ultrasonic pretreatment (40 min), cracks appeared on the surface of XAC; microparticles and small fragments increased the specific surface area of XAC molecules, increasing the probability of contact between the substrate and the enzyme, thereby enhancing the hydrolysis of the enzyme.

Xylan exists in one form and can be linked to other xylan structures and lignin by linking the arabinose-based ferulic acid bridge on the xylan backbone, while the lignin-saccharide complex in the corncob mostly composed of lignin-xylan complex (Van et al., 2011; Ju et al., 2013). Based on the SEM micrographs obtained in this study and calculation of the yield of XOS, we believe that sonication mainly resulted in fiber disruption, which eased subsequent enzymatic hydrolysis. This was in agreement with the observations of Jiang et al. who compared the effects of ultrasound on the functional and structural properties of black-bean protein isolate dispersions (Jiang et al., 2014).



CONCLUSION

An acidic xylanase was purified and its properties were studied. Low intensity ultrasound had a pronounce effect on enzymatic hydrolysis of XAC, and increased XOS yield by 61.80% compared to non-pretreated xylanase. The results also showed that separate pretreatment of both xylanase and its substrate accelerated the hydrolysis. Ultrasonic treatment altered the molecular structure and kinetic parameters of xylanase. Evaluation of the effect of pre-sonication of xylan confirmed that the action of ultrasound on the substrate chain destroyed the molecular aggregation and made it easy to carry out enzymatic reaction.

DATA AVAILABILITY STATEMENT

The original contributions presented in the study are included in the article/Supplementary Material, further inquiries can be directed to the corresponding authors.

REFERENCES

- Aachary, A. A., and Prapulla, S. G. (2009). Value Addition to Corncob: Production and Characterization of Xylooligosaccharides from Alkali Pretreated Lignin-Saccharide Complex Using *Aspergillus oryzae* MTCC 5154. *Bioresour. Technology* 100, 991–995. doi:10.1016/j.biortech.2008.06.050
- Akpinar, O., Erdogan, K., Bakir, U., and Yilmaz, L. (2010). Comparison of Acid and Enzymatic Hydrolysis of Tobacco Stalk Xylan for Preparation of Xylooligosaccharides. *LWT - Food Sci. Technology* 43, 119–125. doi:10.1016/j.lwt.2009.06.025
- Alvira, P., Tomás-Pejó, E., Ballesteros, M., and Negro, M. J. (2010). Pretreatment Technologies for an Efficient Bioethanol Production Process Based on Enzymatic Hydrolysis: A Review. *Bioresour. Technology* 101, 4851–4861. doi:10.1016/j.biortech.2009.11.093
- Amel, B.-D., Nawel, B., Khelifa, B., Mohammed, G., Manon, J., Salima, K.-G., et al. (2016). Characterization of a Purified Thermostable Xylanase from *Caldicoprobacter Algeriensis* Sp. Nov. Strain TH7C1T. *Carbohydr. Res.* 419, 60–68. doi:10.1016/j.carres.2015.10.013
- Badiei, M., Asim, N., Jahim, J. M., and Sopian, K. (2014). Comparison of Chemical Pretreatment Methods for Cellulosic Biomass. *APCBEE Proced.* 9, 170–174. doi:10.1016/j.apcbee.2014.01.030
- Bailey, M. J., Biely, P., and Poutanen, K. (1992). Interlaboratory Testing of Methods for Assay of Xylanase Activity. *J. Biotechnol.* 23, 257–270. doi:10.1016/0168-1656(92)90074-J
- Chapla, D., Pandit, P., and Shah, A. (2012). Production of Xylooligosaccharides from Corncob Xylan by Fungal Xylanase and Their Utilization by Probiotics. *Bioresour. Technology* 115, 215–221. doi:10.1016/j.biortech.2011.10.083
- Chemat, F., Rombaut, N., Sicaire, A.-G., Meullemiestre, A., Fabiano-Tixier, A.-S., and Abert-Vian, M. (2017). Ultrasound Assisted Extraction of Food and Natural Products. Mechanisms, Techniques, Combinations, Protocols and Applications. A Review. *Ultrason. Sonochem.* 34, 540–560. doi:10.1016/j.ultrasonch.2016.06.035
- Dalagnol, L. M. G., Silveira, V. C. C., da Silva, H. B., Manfro, V., and Rodrigues, R. C. (2017). Improvement of Pectinase, Xylanase and Cellulase Activities by Ultrasound: Effects on Enzymes and Substrates, Kinetics and Thermodynamic Parameters. *Process Biochem.* 61, 80–87. doi:10.1016/j.procbio.2017.06.029
- de Figueiredo, F. C., Carvalho, A. F. A., Brienzo, M., Campioni, T. S., and de Oliveira-Neto, P. (2017). Chemical Input Reduction in the Arabinoxylan and Lignocellulose Alkaline Extraction and Xylooligosaccharides Production. *Bioresour. Technology* 228, 164–170. doi:10.1016/j.biortech.2016.12.097
- de Freitas, C., Carmona, E., and Brienzo, M. (2019). Xylooligosaccharides Production Process from Lignocellulosic Biomass and Bioactive Effects. *Bioactive Carbohydrates and Dietary Fibre* 18, 100184. doi:10.1016/j.bcdf.2019.100184
- de Freitas, C., Terrone, C. C., Masarin, F., Carmona, E. C., and Brienzo, M. (2021). *In Vitro* study of the Effect of Xylooligosaccharides Obtained from Banana Pseudostem Xylan by Enzymatic Hydrolysis on Probiotic Bacteria. *Biocatal. Agric. Biotechnol.* 33, 101973. doi:10.1016/j.bcab.2021.101973
- Farzadkia, M., Rashvanlou, R. B., Rezaee, A., Gholami, M., Kermani, M., and Pasalari, H. (2021). The Influence of Combined Low-Strength Ultrasonics and Micro-aerobic Pretreatment Process on Methane Generation and Sludge Digestion: Lipase Enzyme, Microbial Activation, and Energy Yield. *Ultrason. Sonochem.* 73, 105531. doi:10.1016/j.ultrasonch.2021.105531
- Gallego-Juárez, J. A., Rodríguez, G., Acosta, V., and Riera, E. (2010). Power Ultrasonic Transducers with Extensive Radiators for Industrial Processing. *Ultrason. Sonochem.* 17, 953–964. doi:10.1016/j.ultrasonch.2009.11.006
- Gaquere-Parker, A., Taylor, T., Hutson, R., Rizzo, A., Folds, A., Crittenden, S., et al. (2018). Low Frequency Ultrasonic-Assisted Hydrolysis of Starch in the Presence of α -amylase. *Ultrason. Sonochem.* 41, 404–409. doi:10.1016/j.ultrasonch.2017.10.007
- Jadhav, H. B., Gogate, P. R., Waghmare, J. T., and Annature, U. S. (2021). Intensified Synthesis of palm Olein Designer Lipids Using Sonication. *Ultrason. Sonochem.* 73, 105478. doi:10.1016/j.ultrasonch.2021.105478
- Jian, S., Wenyi, T., Wuyong, C., et al. (2008). Ultrasound-accelerated enzymatic hydrolysis of solid leather waste. *J. Cleaner Prod.* 16, 591–597. doi:10.1016/j.jclepro.2006.12.005
- Jiang, L., Wang, J., Li, Y., Wang, Z., Liang, J., Wang, R., et al. (2014). Effects of Ultrasound on the Structure and Physical Properties of Black Bean Protein Isolates. *Food Res. Int.* 62, 595–601. doi:10.1016/j.foodres.2014.04.022
- Joshi, S. M., and Gogate, P. R. (2019). Intensifying the Biogas Production from Food Waste Using Ultrasound: Understanding into Effect of Operating Parameters. *Ultrason. Sonochem.* 59, 104755–104762. doi:10.1016/j.ultrasonch.2019.104755
- Ju, X., Engelhard, M., and Zhang, X. (2013). An Advanced Understanding of the Specific Effects of Xylan and Surface Lignin Contents on Enzymatic Hydrolysis of Lignocellulosic Biomass. *Bioresour. Technology* 132, 137–145. doi:10.1016/j.biortech.2013.01.049
- Kalle, F., Driss, D., Chaari, F., Zouari-Ellouzi, S., Chaabouni, M., Ghorbel, R., et al. (2016). Statistical Optimization of Low-Cost Production of an Acidic Xylanase by *Bacillus Mojavensis* UEB-FK: Its Potential Applications. *Biocatal. Agric. Biotechnol.* 5, 1–10. doi:10.1016/j.bcab.2015.11.005
- Khangwal, I., Nath, S., Kango, N., and Shukla, P. (2020). Endo-xylanase Induced Xylooligosaccharide Production from Corn Cobs, its Structural Features, and

AUTHOR CONTRIBUTIONS

MZ, GF, and CT drafted the manuscript. CT and XL supervision. All authors listed have edited the manuscript and made substantial and direct contribution to the work. All authors gave approval for publication of the manuscript.

FUNDING

The work described in this paper was fully supported by a grant from The National Key Research and Development Program of China (No. 2017YFD0400206), the National Natural Science Foundation of China (No. 31671793, No. 31201449, No. 31830069, No. 31371723), the Key projects jointly funded by Beijing Natural Science Foundation and Beijing Municipal Education Commission (No. KZ202010011018), and the Foundation of Beijing Technology and Business University (No. PXM 2017_014213_000036, No. PXM 2017_014213_000036).

- Concentration-dependent Antioxidant Activities. *Biomass Conv. Bioref.* 17, 1–11. doi:10.1007/s13399-020-00997-3
- Khangwal, I., and Shukla, P. (2019). Combinatory Biotechnological Intervention for Gut Microbiota. *Appl. Microbiol. Biotechnol.* 103, 3615–3625. doi:10.1007/s00253-019-09727-w
- Kumar, V., and Satyanarayana, T. (2015). Generation of Xylooligosaccharides from Microwave Irradiated Agroresidues Using Recombinant Thermo-Alkali-Stable Endoxylanase of the Polyextremophilic Bacterium *Bacillus Halodurans* Expressed in *Pichia pastoris*. *Bioresour. Technology* 179, 382–389. doi:10.1016/j.biortech.2014.12.049
- Laemmli, U. K. (1970). Cleavage of Structural Proteins during the Assembly of the Head of Bacteriophage T4. *Nature* 227, 680–685. doi:10.1038/227680a0
- Larsen, L. R., van der Weem, J., Caspers-Weiffenbach, R., Schieber, A., and Weber, F. (2021). Effects of Ultrasound on the Enzymatic Degradation of Pectin. *Ultrason. Sonochem.* 72, 105465. doi:10.1016/j.ultsonch.2021.105465
- Li, H., Voutilainen, S., Ojamo, H., and Turunen, O. (2015). Stability and Activity of *Dictyoglomus Thermophilum* GH11 Xylanase and its Disulphide Mutant at High Pressure and Temperature. *Enzyme Microb. Technology* 70, 66–71. doi:10.1016/j.enzmtec.2014.12.011
- Liu, H. M., Xie, X. A., Li, M. F., and Sun, R. C. (2012). Hydrothermal liquefaction of cypress: effects of reaction conditions on 5-lump distribution and composition. *J. Anal. Appl. Pyrolysis.* 94, 177–183. doi:10.1016/j.jaap.2011.12.007
- Liu, Q., Fan, H., Mou, H., Liu, J., Huang, J., Dong, X., et al. (2021). Preparation and Characterization of Xylan by an Efficient Approach with Mechanical Pretreatments. *Ind. Crops Prod.* 165, 113420. doi:10.1016/j.indcrop.2021.113420
- Longue Júnior, D., Ayoub, A., Venditti, R. A., Jameel, H., Colodette, J. L., and Chang, H.-m. (2013). Ethanol Precipitation of Hetero-Polysaccharide Material from Hardwood by Alkaline Extraction Prior to the Kraft Cooking Process. *Bioresources* 8, 5319–5332. doi:10.15376/biores.8.4.5319-5332
- Lowry, O., Rosebrough, N., Farr, A. L., and Randall, R. (1951). Protein Measurement with the Folin Phenol Reagent. *J. Biol. Chem.* 193, 265–275. doi:10.1515/bchm2.1951.286.1-6.27010.1016/s0021-9258(19)52451-6
- Moniz, P., Ho, A. L., Duarte, L. C., Kolida, S., Rastall, R. A., Pereira, H., et al. (2016). Assessment of the Bifidogenic Effect of Substituted Xylo-Oligosaccharides Obtained from Corn Straw. *Carbohydr. Polym.* 136, 466–473. doi:10.1016/j.carbpol.2015.09.046
- Pawar, S. V., and Rathod, V. K. (2018). Ultrasound Assisted Process Intensification of Uricase and Alkaline Protease Enzyme Co-production in *Bacillus Licheniformis*. *Ultrason. Sonochem.* 45, 173–179. doi:10.1016/j.ultsonch.2018.03.004
- Rashid, R., Ejaz, U., Ali, F. I., Hashmi, I. A., Bari, A., Liu, J., et al. (2020). Combined Pretreatment of Sugarcane Bagasse Using Alkali and Ionic Liquid to Increase Hemicellulose Content and Xylanase Production. *BMC Biotechnol.* 20, 64. doi:10.1186/s12896-020-00657-4
- Sajjadi, B., Asgharzadehahmadi, S., Asaithambi, P., Raman, A. A. A., and Parthasarathy, R. (2017). Investigation of Mass Transfer Intensification under Power Ultrasound Irradiation Using 3D Computational Simulation: A Comparative Analysis. *Ultrason. Sonochem.* 34, 504–518. doi:10.1016/j.ultsonch.2016.06.026
- Schwarz, W. H., Bronnenmeier, K., Gräbnitz, F., and Staudenbauer, W. L. (1987). Activity Staining of Cellulases in Polyacrylamide Gels Containing Mixed Linkage β -glucans. *Anal. Biochem.* 164, 72–77. doi:10.1016/0003-2697(87)90369-1
- Uma, S., Bandyopadhyay, T., and Bhunia, B. (2016). Optimization of Nutritional and Physicochemical Requirements on Acidic Xylanase Production from *Aspergillus niger* KP874102.1. *Mater. Today Proc.* 3, 3367–3374. doi:10.1016/j.matpr.2016.10.018
- Subhedar, P. B., and Gogate, P. R. (2014). Enhancing the Activity of Cellulase Enzyme Using Ultrasonic Irradiations. *J. Mol. Catal. B: Enzymatic* 101, 108–114. doi:10.1016/j.molcatb.2014.01.002
- Szabo, O. E., and Csiszar, E. (2017). Some Factors Affecting Efficiency of the Ultrasound-Aided Enzymatic Hydrolysis of Cotton Cellulose. *Carbohydr. Polym.* 156, 357–363. doi:10.1016/j.carbpol.2016.09.039
- Trujillo, F. J., and Knoerzer, K. (2011). A Computational Modeling Approach of the Jet-like Acoustic Streaming and Heat Generation Induced by Low Frequency High Power Ultrasonic Horn Reactors. *Ultrason. Sonochem.* 18, 1263–1273. doi:10.1016/j.ultsonch.2011.04.004
- Van Dongen, F. E. M., and Van Eylen, D. (2011). Characterization of substituents in xylans from corn cobs and stover. *Carbohydr. Polym.* 86, 722–731. doi:10.1016/j.carbpol.2011.05.007
- Wang, D., Ma, X., Yan, L., Chantapakul, T., Wang, W., Ding, T., et al. (2017). Ultrasound Assisted Enzymatic Hydrolysis of Starch Catalyzed by Glucoamylase: Investigation on Starch Properties and Degradation Kinetics. *Carbohydr. Polym.* 175, 47–54. doi:10.1016/j.carbpol.2017.06.093
- Wang, S.-L., Yen, Y.-H., Shih, I.-L., Chang, A. C., Chang, W.-T., Wu, W.-C., et al. (2003). Production of Xylanases from rice Bran by *Streptomyces Actuosus* A-151. *Enzyme Microb. Technology* 33, 917–925. doi:10.1016/S0141-0229(03)00246-1
- Yamani, L. N., Kristanti, A. N., and Puspaningsih, N. N. (2016). THE PRELIMINARY STUDY OF ANTIOXIDANT ACTIVITY FROM XYLO-OLIGOSACCHARIDE OF CORNCOB (ZEA MAYS) HYDROLYSIS PRODUCT WITH ENDO- β -XYLANASE ENZYME. *Ijttd* 3, 112–117. doi:10.20473/ijtd.v3i2.219
- You, C., Huang, Q., Xue, H., Yang, X., Lu, H., Zhu, L., et al. (2010). Potential hydrophobic interaction between two cysteines in interior hydrophobic region improves thermostability of a family 11 xylanase from *Neocallimastix Patriciarum*. *Biotechnol. Bioeng.* 105, 861–870. doi:10.1002/bit.22623
- Zhang, J., Wang, Y.-H., Wei, Q.-Y., Du, X.-J., and Qu, Y.-S. (2018). Investigating Desorption during Ethanol Elution to Improve the Quality and Antioxidant Activity of Xylo-Oligosaccharides from Corn Stalk. *Bioresour. Technology* 249, 342–347. doi:10.1016/j.biortech.2017.09.203
- Zhang, W., Johnson, A. M., Barone, J. R., and Renneckar, S. (2016). Reducing the Heterogeneity of Xylan through Processing. *Carbohydr. Polym.* 150, 250–258. doi:10.1016/j.carbpol.2016.05.013
- Zhao, Y., Xu, H., Wang, K., Lu, K., Qu, Y., Zhu, L., et al. (2019). Enhanced Furfural Production from Biomass and its Derived Carbohydrates in the Renewable Butanone-Water Solvent System. *Sustainable Energ. Fuels* 3, 3208–3218. doi:10.1039/c9se00459a

Conflict of Interest: The authors declare that the research was conducted in the absence of any commercial or financial relationships that could be construed as a potential conflict of interest.

Publisher's Note: All claims expressed in this article are solely those of the authors and do not necessarily represent those of their affiliated organizations, or those of the publisher, the editors and the reviewers. Any product that may be evaluated in this article, or claim that may be made by its manufacturer, is not guaranteed or endorsed by the publisher.

Copyright © 2021 Zhou, Fan, Xia, Zhang, Teng and Li. This is an open-access article distributed under the terms of the Creative Commons Attribution License (CC BY). The use, distribution or reproduction in other forums is permitted, provided the original author(s) and the copyright owner(s) are credited and that the original publication in this journal is cited, in accordance with accepted academic practice. No use, distribution or reproduction is permitted which does not comply with these terms.



Insight in the Recent Application of Polyphenols From Biomass

Bowen Yan^{1†}, Zhefan Stephen Chen^{2†}, Yingying Hu¹ and Qiang Yong^{1*}

¹Co-Innovation Center for Efficient Processing and Utilization of Forest Products, College of Chemical Engineering, Nanjing Forestry University, Nanjing, China, ²Nexus of Rare Neurodegenerative Diseases, School of Life Sciences, Faculty of Science, The Chinese University of Hong Kong, Hong Kong, SAR China

OPEN ACCESS

Edited by:

Jia-Long Wen,
Beijing Forestry University, China

Reviewed by:

Cailli Fu,
National University of Singapore
Suzhou Research Institute, China
Chuan-Ling Si,
Tianjin University of Science and
Technology, China
Wenhui Geng,
North Carolina State University,
United States

*Correspondence:

Qiang Yong
swhx@njfu.com.cn

[†]These authors have contributed
equally to this work and share first
authorship

Specialty section:

This article was submitted to
Bioprocess Engineering,
a section of the journal
Frontiers in Bioengineering and
Biotechnology

Received: 05 August 2021

Accepted: 31 August 2021

Published: 13 September 2021

Citation:

Yan B, Chen ZS, Hu Y and Yong Q
(2021) Insight in the Recent Application
of Polyphenols From Biomass.
Front. Bioeng. Biotechnol. 9:753898.
doi: 10.3389/fbioe.2021.753898

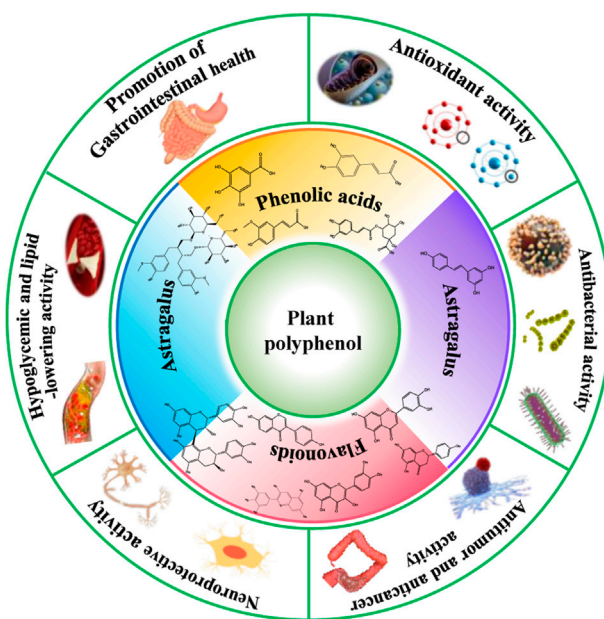
Biomass polyphenols are bio-active macromolecules with distinct chemical structures in a variety of biomass. In recent years, the study of biomass polyphenols and their application in food and medicine fields has become a research hotspot, which predominantly focuses on the preparation, purification, structural identifications, and measurements of biological activities. Many studies describe methodologies for extraction and application of polyphenols, but comprehensive work to review its physiological activities like drugs and health products are lacking. This paper comprehensively unlocks the bioactivities of antioxidant, antibacterial, antitumor, anticancer, neuroprotection, control of blood sugar, regulation of blood fat, and promotion of gastrointestinal health functions of polyphenols from different biomass sources. This review will serve as an illuminating resource for the global scientific community, especially for those who are actively working to promote the advances of the polyphenols research field.

Keywords: biomass, polyphenols, biological application, bioactivities, health functions

INTRODUCTION

The growth and development of biomass are sustained by the regulation of metabolism and resistance against different biological stresses. The endogenous metabolites of biomass are composed of primary and secondary metabolites. In the different biomass, the major constituents are cellulose, hemicellulose, lignin, which can be applied to prepare various value-added products and bio-materials (Sun et al., 2019; Zhou et al., 2019; Chen et al., 2020; Geng et al., 2020; Chen et al., 2021; Liu et al., 2021; Luo et al., 2021). Apart from these constituents, there is existed various minor constituents, such as flavonoids and polyphenols (Si et al., 2009; Gironi and Piemonte, 2011; Quideau et al., 2011; Goodman, 2020). Biomass polyphenols are one type of secondary metabolites synthesized primarily through the shikimic acid and phenylpropane pathways (Hidalgo-Liberona et al., 2020; Wang et al., 2020). Biomass polyphenols are widely found in plant skins, roots, leaves, and fruits, with an abundance of as much as 20% by weight (Quideau et al., 2011).

There has been a long history of utilization of biomass polyphenols, which have been used in tanning and as medicines starting from ancient times (Quideau et al., 2011). The natural feelings and intrinsic properties of biomass polyphenols make them remarkable amongst plant-derived products. In recent years, biomass polyphenols have attracted much more attention in green/sustainable scientific fields due to their broad distribution, natural abundance, diverse chemical structures, and biological functions. A range of studies has demonstrated that biomass polyphenols comprise multiple phenolic hydroxyl groups, which have been reported to elicit prominent physiological functions such as free radical scavenging and radical sequestration activities (Gironi and Piemonte, 2011; Dong et al., 2020; Pei et al., 2020). These functionalities thus highlight biomass polyphenols as effective antioxidants. In addition to executing antioxidant activities, biomass polyphenols dramatically inhibit the growth of different strains of bacteria,



GRAPHICAL ABSTRACT |

fungi, and viruses while not affecting the growth and development of beneficial microorganisms under weak acidic and neutral environments. This indicates the potential applications of biomass polyphenols as bacteriostatic and anti-tumor agents. Moreover, biomass polyphenols also effectively protect against cardiovascular diseases via lowering the levels of several key pathogenic factors in the blood, including blood lipid, oxidation of low-density lipoprotein, and blood pressure (Gironi and Piemonte, 2011; Quideau et al., 2011; Camargo et al., 2019; Delgado et al., 2019; Michaličková et al., 2019).

BIOMASS POLYPHENOLS

Biomass polyphenols are a class of natural compounds widely distributed in biomass with an abundance second to lignin, cellulose, and hemicellulose. Polyphenols are predominantly accumulated in the leaves, vascular tissues, bark, immature fruits, seed coat, and disinfected tissues of biomass. China is rich in biomass polyphenol resources varieties (Figure 1), including Larch (100–150 mg/g, Yashunsky et al., 2014), Black wax (20–50 mg/g, Xu et al., 2016), Waxberry (20–50 mg/g, Chen et al., 2002), Yu Gan (200–300 mg/g, Yang and Liu, 2019), Houpi Xia (400–1,500 mg/g, Dai et al., 2006), Mangrove (500–600 mg/g, Dahibhate et al., 2020), Gallnut (300–500 mg/g, Ge et al., 2015).

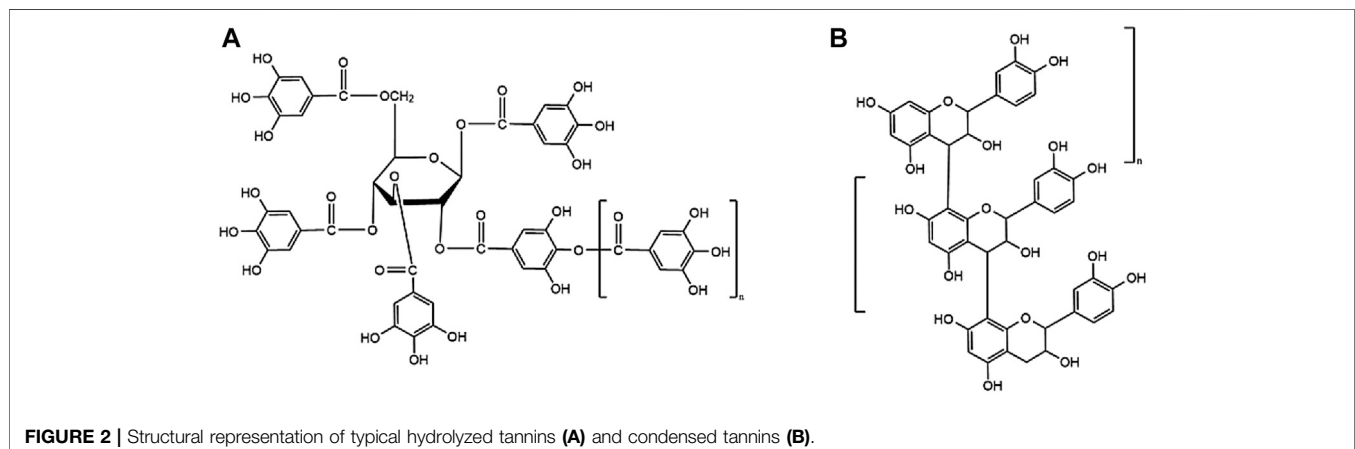
Structure of Polyphenols

Polyphenols share common structural features, their basic framework includes the polyhydroxy substitution of a benzene ring, as well as the absence of any nitrogen functional groups. Biomass polyphenols can be divided into the classes of 1) hydrolyzed tannins (gallate polyphenols) and 2) condensed tannins (polyflavanol polyphenols or proanthocyanidins) (Gironi and Piemonte, 2011). Hydrolyzed tannins are products of tannin hydrolysis, revolving around cleavage

ester linkages. Condensed tannins are mainly composed of polyflavanol polyphenols or proanthocyanidins, which contain hydroxyl flavanol monomers connected by C-C bonds (Porter, 1992). Since hydrolyzed tannins and condensed tannins are completely distinct in the aspect of the unit skeleton, there are significant differences in their functional properties and applications (Figure 2). For example, hydrolyzed tannins are unstable and prone to be hydrolyzed under various conditions (acid, alkali, and under the presence of certain enzymes). Condensed tannins are not readily hydrolyzed, but can be further condensed into insoluble upon contact with a strong acid (Gessner and Steiner, 2005). When polyphenols interact with proteins, alkaloids, or polysaccharides, the polyphenol molecules initially approach the surface of protein molecules through hydrophobic bonds. The entry of polyphenols to the hydrophobic bag enables the following formation of multi-point hydrogen bonds. Due to a large number of coordination groups, most metal ions also tend to form precipitates if allowed to complex with polyphenols. Under alkaline conditions, polyphenols and metal ions readily form polycomplexes. In addition, the phenolic hydroxyl in the phenolic structure of biomass polyphenols (catechol or catechol) is easily oxidized to the quinone structure *via* consuming oxygen in the environment (Zhang et al., 2005).

Classification of Polyphenols

More than 8,000 different kinds of polyphenols and their derivatives have been identified in the biomass kingdom (Boadas-Vaello et al., 2017). The name of polyphenols is assigned due to the presence of multiple phenolic groups in their chemical structures. In terms of structural differences, polyphenols can be further divided into four categories: phenolic acids, astragalus, lignans, and flavonoids (Table 1). A couple of studies have demonstrated the dominant biomass polyphenols that are found in common foods, including gallic catechins in green tea, resveratrol in grapes, capsaicin in chilis and peppers, curcumin in turmeric, genistein in soybean, and



gingerol in ginger (Bhuyan, 2018). Investigation of the biological outcomes of these particular edible goods allows for a better understanding of the structural details related to the functionalities of polyphenols.

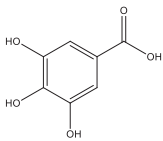
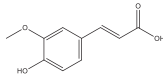
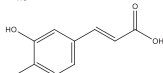
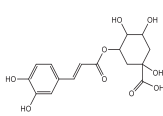
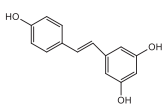
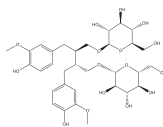
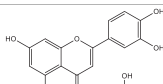
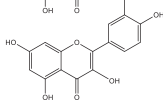
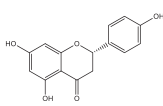
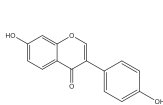
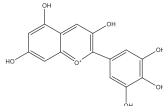
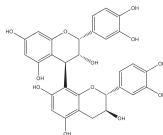
BIOACTIVITY OF POLYPHENOLS

Polyphenols are usually ingested as mixtures of different compounds that are immersed in a complex food substrate. The material then undergoes digestion, which exerts changes in structure and activity, before the mixture eventually reaches and acts upon target organs. After ingestion, absorption from the digestive tract usually requires intestinal enzymes, such as lactase rhizopericoside hydrolase and cytosolute

β -glucosidase, to hydrolyze glycoside binders and produce the corresponding aglycones (Day et al., 2000; Gee et al., 2000). These aglycones can be further metabolized by second-stage enzymes to produce methylated, sulfurated, and gluconalized compounds (Manach et al., 2004). Meanwhile, polyphenols that are not absorbed in the small intestine reach the colon, where they are converted into simpler metabolites by colonic microbiota and consequently being absorbed and get involved in further metabolic reactions (Liu et al., 2018).

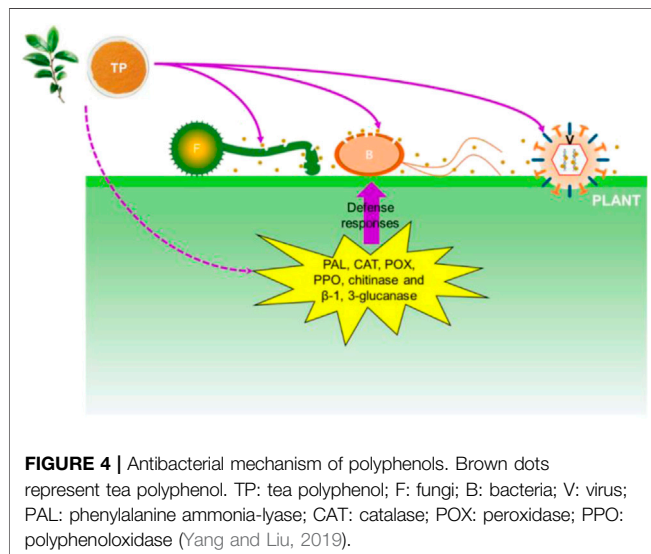
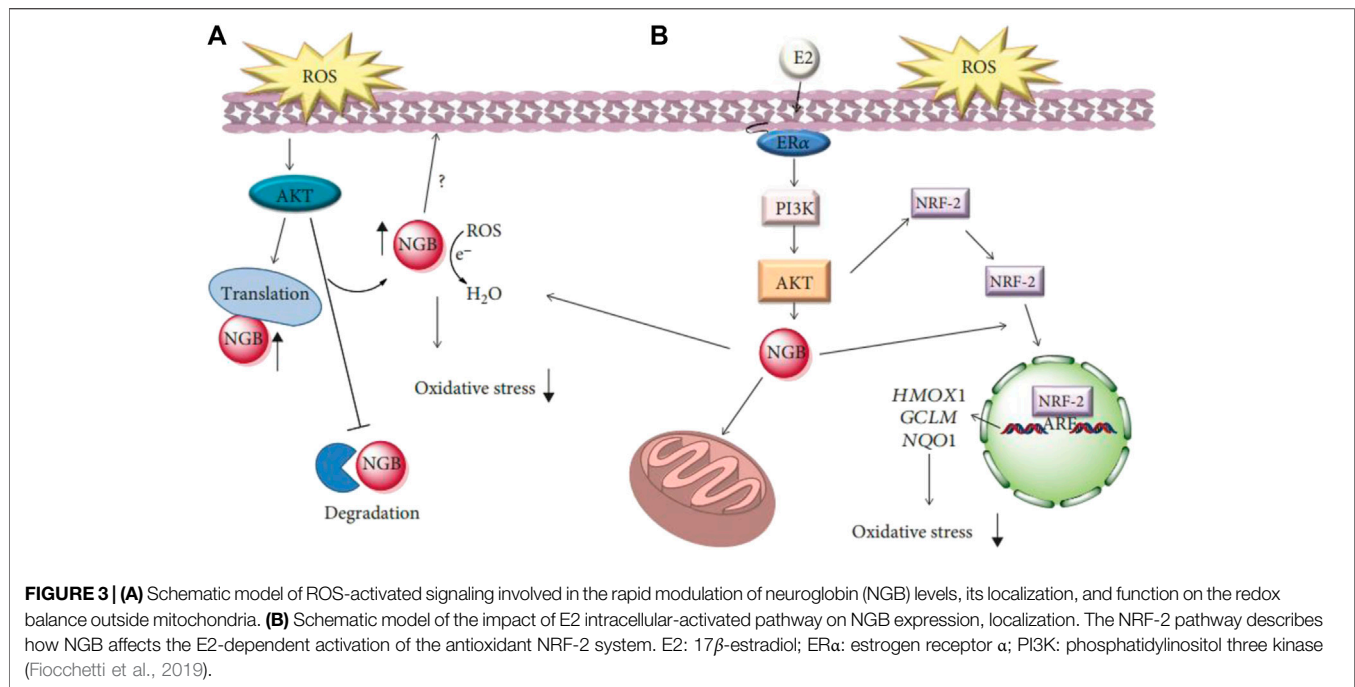
Due to the diversity of biomass polyphenols, a variety of biological activities has been reported, including antioxidant (Hu et al., 2020; Ji et al., 2020), anti-inflammatory (Myint et al., 2021), bacteriostatic (Martin and Bolling, 2015; Gullon et al., 2016; Liu et al., 2019), anti-tumor (Sharma et al., 2017;

TABLE 1 | Classification of polyphenols from different biomass.

Classification of polyphenols	Representative compounds	Structure	Biomass	References
Phenolic acids	Gallic acid		Gallnut, sumac, tea plant	Asnaashari et al., 2014; Wang et al., 2013
	Ferulic acid		<i>Ferula</i> , ligustici, angelica	Zheng et al. (2021)
	Caffeic acid		Coffee, Wine	
	Chlorogenic acid		Honeysuckle, eucommia ulmoides leaves, hawthorn fruit	
<i>Astragalus</i>	Resveratrol		Peanut, mulberry, grape	Zheng et al., 2021; Hiradate et al., 2002
Lignans	Flaxseed lignans		Flaxseed, sesame	Zheng et al. (2021)
Flavonoids	Luteolin, apigenin		Parsley, dragonhead, Chili	Zheng et al. (2021)
	Quercetin, rutin		Apple, onions, Vegetables	
	Nobiletin, naringenin		Citrus fruits	
	Daidzein, puerarin		Legumes	
	Delphinidin, scabiolide		Fruits and vegetables with bright colors	
	Proanthocyanidin		Blueberry, grape pip	

Sajadimajd et al., 2020), regulation of intestinal flora (Cardona et al., 2013; Suzuki, 2013) and prevention of cardiovascular diseases (Kang, 2013; Tangney and Rasmussen, 2013; Kitai

and Tang, 2017; Orr et al., 2020). Biomass polyphenols have also been widely used in the fields of the development of drugs and health products.



Antioxidant Activity

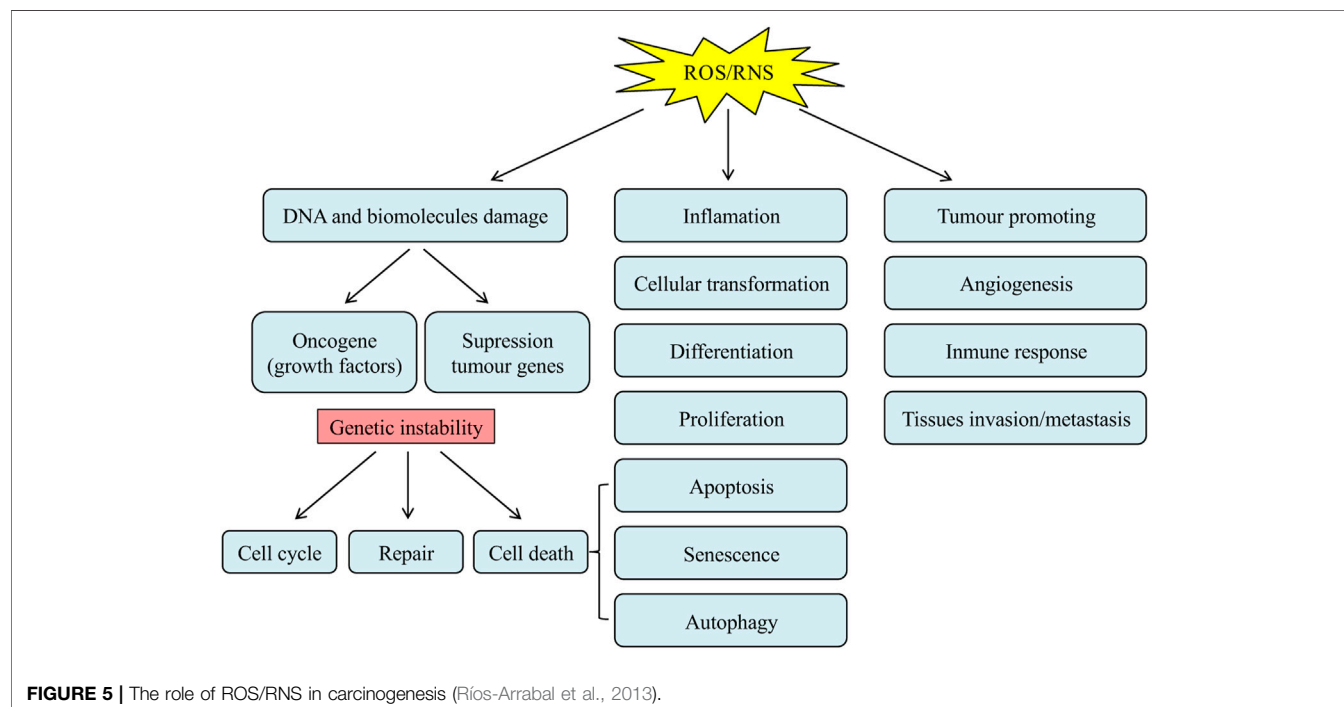
Redox is an essential class of metabolic reaction that occurs in living organisms. However, when the electron flow becomes decoupled, the generation of harmful free radicals results in detrimental outcomes (Fiedor and Burda, 2014; Zhao et al., 2021). Free radicals are atoms, molecules, or ions with unpaired electrons. They are highly unstable, will rapidly attack molecules in adjacent cells, and are prone to chemically react with other molecules (Yu et al., 2020). These reactions in turn contribute to various forms of impairments to cells. Most of the impairments can be repaired, but the entire reaction can be avoided if the free radical interacts with an antioxidant in cells. Antioxidants

play a vital role in inhibiting molecular oxidation reactions to reduce the harmful accumulation of reactive oxygen species (Fiedor and Burda, 2014). Antioxidants also protect human somatic cells from the deteriorating effects of free radicals and reactive oxygen species (ROS) by altering the expression of sensor proteins that are involved in oxidative stress (Figure 3) (Fiocchetti et al., 2019). The different kinds of chronic diseases and the process of lipid peroxidation are thus delayed. In recent years, there has been a great interest in unveiling natural plant-derived novel and safe dietary antioxidants.

Biomass polyphenols have strong activity due to their ability to delocalize uncoupled electrons, which can scavenge free radicals, chelate metal ions and inhibiting oxidase activity, and protect endogenous antioxidant enzymes in the body (Kim et al., 2014; Croft, 2016). Most natural antioxidants are phenolic compounds. The most important natural antioxidants are tocopherols, flavonoids, and phenolic acids. Among the phenolic hydroxyl groups, the phenolic hydroxyl group is the most easily oxidized, exhibiting the capacity to capture free radicals such as ROS and active nitrogen species (Geng et al., 2016; Zheng et al., 2021). This functionality enables polyphenols to scavenge free radicals and quench ROS, thus providing strong antioxidant capacity (Fraga, 2007; Dugasani et al., 2010; Losada and Dí az, 2017). These antioxidants, which are commonly used as food supplements, prevent the free radical chain reaction of oxidation and inhibit the initiation and propagation steps. All of these lead to the termination of the reaction and delay of the oxidation process. Antioxidants have the unique property of extending the shelf life of foods without any adverse effect on their sensory or nutritional qualities. Antioxidants used as food additives are non-toxic and effective at low

TABLE 2 | Antibacterial effect of different polyphenols.

Type of polyphenols	Biomass	Bacteria types	References
Polyphenol	Tea	<i>Proteus vulgaris</i> , <i>Staphylococcus aureus</i>	Pani et al. (2014)
	Apple	<i>Bacillus</i> , <i>Escherichia coli</i> <i>Pseudomonas</i> , <i>Bacillus subtilis</i>	Gullon et al. (2016)
	Pomegranate fruit slag	<i>Salmonella</i> , <i>Escherichia coli</i>	Salto and Lopez (2016)
Teucrium polium Flavonoids	Teucrium polium	<i>Staphylococcus aureus</i>	Hafsa and Ibrahim (2017)
Oligomeric proanthocyanidins	Trester	<i>Streptococcus</i> , <i>Escherichia coli</i>	Hafsa and Ibrahim (2017)
Flavonoid	Olive	<i>Staphylococcus epidermidis</i>	Williams et al. (2017)
Polyphenol	Curry Leaves	<i>Staphylococcus aureus</i>	Hafsa and Ibrahim (2017)
Flavonoid	Hawthorn	<i>Staphylococcus aureus</i>	Yang and Zhang (2019)



concentrations. Other outstanding properties include high stability, robustness to the various stages of food processing, possess no smell, taste, or color, are easy to be mixed into foodstuffs, and have sufficient solubility.

Biomass polyphenols have been widely used in various fields due to their strong antioxidant activities. Hu et al. (2020) impregnated tea polyphenols (Gallic acid) into tea seed oil with ethanol and removed the ethanol by vacuum distillation to produce tea polyphenol colloids. It was found that no chemical changes occurred after the addition of tea polyphenols to tea seed oil. The antioxidant stability of colloidal tea polyphenols in tea seed oil was superior to that of synthetic antioxidants and tea polyphenol palmitate, and the optimal addition of tea polyphenols to tea seed oil ranged from 0.1–0.2 g/kg. Ji et al. (2020) found that the major phenolics in sea buckthorn were flavonoids, phenolic acids, and tannins, which showed antioxidant functions *via* regulating the activities of cellular enzymes. Myint et al. (2021) found that stevia leaves were demonstrated to possess the highest antioxidant capacity

among plant foods due to the abundance of polyphenols (PPS). The stevia leaves PPS showed antioxidant activity similar to epigallocatechin gallate (EGCG), and their antioxidant activity, hydrophilic activity, and stability are stronger than ascorbic acid (VC), vitamin E, and chlorogenic acid. The antioxidant activity of stevia leaves PPS is stable under various physical conditions, except for in the presence of potassium sorbate or sucrose. In addition, the combination of PPS and VC improves their antioxidant stabilities. Taken together, PPS has the potential to be a natural, inexpensive, and abundant antioxidant for use in pharmaceuticals and cosmetics. In animal studies, Gerasopoulos et al. (2015) have included polyphenols extracted from olive oil processing wastewater to feed 20-day-old piglets for 30 days. The authors found that the polyphenol-rich diet significantly increased levels of total antioxidant capacity, catalase activity, and glutathione in the pig's blood, as well as reducing oxidative stress. Liu et al. (2018) and Cimmino et al. (2018) showed that biomass polyphenols reduced the content of malondialdehyde in

mutton, the fat oxidation was inhibited followed by the improvement of meat quality. More importantly, the biomass flavonoid polyphenol fisetin has been shown to relieve allodynia in a reserpine-induced rat model with fibromyalgia, hyperalgesia, and depression. Through evaluating multiple parameters, the researchers suggest that fisetin lowered biogenic amine (5-hydroxytryptamine, noradrenaline, and dopamine) levels, inhibited the oxidation of nitroso stress to downregulate ROS level, to exert its resistance to hurt feelings and antidepressant potential.

In conclusion, biomass polyphenols show prominent antioxidant performance and free radical scavenging capabilities, which is of great significance to broadening their fields of research and various applications.

Antibacterial Activity

In recent years, consumers are increasingly intended to use natural extracts and other substances as potential antibiotics to inhibit the growth of pathogenic bacteria due to the concerns on the destruction of nutrition by sterilization technology and the abuse of synthetic antibiotics, as shown in **Table 2** (Xu et al., 2019; Liu W. et al., 2020). Polyphenols are considered to be one of the intriguing natural extracts to hinder the growth and proliferation of bacteria *via* multiple modes of action, which include alteration of the bacterial membrane permeabilization, inhibition of the bacterial DNA gyrase, interference with the energy metabolism, and perturbation of the functions of bacterial porins (An et al., 2004; Gradisar et al., 2007; Wang et al., 2020; Yun et al., 2021). In addition, the presence of phenolic hydroxyl groups potentiates the antibacterial activities of polyphenols on damaging the structural integrity and functionality of bacterial membranes (Sousa et al., 2015).

Emerging evidence has demonstrated the beneficial effect of biomass polyphenols against bacteria. Pani et al. (2014) studied the toxicities of 29 polyphenols at different concentrations of the monophototoxin produced from *Fusarium oxysporum* in wheat. Most of the polyphenols exhibited an inhibitory rate of 70% against deoxynivalenol ranging from 1 to 1.5 mM. A series of biomass polyphenols shows prominent inhibition on distinct strains of bacteria, fungi, and yeasts. Tea polyphenols are a kind of antimicrobial agent with a broad inhibitory spectrum on multiple pathogenic bacteria, such as *Proteus* common, *Staphylococcus epidermidis*, and *Staphylococcus aureus*. In addition, apple polyphenol extract elicits a suppression effect on the growth of *Bacillus aerobics*, *Escherichia coli*, *Pseudomonas*, and *Bacillus subtilis*. Pomegranate pulp is rich in eight different kinds of polyphenol compounds, all of which exert strong bacteriostatic abilities against *Salmonella* and *Escherichia coli* (Gullon et al., 2016). Flavonoids alone or in combination with known therapeutic agents effectively control *S. aureus* infection (Elmasri et al., 2015). More interestingly, Williams et al. (2017) found that oligoproanthocyanidins in grape dregs modulate intestinal microflora and alleviates intestinal *Ascaris suum* infection when grape dregs were added to the pig's diet. When 10–40 g/kg grape seed powder was added to the chicken diet, it was found that the total number of *Streptococcus*, *Escherichia coli*, and microbial colonies in the chicken intestines decreased while

the number of beneficial lactic acid bacteria increased in a dose-dependent manner (Hafsa and Ibrahim, 2017). Bearing this antibacterial activity in mind, researchers have endeavored to further investigate the mechanisms behind polyphenols' bacteriostatic functionality.

Yang and Zhang (2019) delineated the bacteriostatic mechanism of tea polyphenols as shown in **Figure 4**. Their results showed that the electrolyte leakage rate of bacteria was significantly enhanced after treatment with different concentrations of tea polyphenols, indicating the impairment of bacterial membrane permeability in the presence of polyphenols. The bacterial membrane is mainly composed of lipid bilayers containing hydrophilic and hydrophobic ends. The binding between phenolic hydroxyl groups and hydrophilic ends triggers agglomeration of membrane lipids, thus destroying the bacterial membrane. Intriguingly, when inoculated in plants and fruits, polyphenolic compounds induce the activities of a couple of antibacterial enzymes, including phenylalanine aminase, catalase, peroxidase, polyphenol oxidase, chitinase and β -1, 3-glucanase, thereby improving the antibacterial abilities of plants and fruits (Ramadas et al., 2020).

Currently, the studies on the antibacterial properties of biomass polyphenols continue to be carried out in breadth and depth. However, the structure-function relationship of polyphenols and the combinational applications of polyphenols with more prominent antibacterial effects require further investigation.

Antitumor and Anticancer Activity

Reactive oxygen free radicals are the metabolites of the Redox reaction in biological organisms. Under normal physiological conditions, the generation and scavenging of free radicals are finely balanced in a dynamic equilibrium. However, when the imbalance occurs, excessive free radicals will deteriorate the organisms, leading to aging and the increased incidence of a range of disorders (Zhang et al., 2020; Wang et al., 2021). The accumulation of free radicals generates direct damage on the genetic materials and other biological macromolecules, including the aberrant gene transcriptional activation, changes in the structural and functional identities of proteins, breakage, and polymerization of peptide bonds, and lipid peroxidation, leading to the occurrence of tumors and cancers (**Figure 5**) (Ríos-Arrabal et al., 2013). Polyphenols have attracted broad attention in cancer therapeutics due to their chemopreventive roles as both blocking and suppressing agents (Sharma et al., 2017; Sajadimajd et al., 2020). In terms of their blocking functions, polyphenols can avoid the activation of carcinogens, prevent the reactive carcinogens from interacting with critical DNA sites, and facilitate the metabolic clearance of carcinogens. Moreover, polyphenols are capable of suppressing oncogenesis and cancer progression, to elicit their chemopreventive functions on multiple stages of carcinogenesis (Zhou et al., 2016).

Vegetables and fruits contain a wide variety of polyphenols, and studies have reported that regular consumption of fruits, vegetables, and nuts reduces the risk of various types of cancer, especially with a significant impact on gastric, esophageal, lung, oral, pharyngeal, pancreatic and colon cancers (Yi et al., 2019).

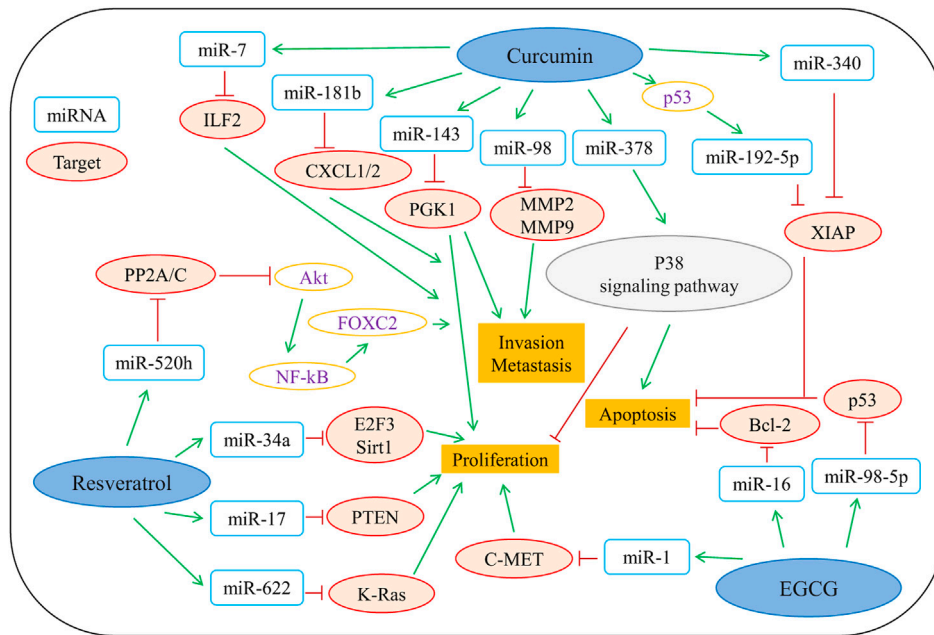


FIGURE 6 | Representative polyphenols that are involved in regulating the antitumor mechanisms of microRNAs. miR, microRNA; ILF2, Interleukin enhancer binding factor 2; CXCL1/2, chemokine (C-X-C motif) ligands 1/2; PGK1, phosphoglycerate kinase 1; MMP2/9, matrix metalloproteinase 2/9; XIAP, X-linked inhibitor of apoptosis; PP2A/C, protein phosphatase 2A/C; E2F3, E2F transcription factor 3; Sirt1, Sirtuin type 1; PTEN, phosphatase and tensin homolog; K-Ras, kirsten rat sarcoma; C-MET, cellular-mesenchymal epithelial transition factor; Bcl-2, B-cell lymphoma-2; p53, protein 53; P38 signaling pathway, protein 38 signaling pathway. reproduced with copyright permission from Elsevier (Yi et al., 2019).

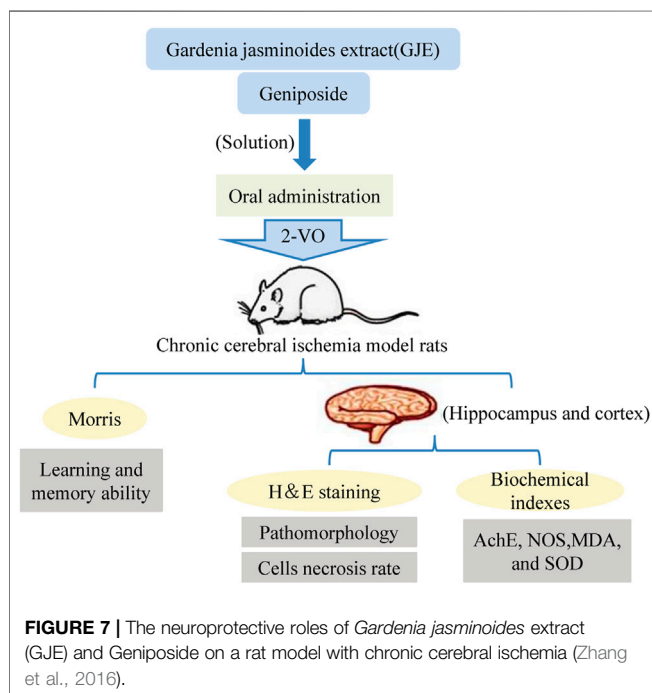
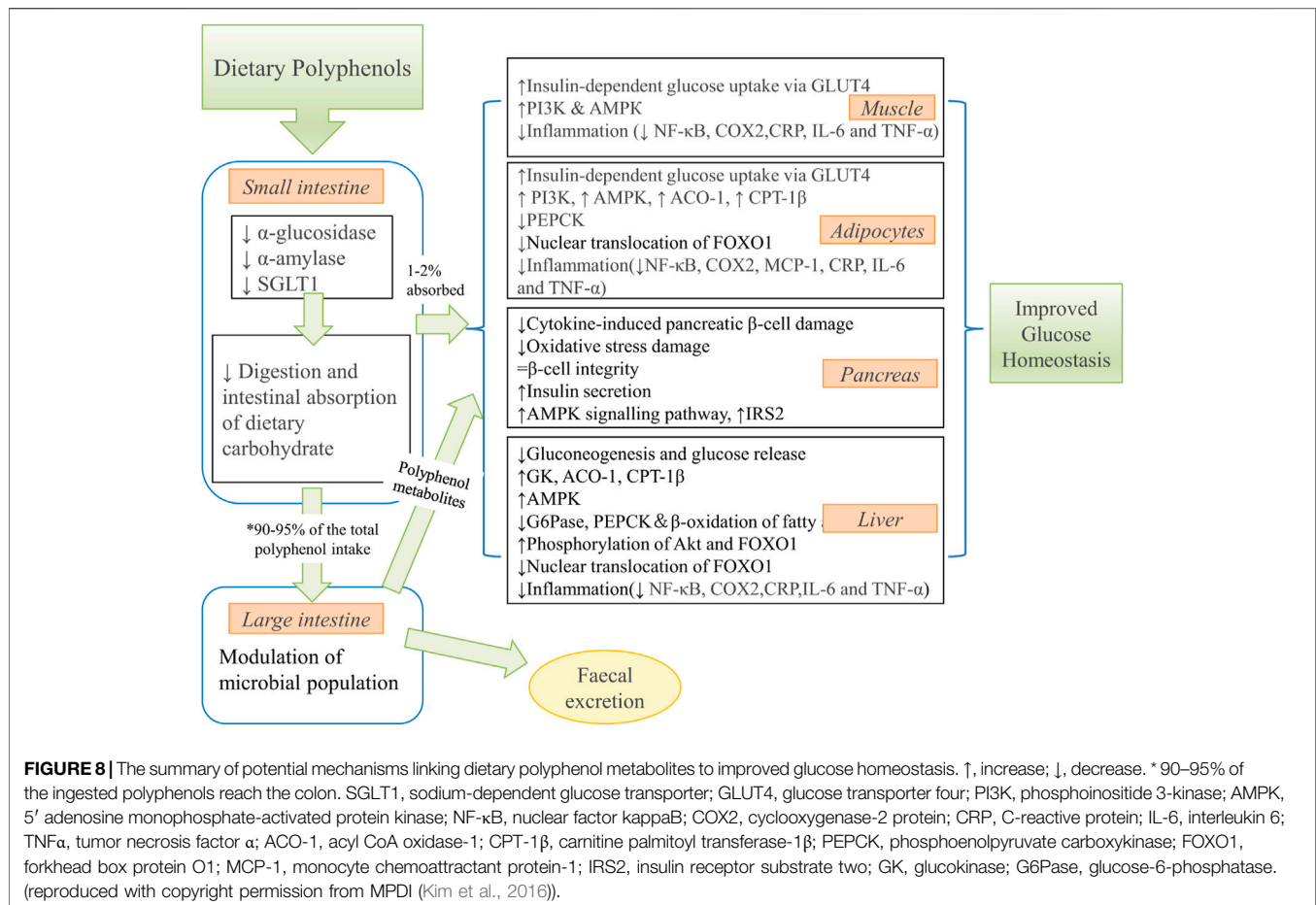


FIGURE 7 | The neuroprotective roles of *Gardenia jasminoides* extract (GJE) and Geniposide on a rat model with chronic cerebral ischemia (Zhang et al., 2016).

Epidemiological and experimental studies have shown that consumption of food and beverages rich in polyphenols (such as catechins, flavonoids, and anthocyanins) is closely associated

with a lower incidence of cancer (Naasani et al., 2003). Animal experiments have also demonstrated that food polyphenols effectively suppress chemical-induced tumors and inhibit tumor developments at multiple stages (Sharma et al., 2017; Sajadimajd et al., 2020). An increasing number of studies highlight the role of biomass polyphenols as potential anticancer cell mutagens. Han et al. (2019) showed that cranberry-extracted polyphenols are bioactive anticancer components, and they have dramatic capacities towards inhibiting the viability and colony formation of human colon cancer cells HCT116. Mechanistically, treatment of polyphenols caused the cell cycle arrest at G0/G1 phase and subsequently led to the induction of cell apoptosis. There is ample evidence showing that polyphenols target a variety of molecules that are involved in multiple cellular signaling pathways. Emerging evidence has shown that non-coding RNAs function as oncogenes or tumor suppressors in the regulation of tumorigenesis and tumor progression (Yi et al., 2019). The antitumor mechanisms of polyphenols are multi-targeted and include the activation of different pathways to induce apoptosis in cancer cells. Moreover, three predominant epigenetic changes (alterations in chromatin structure, DNA methylation, and regulation by microRNAs) are also involved in tumor cells treated with biomass polyphenols. As shown in Figure 6 (Yi et al., 2019), EGCG, curcumin, and resveratrol regulate multiple classes of miRNAs to elicit their antitumor potentials.

Although multiple targets have been identified in terms of the antitumor/anticancer activities of the biomass polyphenols, the



detailed mechanisms of how polyphenols are capable of controlling the expression of these genes/miRNAs remain elusive. It would therefore be interesting to select single or high purity polyphenols from natural product resources with strong antitumor/anticancer activities to further investigate their relationships with antitumor factors.

Neuroprotective Activity

The incidence of neurodegenerative disorders, such as Alzheimer's disease and Parkinson's disease, gradually increases with age (Remington et al., 2010; Figueira et al., 2017; Li, 2018). These types of disorders share common pathological hallmarks, including oxidative stress, neuroinflammation, protein aggregation, and mitochondrial dysfunction (Gu et al., 2021). Given their roles in mediating essential biological processes, including signal transduction, cell proliferation and apoptosis, and cell differentiation, polyphenols have been long taken as potential neuroprotective agents. More importantly, the neuroprotective function of polyphenols has been suggested to be associated with their antioxidant activities, especially towards scavenging ROS and nitric oxide (Zhen and Liu, 2018).

A growing number of studies have provided experimental evidence that the consumption of polyphenol-rich berry fruits is

beneficial to the nervous system and shows the potential to mitigate age-dependent neurodegeneration *via* alleviating cognitive and motor dysfunctions (Figueira et al., 2017; Tavares et al., 2013). Moreover, the neuroprotective function has also been demonstrated on *Gardenia jasminoides* extract (GJE). The medium dose of GJE treatment showed the most effective inhibition of neuronal necrosis in different brain regions of the rat model of chronic cerebral ischemia (Figure 7) (Zhang et al., 2016). Green tea polyphenols have been demonstrated to play a neuroprotective role due to their antioxidant and anti-inflammatory properties (Sutherland et al., 2006; Song et al., 2019). Zhang et al. (2010) showed that a 30-days treatment with green tea polyphenols (200 mg/kg, twice a day) prominently restored blood-brain barrier permeability, rescued cerebral infarction and improved neurological functions in rats underwent cerebral ischemia. Moreover, the induction of caveolin-1 mRNA and hyperphosphorylation of extracellular signal-regulated kinase 1/2, markers of cerebral ischemia, were also found ameliorated in cerebral ischemic tissue. Liu et al. (2019) isolated four catechins, including two new catechin derivatives, from Anhua dark tea. The study showed that the compounds exhibited optimal neuroprotective effects by inhibiting N-methyl-D-aspartate (NMDA) receptors. It protected SH-SY5Y cells from NMDA-induced injury and

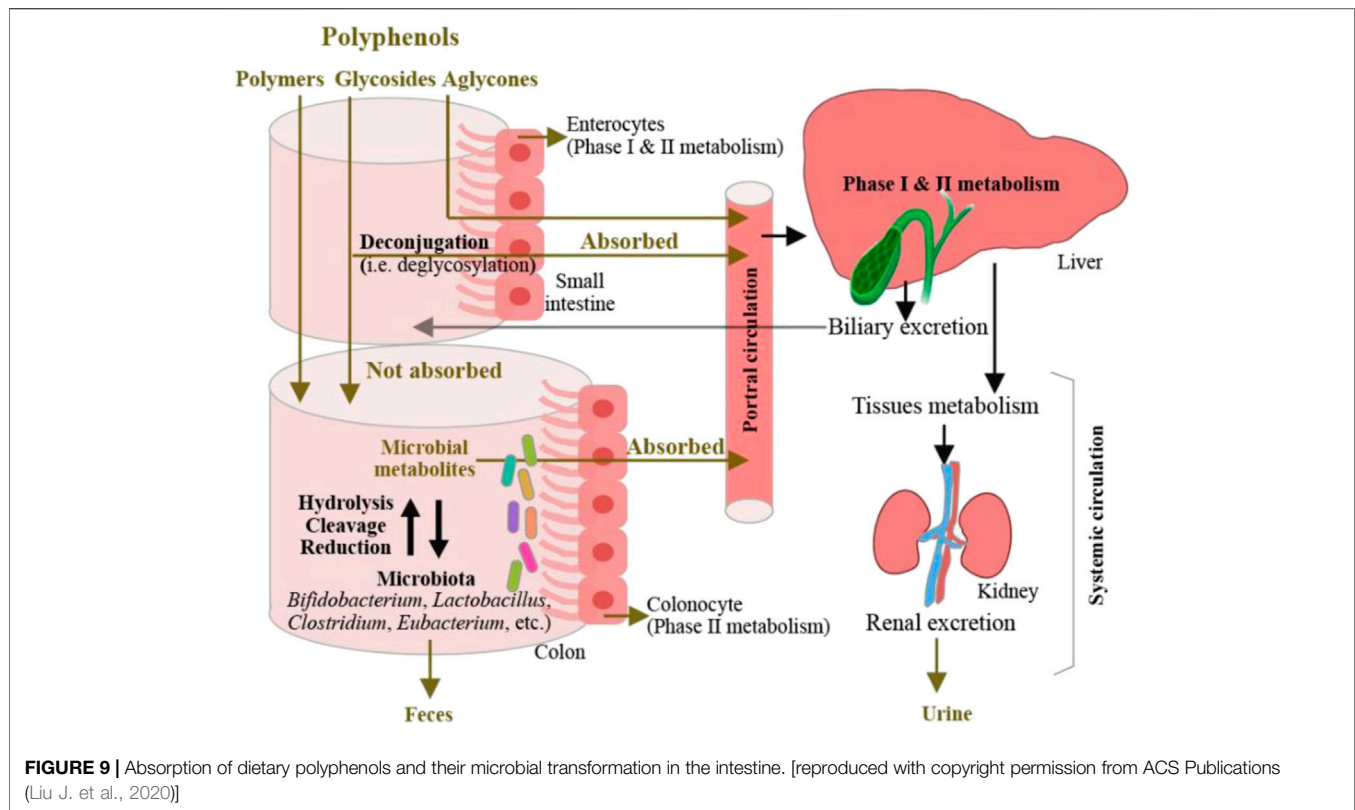


FIGURE 9 | Absorption of dietary polyphenols and their microbial transformation in the intestine. [reproduced with copyright permission from ACS Publications (Liu J. et al., 2020)]

apoptosis by regulating NR2B expression and activating PI3K/Akt signaling pathway. These compounds are expected to be effective therapeutic agents for the prevention of excitatory brain injury. Taken together, these findings emphasize that the antioxidant, anti-apoptotic, and reduction of brain edema activities of tea polyphenols are prerequisites for their neuroprotective functions.

Hypoglycemic and Lipid-Lowering Activity

High blood lipid content is one of the essential risk factors of fatty liver, cerebral infarction, coronary heart disease, and the formation of vascular sclerosis. Excessive accumulation of blood glucose in diabetic patients easily leads to acute severe metabolic disorders, for example, life-threatening hyperosmolar hyperglycemia syndrome. In the meantime, diabetic patients also suffer from infectious diseases, which lead to chronic complications including microangiopathy, diabetic nephropathy, and diabetic retinopathy. The nervous system complications may also be accompanied, such as peripheral neuropathy, autonomic neuropathy, and diabetic feet. All of these symptoms and complications severely ruin the quality of life of diabetic patients (Monika L. et al., 2019). Diabetic patients with combined neuropathy also develop pancreatic sclerosis and atrophy (He et al., 2020). Medicinal biomass has been applied to control diabetes and hyperlipidemia in different countries (Sugiyama et al., 2007; Yang et al., 2010; Saeed et al., 2012), and has become the major source of safe and effective hypoglycemic and hyperlipidemic drugs. Importantly, the hypoglycemic activity has been assigned to biomass

polyphenols due to their capabilities in exerting antioxidant functions, promoting the synthesis and secretion of insulin, perturbing the activities of intestinal digestive enzymes, and inhibiting the glucose transport (Mahmood et al., 2013).

Chakraborty et al. (2012) emphasized that the role of 6-gingerol in controlling insulin responsiveness *via* regulating insulin secretion of mouse pancreas is essential for protecting the hyperglycemia and oxidative stress caused by arsenic. When the mice were fed with 6-gingerol for 12 days, Singh et al. (2009) reported a significant reduction of fasting blood glucose, accompanied by increased glucose tolerance and downregulation of plasma triglyceride (TG), total cholesterol (TC), insulin, low-density lipoprotein cholesterol (LDL-C) and free fatty acid (FFA) levels. These findings support the anti-hyperglycemia and cholesterol-lowering activities of 6-gingerol. The other kinds of biomass polyphenols function to increase insulin sensitivity and improve insulin resistance. Manzano et al. (Manzano et al., 2016) showed that apple polyphenols (APE, mainly quercetin and rutin) have therapeutic potential in the rat model of insulin resistance. Nutritional intervention with APE resulted in increased insulin sensitivity and a 45% increase in glucose infusion rate (GIR). Furthermore, *in vitro* results showed a synergistic effect between APE and insulin to increase glucose uptake through GLUT4 translocation in muscle cells. This translocation is mediated by the phosphatidylinositol 3-kinase (PI3K) and peroxisome proliferator-activated receptor- γ (PPAR γ) signaling pathways. Xiong et al. (2020) also demonstrated that catechins, procyanidin A1 and procyanidin A2 extracted from lychee seed LSF could activate the insulin

signaling pathway and inhibit GSK-3 β activity *via* the IRS-1/PI3K/Akt pathway, which in turn inhibited Tau hyperphosphorylation and ultimately improved cognitive function in AD rats. Kim et al. (2016) provided a summary of potential mechanisms by which dietary polyphenol metabolites improve glucose homeostasis (**Figure 8**).

Vroegrijk et al. (2011) found that male C57BL/J6 rats fed with a high-fat diet containing 1% pomegranate seed oil for 12 weeks showed reduced fat content and body weight compared with those fed with a full-fat diet. Additionally, Xu et al. (2009) studied the effect of pomegranate flower extract on hepatic fat accumulation in Zucker diabetic obese rats with severe fatty liver disease and highlighted the hypolipidemic effect of the isolated polyphenols. Yu et al. (2014) found that pomegranate leaves (PGL) have a similar modulating effect on lipid metabolism. Pomegranate leaves and their major active components (ellagic acid, gallic acid, pyrogallol, gallic acid, and tannic acid) showed the effect of inhibiting pancreatic lipase activity *in vitro*. High doses of PGL inhibited intestinal lipase activity while promoting the expression of tight junction proteins, thereby inhibiting lipid absorption and reducing blood serum total cholesterol (TC) and triglyceride (TG) levels to prevent intestinal mucosal damage due to lipid overload.

Green tea polyphenols, grape polyphenols, citrus juice polyphenols, and sand buckthorn leaf polyphenols play similar roles in lowering blood sugar *via* multiple modes of action. In addition, several common fruit and vegetable polyphenols, such as pomegranate polyphenols, tea polyphenols, hawthorn polyphenols, and apple polyphenols, exert similar effects on downregulating TG, TC, and LDL-C levels while upregulating the level of high-density lipoprotein cholesterol. Currently, the study on the mechanisms of glucose- and lipid-lowering capabilities of biomass polyphenols has attracted much more attention but still requires further investigations.

Promotion of Gastrointestinal Health

Intestinal barriers refer to the intact structure and function of the intestine to prevent harmful substances such as bacteria and toxins from passing through the intestinal mucosa and entering other tissues, organs, and blood circulation in the human body. The normal intestinal mucosal barriers are composed of a mechanical barrier, a chemical barrier, an immune barrier, and a biological barrier, and the integrity of each intestinal barrier is indispensable to human health. The intestinal barriers maintain the normal intestinal permeability and regulate the transportation and absorption of nutrients (such as sugar, vitamins, amino acids, fatty acids, and other lipids) and other food-related compounds (such as polyphenols). In addition, intestinal barriers regulate the composition of bacteria from the lumen to the blood flow of transfer (Tangney and Rasmussen, 2013; Hidalgo-Liberona et al., 2020). The intestinal permeability is under control of a complex system of junctions known as tight junctions (TJ), gap junctions, and adhesion junctions. The system has consisted of numerous TJ proteins and junction adhesion molecules that control the flow among adjacent intestinal cells. It has been reported previously that polyphenols can mitigate leaky bowel disease by directly adjusting TJ function, enhancing the synthesis and redistribution of TJ proteins (such as occludin, claudins, and

occludula), and suppressing the activities of different kinases involved in controlling TJ expression (Hidalgo-Liberona et al., 2020).

Gastrointestinal dysfunction is one of the major factors that contribute to type II diabetes, cardiovascular disease, insomnia, obesity, and other disorders (Kang, 2013; Kitai and Tang, 2017; Orr et al., 2020). Therefore, improvement of gastrointestinal function requires much more investigation. Previous studies (Pandey and Rizvi, 2009) have reported that polyphenols show antioxidant, anti-inflammatory, anti-fat, anti-diabetes, cardioprotective, neuroprotective, and anticarcinogenic effects *via* collaborating with the intestinal microbiota. Biomass polyphenols influence the activities of intestinal microflora, repair gastrointestinal mucosal damage, optimize the intestinal structure, and interact with other macromolecules to affect gastrointestinal function. Chen et al. (2018) showed that the addition of chlorogenic acid to weaning piglets led to an increase of immune globulin level, the expression of antiapoptotic protein B-cell lymphoma-2 was simultaneously upregulated in the duodenum and jejunum. This indicates that the intestinal beneficial effect of chlorogenic acid depends on the enhancement of immune function and suppression of excessive intestinal epithelial cell apoptosis. Liao et al. (2016) showed that upon treatment of tea polyphenols, the reduction of atherosclerosis plaque in mice negatively correlated with the increased number of bifidobacteria in their intestine, suggesting that tea polyphenols promote the proliferation of bifidobacteria and prevent lipid metabolism, thereby suppressing atherosclerosis. Biomass polyphenols were found to accelerate beneficial bacteria proliferation to improve the function of the intestines and stomach and repair the damaged intestinal cells. Zhao et al. (2018) showed that when treated with bitter butyl tea polyphenols, the reduction of gastric acid secretion and increase of gastric juice pH was detected in mice with gastric mucosa damage, indicating that bitter butyl tea polyphenols supplement was an effective approach to combat against gastric mucosa damage. With the increasing number of studies on the relationship between biomass polyphenols and gastrointestinal function, the development and utilization of biomass polyphenols as functional factors for the improvement of gastrointestinal function is expected to be broadened. Liu et al. (2020a) depicted the metabolic mechanisms of dietary polyphenols in the intestine (**Figure 9**). In the body, a small percentage of dietary polyphenols is first absorbed in the small intestine. They are then deconjugated, circulated, and distributed among organs or excreted in the urine. The remaining unabsorbed polyphenols reach the colon where they are catabolized by bacteria to produce metabolites either absorbed or excreted in feces. After intestinal and hepatic Phase I and II metabolism, the microbial-derived polyphenolic metabolites enter the systemic circulation. The metabolites in the liver could be excreted *via* the biliary duct and re-absorbed throughout the enterohepatic recirculation. In animal studies, the addition of polyphenols to diets reduced high-fat diet-induced obesity and modulated the gut microbiota by increasing the growth of short-chain fatty acid-producing bacteria and decreasing the growth of lipopolysaccharide-producing bacteria. More clinical trials are required to investigate the application of dietary

polyphenols as nutritional or functional foods in the prevention and treatment of obesity in humans, and studies that aim at elucidating the mode of action of specific bacteria strains in mediating dietary polyphenols would be necessary.

CONCLUSION AND PERSPECTIVES

Although polyphenols have been considered as chemical impurities, recent studies and findings underlined its biological activities in terms of exerting antioxidant, antibacterial, antitumor, neuroprotection, regulation of blood lipid, and promotion of gastrointestinal health functions. This thus attracts more attention from researchers worldwide to further investigate the pharmacological applications of biomass polyphenols and use them as one of the major components in natural products-derived drugs. More interestingly, given that biomass polyphenols are enriched in daily food, this further highlights the essential contribution of polyphenols to human life and makes biomass polyphenols one of the research hotspots. A range of studies has demonstrated efficient extraction of polyphenols from tea, grape, pomegranate, rapeseed, and other raw materials, which are coincidentally used in medical treatments and as functional food supplements. Many diseases are associated with antioxidants, but given the purity of the extract and the complexity of the structure, polyphenols are currently only used as supplements for the treatment of diseases, and

research into their use as medicines for the treatment of diseases still requires innovative extraction techniques and in-depth research into anti-disease mechanisms, to explore their therapeutic potential. Hence, the mechanisms of polyphenols' pharmacological actions still require further investigation. It is hoped that with the increasing attention from researchers on natural drugs and the progress of scientific technology, more methods of rapid separation and preparation of polyphenols can be developed, and the underlying pharmacological mechanisms of polyphenols will be further elucidated to provide the material basis for further pharmacological examination and clinical investigation.

AUTHOR CONTRIBUTIONS

ZC proposed the idea. BY and YH wrote the manuscript. ZC and QY wrote and revised the manuscript.

FUNDING

This work was supported by Natural Science Foundation of Jiangsu Province (BK20180772) and Qinglan project of Jiangsu Province. ZC was supported by a Postdoctoral Fellowship in Clinical Neurosciences program between The Chinese University of Hong Kong and University of Oxford (Nuffield Department of Clinical Neurosciences and Pembroke College).

REFERENCES

- Abu Hafs, S. H., and Ibrahim, S. A. (2017). Effect of Dietary Polyphenol-Rich Grape Seed on Growth Performance, Antioxidant Capacity and Ileal Microflora in Broiler Chicks. *J. Anim. Physiol. Anim. Nutr.* 102, 268–275. doi:10.1111/jpn.12688
- An, B.-J., Kwak, J.-H., Son, J.-H., Park, J.-M., Lee, J.-Y., Jo, C., et al. (2004). Biological and Anti-microbial Activity of Irradiated green tea Polyphenols. *Food Chem.* 88, 549–555. doi:10.1016/j.foodchem.2004.01.070
- Bhuyan, D. J. (2018). *Phytochemicals Derived from Australian Eucalypts as Anticancer Agents for Pancreatic Malignancies (Doctoral Dissertation)*. Newcastle, England: The University of Newcastle.
- Boadas-Vaello, P., Vela, J. M., and Verdú, E. (2017). New Pharmacological Approaches Using Polyphenols on the Physiopathology of Neuropathic Pain. *Curr. Drug Targets* 18, 160–173. doi:10.2174/1389450117666160527142423
- Cardona, F., Andrés-Lacueva, C., Tulipani, S., Tinahones, F. J., and Queipo-Ortuño, M. I. (2013). Benefits of Polyphenols on Gut Microbiota and Implications in Human Health. *J. Nutr. Biochem.* 24, 1415–1422. doi:10.1016/j.jnutbio.2013.05.001
- Chakraborty, D., Mukherjee, A., Sikdar, S., Paul, A., Ghosh, S., and Khuda-Bukhsh, A. R. (2012). [6]-gingerol Isolated from Ginger Attenuates Sodium Arsenite Induced Oxidative Stress and Plays a Corrective Role in Improving Insulin Signaling in Mice. *Toxicol. Lett.* 210, 34–43. doi:10.1016/j.toxlet.2012.01.002
- Chen, J., Xie, H., Chen, D., Yu, B., Mao, X., Zheng, P., et al. (2018). Chlorogenic Acid Improves Intestinal Development via Suppressing Mucosa Inflammation and Cell Apoptosis in Weaned Pigs. *ACS Omega* 3, 2211–2219. doi:10.1021/acsomega.7b01971
- Chen, J., Yu, Y., Zhu, B., Han, J., Liu, C., Liu, C., et al. (2021). Synthesis of Biocompatible and Highly Fluorescent N-Doped Silicon Quantum Dots from Wheat Straw and Ionic Liquids for Heavy Metal Detection and Cell Imaging. *Sci. Total Environ.* 765, 142754. doi:10.1016/j.scitotenv.2020.142754
- Chen, S., Wang, G., Sui, W., Parvez, A. M., Dai, L., and Si, C. (2020). Novel Lignin-Based Phenolic Nanosphere Supported Palladium Nanoparticles with Highly Efficient Catalytic Performance and Good Reusability. *Ind. Crops Prod.* 145, 112164. doi:10.1016/j.indcrop.2020.112164
- Chen, W., Chen, F., and Tian, J. (2002). Study on Heavy Sulfite Modification and Application of Bayberry Tannin Extract. *Chem. Ind. For. Prod.* 22, 55–58. doi:10.1097/00006982-200202000-00010
- Cimmino, R., Barone, C. M. A., Claps, S., Varricchio, E., Rufrano, D., Caroprese, M., et al. (2018). Effects of Dietary Supplementation with Polyphenols on Meat Quality in Saanen Goat Kids. *Bmc. Vet. Res.* 14, 181. doi:10.1186/s12917-018-1513-1
- Croft, K. D. (2016). Dietary Polyphenols: Antioxidants or Not? *Arch. Biochem. Biophys.* 595, 120–124. doi:10.1016/j.abb.2015.11.014
- Dahibhate, N. L., Kumar, D., and Kumar, K. (2020). Determination of Bioactive Polyphenols in Mangrove Species and Their *In-Vitro* Anti-Candida Activities by Ultra-high-performance Liquid Chromatography - Electrospray Ionization - Tandem Mass Spectrometry (UPLC-ESI-MS/MS). *Anal. Lett.* 54 (4), 608–624. doi:10.1080/00032719.2020.1774600
- Dai, L., Su, X., Lu, Y., Chen, S., and Wu, Z. (2006). Determination of Tannin Content of Valonea Tannin Extracts by Colloidal Titration. *Biomass Chem. Eng.* 40, 15–17.
- Day, A. J., Cañada, F. J., Dī'az, J. C., Kroon, P. A., Mclauchlan, R., Faulds, C. B., et al. (2000). Dietary Flavonoid and Isoflavone Glycosides Are Hydrolysed by the Lactase Site of Lactase Phlorizin Hydrolase. *Febs. Lett.* 468, 166–170. doi:10.1016/s0014-5793(00)01211-4
- de Camargo, A. C., Favero, B. T., Morzelle, M. C., Franchin, M., Alvarez-Parrilla, E., de la Rosa, L. A., et al. (2019). Is Chickpea a Potential Substitute for Soybean? Phenolic Bioactives and Potential Health Benefits. *Ijms* 20 (11), 2644. doi:10.3390/ijms20112644

- de Sousa, J. P., de Oliveira, K. Á. R., de Figueiredo, R. C. B. Q., and de Souza, E. L. (2015). Influence of Carvacrol and 1,8-cineole on Cell Viability, Membrane Integrity, and Morphology of *Aeromonas Hydrophila* Cultivated in a Vegetable-Based Broth. *J. Food Prot.* 78, 424–429. doi:10.4315/0362-028x.jfp-14-242
- Delgado, N. T. B., Rouver, W. N., and Santos, R. L. D. (2019). Protective Effects of Pomegranate in Endothelial Dysfunction. *Curr. Pharm. Design.* 26 (30), 3684–3699.
- Dong, H., Zheng, L., Yu, P., Jiang, Q., Wu, Y., Huang, C., et al. (2020). Characterization and Application of Lignin-Carbohydrate Complexes from Lignocellulosic Materials as Antioxidants for Scavenging *In Vitro* and *In Vivo* Reactive Oxygen Species. *ACS Sust. Chem. Eng.* 8 (1), 256–266. doi:10.1021/acsschemeng.9b05290
- Dugasani, S., Pichika, M. R., Nadarajah, V. D., Balijepalli, M. K., Tandra, S., and Korlakunta, J. N. (2010). Comparative Antioxidant and Anti-inflammatory Effects of [6]-gingerol, [8]-gingerol, [10]-gingerol and [6]-shogaol. *J. Ethnopharmacology* 127 (2), 515–520. doi:10.1016/j.jep.2009.10.004
- Elmasri, W. A., Zhu, R., Peng, W., Al-Hariri, M., Kobeissy, F., Tran, P., et al. (2015). Multitargeted Flavonoid Inhibition of the Pathogenic Bacterium *Staphylococcus aureus*: a Proteomic Characterization. *J. Proteome Res.* 16 (7), 2579–2586. doi:10.1021/acs.jproteome.7b00137
- Fiedor, J., and Burda, K. (2014). Potential Role of Carotenoids as Antioxidants in Human Health and Disease. *Nutrients* 6, 466–488. doi:10.3390/nu6020466
- Figueira, I., Tavares, L., Jardim, C., Costa, I., Terrasso, A. P., Almeida, A. F., et al. (2017). Blood-brain Barrier Transport and Neuroprotective Potential of Blackberry-Digested Polyphenols: an *In Vitro* Study. *Eur. J. Nutr.* 58 (1), 113–130. doi:10.1007/s00394-017-1576-y
- Fiocchetti, M., Fernandez, V. S., Montalesi, E., and Marino, M. (2019). Neuroglobin: a Novel Player in the Oxidative Stress Response of Cancer Cells. *Oxidative Med. Cell Longevity* 2019, 1–9. doi:10.1155/2019/6315034
- Fraga, C. G. (2007). Plant Polyphenols: How to Translate Their *In Vitro* Antioxidant Actions to *In Vivo* Conditions. *Tbmb* 59, 308–315. doi:10.1080/15216540701230529
- Ge, G., Luo, S., and Ta, N. (2015). Extraction of Total Tannins and Determination of Amino Acids in Chinese Gallnut, Cinnamon and Pomegranate Bark. *Inner. Mongolia. Pet. Ind.* 6, 11–13.
- Gee, J. M., Dupont, M. S., Day, A. J., Plumb, G. W., Williamson, G., and Johnson, I. T. (2000). Intestinal Transport of Quercetin Glycosides in Rats Involves Both Deglycosylation and Interaction with the Hexose Transport Pathway. *J. Nutr.* 130, 2765–2771. doi:10.1093/jn/130.11.2765
- Geng, W., Narron, R., Jiang, X., Pawlak, J. J., Chang, H. M., Park, S., et al. (2016). The Influence of Lignin Content and Structure on Hemicellulose Alkaline Extraction for Non-wood and Hardwood Lignocellulosic Biomass. *Cellulose* 26, 3219–3230.
- Geng, W., Venditti, R. A., Pawlak, J. J., Chang, H.-m., Pal, L., and Ford, E. (2020). Carboxymethylation of Hemicellulose Isolated from poplar (*Populus grandidentata*) and its Potential in Water-Soluble Oxygen Barrier Films. *Cellulose* 27, 3359–3377. doi:10.1007/s10570-020-02993-2
- Gerasopoulos, K., Stagos, D., Petrotos, K., Kokkas, S., Kantas, D., Goulas, P., et al. (2015). Feed Supplemented with Polyphenolic Byproduct from Olive Mill Wastewater Processing Improves the Redox Status in Blood and Tissues of Piglets. *Food Chem. Toxicol.* 86, 319–327. doi:10.1016/j.fct.2015.11.007
- Gessner, M. O., and Steiner, D. (2005). *Acid Butanol Assay for Proanthocyanidins (Condensed Tannins). Methods to Study Litter Decomposition*. Springer Netherlands.
- Gironi, F., and Piemonte, V. (2011). Temperature and Solvent Effects on Polyphenol Extraction Process from Chestnut Tree wood. *Chem. Eng. Res. Des.* 89, 857–862. doi:10.1016/j.cherd.2010.11.003
- Goodman, B. A. (2020). Utilization of Waste Straw and Husks from rice Production: A Review. *J. Bioresources Bioproducts* 5 (3), 143–162. doi:10.1016/j.jobab.2020.07.001
- Gradisar, H., Pristovsek, P., Plaper, A., and Jerala, R. (2007). Green tea Catechins Inhibit Bacterial DNA Gyrase by Interaction with its ATP Binding Site. *J. Med. Chem.* 50, 264–271. doi:10.1021/jm060817o
- Gu, J., Guo, M., Huang, C., Wang, X., Zhu, Y., Wang, L., et al. (2021). Titanium Dioxide Nanoparticle Affects Motor Behavior, Neurodevelopment and Axonal Growth in Zebrafish (*Danio rerio*) Larvae. *Sci. Total Environ.* 754, 142315. doi:10.1016/j.scitotenv.2020.142315
- Gullon, B., Pintado, M. E., Pérez-Álvarez, J. A., and Viuda-Martos, M. (2016). Assessment of Polyphenolic Profile and Antibacterial Activity of Pomegranate Peel (*Punica Granatum*) Flour Obtained from Co-product of Juice Extraction. *Food Control* 59, 94–98. doi:10.1016/j.foodcont.2015.05.025
- Han, Y., Huang, M., Li, L., Cai, X., Gao, Z., Li, F., et al. (2019). Non-extractable Polyphenols from Cranberries: Potential Anti-inflammation and anti-colon-cancer Agents. *Food Funct.* 10, 7714–7723. doi:10.1039/c9fo01536a
- He, Y., Jin, Y., Li, X., Wu, L., and Jin, C. (2020). Quantification of Pancreatic Elasticity in Type 2 Diabetes: a New Potential Imaging Marker for Evaluation of Microangiopathy. *Eur. J. Radiol.* 124, 108827. doi:10.1016/j.ejrad.2020.108827
- Hidalgo-Liberona, N., González-Domínguez, R., Vegas, E., Riso, P., Del Bo', C., Bernardi, S., et al. (2020). Increased Intestinal Permeability in Older Subjects Impacts the Beneficial Effects of Dietary Polyphenols by Modulating Their Bioavailability. *J. Agric. Food Chem.* 68, 12476–12484. doi:10.1021/acs.jafc.0c04976
- Hu, L. W., Li, T., Luo, Q., and Zhang, J. S. (2020). Antioxidant Stability of Colloidal tea Polyphenols in tea Seed Oil. *J. Food Process. Pres.* 45 (2), e15130. doi:10.1111/jfpp.15130
- Ji, M., Gong, X., Li, X., Wang, C., and Li, M. (2020). Advanced Research on the Antioxidant Activity and Mechanism of Polyphenols from Hippophae Species—A Review. *Molecules* 25 (4), 917. doi:10.3390/molecules25040917
- Kang, Y. S. (2013). Obesity Associated Hypertension: New Insights into Mechanism. *Electrolyte Blood Press.* 11, 46–52. doi:10.5049/ebp.2013.11.2.46
- Kim, H.-S., Quon, M. J., and Kim, J.-a. (2014). New Insights into the Mechanisms of Polyphenols beyond Antioxidant Properties; Lessons from the green tea Polyphenol, Epigallocatechin 3-gallate: Lessons from the green tea Polyphenol, Epigallocatechin 3-ganate. *Redox Biol.* 2, 187–195. doi:10.1016/j.redox.2013.12.022
- Kim, Y., Keogh, J., and Clifton, P. (2016). Polyphenols and Glycemic Control. *Nutrients* 8 (1), 17. doi:10.3390/nu8010017
- Kitai, T., and Tang, W. H. W. (2017). The Role and Impact of Gut Microbiota in Cardiovascular Disease. *Revista Española de Cardiología (English Edition)* 70, 799–800. doi:10.1016/j.rec.2017.04.007
- Li, J. (2018). Neuroprotective Effect of (-)-Epigallocatechin-3-Gallate on Autoimmune Thyroiditis in a Rat Model by an Anti-inflammation Effect, Anti-apoptosis and Inhibition of TRAIL Signaling Pathway. *Exp. Ther. Med.* 15, 1087–1092. doi:10.3892/etm.2017.5511
- Liao, Z.-L., Zeng, B.-H., Wang, W., Li, G.-H., Wu, F., Wang, L., et al. (2016). Impact of the Consumption of Tea Polyphenols on Early Atherosclerotic Lesion Formation and Intestinal Bifidobacteria in High-Fat-Fed ApoE^{-/-} Mice. *Front. Nutr.* 3, 42. doi:10.3389/fnut.2016.00042
- Liu, D., Meng, S., Xiang, Z., He, N., and Yang, G. (2019). Antimicrobial Mechanism of Reaction Products of *Morus Notabilis* (mulberry) Polyphenol Oxidases and Chlorogenic Acid. *Phytochemistry* 163, 1–10. doi:10.1016/j.phytochem.2019.03.026
- Liu, H. W., Zhao, J. S., Li, K., and Deng, W. (2018). Effects of Chlorogenic Acids-Enriched Extract from *Eucommia Ulmoides* Leaves on Growth Performance, Stress Response, Antioxidant Status and Meat Quality of Lambs Subjected or Not to Transport Stress, Stress Response, Antioxidant Status and Meat Quality of Lambs Subjected or Not to Transport Stress. *Anim. Feed Sci. Tech.* 238, 47–56. doi:10.1016/j.anifeedsci.2018.02.003
- Liu, J., Fan, Y., Kim, D., Zhong, T., Yi, P., Fan, C., et al. (2019). Neuroprotective Effect of Catechins Derivatives Isolated from Anhua Dark tea on NMDA-Induced Excitotoxicity in SH-Sy5y Cells. *Fitoterapia* 137, 104240. doi:10.1016/j.fitote.2019.104240
- Liu, J., He, Z., Ma, N., and Chen, Z.-Y. (2020a). Beneficial Effects of Dietary Polyphenols on High-Fat Diet-Induced Obesity Linking with Modulation of Gut Microbiota. *J. Agric. Food Chem.* 68 (1), 33–47. doi:10.1021/acs.jafc.9b06817
- Liu, K., Du, H., Zheng, T., Liu, H., Zhang, M., Xie, H., et al. (2021). Recent Advances in Cellulose and its Derivatives for Oilfield Applications. *Carbohydr. Polym.* 117740. doi:10.1016/j.carbpol.2021.117740
- Liu, W., Du, H., Zhang, M., Liu, K., Liu, H., Xie, H., et al. (2020b). Bacterial Cellulose-Based Composite Scaffolds for Biomedical Applications: a Review. *ACS Sust. Chem. Eng.* 8 (20), 7536–7562. doi:10.1021/acssuschemeng.0c00125
- Liu, Z., Bruins, M. E., Ni, L., and Vincken, J.-P. (2018). Green and Black tea Phenolics: Bioavailability, Transformation by Colonic Microbiota, and Modulation of Colonic Microbiota. *J. Agric. Food Chem.* 66, 8469–8477. doi:10.1021/acs.jafc.8b02233

- Losada-Barreiro, S., and Bravo-Díaz, C. (2017). Free Radicals and Polyphenols: the Redox Chemistry of Neurodegenerative Diseases. *Eur. J. Med. Chem.* 133, 379–402. doi:10.1016/j.ejmech.2017.03.061
- Luo, Y., Li, Y., Cao, L., Zhu, J., Deng, B., Hou, Y., et al. (2021). High Efficiency and Clean Separation of eucalyptus Components by Glycolic Acid Pretreatment. *Bioresour. Tech.* 341, 125757. doi:10.1016/j.biortech.2021.125757
- Mahmood, D. F. D., Abderrazak, A., El Hadri, K., Simmet, T., and Rouis, M. (2013). The Thioredoxin System as a Therapeutic Target in Human Health and Disease. *Antioxid. Redox Signaling* 19 (11), 1266–1303. doi:10.1089/ars.2012.4757
- Manach, C., Scalbert, A., Morand, C., Rémésy, C., and Jiménez, L. (2004). Polyphenols: Food Sources and Bioavailability. *Am. J. Clin. Nutr.* 79, 727–747. doi:10.1093/ajcn/79.5.727
- Martin, D. A., and Bolling, B. W. (2015). A Review of the Efficacy of Dietary Polyphenols in Experimental Models of Inflammatory Bowel Diseases. *Food Funct.* 6, 1773–1786. doi:10.1039/c5fo00202h
- Michaličková, D., Belović, M., Ilić, N., Kotur-Stevuljević, J., Slanař, O., and Šobajić, S. (2019). Comparison of Polyphenol-Enriched Tomato Juice and Standard Tomato Juice for Cardiovascular Benefits in Subjects with Stage 1 Hypertension: a Randomized Controlled Study. *Plant Food Hum. Nutr.* 74 (1), 122–127.
- Monika, L., Heidemarie, A., Claudia, F., Markus, K., Wolfgang, S., and Gerd, K. (2019). Diabetische neuropathie und diabetischer fuß (update 2019). *Wien. Klin. Wochenschr.* 131, 141–150.
- Myint, K. Z., Zhou, Z. Y., Xia, Y. M., Fang, Y., Wu, M. N., Song, Z., et al. (2021). Stevia Polyphenols: A Stable Antioxidant that Presents a Synergistic Effect with Vitamin C. *J. Food Process. Pres.* 45 (4), e15317. doi:10.1111/jfpp.15317
- Naasani, I., Oh-Hashi, F., Oh-Hara, T., Feng, W. Y., Johnston, J., Chan, K., et al. (2003). Blocking Telomerase by Dietary Polyphenols Is a Major Mechanism for Limiting the Growth of Human Cancer Cells *In Vitro* and *In Vivo*. *Cancer Res.* 63, 824–830.
- Orr, W. C., Fass, R., Sundaram, S. S., and Scheimann, A. O. (2020). The Effect of Sleep on Gastrointestinal Functioning in Common Digestive Diseases. *Lancet Gastroenterol. Hepatol.* 5, 616–624. doi:10.1016/s2468-1253(19)30412-1
- Pandey, K. B., and Rizvi, S. I. (2009). Plant Polyphenols as Dietary Antioxidants in Human Health and Disease. *Oxidative Med. Cell Longevity* 2, 270–278. doi:10.4161/oxim.2.5.9498
- Pani, G., Scherm, B., Azara, E., Balmas, V., Jahanshiri, Z., Carta, P., et al. (2014). Natural and Natural-like Phenolic Inhibitors of Type B Trichothecene *In Vitro* Production by the Wheat (*Triticum* sp.) Pathogen fusarium Culmorum. *J. Agric. Food Chem.* 62, 4969–4978. doi:10.1021/jf500647h
- Pei, W., Chen, Z. S., Chan, H. Y. E., Zheng, L., Liang, C., and Huang, C. (2020). Isolation and Identification of a Novel Anti-protein Aggregation Activity of Lignin-Carbohydrate Complex from Chionanthus Retusus Leaves. *Front. Bioeng. Biotechnol.* 8, 573991. doi:10.3389/fbioe.2020.573991
- Porter, L. J. (1992). Structure and Chemical Properties of the Condensed Tannins. *Plant Polyphenols*, 245–258. doi:10.1007/978-1-4615-3476-1_14
- Quideau, S., Deffieux, D., Douat-casassus, C., and Pouységu, L. (2011). Plant Polyphenols: Chemical Properties, Biological Activities, and Synthesis, Biological Activities, and Synthesis. *Angew. Chem. Int. Ed.* 50, 586–621. doi:10.1002/anie.201000044
- Ramadas, D., Kowti, R., Ramesh, B., Nune, S. K., Joshi, V., and District, M. (2020). Antibacterial Effect of Polyphenols Enriched Drumstick Plant Leaves (*Moringa Oleifera*) Extract: A Research Study. *Int. J. Innovative Sci. Res. Tech.* 5, 1281–1283.
- Remington, R., Chan, A., Lepore, A., Kotlya, E., and Shea, T. B. (2010). Apple Juice Improved Behavioral but Not Cognitive Symptoms in Moderate-To-Late Stage Alzheimer's Disease in an Open-Label Pilot Study. *Am. J. Alzheimers Dis. Other Demen.* 25, 367–371. doi:10.1177/1533317510363470
- Ríos-Arrabal, S., Artacho-Cordón, F., León, J., Román-Marinetto, E., del Mar Salinas-Asensio, M., Calvente, I., et al. (2013). Involvement of Free Radicals in Breast Cancer. *SpringerPlus* 2, 404. doi:10.1186/2193-1801-2-404
- Saeed, S., Mosa-Al-Reza, H., Fatemeh, A., and Saeideh, D. (2012). Antihyperglycemic and Antihyperlipidemic Effects of Guar Gum on Streptozotocin-Induced Diabetes in Male Rats. *Phcog Mag.* 8, 65–72. doi:10.4103/0973-1296.93328
- Sajadimajd, S., Bahramsoltani, R., Iranpanah, A., Kumar Patra, J., Das, G., Gouda, S., et al. (2020). Advances on Natural Polyphenols as Anticancer Agents for Skin Cancer. *Pharmacol. Res.* 151, 104584. doi:10.1016/j.phrs.2019.104584
- Salto, R., and Lopez, J. (2016). Apple Polyphenol Extract Improves Insulin Sensitivity *In Vitro* and *In Vivo* in Animal Models of Insulin Resistance. *Nutr. Metab.* 13, 1–10.
- Sharma, P., Montes de Oca, M. K., Alkeswani, A. R., McClees, S. F., Das, T., Elmetts, C. A., et al. (2017). Tea Polyphenols for the Prevention of UVB-Induced Skin Cancer. *Photodermatol. Photoimmunol Photomed.* 34 (1), 50–59. doi:10.1111/pphp.12356
- Si, C.-L., Kim, J.-K., Bae, Y.-S., and Li, S.-M. (2009). Phenolic Compounds in the Leaves of Populus Ussuriensis and Their Antioxidant Activities. *Planta Med.* 75, 1165–1167. doi:10.1055/s-0029-1185476
- Singh, A., Akanksha Singh, N., Maurya, R., and Srivastava, A. K. (2009). Anti-hyperglycaemic, Lipid Lowering and Anti-oxidant Proper- Ties of (6)-gingerol in Db/db Mice. *Int. J. Med. Med. Sci.* 1 (12), 536–544.
- Song, Y., Li, X., Gong, X., Zhao, X., Ma, Z., Xia, T., et al. (2019). Green tea Polyphenols Improve Isoflurane-Induced Cognitive Impairment via Modulating Oxidative Stress. *J. Nutr. Biochem.* 73, 108213. doi:10.1016/j.jnutbio.2019.07.004
- Sugiyama, H., Akazome, Y., Shoji, T., Yamaguchi, A., Yasue, M., Kanda, T., et al. (2007). Oligomeric Procyanidins in Apple Polyphenol Are Main Active Components for Inhibition of Pancreatic Lipase and Triglyceride Absorption. *J. Agric. Food Chem.* 55, 4604–4609. doi:10.1021/jf070569k
- Sun, S., Zhang, M., Umemura, K., and Zhao, Z. (2019). Investigation and Characterization of Synthesis Conditions on Sucrose-Ammonium Dihydrogen Phosphate (SADP) Adhesive: Bond Performance and Chemical Transformation. *Materials* 12, 4078. doi:10.3390/ma12244078
- Sutherland, B. A., Rahman, R. M. A., and Appleton, I. (2006). Mechanisms of Action of green tea Catechins, with a Focus on Ischemia-Induced Neurodegeneration. *J. Nutr. Biochem.* 17 (5), 291–306. doi:10.1016/j.jnutbio.2005.10.005
- Suzuki, T. (2013). Regulation of Intestinal Epithelial Permeability by Tight Junctions. *Cell. Mol. Life Sci.* 70, 631–659. doi:10.1007/s00018-012-1070-x
- Tangney, C. C., and Rasmussen, H. E. (2013). Polyphenols, Inflammation, and Cardiovascular Disease. *Curr. Atheroscler. Rep.* 15, 324. doi:10.1007/s11883-013-0324-x
- Tavares, L., Figueira, I., Mcdougall, G. J., Vieira, H. L. A., Stewart, D., Alves, P. M., et al. (2013). Neuroprotective Effects of Digested Polyphenols from Wild Blackberry Species. *Eur. J. Nutr.* 52, 225–236. doi:10.1007/s00394-012-0307-7
- Vroegrijk, I. O. C. M., van Diepen, J. A., van den Berg, S., Westbroek, I., Keizer, H., Gambelli, L., et al. (2011). Pomegranate Seed Oil, a Rich Source of Punicic Acid, Prevents Diet-Induced Obesity and Insulin Resistance in Mice. *Food Chem. Toxicol.* 49, 1426–1430. doi:10.1016/j.fct.2011.03.037
- Wang, P., Yin, B., Dong, H., Zhang, Y., Zhang, Y., Chen, R., et al. (2020). Coupling biocompatible au nanoclusters and cellulose nanofibrils to prepare the antibacterial nanocomposite films. *Front. Bioeng. Biotechnol.* 8, 986. doi:10.3389/fbioe.2020.00986
- Wang, X., Tang, S., Chai, S., Wang, P., Qin, J., Pei, W., et al. (2021). Preparing Printable Bacterial Cellulose Based Gelatin Gel to Promote *In Vivo* Bone Regeneration. *Carbohydr. Polym.* 270 (15), 118342. doi:10.1016/j.carbpol.2021.118342
- Wang, Z., Li, S., Ge, S., and Lin, S. (2020). Review of Distribution, Extraction Methods, and Health Benefits of Bound Phenolics in Food Plants. *J. Agric. Food Chem.* 68, 3330–3343. doi:10.1021/acs.jafc.9b06574
- Williams, A. R., Krych, L., Fauzan Ahmad, H., Nejsum, P., Skovgaard, K., Nielsen, D. S., et al. (2017). A Polyphenol-Enriched Diet and ascaris Suum Infection Modulate Mucosal Immune Responses and Gut Microbiota Composition in Pigs. *Plos One* 12, e0186546. doi:10.1371/journal.pone.0186546
- Xiong, R., Wang, X.-L., Wu, J.-M., Tang, Y., Qiu, W.-Q., Shen, X., et al. (2020). Polyphenols Isolated from Lychee Seed Inhibit Alzheimer's Disease-Associated Tau through Improving Insulin Resistance via the IRS-1/PI3K/Akt/GSK-3 β Pathway. *J. Ethnopharmacology* 251, 112548. doi:10.1016/j.jep.2020.112548
- Xu, H., Zhang, D., and Li, J. (2019). Antibacterial Nanoparticles with Universal Adhesion Function Based on Dopamine and Eugenol. *J. Bioresour. Bioprod.* 4 (3), 177–182.

- Xu, K. Z.-Y., Zhu, C., Kim, M. S., Yamahara, J., and Li, Y. (2009). Pomegranate Flower Ameliorates Fatty Liver in an Animal Model of Type 2 Diabetes and Obesity. *J. Ethnopharmacology* 123, 280–287. doi:10.1016/j.jep.2009.03.035
- Xu, L., Yang, Y., and Wang, F. (2016). Callus culture of acacia mearnsii de wilde and analysis on proanthocyanidin. *Chem. Ind. For. Prod.* 36, 53–59.
- Yang, B., and Liu, X. (2019). Extraction and Antioxidant Activity of Polyphenols from phyllanthus Emblica. *Food Ind. Sci. Technol.* 40, 151–155.
- Yang, D.-J., Chang, Y.-Y., Hsu, C.-L., Liu, C.-W., Lin, Y.-L., Lin, Y.-H., et al. (2010). Antiobesity and Hypolipidemic Effects of Polyphenol-Rich Longan (Dimocarpus Longans Lour.) Flower Water Extract in Hypercaloric-Dietary Rats. *J. Agric. Food Chem.* 58, 2020–2027. doi:10.1021/jf903355q
- Yang, Y., and Zhang, T. (2019). Antimicrobial Activities of tea Polyphenol on Phytopathogens: A Review. *Molecules* 24, 816. doi:10.3390/molecules24040816
- Yashunsky, D. V., Men'shov, V. M., Tsvetkov, D. E., Tsvetkov, Y. E., Bel'ko, A. A., Vasiyarov, G. G., et al. (2014). Analysis of Content of (-)-secoisolaricresinol and Related Polyphenols in Different Morphological Parts and Anatomical Structures of Larch wood from Siberia. *Russ. Chem. Bull.* 63 (11), 2571–2576. doi:10.1007/s11172-014-0780-7
- Yi, J., Li, S., Wang, C., Cao, N., Qu, H., Cheng, C., et al. (2019). Potential Applications of Polyphenols on Main ncRNAs Regulations as Novel Therapeutic Strategy for Cancer. *Biomed. Pharmacother.* 113, 108703. doi:10.1016/j.biopha.2019.108703
- Yu, P., Zheng, L., Wang, P., Chai, S., Zhang, Y., Shi, T., et al. (2020). Development of a Novel Polysaccharide-Based Iron Oxide Nanoparticle to Prevent Iron Accumulation-Related Osteoporosis by Scavenging Reactive Oxygen Species. *Int. J. Biol. Macromolecules* 165, 1634–1645. doi:10.1016/j.ijbiomac.2020.10.016
- Yu, Z., Zhang, Z., Wang, Z., Wang, G., Wang, G., and Liu, Z. (2014). The Extraction Technology and Antioxidant Activity of Polyphenol from Larch. *Food Sci. Tech.* 39, 207–212. doi:10.1021/acsomega.9b02071
- Yun, J., Wei, L., Li, W., Gong, D., Qin, H., Feng, X., et al. (2021). Isolating High Antimicrobial Ability Lignin from Bamboo Kraft Lignin by Organosolv Fractionation. *Front. Bioeng. Biotech.* 9, 683796. doi:10.3389/fbioe.2021.683796
- Zhang, H., Lai, Q., Li, Y., Liu, Y., and Yang, M. (2016). Learning and Memory Improvement and Neuroprotection of Gardenia Jasminoides (Fructus Gardenia) Extract on Ischemic Brain Injury Rats. *J. Ethnopharmacol.* 196, 225–235. doi:10.1016/j.jep.2016.11.042
- Zhang, L. L., Zhang, L. F., and Xu, J. G. (2020). Chemical Composition, Antibacterial Activity and Action Mechanism of Different Extracts from Hawthorn (Crataegus Pinnatifida Bge.). *Sci. Rep.* 10 (1), 8876–8913. doi:10.1038/s41598-020-65802-7
- Zhang, L., Sun, C., Li, J., and Liu, Y. (2005). Research Status and Development prospect of Plant Polyphenols. *For. Sci.* 41, 157–162.
- Zhang, S., Liu, Y., Zhao, Z., and Xue, Y. (2010). Effects of green tea Polyphenols on Caveolin-1 of Microvessel Fragments in Rats with Cerebral Ischemia. *Neurol. Res.* 32, 963–970. doi:10.1179/016164110x12700393823570
- Zhao, X., Huang, C., Xiao, D., Wang, P., Luo, X., Liu, W., et al. (2021). Melanin-inspired Design: Preparing Sustainable Photothermal Materials from Lignin for Energy Generation. *ACS Appl. Mater. Inter.* 13 (6), 7600–7607. doi:10.1021/acsami.0c21256
- Zhao, X., Sun, P., Li, G., Yi, R., Qian, Y., and Park, K.-Y. (2018). Polyphenols in Kuding tea Help Prevent Hcl/ethanol-Induced Gastric Injury in Mice. *Food Funct.* 9, 1713–1725. doi:10.1039/c7fo01754e
- Zhen, N., and Liu, M. (2018). Research Progress on Neuroprotective Effects of Polyphenols. *South Forum* 49, 30–31.
- Zheng, L., Yu, P., Zhang, Y., Wang, P., Yan, W., Guo, B., et al. (2021). Evaluating the Bio-Application of Biomacromolecule of Lignin-Carbohydrate Complexes (LCC) from Wheat Straw in Bone Metabolism via ROS Scavenging. *Int. J. Biol. Macromolecules* 176, 13–25. doi:10.1016/j.ijbiomac.2021.01.103
- Zhou, Q., Bennett, L. L., and Zhou, S. (2016). Multifaceted Ability of Naturally Occurring Polyphenols against Metastatic Cancer. *Clin. Exp. Pharmacol. Physiol.* 43 (4), 394–409. doi:10.1111/1440-1681.12546
- Zhou, X., Hua, X., Zhou, X., Xu, Y., and Zhang, W. (2019). Continuous Co-production of Biomass and Bio-Oxidized Metabolite (Sorbitol) Using Gluconobacter Oxydans in a High-Oxygen Tension Bioreactor. *Bioresour. Tech.* 277, 221–224. doi:10.1016/j.biortech.2019.01.046

Conflict of Interest: The authors declare that the research was conducted in the absence of any commercial or financial relationships that could be construed as a potential conflict of interest.

Publisher's Note: All claims expressed in this article are solely those of the authors and do not necessarily represent those of their affiliated organizations, or those of the publisher, the editors and the reviewers. Any product that may be evaluated in this article, or claim that may be made by its manufacturer, is not guaranteed or endorsed by the publisher.

Copyright © 2021 Yan, Chen, Hu and Yong. This is an open-access article distributed under the terms of the Creative Commons Attribution License (CC BY). The use, distribution or reproduction in other forums is permitted, provided the original author(s) and the copyright owner(s) are credited and that the original publication in this journal is cited, in accordance with accepted academic practice. No use, distribution or reproduction is permitted which does not comply with these terms.



Prospects and Applications of Biomass-Based Transparent Wood: An Architectural Glass Perspective

Jing Wang* and Jian'gang Zhu*

College of Furnishings and Industrial Design, Nanjing Forestry University, Nanjing, China

OPEN ACCESS

Edited by:

Jia-Long Wen,
Beijing Forestry University, China

Reviewed by:

Yan Xia,
Southwest Forestry University, China
Yi Liu,
Beijing Forestry University, China

*Correspondence:

Jing Wang
WangJing_9711@163.com
Jian'gang Zhu
austin_zhu@njfu.edu.cn

Specialty section:

This article was submitted to
Green and Sustainable Chemistry,
a section of the journal
Frontiers in Chemistry

Received: 26 July 2021

Accepted: 06 October 2021

Published: 20 October 2021

Citation:

Wang J and Zhu J (2021) Prospects
and Applications of Biomass-Based
Transparent Wood: An Architectural
Glass Perspective.
Front. Chem. 9:747385.
doi: 10.3389/fchem.2021.747385

This paper briefly discussed the research progress of biomass-based transparent wood (BBTW), and summarized the key technologies and potential application prospects of BBTW in replacing architectural glass. Based on the introduction of the preparation process of BBTW, the advantages of BBTW and their feasibility to replace architectural glass are illustrated with a view to the requirements and conditions of architectural glass for different use functions. The limitations of BBTW are discussed and the development prospects of BBTW are also prospected. The research shows that BBTW has the advantages of green and renewable materials that can meet the requirements of good lighting conditions, flame retardant, heat insulation and safety, which are in line with the sustainable development trend. Further studies are needed to continuously break through its limitations with an aim to expand the application of this new biomass-based material.

Keywords: biomass materials, transparent materials, transparent wood, green and renewable energy, architectural glass ;

INTRODUCTION

Biomass materials are new materials with excellent performance and high added value that are processed and manufactured by a series of high technology means using woody, grassy and vine plants (Sun and Liu, 2019; Wu et al., 2020; Zhao et al., 2020a; 2020b). Biomass materials are widely available and renewable, with low processing costs. In the current situation of depletion of non-renewable resources, the development and utilization of new materials can effectively alleviate the serious problems of energy tension and environmental pollution if renewable biomass materials are used as the “cornerstone” of new materials instead of traditional petrochemical and mineral-based materials (Liu et al., 2019; Wang et al., 2019; Chen L. et al., 2020).

Therefore, the research of biomass materials has received a lot of attention from scholars at home and abroad in recent years, such as transparent wood, wood sponge, straw plate, etc. Among them, biomass-based transparent wood (BBTW), as an emerging result of biomass materials research, have been widely studied for their light weight, light transmission, environmental protection, and high mechanical strength (Zhou and Wu, 2020). BBTW are mainly prepared renewable natural plant materials as raw materials and modifying their intrinsic structures or compounding them with other materials to achieve their light transmission and other functions.

At present, BBTW are still in the development and exploration stage, and the related research is focused on the preparation, but not yet put into actual production. The current researchs for BBTW are mainly focused on replacing architectural glass, luminescent materials, energy storage, battery substrates and other fields. This paper briefly discussed the research progress of BBTW, and summarizes the key technologies and potential application prospects of BBTW in replacing architectural glass.

TABLE 1 | BBTW prepared by different methods.

Raw material	Delignin method	The transparency method	References
Balsa wood	NaClO ₂	PMMA	Chen et al. (2019)
Basswood	NaClO ₂	Epoxy resin	Mi et al. (2020b)
Basswood	Alkaline H ₂ O ₂	Epoxy resin	Li et al. (2016)
Basswood	NaClO ₂	Mechanical thermal pressure	Zhu et al. (2018)
Balsa wood	Sodium subchlorite + alkaline H ₂ O ₂	Sulcanol – Alene	Hoglund et al. (2020)
Balsa wood	NaClO ₂	PVA	Mi et al. (2020a)
Balsa wood	DES/Alkaline H ₂ O ₂	PAA	Bi et al. (2018)
Balsa wood	PAA	Limonene acrylate	Montanari et al. (2021)

TABLE 2 | Minimum visible light transmittance of colorless transparent flat glass (Wang et al., 2020).

Nominal thickness/mm	Minimum value of visible light transmission ratio/%
2	89
3	88
4	87
5	86
6	85
8	83
10	81
12	79
15	76
19	72
22	69
25	67

PREPARATION OF BBTW AND LIGHT TRANSMISSION PRINCIPLE

The development history of BBTW can be divided into three stages. 1) The first stage is the pre-exploration of the BBTW. In 1998, (Murayama et al., 1998) were the first to report the use of nanocellulose to prepare a translucent paper with high tensile strength. Following this innovation, many domestic and foreign scholars have initiated research on transparent paper. However, the process of preparing transparent paper has limitations such as high energy consumption and time consuming. 2) The second stage is the period of rapid development of BBTW. A new type of transparent wood (TW) was reported by Liangbing Hu's team in 2016. As a result, the preparation of TW gradually became a research hotspot. 3) The third stage is the period of improvement and enhancement of the transparency of TW. In recent years, many scholars have also conducted research on the transparency of TW other than wood and proposed many methods to improve the performance of BBTW.

Natural wood contains lignin and other light-absorbing components, and the porous structure of the wood will scatter visible light, resulting in opacity of the wood, which can not meet the demand for lighting and can not be used as a building glass material. There are two main reasons for the opacity of wood: 1) The wood contains a large amount of light-absorbing substance that is lignin, which accounts for 20–30% of the total weight of wood; 2) The porosity of wood is as high as 30–80%, and a large

number of pores have diameters larger than the wavelength of visible light (380–780 nm), which will cause severe light scattering. Therefore, by removing the lignin in the wood, it is possible to remove the chromogenic substances while retaining the wood skeleton structure. The pore structure in wood mainly includes a microcapillary system (mainly formed by the dynamic connection of tiny pores with a size below 10 nm in the fine running wall) and a large capillary system (mainly composed of conduits and screens). These capillary channels are connected to each other, so a transparent resin with a very high refractive index matching with the cellulose can be injected into it to fill the pores in the wood, thereby achieving transparency.

As shown in **Table 1**, BBTW were prepared by different preparation methods. The preparation of BBTW is divided into two main steps, preparation of delignified biobased templates (DBT) and impregnation of resins with matching refractive indices. The main methods for preparing DBT are acid, alkali, bioenzymatic and lignin modification methods. Sodium hypochlorite solution is usually used as a high frequency reagent for acid delignification. Sodium hypochlorite destroys the aromatic ring structure of lignin by oxidation and chlorination, thus achieving the effect of lignin removal. The most commonly used reagent for alkali delignification is a mixture of sodium hydroxide and sodium sulfite solution. In addition to the common treatment with sodium hydroxide solution, other alkaline solutions have also been used. Biological enzymatic delignification is a green delignification process, which degrades lignin by enzymes in order to achieve the purpose of delignification. By modifying the lignin, the chromophore groups are removed to achieve bleaching. After obtaining DBT, it is necessary to impregnate it with a resin matching its refractive index to obtain BBTW. The commonly used resins are: methyl methacrylate (MMA), epoxy resin, polyvinyl alcohol (PVA), and polyvinyl pyrrolidone (PVP). The choice of resins is not limited to the requirement of a high refractive index match with DBT, but is also increasingly focused on the environmental and physical properties of the resin itself. Current polymers are mainly petroleum-based products. One of the challenges is to replace fossil polymers in the manufacture of sustainable TW. Recently, Montanari et al. (2021) have successfully developed an environmentally friendly alternative: limonene acrylate, a monomer made from limonene. A substance extracted from orange juice is used to make a polymer that restores the strength of the delignification and allows light to pass through, producing BBTW.

TABLE 3 | Fire-resistant properties of fireproof glass (China National Standardization Administration Committee 2009b).

Classification name	Fire resistance limit grade (h)	Fire-resistant performance requirements
Heat-insulating fireproof glass (Class A)	3.00	Fire resistance and heat insulation time \geq 3.00 h , and fire resistance integrity time \geq 3.00 h
	2.00	Fire resistance and heat insulation time \geq 2.00 h , and fire resistance integrity time \geq 2.00 h
	1.50	Fire resistance and heat insulation time \geq 1.50 h , and fire resistance integrity time \geq 1.50 h
	1.00	Fire resistance and heat insulation time \geq 1.00 h , and fire resistance integrity time \geq 1.00 h
	0.50	Fire resistance and heat insulation time \geq 0.50 h , and fire resistance integrity time \geq 0.50 h

TABLE 4 | Technical conditions for insulating glass (Ministry of Industry and Information Technology of the People's Republic of China 2015).

Types	Levels	Technical conditions		
		K(W/m ² ·K)	LSG	GIR
Thermal insulation type BW	BW1	≤ 1.8	≥ 1.0	—
	BW2	≤ 1.5	≥ 1.0	—
	BW3	≤ 1.0	≥ 1.0	—
thermal insulation type GR	GR1	≤ 2.5	≥ 1.0	≤ 0.40
	GR2	≤ 2.2	≥ 1.5	≤ 0.20
	GR3	≤ 2.0	≥ 1.9	≤ 0.05
thermal insulation type BG	BG1	≤ 2.0	≥ 1.0	≤ 0.40
	BG2	≤ 1.8	≥ 1.5	≤ 0.20
	BG3	≤ 1.5	≥ 1.9	≤ 0.05

REQUIREMENTS AND LIMITATIONS OF ARCHITECTURAL GLASS

Requirements for Flat Glass in Architectural Glass

GB116114-2009 (China National Standardization Administration Committee 2010) provides relevant regulations on some properties of flat glass in building glass doors and windows. The standard specifies the minimum value of visible light transmission ratio of flat glass of different nominal thickness in architectural glass. The transmission ratio, also known as transparency, transmittance or transmission coefficient, is the ratio of transmitted luminous flux to incident luminous flux (Wang et al., 2020). As shown in **Table 2**, the minimum value of the visible transmittance ratio is 89% when the nominal thickness of flat glass is 2 mm, and as the nominal thickness increases, the minimum value of visible transmittance ratio is gradually reduced, and the minimum value of visible transmittance ratio should reach 67% when the engineering thickness of flat glass reaches 25 mm.

Requirements for Fireproof Glass in Architectural Glass

GB15763 "Safety Glass for Buildings" (China National Standardization Administration Committee 2009a) contains the following four types of glass: fireproof glass, tempered glass, laminated glass and homogeneous tempered glass. As shown in **Table 3**, the fire resistance performance is specified in GB15763.1-2009 "Fireproof Glass" (China National Standardization Administration Committee 2009b).

And the standard also specifies the impact resistance of single fire glass. Composite fire glass is not destroyed means that the glass after the test to meet one of the following conditions: first, the glass is not broken; second, the glass is broken but the steel ball did not penetrate the specimen (China National Standardization Administration Committee 2009a).

Requirements of Thermal Insulation Glass for Building

JC/T2304-2015 Technical conditions of thermal insulation glass for building (Ministry of Industry and Information Technology of the People's Republic of China 2015) stipulates that there are three types of thermal insulation glass for building, which are thermal insulation type BW, thermal insulation type GR, thermal insulation type BG. As shown in **Table 4**, for the performance of three different types of thermal insulation glass, this standard stipulates its conduction coefficient (K), light to heat ratio (LSG), solar radiation spectrum transmittance ratio (GIR).

Limitations of Architectural Glass

Architectural glass have many advantages, such as high transmittance, strong sense of fashion, good permeability, rich modeling, wide application, etc. However, there are some limitations of glass windows and doors, specifically in the following aspects.

First, they can produce discomfort glare to threaten public safety. Glare is the visual discomfort caused by the extreme contrast of brightness. The human eye can not adapt to this unsuitable brightness distribution, which may give people a sense of nausea and discomfort. In cities, many buildings are decorated with large-format glass windows on their facades, although when the light is strong, the glare from glass windows may be directed to the eyes of surrounding pedestrians and vehicle drivers, causing visual fatigue and even causing traffic accidents.

Second, the high brittleness of glass will make the cracks in glass very easy to expand by the fact of loosen in the crystal structure due to the less dense of crystallization with coarse grains. Therefore, in the handling, installation, and use process of glass, when accidental colliding happens, it is easy to produce fragments, threatening people's safety.

Third, there are drawbacks in the production process of flat glass industry. The SO₂, NO_x emission reduction pressure is still greater, and the energy saving and emission reduction technology needs to be improved (Zhao et al., 2017). As China's flat glass environmental protection facilities put into use for a relatively



FIGURE 1 | Macroscopic observation diagram of TW (Zhu et al., 2016).

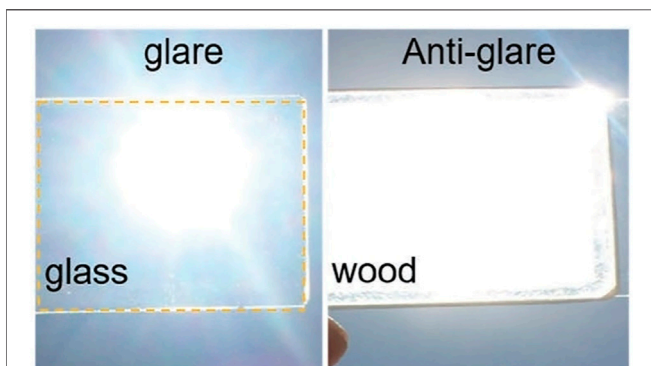


FIGURE 2 | Glare contrast between glass and TW (Li et al., 2016).

short period of time, the periodically “change fire” operation of kiln in the production process always results in unstable concentration of exhaust gas emissions.

ADVANTAGES AND LIMITATIONS OF BBTW AS ALTERNATIVE GLASS MATERIALS

Advantages of BBTW as Alternative Glass Materials

Optical Properties of BBTW Meet the Requirements of Architectural Glass

BBTW should not only meet the basic requirements of glass when used in place of glass for architectural glass, as shown in **Figure 1** (blow), Zhu et al., 2016 prepared 2 mm TW with a transparency of up to 90%, and this study met the requirements of GB116114-2009 on the visible light transmission ratio of flat glass. Therefore, through certain means and techniques, the light transmission ratio of BBTW can reach the requirements of architectural glass.

BBTW also need to compensate on the disadvantages and shortcomings of glass. As shown in **Figure 2** (blow), Li et al., 2016 compared glass and TW against the Sun; glass produces glare due to its extremely uneven brightness, and glare interferes with the

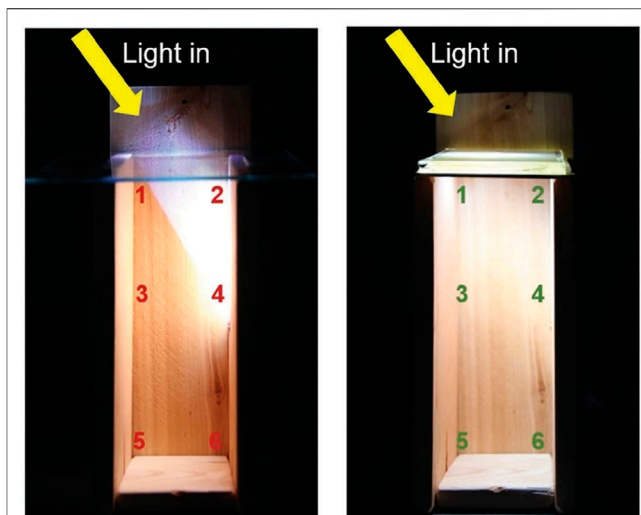


FIGURE 3 | Light contrast between glass and TW (Li et al., 2016).

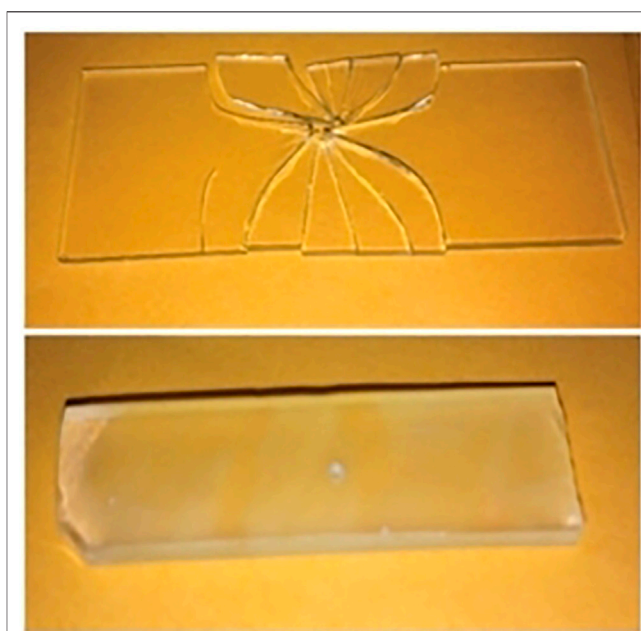


FIGURE 4 | Brittle contrast between glass and TW (Li et al., 2016) (Upper right: glass; Lower right: TW).

clarity of the visual image, while TW has a more uniform and comfortable light due to its uniform texture.

As shown in **Figure 3** (blow), Li et al., 2016 simulated the skylight of a building with glass and TW, and chose six different locations respectively. With glass as the skylight material, the light intensity in the brightest part of the house was 35 times greater than that in the darkest part, and the light was clearly uneven. On the contrary, the difference in light intensity between the brightest and the darkest parts of the house was only 2.3 times when TW was used as the skylight material.

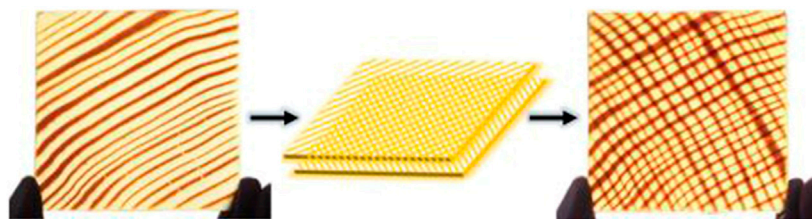


FIGURE 5 | Design of TW (Mi et al., 2020a).

BBTW Is Safer and has Excellent Mechanical Properties

As shown in **Figure 4** (blow), glass immediately shatters into sharp fragments when struck by a falling sharp object. In contrast, even after a sudden impact, TW only bends and splits, rather than shattering into multiple sharp fragments. Therefore, compared to glass materials, BBTW do not have safety hazards caused by shattering. Also, BBTW exhibit excellent mechanical properties. For example, the tensile strength of transparent bamboo (TB) prepared by Wang et al. (2018) reached 92 MPa; the maximum tensile strength of TW prepared by Wu et al. (2019) reached 165.1 ± 1.5 MPa.

Green Production Process

Green process technology is in the key part of the whole process of product life cycle and is the key process to make a green product. In the production process of flat glass, the emission of pollutants and the loss of energy are very huge (Zhao et al., 2019). In contrast, the process of biomass material transparency is free from the emission of toxic and harmful gases. For example, the epoxy resin as impregnating material is free from irritating odor. Recently, Montanari et al. (2021) have successfully developed an environmentally friendly alternative: limonene acrylate, a monomer made from limonene. Besides, the biomass used as raw materials have the advantages of being very widely sourced, green and renewable, which are in line with the trend of sustainable development.

Higher Aesthetic Value

Wood materials not only have practical value but also have high aesthetic value in terms of texture, and the patterns formed by the different arrangement of cell distribution are variable (Yin and Liu, 2020). Compared to glass, most wood materials have a unique texture that is maintained after the transparency treatment, and more types of patterns can be achieved by superimposing two layers of transparent wood. As shown in **Figure 5** (blow), Ruiyu Mi et al. (2020a) designed various lattice patterns by stacking two layers of TW rotated at opposite angles. In addition, using this universal manufacturing method, the BBTW developed from wood with natural texture can increase the aesthetic value of the building.

Good Thermal Insulation Properties

Zhang Y. et al. (2018) compared the radial thermal conductivity of glass, TW, transparent wood fiber (TWF) and unmodified

wood (UW), and the thermal conductivity of glass, TW, TWF and UW were 1.033, 0.164, 0.178 and $0.124 \text{ W m}^{-1} \text{ K}^{-1}$. The thermal conductivity of TWF and TW was significantly lower than that of glass and slightly higher than that of UW. As shown in **Table 5**, the thermal conductivity of the transparent materials prepared from different biomass materials were all significantly lower, which fully satisfied the requirements for thermal conductivity of thermal insulation glass in the above Technical Conditions for Thermal Insulation Glass for Buildings. Wang et al. (2018) found that transparent wood has better thermal insulation performance. Under the condition of an external temperature of 4°C , the indoor temperature of a simulated house using transparent wood dropped from 35°C to 20.1°C . At the same time, the simulation using glass The indoor temperature of the house dropped from 35.1°C to 9.1°C . Applying BBTW to replace architectural glass will help slow down internal temperature fluctuations and reduce energy consumption.

Challenges for BBTW to Replace Architectural Glass

Increasing the Width

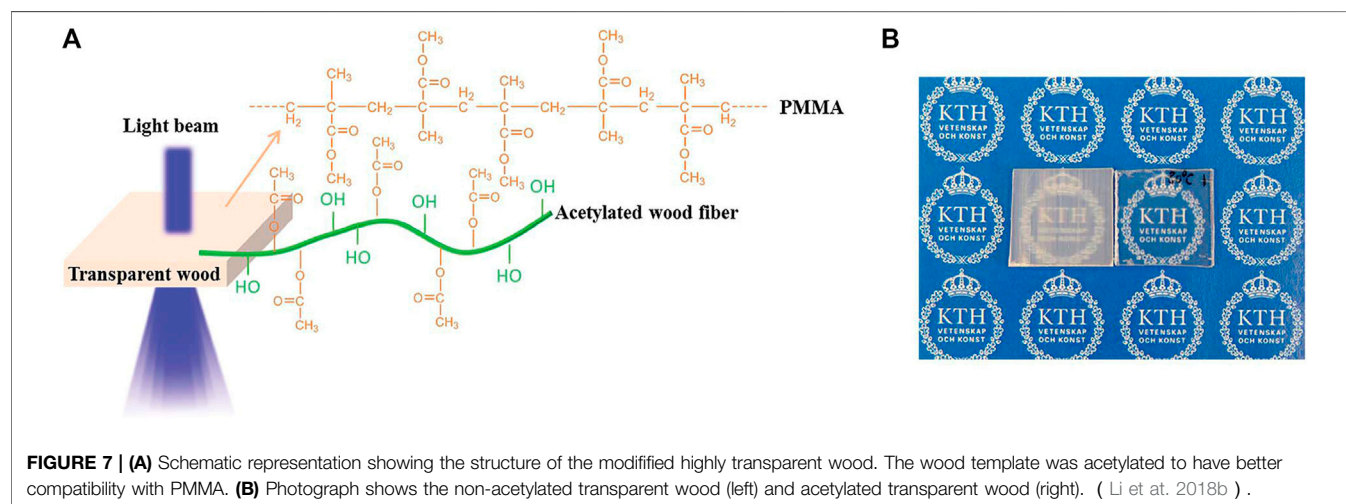
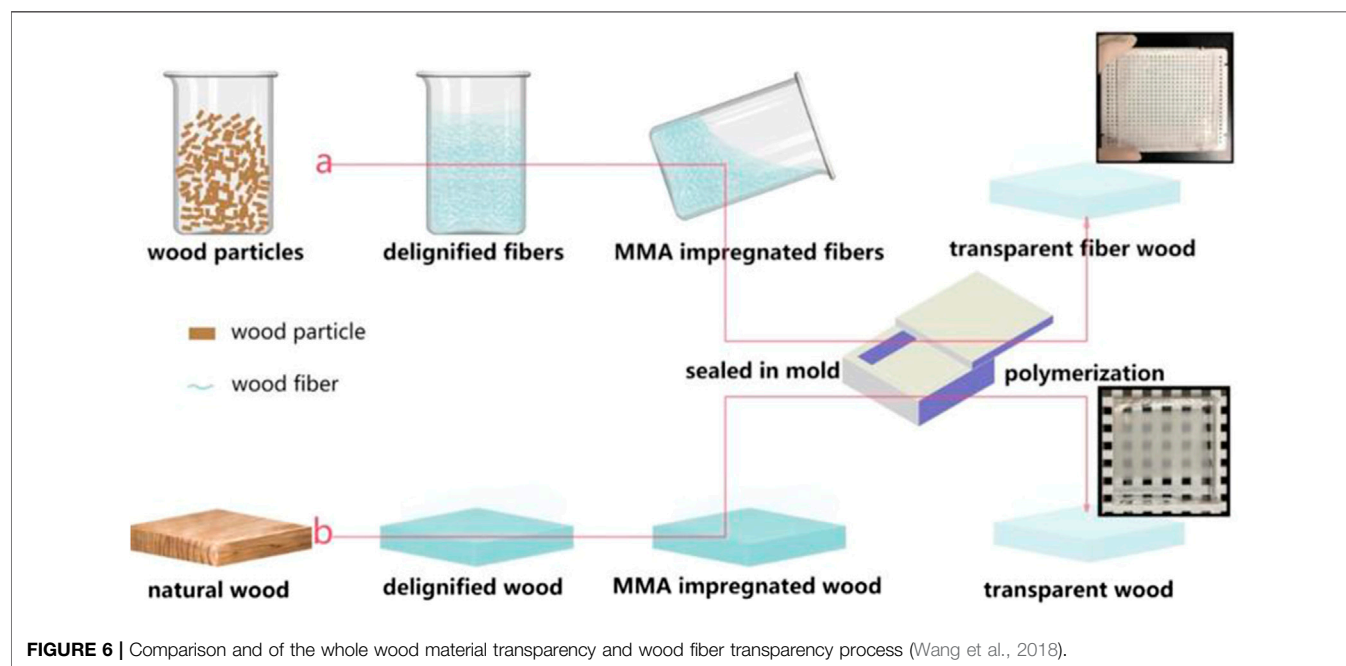
At present, the research on the BBTW is still in the laboratory stage, and the size of the prepared BBTW is limited. If BBTW are to be used in architectural glass, the first thing to consider is to increase the width. Since it takes more time to delignify a large size biomass material (e.g. a whole piece of wood or a whole section of bamboo) and it is difficult to fill it completely with resin when impregnating it, it is inevitably more difficult to prepare a whole biomass material directly for direct transparent processing. The whole biomass material can be processed into fibers and the biomass fibers can be transparently treated, which can reduce the preparation difficulty and at the same time can prepare BBTW of arbitrary size to adapt to the dimensional changes of architectural glass in different scenarios. As could be seen from **Figure 6** (blow), Wang xuan et al. (2018) prepared TW by this method not only with the size of $300 \text{ mm} \times 300 \text{ mm} \times 10 \text{ mm}$ and 68% light transmission, but also with high preparation efficiency, which is suitable for mass production.

Improve Light Transmission

Although the light transmittance of existing BBTW is being improved, there is still a gap between them and the standard of flat glass used in architectural glass. Therefore, it is crucial to

TABLE 5 | Comparison of thermal conductivity of transparent materials prepared from different materials.

Material type	Polymer	Radial thermal conductivity ($\text{W m}^{-1}\text{K}^{-1}$)	References
Basswood	Epoxy resin	0.32	Li et al. (2016)
Douglas-fir	Epoxy resin	0.24	Mi et al. (2020b)
Poplar	PMMA	0.164	Zhang Yaoli et al. (2018)
Balsa	PMMA	0.23	Li et al. (2019)
Pine wood	Epoxy resin	0.2	Zhang et al. (2020)



improve the light transmission of BBTW. The reason why the light transmission of BBTW can not reach the standard of flat glass is due to the debonding phenomenon at the interface of various parts of the composite material, i.e., cracks at the interface

between the polymer and the cell wall of the biomass material, which leads to light scattering or reflection, thus reducing the light transmission of BBTW. This limitation can be improved by acetylation treatment. Li et al. (2018a) prepared high

transmittance BBTW with a thickness of 1.5 mm and 93% light transmission by acetylation treatment of TW (see **Figure 7B** blow). As shown in **Figure 7A**, acetylation treatment is the reaction of introducing acetyl $\text{CH}_3\text{CO}-$ on the nitrogen, oxygen, and carbon atoms in the molecules of organic compounds. The acetylation treatment increases the compatibility of the cell wall of the biomass material with the polymer, thus increasing the light transmission.

Improve Flame Retardancy

Flame retardancy is also a key performance indispensable for architectural glass. Improving the flame retardancy of BBTW can be achieved by adding flame retardant materials for fire protection purposes. For example, polyimide can be added to biomass materials in the process of transparency. Polyimide (PI) is a polymer with imide ring on the main chain, which has the advantages of high thermal stability, excellent mechanical strength, radiation resistance, non-toxicity, and self-extinguishing, etc. Chen et al. (2020b) demonstrated that after adding PI, BBTW maintain good self-extinguishing performance within 2 s after leaving the fire source, the reason is that the thermal decomposition temperature of PI is generally 500°C , and the decomposition products are mainly non-polluting, non-combustible nitrogen-containing gases, which can both dilute the concentration of combustible gases and achieve the pursuit of flame retardancy.

Smart Dimming

If BBTW are used to replace architectural glass, they should not only meet some basic performance requirements, but also conform to the current concept and development trend of smart home. For example, it needs to have the function of adjustable haze, so that it can meet the role of privacy protection in certain scenarios and can be switched for different needs and different scenarios. Qiu et al. (2020) prepared TW with thermally reversible optical properties by infiltrating copolymers of monomer styrene (St), butyl acrylate (BA), and octadecene (ODE) into the treated wood. The introduction of ODE chains leads to TW with repeatable optical properties. With increasing temperature, TW can change repeatedly from lower visibility (transmittance: 23.7%, haze: 8.3%) to transparency (transmittance: 74.9%, haze: 36%), with the opposite change occurring during cooling. This technique promotes the potential application of BBTW as a material for smart windows and doors.

Self-Cleaning Properties

In addition to some basic performance, BBTW can also add some other functions to extend the life cycle of BBTW. For example, self-cleaning function is very important. If architectural glass is to be self-cleaning, it needs to be coated with hydrophobic paint on the surface of the glass. Hydrophobic paint is sprayed on the glass surface, and a durable nano protective film can be formed within a few seconds, which plays a role of self-cleaning and care. The unique nano-structured protective film imitates the super hydrophobic and self-cleaning function of the natural lotus

leaf. The water droplets on the coating surface slide quickly as if falling on the lotus leaf, and the coating surface is kept clean. However, BBTW itself has self-cleaning properties. For example, the transparent luminous wood prepared by Salhah et al. (2021) has superhydrophobic activity, and the water contact angle of the transparent luminous wood is increased from 151.9° to 162.8° , which has extremely superior self-cleaning characteristics.

UV and IR Shielding Performance

Ordinary architectural glass does not have the ability to resist ultraviolet radiation, which will accelerate the aging of human skin. Antimony-doped tin oxide (ATO) particles have excellent ultraviolet and near-infrared shielding properties, and are usually used in shielding glass. Qiu et al. (2019) used modified antimony-doped tin oxide (ATO) Preparation of ATO/transparent wood. When the addition amount of ATO is 0.7% (wt), the UV shielding effect of ATO/transparent wood is as high as 80%. When applied to windows, it can reduce the damage of ultraviolet rays to human skin.

FUTURE PROSPECTS OF BBTW

General Windows and Doors

A well-lit environment can bring more comfortable living experience, while on the contrary, a poorly lit environment can have a negative impact on the human body and mind. Compared with glass, BBTW could meet the conditions of no glare and uniform light exposure, which are important for lighting in houses. BBTW can be used so that artificial lighting can be partially replaced by sunlight to reduce energy (Li et al., 2018b). This initiative is in line with the current concept of green development and sustainability. BBTW are also highly non-toxic and can ensure a more uniform and soft transmission of light, thus protecting interior privacy. However, its application to ordinary windows and doors also needs to be continuously increased and improved light transmission rate, so as to meet the conditions of use of flat glass. Attention should also be paid to the requirement of flame retardancy by adding thermal insulation and fire retardant reagents. The application of BBTW as an alternative to colorless transparent flat glass in architectural glass is promising.

Thermal Insulated Windows and Doors

In addition to ordinary flat glass, BBTW can be used for thermal insulated windows and doors applications. Li et al. (2018a) prepared TW for thermal insulated windows in buildings. Compared to glass windows, transparent wood windows have less temperature change under continuous solar radiation, which contributes to energy saving and environmental protection. The use of transparent cross-laminated wood can be considered to enhance the stability of the structure, but still sufficient thermal resistance (V Karl'a 2019.) Energy-efficient buildings with BBTW as insulated windows and doors consume less energy, which not only significantly reduces electricity consumption, but also promotes natural and comfortable interior lighting.

Intelligent Doors and Windows

With the continuous improvement of people's living standards, the concept of smart home has come into being, and smart windows and doors are an indispensable part of it (Cao et al., 2018). The application of BBTW in smart windows and doors has the following target directions. First, when the ambient temperature of biomass transparent windows and doors is adjusted, the light transmittance and haze of the windows and doors will change accordingly. For example, when reaching a higher temperature, the light transmittance of windows and doors decreases and the haze increases, which can protect the privacy of users, and when the temperature decreases, the light transmittance of windows and doors increases, the haze decreases and the lighting is good. Secondly, BBTW can be used as a smart door and window to protect against ultraviolet rays to protect the indoor environment and protect the skin health of the occupants, and delay skin aging.

Replacement of Glass Curtain Wall

Building glass curtain wall uses a lot of glass materials, a certain extent that can meet the role of beautifying the appearance of the building, but its disadvantages can not be underestimated. Glass curtain wall will not only cause light pollution, but also security risks. Due to the long-term adverse effects of the natural environment, the structure of the glass curtain wall is easy to aging, resulting in the fall of the glass curtain wall. BBTW not only has aesthetic value, but also has unique texture and color. At the same time, the texture of BBTW is even, even if it is impacted, it will not break into sharp pieces. Due to its excellent optical performance, fire and heat insulation performance and high safety factor, BBTW has a broad prospect in replacing building glass curtain wall.

CONCLUSION

Compared with the steel and concrete structures commonly used in modern architecture, house components made of wood

materials can make occupants closer to nature and more relaxed. At the same time, BBTW meet the requirements of good lighting conditions as well as flame retardancy, heat insulation and safety, and have the advantages of very wide material sources, green and renewable, which are in line with the trend of sustainable development. However, due to issues such as process, time, cost and safety, there is still a certain gap between transparent wood and actual large-scale application. Improving the transparency of large-size materials and finding industrialized production methods are the hotspots and difficulties in the current research on transparent wood. Judging from the current research, two problems need to be solved 1) to achieve large-size and high light transmittance biomass-based transparent wood; 2) to find new ideas for preparation, adding more functions, intelligence, composite and other related content, Such as phase change energy storage, electric heating, flame retardant, self-cleaning, smart dimming, decoration, etc. The application of biomass-based transparent wood in architectural glass need gain more experience that would be replicable and scalable in the future with an aim to achieve large-scale and batch production and achieve sustainable development.

AUTHOR CONTRIBUTIONS

WJ and ZJ contributed to conception and design of the study. ZJ organized the frame. WJ wrote the first draft of the manuscript. ZJ wrote sections of the manuscript. All authors contributed to manuscript revision, read, and approved the submitted version.

FUNDING

The authors are grateful the support of the Joint Research program of Sino-foreign Cooperation in Running Schools of Jiangsu Province, China.

REFERENCES

- Bi, Z., Li, T., Su, H., Ni, Y., and Yan, L. (2018). Transparent wood Film Incorporating Carbon Dots as Encapsulating Material for white Light-Emitting Diodes. *ACS Sustainable Chem. Eng.* 6 (7), 9314–9323. doi:10.1021/acssuschemeng.8b01618
- Cao, Y., Mei, J., and Dong, Z. (2018). Intelligent Door and Window System. *Digital Technology Appl.* 36 (8), 821. doi:10.19695/j.cnki.cn12-1369.2018.08.04
- Chen, H., Baitenov, A., Li, Y., Vasileva, E., Popov, S., Sychugov, I., et al. (2019). Thickness Dependence of Optical Transmittance of Transparent Wood: Chemical Modification Effects. *ACS Appl. Mater. Inter.* 11, 35451–35457. doi:10.1021/acsmi.9b11816
- Chen, L., Xu, Z., Wang, F., Duan, G., Xu, W., Zhang, G., et al. (2020a). A Flame-Retardant and Transparent wood/polyimide Composite with Excellent Mechanical Strength. *Composites Commun.* 20, 100355. doi:10.1016/j.coco.2020.05.001
- Chen, Z., Gao, H., Li, W., Li, S., Liu, S., and Li, J. (2020b). Advances in Research on Biomass-Based Photographic Materials. *J. For. Eng.* 5 (3), 1–12. doi:10.13360/j.issn.2096-1359.201906020
- China National Standardization Administration Committee (2010). *GB11614-2009 Code for Flat Glass*. China: China Standard Press. (In Chinese).
- China National Standardization Administration Committee (2009a). *GB15763 Code for Safety Glass for Buildings*. China: China Standard Press. (In Chinese).
- China National Standardization Administration Committee (2009b). *GB15763.1-2009 Code for Flame Resistant Glass*. China: China Standard Press. (In Chinese).
- Höglund, M., Johansson, M., Sychugov, I., and Berglund, L. A. (2020). Transparent Wood Biocomposites by Fast UV-Curing for Reduced Light-Scattering through Wood/Thiol-ene Interface Design. *ACS Appl. Mater. Inter.* 12 (41), 46914–46922. doi:10.1021/acsmi.0c12505
- Karl'a, V. (2019). Update on Research on Transparent wood. *IOP Conf. Ser. Mater. Sci. Eng.* 566, 012015. doi:10.1088/1757-899X/566/1/012015
- Li, T., Zhu, M., Yang, Z., Song, J., Dai, J., Yao, Y., et al. (2016). Wood Composite as an Energy Efficient Building Material: Guided Sunlight Transmittance and Effective thermal Insulation. *Adv. Energ. Mater.* 6 (22), 1601122. doi:10.1002/aenm.201601122
- Li, Y., Cheng, M., Jungstedt, E., Xu, B., Sun, L., and Berglund, L. (2019). Optically Transparent wood Substrate for Perovskite Solar Cells. *ACS Sustainable Chem. Eng.* 7 (6), 6061–6067. doi:10.1021/acssuschemeng.8b06248
- Li, Y., Vasileva, E., Sychugov, I., Popov, S., and Berglund, L. (2018a). Optically Transparent wood: Recent Progress, Opportunities, and Challenges. *Adv. Opt. Mater.* 6 (14), 1800059. doi:10.1002/adom.201800059
- Li, Y., Yang, X., Fu, Q., Rojas, R., Yan, M., and Berglund, L. (2018b). Towards Centimeter Thick Transparent wood through Interface Manipulation. *J. Mater. Chem. A* 6 (3), 1094–1101. doi:10.1039/c7ta09973h

- Liu, Y., Wu, Z., and Xu, W. (2019). Application of Life Cycle Evaluation in Furniture Industry. *World For. Res.* 2, 56–60. doi:10.13348/j.cnki.sjlyyj.2019.0016.y
- Mi, R., Chen, C., Keplinger, T., Pei, Y., He, S., Liu, D., et al. (2020a). Scalable Aesthetic Transparent wood for Energy Efficient Buildings. *Nat. Commun.* 11 (1), 3836. doi:10.1038/s41467-020-17513-w
- Mi, R., Li, T., Dalgo, D., Chen, C., Kuang, Y., He, S., et al. (2020b). A clear, strong, and Thermally Insulated Transparent wood for Energy Efficient Windows. *Adv. Funct. Mater.* 30 (1), 1907511. doi:10.1002/adfm.201907511
- Ministry of Industry and Information Technology of the People's Republic of China (2015). *JC/T2304-2015 Code for Technical Conditions for Building Thermal Insulation Glass*. China: China Building Materials Industry Press. (In Chinese).
- Montanari, C., Ogawa, Y., Olsen, P., and Berglund, L. A. (2021). High Performance, Fully Bio-Based, and Optically Transparent Wood Biocomposites. *Adv. Sci.* 8 (12), 2100559. doi:10.1002/ADVS.202100559
- Murayama, T., Taniguchi, Y., and Iwasawa, K. (1998). High-Ionization Nuclear Emission-Line Region in the Seyfert Galaxy Tololo 0109–383. *Astronomical J.* 115, 460–471. doi:10.1086/300218
- Qiu, Z., Wang, S., Wang, Y., Li, J., Xiao, Z., Wang, H., et al. (2020). Transparent wood with Thermo-Reversible Optical Properties Based on Phase-Change Material. *Composites Sci. Technology* 200, 108407. doi:10.1016/j.compscitech.2020.108407
- Qiu, Z., Xiao, Z., Gao, L., Li, J., Wang, H., Wang, Y., et al. (2019). Transparent wood Bearing a Shielding Effect to Infrared Heat and Ultraviolet via Incorporation of Modified Antimony-Doped Tin Oxide Nanoparticles. *Composites Sci. Technology* 172, 43–48. doi:10.1016/j.compscitech.2019.01.005
- Sun, M., and Liu, Y. (2019). Ecological Design Based on Life Cycle of Furniture Products. *Study Furniture and Interior Decoration* 6, 74–76. doi:10.16771/j.cn43-1247/ts.2019.06.019
- Wang, G., Zhu, J., Hou, H., and Li, X. (2019). A Case Study on the Implementation of green Manufacturing Technology System in Furniture Enterprises (Part II). *Furniture* 6, 85–90. doi:10.16610/j.cnki.jiaju.2019.06.018
- Wang, X., Zhan, T., Liu, Y., Shi, J., Pan, B., Zhang, Y., et al. (2018). Large-Size Transparent Wood for Energy-Saving Building Applications. *ChemSusChem* 11 (23), 4086–4093. doi:10.1002/cssc.201801826
- Wang, Y., Wu, Y., Zhou, J., Huang, Q., Lian, X., and Li, J. (2020). Preparation and Properties of Two Transparent wood. *Study J. Southwest For. Univ.* 5, 151–158. doi:10.11929/j.swfu.201910040
- Wu, Y., Wang, Y., Yang, F., Wang, J., and Wang, X. (2020). Study on the Properties of Transparent Bamboo Prepared by Epoxy Resin Impregnation. *Polymers* 12 (4), 863. doi:10.3390/polym12040863
- Wu, Y., Wu, J., Yang, F., Tang, C., and Huang, Q. (2019). Effect of H₂O₂ Bleaching Treatment on the Properties of Finished Transparent Wood. *Polymers* 11 (5), 776. doi:10.3390/polym11050776
- Yin, Q., and Liu, H. (2020). Application of wood Material in Automobile interior. *Study For. Machinery Woodworking Equipment* 11, 51–53. doi:10.13279/j.cnki.fmwe.2020.0134
- Zhang, L., Wang, A., Zhu, T., Chen, Z., Wu, Y., and Gao, Y. (2020). Transparent wood Composites Fabricated by Impregnation of Epoxy Resin and W-Doped VO₂ Nanoparticles for Application in Energy-Saving Windows. *ACS Appl. Mater. Inter.* 12 (31), 34777–34783. doi:10.1021/acsami.0c06494
- Zhao, P., Li, F., Zhang, N., and Li, K. (2019). Investigation and Analysis on Safety Production Status of Flat Glass Industry. *Sci. Technology Wind* 11, 143. doi:10.19392/j.cnki.1671-7341.201911121
- Zhao, W., Ni, S., Wang, H., and Feng, H. (2017). Problems and Countermeasures of Air Pollution Prevention and Control in Flat Glass Industry. *J. China Inst. Environ. Management* 5, 78–81. doi:10.13358/j.issn.1008-813x.2017.05.20
- Zhao, Z., Huang, C., Wu, D., Chen, Z., Zhu, N., Gui, C., et al. (2020a). Utilization of Enzymatic Hydrolysate from Corn stover as a Precursor to Synthesize an Eco-Friendly Plywood Adhesive. *Ind. Crops Prod.* 152, 112501. doi:10.1016/j.indcrop.2020.112501
- Zhao, Z., Wu, D., Huang, C., Zhang, M., Umemura, K., and Yong, Q. (2020b). Utilization of Enzymatic Hydrolysate from Corn stover as a Precursor to Synthesize an Eco-Friendly Adhesive for Plywood II: Investigation of Appropriate Manufacturing Conditions, Curing Behavior, and Adhesion Mechanism. *J. Wood Sci.* 66 (1), 85. doi:10.1186/s10086-020-01933-9
- Zhou, J., and Wu, Y. (2020). Advances in Preparation Technology and Application of Transparent wood. *For. Product. Industry* 10, 17–22. doi:10.19531/j.issn1001-5299.202010004
- Zhu, M., Jia, C., Wang, Y., Fang, Z., Dai, J., Xu, L., et al. (2018). Isotropic Paper Directly from Anisotropic wood: Top-Down green Transparent Substrate toward Biodegradable Electronics. *ACS Appl. Mater. Inter.* 10 (34), 28566–28571. doi:10.1021/acsami.8b08055
- Zhu, M., Song, J., Li, T., Gong, A., Wang, Y., Dai, J., et al. (2016). Highly Anisotropic, Highly Transparent wood Composites. *Adv. Mater.* 28 (26), 5181–5187. doi:10.1002/adma.201600427

Conflict of Interest: The authors declare that the research was conducted in the absence of any commercial or financial relationships that could be construed as a potential conflict of interest.

Publisher's Note: All claims expressed in this article are solely those of the authors and do not necessarily represent those of their affiliated organizations, or those of the publisher, the editors and the reviewers. Any product that may be evaluated in this article, or claim that may be made by its manufacturer, is not guaranteed or endorsed by the publisher.

Copyright © 2021 Wang and Zhu. This is an open-access article distributed under the terms of the Creative Commons Attribution License (CC BY). The use, distribution or reproduction in other forums is permitted, provided the original author(s) and the copyright owner(s) are credited and that the original publication in this journal is cited, in accordance with accepted academic practice. No use, distribution or reproduction is permitted which does not comply with these terms.



Preparation and Application in Water Treatment of Magnetic Biochar

Qingshuang Zhao^{1†}, Ting Xu^{1,2*†}, Xueping Song², Shuangxi Nie², Sun-Eun Choi^{3*} and Chuanling Si^{1,2*}

¹Tianjin Key Laboratory of Pulp and Paper, Tianjin University of Science and Technology, Tianjin, China, ²Guangxi Key Laboratory of Clean Pulp and Papermaking and Pollution Control, College of Light Industry and Food Engineering, Guangxi University, Nanning, China, ³Department of Forest Biomaterials Engineering, College of Forest and Environmental Sciences, Kangwon National University, Chuncheon, South Korea

OPEN ACCESS

Edited by:

Caoxing Huang,
Nanjing Forestry University, China

Reviewed by:

Shiyan Han,
Northeast Forestry University, China
Dong Lv,
City University of Hong Kong, Hong
Kong, SAR China

*Correspondence:

Ting Xu
xuting@tust.edu.cn
Sun-Eun Choi
oregonin@kangwon.ac.kr
Chuanling Si
sichli@tust.edu.cn

[†]These authors have contributed
equally to this work and share first
authorship

Specialty section:

This article was submitted to
Bioprocess Engineering,
a section of the journal
Frontiers in Bioengineering and
Biotechnology

Received: 02 September 2021

Accepted: 07 October 2021

Published: 25 October 2021

Citation:

Zhao Q, Xu T, Song X, Nie S,
Choi S-E and Si C (2021) Preparation
and Application in Water Treatment of
Magnetic Biochar.
Front. Bioeng. Biotechnol. 9:769667.
doi: 10.3389/fbioe.2021.769667

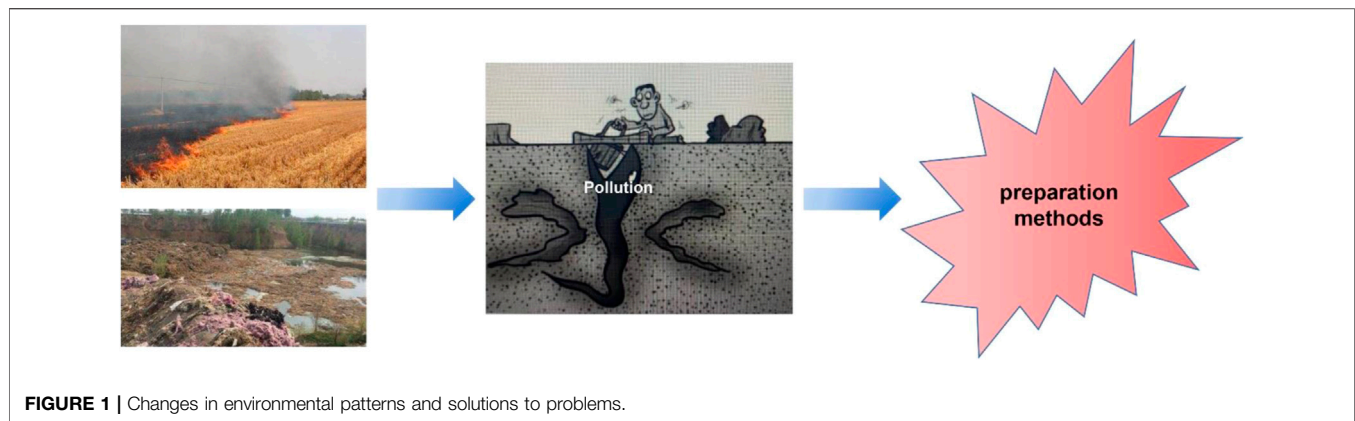
This paper reviews the preparation of magnetic biochar and its application in wastewater treatment, and briefly discusses the adsorption mechanism of biochar to remove pollutants and the modification methods of biochar. Due to the good physical and chemical properties of biochar, including its rough porous structure, it has been widely used to absorb pollutants from water. Magnetic biochar is commonly prepared by combining biochar with magnetic material. The biochar is endowed with the characteristics of the magnetic material, which could effectively solve the problems of difficult recovery and easy loss of adsorbent in water treatment. Magnetic biochar with high carbon content, large specific surface area, magnetic separation, and other excellent properties, has become a hot research topic in recent years. The preparation methods and application properties of magnetic biochar are reviewed. The future research directions of magnetic biochar are put forward to provide directions for further research and application of magnetic biochar materials.

Keywords: magnetic biochar, water treatment, adsorption, magnetic response, adsorption mechanism

INTRODUCTION

In this era of rapid development of the industry, people's needs are constantly increasing to ensure the conditions of cost control to improve the profits of the industry (Yan et al., 2021; Pei et al., 2020a; Dai et al., 2020; Li X. et al., 2019; Si et al., 2009; Yang et al., 2019; Chen et al., 2020a; Liu et al., 2020a). Agricultural waste has received extensive attention due to its wide application and availability (Si et al., 2013; Dai L. et al., 2019; Du et al., 2019; Pei et al., 2020b; Liu et al., 2021c; Liu. et al., 2021e; Ma et al., 2021; Zhang et al., 2021). In these respects, some countries, such as Malaysia, dominated by the department of agriculture, support a most economic turnaround with annual production of more than two million tons of agricultural waste (Yang et al., 2020; Liu et al., 2019; Wang et al., 2019). However, this production is commonly conducted in the open-air, leading to waste being incinerated or dumped in landfill, which can lead to serious environmental problems, such as groundwater pollution or air pollution (Si et al., 2008; Liu et al., 2020b). Materials such as empty fruit bunches, rice husks, and coconut shells were found to be some of the most abundantly available agricultural wastes which contain high amounts of minerals such as silica, magnesium, and potassium along with a high porosity (Laine and Calafat, 1989; Mubarak et al., 2014; Vadivelan et al., 2005; Mubarak et al., 2016; Chen et al., 2020b; Ma et al., 2020; Du et al., 2021).

These agricultural and forestry wastes can be formed into biochar through a common pyrolysis process (Xu, R. et al. 2020b; Cheng, et al. 2020). For example, enhancing the soil fertility for a higher



crop production by increasing the fertilizer's retention time (Liang et al., 2006; Chan et al., 2008), as a dopant to increase the capacitance value of a supercapacitor (Gupta et al., 2015), and as an adsorbent in the removal of various wastewater's contaminants such as lead (Liu and Zhang, 2009), zinc (Chen B. et al., 2011), and natural organic matter (Uchimiya et al., 2010). If the biochar is separated in an aqueous solution, it must be centrifugated (Mukherjee et al., 2011) or activated with a strong base before the biochar can be used in a supercapacitor (Goda et al., 2014; Das et al., 2015). The development of magnetic biochar has overcome this problem, and has been applied in various fields by attaching various metal ions to the surface of biochar to make it magnetic. Magnetic biochar is prepared in the laboratory using conventional heating in an electrical furnace (Zhang et al., 2007; Theydan and Ahmed, 2012; Wang H. et al., 2020), microwave heating in a modified furnace or oven (Wang et al., 2013; Mubarak et al., 2014; Ruthiraan et al., 2015), co-precipitation (Saravanan et al., 2012; Jiang et al., 2015; Yu et al., 2013), and calcination (Gao et al., 2015; Ma et al., 2015). These magnetic biochars adsorb waste water effectively, removing pollutants, such as cadmium (Reddy and Lee, 2014; Mohan et al., 2014), arsenic (Akin et al., 2012; Gao et al., 2015), lead (Wang et al., 2015a; Wang et al., 2015b; Wang et al., 2015), methylene blue (Theydan and Ahmed, 2012; Zhang and Gao, 2013; Mubarak et al., 2014), and phosphate (Chen X. et al., 2011). Besides that, certain selected magnetic biochars showed the excellent capability to be used as electrodes for supercapacitors to increase the capacitance and electrical conductivity value as well (Li and Liu, 2014; Liu et al., 2021a; Xu T. et al., 2021; Du et al., 2022).

This article mainly introduces the preparation method of magnetic biochar and its application in water treatment as well as its wide application in other areas. As shown in **Figure 1**, people throw away rubbish at will, which causes serious environmental pollution (Lin et al., 2020; Liu et al., 2021b). Water resources have also been severely damaged, but the preparation of magnetic biochar can absorb pollutants in the water. Researchers preparing magnetic biochar need to pay attention to its shortcomings, correction methods, and so on. The preparation of biochar by combining magnetic materials

with biochar has become a hot topic for scientists. According to these conditions, the research targets for the future development of magnetic biochar are determined.

PREPARATION METHODS OF MAGNETIC BIOCHAR

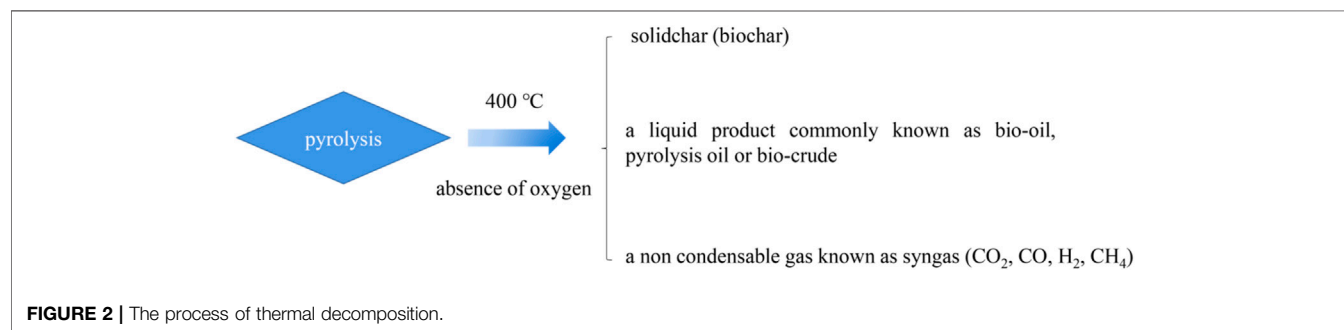
Pyrolysis

In general, pyrolysis refers to the thermal decomposition of organic matter in the absence of oxygen at temperatures over 400°C (Maschio et al., 1992; Thines et al., 2017). Three substances are produced, which consist of a residual solid biochar, a liquid product commonly known as bio-oil, pyrolysis oil, or biocrude, and a non-condensable gas known as syngas, which consists of carbon monoxide (CO), carbon dioxide (CO₂), hydrogen (H₂), and methane (CH₄). The pyrolysis process is generally divided into two stages. In the first stage, heat is transferred to the surface of ions by radiation, from the surface to the interior. During the main pyrolysis and preheating solution, the volatiles and syngas flow through the particles in the void due to the loss of biomass water due to the increase of temperature. The process of heat transfer is a function of time. The second stage of the pyrolysis process begins with the expansion of the solid voids and the conversion of biomass into gas (Blasi, 2008). The expansion of pores provides a site for volatile gases produced during the pyrolysis process. There are three main mechanisms for heat transfer, conduction inside the biomass particle, convection inside the pores of the biomass particle, and the convection and radiation from the surface of the final product.

Accordingly the different operations can be divided into three types: conventional pyrolysis, fast pyrolysis, and flash pyrolysis, as shown in **Table 1**. The heating rate of traditional pyrolysis is relatively slow which allows for the production of solid, liquid, and gaseous products in compelling portions (Goyal et al., 2008). Traditional pyrolysis can be divided into intermittent pyrolysis and continuous pyrolysis. In the latter stage, few internal repeats occur, such as the breaking of bonds, the appearance of free radicals, the elimination of water, and the formation of hydrogen peroxide (Shafizadeh et al., 1982). The main pyrolysis mainly takes place in the second stage of the high-rate decomposition of

TABLE 1 | Operating conditions for different types of pyrolysis processes.

Parameters	Fast pyrolysis	Flash pyrolysis	Conventional pyrolysis
Particle size (mm)	Less than 1	Less than 0.2	5–50
Residence time(s)	0.5–1.0	Less than 0.5	450–550
Heating rate (K/s)	10–200	Less than 1000	0.1–1.0



biomass. The third stage is the slow decomposition of the carbon to form a carbon-rich residue known as biochar. The overall yield of conventional pyrolysis would be approximately 35% biochar, 30% bio-oil, and 35% syngas by mass (Laird et al., 2009). Bio-oil mainly exists in the state of steam and aerosol, and cannot be separated from syngas. If this gas is discharged into the environment, it will cause serious environmental pollution. In contrast, when production is mainly concentrated on liquid or gas products, rapid pyrolysis is chosen (Liu et al., 2021d; Liu W. et al., 2021). In the process of rapid pyrolysis, high operating temperature, short contact time, fine particles, and other operating conditions are required if rapid heating is desired (Babu, 2008). The overall yield of fast pyrolysis would be approximately 50–70% bio-oil, 10–30% biochar, and 15–20% syngas by mass (Babu, 2008). Raw materials need to be dried and ground to a size less than 2 mm before entering the main system of the pyrolysis reactor. However, the temperature of rapid pyrolysis increases rapidly and the particles are sparse. So rapid pyrolysis to produce gaseous products is a good choice (Demirbas et al., 2002). The overall yield of flash pyrolysis would be approximately 60% biochar and 40% volatiles by mass. This process consists of a gasifier which allows a small, limited amount of oxygen to enter the reaction chamber which causes partial combustion of biomass, producing 5–15% char and traces of bio-oil which are referred to as “tar” (Laird et al., 2009). As for laboratory scale, the pyrolysis process is generally done either through conventional heating or microwave heating. The product decomposition diagram is shown in **Figure 2**.

Co-Precipitation

Co-precipitation is the process by which a solute is separated from a solution by means of a carrier, by which the solute is bonded to the solute rather than dissolved in the solution. The solute is called an impurity. This kind of co-precipitation is used in purifying solution and industrial wastewater (Xu R. et al.,

2021). A solute can be co-precipitated out from a solution through three common methods such as inclusion, occlusion, and surface adsorption (Kolthoff, 1932). Inclusion or also known as the formation of mixed crystals is a process which consists of the incorporation of solute in the crystal lattice of the carrier through a hole in which the regular structure of the carrier remains unchanged. This combination forms a mixed crystal in which the amount depends on the adsorption phenomena during the precipitation process.

Apart from that, during the occlusion process, the solute remains incorporated into the crystal lattice of the carrier, instead of the carrier being completely surrounded by the solute during the formation of the crystal matrix, entrapping the solute from returning to the solution. The surface adsorption process on the other describes how the solute is attached to the surface of the carrier and moves out from the solution only when the crystal matrix forms a large surface area and behaves like a flocculated colloid (Wang P. et al., 2020). In general, the precipitation process is a phenomenon that occurs when a substance reaches a certain saturation, followed by the slow growth of the nucleus as the solute diffuses to the surface of the crystal (Sugimoto, 2003). In addition, some organic ions or polymer surface complexing agents can be added to control the size of the magnetic material (Cai and Wan, 2007). Due to the simplicity of the co-precipitation process and the wide range of operating parameters, the required particle size and characteristics can be obtained for the production of magnetic biochar. Massart et al. (Massart, 1981) were first to perform a controlled preparation of superparamagnetic iron oxide particles utilizing the alkaline precipitation of FeCl₃ and FeCl₂ which managed to produce spherical magnetite particles with a diameter in the nanometer scale. In addition, another study by Babes et al. (Babes et al., 1999) showed that if the ratio of Fe²⁺ to Fe³⁺ increased, the particle size of the magnetic biochar increased, but the yield of magnetic biochar decreased (Wang et al., 2021).

The extensive growth of this simple yet significant method which controls the particle size of magnetic particles being produced provided space for researchers to perform studies on the production of magnetic biochar based on various biomasses. In this regard, Saravanan et al. (Saravanan et al., 2012) discovered diamond glue, took out a little biological sample, and co-precipitated the ammonia solution (2:1) with Fe^{2+} and Fe^{3+} to produce magnetic iron oxide particles. This magnetic material had good thermal stability compared with the star polymer containing iron oxide particles. Similarly, Mohan et al. (Mohan et al., 2011) prepared magnetic biochar from almond shells by chemical precipitation (FeCl_3 and FeSO_4). The magnetic biochar had a spongy porous structure and the non-magnetic biochar had a porous shape. These remarkable characteristics provide a good source of magnetic biochar with good adsorption properties.

Reductive Co-Deposition

The reduction co-precipitation process is similar to the co-precipitation process, but the difference is that the transition metal is reduced by a reducing agent such as sodium borohydride or potassium borohydride in the process of binding to the biochar (Wang P. et al., 2020). When the reaction is terminated, the supernatant is removed and the residue is cleaned and dried in a true empty tank to achieve the magnetic biochar. Interestingly, this material is composed of nanoparticles and most of the zero-valent metals, making the magnetic biochar produced highly reductive, and also highly effective at contaminant removal. For example, Zhu et al. (Zhu S. et al., 2018) found that the Cr adsorption capacity of reduced co-precipitated magnetic biochar was 58.82 mg/g, and that most of the Cr (VI) was reduced to Cr (III). Therefore, this method can synthesize magnetic biochar with a better effect and stronger ability to remove pollutants. However, the used reducing agent is harmful and will produce hydrogen during the reduction process, which will pose a certain risk to safety when used on a large scale.

Hydrothermal Carbonization

Hydrothermal carbonization refers to the heterogeneous reaction of biomass and metal ions, because the reaction temperature (100–300°C) is relatively low, the reaction pressure is generated by the reaction itself (An et al., 2019). These conditions are milder than the previous conditions, there is no need to add bases or strong reductants, making the reaction easier. For example, Zhang et al. (Ngarmkam et al., 2011; Bastami and Entezari, 2012) successfully synthesized magnetic biochar by this hydrothermal method from iron-containing sludge and sludge at 473°C, and used the resulting product as a Fenton-like catalyst to completely degrade methylene blue. Similarly, Nethaji et al. (Nethaji et al., 2013) found that magnetic biochar synthesized using this method had a maximum adsorption capacity for Cr (VI) of up to 142.86 mg/g, which was greater than that of most magnetic biochar prepared by co-precipitation (Baig et al., 2014), reductive co-deposition (Devi and Saroha, 2014), or impregnation pyrolysis (Quan et al., 2014).

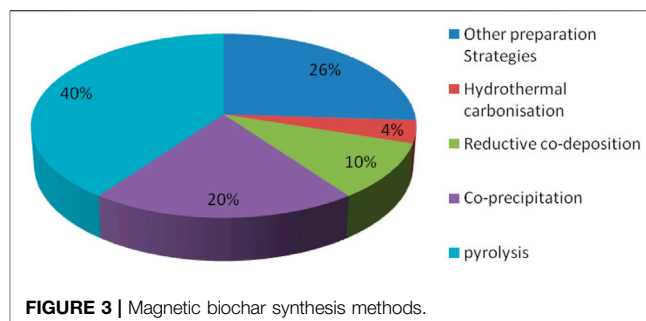


FIGURE 3 | Magnetic biochar synthesis methods.

Other Preparation Strategies

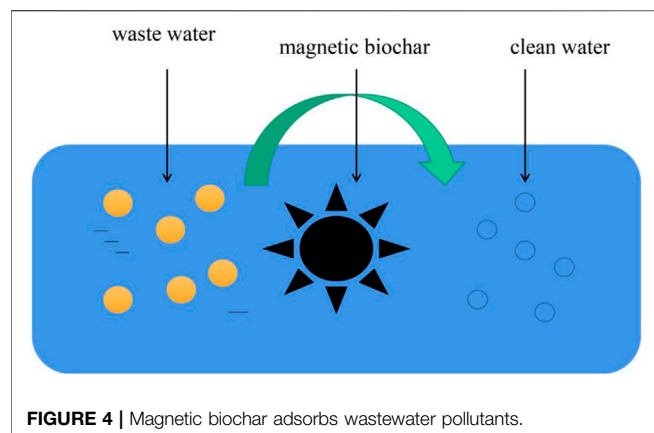
Recently, other methods for preparing magnetic biochar have also been developed, such as ball milling, in which biochar is mechanically mixed with iron oxides in a solvo-free manner (Shang et al., 2016), direct pyrolysis of biomass/metal salts, and cross-linking of biochar and iron oxides (Mojiri et al., 2019). For example, Shang et al. (Shang et al., 2019) found that the adsorption capacities of magnetic biochar synthesized by ball-milling of biochar and iron oxide for the pharmaceuticals carbamazepine (CBZ) and tetracycline were 62.7 mg/g and 94.2 mg/g, respectively. In addition, Dai et al. (Dai S.-j. et al., 2019) demonstrated that the herbicides dichlorophenol and atrazine were very efficiently removed by magnetic biochar synthesized by the molten salt method.

To improve magnetic biochar's ability to heal in the environment more quickly, the researchers treated it with metal or acid or alkali solutions, and also reacted it with different chemical functional groups, in order to improve adsorption selectivity and capacity. A graphical summary of these various methods for the synthesis of magnetic biochar is shown in Figure 3.

Hydrothermal carbonization, reductive co-deposition, co-precipitation, pyrolysis, and other synthetic methods are also used to obtain magnetic biochar. Therefore, the nature of the raw material, the physicochemical properties of the pollutants, and the method operability should be carefully considered when selecting a synthetic approach for magnetic biochar.

APPLICATION OF MAGNETIC BIOCHAR

Magnetic biochar has the potential to be used in purifying the environment, specifically it can be used as an adsorbent, catalyst, soil remediation agent, etc. The need for clean water is a necessity in every part of the world. The main cause of water pollution may be untreated discharge of heavy metals into nearby water sources by mining, batteries, metal plating, or hazardous wastewater such as organic matter and dyes from the textile industry (Li et al., 2020). Therefore, in order to provide clean water for users, a variety of wastewater treatment technologies are chosen such as ion exchange, membrane filtration, biological treatment, and adsorption to solve this problem.



Adsorbent

Adsorption of Heavy Metals

Heavy metals in the environment also have different states. According to the characteristics of these states, heavy metals are classified as anion or cation type. The adsorption capacity of magnetic biochar for chromium is between 8.35 mg/g to 220 mg/g, which proved that the adsorption performance of magnetic biochar was greatly affected by raw materials (Ifthikar et al., 2017). The mechanism by which Cr (VI) is removed by magnetic biochar involves electrostatic adsorption, reduction, ion exchange, complexation with functional groups, and co-precipitation. The adsorption capacity of magnetic biochar is different with the difference of valence, being 1.305–45.8 mg/g and 1.630–10.07 mg/g. For the removal of As, the adsorption mechanism of magnetic biochar is mainly electrostatic adsorption and functional group complexation, among which iron oxide plays a key role (Lu et al., 2004).

The cationic heavy metal pollutants removed by magnetic biochar are mainly Cd (II), Pb (II), Cu (II), Ni (II), Sb (II), Sn (II), and Hg (II), and the efficiency of their removal is influenced by their different physical and chemical properties (Sozeri et al., 2013). The removal mechanism of metal cations by magnetic biochar is as follows: 1) electrostatic adsorption; 2) ion exchange; 3) surface complexation; 4) π - π interaction; 5) internal spherical complexation; 6) hydrogen bonding; and 7) co-deposition. Magnetic biochar is also used for the removal of multiple heavy metals. In systems polluted with multiple heavy metal species, the various heavy metals compete for adsorption sites, which affects the overall adsorption behavior of the magnetic biochar.

Adsorption of Nuclear Waste Pollutants

In recent years, magnetic biochar has become more widely used to remove pollutants from nuclear waste U (VI) and Eu (III) (Hu et al., 2018). For example, Zhu et al. (Zhu Y. et al., 2018) found that the maximum adsorption capacity of magnetic biochar to Eu was 105.53 mg/g, and concluded that the mechanism of magnetic biochar's removal of pollutants was surface and inner sphere complexation. At the same time, Li M. et al.'s (Li M. et al., 2019) research results showed that the maximum adsorption capacity of magnetic biochar for U is 52.63 mg/g, and its pollutant removal

mechanism is inner sphere complexation. It can be seen from these that the pollutants from nuclear waste can be effectively removed by magnetic biochar, which is a process of enrichment, when the complex charge of these pollutants in magnetic biochar is relatively high. Therefore, what to do with magnetic biochar, which contains pollutants that absorb nuclear waste, also remains a challenge. The schematic diagram of purifying wastewater with magnetic biochar is shown in **Figure 4**.

Adsorption of Organic Pollutants

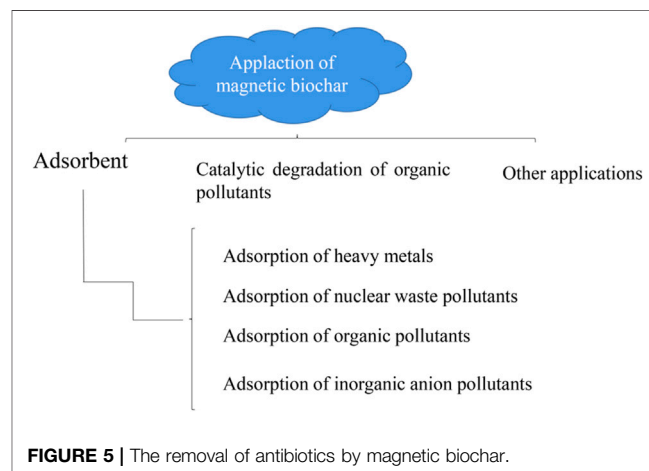
Magnetic biochar showed a good adsorption performance for organic pollutants, and the removal of organic pollutants by magnetic biochar was mainly antibiotics, organic dyes, pesticides, and organochlorine compounds (Kumar et al., 2020). Meng et al. (Meng et al., 2015) summarized the adsorption effect of magnetic biochar on antibiotics. According to these data, tetracycline is the most common removal, with adsorption loads ranging from 33.1 mg/g to 297.61 mg/g, followed by methanoxazole, with adsorption loads ranging from 5.19 to 212.8 mg/g. It mainly summarized the mechanism of antibiotic removal by magnetic biochar and these involve hydrogen bonding, π - π interactions, pore-filling effects, electrostatic adsorption, and hydrophobic interactions.

The organic dyes that are adsorbed by magnetic biochar are rhodamine B, methylene blue, malachite green, acid orange 7 (AO-7), and orange-G. The saturated adsorption capacity of magnetic biochar for these dyes ranged from 31.25 to 388.65 mg/g, while the mechanism of adsorption of dyes by magnetic biochar was less discussed.

At the same time, magnetic biochar can also remove other organic pollutants, such as pesticides, phenol, organochlorine, and hormones. The adsorption capacity varies from 3.46 to 169.7 mg/g. The removal mechanisms of these substances by magnetic biochar involve hydrogen bonding, π - π interactions, pore-filling effects, electrostatic adsorption, hydrophobic interactions, and reductive dehalogenation (Mun et al., 2013).

Adsorption of Inorganic Anion Pollutants

Magnetic biochar can also be used to remove inorganic pollutants such as phosphate, nitrate, fluoride, etc. (Cai et al., 2017; Xu et al.,



2020a). Compared with other pollutants, nitrate has been studied the most, and the adsorption capacity of magnetic biochar is between 1.26 and 474.26 mg/g (Li et al., 2017). The modified magnetic biochar has a good adsorption capacity of phosphate. In addition, the magnetic biochar has a good adsorption capacity of nitrate and fluoride, and the adsorption capacity is about 9 to 15 mg/g. The results show that co-precipitation, electrostatic adsorption, surface complexation, inner sphere complexation, and ligand exchange are present. Finally, due to the ability of magnetic biochar to adsorb a large number of nutrients, it could be used as a slow-release fertilizer to improve the composition of soil elements and soil fertility (Figure 5).

Catalytic Degradation of Organic Pollutants

Magnetic biochar has also been used as a catalyst for hydrogen peroxide, producing a highly reactive oxidizing substance that is used to degrade organic matter. For example, Chen et al. (Chen et al., 2018) found that the antibiotic ofloxacin could be efficiently degraded by magnetic biochar and persulfate. Meanwhile, Zhang et al. (Zhang et al., 2018) demonstrated that methylene blue can be completely removed by magnetic biochar coupled with hydrogen peroxide. Because different organisms have different physical and chemical properties, some organisms cannot remove organic pollutants at all by using female organisms. So, we can take advantage of the function of the female organism, the catalytic property, which is to produce hydroxyl radicals inside of the organism in time, to produce strong oxidizing radicals that attack organic pollutants freely, in a way that maximizes the function of the magnetic biochar. If it is difficult to remove organic pollutants by using magnetic biological carbon, its catalytic properties can be considered to achieve efficient degradation of organic pollutants.

Other Applications

In addition to the above functions, magnetic biochar can also be used as a photocatalytic carrier, for example, Li M. et al. (Li M. et al., 2019) prepared the $\text{Fe}_3\text{O}_4/\text{BiOBr}/\text{BC}$ photocatalyst using magnetic biochar as a carrier and found that its removal efficiency of propranolol was nearly 95%. Similarly, magnetic biochar can effectively recover precious metals by adsorption and enrichment. For example, Zhang et al. (Zhang et al., 2019) found that the adsorption capacity of magnetic biochar for silver ions was 818.4 mg/g.

It is very interesting that Qin et al. (Qin et al., 2017) used magnetic organisms in the process of anaerobic digestion, but as an additive, they found that a small amount of magnetic biochar promoted the production of methane on anaerobic digestion, and finally found methanogenic bacteria that produced methane, which facilitated recycling. And finally, female organisms could not just be used for environmental remediation, but also for energy storage (Hu et al., 2019; Lu et al., 2019). For example, Thines et al. (Thines et al., 2017) found that the density capacitance and energy could be increased when magnetic biological carbon was used as an electric conductor. Meanwhile, Jiang et al.'s (Jiang et al., 2019) research results showed that hydrogen could be effectively recovered in the process of removing nitrophenol. Although magnetic biochar

has a good adsorption effect, due to the release of a lot of heat in the preparation process, the yield is low, and the adsorption may not be complete, difficult to recover, and may cause secondary pollution to the environment. The large-scale application of magnetic biochar is limited.

CONCLUSION AND PROSPECTS

The remarkable properties of magnetic biochar and its special role in related industrial production have attracted great attention. In fact, demand for magnetic biochar has been growing over the past few years. However, this extensive demand is faced with the innovation and breakthrough of the preparation technology, and the solution of the current key technology and restriction links is conducive to the further large-scale production of magnetic biological carbon. In fact, the successful experience gives people a profound enlightenment, one to optimize the choice of production materials. As mentioned earlier, a large amount of agricultural waste can be used to produce magnetic biological carbon, and the expansion potential is huge. Second, the production process should be selected reasonably. For the production of magnetic biochar from agricultural wastes, new processes should be established based on actual conditions. In terms of selection criteria, not only the characterization elements of raw materials should be considered, but also important factors such as moisture content, ash content, carbon content, and surface area should be fully considered. These elements have a direct effect on the morphology and properties of the produced magnetic biochar, and will play a crucial role.

Therefore, the production of magnetic biochar from agricultural waste must be thoroughly understood and analyzed before it is developed into magnetic biochar. In addition, agricultural wastes must be pre-treated with particular care to avoid the spread of harmful pollutants from these wastes and their spread into the surrounding environment through water or air sources. At the same time, it is necessary to fully consider the transportation cost of batch scale and the cost of pretreatment when producing magnetic biochar from various agricultural wastes. It is very important to choose an open site for the treatment of agricultural waste. Through the combustion treatment, the prevention and control of gas pollution should be fully considered. The negative impact on the surrounding environment can be effectively reduced during the production of magnetic biochar through the application of new processes. Magnetic biochar can be produced by new environmental protection technology and strive to become an environmentally friendly product. On the other hand, after the successful development of magnetic biochar, the problems of marketing must be fully considered. The production of magnetic biochar from agricultural waste and its application in wastewater treatment or the electrolysis industry need a process of application and effect approval. It is necessary to organize effective verification tests, especially to carry out cooperation between science and enterprise, and to carry out series promotion and application in combination with production practice. If

magnetic biochar products are successful in specific applications, more enterprises will invest in this environmental protection industry, which will further promote the development of the magnetic biochar industry for agricultural waste development. At the same time, the application of magnetic biochar can be expanded by coating other carbon materials such as carbon nanotubes or graphene or polymers to improve its performance and expand its application in other industries.

In fact, the wide application of biochar in different industries requires continuous improvement, and research and development of new magnetic biochar production is very necessary. It is undoubtedly a new attempt to produce magnetic biochar with specific properties by improving the production method and improving the adsorption characteristics of biological carbon. Three main production methods have been identified as successful in producing effective forms of magnetic biochar with high porosity, magnetic strength, and significant morphology, which can perform well in related applications. It has been proved that magnetic biochar produced from various types of agricultural wastes has a high adsorption capacity to lead, chromium, copper, tetracycline, methylene blue, and crystal violet. In addition, magnetic biochar loaded with different metal salt ions also has high capacity, high density, and high efficiency. Therefore, the production of magnetic biochar by different production methods can open up a new recycling method for the full utilization of

abundant agricultural wastes, and its application prospect is very broad.

AUTHOR CONTRIBUTIONS

Writing original draft: QZ and TX; Supervision: XS and SN; Review and editing: CS, S-EC.

FUNDING

This work was supported by the National Natural Science Foundation of China (32071720). This work was also supported by 2021 Universities leading lab-specific start-ups through the National Research Foundation of Korea (NRF) grant funded by the Korea government (MSIT), the “Beyond Research Innovation and Development for Good Enterprises +” Project, supported by the Ministry of Education (MOE), and partially supported by the Technology Development Program (S3030198) funded by the Ministry of SMEs and Startups (MSS, Korea) to S-EC. In addition, the grants (Nos. 2021KF02, 2021KF32) from the Foundation of Guangxi Key Laboratory of Clean Pulp and Papermaking and Pollution Control, College of Light Industry and Food Engineering, Guangxi University were much appreciated.

REFERENCES

- Akin, I., Arslan, G., Tor, A., Ersoz, M., and Cengeloglu, Y. (2012). Arsenic(V) Removal from Underground Water by Magnetic Nanoparticles Synthesized from Waste Red Mud. *J. Hazard. Mater.* 235–236, 62–68. doi:10.1016/j.jhazmat.2012.06.02410.1016/j.jhazmat.2012.06.024
- An, L., Si, C., Wang, G., Sui, W., and Tao, Z. (2019). Enhancing the Solubility and Antioxidant Activity of High-Molecular-Weight Lignin by Moderate Depolymerization via *In Situ* Ethanol/acid Catalysis. *Ind. Crops Prod.* 128, 177–185. doi:10.1016/j.indcrop.2018.11.009
- Babes, L., Denizot, B., Tanguy, G., Lejeune, J. J., and Jallet, P. (1999). Synthesis of Iron Oxide Nanoparticles Used as MRI Contrast Agents: a Parametric Study. *J. Colloid Interf. Sci.* 212, 474–482. doi:10.1006/jcis.1998.6053
- Babu, B. V. (2008). Biomass Pyrolysis: a State-Of-The-Art Review. *Biofuels, Bioprod. Bioref.* 2, 393–414. doi:10.1002/bbb.92
- Baig, S. A., Zhu, J., Muhammad, N., Sheng, T., and Xu, X. (2014). Effect of Synthesis Methods on Magnetic Kans Grass Biochar for Enhanced As(III, V) Adsorption from Aqueous Solutions. *Biomass and Bioenergy* 71, 299–310. doi:10.1016/j.jenvman.2017.03.08510.1016/j.biombioe.2014.09.027
- Bastami, T. R., and Entezari, M. H. (2012). Activated Carbon from Carrot Dross Combined with Magnetite Nanoparticles for the Efficient Removal of P-Nitrophenol from Aqueous Solution. *Chem. Eng. J.* 210, 510–519. doi:10.1016/j.cej.2012.08.011
- Cai, R., Wang, X., Ji, X., Peng, B., Tan, C., and Huang, X. (2017). Phosphate Reclaim from Simulated and Real Eutrophic Water by Magnetic Biochar Derived from Water Hyacinth. *J. Environ. Manage.* 187, 212–219. doi:10.1016/j.jenvman.2016.11.047
- Cai, W., and Wan, J. (2007). Facile Synthesis of Superparamagnetic Magnetite Nanoparticles in Liquid Polyols. *J. Colloid Interf. Sci.* 305, 366–370. doi:10.1016/j.jcis.2006.10.023
- Chan, K. Y., Van Zwieten, L., Meszaros, I., Downie, A., and Joseph, S. (2007). Agronomic Values of Greenwaste Biochar as a Soil Amendment. *Soil Res.* 45, 629–634. doi:10.1071/SR07109
- Chen, B., Chen, Z., and Lv, S. (2011a). A Novel Magnetic Biochar Efficiently Sorbs Organic Pollutants and Phosphate. *Bioresour. Technol.* 102, 716–723. doi:10.1016/j.biortech.2010.08.067
- Chen, L., Yang, S., Zuo, X., Huang, Y., Cai, T., and Ding, D. (2018). Biochar Modification Significantly Promotes the Activity of Co3O4 towards Heterogeneous Activation of Peroxymonosulfate. *Chem. Eng. J.* 354, 856–865. doi:10.1016/j.cej.2018.08.098
- Chen, S., Wang, G., Sui, W., Parvez, A. M., Dai, L., and Si, C. (2020b). Novel Lignin-Based Phenolic Nanosphere Supported Palladium Nanoparticles with Highly Efficient Catalytic Performance and Good Reusability. *Ind. Crops Prod.* 145, 112164. doi:10.1016/j.indcrop.2020.112164
- Chen, S., Wang, G., Sui, W., Parvez, A. M., and Si, C. (2020a). Synthesis of Lignin-Functionalized Phenolic Nanosphere Supported Ag Nanoparticles with Excellent Dispersion Stability and Catalytic Performance. *Green. Chem.* 22, 2879–2888. doi:10.1039/c9gc04311j
- Chen, X., Chen, G., Chen, L., Chen, Y., Lehmann, J., McBride, M. B., et al. (2011b). Adsorption of Copper and Zinc by Biochars Produced from Pyrolysis of Hardwood and Corn Straw in Aqueous Solution. *Bioresour. Technol.* 102, 8877–8884. doi:10.1016/j.biortech.2011.06.07810.1016/j.biortech.2011.06.078
- Cheng, Z., Meng, J., and Wang, X. (2020). Preparation of Wood-Based Filter Loaded with Ag Nanoparticles and Its Catalytic Degradation Performance on Organic Dye. *J. Forest. Eng.* 50 (6), 94–98. doi:10.13360/j.issn.2096-1359.202004005
- Dai, L., Ma, M., Xu, J., Si, C., Wang, X., Liu, Z., et al. (2020). All-Lignin-Based Hydrogel with Fast pH-Stimuli Responsiveness for Mechanical Switching and Actuation. *Chem. Mater.* 32, 4324–4330. doi:10.1021/acs.chemmater.0c01198
- Dai, L., Zhu, W., Lu, J., Kong, F., Si, C., and Ni, Y. (2019a). A Lignin-Containing Cellulose Hydrogel for Lignin Fractionation. *Green. Chem.* 21, 5222–5230. doi:10.1039/c9gc01975h
- Dai, S.-j., Zhao, Y.-c., Niu, D.-j., Li, Q., and Chen, Y. (2019b). Preparation and Reactivation of Magnetic Biochar by Molten Salt Method: Relevant Performance for Chlorine-Containing Pesticides Abatement. *J. Air Waste Manage. Assoc.* 69, 58–70. doi:10.1080/10962247.2018.1510441

- Das, O., Sarmah, A. K., and Bhattacharyya, D. (2015). A Novel Approach in Organic Waste Utilization through Biochar Addition in wood/polypropylene Composites. *Waste Manage.* 38, 132–140. doi:10.1016/j.wasman.2015.01.015
- Demirbas, A., and Arin, G. (2002). An Overview of Biomass Pyrolysis. *Energy Sources* 24, 471–482. doi:10.1080/00908310252889979
- Devi, P., and Saroha, A. K. (2014). Synthesis of the Magnetic Biochar Composites for Use as an Adsorbent for the Removal of Pentachlorophenol from the Effluent. *Bioresour. Technol.* 169, 525–531. doi:10.1016/j.biortech.2014.07.062
- Diblasi, C. (2008). Modeling Chemical and Physical Processes of wood and Biomass Pyrolysis. *Prog. Energ. Combustion Sci.* 34, 47–90. doi:10.1016/j.pecs.2006.12.001
- Du, H., Liu, W., Zhang, M., Si, C., Zhang, X., and Li, B. (2019). Cellulose Nanocrystals and Cellulose Nanofibrils Based Hydrogels for Biomedical Applications. *Carbohydr. Polym.* 209, 130–144. doi:10.1016/j.carbpol.2019.01.020
- Du, H., Parit, M., Liu, K., Zhang, M., Jiang, Z., Huang, T.-S., et al. (2021). Multifunctional Cellulose Nanopaper with superior Water-Resistant, Conductive, and Antibacterial Properties Functionalized with Chitosan and Polypyrrole. *ACS Appl. Mater. Inter.* 13 (27), 32115–32125. doi:10.1021/acsami.1c06647
- Du, H., Zhang, M., Liu, K., Parit, M., Jiang, Z., Zhang, X., et al. (2022). Conductive PEDOT:PSS/cellulose Nanofibril Paper Electrodes for Flexible Supercapacitors with superior Areal Capacitance and Cycling Stability. *Chem. Eng. J.* 428, 131994. doi:10.1016/j.cej.2021.121994
- Gao, H., Lv, S., Dou, J., Kong, M., Dai, D., Si, C., et al. (2015). The Efficient Adsorption Removal of Cr(VI) by Using Fe₃O₄ Nanoparticles Hybridized with Carbonaceous Materials. *RSC Adv.* 5, 60033–60040. doi:10.1039/C5RA10236G
- Goda, K., Sreekala, M. S., Malhotra, S. K., Joseph, K., and Thomas, S. (2014). Advances in Polymer Composites: Biocomposites-State of the Art, New Challenges, and Opportunities. *Polym. Composites*, 1–10. doi:10.1002/9783527674220.ch1
- Goyal, H. B., Seal, D., and Saxena, R. C. (2008). Bio-fuels from Thermochemical Conversion of Renewable Resources: a Review. *Renew. Sustain. Energ. Rev.* 12, 504–517. doi:10.1016/j.rser.2006.07.014
- Gupta, R. K., Dubey, M., Kharel, P., Gu, Z., and Fan, Q. H. (2015). Biochar Activated by Oxygen Plasma for Supercapacitors. *J. Power Sourc.* 274, 1300–1305. doi:10.1016/j.jpowsour.2014.10.169
- Harikishore Kumar Reddy, D., and Lee, S.-M. (2014). Magnetic Biochar Composite: Facile Synthesis, Characterization, and Application for Heavy Metal Removal. *Colloids Surf. A: Physicochemical Eng. Aspects* 454, 96–103. doi:10.1016/j.colsurfa.2014.03.105
- Hu, L., Du, H., Liu, C., Zhang, Y., Yu, G., Zhang, X., et al. (2019). Comparative Evaluation of the Efficient Conversion of Corn Husk Filament and Corn Husk Powder to Valuable Materials via a Sustainable and Clean Biorefinery Process. *ACS Sustain. Chem. Eng.* 7, 1327–1336. doi:10.1021/acssuschemeng.8b05017
- Hu, Q., Zhu, Y., Hu, B., Lu, S., and Sheng, G. (2018). Mechanistic Insights into Sequestration of U(VI) toward Magnetic Biochar: Batch, XPS and EXAFS Techniques. *J. Environ. Sci.* 70, 217–225. doi:10.1016/j.jes.2018.01.013
- Ifthikar, J., Wang, J., Wang, Q., Wang, T., Wang, H., Khan, A., et al. (2017). Highly Efficient lead Distribution by Magnetic Sewage Sludge Biochar: Sorption Mechanisms and Bench Applications. *Bioresour. Technol.* 238, 399–406. doi:10.1016/j.biortech.2017.03.133
- Jiang, S.-F., Xi, K.-F., Yang, J., and Jiang, H. (2019). Biochar-supported Magnetic noble Metallic Nanoparticles for the Fast Recovery of Excessive Reductant during Pollutant Reduction. *Chemosphere* 227, 63–71. doi:10.1016/j.chemosphere.2019.04.044
- Jiang, Y., Gong, J.-L., Zeng, G.-M., Ou, X.-M., Chang, Y.-N., Deng, C.-H., et al. (2016). Magnetic Chitosan-Graphene Oxide Composite for Anti-microbial and Dye Removal Applications. *Int. J. Biol. Macromolecules* 82, 702–710. doi:10.1016/j.jbiomac.2015.11.021
- Kolthoff, I. M. (1932). Theory of Coprecipitation. The Formation and Properties of Crystalline Precipitates. *J. Phys. Chem.* 36, 860–881. doi:10.1021/j150333a008
- Kumar, A., Sharma, G., Naushad, M., Al-Muhtaseb, A. a. H., García-Peñas, A., Mola, G. T., et al. (2020). Bio-inspired and Biomaterials-Based Hybrid Photocatalysts for Environmental Detoxification: A Review. *Chem. Eng. J.* 382, 122937. doi:10.1016/j.cej.2019.122937
- Laine, J., Calafat, A., and Labady, M. (1989). Preparation and Characterization of Activated Carbons from Coconut Shell Impregnated with Phosphoric Acid. *Carbon* 27, 191–195. doi:10.1016/0008-6223(89)90123-1
- Laird, D. A., Brown, R. C., Amonette, J. E., and Lehmann, J. (2009). Review of the Pyrolysis Platform for Coproducing Bio-Oil and Biochar. *Biofuels, Bioprod. Bioref.* 3, 547–562. doi:10.1002/bbb.169
- Li, H., Mahyoub, S. A. A., Liao, W., Xia, S., Zhao, H., Guo, M., et al. (2017). Effect of Pyrolysis Temperature on Characteristics and Aromatic Contaminants Adsorption Behavior of Magnetic Biochar Derived from Pyrolysis Oil Distillation Residue. *Bioresour. Technol.* 223, 20–26. doi:10.1016/j.biortech.2016.10.033
- Li, M., Liu, H., Chen, T., Dong, C., and Sun, Y. (2019a). Synthesis of Magnetic Biochar Composites for Enhanced Uranium(VI) Adsorption. *Sci. Total Environ.* 651, 1020–1028. doi:10.1016/j.scitotenv.2018.09.259
- Li, X., Lu, X., Nie, S., Liang, M., Yu, Z., Duan, B., et al. (2020). Efficient Catalytic Production of Biomass-Derived Levulinic Acid over Phosphotungstic Acid in Deep Eutectic Solvent. *Ind. Crops Prod.* 145, 112154. doi:10.1016/j.indcrop.2020.112154
- Li, X., Xu, R., Yang, J., Nie, S., Liu, D., Liu, Y., et al. (2019b). Production of 5-hydroxymethylfurfural and Levulinic Acid from Lignocellulosic Biomass and Catalytic Upgradation. *Ind. Crops Prod.* 130, 184–197. doi:10.1016/j.indcrop.2018.12.082
- Li, Y., and Liu, X. (2014). Activated carbon/ZnO Composites Prepared Using Hydrochars as Intermediate and Their Electrochemical Performance in Supercapacitor. *Mater. Chem. Phys.* 148, 380–386. doi:10.1016/j.matchemphys.2014.07.058
- Liang, B., Lehmann, J., Solomon, D., Kinyangi, J., Grossman, J., O'Neill, B., et al. (2006). Black Carbon Increases Cation Exchange Capacity in Soils. *Soil Sci. Soc. Am. J.* 70, 1719–1730. doi:10.2136/sssaj2005.0383
- Lin, W., Xing, S., Jin, Y., Lu, X., Huang, C., and Yong, Q. (2020). Insight into Understanding the Performance of Deep Eutectic Solvent Pretreatment on Improving Enzymatic Digestibility of Bamboo Residues. *Bioresour. Technol.* 306, 123163. doi:10.1016/j.biortech.2020.123163
- Liu, H., Du, H., Zheng, T., Liu, K., Ji, X., Xu, T., et al. (2021a). Cellulose Based Composite Foams and Aerogels for Advanced Energy Storage Devices. *Chem. Eng. J.* 426, 130817. doi:10.1016/j.cej.2021.130817
- Liu, H., Xu, T., Liu, K., Zhang, M., Liu, W., Li, H., et al. (2021b). Lignin-based Electrodes for Energy Storage Application. *Ind. Crops Prod.* 165, 113425. doi:10.1016/j.indcrop.2021.113425
- Liu, K., Du, H., Zheng, T., Liu, H., Zhang, M., Zhang, R., et al. (2021c). Recent Advances in Cellulose and its Derivatives for Oilfield Applications. *Carbohydr. Polym.* 259, 117740. doi:10.1016/j.carbpol.2021.117740
- Liu, K., Du, H., Zheng, T., Liu, W., Zhang, M., Liu, H., et al. (2021d). Lignin-containing Cellulose Nanomaterials: Preparation and Applications. *Green. Chem.* doi:10.1039/d1gc02841c
- Liu, S., Du, H., Liu, K., Ma, M.-G., Kwon, Y.-E., Si, C., et al. (2021e). Flexible and Porous Co₃O₄-Carbon Nanofibers as Binder-free Electrodes for Supercapacitors. *Adv. Compos. Hybrid. Mater.* 4. doi:10.1007/s42114-021-00344-8
- Liu, W., Du, H., Liu, H., Xie, H., Xu, T., Zhao, X., et al. (2020b). Highly Efficient and Sustainable Preparation of Carboxylic and Thermostable Cellulose Nanocrystals via FeCl₃-Catalyzed Innocuous Citric Acid Hydrolysis. *ACS Sustain. Chem. Eng.* 8, 16691–16700. doi:10.1021/acssuschemeng.0c06561
- Liu, W., Du, H., Liu, K., Liu, H., Xie, H., Si, C., et al. (2021f). Sustainable Preparation of Cellulose Nanofibrils via Choline Chloride-Citric Acid Deep Eutectic Solvent Pretreatment Combined with High-Pressure Homogenization. *Carbohydr. Polym.* 267, 118220. doi:10.1016/j.carbpol.2021.118220
- Liu, W., Du, H., Zhang, M., Liu, K., Liu, H., Xie, H., et al. (2020a). Bacterial Cellulose-Based Composite Scaffolds for Biomedical Applications: A Review. *ACS Sustain. Chem. Eng.* 8, 7536–7562. doi:10.1021/acssuschemeng.0c00125
- Liu, W., Si, C., Du, H., Zhang, M., Zhang, X., Xie, H., et al. (2019). Advance in Preparation of Nanocellulose-Based Hydrogels and Their Biomedical Applications. *J. Forest. Eng.* 4 (5), 11–19. doi:10.13360/j.issn.2096-1359.2019.05.002
- Liu, Z., and Zhang, F.-S. (2009). Removal of lead from Water Using Biochars Prepared from Hydrothermal Liquefaction of Biomass. *J. Hazard. Mater.* 167, 933–939. doi:10.1016/j.jhazmat.2009.01.085

- Lu, A.-H., Schmidt, W., Matoussevitch, N., Bönnemann, H., Spliethoff, B., Tesche, B., et al. (2004). Nanoengineering of a Magnetically Separable Hydrogenation Catalyst. *Angew. Chem.* 116, 4403–4406. doi:10.1002/chin.20044323110.1002/ange.200454222
- Lu, J., Zhu, W., Dai, L., Si, C., Si, C., and Ni, Y. (2019). Fabrication of Thermo- and pH-Sensitive Cellulose Nanofibrils-Reinforced Hydrogel with Biomass Nanoparticles. *Carbohydr. Polym.* 215, 289–295. doi:10.1016/j.carbpol.2019.03.100
- Ma, C., Ma, M. G., Si, C., Ji, X. X., and Wan, P. (20210095). Flexible MXene-Based Composites for Wearable Devices. *Adv. Funct. Mater.* 31, 2009524. doi:10.1002/adfm.202009524
- Ma, C., Yuan, Q., Du, H., Ma, M.-G., Si, C., and Wan, P. (2020). Multiresponsive MXene (Ti₃C₂Tx)-Decorated Textiles for Wearable Thermal Management and Human Motion Monitoring. *ACS Appl. Mater. Inter.* 12, 34226–34234. doi:10.1021/acsami.0c10750
- Ma, H., Li, J.-B., Liu, W.-W., Miao, M., Cheng, B.-J., and Zhu, S.-W. (2015). Novel Synthesis of a Versatile Magnetic Adsorbent Derived from Corn cob for Dye Removal. *Bioresour. Technol.* 190, 13–20. doi:10.1016/j.biortech.2015.04.048
- Maschio, G., Koufopoulos, C., and Lucchesi, A. (1992). Pyrolysis, a Promising Route for Biomass Utilization. *Bioresour. Technol.* 42, 219–231. doi:10.1016/0960-8524(92)90025-s
- Massart, R. (1981). Preparation of Aqueous Magnetic Liquids in Alkaline and Acidic media. *IEEE Trans. Magn.* 17, 1247–1248. doi:10.1109/tmag.1981.1061188
- Meng, Y., Chen, D., Sun, Y., Jiao, D., Zeng, D., and Liu, Z. (2015). Adsorption of Cu²⁺ Ions Using Chitosan-Modified Magnetic Mn Ferrite Nanoparticles Synthesized by Microwave-Assisted Hydrothermal Method. *Appl. Surf. Sci.* 324, 745–750. doi:10.1016/j.apsusc.2014.11.028
- Mojiri, A., Andasht Kazeroon, R., and Gholami, A. (2019). Cross-Linked Magnetic Chitosan/Activated Biochar for Removal of Emerging Micropollutants from Water: Optimization by the Artificial Neural Network. *Water* 11 (3), 551. doi:10.3390/w11030551
- Mohan, D., Kumar, H., Sarswat, A., Alexandre-Franco, M., and Pittman, C. U. (2014). Cadmium and Lead Remediation Using Magnetic Oak Wood and Oak Bark Fast Pyrolysis Biochars. *Chem. Eng. J.* 236, 513–528. doi:10.1016/j.cej.2013.09.057
- Mohan, D., Sarswat, A., Singh, V. K., Alexandre-Franco, M., and Pittman, C. U. (2011). Development of Magnetic Activated Carbon from almond Shells for Trinitrophenol Removal from Water. *Chem. Eng. J.* 172, 1111–1125. doi:10.1016/j.cej.2011.06.054
- Mubarak, N. M., Kundu, A., Sahu, J. N., Abdullah, E. C., and Jayakumar, N. S. (2014). Synthesis of palm Oil Empty Fruit bunch Magnetic Pyrolytic Char Impregnating with FeCl₃ by Microwave Heating Technique. *Biomass and Bioenergy* 61, 265–275. doi:10.1016/j.biombioe.2013.12.021
- Mubarak, N. M., Sahu, J. N., Abdullah, E. C., and Jayakumar, N. S. (2016). Palm Oil Empty Fruit bunch Based Magnetic Biochar Composite Comparison for Synthesis by Microwave-Assisted and Conventional Heating. *J. Anal. Appl. Pyrolysis* 120, 521–528. doi:10.1016/j.jaap.2016.06.026
- Mukherjee, A., Zimmerman, A. R., and Harris, W. (2011). Surface Chemistry Variations Among a Series of Laboratory-Produced Biochars. *Geoderma* 163, 247–255. doi:10.1016/j.geoderma.2011.04.021
- Mun, S. P., Cai, Z., and Zhang, J. (2013). Magnetic Separation of Carbon-Encapsulated Fe Nanoparticles from Thermally-Treated wood Char. *Mater. Lett.* 96, 5–7. doi:10.1016/j.matlet.2013.01.006
- Nethaji, S., Sivasamy, A., and Mandal, A. B. (2013). Preparation and Characterization of Corn Cob Activated Carbon Coated with Nano-Sized Magnetite Particles for the Removal of Cr(VI). *Bioresour. Technol.* 134, 94–100. doi:10.1016/j.biortech.2013.02.012
- Ngarmkam, W., Sirisathitkul, C., and Phakakornkule, C. (2011). Magnetic Composite Prepared from Palm Shell-based Carbon and Application for Recovery of Residual Oil from POME. *J. Environ. Manage* 92, 472–479. doi:10.1016/j.jenvman.2010.08.031
- Pei, W., Chen, Z. S., Chan, H. Y. E., Zheng, L., Liang, C., and Huang, C. (2020a). Isolation and Identification of a Novel Anti-protein Aggregation Activity of Lignin-Carbohydrate Complex from Chionanthus Retusus Leaves. *Front. Bioeng. Biotechnol.* 8, 573991. doi:10.3389/fbioe.2020.573991
- Pei, W., Shang, W., Liang, C., Jiang, X., Jiang, X., Huang, C., et al. (2020b). Using Lignin as the Precursor to Synthesize Fe₃O₄@lignin Composite for Preparing Electromagnetic Wave Absorbing Lignin-Phenol-Formaldehyde Adhesive. *Ind. Crops Prod.* 154, 112638. doi:10.1016/j.indcrop.2020.112638
- Qin, Y., Wang, H., Li, X., Cheng, J. J., and Wu, W. (2017). Improving Methane Yield from Organic Fraction of Municipal Solid Waste (OFMSW) with Magnetic rice-straw Biochar. *Bioresour. Technol.* 245, 1058–1066. doi:10.1016/j.biortech.2017.09.047
- Quan, G., Sun, W., and Yan, J. (2014). Nanoscale Zerovalent Iron Supported on Biochar: Characterization and Reactivity for Degradation of Acid Orange 7 from Aqueous Solution. *Water, Air, and Soil Pollution* 225, 2195. doi:10.1007/s11270-014-2195-3
- Ruthiraan, M., Mubarak, N. M., Thines, R. K., Abdullah, E. C., Sahu, J. N., Jayakumar, N. S., et al. (2015). Comparative Kinetic Study of Functionalized Carbon Nanotubes and Magnetic Biochar for Removal of Cd²⁺ Ions from Wastewater. *Korean J. Chem. Eng.* 32, 446–457. doi:10.1007/s11814-014-0260-7
- Saravanan, P., Vinod, V. T. P., Sreedhar, B., and Sashidhar, R. B. (2012). Gum Kondagogu Modified Magnetic Nano-Adsorbent: An Efficient Protocol for Removal of Various Toxic Metal Ions. *Mater. Sci. Eng. C* 32, 581–586. doi:10.1016/j.msec.2011.12.015
- Shang, J., Pi, J., Zong, M., Wang, Y., Li, W., and Liao, Q. (2016). Chromium Removal Using Magnetic Biochar Derived from Herb-Residue. *J. Taiwan Inst. Chem. Eng.* 68, 289–294. doi:10.1016/j.jtice.2016.09.012
- Shafizadeh, F. (1982). Introduction to Pyrolysis of Biomass. *J. Anal. Appl. Pyrolysis* 3, 283–305. doi:10.1016/0165-2370(82)80017-X
- Si, C.-L., Kim, J.-K., Bae, Y.-S., and Li, S.-M. (2009). Phenolic Compounds in the Leaves of Populus Ussuriensis and Their Antioxidant Activities. *Planta Med.* 75, 1165–1167. doi:10.1055/s-0029-1185476
- Si, C.-L., Liu, Z., Kim, J.-K., and Bae, Y.-S. (2008). Structure Elucidation of Phenylethanoid Glycosides from Paulownia Tomentosa Steud. Var. Tomentosa wood. *Holzforchung* 62, 197–200. doi:10.1515/hf.2008.047
- Si, C.-L., Shen, T., Jiang, Y.-Y., Wu, L., Yu, G.-J., Ren, X.-D., et al. (2013). Antioxidant Properties and Neuroprotective Effects of Isocampneoside II on Hydrogen Peroxide-Induced Oxidative Injury in PC12 Cells. *Food Chem. Toxicol.* 59, 145–152. doi:10.1016/j.fct.2013.05.051
- Sozeri, H., Kurtan, U., Topkaya, R., Baykal, A., and Toprak, M. S. (2013). Polyaniline (PANI)-Co_{0.5}Mn_{0.5}Fe₂O₄ Nanocomposite: Synthesis, Characterization and Magnetic Properties Evaluation. *Ceramics Int.* 39, 5137–5143. doi:10.1016/j.ceramint.2012.12.009
- Sugimoto, T. (2003). Formation of Monodispersed Nano- and Micro-particles Controlled in Size, Shape, and Internal Structure. *Chem. Eng. Technol.* 26, 313–321. doi:10.1002/ceat.200390048
- Theydan, S. K., and Ahmed, M. J. (2012). Adsorption of Methylene Blue onto Biomass-Based Activated Carbon by FeCl₃ Activation: Equilibrium, Kinetics, and Thermodynamic Studies. *J. Anal. Appl. Pyrolysis* 97, 116–122. doi:10.1016/j.jaap.2012.05.008
- Thines, K. R., Abdullah, E. C., Mubarak, N. M., and Ruthiraan, M. (2017). In-situ Polymerization of Magnetic Biochar - Polypyrrole Composite: A Novel Application in Supercapacitor. *Biomass and Bioenergy* 98, 95–111. doi:10.1016/j.biombioe.2017.01.019
- Thines, K. R., Abdullah, E. C., Ruthiraan, M., Mubarak, N. M., and Tripathi, M. (2016). A New Route of Magnetic Biochar Based Polyaniline Composites for Supercapacitor Electrode Materials. *J. Anal. Appl. Pyrolysis* 121, 240–257. doi:10.1016/j.jaap.2016.08.004
- Uchimiya, M., Lima, I. M., Klasson, K. T., and Wartelle, L. H. (2010). Contaminant Immobilization and Nutrient Release by Biochar Soil Amendment: Roles of Natural Organic Matter. *Chemosphere* 80, 935–940. doi:10.1016/j.chemosphere.2010.05.020
- Vadivelan, V., and Kumar, K. V. (2005). Equilibrium, Kinetics, Mechanism, and Process Design for the Sorption of Methylene Blue onto Rice Husk. *J. Colloid Interface Sci.* 286, 90–100. doi:10.1016/j.jcis.2005.01.007
- Wang, H., Du, H., Liu, K., Liu, H., Xu, T., Zhang, S., et al. (2021). Sustainable Preparation of Bifunctional Cellulose Nanocrystals via Mixed H₂SO₄/formic Acid Hydrolysis. *Carbohydr. Polym.* 266, 118107. doi:10.1016/j.carbpol.2021.118107
- Wang, H., Xie, H., Du, H., Wang, X., Liu, W., Duan, Y., et al. (2020a). Highly Efficient Preparation of Functional and Thermostable Cellulose Nanocrystals via H₂SO₄ Intensified Acetic Acid Hydrolysis. *Carbohydr. Polym.* 239, 116233. doi:10.1016/j.carbpol.2020.116233

- Wang, M. C., Sheng, G. D., and Qiu, Y. P. (2015). A Novel Manganese-Oxide/biochar Composite for Efficient Removal of Lead(II) from Aqueous Solutions. *Int. J. Environ. Sci. Technol.* 12, 1719–1726. doi:10.1007/s13762-014-0538-7
- Wang, P., Yin, B., Dong, H., Zhang, Y., Zhang, Y., Chen, R., et al. (2020b). Coupling Biocompatible Au Nanoclusters and Cellulose Nanofibrils to Prepare the Antibacterial Nanocomposite Films. *Front. Bioeng. Biotechnol.* 8, 986. doi:10.3389/fbioe.2020.00986
- Wang, S., Gao, B., Li, Y., Mosa, A., Zimmerman, A. R., Ma, L. Q., et al. (2015a). Manganese Oxide-Modified Biochars: Preparation, Characterization, and Sorption of Arsenate and lead. *Bioresour. Technol.* 181, 13–17. doi:10.1016/j.biortech.2015.01.044
- Wang, S., Gao, B., Zimmerman, A. R., Li, Y., Ma, L., Harris, W. G., et al. (2015b). Removal of Arsenic by Magnetic Biochar Prepared from Pinewood and Natural Hematite. *Bioresour. Technol.* 175, 391–395. doi:10.1016/j.biortech.2014.10.104
- Wang, W., Wang, X., Wang, X., Yang, L., Wu, Z., Xia, S., et al. (2013). Cr(VI) Removal from Aqueous Solution with Bamboo Charcoal Chemically Modified by Iron and Cobalt with the Assistance of Microwave. *J. Environ. Sci.* 25, 1726–1735. doi:10.1016/S1001-0742(12)60247-2
- Wang, X., Li, X., Ge, W., and Yang, Y. (2019). Progress in Biomass-Derived Carbon Materials/MnO₂ Composite and Its Application in Supercapacitors. *J. Forest. Eng.* 4 (6), 1–10. doi:10.13360/j.issn.2096-1359.2019.06.001
- Xu, J., Li, C., Dai, L., Xu, C., Zhong, Y., Yu, F., et al. (2020a). Biomass Fractionation and Lignin Fractionation towards Lignin Valorization. *ChemSusChem* 13, 4284–4295. doi:10.1002/cssc.202001491
- Xu, R., Du, H., Liu, C., Liu, H., Wu, M., Zhang, X., et al. (2021a). An Efficient and Magnetic Adsorbent Prepared in a Dry Process with Enzymatic Hydrolysis Residues for Wastewater Treatment. *J. Clean. Prod.* 313, 127834. doi:10.1016/j.jclepro.2021.127834
- Xu, R., Si, C., Kong, F., and Li, X. (2020b). Synthesis of γ -valerolactone and Its Application in Biomass Conversion. *Forest. Eng.* 5 (2), 20–28. doi:10.13360/j.issn.2096-1359.201904004
- Xu, T., Du, H., Liu, H., Liu, W., Zhang, X., Si, C., et al. (2021b). Advanced Nanocellulose-Based Composites for Flexible Functional Energy Storage Devices. *Adv. Mater.*, 2101368. doi:10.1002/adma.202101368
- Yan, B., Chen, Z. S., Hu, Y., and Yong, Q. (2021). Insight in the Recent Application of Polyphenols From Biomass. *Front. Bioeng. Biotechnol.* 9, 753898. doi:10.3389/fbioe.2021.753898
- Yang, J., Si, C., Liu, K., Liu, H., Li, X., Liang, M., et al. (2020). Production of Levulinic Acid from Lignocellulosic Biomass and Application. *J. Forest. Eng.* 5 (5), 21–27. doi:10.13360/j.issn.2096-1359.201905013
- Yang, X., Xie, H., Du, H., Zhang, X., Zou, Z., Zou, Y., et al. (2019). Facile Extraction of Thermally Stable and Dispersible Cellulose Nanocrystals with High Yield via a green and Recyclable FeCl₃-Catalyzed Deep Eutectic Solvent System. *ACS Sustain. Chem. Eng.* 7, 7200–7208. doi:10.1021/acssuschemeng.9b00209
- Yu, J.-X., Wang, L.-Y., Chi, R.-A., Zhang, Y.-F., Xu, Z.-G., and Guo, J. (2013). Competitive Adsorption of Pb²⁺ and Cd²⁺ on Magnetic Modified Sugarcane Bagasse Prepared by Two Simple Steps. *Appl. Surf. Sci.* 268, 163–170. doi:10.1016/j.apsusc.2012.12.047
- Zhang, G., Qu, J., Liu, H., Cooper, A. T., and Wu, R. (2007). CuFe₂O₄/activated Carbon Composite: A Novel Magnetic Adsorbent for the Removal of Acid orange II and Catalytic Regeneration. *Chemosphere* 68, 1058–1066. doi:10.1016/j.chemosphere.2007.01.081
- Zhang, H., Xue, G., Chen, H., and Li, X. (2018). Magnetic Biochar Catalyst Derived from Biological Sludge and Ferric Sludge Using Hydrothermal Carbonization: Preparation, Characterization and its Circulation in Fenton Process for Dyeing Wastewater Treatment. *Chemosphere* 191, 64–71. doi:10.1016/j.chemosphere.2017.10.026
- Zhang, L., Guo, J., Huang, X., Wang, W., Sun, P., Li, Y., et al. (2019). Functionalized Biochar-Supported Magnetic MnFe₂O₄ Nanocomposite for the Removal of Pb(II) and Cd(II). *RSC Adv.* 9, 365–376. doi:10.1039/c8ra09061k
- Zhang, M., Du, H., Liu, K., Nie, S., Xu, T., Zhang, X., et al. (2021). Fabrication and Applications of Cellulose-Based Nanogenerators. *Adv. Compos. Hybrid. Mater.* doi:10.1007/s42114-021-00312-2
- Zhang, M., and Gao, B. (2013). Removal of Arsenic, Methylene Blue, and Phosphate by biochar/AlOOH Nanocomposite. *Chem. Eng. J.* 226, 286–292. doi:10.1016/j.cej.2013.04.077
- Zhu, S., Huang, X., Wang, D., Wang, L., and Ma, F. (2018a). Enhanced Hexavalent Chromium Removal Performance and Stabilization by Magnetic Iron Nanoparticles Assisted Biochar in Aqueous Solution: Mechanisms and Application Potential. *Chemosphere* 207, 50–59. doi:10.1016/j.chemosphere.2018.05.046
- Zhu, Y., Zheng, C., Wu, S., Song, Y., and Hu, B. (2018b). Interaction of Eu(III) on Magnetic Biochar Investigated by Batch, Spectroscopic and Modeling Techniques. *J. Radioanal. Nucl. Chem.* 316, 1337–1346. doi:10.1007/s10967-018-5839-8

Conflict of Interest: The authors declare that the research was conducted in the absence of any commercial or financial relationships that could be construed as a potential conflict of interest.

Publisher's Note: All claims expressed in this article are solely those of the authors and do not necessarily represent those of their affiliated organizations, or those of the publisher, the editors and the reviewers. Any product that may be evaluated in this article, or claim that may be made by its manufacturer, is not guaranteed or endorsed by the publisher.

Copyright © 2021 Zhao, Xu, Song, Nie, Choi and Si. This is an open-access article distributed under the terms of the Creative Commons Attribution License (CC BY). The use, distribution or reproduction in other forums is permitted, provided the original author(s) and the copyright owner(s) are credited and that the original publication in this journal is cited, in accordance with accepted academic practice. No use, distribution or reproduction is permitted which does not comply with these terms.



Effects of P-Coumarate 3-Hydroxylase Downregulation on the Compositional and Structural Characteristics of Lignin and Hemicelluloses in Poplar Wood (*Populus alba* × *Populus glandulosa*)

OPEN ACCESS

Edited by:

Chao Zhao,
Zhejiang A&F University, China

Reviewed by:

Zhouyang Xiang,
South China University of Technology,
China
Wu Lan,
South China University of Technology,
China
Zhiwen Wang,
University of Groningen, Netherlands

*Correspondence:

Cheng-Ye Ma
chengye.ma@foxmail.com
Jia-Long Wen
wenjialong@bjfu.edu.cn

Specialty section:

This article was submitted to
Bioprocess Engineering,
a section of the journal
Frontiers in Bioengineering and
Biotechnology

Received: 06 October 2021

Accepted: 22 October 2021

Published: 15 November 2021

Citation:

Peng X-P, Bian J, Yao S-Q, Ma C-Y
and Wen J-L (2021) Effects of P-
Coumarate 3-Hydroxylase
Downregulation on the Compositional
and Structural Characteristics of Lignin
and Hemicelluloses in Poplar Wood
(*Populus alba* × *Populus glandulosa*).
Front. Bioeng. Biotechnol. 9:790539.
doi: 10.3389/fbioe.2021.790539

Xiao-Peng Peng¹, Jing Bian², Shuang-Quan Yao³, Cheng-Ye Ma^{2*} and Jia-Long Wen^{2*}

¹State Key Laboratory of Tree Genetics and Breeding, Key Laboratory of Tree Breeding and Cultivation of the National Forestry and Grassland Administration, Research Institute of Forestry, Chinese Academy of Forestry, Beijing, China, ²Beijing Key Laboratory of Lignocellulosic Chemistry, Beijing Forestry University, Beijing, China, ³Guangxi Key Laboratory of Clean Pulp and Papermaking and Pollution Control, College of Light Industry and Food Engineering, Guangxi University, Nanning, China

Elucidating the chemical and structural characteristics of hemicelluloses and lignin in the *p*-coumarate 3-hydroxylase (C3H) down-regulated poplar wood will be beneficial to the upstream gene validation and downstream biomass conversion of this kind of transgenic poplar. Herein, the representative hemicelluloses and lignin with unaltered structures were prepared from control (CK) and C3H down-regulated 84K poplars. Modern analytical techniques, such as ¹³C NMR, 2D-HSQC NMR, and gel chromatography (GPC), were performed to better delineate the structural changes of hemicelluloses and lignin caused by transgenesis. Results showed that both the hemicelluloses (H_{CK} and H_{C3H}) extracted from control and C3H down-regulated poplar wood have a chain backbone of (1→4)-β-D-Xylan with 4-O-Me-α-D-GlcpA as side chain, and the branch degree of the H_{C3H} is higher than that of H_{CK}. With regarding to the lignin macromolecules, NMR results demonstrated that the syringyl/guaiacyl (S/G) ratio and dominant substructure β-O-4 linkages in C3H down-regulated poplar were lower than those of control poplar wood. By contrast, native lignin from C3H down-regulated poplar wood exhibited higher contents of *p*-hydroxybenzoate (PB) and *p*-hydroxyphenyl (H) units. In short, C3H down-regulation resulted in the chemical and structural changes of the hemicelluloses and lignin in these poplar wood. The identified structures will facilitate the downstream utilization and applications of lignocellulosic materials in the biorefinery strategy. Furthermore, this study could provide some illuminating results for genetic breeding on the improvement of wood properties and efficient utilization of poplar wood.

Keywords: C3H down-regulation, hemicelluloses, lignin, NMR, structural characteristics

INTRODUCTION

With the consumption of petrochemical resources and environmental concerns related to global warming and pollution, the search and development of renewable alternatives to petroleum-based resources have gained worldwide attraction (Himmel et al., 2007; Ragauskas et al., 2014). Lignocellulosic biomass represents a readily available renewable feedstock with the potential to be converted into a variety of fuels and chemicals (Ragauskas et al., 2006). Lignocellulosic biomass consists of three main components: lignin, hemicelluloses, and cellulose (Wang et al., 2019). Cellulose is a homopolymer which accounts for 30–50 wt% in lignocellulose, consisting of β -D-glucopyranose units linked by glycosidic bonds. Meanwhile, cellulose can be hydrolyzed enzymatically or chemically to obtain glucose, which can be further used to produce bioethanol and platform chemicals (Ma et al., 2021b). Hemicelluloses are amorphous polymers (15–30 wt% of lignocellulosic biomass) and consisted of C5 and C6 sugars. Due to the higher reactive activation than cellulose, hemicelluloses are easier to remove from lignocellulose to produce furfural and related chemicals (Peng et al., 2009). In addition, lignin is composed of aromatic monomers, which is an amorphous polymer accounting for 15–30 wt% in biomass (Wen et al., 2013b; Ragauskas et al., 2014).

Lignocelluloses are the largest renewable resource on Earth, which are considered to replace fossil-based products to produce chemicals, energy product, and fuels as the ideal raw materials (Sanderson, 2011; Isikgor and Becer, 2015; Wang et al., 2020). For a long time, lignocellulosic biomass has been considered a potential sustainable mixed sugar source, which can be used to ferment biomaterials and biofuels. (Ragauskas et al., 2014). However, “biomass recalcitrance” is created by tight binding of cellulose, hemicelluloses, and lignin, which is also the major obstacle for biorefinery (Himmel et al., 2007). The high cost of lignocellulose conversion is largely due to “biomass recalcitrance” (Zhao et al., 2012). Cellulose is difficult to be enzymatically hydrolyzed without pretreatment in woody biomass, which results from the existence of “biomass recalcitrance” (Ding et al., 2012; Sun et al., 2016). Ding et al. also pointed out that the ideal pretreatment should involve removing lignin as much as possible and reducing the modification of polysaccharides (Ding et al., 2012). “Biomass recalcitrance” must be reduced through pretreatment (Zhu and Pan, 2010; Pu et al., 2013). The second generation of biotechnological biofuel is liquid fuels (e.g., ethanol et al.) (Stephanopoulos, 2007; de Souza et al., 2014). The engineering feedstock crops will cost-competitively take the place of the fossil fuels to produce biofuels due to susceptible pretreatment and hydrolysis (Zhou et al., 2011). Lignin is the most abundant natural aromatic in plants because of its vital biological functions such as water retention and mechanical support. However, lignin can also inhibit saccharification by adsorbing hydrolytic enzymes (Alvira et al., 2010; Zheng et al., 2021). If lignin content and components can be reduced and altered by inhibiting the expression of critical genes in the lignin biosynthetic pathway, it will improve the efficiency of biorefinery and lower the cost (Sikarwar et al., 2016).

Lignin is a natural aromatic polymer composed of sinapyl alcohols, coniferyl, and hydroxycinnamyl (Vanholme et al., 2012a; Rinaldi et al., 2016; Vanholme et al., 2019; Zhao et al., 2020; Yang et al., 2021). The establishment of a suitable mass flux in the lignin biosynthesis pathway has become a new strategy for modifying lignin content (Boerjan et al., 2003). Realization of this strategy requires a comprehensive knowledge of lignin biosynthesis (Simmons et al., 2010). Researchers have made tremendous efforts to tailor the composition, structures, and reactivity of lignocellulose, especially lignin (Pilate et al., 2002). The lignin structure, composition, and content may vary among plant species and individuals, and even tissues of the same individual plant. Lignin biosynthesis is a complex process common to all vascular plants (Peng et al., 2014). Fortunately, the genes involved in this pathway have been studied and homologous genes for respective key genes are also known. There have been performed on genome-wide, transcript-, protein-, and metabolite-level studies, as well as the regulatory cascade of upstream transcription factors of these gene families, especially in *Arabidopsis* and poplar (Vanholme et al., 2012a; Vanholme et al., 2012b). The important enzymes in the phenylpropanoid biosynthetic pathway are hydroxycinnamoyl CoA: P-coumarate 3-hydroxylase (C3H), which could divert the pathway away from H lignin and toward S and G lignin (Franke et al., 2002a; Franke et al., 2002b; Wagner et al., 2007; Ralph et al., 2012). However, the compositional and structural characteristics of hemicelluloses and lignin from C3H-downregulated hardwood (poplar) have not been systematically characterized and researched. Herein, the effects of C3H downregulation on poplar hemicelluloses and lignin structures were investigated to determine how the genetic modification affects the hemicelluloses and lignin structures.

In this study, coumaroyl shikimate 3-hydroxylase (C3H) was cloned and constructed into RNAi vectors. Meanwhile, poplar was transformed by the leaf-disc method. A total of C3H-RNAi transgenic lines were obtained and vegetatively propagated by cutting for each line in the greenhouse. To illustrate the effects of C3H downregulation on the compositional and structural characteristics of lignin and hemicelluloses in poplar wood (*Populus alba* \times *Populus glandulosa*), representative hemicelluloses and lignin samples were firstly isolated, and modern analytical techniques (high-performance anion exchange chromatography (HPAEC), ^{13}C NMR, 2D-HSQC NMR, and gel chromatography (GPC) techniques) were applied to comprehensively delineate the chemical and structural changes of hemicelluloses and lignin caused by downregulation of the C3H gene. In short, this study is expected to provide some enlightenment for genetic breeding on the improvement of wood properties and efficient utilization of poplar wood in the current biorefinery engineering of woody biomass.

MATERIALS AND METHODS

Materials

Control 84K (CK) and downregulated C3H transgenic poplar 84K (*Populus alba* \times *Populus glandulosa*, 4 years) were cultivated

at the Chinese Academy of Forestry Sciences, and the detail regarding the procurement of wood was described in the ESI section. Especially, the gene-specific fragments were constructed into the RNAi plant expression vector by the double-digestion technique to obtain the RNAi expression vector of the C3H gene (**Supplementary Figure S1**). The *Populus alba* × *Populus glandulosa* clone 84K was used as transgenic poplar receptor material. Then, the resistant plants were obtained by the *Agrobacterium tumefaciens*-mediated transformation of leaf disc. That includes *Agrobacterium* culture, infection, coculture, selective culture, screening medium, and rooting culture (**Supplementary Figure S2**). The transplanted greenhouse was identified by PCR after the NPT-II gene and the target gene fragment, and the greenhouse was cut and propagated at low temperature and then the transgenic plants were obtained. The poplars were debarked and smashed into small pieces, then sieved to obtain 40–60 mesh particles. The composition of CK and C3H transgenics was determined by the National Renewable Energy Laboratory (NREL) standard analytical procedure (Sluiter et al., 2008). All the chemicals used in the experiment were of analytical grade.

Determination of Klason lignin content

The determination of the Klason lignin content of CK and C3H poplar particles was based on the NREL standard analytical procedure (Sluiter et al., 2008). In detail, 0.3 g poplar sample was added to 72% H₂SO₄ to hydrolyze at 30°C for 1 h. Then, the solution was added with 84 ml deionized water for further hydrolysis at 121°C for 1 h. After the hydrolysis, the solution was filtrated using a G3 sand core funnel. The mass change before and after filtration was the weight of the Klason lignin.

Isolation of representative hemicelluloses

Firstly, the control and C3H-downregulated poplar were delignified with acidic sodium chlorite solution (adjusted by acetic acid, pH 3.8–4.0) at 75°C for 2 h according to an earlier described procedure (Bian et al., 2012). As shown in **Supplementary Figure S3**, the delignified material (holocellulose) was extracted with 10% potassium hydroxide for 10 h (1:20 g ml⁻¹) at room temperature. The liquid fractions were collected and adjusted to pH 5.5–6.0 with acetic acid. Then, the neutral solution was concentrated and precipitated in ethanol (three equivalent volumes). After filtration, the precipitates were redissolved in distilled water and dialyzed against water. After the freeze-dried process, the KOH-extracted hemicelluloses were obtained (named H_{CK} and H_{C3H}, respectively).

Preparation of representative native lignin

To delineate the structural characteristics of the native lignin in the raw material, double enzymatic lignins (DELs) from CK and C3H were prepared. The detailed preparation process was according to our previous publications (Chen et al., 2017a; Ma et al., 2020). As shown in **Supplementary Figure S4**, the ball-milled powder (5 g) was mixed with the desired amount of sodium acetate buffer (pH 4.8) with a solid-to-liquid ratio of 1:20 (g/ml) and cellulase (35 FPU/g substrate). Then, the mixture

was incubated at 50°C in a rotary shaker with a rotational velocity of 150 rpm for 48 h. Next, the mixture was centrifuged and the residue was washed thoroughly with sodium acetate buffer (pH 4.8) to remove the hydrolyzed carbohydrates and then freeze-dried. Finally, the dried residual solid was repeatedly subjected to ball-milling for 2 h and enzymatic hydrolysis again, as in the abovementioned processes. After washing with acidic water (pH 2.0) and freeze-drying, DEL samples were obtained (named DEL_{CK} and DEL_{C3H}). To increase the solubility of lignin in tetrahydrofuran (THF) for the determination of molecular weights by GPC technique, the acetylation of lignin was performed as previously described (Wang et al., 2017). All experiments in this study were conducted in duplicate, and the results reported were the average values.

Methods

Sugar analysis (neutral sugars and uronic acids) was conducted by high-performance anion-exchange chromatography (HPAEC) in a Dionex ICS-3000 system (Dionex Corporation, Sunnyvale, CA, USA) equipped with a CarboPac PA1 (4 × 250 mm) column. The weight-average (*M_w*) and number-average (*M_n*) molecular weights of the samples were determined by gel permeation chromatography (GPC) (Agilent 1200, Agilent Technologies, Santa Clara, CA, USA) with an ultraviolet (UV) detector at 240 nm. The column used was a PL-gel 10 mm mixed-B 7.5 mm i.d. column, which was calibrated with PL polystyrene standards according to a previous report (Chen et al., 2017b). The NMR spectra of the samples were recorded at 25°C in DMSO-*d*₆ (or D₂O) on a Bruker AVIII 400 MHz spectrometer according to published procedures (Wen et al., 2013b; Wen et al., 2014). In detail, about 25 mg of lignin and hemicelluloses was dissolved in 0.5 ml of DMSO-*d*₆ and D₂O, respectively. For quantitative 2D-HSQC spectra, the Bruker standard pulse program hsqcetgpsi was used for HSQC experiments. The spectral widths were 5,000 Hz and 20,000 Hz for the ¹H- and ¹³C-dimensions, respectively. The number of collected complex points was 1,024 for ¹H-dimension with a recycle delay of 1.5 s. The number of transients was 64, and 256-time increments were always recorded in the ¹³C-dimension. The ¹J_{CH} used was 145 Hz. Prior to Fourier transformation, the data matrixes were zero filled up to 1,024 points in the ¹³C-dimension. Data processing was performed using standard Bruker Topspin-NMR software.

RESULTS AND DISCUSSION

Transcriptional abundance, plant height, and composition analysis

The inhibitory intensity of the gene is determined by detecting the expression level of the target gene at the transgenic plant. The expression of the transgene gene seriously affects the analysis of the subsequent result. Therefore, it is very important to detect the expression level of the transgenic gene. There are many ways to identify plant transgene expression at the transcriptional level, and a method for determining its specific mRNA is usually used. As shown in **Supplementary Figure S5**, the transcription level of the C3H gene in transgenic poplar was decreased in comparison

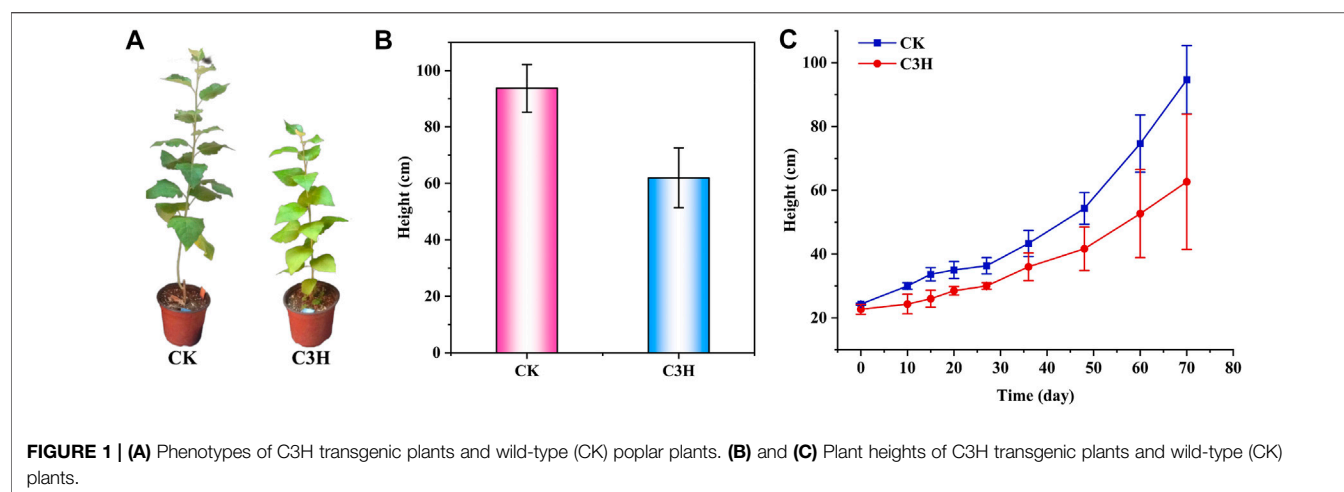


TABLE 1 | Composition analysis of CK and C3H.

Sample	Lignin ^a	Cellulose	Hemicelluloses
CK	25.94 ± 0.21	42.94 ± 0.32	22.15 ± 0.38
C3H	20.52 ± 0.38	44.29 ± 0.44	23.74 ± 0.42

^aLignin, Klason lignin.

with wild-type poplar (0.27). The expression of transgenic poplar was significantly reduced, and the average reduction was about 80%, indicating that the expression of the C3H gene was inhibited in transgenic CK.

According to **Figure 1B**, the plant height of wild-type plants (CK) was between 83 and 104 cm, the plant height of transgenic plants (C3H) was between 39 and 82 cm, and the average plant height was 61.93 cm. It was found that the height of transgenic poplars was lower than that of the CK, and the stems were browned to some extent (**Figures 1A–C**). Simultaneously, the results showed that the transgenic poplar woods had a significant decrease at different growth stages as compared to CK, and the height of C3H poplar decreased by about 34% under the same growing period. When the lignin synthetase was inhibited, it was bound to affect the growth of plant height, because lignin played a certain role in mechanical support. Hu and coauthors found that 4CL was a key gene lying upstream of C3H to adjust the lignin content (Hu et al., 1999). The 4CL suppression resulted in as much as a 45% reduction in total cell wall lignin and reportedly no impairment in growth (Hu et al., 1999). On the contrary, reductions in C3H resulted in varying effects on growth properties (Coleman et al., 2008). In this study, it was found that C3H downregulation could lead to the impairment in growth, which resulted in the relatively short plant height of C3H down-regulated poplar as compared to that of control (CK).

As shown in **Table 1**, regarding the chemical composition of CK and C3H, it was found that the content of Klason lignin in CK poplar wood was 25.94%, while the content of lignin was slightly decreased to 20.52% in C3H, which was slightly inconsistent with the previous reports (Pu et al., 2009; Ralph et al., 2012; Ma et al., 2021a). The reason for that was that C3H downregulation will

TABLE 2 | Monosaccharide content of the KOH-extracted hemicelluloses.

Sample	Molar composition (%)							
	Rha ^a	Ara	Gal	Glu	Xyl	Man	UA	UA/Xyl
H _{CK}	2.99	1.31	2.19	1.72	85.43	3.15	3.21	0.04
H _{C3H}	2.90	1.02	2.04	1.12	85.61	2.90	4.41	0.05

^aAbbreviation: Rha, rhamnose; Ara, arabinose; Gal, galactose; Glu, glucose; Xyl, xylose; UA, uronic acid.

inhibit the synthesis of lignin (Peng et al., 2016). By contrast, the contents of hemicelluloses and cellulose in the C3H-downregulated poplar woods slightly increased as compared to those of wild poplar (CK). In short, compositional analysis indicated that downregulation of C3H resulted in the slight changes of chemical composition of poplar wood, such as the decrease in lignin content.

Effects of C3H downregulation on the compositional and structural characteristics of hemicelluloses

Monosaccharide analysis of the hemicelluloses

To survey the structural differences of the hemicelluloses during the C3H downregulation process, the scheme of hemicellulose isolation is illustrated in **Supplementary Figure S3**. Hemicelluloses are consisted of pentose and hexose, such as arabinose, rhamnose, glucose, xylose, mannose, galactose, and a small amount of glucuronic acid and galacturonic acid (Peng et al., 2012; Peng et al., 2009). **Table 2** shows the neutral sugar and uronic acid contents of the CK and C3H hemicellulose samples. As illustrated in **Table 2**, the main glycosyl units of the hemicellulose were xylose (85.43%–85.61%), containing glucose (1.12%–1.72%), mannose (2.90%–3.15%), uronic acid (3.21%–4.41%), and a little of rhamnose (2.90%–2.99%), arabinose (1.02%–1.31%), and galactose (2.04%–2.19%), respectively. The xylose content of H_{CK} and H_{C3H} was 85.43% and 85.61%, respectively. Additionally, these hemicelluloses also contain 3.21% and 4.41% uronic acid

TABLE 3 | Weight-average (M_w) and number-average (M_n) molecular weights and polydispersity (M_w/M_n) of the hemicelluloses and lignin fractions.

	H _{CK}	H _{C3H}	DEL _{CK}	DEL _{C3H}
M_w	30,720	39,800	8,020	7,410
M_n	14,600	21,150	4,220	4,080
M_w/M_n	2.10	1.88	1.90	1.81

(UA), indicating that H_{CK} and H_{C3H} mainly belonged to glucuronic acid-type xylan, and the other glycosyl groups can serve as a side chain attached to the main chain. A recent publication regarding the hardwood hemicelluloses demonstrated that hemicelluloses from hardwood were mainly composed of xylan-type and small amounts of mannan-type hemicelluloses (Qaseem et al., 2021). However, in this study, the monosaccharide analysis of the hemicelluloses showed that KOH-extracted hemicelluloses were principally the xylan-type hemicelluloses. This discrepancy is probably related to the tree species and the extraction method of hemicelluloses. However, the detailed composition and structural features of the hemicelluloses still need to be confirmed *via* NMR characterization. Additionally, the ratio of uronic acid to xylose (UA/Xyl) can contribute to understanding the degree of linearity or branching of hemicelluloses (Wen et al., 2010; Peng et al., 2012). It can be seen from the uronic acid/xylose ratio that H_{C3H} (UA/Xyl, 0.04) had a more linear chain than H_{CK} (UA/Xyl, 0.05), implying that hemicelluloses from C3H-downregulated poplar wood had more linear structures. However, the differences in monosaccharide components of hemicelluloses from CK and C3H were not particularly pronounced. The structural characteristics of the hemicellulose from CK and C3H down-regulated poplar wood samples will be discussed in the following NMR analysis.

Molecular weights and NMR analysis of the hemicelluloses

The weight-average molecular weight (M_w), number-average molecular weight (M_n), and polydispersity (M_w/M_n) of the hemicelluloses are shown in **Table 3**. The M_w of H_{CK} and H_{C3H} were 30,720, and 39,800 g/mol, indicating that the M_w of H_{CK} was less than that of H_{C3H}. The polydispersity index (PDI) of H_{CK} (2.10) was higher than that of H_{C3H} (1.88), implying that H_{C3H} has a narrow molecular weight distribution and H_{C3H} exhibits a relatively homogeneous structure.

For further understanding of the structural characteristics of hemicelluloses, H_{CK} and H_{C3H} were characterized by NMR techniques (Peng et al., 2010; Wen et al., 2010; Bian et al., 2012). The NMR techniques can obtain valuable information about the backbone of the hemicelluloses and their branching side chains. **Figure 2** shows the ¹³C NMR spectra of the CK and C3H hemicelluloses (H_{CK} and H_{C3H}). For ¹³C NMR spectra, all hemicelluloses had strong signals at 74.92, 63.35, 75.99, 73.32, and 102.34 ppm, which were characteristic of the C-3, C-5, C-4, C-2, and C-1 positions of the (1→4)-linked-β-D-xylopyranoside units. Additionally, the -OCH₃, C-2, C-4, C-3, C-1, C-6, and C-5

of the 4-O-methyl-α-glucuronic acid units were located at 59.60, 71.86, 82.64, 72.39, 97.55, 177.03, and 72.25 ppm, respectively. The hemicelluloses from CK and C3H-downregulated poplar wood exhibited similar chemical shifts, suggesting that these hemicelluloses had the same structural characteristics. Especially, as compared with H_{CK}, the ¹³C NMR spectra of H_{C3H} showed a weak signal at 168.41 ppm, which was the characteristic signal of the free *p*-hydroxybenzoic acid (PB). This phenomenon suggested that the C3H-downregulated poplar contained more *p*-hydroxybenzoic acid, which will also be demonstrated by 2D-HSQC NMR below. In fact, C3H poplar wood contained more PB units (especially for lignin); thus, a bit of *p*-hydroxybenzoic acid in the cell wall after KOH extraction was co-precipitated with the hemicelluloses.

To further uncover the molecular structural characteristics of H_{CK} and H_{C3H}, the 2D-HSQC NMR spectral analysis of these hemicelluloses was performed and the spectra were assigned according to the previous publication (Wen et al., 2010). As shown in **Figure 3**, the prominent signals corresponding to the (1→4)-β-D-Xylp backbone and 4-O-Me-α-D-GlcpA side chain in all the spectra were found. Especially, the main cross-peaks of C₁-H₁, C₄-H₄, C₃-H₃, C₂-H₂, and C₅-H₅ of the (1→4)-linked-β-D-Xylp units were distributed at δC/δH 102.2/4.28, 76.0/3.63, 75.0/3.34, 73.1/3.13, 63.2/3.93, and 3.27. Additionally, a distinguishable cross-peak at 60.1/3.32 was assigned to the methoxy group (-OCH₃) in 4-O-methyl-D-glucuronic acid. For 4-O-methyl-D-glucuronic acid, the signals appear at δC/δH 97.31/5.14 (C₁-H₁) and δC/δH 71.6/3.41 (C₂-H₂), δC/δH 72.16/3.62 (C₃-H₃), δC/δH 82.48/3.07 (C₄-H₄), δC/δH 72.0/4.20 (C₅-H₅) (Yuan et al., 2010). According to the existing literature concerning the NMR linkages between the monosaccharides (Peng et al., 2010), it could be found that the KOH-extracted hemicelluloses from these poplar woods were mainly composed of a linear backbone of (β-1→4)-Xylp residues, and the xylose was substituted by 4-O-methyl-α-D-GlcpA at the C₂ position. Based on the results of NMR and sugar analysis of the hemicelluloses, it was suggested that H_{CK} and H_{C3H} were mainly composed of the 4-O-Me-α-D-GlcpA side chains attached to a linear backbone of (1→4)-β-D-Xylp.

Effects of C3H downregulation on the molecular weights and structural characteristics of native lignin

In fact, C3H downregulation mainly affects the biosynthesis of the lignin macromolecule. Herein, the effects of C3H downregulation on the molecular weights and structural characteristics of native lignin were investigated and discussed in detail. The M_w and M_n and polydispersity index (M_w/M_n) of DEL_{CK} and DEL_{C3H} are displayed in **Table 3**. The M_w of DEL_{CK} and DEL_{C3H} was 8,020 and 7,410 g/mol, respectively. The higher M_w of lignin was partly related to the relatively high β-O-4 content, as observed previously (Wen et al., 2013). DEL_{C3H} had relatively lower molecular weight distributions (1.81) as compared to DEL_{CK} (1.90), implying that the downregulation of C3H facilitates the formation of relatively homogeneous lignin

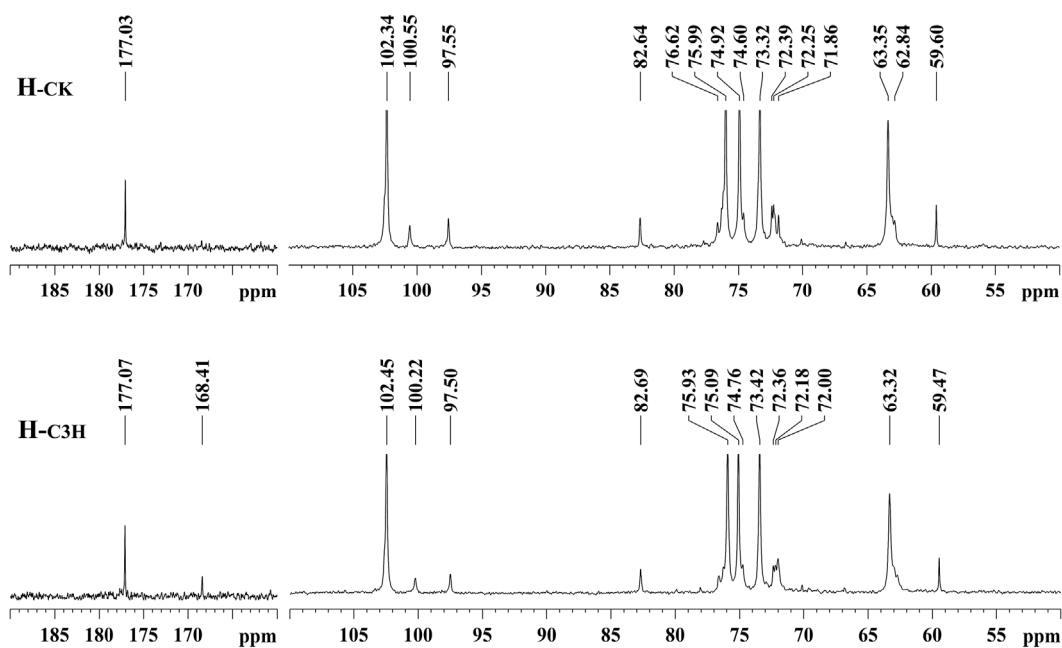


FIGURE 2 | ^{13}C NMR spectra of the hemicelluloses.

fractions. This phenomenon was similar to that of hemicellulose, implying that downregulation of C3H led to the homogenization of biomacromolecules.

To demonstrate the structural differences of native lignin between control 84K poplar (CK) and C3H-downregulated poplar (C3H) samples, the lignin samples were analyzed by the 2D HSQC NMR technique. These differences could provide some fundamental basis for obtaining ideal lignin sources for subsequent lignin valorization (Wen et al., 2013a). **Figure 4** shows the chemical composition (aromatic region) and interunit linkages (side-chain region) in the 2D-HSQC spectra of DEL_{CK} and DEL_{C3H} according to the previous signal assignments (Wen et al., 2015). In the side-chain regions ($\delta\text{C}/\delta\text{H}$ 49–92/2.5–5.7) of the 2D-HSQC spectra, the linkages of β -O-4 aryl ethers (A), resinols (B), and phenylcoumarans (C) could be obviously observed. It was found that DEL_{C3H} and DEL_{CK} exhibited similar but discriminative spectral patterns. Cross-signals of β -O-4 and -OCH₃ ($\delta\text{C}/\delta\text{H}$ 55.7/3.70) were the prominent signals. $\delta\text{C}/\delta\text{H}$ 71.9/4.87 were cross-signals of C $_{\alpha}$ -H $_{\alpha}$ correlations in the β -O-4 linkages, while the β -O-4 linkages (C $_{\beta}$ -H $_{\beta}$) linked to G and S units can be distinguished at $\delta\text{C}/\delta\text{H}$ 83.5/4.34 and 85.7/4.12. $\delta\text{C}/\delta\text{H}$ 59.5/3.71–3.40 was assigned C $_{\gamma}$ -H $_{\gamma}$ correlations in the β -O-4 substructures. Meanwhile, the content of β -O-4 linkages in DEL_{C3H} was higher than that of DEL_{CK}, which was consistent with the results in a previous publication (Ma et al., 2021a). In addition, $\delta\text{C}/\delta\text{H}$ 62.9/4.40 was assigned C $_{\gamma}$ -H $_{\gamma}$ correlations in γ -acylated lignin units (A'). This indicated that those lignin samples were partially γ -carbon acylated in β -O-4 aryl ether linkages and *p*-hydroxybenzoates (PB). In a recent publication, whether *p*-hydroxybenzoates acylate solely S units in transgenics poplar has not been

confirmed (Ralph et al., 2012). Resinols (β - β , substructures B) can be easily identified in the spectra in conspicuous amounts. $\delta\text{C}/\delta\text{H}$ 84.8/4.67, 53.4/3.04, and 71.1/3.80–4.19 were assigned their C $_{\alpha}$ -H $_{\alpha}$, C $_{\beta}$ -H $_{\beta}$ and the double C $_{\gamma}$ -H $_{\gamma}$ correlations, respectively. The weak signal of C $_{\alpha}$ -H $_{\alpha}$ correlations of phenylcoumarans (β -5, $\delta\text{C}/\delta\text{H}$, 86.8/5.49) suggested that the low content of β -5 linkages (DEL_{CK} 1.18/100Ar, DEL_{C3H} 1.14/100Ar). This phenomenon could be attributed to the reduction of G units (relative to per 100Ar) as compared to that of CK based on a publication (Wang et al., 2018), in which it was reported that phenylcoumaran (β -5) was derived from the coupling of a monolignol with G units.

In the aromatic regions ($\delta\text{C}/\delta\text{H}$ 100–135/5.7–8.0) of the 2D-HSQC NMR spectra (**Figure 4**), the chemical composition in the lignin samples (DEL_{CK} and DEL_{C3H}) can be clearly observed, such as syringyl (S) and guaiacyl (G) lignin units and some other lignin substructures. The C $_{2,6}$ -H $_{2,6}$ correlation at $\delta\text{C}/\delta\text{H}$ 103.8/6.68 represented the prominent signal for S-type lignin units, whereas the signal at $\delta\text{C}/\delta\text{H}$ 106.2/7.18 was observed for the C $_{\alpha}$ -oxidized S-units (S'). Additionally, the different correlations of C $_{2}$ -H $_{2}$ ($\delta\text{C}/\delta\text{H}$ 110.9/6.97), C $_{5}$ -H $_{5}$ ($\delta\text{C}/\delta\text{H}$ 114.8/6.77), and C $_{6}$ -H $_{6}$ ($\delta\text{C}/\delta\text{H}$ 118.8/6.78) belonged to G-type lignin units. Specially, H $_{2,6}$ signals were detected at $\delta\text{C}/\delta\text{H}$ 127.7/7.15, which increased from 0.6 to 1.1/100Ar, suggesting a striking elevation of *p*-hydroxyphenyl (H) units in transgenic poplar. The relative abundances of different linkages in lignin were quantified according to the previous literatures (Ma et al., 2021a; Wen et al., 2013a). The changes of the S/G ratio can intuitively reflect the compositional change of lignin samples. As is shown in **Table 4**, the S/G ratio in DEL_{CK} was 2.82, while the S/G ratio for DEL_{C3H} was 2.48. Interestingly, the relative content

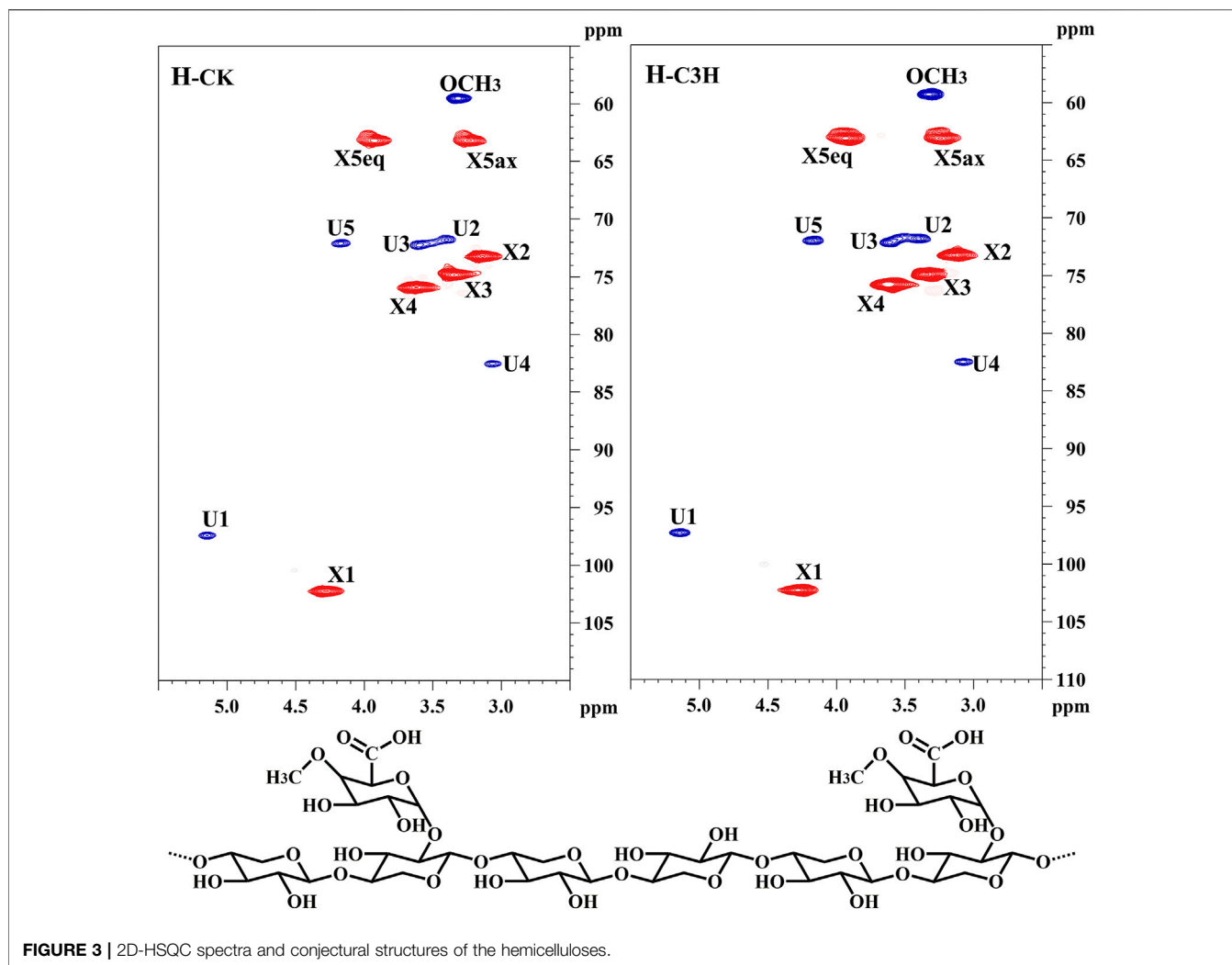


FIGURE 3 | 2D-HSQC spectra and conjectural structures of the hemicelluloses.

of H-type lignin in DEL_{C3H} (1.11/100Ar) was higher than that in DEL_{CK} (0.6/100Ar). This fact suggested that H-type lignin units have been elevated in C3H-downregulated poplar. Similarly, this phenomenon had been reported in a previous study, in which the increased amount of *p*-hydroxyphenyl unit was observed as well as a concomitant decrease of guaiacyl and syringyl units (Pu et al., 2009). In this study, the spectra shown in **Figure 4** clearly showed the enhancement of PB content in DEL_{C3H}. Precisely, the integral value of PB increased from 14.17 to 16.37/100Ar (as shown in **Table 4**), which was in agreement with a previous study (Ralph et al., 2012). In short, the C3H downregulated could increase the content of H units and *p*-hydroxybenzoate (PB) units in lignin. These results were also in line with the ¹³C-NMR section of H-C_{3H}, in which more PB units were detected. In short, 2D-HSQC spectra of native lignin and hemicellulose samples demonstrated that C3H downregulation indeed altered the chemical and structural features of these natural macromolecules to different extents. Due to these differences in composition and structure, the processing performance of transgenic poplar wood will be affected and the corresponding investigations are being explored.

Implications

The elevated lignin in the *p*-hydroxyphenyl (H) unit is produced by the downregulation of C3H in poplar wood, and the lignin content is also significantly reduced. A previous study investigated the effects of C3H downregulation on the lignin in alfalfa (Ralph et al., 2006). Ralph and coauthors found that the lignins rich in *p*-hydroxyphenyl units were produced by C3H downregulation, but the S/G ratio changed only slightly in alfalfa. Conversely, the S/G ratio of lignin was increased in the C3H downregulation poplar. Most of the relative H unit elevation was at the expense of G units rather than S units in poplar (Ralph et al., 2012). In general, genetic modification during lignin biosynthesis led to dwarfing or developmental abnormalities of the transgenic plants (Bonawitz and Chapple, 2013). However, with the growth and development of the plant, the transgenic poplar probably restores growth if there is an active cell wall feedback signaling responsible for dwarfing existing in lignin-deficient mutants (Bonawitz and Chapple, 2013). Simultaneously, as a pendant group, the PB content in lignin was increased in C3H poplar as compared to CK wood. However, the related transferase in poplar has not been identified. The identified transferase will



Sample	DEL _{CK}	DEL _{C3H}
β-O-4 ^a	57.79	56.78
β-β	13.02	10.76
β-5	1.18	1.14
PB	14.17	16.37
S/G ^b	2.82	2.48
S/G/H	73.4/26/0.6	70.5/28.4/1.1

^bS/G ratio obtained by this equation: S/G ratio = 0.5I (S_{2,6})/I (G₂).

CONCLUSION

of H_{CK} was more than that of H_{C3H} . Meanwhile, the downregulation of C3H could decrease the lignin content. Results showed that native lignin of CK and C3H exhibited similar structural features; nevertheless, transgenic poplars had relatively lower contents of β -O-4 linkages and S/G ratios as well as a relatively higher content of H-type lignin units. Furthermore, the content of PB content in poplar wood was increased in the lignin from C3H-downregulated poplar. In short, understanding the structural characteristics of native hemicelluloses and lignin from control and transgenic poplar is conducive to selecting optimal hemicelluloses and lignin characteristics required for downstream applications and utilization of lignocellulosic materials in the biorefinery strategy.

DATA AVAILABILITY STATEMENT

The original contributions presented in the study are included in the article/**Supplementary Material**; further inquiries can be directed to the corresponding authors.

AUTHOR CONTRIBUTIONS

C-YM and J-LW contributed to conception and design of the study. X-PP and C-YM operated the experiment, performed statistical analysis and wrote the first draft of the manuscript. C-YM, JB, S-QY, and J-LW wrote sections of the manuscript. All

authors contributed to manuscript revision and read and approved the submitted version.

FUNDING

This work was supported by the National Key Program on Transgenic Research (2018ZX08020002), the National Natural Science Foundation of China (31872698; 32071854), Beijing Forestry University Outstanding Young Talent Cultivation Project (2019JQ03006), the Foundation of Guangxi Key Laboratory of Clean Pulp and Papermaking and Pollution

REFERENCES

- Alvira, P., Tomás-Pejó, E., Ballesteros, M., and Negro, M. J. (2010). Pretreatment Technologies for an Efficient Bioethanol Production Process Based on Enzymatic Hydrolysis: A Review. *Bioresour. Technol.* 101 (13), 4851–4861. doi:10.1016/j.biortech.2009.11.093
- Bian, J., Peng, F., Peng, P., Xu, F., and Sun, R.-C. (2012). Chemical Composition and Structural Feature of *Populus Gansuensis* Hemicellulosic Polymers. *J. Appl. Polym. Sci.* 124 (4), 3154–3164. doi:10.1002/app.34835
- Boerjan, W., Ralph, J., and Baucher, M. (2003). Lignin Biosynthesis. *Annu. Rev. Plant Biol.* 54 (1), 519–546. doi:10.1146/annurev.arplant.54.031902.134938
- Bonawitz, N. D., and Chapple, C. (2013). Can Genetic Engineering of Lignin Deposition Be Accomplished without an Unacceptable Yield Penalty? *Curr. Opin. Biotechnol.* 24 (2), 336–343. doi:10.1016/j.copbio.2012.11.004
- Chen, T.-Y., Wang, B., Wu, Y.-Y., Wen, J.-L., Liu, C.-F., Yuan, T.-Q., et al. (2017a). Structural Variations of Lignin Macromolecule from Different Growth Years of Triploid of *Populus tomentosa* Carr. *Int. J. Biol. Macromolecules* 101, 747–757. doi:10.1016/j.ijbiomac.2017.03.146
- Chen, T.-Y., Wen, J.-L., Wang, B., Wang, H.-M., Liu, C.-F., and Sun, R.-C. (2017b). Assessment of Integrated Process Based on Autohydrolysis and Robust Delignification Process for Enzymatic Saccharification of Bamboo. *Bioresour. Technol.* 244, 717–725. doi:10.1016/j.biortech.2017.08.032
- Coleman, H. D., Samuels, A. L., Guy, R. D., and Mansfield, S. D. (2008). Perturbed Lignification Impacts Tree Growth in Hybrid Poplar-A Function of Sink Strength, Vascular Integrity, and Photosynthetic Assimilation. *Plant Physiol.* 148 (3), 1229–1237. doi:10.1104/pp.108.125500
- de Souza, R. O. M. A., Miranda, L. S. M., and Luque, R. (2014). Bio(chemo) technological Strategies for Biomass Conversion into Bioethanol and Key Carboxylic Acids. *Green. Chem.* 16 (5), 2386–2405. doi:10.1039/c3gc41885e
- Ding, S.-Y., Liu, Y.-S., Zeng, Y., Himmel, M. E., Baker, J. O., and Bayer, E. A. (2012). How Does Plant Cell wall Nanoscale Architecture Correlate with Enzymatic Digestibility? *Science* 338 (6110), 1055–1060. doi:10.1126/science.1227491
- Franke, R., Hemm, M. R., Denault, J. W., Ruegger, M. O., Humphreys, J. M., and Chapple, C. (2002a). Changes in Secondary Metabolism and Deposition of an Unusual Lignin in the Ref8 Mutant of *Arabidopsis*. *Plant J.* 30 (1), 47–59. doi:10.1046/j.1365-3113x.2002.01267.x
- Franke, R., Humphreys, J. M., Hemm, M. R., Denault, J. W., Ruegger, M. O., Cusumano, J. C., et al. (2002b). The *Arabidopsis* REF8 Gene Encodes the 3-Hydroxylase of Phenylpropanoid Metabolism. *Plant J.* 30 (1), 33–45. doi:10.1046/j.1365-3113x.2002.01266.x
- Himmel, M. E., Ding, S.-Y., Johnson, D. K., Adney, W. S., Nimlos, M. R., Brady, J. W., et al. (2007). Biomass Recalcitrance: Engineering Plants and Enzymes for Biofuels Production. *Science* 315 (5813), 804–807. doi:10.1126/science.1137016
- Hu, W.-J., Harding, S. A., Lung, J., Popko, J. L., Ralph, J., Stokke, D. D., et al. (1999). Repression of Lignin Biosynthesis Promotes Cellulose Accumulation and Growth in Transgenic Trees. *Nat. Biotechnol.* 17 (8), 808–812. doi:10.1038/11758
- Isikgor, F. H., and Becer, C. R. (2015). Lignocellulosic Biomass: A Sustainable Platform for the Production of Bio-Based Chemicals and Polymers. *Polym. Chem.* 6 (25), 4497–4559. doi:10.1039/c5py00263j
- Ma, C.-Y., Gao, X., Peng, X.-P., Gao, Y.-F., Liu, J., Wen, J.-L., et al. (2021a). Microwave-Assisted Deep Eutectic Solvents (DES) Pretreatment of Control and Transgenic Poplars for Boosting the Lignin Valorization and Cellulose Bioconversion. *Ind. Crops Prod.* 164, 113415. doi:10.1016/j.indcrop.2021.113415
- Ma, C.-Y., Wang, H.-M., Wen, J.-L., Shi, Q., Wang, S.-F., Yuan, T.-Q., et al. (2020). Structural Elucidation of Lignin Macromolecule from Abaca during Alkaline Hydrogen Peroxide Delignification. *Int. J. Biol. Macromolecules* 144, 596–602. doi:10.1016/j.ijbiomac.2019.12.080
- Ma, C.-Y., Xu, L.-H., Zhang, C., Guo, K.-N., Yuan, T.-Q., and Wen, J.-L. (2021b). A Synergistic Hydrothermal-Deep Eutectic Solvent (DES) Pretreatment for Rapid Fractionation and Targeted Valorization of Hemicelluloses and Cellulose from Poplar Wood. *Bioresour. Technol.* 341, 125828. doi:10.1016/j.biortech.2021.125828
- Peng, F., Peng, P., Xu, F., and Sun, R.-C. (2012). Fractional Purification and Bioconversion of Hemicelluloses. *Biotechnol. Adv.* 30 (4), 879–903. doi:10.1016/j.biotechadv.2012.01.018
- Peng, F., Ren, J.-L., Xu, F., Bian, J., Peng, P., and Sun, R.-C. (2009). Comparative Study of Hemicelluloses Obtained by Graded Ethanol Precipitation from Sugarcane Bagasse. *J. Agric. Food Chem.* 57 (14), 6305–6317. doi:10.1021/jf900986b
- Peng, F., Ren, J.-L., Xu, F., Bian, J., Peng, P., and Sun, R.-C. (2010). Fractionation of Alkali-Solubilized Hemicelluloses from Delignified *Populus Gansuensis*: Structure and Properties. *J. Agric. Food Chem.* 58 (9), 5743–5750. doi:10.1021/jf1003368
- Peng, X.-P., Sun, S.-L., Wen, J.-L., Yin, W.-L., and Sun, R.-C. (2014). Structural Characterization of Lignins from Hydroxycinnamoyl Transferase (HCT) Down-Regulated Transgenic Poplars. *Fuel* 134, 485–492. doi:10.1016/j.fuel.2014.05.069
- Peng, X.-P., Wang, B., Wen, J.-L., Yang, S.-Z., Lu, M.-Z., and Sun, R.-C. (2016). Effects of Genetic Manipulation (HCT and C3H Down-Regulation) on Molecular Characteristics of Lignin and its Bioconversion to Fermentable Sugars. *Cellulose Chem. Technol.* 50, 649–658.
- Pilate, G., Guiney, E., Holt, K., Petit-Conil, M., Lapierre, C., Leplé, J.-C., et al. (2002). Field and Pulping Performances of Transgenic Trees with Altered Lignification. *Nat. Biotechnol.* 20 (6), 607–612. doi:10.1038/nbt0602-607
- Pu, Y., Hu, F., Huang, F., Davison, B. H., and Ragauskas, A. J. (2013). Assessing the Molecular Structure Basis for Biomass Recalcitrance during Dilute Acid and Hydrothermal Pretreatments. *Biotechnol. Biofuels* 6 (1), 15–13. doi:10.1186/1754-6834-6-15
- Pu, Y., Chen, F., Ziebell, A., Davison, B. H., and Ragauskas, A. J. (2009). NMR Characterization of C3H and HCT Down-Regulated Alfalfa Lignin. *Bioenerg. Res.* 2 (4), 198–208. doi:10.1007/s12155-009-9056-8
- Qaseem, M. F., Shaheen, H., and Wu, A.-M. (2021). Cell Wall Hemicellulose for Sustainable Industrial Utilization. *Renew. Sustain. Energy Rev.* 144, 110996. doi:10.1016/j.rser.2021.110996
- Ragauskas, A. J., Beckham, G. T., Biddy, M. J., Chandra, R., Chen, F., Davis, M. F., et al. (2014). Lignin Valorization: Improving Lignin Processing in the Biorefinery. *Science* 344 (6185), 1246843. doi:10.1126/science.1246843
- Ragauskas, A. J., Williams, C. K., Davison, B. H., Britovsek, G., Cairney, J., Eckert, C. A., et al. (2006). The Path Forward for Biofuels and Biomaterials. *Science* 311 (5760), 484–489. doi:10.1126/science.1114736

SUPPLEMENTARY MATERIAL

The Supplementary Material for this article can be found online at: <https://www.frontiersin.org/articles/10.3389/fbioe.2021.790539/full#supplementary-material>

- Ralph, J., Akiyama, T., Coleman, H. D., and Mansfield, S. D. (2012). Effects on Lignin Structure of Coumarate 3-Hydroxylase Downregulation in Poplar. *Bioenerg. Res.* 5 (4), 1009–1019. doi:10.1007/s12155-012-9218-y
- Ralph, J., Akiyama, T., Kim, H., Lu, F., Schatz, P. F., Marita, J. M., et al. (2006). Effects of Coumarate 3-Hydroxylase Down-Regulation on Lignin Structure. *J. Biol. Chem.* 281 (13), 8843–8853. doi:10.1074/jbc.m511598200
- Rinaldi, R., Jastrzebski, R., Clough, M. T., Ralph, J., Kennema, M., Bruijninckx, P. C. A., et al. (2016). Paving the Way for Lignin Valorisation: Recent Advances in Bioengineering, Biorefining and Catalysis. *Angew. Chem. Int. Ed.* 55 (29), 8164–8215. doi:10.1002/anie.201510351
- Sanderson, K. (2011). Lignocellulose: A Chewy Problem. *Nature* 474 (7352), S12–S14. doi:10.1038/474s012a
- Sikarwar, V. S., Zhao, M., Clough, P., Yao, J., Zhong, X., Memon, M. Z., et al. (2016). An Overview of Advances in Biomass Gasification. *Energy Environ. Sci.* 9 (10), 2939–2977. doi:10.1039/c6ee00935b
- Simmons, B. A., Loqué, D., and Ralph, J. (2010). Advances in Modifying Lignin for Enhanced Biofuel Production. *Curr. Opin. Plant Biol.* 13 (3), 312–319. doi:10.1016/j.pbi.2010.03.001
- Sluiter, A., Hames, B., Ruiz, R., Scarlata, C., Sluiter, J., Templeton, D., et al. (2008). Determination of Structural Carbohydrates and Lignin in Biomass. *Lab. Anal. procedure* 1617 (1), 1–16.
- Stephanopoulos, G. (2007). Challenges in Engineering Microbes for Biofuels Production. *Science* 315 (5813), 801–804. doi:10.1126/science.1139612
- Sun, S., Sun, S., Cao, X., and Sun, R. (2016). The Role of Pretreatment in Improving the Enzymatic Hydrolysis of Lignocellulosic Materials. *Bioresour. Technol.* 199, 49–58. doi:10.1016/j.biortech.2015.08.061
- Vanholme, R., De Meester, B., Ralph, J., and Boerjan, W. (2019). Lignin Biosynthesis and its Integration into Metabolism. *Curr. Opin. Biotechnol.* 56, 230–239. doi:10.1016/j.copbio.2019.02.018
- Vanholme, R., Morreel, K., Darrah, C., Oyarce, P., Grabber, J. H., Ralph, J., et al. (2012a). Metabolic Engineering of Novel Lignin in Biomass Crops. *New Phytol.* 196 (4), 978–1000. doi:10.1111/j.1469-8137.2012.04337.x
- Vanholme, R., Storme, V., Vanholme, B., Sundin, L., Christensen, J. H., Goeminne, G., et al. (2012b). A Systems Biology View of Responses to Lignin Biosynthesis Perturbations in Arabidopsis. *The Plant Cell* 24 (9), 3506–3529. doi:10.1105/tpc.112.102574
- Wagner, M. S., Wajner, S. M., Dora, J. M., and Maia, A. L. (2007). Regulation of Dio2 Gene Expression by Thyroid Hormones in Normal and Type 1 Deiodinase-Deficient C3H Mice. *J. Endocrinol.* 193 (3), 435–444. doi:10.1677/joe-07-0099
- Wang, H.-M., Wang, B., Wen, J.-L., Wang, S.-F., Shi, Q., and Sun, R.-C. (2018). Green and Efficient Conversion Strategy of Eucalyptus Based on Mechanochemical Pretreatment. *Energy Convers. Manage.* 175, 112–120. doi:10.1016/j.enconman.2018.09.002
- Wang, H.-M., Wang, B., Wen, J.-L., Yuan, T.-Q., and Sun, R.-C. (2017). Structural Characteristics of Lignin Macromolecules from Different Eucalyptus Species. *ACS Sustain. Chem. Eng.* 5 (12), 11618–11627. doi:10.1021/acsschemeng.7b02970
- Wang, H.-M., Wang, B., Yuan, T.-Q., Zheng, L., Shi, Q., Wang, S.-F., et al. (2020). Tunable, UV-Shielding and Biodegradable Composites Based on Well-Characterized Lignins and Poly(Butylene Adipate-Co-Terephthalate). *Green. Chem.* 22 (24), 8623–8632. doi:10.1039/d0gc03284k
- Wang, H., Wang, B., Sun, D., Shi, Q., Zheng, L., Wang, S., et al. (2019). Unraveling the Fate of Lignin from Eucalyptus and Poplar during Integrated Delignification and Bleaching. *ChemSusChem* 12 (5), 1059–1068. doi:10.1002/cssc.201802592
- Wen, J.-L., Sun, S.-L., Xue, B.-L., and Sun, R.-C. (2013a). Quantitative Structural Characterization of the Lignins from the Stem and Pith of Bamboo (*Phyllostachys Pubescens*). *Holzforschung* 67 (6), 613–627. doi:10.1515/hf-2012-0162
- Wen, J.-L., Sun, S.-L., Xue, B.-L., and Sun, R.-C. (2013b). Quantitative Structures and Thermal Properties of Birch Lignins after Ionic Liquid Pretreatment. *J. Agric. Food Chem.* 61 (3), 635–645. doi:10.1021/jf3051939
- Wen, J.-L., Sun, S.-L., Yuan, T.-Q., and Sun, R.-C. (2015). Structural Elucidation of Whole Lignin from Eucalyptus Based on Preswelling and Enzymatic Hydrolysis. *Green. Chem.* 17 (3), 1589–1596. doi:10.1039/c4gc01889c
- Wen, J.-L., Sun, S.-L., Yuan, T.-Q., Xu, F., and Sun, R.-C. (2014). Understanding the Chemical and Structural Transformations of Lignin Macromolecule during Torrefaction. *Appl. Energy* 121, 1–9. doi:10.1016/j.apenergy.2014.02.001
- Wen, J.-L., Sun, Y.-C., Xu, F., and Sun, R.-C. (2010). Fractional Isolation and Chemical Structure of Hemicellulosic Polymers Obtained from Bambusa Rigida Species. *J. Agric. Food Chem.* 58 (21), 11372–11383. doi:10.1021/jf1032153
- Wen, J.-L., Xue, B.-L., Xu, F., Sun, R.-C., and Pinkert, A. (2013). Unmasking the Structural Features and Property of Lignin from Bamboo. *Ind. Crops Prod.* 42, 332–343. doi:10.1016/j.indcrop.2012.05.041
- Yang, L., Lin, M., Zhang, H., Wang, C., Shi, L., Lan, W., et al. (2021). Ferulate-Sinapyl Alcohol Cross-Coupling Reaction Improves the Understanding of Grass Cell Wall Lignification. *Ind. Crops Prod.* 168, 113587. doi:10.1016/j.indcrop.2021.113587
- Yuan, T.-Q., Xu, F., He, J., and Sun, R.-C. (2010). Structural and Physico-Chemical Characterization of Hemicelluloses from Ultrasound-Assisted Extractions of Partially Delignified Fast-Growing Poplar Wood through Organic Solvent and Alkaline Solutions. *Biotechnol. Adv.* 28 (5), 583–593. doi:10.1016/j.biotechadv.2010.05.016
- Zhao, C., Hu, Z., Shi, L., Wang, C., Yue, F., Li, S., et al. (2020). Profiling of the Formation of Lignin-Derived Monomers and Dimers from Eucalyptus Alkali Lignin. *Green. Chem.* 22 (21), 7366–7375. doi:10.1039/d0gc01658f
- Zhao, X., Zhang, L., and Liu, D. (2012). Biomass Recalcitrance. Part I: The Chemical Compositions and Physical Structures Affecting the Enzymatic Hydrolysis of Lignocellulose. *Biofuels, Bioprod. Bioref.* 6 (4), 465–482. doi:10.1002/bbb.1331
- Zheng, Y., Yu, Y., Lin, W., Jin, Y., Yong, Q., and Huang, C. (2021). Enhancing the Enzymatic Digestibility of Bamboo Residues by Biphasic Phenoxymethanol-Acid Pretreatment. *Bioresour. Technol.* 325, 124691. doi:10.1016/j.biortech.2021.124691
- Zhou, C.-H., Xia, X., Lin, C.-X., Tong, D.-S., and Beltrami, J. (2011). Catalytic Conversion of Lignocellulosic Biomass to Fine Chemicals and Fuels. *Chem. Soc. Rev.* 40 (11), 5588–5617. doi:10.1039/c1cs15124j
- Zhu, J. Y., and Pan, X. J. (2010). Woody Biomass Pretreatment for Cellulosic Ethanol Production: Technology and Energy Consumption Evaluation☆. *Bioresour. Technol.* 101 (13), 4992–5002. doi:10.1016/j.biortech.2009.11.007

Conflict of Interest: The authors declare that the research was conducted in the absence of any commercial or financial relationships that could be construed as a potential conflict of interest.

Publisher's Note: All claims expressed in this article are solely those of the authors and do not necessarily represent those of their affiliated organizations, or those of the publisher, the editors, and the reviewers. Any product that may be evaluated in this article, or claim that may be made by its manufacturer, is not guaranteed or endorsed by the publisher.

Copyright © 2021 Peng, Bian, Yao, Ma and Wen. This is an open-access article distributed under the terms of the Creative Commons Attribution License (CC BY). The use, distribution or reproduction in other forums is permitted, provided the original author(s) and the copyright owner(s) are credited and that the original publication in this journal is cited, in accordance with accepted academic practice. No use, distribution or reproduction is permitted which does not comply with these terms.



Research Progress on Cell Membrane-Coated Biomimetic Delivery Systems

Mengyu Guo^{1,2}, Chenjie Xia^{1,2†}, Yu Wu^{1,2}, Nong Zhou^{3†*}, Zhipeng Chen^{1,2} and Weidong Li^{1,2*}

¹College of Pharmacy, Nanjing University of Chinese Medicine, Nanjing, China, ²Engineering Center of State Ministry of Education for Standardization of Chinese Medicine Processing, Nanjing University of Chinese Medicine, Nanjing, China, ³The Chongqing Engineering Laboratory for Green Cultivation and Deep Processing of Three Gorges Reservoir Area's Medicinal Herbs, College of Food and Biology Engineering, Chongqing Three Gorges University, Chongqing, China

OPEN ACCESS

Edited by:

Tajalli Keshavarz,
University of Westminster,
United Kingdom

Reviewed by:

Anna Rafaela Cavalcante Braga,
Federal University of São Paulo, Brazil
Miguel Ladero,
Complutense University of Madrid,
Spain

*Correspondence:

Nong Zhou
erhaizn@126.com
Weidong Li
liweidong0801@163.com

[†]These authors share senior authorship

Specialty section:

This article was submitted to
Bioprocess Engineering,
a section of the journal
Frontiers in Bioengineering and
Biotechnology

Received: 09 September 2021

Accepted: 29 October 2021

Published: 16 November 2021

Citation:

Guo M, Xia C, Wu Y, Zhou N, Chen Z
and Li W (2021) Research Progress on
Cell Membrane-Coated Biomimetic
Delivery Systems.
Front. Bioeng. Biotechnol. 9:772522.
doi: 10.3389/fbioe.2021.772522

Cell membrane-coated biomimetic nanoplateforms have many inherent properties, such as bio-interfacing abilities, self-identification, and signal transduction, which enable the biomimetic delivery system to escape immune clearance and opsonization. This can also maximize the drug delivery efficiency of synthetic nanoparticles (NPs) and functional cell membranes. As a new type of delivery system, cell membrane-coated biomimetic delivery systems have broadened the prospects for biomedical applications. In this review, we summarize research progress on cell membrane biomimetic technology from three aspects, including sources of membrane, modifications, and applications, then analyze their limitations and propose future research directions.

Keywords: cell membrane, biomimetic, drug delivery, nanomedicine, nanobiotechnology

INTRODUCTION

Traditional drug delivery primarily involves oral, intravascular, muscular, inhalational, or subcutaneous routes. In these drug delivery methods, the delivered drugs pass through the circulation, following which most are eliminated by the kidney resulting in undesirable pharmacokinetics. However, nanoparticles (NPs) can be utilized to overcome this issue. Synthetic NPs have the advantages of increased drug loading, special release properties, and diverse engineering functions; therefore, they are widely studied and used in biomedicine (Swain et al., 2016). However, there remain limitations such as immunogenicity in applying NPs (Blackman et al., 2021). NPs are initially coated with a variety of polymer molecules, including natural substances such as polysaccharides or semi-synthetic substances such as polymers, which are used to make the NPs as biofriendly and immune system evasive as possible. However, the use of polymer invisibility cloaks, such as polyethylene glycol, cannot completely avoid immune clearance, and NPs can still activate the human complement system (Tasciotti et al., 2008; Chiappini et al., 2010; van de Ven et al., 2012). This necessitates the design of novel drug carriers which can potentially improve drug loading capabilities, the ability to avoid immune clearance, self-targeting functions, and controllable drug release activity.

Cells are the basic unit of life's activities and it the normal functioning of individual cells and cellular systems is crucial for a living body. Researchers have sought inspiration from and attempted to imitate natural cells to construct bionic nano-drug delivery carriers. A biomimetic system coated by a cell membrane, was first established by Hu et al. (2011); they coated erythrocyte membranes with prepared polymer NPs to achieve the biocompatibility of NPs. Since then, this area of research has evolved to allow cell membranes to play additional roles as

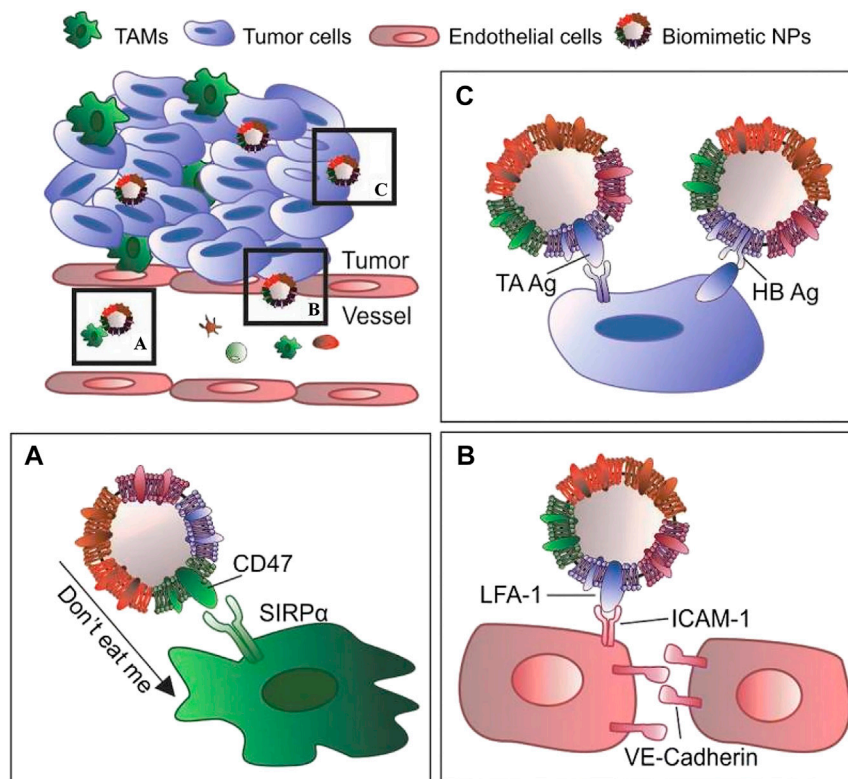


FIGURE 1 | The main functions of the outer cell membrane include: **(A)** protecting drug-carrying NPs from the body's immune system; **(B)** specific binding with the target cell receptor to achieve of activation or inhibition; **(C)** specifically target tissues and lesion sites to improve efficiency of drug delivery system (Reproduced from Pasto et al., 2019).

protective carriers. Herein, we review cell membrane sources, membrane modifications, and applications of cell membrane-coated biomimetic systems.

MEMBRANE SOURCES

The outer cell membrane is not only a simple drug carrier but also a valid shield, and its primary functions include protecting drug-carrying NPs from the body's immune system, acting as a drug delivery system, and maintaining maximum efficacy. Other functions include targeting, allowing the drug to target specific tissues and lesion sites, and creating a highly efficient drug delivery system (Pasto et al., 2019) (**Figure 1**). The functions depend on the presence of specific, active membrane proteins.

Current research on cell membranes includes erythrocyte membranes, leukocyte membranes, platelet membranes, stem cell membranes, cancer cell membranes, and hybrid membranes (Liu et al., 2019; Dash et al., 2020) (**Figure 2**). The complex antigenic characteristics presented on the membrane result in the display of different properties by each type of membrane. Each classification describes different biomimetic properties, and we have summarized the primary features to facilitate convenient comparison (**Table 1**).

Erythrocytes

Red blood cells (RBCs) are natural cells with a long circulation time through the body. Their circulation life is up to 100–130 days (Kuhn et al., 2017), and they are the most abundant of all blood cells. Some of their advantageous features are: good plasticity and elasticity, oxygen carrying and some immune capacity, and the ability to pass through capillaries with smaller diameters by changing their shape (Tan et al., 2013; Wicki et al., 2015). One of the reasons RBCs are considered an ideal membrane modifier is because the surface of the RBC membrane is rich in proteins, glycans, and receptors that can bypass attacks by the immune system (Rao et al., 2017; Ren et al., 2017; Su et al., 2017). For example, one of the most representative markers, CD47, is an immunomodulatory protein that acts on the inhibitory receptor SIRPα to prevent clearance from the bloodstream by macrophages (Oldenborg et al., 2000; Legrand et al., 2011; Xie et al., 2019). The RBC membrane was the first to be used to form cell membrane-coated NPs, which Hu et al. (2011) first obtained and successfully prepared utilizing the “invisibility” function and circulation properties of the RBC membrane in 2011. Wang et al. (2019) achieved the targeted release of encapsulated drug-loaded NPs by utilizing the biomimetic properties of the RBC membrane interface to reduce phagocytosis by macrophages and enhance the accumulation of NPs in atherosclerotic plaques.

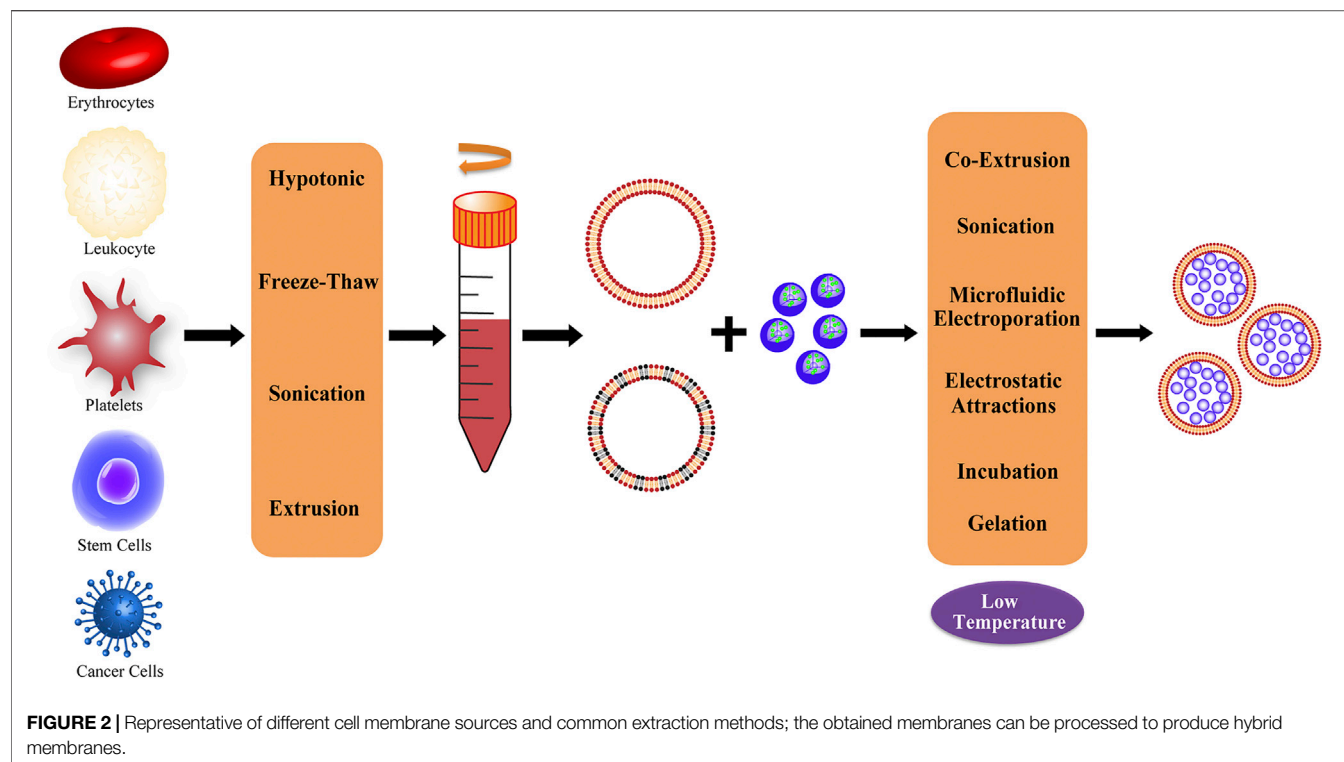


TABLE 1 | Summary of the differences among different cell membranes.

Source cell	Main properties	Targeting ability	Representative protein
Erythrocytes	Long circulation life The most abundant blood cell Immune evasion	RES-targeting	CD47
Leukocyte	Recognize inflammation Circulating tumor cells Immune evasion	Inflammatory-targeting; Diseased-sites	CD47, CD45, LFA-1, Mac-1
Platelets	The smallest circulating blood cell Adhesion to other cells Accumulate in diseased region Immune evasion	Tumor targeting; Injured-sites	P-Selectin, CD41, CD42b, CD61
Stem cells	Multipotent differentiation Self-replication Tumor-specific targeted Immune evasion	Tumor targeting	Specific integrins
Cancer cells	Unlimited replication Homologous targeting Immune evasion	Tumor targeting	Adhesion molecules

Leukocyte

Unlike RBCs, which cannot perform selective targeting, white blood cells (WBCs) are activated by chemokines that are overexpressed in inflammatory tissue, and can recognize inflammation and purposefully accumulate in the lesion area, representing a pivotal marker of the response to disease (Gao et al., 2016b). WBCs, including granulocytes, monocytes, and lymphocytes, can also migrate between extravascular tissues and vessels. Moreover, they have been reported to have targeting abilities against circulating tumor cells through inherent cell

adhesion molecules on their membranes (Corbo et al., 2015). Similar to other cells, WBCs are also rich in active functional proteins, such as CD47 and CD45, which confer immune tolerance (Molinaro et al., 2016; Martinez et al., 2018), and lymphocyte function-associated antigen 1 (LFA-1) and macrophage-1 (Mac-1), which allow binding to inflamed endothelium and tumor targeting (Parodi et al., 2013; Palomba et al., 2016). Targeted NPs were prepared for esophageal cancer, including tests using doxorubicin (DOX) and small interfering RNA that interfered with the overexpression of the *LPCAT1* gene.

To improve targeting and anti-tumor effects, a white cell membrane coating was used to demonstrate that the coated NPs had more significant anti-tumor proliferation, migration, and metastasis, which was mainly attributed to LFA-1 expressed by WBCs. LFA-1 significantly promotes adhesion between cells and promotes the tumor penetration and internalization ability of the bionic system (Jun et al., 2020).

Platelets

Platelets are the smallest circulating blood cells and cytoplasmic fragments produced by mature megakaryocytes in the bone marrow (Fang et al., 2014); they play a crucial role in vascular injury, wound healing, inflammatory reactions, and hemostasis after thrombosis (Harker et al., 2000). Platelets have complex properties; for example, there are many proteins on the surface of platelets that can adhere to other cells. Therefore, platelets are closely related to cancer, cardiovascular disease, infection, and other diseases. Especially in cancer, platelets can be recalled and accumulate due to inflammation in the tumor. CD40L, an inflammatory enhancer protein, plays an important role in T cell immunity and dendritic cell maturation (Hu et al., 2017). P-selectin, mainly found in endothelial cells and platelets, is a cell adhesion protein that interacts with cancer cells. It can be exposed on the surface of platelet membranes and specifically binds to the CD44 receptor on the surface of cancer cells (Bergstrand et al., 2019). Additionally, CD41, CD42b, CD61, and platelet membrane glycans are important active components in the interaction between platelets and tumor cells (Li et al., 2016). Activation of these representative proteins mediates NP accumulation at the tumor site, which reduces vascular inflammation and increases drug accumulation and therapeutic effects. Inspired by these properties of platelets, Hu et al. (2015) developed a functional NP-coated platelet membrane to enhance anti-tumor efficacy, which has targeting and site-specific abilities allowing the delivery of extracellular drugs and intracellular small molecules. Moreover, the biomimetic delivery system can effectively clear circulating tumor cells from the body and inhibit the occurrence of tumor metastasis (Hu et al., 2015).

Stem Cells

Stem cells are multi-potential differentiated cells that have a strong ability to self-replicate. Many types of stem cells, such as bone marrow mesenchymal stem cells and neural stem cells, have been proven to have the ability to target tumors and are widely used in tumor-specific targeted transport. Mesenchymal stem cells (MSCs) exist in diverse tissues and retain their original biological properties after extraction, even after continuous subculture and cryopreservation (Timaner et al., 2018). In addition, MSCs possess an effective homing ability which is believed to be the cause of chemotaxis to the site of injury or stimulation. The tumor-targeting of MSCs is associated with surface-specific integrins (Toledano Furman et al., 2013). In addition, the NP bionic system prepared using MSC membranes can effectively avoid clearance by the immune system, enhance the tumor-targeting and anti-tumor

chemotherapy efficacy of loaded doxorubicin (DOX), and also exhibits long-term stability (Gao et al., 2016a).

Cancer Cells

Compared with blood cells, cancer cells have unique unlimited replication potential and homologous targeting ability. Because of the proliferation ability of cancer cells, it is easy to obtain cancer cells through cell culture *in vitro*, rather than from autologous plasma or donors (Hanahan and Weinberg, 2011). Biomimetic membrane carriers can camouflage nanodrugs as cancer cells, and use the characteristics of mutual recognition and adhesion of molecules on the surface of cancer cells to actively target drugs to the lesions, thereby achieving drug enrichment and effective treatment. Zhu et al. (2016) encapsulated NPs with specific cell membranes of multiple tumor cell lines, and *in vitro* experiments indicated good self-recognition internalization and immune evasion of the source tumor cell lines. More importantly, the same tumor cell line enables highly tumor-selective self-targeting of homologous tumors *in vivo*, even in the context of a heterotypic tumor (Zhu et al., 2016).

Hybrid Cells

With the deepening of research and the expansion of applications, certain limitations associated with the use of a single membrane have been identified; thus, researchers have been working to develop two types of membrane fusion coatings, thereby integrating additional advantages and enabling NPs to inherit and amplify the characteristics of both source cells (Zhu et al., 2016; Liang et al., 2018). Dehaini et al. (2017) first adopted the fusion cell membrane strategy, proving that a mixed membrane using RBC and platelet membrane-coated PLGA NPs possesses the dual functions of prolonging blood circulation time and targeting tumors. The mixed cell membrane-modified drug-loaded nanosystem further improved the functionalization of the original drug-loaded nanosystem. Bu et al. (2019) developed Fe₃O₄ NPs encapsulated by tumor stem cell and platelet fusion membranes which have strong immune evasion, tumor-targeting activity, magnetic resonance imaging and photothermal therapy function, and can be used to enhance photothermal therapy for head and neck squamous cell carcinoma. Therefore, it is reasonable to conjecture that the hybrid membrane is powerful and has the potential to produce a new nanosystem of multi-membrane coatings with the potential to surpass their single-membrane counterparts.

MODIFICATION OF CELL MEMBRANE

The cell membrane is composed of lipids, polysaccharides, and proteins, and the functions entrusted to NPs mostly depend on their surface functional proteins. With the latest developments in materials and medical science, the targeting and monitoring operations of nanoplatforms based on cell membranes are increasing. To improve the characteristics of membrane-coated NPs compared to those of natural cell membranes and conduct more precise targeted research and treatment, the modification of

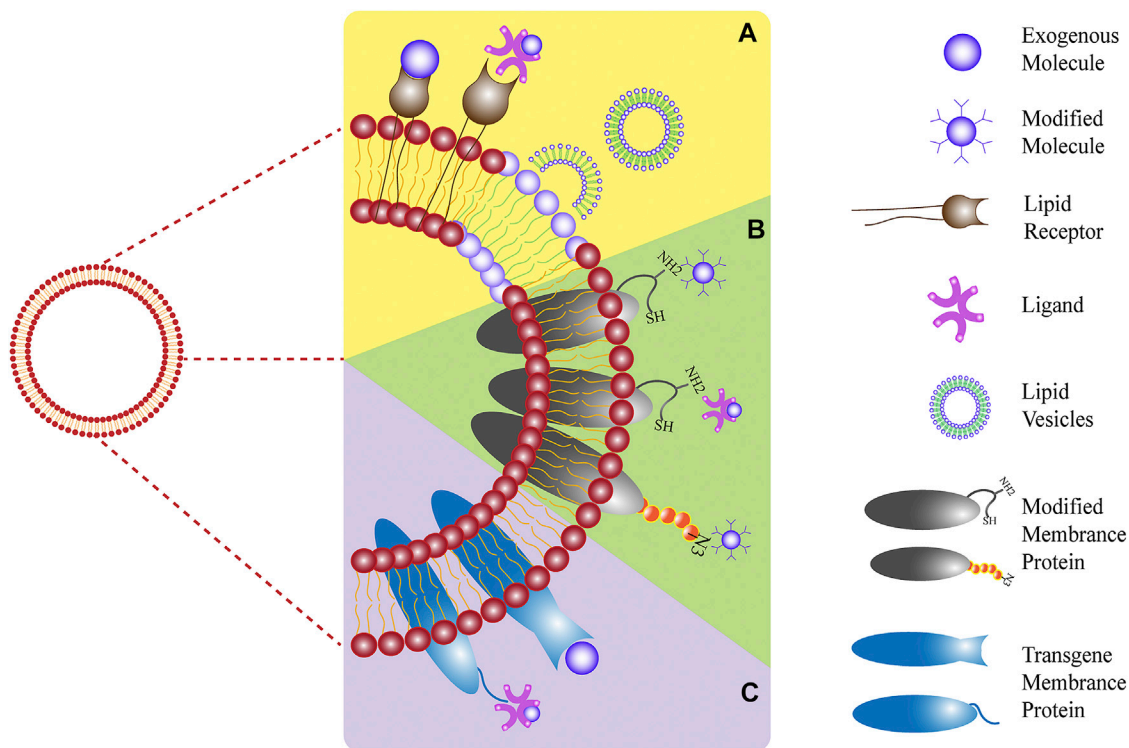


FIGURE 3 | Three modification strategies: **(A)** physical, **(B)** chemical, and **(C)** biological methods.

cell membranes is a new research direction with substantial potential (Mayor and Etienne-Manneville, 2016; Lim and June, 2017; Yan et al., 2019). Generally, modifications to cell membranes can be roughly divided into three main sections: physical, chemical, and genetic engineering (Bachir et al., 2017) (summarized in **Figure 3**).

Physical Engineering of Cell Membranes

The physical engineering of cell membranes involves the utilization of lipid structure and membrane fluidity to naturally anchor targeted groups to the cell membrane through lipid-lipid interactions (Escribá et al., 2015). A design for targeted or therapeutic cell membrane can be achieved by inserting the hydrophobic lipid portion, with targeting or therapeutic molecules, into the outer lobule of the lipid bilayer. In addition, exogenous receptors can be inserted into the cell membrane to specifically bind to representative molecules, such as the ligands of probes, therapeutic drugs, and biological macromolecules. Moreover, the fusion of lipid vesicles containing target molecules with cell membranes is a feasible method. For example, glycosylphosphatidylinositol-fused proteins can be designed to attach to the cell membrane, and liposomes can be introduced to fuse with vesicles derived from cell membranes to promote the encapsulation and controlled release of small molecules (Escribá et al., 2015; Saha et al., 2016). It has been reported that vesicles derived from RBC membranes were first fused with cholesterol to encapsulate the chemotherapeutic drug DOX and the antibiotic vancomycin,

which exhibited a pH-dependent drug release behavior. And the Exogenous cholesterol supplementation can effectively maintain the pH gradient and drive drug loading (Zhang et al., 2017) (**Figure 4**). There have also been studies using the method of lipid insertion to achieve recombinant proteins that improve the targeting ability of the membrane bionic system (Zhang Z. et al., 2018). Overall, the physical engineering strategy is convenient and compatible with other membrane modification schemes. However, potential instability of the inserted molecule and a negative effect of the inserted molecule on the overall stability, may limit the effectiveness of this strategy.

Chemical Engineering of Cell Membranes

Chemical engineering strategies can be used to conveniently endow cells with new functions while preserving their biological competence. Chemical engineering strategies mainly target the primary amine and thiol residues of membrane-associated proteins and the hydroxyl residues of polysaccharides, which can be used as active sites for various covalent conjugation schemes (Sletten and Bertozzi, 2009). For example, through amidation reactions, functional molecules containing carboxyl groups can be combined with the amino residues of cell membranes. It has been reported that tetraacetyl-N-azidoacetylmannosamine-mediated click chemoselective labeling of target cells with azide groups is followed by click chemistry to enhance the accumulation of conjugates (Wang et al., 2017) (**Figure 5**). Moreover, the strategy of modifying RBC membranes with human recombinant hyaluronidase enabled

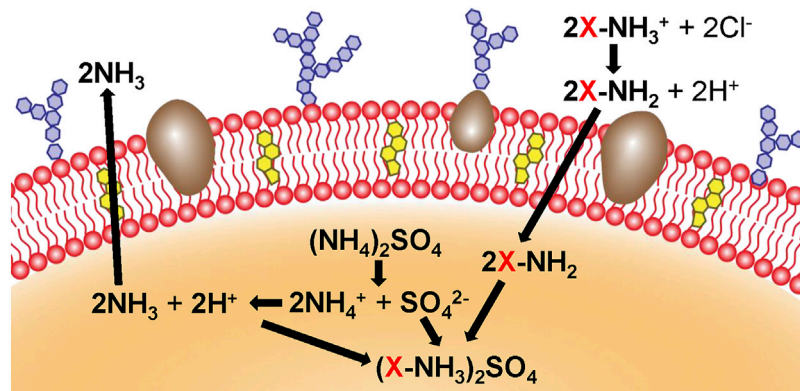


FIGURE 4 | Cholesterol (yellow) and ammonium sulfate (orange) are used to generate a pH gradient, which contributes to the accumulation of the drug in cholesterol-rich RBC vesicles (Reproduced from Zhang et al., 2017).

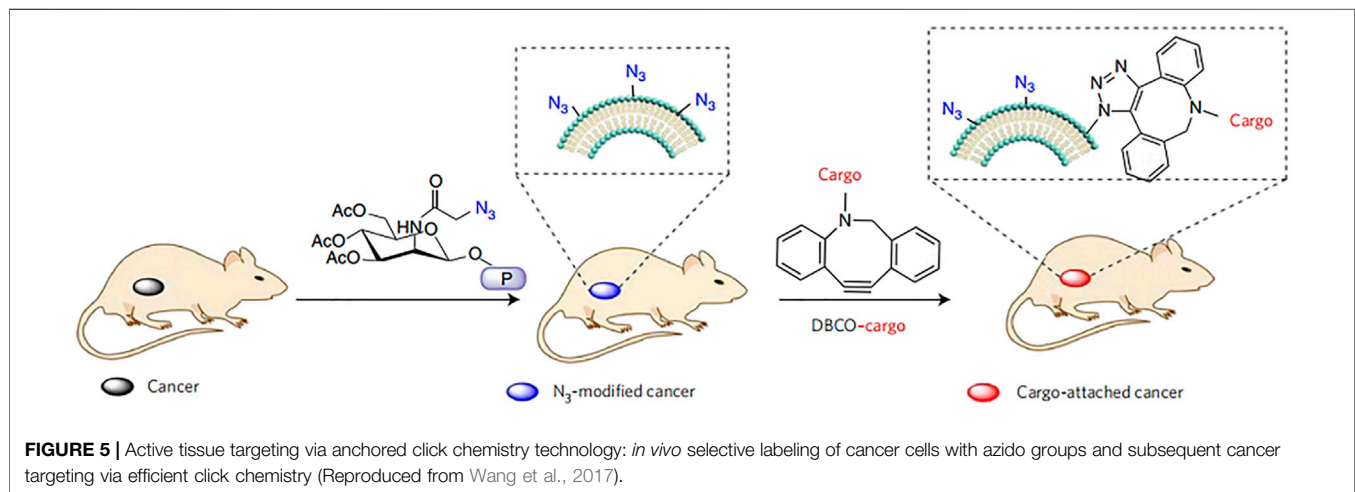


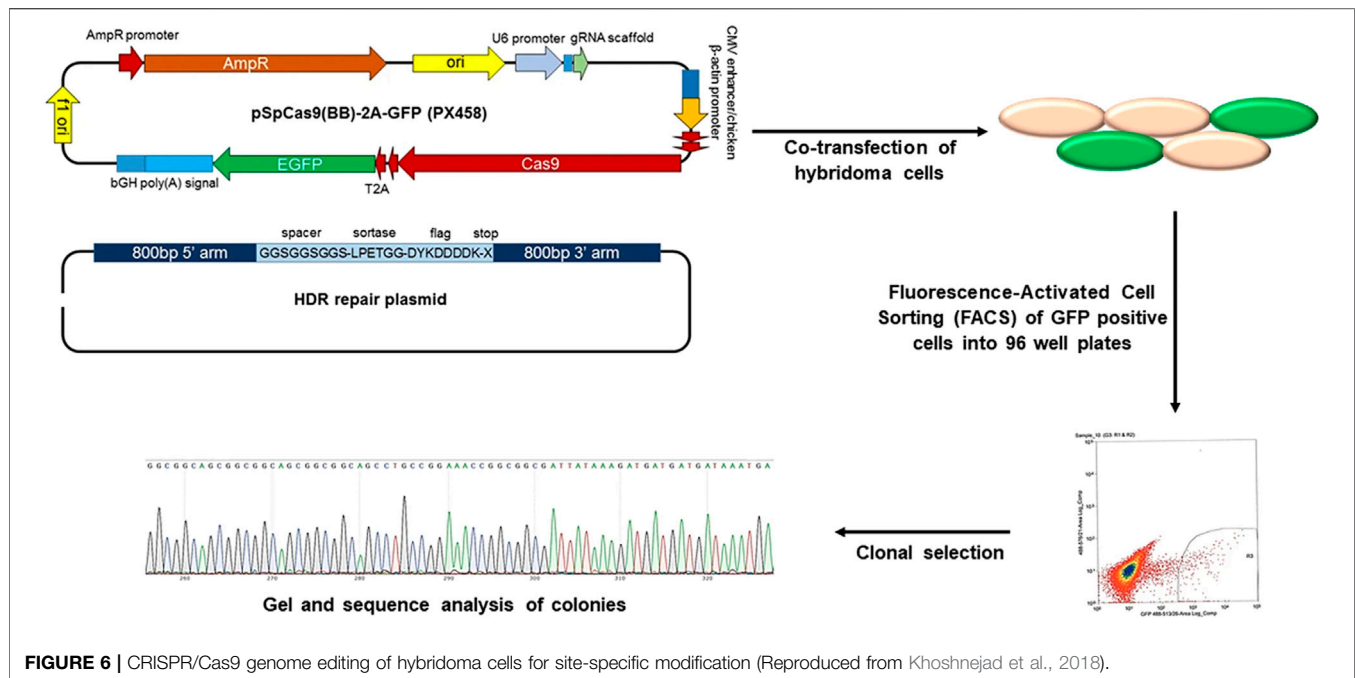
FIGURE 5 | Active tissue targeting via anchored click chemistry technology: *in vivo* selective labeling of cancer cells with azido groups and subsequent cancer targeting via efficient click chemistry (Reproduced from Wang et al., 2017).

human recombinant hyaluronidase PH20 to be stably fixed to the extracellular domain of erythrocyte membrane proteins via the cell impermeable linker NHS-PEG-maleimide. Because hyaluronidase overexpression has been found in cancer studies and can reduce the effective drug concentration of treatment, anchoring hyaluronidase to NP-coated cell membranes could potentially improve the spread of NPs in tumors and increase the access of biomimetic systems to tumor cells (Zhou et al., 2016). Thus, chemical strategies are generally convenient and can provide cells with new functions while maintaining their biological functions. However, a limitation is the lack of specificity of the reaction, which may impair the biological activity of the natural protein and affect the original function.

Biological Engineering of Cell Membranes

Genetic engineering is the selective introduction of the desired protein or peptide into the cell membrane through the transfection or transduction of non-viral or viral vectors (Choi et al., 2008; Levy et al., 2013). This strategy is widely used to modify cell membranes with fused motifs for targeting

and therapeutic applications (Kell et al., 2015). The thioester acyl residues of the LPETGG motif cleaved by sortase A can connect the N-terminal glycine-functionalized peptide to the cell membrane (Chen et al., 2005). Furthermore, the clustered regularly spaced short palindromic repeats (CRISPR)/CRISPR-associated protein 9 (Cas9) system can be used to promote the introduction of receptor peptides, which allows targeted genome editing with specific guide RNA. The LPXTG motif is genetically expressed on the RBC membrane through the CRISPR/Cas9 system, and the immunodominant peptide containing appropriately exposed N-terminal glycine can be covalently linked with the LPXTG motif with the help of sortase A. This system demonstrated therapeutic efficacy in autoimmune encephalomyelitis (Figure 6) (Khoshnejad et al., 2018; Lao et al., 2018). In general, genetically engineered cell membranes have higher specificity, which could result in more precise cell membrane engineering by combining other chemical or physical strategies. However, both viral and non-viral methods may cause uncontrolled toxicity or immunogenicity.



APPLICATION OF CELL MEMBRANE BIOMIMETIC SYSTEMS

Cancer Treatment

The treatment of cancer has always been a major focus and difficulty in scientific research, and the generation of new scientific technologies can be applied to basic research. Previously, although the drug delivery of NPs improved drug loading and control the release of drugs, the targeting and immune clearance of foreign substances prevented the NPs from being widely implemented in clinical applications, despite promising results in a large number of basic studies (Narain et al., 2017; Yaman et al., 2020). To some extent, the cell membrane biomimetic system technology can improve the deficiencies exhibited by simple NPs. The homologous binding of cancer cells leads to the growth of a tumor mass when cancer cells adhere to each other. Therefore, for the delivery of anticancer drugs, membrane coatings with homomorphic binding mechanisms can target cancer cells (Yaman et al., 2020).

As a shield for NPs carrying drugs, the most practical function of the cell membrane is to reduce the clearance rate *in vivo* and homologous targeting of cancer cell membranes. Bahmani et al. (2021) used a platelet membrane to wrap R848 (toll-like receptor agonists) and fuse the platelet membrane with NPs through ultrasound. An *in vitro* study demonstrated that the system can greatly increase the activity of R848 because of the biomimetic stealth effect produced by the platelet membrane and that coated R848 is more likely to be absorbed by cancer cells and has a longer drug retention time (Bahmani et al., 2021).

Another branch of tumor therapy is photothermal therapy (PTT), which uses the targeting property of photosensitizers after entering the body to absorb infrared light from external

interference and convert light energy into heat energy to generate heat in the body. This method is simple and non-invasive and is considered as an adjuvant therapy to enhance chemotherapy and radiotherapy (Yang et al., 2017). A system using both platelet-coated DOX and the photothermal agent IR780 was designed. *In vivo* experiments used near-infrared fluorescence imaging to detect NPs *in vivo* and assess tumor targeting and biological distribution, and showed that the system has a longer retention time and accumulation effect. Further evaluation of the combined thermal therapy and tumor-targeting system found that the tumor growth in the laser NP group was completely restrained compared with the system without thermal ablation (Pei et al., 2020).

The single-membrane approach can no longer meet the needs of research, and the emergence of hybrid membranes combined with various cell membrane functions has excellent prospects. Sun et al. (2020) used the homologous specificity of cancer cell membranes combined with the long cycle time of erythrocyte membranes to prepare mixed membranes coated with DOX-loaded gold nanocages, forming a biomimetic system constructed using a hybrid membrane. This hybrid membrane biological system has a higher stability in maintaining the stable encapsulation of drugs before radiation. The release of DOX was less than 20% within 24 h, and the release of drugs was significantly increased to more than 80% when receiving external near-infrared radiation. Moreover, hybrid membrane-coated NPs exhibit better cellular internalization behavior (Sun et al., 2020).

Photodynamic therapy (PDT) is a new choice for cancer treatment. Its anti-tumor effect depends on reactive oxygen species and singlet oxygen produced in the photodynamic reaction, which can producing oxidative reactions and cytotoxicity to kill cells. This process consumes oxygen, so it

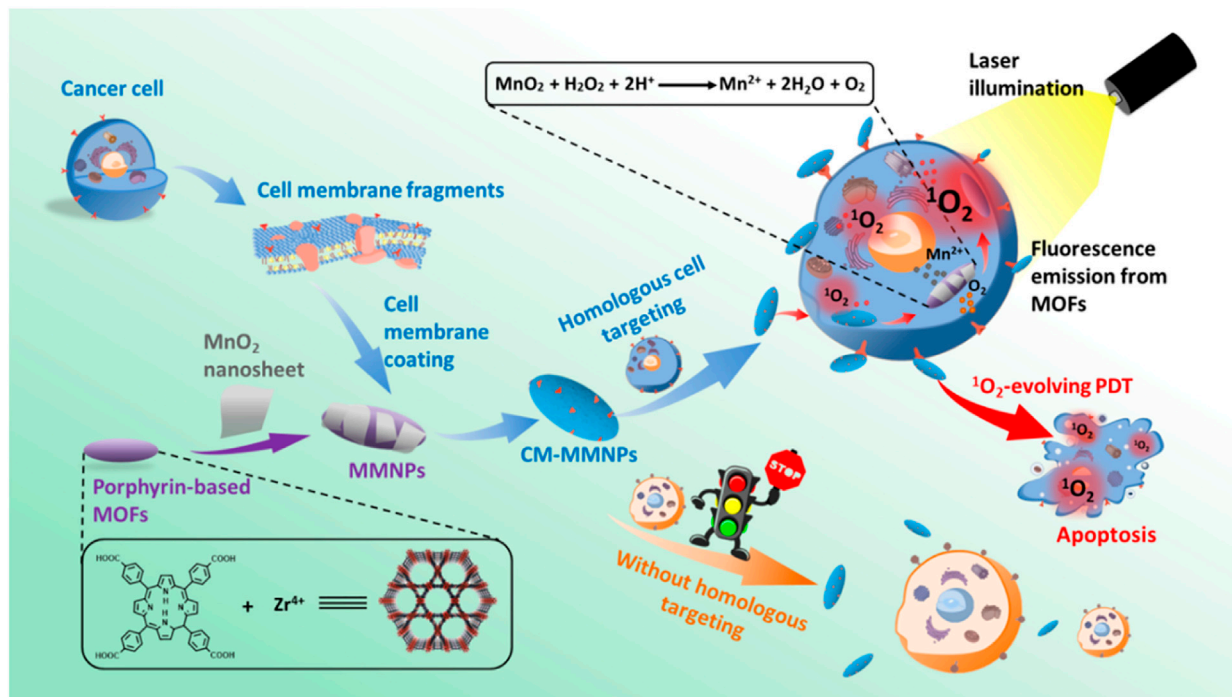


FIGURE 7 | Construction of a biomimetic system with homologous targeting, MRI/fluorescence dual-mode imaging, and PDT (Reproduced from Zhang et al., 2019).

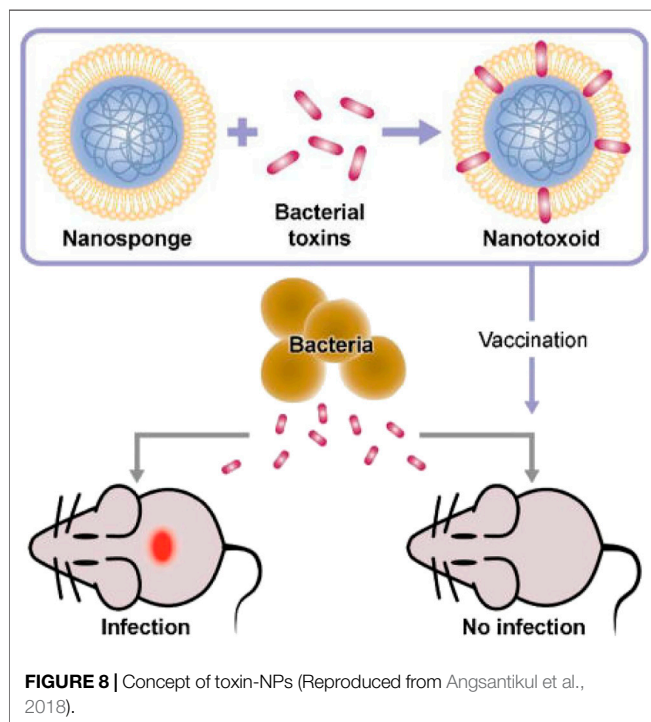


FIGURE 8 | Concept of toxin-NPs (Reproduced from Angsantikul et al., 2018).

needs to overcome a certain hypoxic microenvironment. Perfluorocarbons are ideal carriers of oxygen delivery to enhance PDT, and exhibit increased stability when combined

with the photosensitizer indocyanine green (ICG) containing human serum albumin. The cancer cell membrane is used for targeting and immune escape, and a biomimetic system has been prepared for scanning imaging and photodynamic therapy. The experimental results showed that the system had a higher oxygen capacity, and fluorescence imaging *in vivo* showed that the fluorescence intensity of the system was stronger and exhibited increased duration, and that the system could significantly inhibit tumor growth (Fang et al., 2021). Zhang et al. (2019) developed novel O_2 -evolved PDT NPs for homologous cancer cell targeting and dual-mode imaging (magnetic resonance imaging and fluorescence imaging). The system comprises a metal-organic framework nucleus coated with a manganese dioxide nanosheet and a cancer cell membrane shell. MnO_2 layers expressed both H^+ and H_2O , and the resulting Mn^{2+} can also be used as an optimal MR contrast agent. The introduction of membranes results in improved stability and integrity during endocytosis, as well as strong targeting of homologous cells (Zhang et al., 2019) (Figure 7).

Detoxification

Membrane-coated NPs offer a novel strategy to intercept and neutralize bacterial toxins by exploiting the natural affinity of bacterial toxins to the cell membrane. This toxin-NP assembly, known as nanotoxoid, is capable of rapidly loading different types of toxins and has been developed to effectively prevent bacterial infections (Angsantikul et al., 2018) (Figure 8).

Pore-forming toxins are virulence factors secreted by bacteria that can cause considerable damage to host cells by

damaging target cell membranes. Therefore, neutralizing or inhibiting the expression of poretoxins is the primary method of improving their antibacterial ability (Kong et al., 2016; Dickey et al., 2017). RBCs have “adsorption” effects on these toxins, and NPs coated with RBCs inherit this function, and thus can be used as a valuable treatment. These particles are called “nano-sponges” and can act as decoys, retaining the toxin inserted into the RBCs and preventing them from lysing cells. This bioactivated toxin nano-sponge offers a detoxification treatment that could potentially treat a variety of injuries and diseases caused by pore-forming toxins. For example, nano-sponges can significantly reduce the toxicity of staphylococcal α -hemolysin and improve the survival rate of mice (Hu et al., 2013). NPs coated by erythrocyte membranes absorb and neutralize bacterial factors associated with bacterial infection; for example, a broad spectrum of programmed toxins can be nonspecifically absorbed and neutralized. Chen et al. (2019) developed and characterized NP-coated RBCs against whole secreted proteins from methicillin-resistant *Staphylococcus aureus* to explore the therapeutic effect of biomimetic systems, and *in vivo* and *in vitro* experiments were conducted assaying hemolytic activity to evaluate the therapeutic effect in WSP-induced lethal phenomena. In addition, they preliminarily explored the mechanism conferring immunity from toxins, and found that it was related to the permeability of the pulmonary endothelium. The molecular mechanism was attributed to the rapid activation of NF- κ B (Chen et al., 2019).

In addition, NPs coated on bacterial membranes can stimulate the immune system by simulating the natural bacterial antigens and potentially enhance the immune ability of the body to resist foreign microorganisms (Leleux and Roy, 2013). Gao et al. (2015) developed a natural bacterial membrane collected from bacterial outer membrane vesicles fused onto gold NPs, which showed significantly enhanced stability. When subcutaneously injected, these NPs can rapidly induce the activation and maturation of lymph node dendritic cells. Additionally, immunization with a biomimetic system produced a strong and persistent antibody response with an affinity higher than that induced by membrane vesicles alone (Gao et al., 2015).

Immune Modulation

Immunity and inflammation are highly correlated; to some extent, inflammation is a form of self-defense, eliminating necrotic cells and tissue. However, in some cases, inflammation can be harmful, such as attacks on healthy organizations (Jin et al., 2018). Autoimmune diseases are caused by an immune response to native components of the body. Under the influence of certain factors, the body's tissue or the immune system itself can exhibit abnormalities, causing the immune system to mistake its own components as foreign and attack. At this time, the immune system produces antibodies and active lymphocytes aimed at components of the body itself, damaging its own tissues and organs and leading to disease. It is often characterized by the opsonization of target cells by pathological autoantibodies produced by B cells (Eggert et al., 2010).

Cell membrane-coated NPs reserve and present the antigen protein inherited from the cell membrane surface. Therefore, membrane-coated NPs have the ability to act as antibody bait to improve disease parameters, primarily in the context of type II immune hypersensitivity. The pathological immune response is primarily caused by cell lysis or tissue damage, such as in autoimmune hemolytic anemia. Copp et al. (2014) explored the ability of targeted RBC-coated NPs to eliminate viral antibodies, as an alternative target to protect normally circulating RBCs in the body, theoretically eliminating the need for immunodrug therapy and reducing the burden of disease.

Rheumatoid arthritis (RA) is a widespread and devastating autoimmune disease. Zhang Q. et al. (2018) designed a neutrophil membrane reprocessing system, which is a human peripheral blood neutrophil membrane coated onto complex NPs that was used for the treatment of RA (Figure 9). In response to cytokine inducers produced in RA, neutrophils accumulate to produce micro-vesicles that enter the cartilage. The combination with NPs cores can neutralize proinflammatory factors, inhibit synovial inflammation, and target the cartilage matrix, resulting in a promising therapeutic effect (Zhang Q. et al., 2018).

Zhang G. et al. (2020) developed NPs encapsulated by CD4⁺ T cells with a polymerist core which were able to target the HIV particle and neutralize not only free HIV but also cell-associated HIV through autophagy. Specifically, CD4⁺ T cells express CCR5 and CXCR4, which are necessary for binding to HIV; thus, the NP-coated T cells were able to selectively bind HIV and also inhibit HIV infection in a dose-dependent manner in human peripheral blood mononuclear cells and mononuclear cell-derived macrophages (Wei et al., 2018; Zhang G. et al., 2020).

Imaging

The most important roles of cell membrane coating in the imaging field are biocompatibility and homologous targeting of NPs combining photosensitizers and drugs. Li et al. (2020) coated UCNPs with RBCs to ameliorate the limitations of *in vivo* clearance time and immune response, and preserved both the optical properties of UCNPs and the immune properties of the cell membrane, thus achieving targeted multimodal imaging. This biomimetic system can be used in magnetic resonance imaging and micro PET/CT imaging of a 4T1 breast tumor mouse model, and showed desirable imaging results and no apparent toxicity *in vivo* (Li et al., 2020).

Using homologous targeting of cancer cell membranes, the NP-loaded ICG and coated cancer cell membrane, called ICNPS, was prepared by Chen et al. (2016) ICNPS achieved dual-modal imaging using (NIR)-FL/PA. *In vitro* cell experiments showed that ICG had strong fluorescence imaging ability, cell uptake, and targeting and accumulation ability *in vivo*. This bionic system also exhibits potential as photothermal therapy (Chen et al., 2016). Rao et al. (2016) also used cancer cell membranes to wrap UCNPs, protect UCNPs from immune clearance, and convert near-infrared radiation into visible light for tumor imaging *in vivo* (Rao et al., 2016) (Figure 10).

Moreover, the ability to target specific locations leads NPs coated with cell membrane systems to be utilized for imaging and

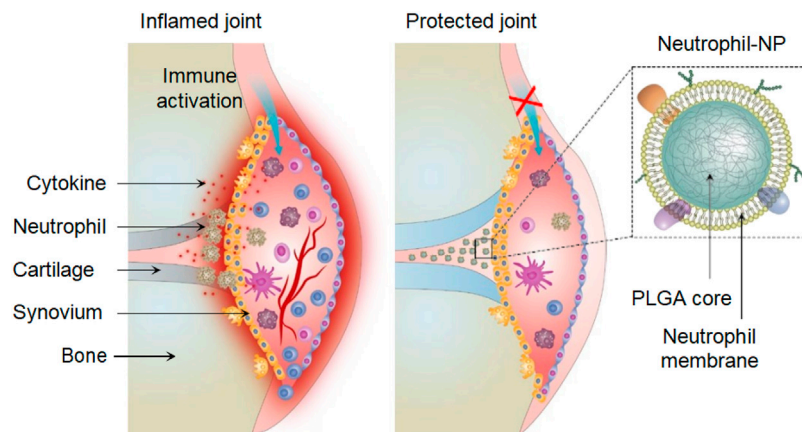


FIGURE 9 | Neutrophil-NPs inhibit synovial inflammation and ameliorate joint destruction in inflammatory arthritis (Reproduced from Zhang Q. et al., 2018).

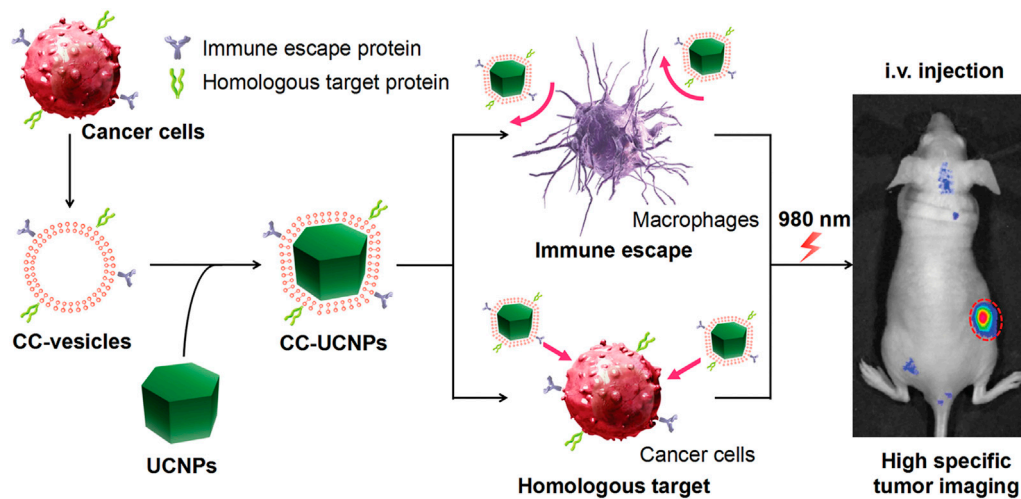


FIGURE 10 | Cancer cell membrane coated UCNP system produce a biomimetic system that exhibit immune escape and homologous targeting capabilities for highly specific tumor imaging (Reproduced from Rao et al., 2016).

PTT. A fibroblast cell membrane with nanomicelles bonded to the biomimetic semiconducting polymer NPs was developed by Li et al. (2018) and called the AF-SPN system. This system can specifically target cancer-associated fibroblasts in the tumor microenvironment and enhance the photothermal characteristics of multimodal cancer. The homologous targeting mechanism enables the bionic system to specifically target tumor-associated fibroblasts, protect SPN to provide better optical signals for tumor detection, and to generate photothermal and photodynamic therapy. The camouflage of cell membranes does not affect the near-infrared fluorescence, photothermal, or photodynamic properties, and the biomimetic system can preferentially target cancer-associated fibroblasts (Li et al., 2018).

However, based on the imaging requirements, the most fundamental improvement method is to modify NPs. To develop more advanced nanoprobes to improve the imaging

depth and stability, and to achieve further breakthroughs with the biocompatibility and targeting ability conferred by the cell membrane. For example, Lv et al. (2018) developed a biosystem nanoprobe characterized by the realization of two-photon absorption and Forster resonance energy transfer processes, achieving superior fluorescence performance, including high-resolution visualization of the fine structure of tumor tissue *in vivo*. The cancer cell membrane coating provides biocompatibility with the nanoprobe (Lv et al., 2018).

Therefore, cell-membrane-coated biomimetic delivery systems are widely used. Additionally, the use of Chinese medicine is a good representative of natural medicine, and the excavation and utilization of the active ingredients is a promising breakthrough in Chinese medicine. However, innovative development and utilization of Chinese medicine is often limited by their solubility, stability, and toxicity. Large-sized

TABLE 2 | Summary of Chinese medicine ingredients used in cell membrane coating research.

Drugs	Membrane	Indications	Strategy	Reference
Curcumin	Cancer cell membrane	Breast cancer	Improve the biosafety and stability of combination photochemotherapy for breast cancer	Zhang et al. (2021)
Curcumin	RBC membrane	Alzheimer's disease	Load antioxidants into RBC membrane-camouflaged human serum albumin NPs containing T807 and triphenylphosphine, which promote sustained drug release and improve biocompatibility and long-term circulation	Gao et al. (2020)
Curcumin and Angelica polysaccharide	RBC membrane	Hepatocellular Carcinoma	Use cell membrane to avoid immune system clearance	Guo et al. (2021)
Tanshinone IIA	RBC membrane		Prolong the circulation time and prevent oxidative stress at the cellular level by protecting encapsulated drug STS from RES clearance	Dong et al. (2017)
Gambogic acid	RBC membrane	Colorectal cancer	Extend circulation time <i>in vivo</i> with improved biocompatibility and stability	Zhang et al. (2020b)
Paclitaxel	Macrophage cell membrane	Melanoma	Improve delivery to cancer metastatic sites	Cao et al. (2020)
Chikusetsusapo-nin Iva	Hybrid cell membrane (RBC membrane and cancer cell membrane)	Breast cancer	Increase immune evasion and targeting ability at the tumor site	Xie et al. (2021)
Resveratrol	RBC membrane	Alzheimer's disease	Load antioxidants into RBC membrane-camouflaged NPs bearing rabies virus glycoprotein and triphenylphosphine cation, which promote sustained drug release and improve biocompatibility and long-term circulation	Han et al. (2020)

materials in drug delivery pose some challenges, including *in vivo* stability, bioavailability, solubility, and target-specific delivery problems. Designing cell membrane-coated biomimetic delivery systems by applying cell membrane bionic carriers to deliver active substances may offer a good solution. Research in this field is gradually emerging, and we summarize the application of biomimetic delivery systems to Chinese medicine ingredients combined with cell membranes in **Table 2**.

CONCLUSION AND PERSPECTIVES

This review introduces different cell membranes used in cell membrane technology, including erythrocyte membranes, leukocyte membranes, platelet membranes, stem cell membranes, cancer cell membranes, and hybrid membranes. With the widespread application of cell membrane biomimetic technology, modifications of cell membranes are being widely investigated as potential strategies. There are three main types of cell membrane modifications based on the strategy used for modifications: physical, chemical, and biological engineering. The physical engineering of cell membranes mainly uses lipid structure and membrane fluidity to anchor targeted groups to the cell membrane; chemical engineering strategies mainly target active chemical bond reaction sites for various covalent conjugation schemes; and the biological engineering strategies can selectively introduce the desired protein or peptide into the cell membrane through the transfection or transduction of non-viral or viral vectors.

An increasing number of studies are focused on cell membrane encapsulating NPs, which are mainly used for cancer treatment, drug delivery, detoxification, immune regulation, and imaging. Among these, specific targeting is the

most important central role in cancer and imaging. In addition, by taking advantage of the inevitable action between toxins and the cell membrane, the cell membrane can be used as a broad-spectrum detoxification agent. Regarding immunity, in addition to the inherent targeting effect of cell membranes, many studies have been carried out in the field of autoimmune diseases using antigen-specific approaches, which are expected to further solve the problem of immunity.

Despite the advantages of cell membrane bionic technology, further improvements are still required. There remains substantial scope for the development and application of engineered cell membrane-based nanotherapeutics. Moreover, there are additional problems that remain to be solved.

First, membrane biomimetic technology is mainly derived from various animals; that is, the membrane is obtained from the animal body, which is dependent on the animal model used in *in vivo* and *in vitro* experimental studies, and the specific clinical efficacy remains to be verified. Studies have used human cells to study human glioblastoma U87 and U87-CXCR4 cell lines at the animal level (Jin et al., 2019). Although the technique does not have extensive clinical applications, its rapid development provides a new direction for the refinement of individual medicine in the future.

Second, the quality control of cell membranes seems to have been ignored. Determining and controlling the critical quality attributes of cell membranes warrants additional research. The characterization of functional proteins on the surface of cell membranes, which is an important source of targeting and homology, is an important indicator in all studies. The source of cell membranes produces differences not only in the different cell types used, but also for in the same types of cells when used from different species. Microscopic characterization is still insufficient to characterize the varying properties of different

cell membranes. Many research groups are continuously working to refine and upgrade existing methods and standards to develop industry-wide benchmarks and manufacturing principles. In addition, as for the current cell culture and membrane derivative technology, whether the combination technology of membrane and NPs can cope with high-throughput culture and preparation, and whether the changes in experimental conditions requires the consideration of new standards to measure the purity of membrane derivation remains to be seen.

The membrane modification process is equivalent to killing the cells and resplicing the fragments. Identifying strategies to deal with the body's removal of cell fragments and better simulate the function of living cells, rather than simple cell membrane extraction and separation, can further improve the function of the membrane bionic system.

Owing to the limited membrane sources, the functional components of the cell membrane can be identified *in vitro* to facilitate clinical transformation. Although there are plans to integrate the active proteins of the cell membrane into the

synthetic phospholipid bilayer and use the generated bionic vesicles to achieve targeting (Molinaro et al., 2016), further research in this area is needed.

We hope that by exploring the relationship between critical quality attributes and the function of the carrier and establishing the standardization of cell membrane sources, we can accelerate the clinical transformation of cell membrane-coated NPs, which will have a positive impact on human health and be of great economic value.

AUTHOR CONTRIBUTIONS

MG, CX, ZC, YW, and WL designed the structure of the manuscript and drafted the manuscript. MG and CX performed the literature search and contributed to writing the manuscript. MG, CX, NZ, WL, and ZC reviewed and revised the manuscript. All authors contributed to manuscript revision, read, and approved the submitted version.

REFERENCES

- Angsantikul, P., Fang, R. H., and Zhang, L. (2018). Toxoid Vaccination against Bacterial Infection Using Cell Membrane-Coated Nanoparticles. *Bioconjug. Chem.* 29 (3), 604–612. doi:10.1021/acs.bioconjchem.7b00692
- Bachir, A. I., Horwitz, A. R., Nelson, W. J., and Bianchini, J. M. (2017). Actin-Based Adhesion Modules Mediate Cell Interactions with the Extracellular Matrix and Neighboring Cells. *Cold Spring Harb Perspect. Biol.* 9 (7), a023234. doi:10.1101/cshperspect.a023234
- Bahmani, B., Gong, H., Luk, B. T., Haushalter, K. J., DeTeresa, E., Previti, M., et al. (2021). Intratumoral Immunotherapy Using Platelet-Cloaked Nanoparticles Enhances Antitumor Immunity in Solid Tumors. *Nat. Commun.* 12 (1), 1999. doi:10.1038/s41467-021-22311-z
- Bergstrand, J., Xu, L., Miao, X., Li, N., Öktem, O., Franzén, B., et al. (2019). Super-resolution Microscopy Can Identify Specific Protein Distribution Patterns in Platelets Incubated with Cancer Cells. *Nanoscale* 11 (20), 10023–10033. doi:10.1039/c9nr01967g
- Blackman, L. D., Qu, Y., Cass, P., and Locock, K. E. S. (2021). Approaches for the Inhibition and Elimination of Microbial Biofilms Using Macromolecular Agents. *Chem. Soc. Rev.* 50 (3), 1587–1616. doi:10.1039/d0cs00986e
- Bu, L. L., Rao, L., Yu, G. T., Chen, L., Deng, W. W., Liu, J. F., et al. (2019). Cancer Stem Cell-Platelet Hybrid Membrane-Coated Magnetic Nanoparticles for Enhanced Photothermal Therapy of Head and Neck Squamous Cell Carcinoma. *Adv. Funct. Mater.* 29 (10), 1807733. doi:10.1002/adfm.201807733
- Cao, X., Tan, T., Zhu, D., Yu, H., Liu, Y., Zhou, H., et al. (2020). Paclitaxel-Loaded Macrophage Membrane Camouflaged Albumin Nanoparticles for Targeted Cancer Therapy. *Ijn* 15, 1915–1928. doi:10.2147/ijn.S244849
- Chen, I., Howarth, M., Lin, W., and Ting, A. Y. (2005). Site-specific Labeling of Cell Surface Proteins with Biophysical Probes Using Biotin Ligase. *Nat. Methods* 2 (2), 99–104. doi:10.1038/nmeth735
- Chen, Y., Zhang, Y., Chen, M., Zhuang, J., Fang, R. H., Gao, W., et al. (2019). Biomimetic Nanosponges Suppress *In Vivo* Lethality Induced by the Whole Secreted Proteins of Pathogenic Bacteria. *Small* 15 (6), 1804994. doi:10.1002/smll.201804994
- Chen, Z., Zhao, P., Luo, Z., Zheng, M., Tian, H., Gong, P., et al. (2016). Cancer Cell Membrane-Biomimetic Nanoparticles for Homologous-Targeting Dual-Modal Imaging and Photothermal Therapy. *ACS Nano* 10 (11), 10049–10057. doi:10.1021/acs.nano.6b04695
- Chiappini, C., Tasciotti, E., Fakhoury, J. R., Fine, D., Pullan, L., Wang, Y.-C., et al. (2010). Tailored Porous Silicon Microparticles: Fabrication and Properties. *Chemphyschem* 11 (5), 1029–1035. doi:10.1002/cphc.200900914
- Choi, J.-J., Yoo, S.-A., Park, S.-J., Kang, Y.-J., Kim, W.-U., Oh, I.-H., et al. (2008). Mesenchymal Stem Cells Overexpressing Interleukin-10 Attenuate Collagen-Induced Arthritis in Mice. *Clin. Exp. Immunol.* 153 (2), 269–276. doi:10.1111/j.1365-2249.2008.03683.x
- Copp, J. A., Fang, R. H., Luk, B. T., Hu, C.-M. J., Gao, W., Zhang, K., et al. (2014). Clearance of Pathological Antibodies Using Biomimetic Nanoparticles. *Proc. Natl. Acad. Sci. USA* 111 (37), 13481–13486. doi:10.1073/pnas.1412420111
- Corbo, C., Parodi, A., Evangelopoulos, M., Engler, D., Matsunami, R., Engler, A., et al. (2015). Proteomic Profiling of a Biomimetic Drug Delivery Platform. *Cdt* 16 (13), 1540–1547. doi:10.2174/1389450115666141109211413
- Dash, P., Piras, A. M., and Dash, M. (2020). Cell Membrane Coated Nanocarriers - an Efficient Biomimetic Platform for Targeted Therapy. *J. Controlled Release* 327, 546–570. doi:10.1016/j.jconrel.2020.09.012
- Dehaini, D., Wei, X., Fang, R. H., Masson, S., Angsantikul, P., Luk, B. T., et al. (2017). Erythrocyte-Platelet Hybrid Membrane Coating for Enhanced Nanoparticle Functionalization. *Adv. Mater.* 29 (16), 1606209. doi:10.1002/adma.201606209
- Dickey, S. W., Cheung, G. Y. C., and Otto, M. (2017). Different Drugs for Bad Bugs: Antivirulence Strategies in the Age of Antibiotic Resistance. *Nat. Rev. Drug Discov.* 16 (7), 457–471. doi:10.1038/nrd.2017.23
- Dong, X., Niu, Y., Ding, Y., Wang, Y., Zhao, J., Leng, W., et al. (2017). Formulation and Drug Loading Features of Nano-Erythrocytes. *Nanoscale Res. Lett.* 12 (1), 202. doi:10.1186/s11671-017-1980-5
- Eggert, M., Zettl, U. K., and Neeck, G. (2010). Autoantibodies in Autoimmune Diseases. *Cpd* 16 (14), 1634–1643. doi:10.2174/138161210791164144
- Escribá, P. V., Busquets, X., Inokuchi, J.-i., Balogh, G., Török, Z., Horváth, I., et al. (2015). Membrane Lipid Therapy: Modulation of the Cell Membrane Composition and Structure as a Molecular Base for Drug Discovery and New Disease Treatment. *Prog. Lipid Res.* 59, 38–53. doi:10.1016/j.plipres.2015.04.003
- Fang, H., Gai, Y., Wang, S., Liu, Q., Zhang, X., Ye, M., et al. (2021). Biomimetic Oxygen Delivery Nanoparticles for Enhancing Photodynamic Therapy in Triple-Negative Breast Cancer. *J. Nanobiotechnol* 19 (1), 81. doi:10.1186/s12951-021-00827-2
- Fang, R. H., Hu, C.-M. J., Luk, B. T., Gao, W., Copp, J. A., Tai, Y., et al. (2014). Cancer Cell Membrane-Coated Nanoparticles for Anticancer Vaccination and Drug Delivery. *Nano Lett.* 14 (4), 2181–2188. doi:10.1021/nl500618u
- Gao, C., Lin, Z., Jurado-Sánchez, B., Lin, X., Wu, Z., and He, Q. (2016a). Stem Cell Membrane-Coated Nanogels for Highly Efficient *In Vivo* Tumor Targeted Drug Delivery. *Small* 12 (30), 4056–4062. doi:10.1002/smll.201600624
- Gao, C., Wang, Y., Sun, J., Han, Y., Gong, W., Li, Y., et al. (2020). Neuronal Mitochondria-Targeted Delivery of Curcumin by Biomimetic Engineered

- Nanosystems in Alzheimer's Disease Mice. *Acta Biomater.* 108, 285–299. doi:10.1016/j.actbio.2020.03.029
- Gao, C., Wu, Z., Lin, Z., Lin, X., and He, Q. (2016b). Polymeric Capsule-Cushioned Leukocyte Cell Membrane Vesicles as a Biomimetic Delivery Platform. *Nanoscale* 8 (6), 3548–3554. doi:10.1039/c5nr08407e
- Gao, W., Fang, R. H., Thamphiwatana, S., Luk, B. T., Li, J., Angsantikul, P., et al. (2015). Modulating Antibacterial Immunity via Bacterial Membrane-Coated Nanoparticles. *Nano Lett.* 15 (2), 1403–1409. doi:10.1021/nl504798g
- Guo, C., Hou, X., Liu, Y., Zhang, Y., Xu, H., Zhao, F., et al. (2021). Novel Chinese Angelica Polysaccharide Biomimetic Nanomedicine to Curcumin Delivery for Hepatocellular Carcinoma Treatment and Immunomodulatory Effect. *Phytomedicine* 80, 153356. doi:10.1016/j.phymed.2020.153356
- Han, Y., Chu, X., Cui, L., Fu, S., Gao, C., Li, Y., et al. (2020). Neuronal Mitochondria-Targeted Therapy for Alzheimer's Disease by Systemic Delivery of Resveratrol Using Dual-Modified Novel Biomimetic Nanosystems. *Drug Deliv.* 27 (1), 502–518. doi:10.1080/10717544.2020.1745328
- Hanahan, D., and Weinberg, R. A. (2011). Hallmarks of Cancer: the Next Generation. *Cell* 144 (5), 646–674. doi:10.1016/j.cell.2011.02.013
- Harker, L. A., Roskos, L. K., Marzec, U. M., Carter, R. A., Cherry, J. K., Sundell, B., et al. (2000). Effects of Megakaryocyte Growth and Development Factor on Platelet Production, Platelet Life Span, and Platelet Function in Healthy Human Volunteers. *Blood* 95 (8), 2514–2522. doi:10.1182/blood.v95.8.2514.008k25_2514_2522
- Hu, C.-M. J., Fang, R. H., Copp, J., Luk, B. T., and Zhang, L. (2013). A Biomimetic Nanosponge that Absorbs Pore-Forming Toxins. *Nat. Nanotech* 8 (5), 336–340. doi:10.1038/nnano.2013.54
- Hu, C.-M. J., Zhang, L., Aryal, S., Cheung, C., Fang, R. H., and Zhang, L. (2011). Erythrocyte Membrane-Camouflaged Polymeric Nanoparticles as a Biomimetic Delivery Platform. *Proc. Natl. Acad. Sci.* 108 (27), 10980–10985. doi:10.1073/pnas.1106634108
- Hu, Q., Sun, W., Qian, C., Bomba, H. N., Xin, H., and Gu, Z. (2017). Relay Drug Delivery for Amplifying Targeting Signal and Enhancing Anticancer Efficacy. *Adv. Mater.* 29 (13), 1605803. doi:10.1002/adma.201605803
- Hu, Q., Sun, W., Qian, C., Wang, C., Bomba, H. N., and Gu, Z. (2015). Anticancer Platelet-Mimicking Nanovehicles. *Adv. Mater.* 27 (44), 7043–7050. doi:10.1002/adma.201503323
- Jin, J., Krishnamachary, B., Barnett, J. D., Chatterjee, S., Chang, D., Mironchik, Y., et al. (2019). Human Cancer Cell Membrane-Coated Biomimetic Nanoparticles Reduce Fibroblast-Mediated Invasion and Metastasis and Induce T-Cells. *ACS Appl. Mater. Inter.* 11 (8), 7850–7861. doi:10.1021/acsami.8b22309
- Jin, K., Luo, Z., Zhang, B., and Pang, Z. (2018). Biomimetic Nanoparticles for Inflammation Targeting. *Acta Pharmaceutica Sinica B* 8 (1), 23–33. doi:10.1016/j.apsb.2017.12.002
- Jun, Y., Tang, Z., Luo, C., Jiang, B., Li, X., Tao, M., et al. (2020). Leukocyte-Mediated Combined Targeted Chemo and Gene Therapy for Esophageal Cancer. *ACS Appl. Mater. Inter.* 12 (42), 47330–47341. doi:10.1021/acsami.0c15419
- Kell, D. B., Swainston, N., Pir, P., and Oliver, S. G. (2015). Membrane Transporter Engineering in Industrial Biotechnology and Whole Cell Biocatalysis. *Trends Biotechnol.* 33 (4), 237–246. doi:10.1016/j.tibtech.2015.02.001
- Khoshnejad, M., Brenner, J. S., Motley, W., Parhiz, H., Greineder, C. F., Villa, C. H., et al. (2018). Molecular Engineering of Antibodies for Site-specific Covalent Conjugation Using CRISPR/Cas9. *Sci. Rep.* 8 (1), 1760. doi:10.1038/s41598-018-19784-2
- Kong, C., Neoh, H.-m., and Nathan, S. (2016). Targeting *Staphylococcus aureus* Toxins: A Potential Form of Anti-virulence Therapy. *Toxins* 8 (3), 72. doi:10.3390/toxins8030072
- Kuhn, V., Diederich, L., Keller, T. C. S., Kramer, C. M., Lückstädt, W., Panknin, C., et al. (2017). Red Blood Cell Function and Dysfunction: Redox Regulation, Nitric Oxide Metabolism, Anemia. *Antioxid. Redox Signaling* 26 (13), 718–742. doi:10.1089/ars.2016.6954
- Lao, Y.-H., Li, M., Gao, M. A., Shao, D., Chi, C.-W., Huang, D., et al. (2018). HPV Oncogene Manipulation Using Nonvirally Delivered CRISPR/Cas9 or *Natronobacterium gregoryi* Argonaute. *Adv. Sci.* 5 (7), 1700540. doi:10.1002/adv.201700540
- Legrand, N., Huntington, N. D., Nagasawa, M., Bakker, A. Q., Schotte, R., Strick-Marchand, H., et al. (2011). Functional CD47/signal Regulatory Protein Alpha (SIRPα) Interaction Is Required for Optimal Human T- and Natural Killer (NK) Cell Homeostasis *In Vivo*. *Proc. Natl. Acad. Sci. USA* 108 (32), 13224–13229. doi:10.1073/pnas.1101398108
- Leleux, J., and Roy, K. (2013). Micro and Nanoparticle-Based Delivery Systems for Vaccine Immunotherapy: an Immunological and Materials Perspective. *Adv. Healthc. Mater.* 2 (1), 72–94. doi:10.1002/adhm.201200268
- Levy, O., Zhao, W., Mortensen, L. J., Leblanc, S., Tsang, K., Fu, M., et al. (2013). mRNA-Engineered Mesenchymal Stem Cells for Targeted Delivery of Interleukin-10 to Sites of Inflammation. *Blood* 122 (14), e23–e32. doi:10.1182/blood-2013-04-495119
- Li, J., Ai, Y., Wang, L., Bu, P., Sharkey, C. C., Wu, Q., et al. (2016). Targeted Drug Delivery to Circulating Tumor Cells via Platelet Membrane-Functionalized Particles. *Biomaterials* 76, 52–65. doi:10.1016/j.biomaterials.2015.10.046
- Li, J., Zhen, X., Lyu, Y., Jiang, Y., Huang, J., and Pu, K. (2018). Cell Membrane Coated Semiconducting Polymer Nanoparticles for Enhanced Multimodal Cancer Phototheranostics. *ACS Nano* 12 (8), 8520–8530. doi:10.1021/acsnano.8b04066
- Li, M., Fang, H., Liu, Q., Gai, Y., Yuan, L., Wang, S., et al. (2020). Red Blood Cell Membrane-Coated Upconversion Nanoparticles for Pretargeted Multimodality Imaging of Triple-Negative Breast Cancer. *Biomater. Sci.* 8 (7), 1802–1814. doi:10.1039/d0bm00029a
- Liang, H., Huang, K., Su, T., Li, Z., Hu, S., Dinh, P.-U., et al. (2018). Mesenchymal Stem Cell/Red Blood Cell-Inspired Nanoparticle Therapy in Mice with Carbon Tetrachloride-Induced Acute Liver Failure. *ACS Nano* 12 (7), 6536–6544. doi:10.1021/acsnano.8b00553
- Lim, W. A., and June, C. H. (2017). The Principles of Engineering Immune Cells to Treat Cancer. *Cell* 168 (4), 724–740. doi:10.1016/j.cell.2017.01.016
- Liu, Y., Luo, J., Chen, X., Liu, W., and Chen, T. (2019). Cell Membrane Coating Technology: A Promising Strategy for Biomedical Applications. *Nano-micro Lett.* 11 (1), 100. doi:10.1007/s40820-019-0330-9
- Lv, Y., Liu, M., Zhang, Y., Wang, X., Zhang, F., Li, F., et al. (2018). Cancer Cell Membrane-Biomimetic Nanoprobes with Two-Photon Excitation and Near-Infrared Emission for Intravital Tumor Fluorescence Imaging. *ACS Nano* 12 (2), 1350–1358. doi:10.1021/acsnano.7b07716
- Martinez, J. O., Molinaro, R., Hartman, K. A., Boada, C., Sukhovshin, R., De Rosa, E., et al. (2018). Biomimetic Nanoparticles with Enhanced Affinity towards Activated Endothelium as Versatile Tools for Theranostic Drug Delivery. *Theranostics* 8 (4), 1131–1145. doi:10.7150/thno.22078
- Mayor, R., and Etienne-Manneville, S. (2016). The Front and Rear of Collective Cell Migration. *Nat. Rev. Mol. Cell Biol.* 17 (2), 97–109. doi:10.1038/nrm.2015.14
- Molinaro, R., Corbo, C., Martinez, J. O., Taraballi, F., Evangelopoulos, M., Minardi, S., et al. (2016). Biomimetic Proteolipid Vesicles for Targeting Inflamed Tissues. *Nat. Mater.* 15 (9), 1037–1046. doi:10.1038/nmat4644
- Narain, A., Asawa, S., Chhabria, V., and Patil-Sen, Y. (2017). Cell Membrane Coated Nanoparticles: Next-Generation Therapeutics. *Nanomedicine* 12 (21), 2677–2692. doi:10.2217/nnm-2017-0225
- Oldenborg, P.-A., Zheleznyak, A., Fang, Y.-F., Lagenaur, C. F., Gresham, H. D., and Lindberg, F. P. (2000). Role of CD47 as a Marker of Self on Red Blood Cells. *Science* 288 (5473), 2051–2054. doi:10.1126/science.288.5473.2051
- Palomba, R., Parodi, A., Evangelopoulos, M., Acciardo, S., Corbo, C., de Rosa, E., et al. (2016). Biomimetic Carriers Mimicking Leukocyte Plasma Membrane to Increase Tumor Vasculature Permeability. *Sci. Rep.* 6, 34422. doi:10.1038/srep34422
- Parodi, A., Quattrocchi, N., van de Ven, A. L., Chiappini, C., Evangelopoulos, M., Martinez, J. O., et al. (2013). Synthetic Nanoparticles Functionalized with Biomimetic Leukocyte Membranes Possess Cell-like Functions. *Nat. Nanotech* 8 (1), 61–68. doi:10.1038/nnano.2012.212
- Pasto, A., Giordano, F., Evangelopoulos, M., Amadori, A., and Tasciotti, E. (2019). Cell Membrane Protein Functionalization of Nanoparticles as a New Tumor-targeting Strategy. *Clin. Translational Med.* 8 (1), 8. doi:10.1186/s40169-019-0224-y
- Pei, W., Huang, B., Chen, S., Wang, L., Xu, Y., and Niu, C. (2020). Platelet-Mimicking Drug Delivery Nanoparticles for Enhanced Chemo-Photothermal Therapy of Breast Cancer. *Ijn* 15, 10151–10167. doi:10.2147/ijn.S285952
- Rao, L., Bu, L.-L., Cai, B., Xu, J.-H., Li, A., Zhang, W.-F., et al. (2016). Cancer Cell Membrane-Coated Upconversion Nanoprobes for Highly Specific Tumor Imaging. *Adv. Mater.* 28 (18), 3460–3466. doi:10.1002/adma.201506086

- Rao, L., Meng, Q.-F., Bu, L.-L., Cai, B., Huang, Q., Sun, Z.-J., et al. (2017). Erythrocyte Membrane-Coated Upconversion Nanoparticles with Minimal Protein Adsorption for Enhanced Tumor Imaging. *ACS Appl. Mater. Inter.* 9 (3), 2159–2168. doi:10.1021/acsami.6b14450
- Ren, H., Liu, J., Li, Y., Wang, H., Ge, S., Yuan, A., et al. (2017). Oxygen Self-Enriched Nanoparticles Functionalized with Erythrocyte Membranes for Long Circulation and Enhanced Phototherapy. *Acta Biomater.* 59, 269–282. doi:10.1016/j.actbio.2017.06.035
- Saha, S., Anilkumar, A. A., and Mayor, S. (2016). GPI-anchored Protein Organization and Dynamics at the Cell Surface. *J. Lipid Res.* 57 (2), 159–175. doi:10.1194/jlr.R062885
- Sletten, E. M., and Bertozzi, C. R. (2009). Bioorthogonal Chemistry: Fishing for Selectivity in a Sea of Functionality. *Angew. Chem. Int. Ed.* 48 (38), 6974–6998. doi:10.1002/anie.200900942
- Su, J., Sun, H., Meng, Q., Zhang, P., Yin, Q., and Li, Y. (2017). Enhanced Blood Suspensibility and Laser-Activated Tumor-specific Drug Release of Theranostic Mesoporous Silica Nanoparticles by Functionalizing with Erythrocyte Membranes. *Theranostics* 7 (3), 523–537. doi:10.7150/thno.17259
- Sun, M., Duan, Y., Ma, Y., and Zhang, Q. (2020). Cancer Cell-Erythrocyte Hybrid Membrane Coated Gold Nanocages for Near Infrared Light-Activated Photothermal/Radio/Chemotherapy of Breast Cancer. *Ijn* 15, 6749–6760. doi:10.2147/ijn.S266405
- Swain, S., Sahu, P., Beg, S., and Babu, S. (2016). Nanoparticles for Cancer Targeting: Current and Future Directions. *Cdd* 13 (8), 1290–1302. doi:10.2174/1567201813666160713121122
- Tan, S., Li, X., Guo, Y., and Zhang, Z. (2013). Lipid-enveloped Hybrid Nanoparticles for Drug Delivery. *Nanoscale* 5 (3), 860–872. doi:10.1039/c2nr32880a
- Tasciotti, E., Liu, X., Bhavane, R., Plant, K., Leonard, A. D., Price, B. K., et al. (2008). Mesoporous Silicon Particles as a Multistage Delivery System for Imaging and Therapeutic Applications. *Nat. Nanotech* 3 (3), 151–157. doi:10.1038/nnano.2008.34
- Timaner, M., Letko-Khait, N., Kotsofruk, R., Benguigui, M., Beyar-Katz, O., Rachman-Tzemah, C., et al. (2018). Therapy-Educated Mesenchymal Stem Cells Enrich for Tumor-Initiating Cells. *Cancer Res.* 78 (5), 1253–1265. doi:10.1158/0008-5472.Can-17-1547
- Toledano Furman, N. E., Lupu-Haber, Y., Bronshtein, T., Kaneti, L., Letko, N., Weinstein, E., et al. (2013). Reconstructed Stem Cell Nanoghosts: a Natural Tumor Targeting Platform. *Nano Lett.* 13 (7), 3248–3255. doi:10.1021/nl401376w
- van de Ven, A. L., Kim, P., Haley, O. H., Fakhoury, J. R., Adriani, G., Schmulen, J., et al. (2012). Rapid Tumorotropic Accumulation of Systemically Injected Plateloid Particles and Their Biodistribution. *J. Controlled Release* 158 (1), 148–155. doi:10.1016/j.jconrel.2011.10.021
- Wang, H., Wang, R., Cai, K., He, H., Liu, Y., Yen, J., et al. (2017). Selective *In Vivo* Metabolic Cell-Labeling-Mediated Cancer Targeting. *Nat. Chem. Biol.* 13 (4), 415–424. doi:10.1038/nchembio.2297
- Wang, Y., Zhang, K., Qin, X., Li, T., Qiu, J., Yin, T., et al. (2019). Biomimetic Nanotherapies: Red Blood Cell Based Core-Shell Structured Nanocomplexes for Atherosclerosis Management. *Adv. Sci.* 6 (12), 1900172. doi:10.1002/adv.201900172
- Wei, X., Zhang, G., Ran, D., Krishnan, N., Fang, R. H., Gao, W., et al. (2018). T-Cell-Mimicking Nanoparticles Can Neutralize HIV Infectivity. *Adv. Mater.* 30 (45), 1802233. doi:10.1002/adma.201802233
- Wicki, A., Witzigmann, D., Balasubramanian, V., and Huwyler, J. (2015). Nanomedicine in Cancer Therapy: Challenges, Opportunities, and Clinical Applications. *J. Controlled Release* 200, 138–157. doi:10.1016/j.jconrel.2014.12.030
- Xie, J., Shen, Q., Huang, K., Zheng, T., Cheng, L., Zhang, Z., et al. (2019). Oriented Assembly of Cell-Mimicking Nanoparticles via a Molecular Affinity Strategy for Targeted Drug Delivery. *ACS Nano* 13 (5), 5268–5277. doi:10.1021/acsnano.8b09681
- Xie, Q., Liu, Y., Long, Y., Wang, Z., Jiang, S., Ahmed, R., et al. (2021). Hybrid-cell Membrane-Coated Nanocomplex-Loaded Chikusetsusaponin IVa Methyl Ester for a Combinational Therapy against Breast Cancer Assisted by Ce6. *Biomater. Sci.* 9 (8), 2991–3004. doi:10.1039/d0bm02211j
- Yaman, S., Chintapala, U., Rodriguez, E., Ramachandramoorthy, H., and Nguyen, K. T. (2020). Cell-mediated and Cell Membrane-Coated Nanoparticles for Drug Delivery and Cancer Therapy. *Cdr* 3, 879–911. doi:10.20517/cdr.2020.55
- Yan, H., Shao, D., Lao, Y. H., Li, M., Hu, H., and Leong, K. W. (2019). Engineering Cell Membrane-Based Nanotherapeutics to Target Inflammation. *Adv. Sci.* 6 (15), 1900605. doi:10.1002/adv.201900605
- Yang, Y., Zhu, W., Dong, Z., Chao, Y., Xu, L., Chen, M., et al. (2017). 1D Coordination Polymer Nanofibers for Low-Temperature Photothermal Therapy. *Adv. Mater.* 29 (40), 1703588. doi:10.1002/adma.201703588
- Zhang, D., Ye, Z., Wei, L., Luo, H., and Xiao, L. (2019). Cell Membrane-Coated Porphyrin Metal-Organic Frameworks for Cancer Cell Targeting and O₂-Evolving Photodynamic Therapy. *ACS Appl. Mater. Inter.* 11 (43), 39594–39602. doi:10.1021/acsami.9b14084
- Zhang, G., Campbell, G. R., Zhang, Q., Maule, E., Hanna, J., Gao, W., et al. (2020a). CD4 + T Cell-Mimicking Nanoparticles Broadly Neutralize HIV-1 and Suppress Viral Replication through Autophagy. *mBio* 11 (5). doi:10.1128/mBio.00903-20
- Zhang, Q., Dehaini, D., Zhang, Y., Zhou, J., Chen, X., Zhang, L., et al. (2018a). Neutrophil Membrane-Coated Nanoparticles Inhibit Synovial Inflammation and Alleviate Joint Damage in Inflammatory Arthritis. *Nat. Nanotech* 13 (12), 1182–1190. doi:10.1038/s41565-018-0254-4
- Zhang, X., Angsantikul, P., Ying, M., Zhuang, J., Zhang, Q., Wei, X., et al. (2017). Remote Loading of Small-Molecule Therapeutics into Cholesterol-Enriched Cell-Membrane-Derived Vesicles. *Angew. Chem. Int. Ed.* 56 (45), 14075–14079. doi:10.1002/anie.201707598
- Zhang, Y., He, Z., Li, Y., Xia, Q., Li, Z., Hou, X., et al. (2021). Tumor Cell Membrane-Derived Nano-Trojan Horses Encapsulating Phototherapy and Chemotherapy Are Accepted by Homologous Tumor Cells. *Mater. Sci. Eng. C* 120, 111670. doi:10.1016/j.msec.2020.111670
- Zhang, Z., Li, D., Li, X., Guo, Z., Liu, Y., Ma, X., et al. (2020b). PEI-modified Macrophage Cell Membrane-Coated PLGA Nanoparticles Encapsulating Dendrobium Polysaccharides as a Vaccine Delivery System for Ovalbumin to Improve Immune Responses. *Int. J. Biol. Macromolecules* 165 (Pt A), 239–248. doi:10.1016/j.ijbiomac.2020.09.187
- Zhang, Z., Qian, H., Huang, J., Sha, H., Zhang, H., Yu, L., et al. (2018b). Anti-EGFR-irGD Recombinant Protein Modified Biomimetic Nanoparticles Loaded with Gambogic Acid to Enhance Targeting and Antitumor Ability in Colorectal Cancer Treatment. *Ijn* 13, 4961–4975. doi:10.2147/ijn.S170148
- Zhou, H., Fan, Z., Lemons, P. K., and Cheng, H. (2016). A Facile Approach to Functionalize Cell Membrane-Coated Nanoparticles. *Theranostics* 6 (7), 1012–1022. doi:10.7150/thno.15095
- Zhu, J.-Y., Zheng, D.-W., Zhang, M.-K., Yu, W.-Y., Qiu, W.-X., Hu, J.-J., et al. (2016). Preferential Cancer Cell Self-Recognition and Tumor Self-Targeting by Coating Nanoparticles with Homotypic Cancer Cell Membranes. *Nano Lett.* 16 (9), 5895–5901. doi:10.1021/acs.nanolett.6b02786

Conflict of Interest: The authors declare that the research was conducted in the absence of any commercial or financial relationships that could be construed as a potential conflict of interest.

Publisher's Note: All claims expressed in this article are solely those of the authors and do not necessarily represent those of their affiliated organizations, or those of the publisher, the editors and the reviewers. Any product that may be evaluated in this article, or claim that may be made by its manufacturer, is not guaranteed or endorsed by the publisher.

Copyright © 2021 Guo, Xia, Wu, Zhou, Chen and Li. This is an open-access article distributed under the terms of the Creative Commons Attribution License (CC BY). The use, distribution or reproduction in other forums is permitted, provided the original author(s) and the copyright owner(s) are credited and that the original publication in this journal is cited, in accordance with accepted academic practice. No use, distribution or reproduction is permitted which does not comply with these terms.



Bioprocess of Microbial Melanin Production and Isolation

Kwon-Young Choi^{1,2*}

¹Department of Environmental Engineering, College of Engineering, Ajou University, Suwon, South Korea, ²Department of Environmental and Safety Engineering, College of Engineering, Ajou University, Suwon, South Korea

OPEN ACCESS

Edited by:

Jia-Long Wen,
Beijing Forestry University, China

Reviewed by:

Long Liu,
Jiangnan University, China
Alfredo Martinez,
Universidad Nacional Autónoma de
México, Mexico

*Correspondence:

Kwon-Young Choi
kychoi@ajou.ac.kr

Specialty section:

This article was submitted to
Bioprocess Engineering,
a section of the journal
Frontiers in Bioengineering and
Biotechnology

Received: 26 August 2021

Accepted: 28 October 2021

Published: 16 November 2021

Citation:

Choi K-Y (2021) Bioprocess of
Microbial Melanin Production
and Isolation.
Front. Bioeng. Biotechnol. 9:765110.
doi: 10.3389/fbioe.2021.765110

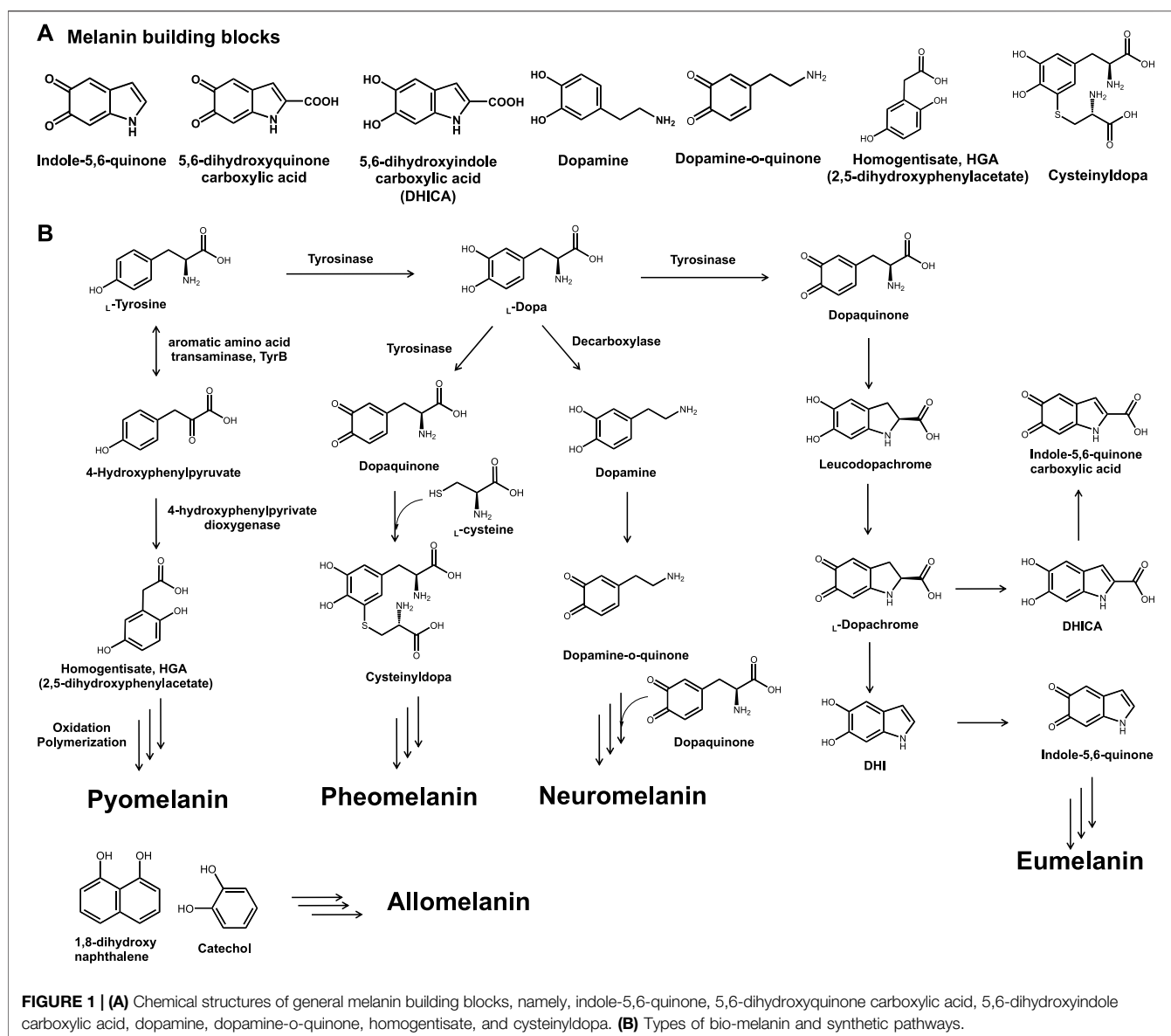
Melanin is one of the most abundant pigments found in the biosphere. Owing to its high biocompatibility and diverse biological activities, it has been widely applied as a functional biomaterial in the cosmetic, pharmaceutical, biopolymer, and environmental fields. In this study, the production of melanin was comprehensively reviewed concerning bioconversion and isolation processes. First, several melanogenic microbes, including fungi and bacteria, were summarized. Melanin production was classified by host and melanin type and was analyzed by titers in g/L in addition to reaction conditions, including pH and temperature. The production was further interpreted using a space-time yields chart, which showed two distinct classifications in productivity, and reaction conditions were analyzed using a pH-temperature-titer chart. Next, the extraction process was summarized by crude and pure melanin preparation procedures, and the extraction yields were highlighted. Finally, the recent applications of melanin were briefly summarized, and prospects for further application and development in industrial applications were suggested.

Keywords: melanin, pigment, space-time yields, extraction, purification

INTRODUCTION

Melanin is a representative brown-black pigment commonly found in most organisms. It is widely found in melanin-producing animal cells as well as in bacteria, fungi, and plants. From the black coloration of a human eye, hair, and skin to the black insect epidermis and oxidation-induced discoloration of fruits, melanin occurs in most of the biosphere (Pralea et al., 2019; Singh et al., 2021). Melanin has long been an important component of living organisms and cells. Melanin synthesis in organisms is primarily involved in the protection of host cells and organisms. This includes protection from UV radiation and energy absorption, protection from external physical changes, and maintenance of intracellular homeostasis through its physiological activity (Bolognese et al., 2019; Seo and Choi, 2020a).

It is structurally complex and has various forms depending on its building blocks (Nosanchuk et al., 2015; Choi et al., 2018). The mechanism of melanin synthesis varies depending on the radical formation; it can be synthesized through the random polymerization of a few building blocks, such as L-tyrosine metabolites of indole-5,6-quinone, 5,6-dihydroxyquinone carboxylic acid, 5,6-dihydroxyindole carboxylic acid (DHICA), dopamine, dopamine-o-quinone, homogentisate, cysteinyllopa, and some phenolic precursors (Figure 1A) (Li et al., 2019; Seo and Choi, 2020b). Depending on the polymerization pathways, building blocks, and enzymes, melanin is classified into several groups, including eumelanin, pyromelanin, pheomelanin, neuromelanin, and allomelanin (Figure 1B) (Powell et al., 2004; Simon and Rozanowska, 2008).



The characteristic features of melanin vary depending on the class. The most common type of eumelanin consists of dihydroxyindole and DHICA, shows brown to black coloration, and can be produced by several microorganisms, including bacteria and fungi (Kuzumaki et al., 1993). Melanogenesis in the human skin, which is initiated by UV exposure, can lead to the formation of skin melanin and yellowish pheomelanin constitutes in the human skin (Wood and Schallreuter, 2006; Wolnicka-Glubisz et al., 2012; Pukalski et al., 2020). In addition, several catechol moieties have been reported to be involved in allomelanin production and can be found in plants and fruits (Varga et al., 2016; McCallum et al., 2021). Neuromelanin, which can be found in the brain, plays a critical role in treating neurodegenerative disorders (Usunoff et al., 2002; Double et al., 2008; Bellinger et al., 2011; Zucca et al., 2017). Similarly, it has been reported that melanin is

involved in several physiological functions and as a result, serious genetic disorders are induced unless melanin is properly produced (Frenk and Lattion, 1982; Schmidt et al., 2015; Suo et al., 2020).

Melanin has been applied in a variety of biological, physiological, and physical materials, despite its complex random polymeric structures, which are responsible for its unique properties and functionality. Accordingly, great efforts have been made to screen melanin-producing strains for melanin production. For example, the isolation of melanin-producing fungal strains and the production of melanin on a large scale have attracted great attention. However, production titers and isolation methods vary depending on the host strain and melanin type. Although fungal strains are good hosts for melanin production, they require a long fermentation period to obtain the desired production titer (Nosanchuk et al., 2015; Cordero and

Casadevall, 2017). In addition, the extraction and purification steps differ depending on the physical properties, such as solubility and the use of the isolated melanin (Pralea et al., 2019; Singh et al., 2021). Bioprocesses in melanin biorefinery include fermentation and extraction processes, which are widely used for biochemical production processes. Also, the treatment process of chemicals such as organic solvent in melanin extraction is included in the melanin biorefinery. Therefore, it is necessary to understand melanin production concerning the biorefinery process.

Several in-depth reviews on the chemical structure, engineering and production, and applications of melanin are available. For example, recent review articles by Pralea et al. and Singh et al. comprehensively reviewed the recent advances in melanin from biosynthesis to the application (Pralea et al., 2019; Park S. et al., 2020; Singh et al., 2021). In this review article, we summarize and highlight melanin bioproduction, including the current status of microbial production, extraction, and purification. In particular, we review the production of melanin from the space-time yield viewpoint, extraction from crude material, and pure melanin preparations. This review shares information on melanin biorefineries and supports the further development and potential applications of melanin.

BIOCONVERSION OF BIOMASS INTO MELANIN

Natural Melanin Sources and Alternatives

There is a variety of melanin sources; several common fruits and vegetables, such as apples, bananas, garlic, persimmons, and potatoes, can produce melanin (Lefevre and Perrett, 2015; Hagiwara et al., 2016; Qi et al., 2020). Melanin can also be obtained from plants, such as *Mucuna monosperma* (Wight) callus (Inamdar et al., 2014). Commercial melanin is prepared from sepia extract or by synthetic means (Prados-Rosales et al., 2015; Schroeder et al., 2015; Srisuk et al., 2016).

Nevertheless, these methods have the disadvantage of high production costs, low maneuverability, and environmental pollution risk. Therefore, the bioproduction of melanin by microorganisms such as fungi and bacteria as alternative melanin sources has attracted great attention. As they grow fast relatively and can be applied to the scale-up process for mass production. Besides, several attempts have been made to isolate melanin-producing strains from various environments to enhance melanin production through reactions and host cell engineering.

Melanin Production by Fungal Strains

To date, several melanin-producing fungal strains have been reported (Rosas et al., 2000; Gomez et al., 2001; Nosanchuk et al., 2002; Morris-Jones et al., 2003; da Silva et al., 2006; Franzen et al., 2006; Nosanchuk et al., 2007; Walker et al., 2010; Nosanchuk et al., 2015). While fungal strains produce different types of melanin, the predominant melanin type is nitrogen-deficient allomelanin (Varga et al., 2016). The key enzymes responsible for melanin synthesis are tyrosinases,

which are copper-dependent biocatalysts involved in ortho-specific hydroxylation and subsequent oxidation of monophenols like tyrosine (Kuzumaki et al., 1993). Laccase is another enzyme, which can catalyze the oxidation of a broad range of substrates like tyrosinase, including dihydroxyphenols and quinones (Nagai et al., 2003). Both enzymes are commonly abundant in plants and fungi rather than in bacteria. Therefore, fungal strains were potential candidate for melanin production. Moreover, the complex and dynamic membrane structure of fungi supplies a more suitable environment for melanin synthesis and deposition. For example, *Cryptococcus neoformans* melanin was reported to be located within the cell walls of branched polysaccharides and protein constructs (Nosanchuk and Casadevall, 2003). In addition, the presence of other cellular organizations, such as fungal vesicles, melanosomes, and anchoring structures, have been reported to assist in the efficient production and localization of fungal melanin (Nosanchuk and Casadevall, 2003; Nosanchuk et al., 2015; Camacho et al., 2019).

It should be noted, however, that the production of melanin-consuming fungus requires a relatively long incubation time due to the low cell growth rate of the fungus; for example, *Auricularia auricula* or *Gliocephalotrichum simplex* produced 2.97 g/L and 6.6 g/L of melanin in 8 and 6 days, respectively (Jalmi et al., 2012; Sun et al., 2016). Interestingly, Ribera et al. reported that 161 days of *Armillaria cepistipes* culture could produce 27.98 g/L of eumelanin, which was the highest as far as our understanding, in a 3% (w/v) tyrosine-supplemented medium (Ribera et al., 2019). However, it took a long time of 161 days to achieve this production titer.

It is possible to produce eumelanin from L-tyrosine and allomelanin via the polyketide pathway (Varga et al., 2016). However, limitations, such as low growth rate, sporulation, low extraction efficiency, and potential pathogenicity of fungal strains, need to be overcome to obtain desirable production titers. Recently, along with the development of genetic manipulation and sequencing technology, it has become possible to increase the productivity of various biochemicals with recombinant fungi through genetic engineering. In line with this, it could be possible to increase fungal melanin production through the expression of an external enzyme.

Melanin Production by Bacterial Strains

Several microbial melanins have also been reported (Cubo et al., 1988; Jalmi et al., 2012; Ganesh Kumar et al., 2013; Surwase et al., 2013; Guo et al., 2014a; Madhusudhan et al., 2014; Tarangini and Mishra, 2014; Perez-Cuesta et al., 2020). Also, it was reported the production of melanin by using wild-type bacteria of *Klebsiella sp.*, *Pseudomonas*, *Streptomyces*, *Bacillus*, *Amorphotheca*, and *Vibrio*, or by the expressing tyrosinase in *E. coli* as summarized in **Table 1** (Tarangini and Mishra, 2014; Oh et al., 2020; Wang et al., 2020; Ahn et al., 2021). Organisms with melanogenic capabilities have also been employed to develop production processes, which included production optimization of melanin by utilizing various carbon sources and culture variables; In particular, tyrosine, peptone, soy peptone, starch, and yeast extract were used as

TABLE 1 | Production of microbial melanin in a biorefinery process.

No	Sources	Melanin type	Host strain	Genes expressed	Substrate (conc.)	Reaction condition	Reaction time	Production	Ref
1	Plant	—	<i>Mucuna monosperma</i> (Wight) callus	—	Tyrosine (1 g/L)	pH 5.5	48 h	0.887 g/L	Inamdar et al. (2014)
2	Fungus	—	<i>Auricularia auricula</i>	Wild type	Tyrosine (1.92 g/L), yeast extract (17.27 g/L), lactose (3.84 g/L)	pH 6, 28°C	8 days	2.97 g/L	Sun et al. (2016)
3	Fungus	Eumelanin	<i>Gliocephalotrichum simplex</i>	Wild type	Tyrosine (2.5% w/v), peptone (1% w/v)	28°C	6 days	6.6 g/L	Jalmi et al. (2012)
4	Fungus	Eumelanin	<i>Armillaria cepistipes</i>	Wild type	Tyrosine (3.0% w/v)	pH 6, 22°C	161 days	27.98 g/L	Ribera et al. (2019)
5	Bacterial	Eumelanin	<i>Klebsiella sp.</i> GSK 46	Wild type	Tyrosine (1 g/L)	pH 7.2, 37°C	3.5 days	0.13 g/L	Sajjan et al. (2010)
6	Bacterial	Eumelanin	<i>Pseudomonas stutzeri</i>	Wild type	Sea-water medium without tyrosine	pH 6.7, 37°C	10 h	6.7 g/L	Ganesh Kumar et al. (2013)
7	Bacterial	Eumelanin	<i>Streptomyces kathirae</i>	Wild type	Amylodextrine (3.3 g/L), yeast extract (5 g/L)	pH 6, 28°C	128 h	13.7 g/L	Guo et al. (2014a)
8	Bacterial	Eumelanin	<i>Bacillus safensis</i>	Wild type	Fruit waste extract	pH 6.84, 30.7°C	24 h	6.96 g/L	Tarangini and Mishra, (2014)
9	Bacterial	Eumelanin	<i>Streptomyces glaucescens</i> NEAE-H	Wild type	Protease-peptone (5 g/L)	30–37°C	6 days	3.16 g/L	El-Naggar and El-Ewasy, (2017)
10	Bacterial	Eumelanin	<i>Streptomyces sp.</i> ZL-24	Wild type	Soy peptone (20.31 g/L)	pH 7, 30°C	5 days	4.24 g/L (189.9 mg/L insoluble)	Wang et al. (2019)
11	Bacterial	Eumelanin	<i>Bacillus subtilis</i> 4NP-BL	Wild type	Starch (15 g/L)	pH 7.2, 28°C	7 days	1.5 g/L	Ghadge et al. (2020)
12	Bacterial	Eumelanin	<i>Escherichia coli</i>	<i>melC</i> , <i>cyp102G4</i>	Tyrosine, Indole	pH 7, 37°C	24 h	3.4 g/L	Park et al. (2020a)
13	Bacterial	Eumelanin	<i>Pseudomonas koreensis</i> UIS 19	Wild type	Molasses 5 Brix (5%), tyrosine (2.5 g/L)	pH 7.5, 30°C	24 h	5.5 g/L	Eskandari and Etemadifar, (2021)
14	Bacterial	Eumelanin	<i>Amorphotheca resiniae</i>	Wild type	Peptone (10 g/L), yeast extract (5 g/L), glucose (20 g/L)	27°C	14 days	4.5 g/L (13.4 mg/L/h)	Oh et al. (2020)
15	Marine Bacterium	Eumelanin	<i>Vibrio natriegens</i>	<i>tyr1</i>	Tyrosine (0.4 g/L)	30°C	2 h	0.45 g/L (0.32 mg/mL/h)	Wang et al. (2020)
16	Bacterial	Pyomelanin	<i>Escherichia coli</i>	<i>4-hppd</i>	Tyrosine (1 mM)	pH 7, 37°C	6 days	0.213 g/L	Bolognese et al. (2019)
17	Bacterial	Pyomelanin	<i>Ralstonia picketti</i>	Wild type	Tyrosine (4 mM)	pH 7, 30°C	62 h	0.09 g/L	Seo and Choi, (2020a)
18	Bacterial	Pyomelanin	<i>Escherichia coli</i>	<i>4-hppd</i>	Tyrosine (4 mM)	pH 7, 30°C	24 h	0.315 g/L (13.1 mg/L/h)	Seo and Choi, (2020a)
19	Bacterial	Pyomelanin	<i>Yarrowia lypolytica</i> W29	4-HPPD	Tyrosine (1 g/L)	pH 7, 37°C	72 h	0.5 g/L	Ben Tahar et al. (2020)
20	Bacterial	Allomelanin	<i>Escherichia coli</i>	<i>fcs/ech</i>	Caffeic acid (5 mM)	pH 7, 37°C	12 h	0.2 g/L (40.9 mg/L/h)	Jang et al. (2018)
21	Bacterial	Allomelanin	<i>Escherichia coli</i>	<i>fcs/ech</i>	Caffeic acid (0.5 mM)	pH 7, 37°C	12 h	0.17 g/L (14.2 mg/L/h)	Ahn et al. (2019)

melC; tyrosinase from *Bacillus megaterium*, *cyp102G4*; cytochrome P450 monooxygenase from *Streptomyces cattleya*, *4-hppd*; 4-hydroxyphenylpyruvate dioxygenase, *tyr1*; tyrosinase from *Bacillus megaterium*.

carbon sources or mixtures. This resulted in the biosynthesis of tyrosine-based eumelanin. The *Klebsiella sp.* GSK46 strain, which was isolated from crop field soil, was able to produce approximately 0.13 g/L of eumelanin when fed with 1 g/L of tyrosine (Sajjan et al., 2010).

However, melanin could be produced even in the absence of tyrosine. For example, marine *Pseudomonas stutzeri*, isolated from seaweed, was found to produce significant amounts of melanin, which was 6.7 g/L within 10 h of incubation in sea water production medium without

tyrosine supplementation (Ganesh Kumar et al., 2013). As fruit waste extract provides good nutrition for biochemical production, it has been utilized for melanin production. Tarangini and Mishra reported that *Bacillus safensis*, isolated from garden soil, could produce 6.96 g/L of melanin within 10 h of incubation (Tarangini and Mishra, 2014; Valdez-Calderón et al., 2020).

Amino acids also have been utilized for melanin production through whole cell biotransformation, in addition to the use of sugar-based fermentation including

glucose, starch, and molasses (Ghadge et al., 2020; Oh et al., 2020; Eskandari and Etemadifar, 2021). For example, Eskandari and Etemadifar reported cost effective melanin production using *Pseudomonas koreensis* UIS19 in a molasses medium with tyrosine supplementation (Mustafa et al., 2020; Eskandari and Etemadifar, 2021). A total of 32 g/L of sugar was consumed to obtain 5.4 g/L of dry cell mass and 0.44 g dry melanin/g weight of yield could be achieved from supplemented tyrosine. In addition, several amino acid-based mediums, such as peptone and yeast extract, were utilized for melanin production using *Streptomyces kathirae*, *Streptomyces glaucescens*, *Streptomyces* sp. ZL-24, and *Amorphoteca resinae*, which resulted in several g/L of melanin (Guo J. et al., 2014; El-Naggar and El-Ewasy, 2017; Wang et al., 2019; Eskandari and Etemadifar, 2021). In particular, melanin production by *S. kathirae* could reach up to 13.7 g/L, but 128 h of incubation was required for the highest titer (Guo J. et al., 2014).

It is worth noting that metal ions are critical for eumelanin production. For example, ferrous and nickel ion supplementation has been reported to drive melanin production by improving tyrosinase activity or by inducing the synthesis of tyrosinase (Wang et al., 2019). According to optimization results, 1.33 g/L FeSO_4 and 3.05 mM NiCl_2 could produce approximately 189.9 mg/L of insoluble melanin and 4.24 g/L of soluble pure melanin. The supplementation of metal ions seemed to have a positive effect on the activation of melanin production; however, the produced melanin was also reported to be able to chelate or absorb metal ions, such as Cu(II) and Zn(II), which would result in a metal-melanin complex and affect its characteristic features (Caldas et al., 2020; He et al., 2020).

Pyomelanin and Allomelanin Production by Bacterial and Recombinant Strains

Another interesting type of melanin produced by bacteria is pyomelanin. Pyomelanin utilizes different synthetic pathways compared to bacterial eumelanin, even though they both are originated from L-tyrosine. The key enzyme in pyomelanin synthesis is the 4-hydroxyphenylpyruvate dioxygenase (4-HPPD) enzyme, which converts 4-hydroxyphenylpyruvate, a transaminated form of tyrosine, into homogentisate, a key intermediate in pyomelanin synthesis (Figure 1B). Recently, *Ralstonia picketti* was isolated and identified as capable of generating pyomelanin in the presence of tyrosine (Seo and Choi, 2020a). In the presence of 4 mM of tyrosine, *R. picketti* could produce about 0.09 g/L of pyomelanin within 62 h of incubation. To verify 4-HPPD-dependent pyomelanin synthesis, the encoding gene was isolated and cloned into *E. coli* BL21 (DE3). And the 4-HPPD overexpressing cells could produce 0.213 g/L of pyomelanin from 1 mM tyrosine within 24 h of incubation, suggesting that recombinant strain development could greatly enhance the production rate and titer (Seo and Choi, 2020a). Similarly, Bolognese

et al. isolated the 4-HPPD enzyme and constructed a pyomelanin-producing recombinant *E. coli* strain that could produce 0.213 g/L of pyomelanin (Bolognese et al., 2019). In addition to bacterial strains, the yeast strain *Yarrowia lypolytica* W29 was isolated and verified to be capable of producing 0.5 g/L of pyomelanin by 1 g/L of tyrosine feeding (Ben Tahar et al., 2020). However, similar to fungal melanin production, a 72 h of incubation period was required to achieve the highest titer.

The development of a recombinant strain to produce allomelanin has also been extensively studied. For example, caffeic acid-based allomelanin production was investigated by our group. Jang et al. first reported the co-expression of feruloyl-CoA synthetase (FCS) and enoyl-CoA hydratase/aldolase (ECH) in an *E. coli* strain that drives allomelanin production in the presence of caffeic acids (Jang et al., 2018). These enzymes have been previously utilized in vanillin synthesis from ferulic acid (Gallage et al., 2014). As caffeic acid has a catechol moiety in its core structure, contrary to ferulic acid of which one hydroxyl group was blocked by the methoxyl group, the enzymatic modification of the other carboxylic moiety could readily lead to the formation of allomelanin. The FCS/ECH overexpressing recombinant strain could produce 0.2 g/L of allomelanin within a 12 h reaction (~40.9 mg/L/h) (Jang et al., 2018). Ahn et al. also used the same strain to produce caffeic acid-based allomelanin and compared its chemical composition with that of other natural and synthetic melanin (Ahn et al., 2019). Interestingly, the caffeic acid-derived allomelanin showed substantial dyeing of the HEMA (hydroxyethyl methacrylate) polymer, which is generally used for soft contact lenses, suggesting the potential application of melanin as a UV-blocking contact lens.

Recombinant strains for melanin synthesis have several advantages, not only in terms of production rates and titers but also regarding extraction and purity. This was evident in studies conducted on the production of eumelanin and pyomelanin (Jang et al., 2018; Ahn et al., 2019; Bolognese et al., 2019; Park H. et al., 2020; Seo and Choi, 2020a). Another advantage is the possibility of an additional supply of melanin building blocks to control melanin chemical structure, this allows for the engineering of functionalities depending on the purpose of use. For example, we reported eumelanin engineering by co-expressing bacterial tyrosinase (MelC) with cytochrome P450 monooxygenase (CYP102G4), which is capable of catalyzing indole C2 hydroxylation (Park H. et al., 2020). The additionally supplied 2-hydroxyindole functioned as a new building block in melanin polymerization and could obtain different physical and electrical characteristics. However, several issues regarding the use of recombinant strains for melanin production should be addressed. For example, there is an issue regarding the safety of genetic engineering for use in cosmetics and pharmaceuticals. In addition, the dependency of the macroscopic structures and physical properties on the producing host should be considered.

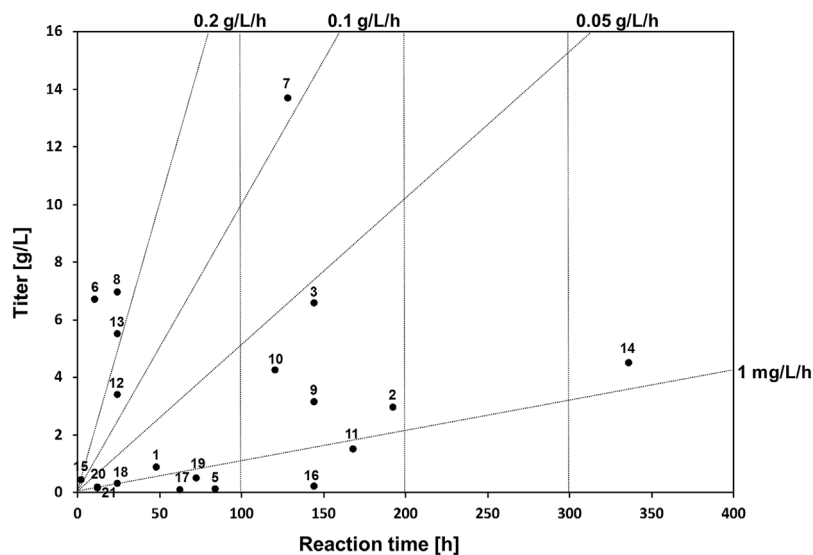


FIGURE 2 | Space-time yield analysis of whole-cell biotransformation in melanin production and reported bioreactor scale by biotransformation yields. The numbers next to the circles indicate the corresponding reference numbers in Table 1.

Understanding the Space-Time Yield of Melanin Bioproduction

To understand the reaction time and titer correlation in melanin production, a space-time yield analysis was conducted. Space-time yield analysis of the summarized microbial melanin production in g/L (closed circle, •) revealed that this biotransformation exhibited not distinct but observable two classes, namely those with a production rate range of less than 0.05 g/L/h and those with a range over 0.1 g/L/h (Figure 2). The first group includes most eumelanin- and pyromelanin-producing bacteria with less than 100 h of reaction time. The second group includes fungi and some *Streptomyces* species with more than 100 h of reaction time (Guo J. et al., 2014; Ribera et al., 2019). In particular, *A. auricula* showed the longest reaction time of 8 days with a moderate production titer (2.97 g/L) (Sun et al., 2016).

The second group had a relatively higher production rate. This group included several bacteria, such as *P. stutzeri*, *P. koreensis*, and *B. safensis*, which could produce more than 5 g/L of melanin within 24 h (Ganesh Kumar et al., 2013; Tarangini and Mishra, 2014; Eskandari and Etemadifar, 2021). Interestingly, melanin production by *S. kathirae*, with a 13.7 g/L titer within 128 h also belongs to this group, as it showed a production rate of more than 0.1 g/L/h (Guo J. et al., 2014). Compared to the fungal host system, the bacterial host system for whole-cell melanin production appears to be advantageous in terms of timescale, depending on the type of target melanin. However, several hurdles must be overcome to utilize bacterial hosts for industrial-scale production. One of the most limiting factors is the necessity of isolation and purification steps in circumstances where the synthesized melanin is not secreted. In addition, an adequate growth medium needs to be optimized to obtain a desirable cell mass.

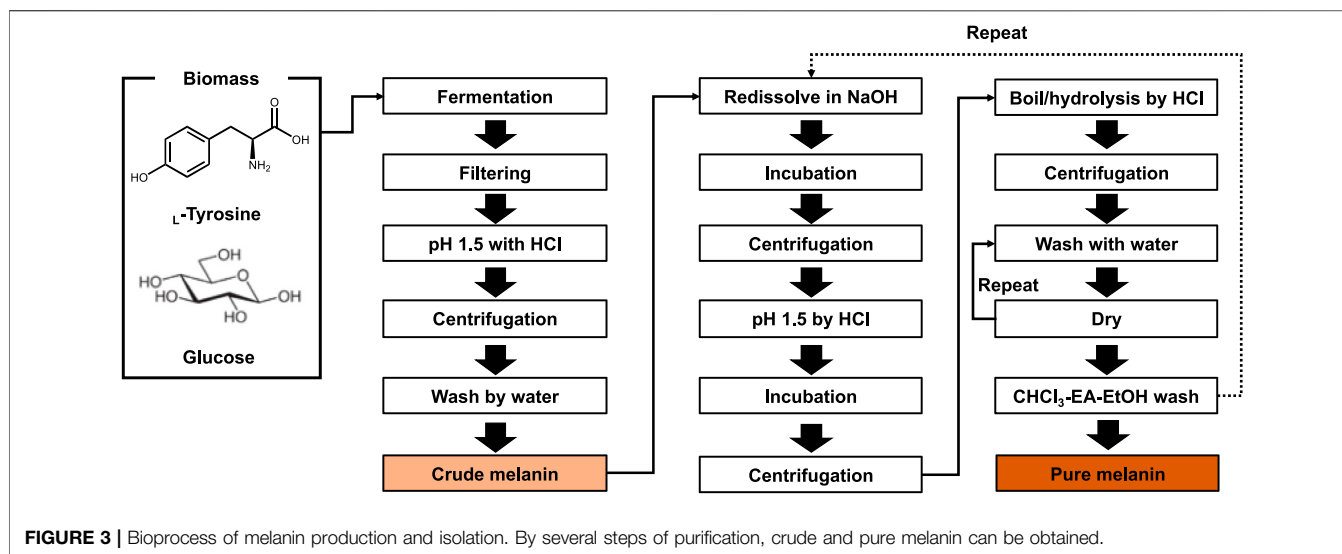
In general, the pH for fungal melanin production was less than 6, whereas it was approximately neutral in bacterial cases.

Although a pH of less than 7 was adopted for bacterial melanin production regarding *P. stutzeri*, *S. kathirae*, and *B. safensis*, which showed more than 5 g/L of production titer, the optimal pH for melanin production varied depending on the host cells (Ganesh Kumar et al., 2013; Guo J. et al., 2014; Eskandari and Etemadifar, 2021). The temperature for melanin synthesis is approximately 28°C for fungi and 30–37°C for bacterial systems. However, there seems to be no significant correlation between melanin production and temperature; rather, it seems more important to secure the maximal cell mass for melanin production under optimized conditions. Therefore, melanin production should be focused on the optimization of production parameters, such as growth medium composition, pH, temperature, extraction parameters, in addition to the design of response surface methodology in order to obtain a higher production titer and rate.

BIOPROCESS FOR MELANIN PRODUCTION; FERMENTATION, EXTRACTION, AND PURIFICATION

Extraction of Melanin From Melanin Production Culture

The basic melanin production process includes host selection, fermentation or biotransformation, followed by securing crude melanin through extraction and purification processes to obtain pure melanin (Figure 3). The method of extracting melanin differs depending on the host cell that is producing melanin, the intracellular localization of melanin, the structural properties of melanin, and the melanin crystal structure. As melanin pigment can easily be found in nature, research on extracting melanin was conducted early on (Aneesh et al., 2020). In



particular, methods for extracting melanin pigment from melanocytes and melanin organs, which are generally extracted by dissolving in an alkali or strong acid solution and heating (Young, 1921; Voss, 1954). For example, crude melanin was obtained by simple alkali extraction; however, the yield was as low as 2.59% (Ma et al., 2018). The extraction and purification process of melanin affects the purity of melanin, depending on the extraction method, the number of repeat cycles, and the form of melanin, namely crude or pure melanin.

Preparation of Crude Melanin From Melanin Extract

The detailed extraction process for microbial melanin production is presented in **Table 2**. Depending on the melanin source, it is divided into extracellular and intracellular melanin. Extracellular melanin extraction methods employ acid precipitation, whereas additional alkali extraction is necessary for intracellular melanin production. To assist alkali extraction, ultrasonic- or microwave-assisted methods were used (450 W for 50 min, or 70 W for 3 min periods with 30 cycles) (Sajjan et al., 2010; Jalmi et al., 2012; Lu et al., 2014; Hou et al., 2019; Liu et al., 2019). According to Hou et al., the ultrasonic-assisted extraction method yielded 37.33% pure melanin, whereas 24.24% was obtained without this step (Hou et al., 2019). Similarly, Lu et al. reported that a purification yield of 11.08% could be achieved through a microwave-assisted extraction method, which was 40.43% higher than that obtained by alkali extraction and acid precipitation. In addition, an additional step of boiling at 80°C for 2 h was employed to increase the extraction yields (Oh et al., 2020).

Before acid precipitation, filtering through various materials, such as 0.45 µm glass fiber, 0.45 µm nitrocellulose membrane, 0.22 µm membrane filter, and Millipore 0.2 µm polyether sulfone membrane, were employed to remove cell debris and byproducts (Jalmi et al., 2012; Ribera et al., 2019; Oh et al., 2020; Wang et al., 2020). To assist precipitation, a boiling or incubation step for several hours may be added (Sajjan et al., 2010; Sun et al., 2016;

Liu et al., 2019). After precipitation, a washing step with deionized water was conducted. Crude melanin could be prepared using these filtration-precipitation-centrifugation-washing procedures (**Figure 3**).

Preparation of Pure Melanin Powder From Crude Melanin

To increase the purity of the isolated crude melanin, several redissolution, precipitation, boiling, and washing steps were employed. In brief, crude melanin was dissolved in NaOH and collected by centrifugation. Thereafter, the pH of the collected sample was adjusted to approximately pH 2 with HCl, followed by incubation. The resuspended melanin was collected by centrifugation and washed several times with deionized water. Finally, the collected melanin was washed with CHCl₃, DCM, EA, and pure EtOH, followed by lyophilization. Depending on the melanin type and condition, extra boiling, acid-hydrolysis, and repetitive washing steps can be added to pure melanin (Sun et al., 2016; Liu et al., 2019; Ribera et al., 2019; Oh et al., 2020).

Several simplified extraction methods have been proposed, however, acid precipitation-pH adjustment-washing-resuspension steps are commonly used (Sajjan et al., 2010; Jalmi et al., 2012; Guo J. et al., 2014; Tarangini and Mishra, 2014; Ghadge et al., 2020; Wang et al., 2020). In addition, other useful technologies have been applied to melanin extraction. For example, enzymatic disruption of the cell membrane using protease or hydrolase enzymes, instead of alkali extraction, has been utilized. Additionally, a variety of organic solvents has been utilized for melanin extraction with excellent yields. With respect to bioprocess, an issue regarding environmental concerns should be considered as such use of organic solvent and effluent disposal for melanin isolation process. As described above, several extraction methods could be applied to different types of melanin and different sources, suggesting that no optimal method can be applied consistently. Depending on the chemical structure, type, solubility, and purpose of use, it

TABLE 2 | Extraction and purification process details in melanin biorefinery.

Sources	Sources	Melanin type	Extraction methods	Performance	Ref
Mushroom	<i>Auricularia auricula-judae</i>	—	69.11°C, 58.66 min, pH 12.81	2.59% yield	Ma et al. (2018)
Mushroom	<i>Inonotus hispidus</i>	—	Sample to liquid (1:50) in NaOH (0.56 mol/L) with ultrasonic waves-assisted extraction (300 W, 70°C, 70 min), collect by centrifugation (10,000 rpm, 10 min)	37.33% yield (24.24% yield w/o ultrasonic)	Hou et al. (2019)
Mushroom	<i>Auricularia auricula</i>	—	Crude melanin: sample to liquid (1:44) in NaOH (0.58 mol/L) with ultrasonic waves-assisted extraction (450 W, 70°C, 50 min), collection by centrifugation, adjust pH to 1.5 with HCl (6 mol/L), incubate at 80°C for 10 h, collect by centrifugation, and wash with deionized water Pure melanin: re-dissolve in NaOH (1.5 mol/L), collect by centrifugation (10,000 rpm, 5 min), adjust pH to 1.5 with HCl (6 mol/L), incubate at 4°C for 5 h, collect by centrifugation (10,000 rpm, 5 min), wash with deionized water to pH 7, wash with CHCl ₃ , DCM, EA, and EtOH, followed by freeze-drying	11.99% yield	Liu et al. (2019)
Mushroom	<i>Lachnum singerianum</i> YM296	—	NaOH concentration, 1.05 mol/L; ratio of raw material to liquid ratio, 1:14.72 (g/ml); microwave time, 118.70 s; and microwave power, 320 W	11.08% yield	Lu et al. (2014)
Fungus	<i>Gliocephalotrichum simplex</i>	Eumelanin	Collect by centrifugation (12,000 g, 15 min), filter using 0.22 µm membrane filters, precipitate using acetic acid (1 M), collect by centrifugation and wash, dry and resolubilize in NaOH (0.1 M, pH 12), adjust pH by HCl (0.1 M)	6.6 g/L	Jalmi et al. (2012)
Fungi	<i>Amorphotheca resiniae</i> KUC3009	Eumelanin-like	Crude melanin: filter through 0.45-µm glass fiber, mix with NH ₃ ·H ₂ O (1 M, 1:1 v/v), boil at 80°C for 2 h, adjust pH to 2 with HCl (6 M), incubate at 21°C for 24 h, and collect by centrifugation Pure melanin: resuspend in HCl (6 M), boil at 100°C for 4 h, rinse repeatedly with deionized water, re-dispersed in deionized water, extract with CHCl ₃ , EA, and EtOH, and lyophilize	4.5 g/L (13.4 mg/L/h)	Oh et al. (2020)
Fungi	<i>Auricularia auricula</i>	Eumelanin	Crude melanin: squeeze through a nylon mesh, adjust pH 1.5 with HCl (6 mol/L), store overnight at 4°C, collect by centrifugation (10,000 rpm, 15 min, at 4 °C), wash with deionized water, and dry Pure melanin: redissolve in NaOH (2 mol/L), stir overnight, collect by centrifugation (10,000 rpm, 15 min, at 4°C), adjust pH to 1.5 by HCl (7 mol/L), incubate at room temperature for 2 h, collect by centrifugation (10,000 rpm, 15 min, at 4°C), hydrolyze with HCl (7 mol/L) at 100°C for 2 h, collect by centrifugation (10,000 rpm, 15 min, at 4°C), wash three times with distilled water, dry and wash with CHCl ₃ , EA, EtOH, dry at room temperature, redissolve in NaOH (2 mol/L), collect by centrifugation (10,000 rpm, 15 min, at 4°C), adjust pH to 1.5, collect by centrifugation (10,000 rpm, 15 min, at 4°C), repeat and dry at 60°C	2.97 g/L	Sun et al. (2016)
Fungi	<i>Armillaria cepistipes</i>	Eumelanin	Raw melanin: filter through a 0.45 µm nitrocellulose membrane, sterilize by autoclaving (20 min, 121°C, 1 bar), and lyophilize (28.0 g/L melanin powder) Pure melanin: adjust pH to 2 by HCl (5 M), collect by centrifugation (8,000 rpm, 15 min), wash with water using four cycles of centrifugation–redispersion (until pH ~6 is reached, vortex, and sonicate), wash with EtOH three times, ethanolic suspension, and lyophilize	17.0 g/L pure melanin from 28.0 g/L raw melanin	Ribera et al. (2019)
Bacterial	<i>Pseudomonas koreensis</i> UIS 19	Eumelanin	Crude melanin: collect by centrifugation (2,600 g, 15 min), wash by EtOH-acetone (1:1) solution, collect by centrifugation (2,600 g, 15 min), boil for 15 min, and dry	0.44 g dry wt/g L-tyrosine	Eskandari and Etemadifar, (2021)
Bacterial	<i>Streptomyces kathirae</i>	Eumelanin	Collect by centrifugation (5,000 g, 15 min), adjust pH to 3, resuspend in HCl (6 M) for 4 h, collect by centrifugation (5,000 g at room temperature), adjust pH to 9 and 3 twice for precipitation, wash with distilled water, collect by centrifugation, and dry at 70°C	13.7 g/L	Guo et al. (2014a)
Bacterial	<i>Streptomyces glaucescens</i> NEAE-H	Eumelanin	Collect by centrifugation (5,000 g, 15 min), adjust pH to 2 by HCl (6 M) for 4 h, collect by centrifugation (9,000 g, 15 min), wash with distilled water for four times, collect by centrifugation (9,000 g, 15 min), and lyophilize	0.35 dry wt/L	El-Naggar and El-Ewasy, (2017)

(Continued on following page)

TABLE 2 | (Continued) Extraction and purification process details in melanin biorefinery.

Sources	Sources	Melanin type	Extraction methods	Performance	Ref
Bacterial	<i>Vibrio natriegens</i>	Eumelanin	Collect by centrifugation, filter through a Millipore 0.2- μ m polyether sulfone membrane, precipitate by HCl (6 N, 10% v/v), wash with deionizing water until neutral pH, and lyophilize	66 mg mel/g CDW/h	Wang et al. (2020)
Bacterial	<i>Bacillus subtilis</i> 4NP-BL	Eumelanin	Collect by centrifugation (6,720 g, 15 min), adjust pH 2 by HCl (6 M), precipitate for 4 h, collect by centrifugation (10,510 g, 15 min), wash with distilled water for four times, collect by centrifugation (10,510 g, 15 min), and vacuum-dry	1.5 g/L	Ghadge et al. (2020)
Bacterial	<i>Bacillus safensis</i>	Eumelanin	Collect by centrifugation (9,200 g, 15 min), suspended in distilled water, collect by centrifugation, adjust pH to 2 by HCl (3 N), incubate for 48 h at RT, repeat, boil for 5 min, and collect by centrifugation (4,600 g, 15 min)	6.96 g/L	Tarangini and Mishra, (2014)
Bacterial	<i>Amorphotheca resiniae</i>	Eumelanin	Collect by centrifugation, filter using 0.45- μ m glass fiber, mix with $\text{NH}_3\text{-H}_2\text{O}$ (1 M, 1:1 v/v), boil at 80°C for 2 h, adjust pH to 2 by HCl (6 M), incubate for 24 h at 21°C, collect by centrifugation, resuspend in HCl (6 M), boil at 100°C for 4 h, rinse repeatedly with deionized water, re-disperse in deionized water, extract with CHCl_3 , EA, and EtOH, and lyophilize	4.5 g/L	Oh et al. (2020)
Bacterial	<i>Klebsiella</i> sp. GSK 46	Eumelanin	Disrupt by Vibracell ultrasonicator in an ice bath (70 W, 30 cycles of 3 min, 1 min off per cycle), adjust pH to 2 by HCl (1 N), boil for 1 h, collect by centrifugation (8,000 g, 10 min), wash three times with HCl (0.1 N, 15 ml) and with water, mix with EtOH (10 ml), boil for 10 min, incubate at room temperature for 24 h, wash with EtOH two times, and dry in air	0.13 g/L	Sajjan et al. (2010)

seems appropriate to use optimized methods specific to each process.

LIMITATIONS OF MICROBIAL MELANIN IN COMMERCIALIZATION AND INDUSTRIAL USES

Despite its high potential as functional biomaterials, its commercialized use has been limited. One possible explanation for that is due to its complexity and diversity in commercialization. As the synthetic route includes radical-based random organization, keeping and controlling of physical properties and biological functionalities consistently is difficult. And this also relates to the difficulties in standardization of melanin quality and performance. Also, as it is produced by microorganisms, whether genetically modified or not, it is limited due to various regulations regarding human toxicity to be applied to physiologically active materials targeting the human body. Along with the harmful of toxic microorganisms, the use of strong acid/base and organic solvent of DCM, EA, and chloroform is surely a burden in effluent disposal and one of the limitations in the commercialization of microbial melanin, and this should be overcome by the engineering of isolation process with eco-friendly manner.

Besides, economics for the melanin production process should be considered. In industrial applications, materials that can produce several g/L of end products with wild-type strains are unusual even if no special genetic engineering is applied. In the biotransformation process, it is critical for the tyrosine

conversion reaction to secure an adequate cell mass and increase the activity of conversion enzymes, such as tyrosinase, laccase, and 4-HPPD. In addition, it is important to increase the production yield of melanin to ensure a competitive market price of melanin using tyrosine as a substrate, as tyrosine has a higher market price than sugar-based biomass. Alternatively, another solution could be the intracellular supply of tyrosine through metabolic engineering from cost-effective carbon sources. The application of melanin to high-value-added fields should also be considered.

APPLICATION OF MELANIN AND FUTURE PERSPECTIVES

Due to its black pigmentation in the skin, inhibition of melanin formation by tyrosinase inhibitors has been focused on for a long time. Such inhibitors are often utilized as ingredients in skin-whitening cosmetics (Cabanes et al., 1994; Netcharoensirisuk et al., 2021). However, interesting features of melanin, including its ability as a UV protector, a radical scavenger, and a chelator against metal ions, have driven melanin production as a functional material with promising cosmetic, pharmaceutical, and environmental applications. In addition, the electron-storing capacity of melanin has enabled its application as an electrode and supercapacitor (Park H. et al., 2020; Hernández-Velasco et al., 2020).

As such, a pigment made by microorganisms is receiving substantial focus. In particular, the use of bio-pigments with

biocompatibility can be used in various fields, such as cosmetics, medicine, pharmaceuticals, and the environment. Highlighting the industrial application of melanin, recently various products have been released in the beauty field of hair care, such as dyeing and shampooing, which utilize water-soluble squid melanin (Aghajanyan et al., 2005; Guo X. et al., 2014; Longo et al., 2017).

As a strategy for securing both the productivity and the high value-added application of melanin in biological processes, the simultaneous production of melanin and biochemicals in a single cell could also be used. For example, Ahn et al. recently reported the co-production of melanin with valuable biochemical, such as cadaverine, which is a diamino pentane obtained from the decarboxylation of lysine (Ahn et al., 2021). According to the study, the produced cadaverine was directly incorporated in melanin polymerization. This co-production process would be a solution to ensure a competitive market price. From a bioprocess point of view, it is appealing to produce biochemicals with such functionality only by single enzyme expression. Research on obtaining excellent functionality through additional building block-based structural modifications in recombinant melanin-producing strains should also be in the spotlight in the future.

CONCLUSION

Melanin is the pigment that is most frequently encountered and is one of the constituents of human skin tissue. Melanogenesis is possible in various organisms, and its mass production has become possible through the

discovery of melanin-producing microorganisms and bioconversion processes. As a result of the study on the complex melanin chemical structure and physicochemical properties, melanin extraction, separation, and purification optimization studies have been conducted. Through these studies, crude melanin and pure melanin can be produced at a level of several g/L. In the biochemical field, there is still a need for research on increased productivity at the level of space-time yields that can be matched in the fine chemical and pharmaceutical industries. Above all, two of the key limitations that need to be overcome for the industrial application of melanin are securing the substrate and securing price competitiveness in the bioconversion process of the tyrosine substrate. In addition, the link between biological function and structural complexity of melanin needs to be better understood to fully reproduce the functional properties of melanin, allowing for its development as an actual biochemical product.

AUTHOR CONTRIBUTIONS

K-YC designed the study and wrote the manuscript.

FUNDING

This work was supported by the National Research Foundation of Korea (NRF) grant funded by the Ministry of Education, Science, and Technology (MEST) (2021R1A2C1007519).

REFERENCES

- Aghajanyan, A. E., Hambardzumyan, A. A., Hovsepyan, A. S., Asaturian, R. A., Vardanyan, A. A., and Saghayan, A. A. (2005). Isolation, Purification and Physicochemical Characterization of Water-soluble *Bacillus Thuringiensis* melanin. *Pigment Cel Res* 18, 130–135. doi:10.1111/j.1600-0749.2005.00211.x
- Ahn, S.-Y., Choi, M., Jeong, D.-W., Park, S., Park, H., Jang, K.-S., et al. (2019). Synthesis and Chemical Composition Analysis of Protocatechualdehyde-Based Novel Melanin Dye by 15T FT-ICR: High Dyeing Performance on Soft Contact Lens. *Dyes Pigment* 160, 546–554. doi:10.1016/j.dyepig.2018.08.058
- Ahn, S. Y., Jang, S., Sudheer, P. D. V. N., and Choi, K. Y. (2021). Microbial Production of Melanin Pigments from Caffeic Acid and L-Tyrosine Using *Streptomyces Glaucoscens* and FCS-ECH-Expressing *Escherichia coli*. *Int. J. Mol. Sci.* 22. doi:10.3390/ijms22052413
- Aneesh, P. A., Anandan, R., Kumar, L. R. G., Ajeeshkumar, K. K., Kumar, K. A., and Mathew, S. (2020). A Step to Shell Biorefinery—Extraction of Astaxanthin-Rich Oil, Protein, Chitin, and Chitosan from Shrimp Processing Waste. *Biomass Convers. Biorefinery*
- Bellinger, F. P., Bellinger, M. T., Seale, L. A., Takemoto, A. S., Raman, A. V., Miki, T., et al. (2011). Glutathione Peroxidase 4 Is Associated with Neuromelanin in Substantia Nigra and Dystrophic Axons in Putamen of Parkinson's Brain. *Mol. Neurodegeneration* 6, 8. doi:10.1186/1750-1326-6-8
- Ben Tahar, I., Kus-Lisiewicz, M., Lara, Y., Javaux, E., and Fickers, P. (2020). Characterization of a Nontoxic Pyomelanin Pigment Produced by the Yeast *Yarrowia Lipolytica*. *Biotechnol. Prog.* 36, e2912. doi:10.1002/btpr.2912
- Bolognese, F., Scanferla, C., Caruso, E., and Orlandi, V. T. (2019). Bacterial Melanin Production by Heterologous Expression of 4-hydroxyphenylpyruvate D-oxxygenase from *Pseudomonas aeruginosa*. *Int. J. Biol. Macromolecules* 133, 1072–1080. doi:10.1016/j.jbiomac.2019.04.061
- Cabanes, J., Chazarra, S., and Garcia-Carmona, F. (1994). Kojic Acid, a Cosmetic Skin Whitening Agent, Is a Slow-Binding Inhibitor of Catecholase Activity of Tyrosinase. *J. Pharm. Pharmacol.* 46, 982–985. doi:10.1111/j.2042-7158.1994.tb03253.x
- Caldas, M., Santos, A. C., Veiga, F., Rebelo, R., Reis, R. L., and Corrello, V. M. (2020). Melanin Nanoparticles as a Promising Tool for Biomedical Applications - a Review. *Acta Biomater.* 105, 26–43. doi:10.1016/j.actbio.2020.01.044
- Camacho, E., Vij, R., Chrissian, C., Prados-Rosales, R., Gil, D., O'Meally, R. N., et al. (2019). The Structural Unit of Melanin in the Cell wall of the Fungal Pathogen *Cryptococcus Neoformans*. *J. Biol. Chem.* 294, 10471–10489. doi:10.1074/jbc.ra119.008684
- Choi, M. H., Choi, A. Y., Ahn, S.-Y., Choi, K.-Y., and Jang, K.-S. J. M. S. L. (2018). Mass Spectrometry-Based Metabolic Signatures of Sex Steroids in Breast Cancer. *Mol. Cell Endocrinol.* 466, 81–85. doi:10.1016/j.mce.2017.09.023
- Cordero, R. J. B., and Casadevall, A. (2017). Functions of Fungal Melanin beyond Virulence. *Fungal Biol. Rev.* 31, 99–112. doi:10.1016/j.fbr.2016.12.003
- Cubo, M. T., Buendia-Claveria, A. M., Beringer, J. E., and Ruiz-Sainz, J. E. (1988). Melanin Production by *Rhizobium* Strains. *Appl. Environ. Microbiol.* 54, 1812–1817. doi:10.1128/aem.54.7.1812-1817.1988
- Da Silva, M. B., Marques, A. F., Nosanchuk, J. D., Casadevall, A., Travassos, L. R., and Taborda, C. P. (2006). Melanin in the Dimorphic Fungal Pathogen *Paracoccidioides Brasiliensis*: Effects on Phagocytosis, Intracellular Resistance and Drug Susceptibility. *Microbes Infect.* 8, 197–205. doi:10.1016/j.micinf.2005.06.018
- Double, K. L., Dedov, V. N., Fedorow, H., Kettle, E., Halliday, G. M., Garner, B., et al. (2008). The Comparative Biology of Neuromelanin and Lipofuscin in the Human Brain. *Cell. Mol. Life Sci.* 65, 1669–1682. doi:10.1007/s00018-008-7581-9
- El-Naggar, N. E.-A., and El-Ewasy, S. M. (2017). Bioproduction, Characterization, Anticancer and Antioxidant Activities of Extracellular Melanin Pigment

- Produced by Newly Isolated Microbial Cell Factories *Streptomyces Glaucescens* NEAE-H. *Sci. Rep.* 7, 42129. doi:10.1038/srep42129
- Eskandari, S., and Etemadifar, Z. (2021). Melanin Biopolymers from Newly Isolated *Pseudomonas Korensis* Strain UIS 19 with Potential for Cosmetics Application, and Optimization on Molasses Waste Medium. *J. Appl. Microbiol.* 131, 1331–1343.
- Franzen, A. J., Cunha, M. M. L., Batista, E. J. O., Seabra, S. H., De Souza, W., and Rozental, S. (2006). Effects of Triclazazole (5-Methyl-1,2,4-Triazol[3,4] Benzothiazole), a Specific DHN-Melanin Inhibitor, on the Morphology of *Fonsecaea Pedrosi* Conidia and Sclerotic Cells. *Microsc. Res. Tech.* 69, 729–737. doi:10.1002/jemt.20344
- Frenk, E., and Lattion, F. (1982). The Melanin Pigmentary Disorder in a Family with Hermansky-Pudlak Syndrome. *J. Invest. Dermatol.* 78, 141–143. doi:10.1111/1523-1747.ep12506274
- Gallage, N. J., Hansen, E. H., Kannangara, R., Olsen, C. E., Motawia, M. S., Jørgensen, K., et al. (2014). Vanillin Formation from Ferulic Acid in Vanilla Planifolia Is Catalysed by a Single Enzyme. *Nat. Commun.* 5, 4037. doi:10.1038/ncomms5037
- Ganesh Kumar, C., Sahu, N., Narender Reddy, G., Prasad, R. B. N., Nagesh, N., and Kamal, A. (2013). Production of Melanin Pigment from *Pseudomonas Stutzeri* Isolated from Red Seaweed *Hypnea Musciformis*. *Lett. Appl. Microbiol.* 57, 295–302. doi:10.1111/lam.12111
- Ghadge, V., Kumar, P., Singh, S., Mathew, D. E., Bhattacharya, S., Nimse, S. B., et al. (2020). Natural Melanin Produced by the Endophytic *Bacillus Subtilis* 4NP-BL Associated with the Halophyte *Salicornia Brachiata*. *J. Agric. Food Chem.* 68, 6854–6863. doi:10.1021/acs.jafc.0c01997
- Gómez, B. L., Nosanchuk, J. D., Díez, S., Youngchim, S., Aisen, P., Cano, L. E., et al. (2001). Detection of Melanin-like Pigments in the Dimorphic Fungal Pathogen *Paracoccidioides Brasiliensis* *In Vitro* and during Infection. *Infect. Immun.* 69, 5760–5767. doi:10.1128/iai.69.9.5760-5767.2001
- Guo, J., Rao, Z., Yang, T., Man, Z., Xu, M., and Zhang, X. (2014a). High-level Production of Melanin by a Novel Isolate of *Streptomyces Kathirae*. *FEMS Microbiol. Lett.* 357, 85–91. doi:10.1111/1574-6968.12497
- Guo, X., Chen, S., Hu, Y., Li, G., Liao, N., Ye, X., et al. (2014b). Preparation of Water-Soluble Melanin from Squid Ink Using Ultrasound-Assisted Degradation and its Anti-oxidant Activity. *J. Food Sci. Technol.* 51, 3680–3690. doi:10.1007/s13197-013-0937-7
- Hagiwara, K., Okura, M., Sumikawa, Y., Hida, T., Kuno, A., Horio, Y., et al. (2016). Biochemical Effects of the Flavanol-Rich Lychee Fruit Extract on the Melanin Biosynthesis and Reactive Oxygen Species. *J. Dermatol.* 43, 1174–1183. doi:10.1111/1346-8138.13326
- He, X., Xie, Q., Fan, J., Xu, C., Xu, W., Li, Y., et al. (2020). Dual-functional Chemosensor with Colorimetric/ratiometric Response to Cu(II)/Zn(II) Ions and its Applications in Bioimaging and Molecular Logic gates. *Dyes Pigm.* 177, 108255. doi:10.1016/j.dyepig.2020.108255
- Hernández-Velasco, P., Morales-Atilano, I., Rodríguez-Delgado, M., Rodríguez-Delgado, J. M., Luna-Moreno, D., Ávalos-Alanís, F. G., et al. (2020). Photoelectric Evaluation of Dye-Sensitized Solar Cells Based on Prodigiosin Pigment Derived from *Serratia marcescens* 11E. *Dyes Pigm.* 177, 108278. doi:10.1016/j.dyepig.2020.108278
- Hou, R., Liu, X., Xiang, K., Chen, L., Wu, X., Lin, W., et al. (2019). Characterization of the Physicochemical Properties and Extraction Optimization of Natural Melanin from *Inonotus Hispidus* Mushroom. *Food Chem.* 277, 533–542. doi:10.1016/j.foodchem.2018.11.002
- Inamdar, S., Joshi, S., Bapat, V., and Jadhav, J. (2014). Innovative Use of *Mucuna Monosperma* (Wight) Callus Cultures for Continuous Production of Melanin by Using Statistically Optimized Biotransformation Medium. *J. Biotechnol.* 170, 28–34. doi:10.1016/j.jbiotec.2013.11.012
- Jalmi, P., Bodke, P., Wahidullah, S., and Raghukumar, S. (2012). The Fungus *Gliocephalotrichum Simplex* as a Source of Abundant, Extracellular Melanin for Biotechnological Applications. *World J. Microbiol. Biotechnol.* 28, 505–512. doi:10.1007/s11274-011-0841-0
- Jang, S., Gang, H., Kim, B.-G., and Choi, K.-Y. (2018). FCS and ECH Dependent Production of Phenolic Aldehyde and Melanin Pigment from L-Tyrosine in *Escherichia coli*. *Enzyme Microb. Tech.* 112, 59–64. doi:10.1016/j.enzmictec.2017.10.011
- Kuzumaki, T., Matsuda, A., Wakamatsu, K., Ito, S., and Ishikawa, K. (1993). Eumelanin Biosynthesis Is Regulated by Coordinate Expression of Tyrosinase and Tyrosinase-Related Protein-1 Genes. *Exp. Cell Res.* 207, 33–40. doi:10.1006/excr.1993.1159
- Lefevre, C. E., and Perrett, D. I. (2015). Fruit over Sunbed: Carotenoid Skin Colouration Is Found More Attractive Than Melanin Colouration. *Q. J. Exp. Psychol.* 68, 284–293. doi:10.1080/17470218.2014.944194
- Li, S., Yang, L., Li, J., Chen, T., and Ye, M. (2019). Structure, Molecular Modification, and Anti-radiation Activity of Melanin from *Lachnum YM156* on Ultraviolet B-Induced Injury in Mice. *Appl. Biochem. Biotechnol.* 188, 555–567. doi:10.1007/s12010-018-2898-9
- Liu, X., Hou, R., Wang, D., Mai, M., Wu, X., Zheng, M., et al. (2019). Comprehensive Utilization of Edible Mushroom *Auricularia Auricula* Waste Residue-Extraction, Physicochemical Properties of Melanin and its Antioxidant Activity. *Food Sci. Nutr.* 7, 3774–3783. doi:10.1002/fsn3.1239
- Longo, D. L., Stefania, R., Callari, C., De Rose, F., Rolle, R., Conti, L., et al. (2017). Water Soluble Melanin Derivatives for Dynamic Contrast Enhanced Photoacoustic Imaging of Tumor Vasculature and Response to Antiangiogenic Therapy. *Adv. Healthc. Mater.* 6, doi:10.1002/adhm.201600550
- Lu, Y., Ye, M., Song, S., Li, L., Shaikh, F., and Li, J. (2014). Isolation, Purification, and Anti-aging Activity of Melanin from *Lachnum Singerianum*. *Appl. Biochem. Biotechnol.* 174, 762–771. doi:10.1007/s12010-014-1110-0
- Ma, Y.-P., Bao, Y.-H., Kong, X.-H., Tian, J.-J., Han, B., Zhang, J.-C., et al. (2018). Optimization of Melanin Extraction from the Wood Ear Medicinal Mushroom, *Auricularia Auricula-Judae* (Agaricomycetes), by Response Surface Methodology and its Antioxidant Activities *In Vitro*. *Int. J. Med. Mushrooms* 20, 1087–1095. doi:10.1615/intjmedmushrooms.2018028694
- Madhusudhan, D. N., Mazhari, B. B., Dastager, S. G., and Agsar, D. (2014). Production and Cytotoxicity of Extracellular Insoluble and Droplets of Soluble Melanin by *Streptomyces Lusitanus* DMZ-3. *Biomed. Res. Int.* 2014, 306895. doi:10.1155/2014/306895
- Mccallum, N. C., Son, F. A., Clemons, T. D., Weigand, S. J., Gnanasekaran, K., Battistella, C., et al. (2021). Allomelanin: A Biopolymer of Intrinsic Microporosity. *J. Am. Chem. Soc.* 143, 4005–4016. doi:10.1021/jacs.1c00748
- Morris-Jones, R., Youngchim, S., Gomez, B. L., Aisen, P., Hay, R. J., Nosanchuk, J. D., et al. (2003). Synthesis of Melanin-like Pigments by *Sporothrix Schenckii* *In Vitro* and during Mammalian Infection. *Infect. Immun.* 71, 4026–4033. doi:10.1128/iai.71.7.4026-4033.2003
- Mustafa, G., Arshad, M., Bano, I., and Abbas, M. (2020). Biotechnological Applications of Sugarcane Bagasse and Sugar Beet Molasses. *Biomass Convers. Biorefinery*
- Nagai, M., Kawata, M., Watanabe, H., Ogawa, M., Saito, K., Takesawa, T., et al. (2003). Important Role of Fungal Intracellular Laccase for Melanin Synthesis: Purification and Characterization of an Intracellular Laccase from *Lentinula Edodes* Fruit Bodies. *Microbiology (Reading)* 149, 2455–2462. doi:10.1099/mic.0.26414-0
- Netchaeronsirak, P., Abrahamian, C., Tang, R., Chen, C.-C., Rosato, A. S., Beyers, W., et al. (2021). Flavonoids Increase Melanin Production and Reduce Proliferation, Migration and Invasion of Melanoma Cells by Blocking Endolysosomal/melanosomal TPC2. *Sci. Rep.* 11, 8515. doi:10.1038/s41598-021-88196-6
- Nosanchuk, J. D., and Casadevall, A. (2003). The Contribution of Melanin to Microbial Pathogenesis. *Cell Microbiol.* 5, 203–223. doi:10.1046/j.1462-5814.2003.00268.x
- Nosanchuk, J. D., Go'mez, B. L., Youngchim, S., Di'ez, S., Aisen, P., Zancopé-Oliveira, R. M., et al. (2002). Histoplasma Capsulatum Synthesizes Melanin-like Pigments *In Vitro* and during Mammalian Infection. *Infect. Immun.* 70, 5124–5131. doi:10.1128/iai.70.9.5124-5131.2002
- Nosanchuk, J. D., Stark, R. E., and Casadevall, A. (2015). Fungal Melanin: What Do We Know about Structure? *Front. Microbiol.* 6, 1463. doi:10.3389/fmicb.2015.01463
- Nosanchuk, J. D., Yu, J.-J., Hung, C.-Y., Casadevall, A., and Cole, G. T. (2007). *Coccidioides Posadasii* Produces Melanin *In Vitro* and during Infection. *Fungal Genet. Biol.* 44, 517–520. doi:10.1016/j.fgb.2006.09.006
- Oh, J.-J., Kim, J. Y., Kwon, S. L., Hwang, D.-H., Choi, Y.-E., and Kim, G.-H. (2020). Production and Characterization of Melanin Pigments Derived from *Amorphotheca Resinae*. *J. Microbiol.* 58, 648–656. doi:10.1007/s12275-020-0054-z
- Park, H., Yang, I., Choi, M., Jang, K.-S., Jung, J. C., and Choi, K.-Y. (2020a). Engineering of Melanin Biopolymer by Co-expression of MeC Tyrosinase with CYP102G4 Monooxygenase: Structural Composition Understanding by 15 Tesla FT-ICR MS Analysis. *Biochem. Eng. J.* 157, 107530. doi:10.1016/j.bej.2020.107530
- Park, S., Lee, C., Lee, J., Jung, S., and Choi, K.-Y. (2020b). Applications of Natural and Synthetic Melanins as Biosorbents and Adhesive Coatings. *Biotechnol. Bioproc. E* 25, 646–654. doi:10.1007/s12257-020-0077-7
- Perez-Cuesta, U., Aparicio-Fernandez, L., Guruceaga, X., Martin-Souto, L., Abad-Díaz-De-Cerio, A., Antoran, A., et al. (2020). Melanin and Pyomelanin in

- Aspergillus fumigatus*: from its Genetics to Host Interaction. *Int. Microbiol.* 23, 55–63. doi:10.1007/s10123-019-00078-0
- Powell, B. J., Baruah, T., Bernstein, N., Brake, K., Mckenzie, R. H., Meredith, P., et al. (2004). A First-Principles Density-Functional Calculation of the Electronic and Vibrational Structure of the Key Melanin Monomers. *J. Chem. Phys.* 120, 8608–8615. doi:10.1063/1.1690758
- Prados-Rosales, R., Toriola, S., Nakouzi, A., Chatterjee, S., Stark, R., Gerfen, G., et al. (2015). Structural Characterization of Melanin Pigments from Commercial Preparations of the Edible Mushroom *Auricularia Auricula*. *J. Agric. Food Chem.* 63, 7326–7332. doi:10.1021/acs.jafc.5b02713
- Pralea, I. E., Moldovan, R. C., Petrache, A. M., Ilies, M., Heghes, S. C., Ielciu, I., et al. (2019). From Extraction to Advanced Analytical Methods: The Challenges of Melanin Analysis. *Int. J. Mol. Sci.* 20. doi:10.3390/ijms20163943
- Pukalski, J., Marcol, N., Wolan, N., Plonka, P. M., Ryszka, P., Kowalski, T., et al. (2020). Detection of a Pheomelanin-like Pigment by EPR Spectroscopy in the Mycelium of *Plenodomus Biglobosus*. *Acta Biochim. Pol.* 67, 295–301. doi:10.18388/abp.2020_5405
- Qi, Y., Liu, J., Liu, Y., Yan, D., Wu, H., Li, R., et al. (2020). Polyphenol Oxidase Plays a Critical Role in Melanin Formation in the Fruit Skin of Persimmon (*Diospyros Kaki* Cv. 'Heishi'). *Food Chem.* 330. 127253. doi:10.1016/j.foodchem.2020.127253
- Ribera, J., Panzarasa, G., Stobbe, A., Osypova, A., Rupper, P., Klose, D., et al. (2019). Scalable Biosynthesis of Melanin by the Basidiomycete *Armillaria Cepistipes*. *J. Agric. Food Chem.* 67, 132–139. doi:10.1021/acs.jafc.8b05071
- Rosas, Á. L., Nosanchuk, J. D., Gómez, B. L., Edens, W. A., Henson, J. M., and Casadevall, A. (2000). Isolation and Serological Analyses of Fungal Melanins. *J. Immunological Methods* 244, 69–80. doi:10.1016/s0022-1759(00)00255-6
- Sajjan, S., Kulkarni, G., Yaligara, V., Kyoung, L., and Karegoudar, T. B. (2010). Purification and Physicochemical Characterization of Melanin Pigment from *Klebsiella* Sp. GSK. *J. Microbiol. Biotechnol.* 20, 1513–1520. doi:10.4014/jmb.1002.02006
- Schmidt, F. M., Nowak, C., Kratzsch, J., Sander, C., Hegerl, U., and Schönknecht, P. (2015). Dynamics of Melanin-Concentrating Hormone (MCH) Serum Levels in Major Depressive Disorder during Antidepressant Treatment. *J. Affective Disord.* 180, 207–213. doi:10.1016/j.jad.2015.03.039
- Schroeder, R. L., Double, K. L., and Gerber, J. P. (2015). Using Sepia Melanin as a PD Model to Describe the Binding Characteristics of Neuromelanin - A Critical Review. *J. Chem. Neuroanat.* 64–65, 20–32. doi:10.1016/j.jchemneu.2015.02.001
- Seo, D., and Choi, K.-Y. (2020a). Heterologous Production of Pyomelanin Biopolymer Using 4-hydroxyphenylpyruvate Dioxygenase Isolated from *Ralstonia Pickettii* in *Escherichia coli*. *Biochem. Eng. J.* 157. 107548. doi:10.1016/j.bej.2020.107548
- Seo, D., and Choi, K.-Y. (2020b). Heterologous Production of Pyomelanin Biopolymer Using 4-hydroxyphenylpyruvate Dioxygenase Isolated from *Ralstonia Pickettii* in *Escherichia coli*. *Biochem. Eng. J.* 157. 107548. doi:10.1016/j.bej.2020.107548
- Simon, J. D., and Rózanowska, M. (2008). Perspectives on the Structure and Function of Melanin. *Pigment Cel Melanoma Res* 21, 346–347. doi:10.1111/j.1755-148x.2008.00455.x
- Singh, S., Nimse, S. B., Mathew, D. E., Dhimmara, A., Sahastrabudhe, H., Gajjar, A., et al. (2021). Microbial Melanin: Recent Advances in Biosynthesis, Extraction, Characterization, and Applications. *Biotechnol. Adv.*, 107773
- Srisuk, P., Corredo, V. M., Leonor, I. B., Palladino, P., and Reis, R. L. (2016). Redox Activity of Melanin from the Ink Sac of *Sepia Officinalis* by Means of Colorimetric Oxidative Assay. *Nat. Product. Res.* 30, 982–986. doi:10.1080/14786419.2015.1079185
- Sun, S., Zhang, X., Chen, W., Zhang, L., and Zhu, H. (2016). Production of Natural Edible Melanin by *Auricularia Auricula* and its Physicochemical Properties. *Food Chem.* 196, 486–492. doi:10.1016/j.foodchem.2015.09.069
- Suo, D., Zeng, S., Zhang, J., Meng, L., and Weng, L. (2020). PM2.5 Induces Apoptosis, Oxidative Stress Injury and Melanin Metabolic Disorder in Human Melanocytes. *Exp. Ther. Med.* 19, 3227–3238. doi:10.3892/etm.2020.8590
- Surwase, S. N., Jadhav, S. B., Phugare, S. S., and Jadhav, J. P. (2013). Optimization of Melanin Production by *Brevundimonas* Sp. SGJ Using Response Surface Methodology. *3 Biotech.* 33, 187–194. doi:10.1007/s13205-012-0082-4
- Tarangini, K., and Mishra, S. (2014). Production of Melanin by Soil Microbial Isolate on Fruit Waste Extract: Two Step Optimization of Key Parameters. *Biotechnol. Rep.* 4, 139–146. doi:10.1016/j.btre.2014.10.001
- Usunoff, K. G., Itzev, D. E., Ovtsharoff, W. A., and Marani, E. (2002). Neuromelanin in the Human Brain: a Review and Atlas of Pigmented Cells in the Substantia Nigra. *Arch. Physiol. Biochem.* 110, 257–369. doi:10.1076/apab.110.4.257.11827
- Valdez-Calderón, A., Barraza-Salas, M., Quezada-Cruz, M., Islas-Ponce, M. A., Angeles-Padilla, A. F., Carrillo-Ibarra, S., et al. (2020). Production of Polyhydroxybutyrate (PHB) by a Novel *Klebsiella pneumoniae* Strain Using Low-Cost media from Fruit Peel Residues. *Biomass Convers. Biorefinery*
- Varga, M., Berkesi, O., Darula, Z., May, N. V., and Palágyi, A. (2016). Structural Characterization of Allomelanin from Black Oat. *Phytochemistry* 130, 313–320. doi:10.1016/j.phytochem.2016.07.002
- Voss, E. (1954). Extraction Trials on Melanin Pigment with Perchloric Acid. *Acta Histochem.* 1, 111–115.
- Walker, C. A., Gómez, B. L., Mora-Montes, H. M., Mackenzie, K. S., Munro, C. A., Brown, A. J. P., et al. (2010). Melanin Externalization in *Candida Albicans* Depends on Cell wall Chitin Structures. *Eukaryot. Cel* 9, 1329–1342. doi:10.1128/ec.00051-10
- Wang, L., Li, Y., and Li, Y. (2019). Metal Ions Driven Production, Characterization and Bioactivity of Extracellular Melanin from *Streptomyces* Sp. ZL-24. *Int. J. Biol. Macromolecules* 123, 521–530. doi:10.1016/j.ijbiomac.2018.11.061
- Wang, Z., Tschirhart, T., Schultzhau, Z., Kelly, E. E., Chen, A., Oh, E., et al. (2020). Melanin Produced by the Fast-Growing Marine Bacterium *Vibrio Natrigens* through Heterologous Biosynthesis: Characterization and Application. *Appl. Environ. Microbiol.* 86. doi:10.1128/AEM.02749-19
- Wolnicka-Glubisz, A., Pecio, A., Podkova, D., Kolodziejczyk, L. M., and Plonka, P. M. (2012). Pheomelanin in the Skin of *Hymenochirus Boettgeri* (Amphibia: Anura: Pipidae). *Exp. Dermatol.* 21, 537–540. doi:10.1111/j.1600-0625.2012.01511.x
- Wood, J. M., and Schallreuter, K. U. (2006). UVA-irradiated Pheomelanin Alters the Structure of Catalase and Decreases its Activity in Human Skin. *J. Invest. Dermatol.* 126, 13–14. doi:10.1038/sj.jid.5700051
- Young, W. J. (1921). The Extraction of Melanin from Skin with Dilute Alkali. *Biochem. J.* 15, 118–122. doi:10.1042/bj0150118
- Zucca, F. A., Segura-Aguilar, J., Ferrari, E., Muñoz, P., Paris, I., Sulzer, D., et al. (2017). Interactions of Iron, Dopamine and Neuromelanin Pathways in Brain Aging and Parkinson's Disease. *Prog. Neurobiol.* 155, 96–119. doi:10.1016/j.pneurobio.2015.09.012

Conflict of Interest: The author declares that the research was conducted in the absence of any commercial or financial relationships that could be construed as a potential conflict of interest.

Publisher's Note: All claims expressed in this article are solely those of the authors and do not necessarily represent those of their affiliated organizations, or those of the publisher, the editors and the reviewers. Any product that may be evaluated in this article, or claim that may be made by its manufacturer, is not guaranteed or endorsed by the publisher.

Copyright © 2021 Choi. This is an open-access article distributed under the terms of the Creative Commons Attribution License (CC BY). The use, distribution or reproduction in other forums is permitted, provided the original author(s) and the copyright owner(s) are credited and that the original publication in this journal is cited, in accordance with accepted academic practice. No use, distribution or reproduction is permitted which does not comply with these terms.



The Kinetics Studies on Hydrolysis of Hemicellulose

Qi Yuan¹, Shan Liu², Ming-Guo Ma^{1*}, Xing-Xiang Ji^{2*}, Sun-Eun Choi^{3*} and Chuanling Si^{4*}

¹Engineering Research Center of Forestry Biomass Materials and Bioenergy, Research Center of Biomass Clean Utilization, Beijing Key Laboratory of Lignocellulosic Chemistry, College of Materials Science and Technology, Beijing Forestry University, Beijing, China, ²State Key Laboratory of Biobased Material and Green Papermaking, Qilu University of Technology (Shandong Academy of Sciences), Jinan, China, ³Department of Forest Biomaterials Engineering, College of Forest and Environmental Sciences, Gangwon National University, Chuncheon, South Korea, ⁴Tianjin Key Laboratory of Pulp and Paper, Tianjin University of Science and Technology, Tianjin, China

OPEN ACCESS

Edited by:

Caoxing Huang,
Nanjing Forestry University, China

Reviewed by:

Liqiu Hu,
Åbo Akademi University, Finland
Jingsan Xu,
Queensland University of Technology,
Australia

*Correspondence:

Ming-Guo Ma
mg_ma@bjfu.edu.cn
Xing-Xiang Ji
jxx@qlu.edu.cn
Sun-Eun Choi
oregonin@kangwon.ac.kr
Chuanling Si
sichli@tust.edu.cn

Specialty section:

This article was submitted to
Green and Sustainable Chemistry,
a section of the journal
Frontiers in Chemistry

Received: 22 September 2021

Accepted: 07 October 2021

Published: 18 November 2021

Citation:

Yuan Q, Liu S, Ma M-G, Ji X-X,
Choi S-E and Si C (2021) The Kinetics
Studies on Hydrolysis
of Hemicellulose.
Front. Chem. 9:781291.
doi: 10.3389/fchem.2021.781291

The kinetics studies is of great importance for the understanding of the mechanism of hemicellulose pyrolysis and expanding the applications of hemicellulose. In the past years, rapid progress has been paid on the kinetics studies of hemicellulose hydrolysis. In this article, we first introduced the hydrolysis of hemicelluloses *via* various strategies such as autohydrolysis, dilute acid hydrolysis, catalytic hydrolysis, and enzymatic hydrolysis. Then, the history of kinetic models during hemicellulose hydrolysis was summarized. Special attention was paid to the oligosaccharides as intermediates or substrates, acid as catalyst, and thermogravimetric as analyzer method during the hemicellulose hydrolysis. Furthermore, the problems and suggestions of kinetic models during hemicellulose hydrolysis was provided. It expected that this article will favor the understanding of the mechanism of hemicellulose pyrolysis.

Keywords: hemicellulose, hydrolysis, kinetics, oligosaccharides, acid, thermogravimetric analyzer

INTRODUCTION

Chemical kinetics explore the reaction rate and reaction mechanism of chemical processes, which is often the decisive factor in the process of chemical production (Bazant, 2013; An et al., 2019; Hu et al., 2019; Li et al., 2019; Kumar et al., 2020). In comparison with chemical thermodynamics, chemical kinetics observe the chemical reaction from a dynamic point of view and studies the required time and micro processes for the transformation of the reaction system (Real et al., 2009; Xu R. et al., 2021), whose object is a non-equilibrium dynamic system. Chemical kinetics were used to explore the mechanism of chemical reaction based on the factors, such as temperature, pressure, catalyst, and solvent (Harvey, 2007; Lu et al., 2019; Ma et al., 2020; Xu R. et al., 2020). One can control the reaction conditions, improve the rate of reaction, reduce byproducts, and improve product quality through the chemical kinetics.

Classical chemical kinetics is based on the original experimental data of concentration and time, and obtains some reaction kinetic parameters including reaction rate constant, activation energy, and pre-exponential factor. The research on the kinetics was widely carried out based on elementary reaction kinetics and active intermediates (Zarea, 2002; Liu S. et al., 2021; Liu et al., 2021; Ma et al., 2021). The reaction intermediates were detected and analyzed to understand the reaction mechanism. The chemical kinetics were widely used in chemical engineering, catalysis, pharmacy, and environment (Yang and Lee, 2005; Zazo et al., 2005; Gillespie, 2007). There are many reports on the application of kinetics in biomass pyrolysis (Ranzi et al., 2008; White et al., 2011; Mishra and Mohanty, 2018). Lignocellulosic biomass is one of the most abundant resources, which is

TABLE 1 | The comparison of four hydrolysis methods.

Hydrolysis methods	Advantage	Disadvantage
Autohydrolysis	Low-cost simple production	Low yield
Dilute acid hydrolysis	wide source of materials low cost	High reaction temperature, more byproducts
Catalytic hydrolysis	Short reaction time; high yield	Corrosive, environmental, and handling problems
Enzymatic hydrolysis	High specificity mild reaction conditions	Long reaction time; high requirements for equipment

a promising source of renewable energy (Du et al., 2019; Liu et al., 2020a; Wang H. et al., 2020; Liu et al., 2021b; Liu et al., 2021c). Lignocellulosic biomass is mainly composed of cellulose, hemicelluloses, and lignin (Liu et al., 2020b; Liu et al., 2020; Liu et al., 2021a; Du et al., 2021b; Liu et al., 2021d; Wang et al., 2021). Hemicellulose is a polysaccharide composed of different types of monosaccharides such as xylose, arabinose, galactose, and so on. The content and composition of hemicellulose vary greatly with plant species, maturity, early and late wood, cell type, and morphological position (Scheller and Ulvskov, 2010). Hemicellulose pyrolysis is a fundamental thermochemical conversion process, which is a very complex reaction (Yang et al., 2007; Du et al., 2021a; Xu T. et al., 2021). Therefore, the exact mechanism for hemicellulose pyrolysis still needs to be explored. Moreover, cellulose is the major source of fermentable sugars for the production of ethanol in biomass, which is protected by a network of lignin and hemicellulose (Girio et al., 2010; Collard and Blin, 2014; Dai et al., 2019; Yang et al., 2019; Chen et al., 2020a; Xu J. et al., 2020). The hemicellulose pyrolysis removes the protecting shield, making the cellulose more susceptible to enzymatic digestion (Chen et al., 2020b; Dai et al., 2020; Huang et al., 2020; Lin et al., 2020; Zhang et al., 2021; Zheng et al., 2021). Therefore, understanding the mechanism of hemicellulose pyrolysis by chemical kinetics is of great importance for the applications of hemicellulose.

The review paper introduced the hydrolysis of hemicelluloses, reviewed the history of kinetic models during hemicellulose hydrolysis, provided the kinetic models, and comparatively evaluated kinetic parameters. The kinetic models were influenced by many parameters such as intermediates, temperature, and catalyst. The oligosaccharides as intermediates or substrates, acid as catalyst, and thermogravimetric as analyzer method were summarized during the hemicellulose hydrolysis. We expect that this review paper would put forward the developments and applications of the hemicelluloses.

HYDROLYSIS OF HEMICELLULOSES

The structure and composition of hemicellulose vary greatly with biomass species, cell type, morphological position, and pyrolysis methods. The pyrolysis, such as autohydrolysis, dilute acid hydrolysis, catalytic hydrolysis, and enzymatic hydrolysis, is an important strategy to obtain hemicellulose and its derivatives for the fabrication of materials and chemicals (Delbecq et al., 2018). **Table 1** displays the comparison of four hydrolysis methods. In the previous review article (Kapu and Trajano, 2014), Kapu and Trajano summarized the hydrolysis mechanism of

polysaccharide in softwoods and bamboo in depth, and overviewed the effects of all temperature, time, acid concentration, size, reactor configuration on the hydrolysis comprehensively, and presented the types, strengths, and weaknesses of kinetic models of the hemicellulose hydrolysis. In Negahdar's work, they reported on aqueous-phase hydrolysis of cellulose and hemicelluloses over molecular acidic catalysts in detail (Negahdar et al., 2016). Three approaches, including the simplest kinetic models, oligosaccharides as intermediates, and oligosaccharides as model compounds, were discussed to understand the reaction mechanism systematically.

The autohydrolysis and dilute acid hydrolysis methods are traditional treatments to extract hemicellulose. For example, aspen wood chip was subjected to autohydrolysis with sulfuric acid to extract hemicelluloses (Al-Dajani et al., 2009). It obtained suitable conditions for the extraction of hemicellulose using H_2SO_4 at a liquor to wood ratio of 4:1 for 4.5 h. In 2016, authors investigated the change in proton concentration for bamboo hemicellulose between autohydrolysis and dilute acid hydrolysis (Kapu et al., 2016). It found that all the acetyl group, ash content, initial acid concentration, and temperature affected the evolution of proton concentration during hydrolysis. The dilute sulfuric acid was used to treat three sugarcane hybrids to explore the removal of hemicellulose on the enzymatic conversion efficiency of glucan (Santos et al., 2018). It obtained the enzymatic glucan conversion of 92%–100% for post-delignification of acid-pretreated samples. A solution of hemicellulosic saccharides was obtained by non-isothermal autohydrolysis from Birch (Rivas et al., 2016). The xylan derived soluble saccharides and furfural with a yield of 80.5% based on the kinetic modeling. It converted 44.8% of substrates in furfural at 170°C with 1% sulfuric acid. Recently, Xu Y. et al. investigated the behavior of *Populus tomentosa* hemicellulose and the formation of furfural in the autohydrolysis process at 160–180°C (Xu Y. et al., 2020). The hemicellulose was converted to corresponding monosaccharides at an ultra-high hydrolysis rate. At 180°C for 2 h, it achieved the hydrolysis rate of 91, 100, 95, 58, and 37%, for xylose, rhamnose, galactose, mannose, and glucose from hemicellulose, respectively.

In addition, both acid hydrolysis and enzymatic hydrolysis were successfully developed to obtain xylooligosaccharides based on the dissolving pulp hemicellulose (Wang et al., 2018; Lin et al., 2019; Gu et al., 2020; Lin et al., 2021). It obtained the highest xylooligosaccharides yield of 45.18% from 1% sulfuric acid at 120°C for 60 min. Meanwhile, it achieved the highest xylooligosaccharides yield of 42.96% for enzymatic hydrolysis. Lopes et al. also demonstrated the separation of hemicellulose-derived sugar of xylose in acidic green ionic liquid (da Costa Lopes and Łukasik, 2018). It achieved very high recovery yields of

90.8 wt% for the ionic liquid and 98.1 wt% for xylose by alumina treatment. Obviously, the acidic green ionic liquid displayed a similar mechanism of hydrolysis of hemicellulose, compared with acid hydrolysis. Relvas, Morais, and Bogel-Lukasik focused on hydrolysis kinetic models of hemicellulose from wheat straw using novel high-pressure CO_2 - H_2O method (Relvas et al., 2015a). The three accurate kinetic models of xylan conversion, arabinoxylan hydrolysis, and acetyl group hydrolysis were developed to describe the effect of CO_2 pressure and reaction time on the intermediate compounds of xylose and arabinose. CO_2 had an effect on the hydrolysis kinetics of hemicellulose as the fastest step of polysaccharide hydrolysis in sugars. The initial kinetic constant of the aforementioned reaction was increased by almost 40% with CO_2 , compared with the water process. Moreover, the high-pressure CO_2 - H_2O method was also applied to selectively hydrolyze hemicellulose of wheat straw in acetic acid with a low concentration (Li M. et al., 2020). The hemicellulose selective hydrolysis was catalyzed by both carbonic acid and acetic acid. It reached the hemicellulose removal ratio of 82.3% using high-pressure acetic acid at 180°C for 1 h.

Recently, there are various reports on the enzymatic hydrolysis of hemicellulose. Ostadjoo et al., 2019 introduced the efficient enzymatic hydrolysis of hemicellulose using xylanase from *Thermomyces lanuginosus* (Ostadjoo et al., 2019). The enzymatic process enabled hydrolysis of hemicellulose to soluble oligoxylosaccharides in >70% yields. CO_2 -assisted hydrothermal method was developed for selective degradation of wheat straw hemicellulose to enhance the enzymatic hydrolysis efficiency for glucose (Wang R. et al., 2020). It obtained the significantly high efficiency of enzymatic hydrolysis due to the loose structure after hemicellulose removal. It achieved more than 72.7% of glucose after enzymatic hydrolysis, compared with merely 30.2% of untreated sample. More recently, the rational protein engineering strategy was developed to increase the catalytic efficiency for hemicellulose hydrolysis (Jaafar et al., 2021). It observed the improved enzyme catalytic reaction for insoluble substrate and the highest hydrolysis of hemicellulose by producing up to 62%, reducing sugar using variant E449D/W453Y. Dutta and Chakraborty reported the kinetics and dynamics of two-phase enzymatic hydrolysis of hemicellulose for biofuel production (Dutta and Chakraborty, 2018). The kinetic constants (K_m , V_{max} , K_x) assume mass transfer disguised values at 0–200 rpm. The mixing strategy increased xylose yields by 6.3–8% and reduced sugar yields by 13–20%.

In essence, acid acted as a catalyst during the acid hydrolysis of hemicellulose. In 2012, Ormsby et al. used solid acid catalysts to selective hemicellulose hydrolysis from both biochar and activated carbon (Ormsby et al., 2012). It observed an 85% conversion of xylan in 2 h for biochar and 57% in 24 h for activated carbon. The temperature increased hydrolysis reaction rate and conversion. In 2015, the solid acid $\text{SO}_4^{2-}/\text{Fe}_2\text{O}_3$ catalyst was found to selectively hydrolyze hemicellulose from wheat straw (Zhong et al., 2015). The hemicellulose hydrolysis yield of 63.5% was observed with a ratio of wheat straw to catalyst (w/w) of 1.95:1 at 142°C for 4.1 h. Dutta and Chakraborty presented a coupled experimental and theoretical

framework for quantifying the two-phase enzymatic hydrolysis kinetics of hemicellulose (Dutta and Chakraborty, 2015). The xylose yield increased product inhibition and decreased reducing sugar yields. Relvas et al. used high-pressure CO_2 as catalyst for selective hydrolysis of wheat straw hemicellulose (Relvas et al., 2015b). The CO_2 induced the *in situ* formation of carbonic acid, obtaining a high dissolution of wheat straw hemicellulose. For high pressure CO_2 , it found a decrease in oligosaccharide content, achieving a maximum monomer sugars of 5.7 g L^{-1} . In 2020, the Keggin-type molybdovanadophosphate heteropolyacids were reported as acid catalysts for the soluble mono and oligosaccharides by hydrolytic conversion of hemicellulose (Shatalov, 2020). Of the total crop xylan, 98.5% was hydrolytically converted into soluble sugars. Moreover, the solid acid sulfated zirconia was used as catalyst for the synthesis of hemicellulose hydrolysate from corncob (Wan et al., 2021). It carried out the soluble sugar concentration of 30.12 g L^{-1} with a yield of 0.33 g g^{-1} corncob and the maximum xylitol yield of 0.76 g g^{-1} from the hemicellulose hydrolysate fermented by *C. Tropicalis*.

DEVELOPMENT OF CONVENTIONAL KINETIC MODELS DURING HEMICELLULOSE HYDROLYSIS

As early as 1945, Saeman did pioneering work in developing the kinetics of hydrolysis of wood chips in dilute acid at 170 – 190°C (Saeman, 1945). The author found that the activation energy was independent of the acid concentration, averaged 42,900 calories. In addition, both the increase in acid concentration and temperature resulted in an increase reaction rate. The improved Saeman model was also applied to study the kinetics of hemicellulosic hydrolysis. From then on, there are many reports on the kinetic research of hemicellulosic hydrolysis using well-known Saeman model. Moreover, more and more scholars paid attention to the kinetic models of hemicellulosic hydrolysis. In 1956, Kobayashi and Sakai explored the hydrolysis rates of pentosan of Buna (*Fagus crenata* Blume) in sulfuric acid at 74, 100, 115, 130, and 147°C (Kobayashi and Sakai, 1956). It found two stages for the hydrolysis of Buna wood pentosan with the same magnitude values for activation energy. Fagan et al. reported the acid hydrolysis kinetics of cellulose in paper refuse in 1971 (Fagan et al., 1971). In general, the hemicelluloses are more hydrolyzed than cellulose. Therefore, it is necessary for utilizing wood as chemicals and fuels to remove the hemicellulose by the pre-hydrolysis step. González et al. applied a kinetic model about the hydrolysis of hemicellulose from wheat straw in sulfuric acid at 34 and 90°C in 1986 (González et al., 1986). It yielded complete solubilization of hemicellulose to xylose and arabinose at 90°C . A two-consecutive reaction mechanism was developed about the kinetic model of acid-catalyzed hydrolysis. Conner and Lorenz used two pre-hydrolysis methods including the Iotech steam explosion process and the Stake process to explore the kinetic modeling of water and dilute acetic acid (5%) pre-hydrolysis of southern red oak wood (Conner and Lorenz, 1986). Kinetic parameters modeled the xylan removal and the occurrence of

xylan oligosaccharides, free xylose, furfural, and degradation products. Thereafter, the famous biphasic model was established including “fast-reacting xylan” and “slow-reacting xylan.” The biphasic model fitted well the experimental data, compared with the Saeman model. In 1997, three different feedstocks of corn stover, poplar, and switchgrass were treated using dilute sulfuric acid (Esteghlalian et al., 1997). The authors applied first-order reactions to model monomeric constituents and degradation of the monomers by hydrolysis of hemicellulose. They used the actual acid concentration to determine the kinetic parameters of the biphasic model, predicting the percentage of as-remaining xylan and xylose. Moreover, Lu and Mosier applied the kinetic model to analyze the maleic acid-catalyzed hemicellulose hydrolysis in corn stover based on the Saeman model and biphasic model (Lu and Mosier, 2008b). It achieved the activation energy of $83.3 \pm 10.3 \text{ kJ mol}^{-1}$ for hemicellulose hydrolysis by maleic acid. It suggested low-temperature reaction conditions for monomeric xylose yield in the maleic acid-catalyzed reaction based on the Saeman model. It achieved around 80%–90% xylose yields at 100–150°C with 0.2 M maleic acid. Furthermore, Sun et al. chose five inorganic salts, such as ZnCl_2 , FeSO_4 , $\text{Fe}_2(\text{SO}_4)_3$, FeCl_3 , and $\text{Fe}(\text{NO}_3)_3$ as catalysts on hemicellulose hydrolysis in control silage (Sun L. et al., 2011). The Saeman model fitted $\text{Fe}(\text{NO}_3)_3$ catalyzed hydrolysis for corn stover silage. It obtained the maximum yields of 81.66% for xylose and 93.36% for initial xylan. It carried out the activation energies from 44.35 to $86.14 \text{ kJ mol}^{-1}$ for hemicellulose hydrolysis in control and from 3.11 to $34.11 \text{ kJ mol}^{-1}$ in acid silage. Liu et al. reported kinetic model of dilute sulfuric acid-catalyzed hemicellulose hydrolysis in sweet sorghum bagasse for xylose production (Liu et al., 2012). It achieved the pre-exponential factors for the “easy-to-hydrolyze” fraction, the “hard-to-hydrolyze” fraction of hemicellulose, and xylose degradation of 3.53×10^6 , 1.80×10^5 , and 0.62 min^{-1} , respectively, and the activation energies of 60.7, 58.1, and 14.5 kJ mol^{-1} , respectively. It yielded the xylose for 60% of hemicellulose weight under 140°C for 50 min. Shi et al. developed the kinetics by dilute-acid pretreatment from corn Stover (Shi et al., 2017). The first-order biphasic model assumed that xylan was composed of two different fragments of fast and slow reacting fractions. The oligomers were used as intermediates in the kinetic model. It observed the low activation energies of xylan hydrolysis. Soleimani et al. explored the kinetics of hemicellulose depolymerization and decomposition in oat hull (Soleimani et al., 2018). The generation of xylose was explained by a single-phase kinetic mechanism with product decomposition (two-step sequential reaction). The single-phase mechanism was used to explain the generation of arabinose, furfural, and acetic acid. A biphasic model was applied to explain the generation of glucose in the hydrolysate due to the fast- and slow-releasing fractions into the liquid phase.

In 2003, Belkacemi and Hamoudi investigated the reaction kinetics and model of enzymatic hydrolysis of hemicellulose from corn stalk (Belkacemi and Hamoudi, 2003). A lumped model based on the Michaelis–Menten approach was used to explain the hydrolysis kinetics of two kinds of corn stalk hemicelluloses, such as xylan and heteropolymers, and three lumped species of

polymeric, oligomers, and monomers. Dussan et al. also described a lumped kinetic model to simulate the pyrolysis of hemicellulose (Dussan et al., 2017). Authors proposed five new model compounds of acetylated glucuronoxylan, arabinoxylan, (galacto) glucomannan, xyloglucans, and beta-glucan toward replicating the pyrolytic reactivity of hemicellulose. Lloyd and Wyman used the depolymerization model to predict thermochemical hydrolysis of hemicellulose by dilute acid and water-only hemicellulose hydrolysis (Lloyd and Wyman, 2003). A kinetic model integrated the polymeric nature of hemicellulose to explain the polymer decomposition. In 2004, Nabarlantz, Farriol, and Montane developed a kinetic model for the autohydrolysis of xylan, which described the yields of the different reaction products and explained the chemical composition changes of the xylo-oligomers due to reaction temperature and time (Nabarlantz et al., 2004). There were two xylan fractions of three monomers (xylose, arabinose, and acetic acid) with different compositions and reactivity toward hydrolysis.

Rissanen et al. reported the extraction of hemicelluloses from spruce at 90 and 110°C (Rissanen et al., 2016). The low temperature dissolution was used to explore the early stage of extraction as the kinetic. Li et al. investigated the kinetics of hemicelluloses removal from the cold caustic extraction (Li et al., 2017). The authors indicated the hemicelluloses removal process with pseudo zero order kinetics including the bulk phase, transition phase, and residual phase. The fundamentals of hemicelluloses removal were explored by the enzymatic peeling method. Yedro et al. explored the extraction kinetics of hemicelluloses from Holm oak in subcritical water (Yedro et al., 2017; Li X. et al., 2020). It achieved the maximum yield (approximately 60%) at 170°C for 20 min. Temperature influenced significantly the hydrolysis rate of the macromolecules. Fernández et al. also applied subcritical water to extract hemicelluloses from stone pine, holm oak, and Norway spruce (Fernández et al., 2018). It observed the high activation energy of 88 kJ mol^{-1} for stone pine, 129 kJ mol^{-1} for Norway spruce, and 153 kJ mol^{-1} for holm oak. Santos-Rocha et al. presented the semi-mechanistic kinetic models of cellulose and hemicellulose for sugarcane straw (Santos-Rocha et al., 2017). The kinetic parameters were explored based on cellobiose, glucose, formic acid, and hydroxymethylfurfural (from cellulosic fraction), and xylose, arabinose, acetic acid, glucuronic acid, and furfural (from hemicellulosic fraction). Kinetic models for both cellulosic and hemicellulosic fractions degradation fitted the experimental data. Köchermann et al. explored kinetics of an aqueous organosolv hemicellulose and D-xylose conversion into furfural between 160 and 200°C using three reaction models (Köchermann et al., 2018). Kinetic models showed slight differences for D-xylose conversion and stronger deviations for furfural formation. The formation of a xylose intermediate showed the best performance. Liu F. et al. carried out the inhibitory effects of acetosyringone on xylanase activity by kinetic experiments (Liu et al., 2020). The acetosyringone obviously inhibited the activity of xylanase in a reversible and noncompetitive binding manner. He et al. developed the dissolution kinetics about the atmospheric sodium

TABLE 2 | The development summary of kinetic models during hemicellulose hydrolysis.

Kinetic models	Proposer	Reference
Saeman model	Saeman	Saeman, 1945
Bidirectional model	Conner	Conner and Lorenz, (1986)
Garrote model	Garrote	Garrote et al. (1999)
Improved bidirectional model	Borrega	Borrega et al. (2011)
Bidirectional dynamic model	Tizazu	Tizazu and Moholkar, (2018)

hydroxide–hydrogen peroxide extraction process of hemicellulose in bagasse pith (He et al., 2020). The activation energy of $22.19 \text{ kJ mol}^{-1}$ indicated the time-dependent dissolution process of hemicellulose, attributing to a diffusion-controlled process. Chen et al. adopted a two-step model to predict the isothermal torrefaction kinetics of cellulose, hemicelluloses, and lignin at 200, 250, and 300°C (Chen et al., 2021). It found hemicelluloses with severe weight loss at 250°C due to the relatively weak structure. It achieved the activation energies of cellulose, hemicelluloses, and lignin in the range of 166–260, 48–55, and $59\text{--}70 \text{ kJ mol}^{-1}$, respectively. **Table 2** demonstrates the development summary of kinetic models during hemicellulose hydrolysis.

Effects of Modeling Hemicellulosic Hydrolysis Kinetics

During the kinetic models for hemicellulose hydrolysis, oligosaccharides are important as intermediates or substrates. In 2005, Carvalheiro et al. reported hemicellulose solubilization and xylo-oligosaccharide production by isothermal autohydrolysis treatments of brewery's spent grain (Carvalheiro et al., 2005). Xylan and arabinan yielded oligosaccharides, monosaccharides (xylose or arabinose), furfural, and other decomposition products in consecutive reaction steps. It developed an arabinoxylan model merging the two proposed models for xylan and arabinan degradation, and including furfural formation from both pentoses. The as-proposed models provided an interpretation of the hydrolytic conversion of xylan and arabinan. In 2006, autohydrolysis of *Arundo donax* L. was reported at $150\text{--}195^\circ\text{C}$ for hydrolyzing hemicelluloses to xylo-oligosaccharides with high yields of oligomers and monomers (Caparros et al., 2006). It developed a conventional kinetic model, explaining the evolution over time of the hemicelluloses and hemicellulose degradation products. Yáñez et al. assessed the suitability of autohydrolysis as a first biorefinery stage using processing of *Acacia dealbata* in aqueous media at $170\text{--}240^\circ\text{C}$ (Yáñez et al., 2009). Xylan (70%) was converted into xylo-oligosaccharide at 215°C . The authors developed first-order pseudohomogeneous kinetics model, describing the *Acacia dealbata* wood solubilization as well as the autohydrolysis of the polysaccharide fractions such as glucan, xylan, arabinosyl, and acetyl substituents of hemicelluloses. In the work of Gullón, they obtained substituted xylo-oligosaccharides and solids in cellulose by the non-isothermal autohydrolysis of rye straw (Gullón et al., 2010). It found 69.2% of the initial xylan into xylo-oligosaccharide at 208°C , containing up to 22.4 g of

oligosaccharide/L. It saccharified 70.6% of cellulose and 63.8% of xylan after 48 h during enzymatic hydrolysis. Kim, Kreke, and Ladisch reported reaction kinetics of xylo-oligosaccharide hydrolysis by dicarboxylic acids (Kim et al., 2013). The hydrolysis of soluble sugar oligomers followed first-order hydrolysis kinetics. The hydrolysis of xylo-oligosaccharide by dicarboxylic acids was modeled using a monophasic model based on Saeman's pseudohomogeneous irreversible first-order reaction kinetics. Branco et al. maximized the yield of oligosaccharides by the selective hemicelluloses removal in autohydrolysis (Branco et al., 2015). It obtained a maximum of 10.4 g L^{-1} of oligosaccharides for a severity factor of 3.6. Gullón et al. reported hemicellulose solubilization and xylo-oligosaccharides production by non-isothermal autohydrolysis treatments of vine shoots (Gullón et al., 2017). The as-proposed kinetic model maximized the oligosaccharide content and minimized the generation of monosaccharides and sugar decomposition products.

In 2008, Lu et al. studied the xylose by the hydrolysis of corn stover in diluted sulfuric acid at 100°C (Lu et al., 2008a). It found the kinetic parameters of mathematical models, predicting the concentrations of xylose, glucose, and furfural in the hydrolysates. Then Jensen et al. compared the kinetic of dilute sulfuric acid hydrolysis of mixtures of hardwoods, softwood, and switchgrass (Jensen et al., 2008). It obtained an activation energy of $76.19 \text{ kJ mol}^{-1}$ for balsam, $133.44 \text{ kJ mol}^{-1}$ for red maple, $141.30 \text{ kJ mol}^{-1}$ for switchgrass, $142.58 \text{ kJ mol}^{-1}$ for aspen, and $171.20 \text{ kJ mol}^{-1}$ for basswood. The acid hydrolysis data confirmed the validity of a pseudo first-order mixture model. After that, Xu et al. researched the kinetics of acid hydrolysis of water-soluble spruce *O*-acetyl galactoglucomannans (Xu et al., 2008). A first-order kinetic model during the acid hydrolysis was used to calculate the reaction rate constants at various pH values and temperatures. It found the activation energy of 150 kJ mol^{-1} for acid hydrolysis of spruce galactoglucomannans from the Arrhenius plot. In 2014, Rissanen et al. reported kinetics modeling of spruce hemicellulose for chemicals (Rissanen et al., 2014). A first-order model was used to perform the overall extraction data, which fitted the experimental data. It found the activation energy of about 120 kJ mol^{-1} for both chip sizes with different reaction rates and the pre-exponential factor.

In 2009, Morinelly et al. investigated the kinetics of dilute acid hydrolysis for aspen, balsam, and switchgrass at various temperatures, acid concentrations, and reaction times (Morinelly et al., 2009). The four-step kinetic model with first-order irreversible rate constants fitted the experimental data. The as-proposed kinetic model described the reaction profiles for xylose monomer by the reaction. Meanwhile, the kinetic model described the oligomer data at early reaction time. Pronyk and Mazza reported the kinetic model of hemicellulose hydrolysis from triticale straw (Pronyk and Mazza, 2010). It observed a dependency about the kinetic rate constants with flow rate. Jin et al. investigated the kinetic of hemicellulose hydrolysis of corn stover in dilute acid (Jin et al., 2011). A first-order reaction model fitted the kinetic data of hemicellulose hydrolysis. It observed over 90% of the xylose monomer yield and below 5.5% of furfural yield. It obtained the activation energy of $111.6 \text{ kJ mol}^{-1}$ for

xylose and 95.7 kJ mol^{-1} for xylose. Patwardhan, Brown, and Shanks explored the fast pyrolysis product distribution of hemicelluloses from switchgrass (Patwardhan et al., 2011). It achieved the primary pyrolysis products of the as-purified hemicellulose in decreasing abundance, such as CO_2 , formic acid, char, DAXP2, xylose, acetol, CO, 2-furaldehyde, and AXP. Shen and Wyman applied the kinetic model to explain the enhanced xylose yields from dilute sulfuric acid using reversible fast-reacting xylan and irreversible slow-reacting xylan (Shen and Wyman, 2011). The xylan removal data were simulated by a kinetic model for dilute acid and hydrothermal pretreatment of corn stover. The oligomeric xylose decomposition controlled hydrothermal autocatalytic reactions from xylan to furfural. However, monomeric xylose decomposition controlled dilute acid-catalytic reactions.

As mentioned above, acid was applied as a catalyst during the hemicellulose hydrolysis in acid system. Grénman et al. investigated the kinetics of aqueous extraction of hemicelluloses from spruce in an intensified reactor system (Grénman et al., 2011). A kinetic model fitted the experimental data. It obtained the activation energy of 135 kJ mol^{-1} . In 2012, Rafiqul and Sakinah also studied the kinetic on acid hydrolysis of Meranti wood sawdust for xylose (Rafiqul and Sakinah, 2012). The kinetic parameters were used to predict the concentration of xylose, glucose, furfural, and acetic acid in the hemicellulosic hydrolysate. It obtained the 6% sulfuric acid and residence time of 20 min. Enslow and Bell reported the kinetics of Brønsted acid-catalyzed hydrolysis of hemicellulose in green 1-ethyl-3-methylimidazolium chloride (Enslow and Bell, 2012). The hemicellulose was hydrolyzed to xylose in 90% yield. In 2013, Rivas et al. researched the kinetics and manufacturing of levulinic acid from pine wood hemicelluloses *via* autohydrolysis in sulfuric acid (Rivas et al., 2013). They applied a model involved to interpret the concentration profiles including the major conversion steps such as oligomers into monosaccharides, hexoses into hydroxymethyl furfural, decomposition of this latter into levulinic and formic acids, dehydration of pentoses into furfural, and conversion of this latter into formic acid. It yielded 66% of the stoichiometric value in levulinic acid under the best conditions. In 2014, kinetic models were developed for the hydrolysis of O-acetyl-galactoglucomannan in homogeneous and heterogeneous catalysts (Salmi et al., 2014). It observed a regular kinetic behavior during the hydrolysis process using homogeneous catalysts (HCl , H_2SO_4 , oxalic acid, and trifluoroacetic acid) and a prominent autocatalytic effect using heterogeneous cation-exchange catalysts (Amberlyst 15 and Smopex 101). The kinetic models for heterogeneous catalysts were based on the reactivity of the non-hydrolyzed sugar units and the rate constant. The kinetic model described the overall kinetics and product distribution in the hydrolysis of water soluble O-acetyl-galactoglucomannan by homogeneous and heterogeneous catalysts. A hydrogen ion catalytic kinetic model was used to predict the time-dependent behavior of xylo-oligomer, xylose, arabinose, and furfural in hydrolysates in hot water pre-extraction of moso bamboo (Hu et al., 2014). The hydrogen ion catalytic kinetic model introduced the time dependence of the hydrogen ion concentration. The authors

calculated the activation energy of 98.2 kJ mol^{-1} for xylan. Moreover, Negahdar et al. investigated the kinetics of the catalytic conversion of cellobiose to sorbitol (Negahdar et al., 2014). In this work, two competing reaction pathways started from cellobiose. It obtained activation energy of 115 kJ mol^{-1} for the hydrolysis of cellobiose and 69 kJ mol^{-1} for subsequent hydrogenation of glucose, and 76 and 103 kJ mol^{-1} with overall high reaction rates at low temperatures for cellobitol formation followed by hydrolysis. Dussan et al. investigated the reaction kinetics of the major components catalyzed by formic acid in the hemicellulose fractions of D-xylose, L-arabinose, and D-glucose (Dussan et al., 2015). The reaction kinetics of solutions were predicted by these models. Chen and Liu used liquid hot water extraction to separate the hemicellulose fraction from dried distiller's grain (Chen and Liu, 2015). A kinetic model was used to introduce the concentration of monomer, oligomer, and sugar units during acid hydrolysis. Santucci et al. evaluated a simplified pseudo-first-order kinetic model for autohydrolysis of hemicelluloses from sugarcane bagasse including all sugars, oligomers, and decomposition products from hemicelluloses (Santucci et al., 2015). Hemicellulose (61.7% of) was converted to oligomeric and monomeric sugars. It obtained an activation energy of $143.1 \text{ kJ mol}^{-1}$ for oligomers, $158.9 \text{ kJ mol}^{-1}$ for monomers, and $138.3 \text{ kJ mol}^{-1}$ for sugar derivatives/decomposition compounds.

The thermogravimetric analyzer (TGA) is a very important method to explore the kinetics of biomass pyrolysis. TGA is a thermal analysis technique used to measure the change in sample mass with temperature through thermobalance and programmed temperature rise method. It can be used to get thermogravimetric curve and weight loss rate curve. By analyzing the curve, the reaction stage can be divided, the corresponding parameters can be calculated, and the pyrolysis law of the sample can be analyzed preliminarily. Rapid progress has been paid on the thermogravimetric kinetic study of hemicellulose hydrolysis. As early as 2011, Chen and Kuo developed the isothermal kinetics to explain the thermal decompositions of hemicellulose, cellulose, lignin, and xylan using TGA (Chen and Kuo, 2011). It achieved the reaction order of hemicellulose, cellulose, lignin, and xylan of 3, 1, 1, and 9, respectively, and the activation energies of 187.06, 124.42, 37.58, and $67.83 \text{ kJ mol}^{-1}$, respectively. This model provided a good evaluation on the thermal degradations of the constituents, expect for cellulose at 300°C and hemicellulose at 275°C . Then Zhou et al. applied TGA and macro-TGA to research kinetics of pyrolysis of hemicellulose, cellulose, and lignin (Zhou et al., 2015). It found the different slow pyrolysis in the TGA and macro-TGA due to the heat transfer process, and the considerable differences of the pyrolysis and fast pyrolysis in macro-TGA. Wang et al. used TGA to explore kinetic of biomass pyrolysis using combined kinetics (Wang et al., 2016). One-step pyrolysis was developed with kinetic parameters of apparent activation energy $221.7 \text{ kJ mol}^{-1}$ and pre-exponential factor $4.17\text{E} + 16 \text{ s}^{-1}$. Combined kinetics three-parallel-reaction model fitted the pyrolysis experimental data. It obtained the activation energy order of three pseudo components: E_{lignin} ($197.3 \text{ kJ mol}^{-1}$) $> E_{\text{cellulose}}$ ($176.3 \text{ kJ mol}^{-1}$) $> E_{\text{hemicellulose}}$ ($151.1 \text{ kJ mol}^{-1}$). The

TABLE 3 | The activation energy ($E/\text{kJ mol}^{-1}$) in comparison with hemicellulose hydrolysis.

E (kJ mol^{-1})	Reference
83.3 ± 10.3	Lu and Mosier, (2008b)
127	Sun et al. (2011b)
187.06	Chen and Kuo, (2011)
135	Grénman et al. (2011)
58.1	Liu et al. (2012)
179.84	Zhang et al. (2014)
151.1	Wang et al. (2016)
162.8	Chen et al. (2017)
95.39	Yeo et al. (2019)
147.2	Qi et al. (2020)
126.31	Zhu and Zhong, (2020)
22.19	He et al. (2020)
48–55	Chen et al. (2021)

pyrolysis of cellulose, hemicellulose, and lignin was comparatively studied using combined kinetics (Yeo et al., 2019). The activation energies for cellulose, hemicellulose, and lignin are 199.66, 95.39, and 174.40 kJ mol^{-1} , respectively. Moreover, their group also applied TGA to investigate kinetics of biomass slow pyrolysis using distributed activation energy model, Fraser–Suzuki deconvolution, and iso-conversional method (Hu et al., 2015). The TGA technique was used to explore pyrolysis kinetics of pine wood, rice husk, and bamboo (*Bambusa chungii*). It obtained the activation energy distribution for pseudo components: E_0 (lignin) > E_0 (cellulose) > E_0 (hemicelluloses), r (lignin) > r (hemicelluloses) > r (cellulose). It achieved the apparent activation energy of $162.84 \pm 26.45 \text{ kJ mol}^{-1}$ for pine wood, $168.63 \pm 28.47 \text{ kJ mol}^{-1}$ for rice husk, and $154.55 \pm 26.49 \text{ kJ mol}^{-1}$ for bamboo, respectively. A TGA was developed to explore the pyrolysis kinetic analysis of the three pseudocomponents of cellulose, hemicellulose, and lignin (Chen et al., 2017). The activation energies of cellulose, hemicellulose, and lignin pyrolysis of 112.6, 162.8, and 156.8 kJ mol^{-1} were obtained using the modulated temperature method. The pyrolytic mechanism of cellulose, hemicellulose, and lignin was investigated using TGA (Yeo et al., 2019). The activation energies for cellulose, hemicellulose, and lignin are 199.66, 95.39, and 174.40 kJ mol^{-1} , respectively. Lei et al. reported thermal pyrolysis kinetics of hemicellulose from *Camellia Oleifera* Shell by TGA (Lei et al., 2019). Thermal pyrolysis kinetics of *Camellia Oleifera* Shell hemicelluloses were investigated based on the Coats–Redfern, Flynn–Wall–Ozawa, and Kissinger–Akahira–Sunose models. The thermal pyrolysis mechanism of *Camellia Oleifera* Shell hemicelluloses was a one-dimensional diffusion reaction analyzed by the Coats–Redfern model. The activation energies of *Camellia Oleifera* Shell hemicelluloses ranged from 175.07 to 247.87 kJ mol^{-1} and from 174.74 to 252.50 kJ mol^{-1} calculated by Flynn–Wall–Ozawa and Kissinger–Akahira–Sunose, respectively. Recently, the TGA method was used to isolate hemicellulose, cellulose, and their mixture (Ding et al., 2020). The activation energy and pre-exponential factor influenced the pyrolysis process of mixture. Díez et al. reported the

determination of hemicellulose, cellulose, and lignin content by TGA and pseudocomponent kinetic model (Díez et al., 2020). It obtained the good characteristic kinetic parameters of each fraction. Zhu and Zhong investigated interactions among biomass components on pyrolysis kinetics including pyrolysis experiments of individual components, synthetic biomass, and natural biomass on a TGA (Zhu and Zhong, 2020). It obtained the sharp pyrolysis behavior of cellulose with low pyrolysis reaction order (1.38), high activation energy (168.61 kJ mol^{-1}), and high pre-exponential factor ($3.50\text{E} + 12/\text{s}$). The pyrolysis behavior of hemicellulose and lignin had a high pyrolysis reaction order (2.30, 1.51), low activation energy (126.31, 87.21 kJ mol^{-1}), and low pre-exponential factor ($9.67\text{E} + 09$, $2.59\text{E} + 05/\text{s}$). **Table 3** presents the comparison for activation energy of hemicellulose hydrolysis.

Besides the kinetic models during hemicellulose hydrolysis, there are reports on the kinetics of dye and hydrogels. In Batzias's work, they explored the simulation of batch and column kinetics of methylene blue and red basic 22 adsorption on mild acid hydrolyzed wheat straw as an adsorbent for wastewater dye removal (Batzias et al., 2009). Moreover, the pH-responsive hemicellulose hydrogels were prepared as carrier for controlled drug delivery (Sun et al., 2013). The swelling kinetics of the hydrogels followed Fickian diffusion process. Sun et al. synthesized stimuli-responsive porous hydrogels from wheat straw hemicellulose using CaCO_3 as porogen for the removal of methylene blue (Sun et al., 2015b). The adsorption data was reported to be fitted to the pseudo-first-order, pseudo-second-order, and intra-particle diffusion kinetics models. The xylan/poly (acrylic acid) magnetic nanocomposite hydrogel was prepared from wheat straw xylan and Fe_3O_4 nanoparticles for methylene blue removal (Sun et al., 2015a). It achieved the adsorption isotherm of the Langmuir model and the pseudo-second-order kinetic model of the adsorption process. Recently, high-performance superabsorbent hydrogels were fabricated by using waste hemicelluloses lye (Liu et al., 2019). It achieved the adsorption kinetics and isotherms of the composites, and the synergy effect of polyvinyl alcohol and bentonite.

CONCLUSION AND OUTLOOK

In summary, there is a long history about kinetics modeling of hemicellulose hydrolysis. Recently, it achieved the obvious development of kinetics modeling of hemicellulose hydrolysis. Various parameters, such as process, intermediates, temperature, catalyst, solvent, and systematic errors, received more attention for the kinetic models. In general, the hemicelluloses have different structures, contents, and compositions with plant species, maturity, early and late wood, cell type, and morphological position. Exploring the kinetics modeling is of great importance for understanding the mechanism of hemicellulose hydrolysis.

The kinetics modeling of hemicellulose hydrolysis still needs to be explored due to the complex structure and composition of hemicellulose. It is often carried out for the hemicellulose hydrolysis in a closed system. It is difficult to obtain the

intrinsic parameters and real mechanism during the hemicellulose hydrolysis. It is also very difficult to study the kinetics of hemicellulose hydrolysis due to its complex reaction process and many influencing factors. The kinetic law based on elementary reaction conforms to the law of mass action. However, the course of most chemical reactions indicated that there existed several steps (elementary reactions) during hemicellulose hydrolysis. Therefore, accurate measurement is very important in kinetics modeling. It is urgent to establish a method for detecting active intermediates from hemicellulose. The kinetics modeling is usually derived from several assumptions. For example, the hydrolysis of xylanase reactions follows the first-order kinetic reaction equation and the hydrolysis of hemicellulose was not affected by other components in the cell wall. Arrhenius equation is a formula for the variation of chemical reaction rate constant with temperature. It should be noted that the activation energy E_a , as a constant independent of temperature, fits the experimental result in a certain temperature range. However, the activation energy is related to temperature in the wide temperature range or complex reaction, which is not applicable to some complex reactions. Moreover, the first premise of Arrhenius formula is that the reactions at different temperatures are consistent. However, the hemicellulose hydrolysis has different reactions at different temperatures. In short, the complexity of hemicellulose hydrolysis, closed system, and kinetics modeling itself cannot be overstated. Obviously, the development of chemical kinetics benefits from the development of modern

detection methods, especially surface analysis and rapid tracking methods. It expected that the kinetics modeling of hemicellulose hydrolysis will favor the applications of hemicellulose in the near future.

AUTHOR CONTRIBUTIONS

QY, SL, and M-GM handled the investigation. X-XJ, S-EC, and CS were in charge of the supervision. QY, SL, and M-GM wrote the original draft. M-GM, X-XJ, S-EC, and CS wrote, reviewed, and edited the manuscript.

FUNDING

The financial support from the National Key R&D Program of China (2019YFC1905901) is gratefully acknowledged, and this work was also partially supported by 2021 Universities Leading Lab-Specific Start-Ups through the National Research Foundation of Korea (NRF) grant funded by the Korea government (MSIT), R&D program for Forest Science Technology (2019151D10-2023-0301) provided by Korea Forest Service (Korea Forestry Promotion Institute), work was also partially supported by the Technology Development Program (S3030198) funded by the Ministry of SMEs and Startups (MSS, Korea) work to S.E.C.

REFERENCES

- Al-Dajani, W. W., Tschirner, U. W., and Jensen, T. (2009). Pre-extraction of Hemicelluloses and Subsequent Kraft Pulping Part II: Acid- and Autohydrolysis. *Tappi J.* 8 (9), 30–37.
- An, L., Si, C., Wang, G., Sui, W., and Tao, Z. (2019). Enhancing the Solubility and Antioxidant Activity of High-Molecular-Weight Lignin by Moderate Depolymerization via *In Situ* Ethanol/acid Catalysis. *Ind. Crops Prod.* 128, 177–185. doi:10.1016/j.indcrop.2018.11.009
- Andrés Fernández, M., Rissanen, J., Pérez Nebreda, A., Xu, C., Willför, S., García Serna, J., et al. (2018). Hemicelluloses from Stone pine, Holm Oak, and Norway spruce with Subcritical Water Extraction – Comparative Study with Characterization and Kinetics. *J. Supercrit. Fluids* 133, 647–657. doi:10.1016/j.supflu.2017.07.001
- Batzias, F., Sidiras, D., Schroeder, E., and Weber, C. (2009). Simulation of Dye Adsorption on Hydrolyzed Wheat Straw in Batch and Fixed-Bed Systems. *Chem. Eng. J.* 148 (2–3), 459–472. doi:10.1016/j.cej.2008.09.025
- Bazant, M. Z. (2013). Theory of Chemical Kinetics and Charge Transfer Based on Nonequilibrium Thermodynamics. *Acc. Chem. Res.* 46 (5), 1144–1160. doi:10.1021/ar300145c
- Belkacemi, K., and Hamoudi, S. (2003). Enzymatic Hydrolysis of Dissolved Corn Stalk Hemicelluloses: Reaction Kinetics and Modeling. *J. Chem. Technol. Biotechnol.* 78 (7), 802–808. doi:10.1002/jctb.865
- Borrega, M., Nieminen, K., and Sixta, H. (2011). Degradation Kinetics of the Main Carbohydrates in Birch wood during Hot Water Extraction in a Batch Reactor at Elevated Temperatures. *Bioresour. Technology* 102 (22), 10724–10732. doi:10.1016/j.biortech.2011.09.027
- Branco, P. C., Dionísio, A. M., Torrado, I., Carneiro, F., Castilho, P. C., and Duarte, L. C. (2015). Autohydrolysis of Annona Cherimola Mill. Seeds: Optimization, Modeling and Products Characterization. *Biochem. Eng. J.* 104, 2–9. doi:10.1016/j.bej.2015.06.006
- Caparrós, S., Garrote, G., Ariza, J., and López, F. (2006). Autohydrolysis of Arundo donax L., a Kinetic Assessment. *Ind. Eng. Chem. Res.* 45 (26), 8909–8920. doi:10.1021/ie061166x
- Carvalho, F., Garrote, G., Parajó, J. C., Pereira, H., and Gírio, F. M. (2005). Kinetic Modeling of Brewerywaste Spent Grain Autohydrolysis. *Biotechnol. Prog.* 21, 233–243. doi:10.1021/bp049764z
- Chen, H., and Liu, S. (2015). A Kinetic Study of DDGS Hemicellulose Acid Hydrolysis and NMR Characterization of DDGS Hydrolysate. *Appl. Biochem. Biotechnol.* 177 (1), 162–174. doi:10.1007/s12010-015-1735-7
- Chen, S., Wang, G., Sui, W., Parvez, A. M., Dai, L., and Si, C. (2020a). Novel Lignin-Based Phenolic Nanosphere Supported Palladium Nanoparticles with Highly Efficient Catalytic Performance and Good Reusability. *Ind. Crops Prod.* 145, 112164. doi:10.1016/j.indcrop.2020.112164
- Chen, S., Wang, G., Sui, W., Parvez, A. M., and Si, C. (2020b). Synthesis of Lignin-Functionalized Phenolic Nanosphere Supported Ag Nanoparticles with Excellent Dispersion Stability and Catalytic Performance. *Green. Chem.* 22, 2879–2888. doi:10.1039/c9gc04311j
- Chen, T., Li, L., Zhao, R., and Wu, J. (2017). Pyrolysis Kinetic Analysis of the Three Pseudocomponents of Biomass-Cellulose, Hemicellulose and Lignin. *J. Therm. Anal. Calorim.* 128 (3), 1825–1832. doi:10.1007/s10973-016-6040-3
- Chen, W.-H., Fong Eng, C., Lin, Y.-Y., Bach, Q.-V., Ashokkumar, V., and Show, P.-L. (2021). Two-step Thermodegradation Kinetics of Cellulose, Hemicelluloses, and Lignin under Isothermal Torrefaction Analyzed by Particle Swarm Optimization. *Energ. Convers. Management* 238, 114116. doi:10.1016/j.enconman.2021.114116
- Chen, W.-H., and Kuo, P.-C. (2011). Isothermal Torrefaction Kinetics of Hemicellulose, Cellulose, Lignin and Xylan Using Thermogravimetric Analysis. *Energy* 36 (11), 6451–6460. doi:10.1016/j.energy.2011.09.022
- Collard, F.-X., and Blin, J. (2014). A Review on Pyrolysis of Biomass Constituents: Mechanisms and Composition of the Products Obtained from the Conversion of Cellulose, Hemicelluloses and Lignin. *Renew. Sustainable Energy Rev.* 38, 594–608. doi:10.1016/j.rser.2014.06.013

- da Costa Lopes, A. M., and Łukasik, R. M. (2018). Separation and Recovery of a Hemicellulose-Derived Sugar Produced from the Hydrolysis of Biomass by an Acidic Ionic Liquid. *ChemSusChem* 11 (6), 1099–1107. doi:10.1002/cssc.201702231
- Dai, L., Ma, M., Xu, J., Si, C., Wang, X., Liu, Z., et al. (2020). All-Lignin-Based Hydrogel with Fast pH-Stimuli Responsiveness for Mechanical Switching and Actuation. *Chem. Mater.* 32, 4324–4330. doi:10.1021/acs.chemmater.0c01198
- Dai, L., Zhu, W., Lu, J., Kong, F., Si, C., and Ni, Y. (2019). A Lignin-Containing Cellulose Hydrogel for Lignin Fractionation. *Green. Chem.* 21, 5222–5230. doi:10.1039/c9gc01975h
- Delbecq, F., Wang, Y., Muralidhara El Ouardi, A. K., El Ouardi, K., Marlair, G., and Len, C. (2018). Hydrolysis of Hemicellulose and Derivatives-A Review of Recent Advances in the Production of Furfural. *Front. Chem.* 6, 146. doi:10.3389/fchem.2018.00146
- Díez, D., Urueña, A., Piñero, R., Barrio, A., and Tamminen, T. (2020). Determination of Hemicellulose, Cellulose, and Lignin Content in Different Types of Biomasses by Thermogravimetric Analysis and Pseudocomponent Kinetic Model (TGA-PKM Method). *Processes* 8 (9), 1048. doi:10.3390/pr8091048
- Ding, Y., Huang, B., Li, K., Du, W., Lu, K., and Zhang, Y. (2020). Thermal Interaction Analysis of Isolated Hemicellulose and Cellulose by Kinetic Parameters during Biomass Pyrolysis. *Energy* 195, 117010. doi:10.1016/j.energy.2020.117010
- dos Santos Rocha, M. S. R., Pratto, B., de Sousa, R., Almeida, R. M. R. G., and Cruz, A. J. G. d. (2017). A Kinetic Model for Hydrothermal Pretreatment of Sugarcane Straw. *Bioresour. Technology* 228, 176–185. doi:10.1016/j.biortech.2016.12.087
- Du, H., Liu, W., Zhang, M., Si, C., Zhang, X., and Li, B. (2019). Cellulose Nanocrystals and Cellulose Nanofibrils Based Hydrogels for Biomedical Applications. *Carbohydr. Polym.* 209, 130–144. doi:10.1016/j.carbpol.2019.01.020
- Du, H., Parit, M., Liu, K., Zhang, M., Jiang, Z., Huang, T.-S., et al. (2021a). Multifunctional Cellulose Nanopaper with superior Water-Resistant, Conductive, and Antibacterial Properties Functionalized with Chitosan and Polypyrrole. *ACS Appl. Mater. Inter.* 13 (27), 32115–32125. doi:10.1021/acsami.1c06647
- Du, H., Zhang, M., Liu, K., Parit, M., Jiang, Z., Zhang, X., et al. (2022b). Conductive PEDOT:PSS/cellulose Nanofibril Paper Electrodes for Flexible Supercapacitors with superior Areal Capacitance and Cycling Stability. *Chem. Eng. J.* 428, 131994. doi:10.1016/j.cej.2021.131994
- Dussan, K., Dooley, S., and Monaghan, R. (2017). Integrating Compositional Features in Model Compounds for a Kinetic Mechanism of Hemicellulose Pyrolysis. *Chem. Eng. J.* 328, 943–961. doi:10.1016/j.cej.2017.07.089
- Dussan, K., Girisuta, B., Lopes, M., Leahy, J. J., and Hayes, M. H. B. (2015). Conversion of Hemicellulose Sugars Catalyzed by Formic Acid: Kinetics of the Dehydration of D-Xylose, L-Arabinose, and D-Glucose. *ChemSusChem* 8 (8), 1411–1428. doi:10.1002/cssc.201403328
- Dutta, S. K., and Chakraborty, S. (2015). Kinetic Analysis of Two-phase Enzymatic Hydrolysis of Hemicellulose of Xylan Type. *Bioresour. Technology* 198, 642–650. doi:10.1016/j.biortech.2015.09.066
- Dutta, S. K., and Chakraborty, S. (2018). Mixing Effects on the Kinetics and the Dynamics of Two-phase Enzymatic Hydrolysis of Hemicellulose for Biofuel Production. *Bioresour. Technology* 259, 276–285. doi:10.1016/j.biortech.2018.03.042
- Enslow, K. R., and Bell, A. T. (2012). The Kinetics of Brønsted Acid-Catalyzed Hydrolysis of Hemicellulose Dissolved in 1-Ethyl-3-Methylimidazolium Chloride. *RSC Adv.* 2 (26), 10028. doi:10.1039/C2RA21650G
- Esteghlalian, A., Hashimoto, A. G., Fenske, J. J., and Penner, M. H. (1997). Modeling and Optimization of the Dilute-Sulfuric-Acid Pretreatment of Corn stover, poplar and Switchgrass. *Bioresour. Technology* 59, 129–136. doi:10.1016/S0960-8524(97)81606-9
- Fagan, R. D., Grethlein, H. E., Converse, A. O., and Porteous, A. (1971). Kinetics of the Acid Hydrolysis of Cellulose Found in Paper Refuse. *Environ. Sci. Technol.* 5 (6), 545–547. doi:10.1021/es60053a006
- Garrote, G., Domínguez, H., and Parajó, J. C. (1999). Hydrothermal Processing of Lignocellulosic Materials. *Holz als Roh- und Werkstoff* 57 (3), 191–202. doi:10.1007/s001070050039
- Gillespie, D. T. (2007). Stochastic Simulation of Chemical Kinetics. *Annu. Rev. Phys. Chem.* 58, 35–55. doi:10.1146/annurev.physchem.58.032806.104637
- Girio, F. M., Fonseca, C., Carvalheiro, F., Duarte, L. C., Marques, S., and Bogel-Lukasik, R. (2010). Hemicelluloses for Fuel Ethanol: A Review. *Bioresour. Technology* 101 (13), 4775–4800. doi:10.1016/j.biortech.2010.01.088
- González, G., López-Santín, J., Caminal, G., and Solà, C. (1986). Dilute Acid Hydrolysis of Wheat Straw Hemicellulose at Moderate Temperature: A Simplified Kinetic Model. *Biotechnol. Bioeng.* 28 (2), 288–293. doi:10.1002/bit.260280219
- González, G., López-Santín, J., Caminal, G., and Solà, C. (1986). Dilute Acid Hydrolysis of Wheat Straw Hemicellulose at Moderate Temperature: A Simplified Kinetic Model. *Biotechnol. Bioeng.* 28 (2), 288–293. doi:10.1002/bit.260280219
- Grenman, H., Eränen, K., Krogell, J., Willför, S., Salmi, T., and Murzin, D. Y. (2011). Kinetics of Aqueous Extraction of Hemicelluloses from Spruce in an Intensified Reactor System. *Ind. Eng. Chem. Res.* 50 (7), 3818–3828. doi:10.1021/ie101946c
- Gu, J., Pei, W., Tang, S., Yan, F., Peng, Z., Huang, C., et al. (2020). Procuring Biologically Active Galactomannans from Spent Coffee Ground (SCG) by Autohydrolysis and Enzymatic Hydrolysis. *Int. J. Biol. Macromolecules* 149, 572–580. doi:10.1016/j.ijbiomac.2020.01.281
- Gullón, B., Eibes, G., Dávila, I., Vila, C., Labidi, J., and Gullón, P. (2017). Valorization of Vine Shoots Based on the Autohydrolysis Fractionation Optimized by a Kinetic Approach. *Ind. Eng. Chem. Res.* 56 (48), 14164–14171. doi:10.1021/acs.iecr.7b02833
- Gullón, B., Yáñez, R., Alonso, J. L., and Parajó, J. C. (2010). Production of Oligosaccharides and Sugars from rye Straw: a Kinetic Approach. *Bioresour. Technology* 101 (17), 6676–6684. doi:10.1016/j.biortech.2010.03.080
- Harvey, J. N. (2007). Understanding the Kinetics of Spin-Forbidden Chemical Reactions. *Phys. Chem. Chem. Phys.* 9 (3), 331–343. doi:10.1039/b614390c
- He, L., Chen, D., Yang, S., Peng, L., Zhang, J., Guan, Q., et al. (2020). Deep Insights into the Atmospheric Sodium Hydroxide-Hydrogen Peroxide Extraction Process of Hemicellulose in Bagasse Pith: Technical Uncertainty, Dissolution Kinetics Behavior, and Mechanism. *Ind. Eng. Chem. Res.* 59 (21), 10150–10159. doi:10.1021/acs.iecr.0c01076
- Hu, H.-C., Chai, X.-S., Zhan, H.-Y., Barnes, D., Huang, L.-L., and Chen, L.-H. (2014). Hydrogen Ion Catalytic Kinetic Model of Hot Water Preextraction for Production of Biochemicals Derived from Hemicellulose Using Moso Bamboo (*Phyllostachys pubescens*). *Ind. Eng. Chem. Res.* 53 (29), 11684–11690. doi:10.1021/ie502261m
- Hu, L., Du, H., Liu, C., Zhang, Y., Yu, G., Zhang, X., et al. (2019). Comparative Evaluation of the Efficient Conversion of Corn Husk Filament and Corn Husk Powder to Valuable Materials via a Sustainable and Clean Biorefinery Process. *ACS Sustainable Chem. Eng.* 7, 1327–1336. doi:10.1021/acscchemeng.8b05017
- Hu, M., Chen, Z., Wang, S., Guo, D., Ma, C., Zhou, Y., et al. (2016). Thermogravimetric Kinetics of Lignocellulosic Biomass Slow Pyrolysis Using Distributed Activation Energy Model, Fraser-Suzuki Deconvolution, and Iso-Conventional Method. *Energ. Convers. Management* 118, 1–11. doi:10.1016/j.enconman.2016.03.058
- Huang, C., Zheng, Y., Lin, W., Shi, Y., Huang, G., and Yong, Q. (2020). Removal of Fermentation Inhibitors from Pre-hydrolysis Liquor Using Polystyrene Divinylbenzene Resin. *Biotechnol. Biofuels* 13, 188. doi:10.1186/s13068-020-01828-3
- Jaafar, N. R., Ayob, S. N., Abd Rahman, N. H., Abu Bakar, F. D., Murad, A. M. A., and Illias, R. M. (2021). Rational Protein Engineering of α -L-arabinofuranosidase from *Aspergillus niger* for Improved Catalytic Hydrolysis Efficiency on Kenaf Hemicellulose. *Process Biochem.* 102, 349–359. doi:10.1016/j.procbio.2020.12.012
- Jensen, J., Morinelly, J., Aglan, A., Mix, A., and Shonnard, D. R. (2008). Kinetic Characterization of Biomass Dilute Sulfuric Acid Hydrolysis: Mixtures of Hardwoods, Softwood, and Switchgrass. *AIChE J.* 54 (6), 1637–1645. doi:10.1002/aic.11467
- Jin, Q., Zhang, H., Yan, L., Qu, L., and Huang, H. (2011). Kinetic Characterization for Hemicellulose Hydrolysis of Corn stover in a Dilute Acid Cycle spray Flow-Through Reactor at Moderate Conditions. *Biomass and Bioenergy* 35 (10), 4158–4164. doi:10.1016/j.biombioe.2011.06.050
- Kapu, N. S., Yuan, Z., Chang, X. F., Beatson, R., Martinez, D. M., and Trajano, H. L. (2016). Insight into the Evolution of the Proton Concentration during Autohydrolysis and Dilute-Acid Hydrolysis of Hemicellulose. *Biotechnol. Biofuels* 9, 224. doi:10.1186/s13068-016-0619-6

- Kim, Y., Kreke, T., and Ladisch, M. R. (2013). Reaction Mechanisms and Kinetics of Xylo-Oligosaccharide Hydrolysis by Dicarboxylic Acids. *Aiche J.* 59 (1), 188–199. doi:10.1002/aic.13807
- Kobayashi, T., and Sakai, Y. (1956). Hydrolysis Rate of Pentosan of Hardwood in Dilute Sulfuric Acid. *Bull. Agric. Chem. Soc. Jpn.* 20 (1), 1–7. doi:10.1080/03758397.1956.10857296
- Köchermann, J., Mühlenberg, J., and Klemm, M. (2018). Kinetics of Hydrothermal Furfural Production from Organosolv Hemicellulose and D-Xylose. *Ind. Eng. Chem. Res.* 57 (43), 14417–14427. doi:10.1021/acs.iecr.8b03402
- Kumar, A., Sharma, G., Naushad, M., Al-Muhtaseb, A. a. H., García-Peñas, A., Mola, G. T., et al. (2020). Bio-inspired and Biomaterials-Based Hybrid Photocatalysts for Environmental Detoxification: A Review. *Chem. Eng. J.* 382, 122937. doi:10.1016/j.cej.2019.122937
- Lei, Z., Wang, S., Fu, H., Gao, W., Wang, B., Zeng, J., et al. (2019). Thermal Pyrolysis Characteristics and Kinetics of Hemicellulose Isolated from Camellia Oleifera Shell. *Bioresour. Technology* 282, 228–235. doi:10.1016/j.biortech.2019.02.131
- Li, J., Hu, H., Li, H., Huang, L., Chen, L., and Ni, Y. (2017). Kinetics and Mechanism of Hemicelluloses Removal from Cellulosic Fibers during the Cold Caustic Extraction Process. *Bioresour. Technology* 234, 61–66. doi:10.1016/j.biortech.2017.03.026
- Li, M., Yang, X., Lu, T., and Zhou, L. (2020a). Selective Hydrolysis of Hemicellulose Component of Wheat Straw in High-pressure CO₂ and Water with Low Concentration of Acetic Acid. *J. Chem. Technol. Biotechnol.* 95 (8), 2237–2242. doi:10.1002/jctb.6411
- Li, X., Lu, X., Nie, S., Liang, M., Yu, Z., Duan, B., et al. (2020b). Efficient Catalytic Production of Biomass-Derived Levulinic Acid over Phosphotungstic Acid in Deep Eutectic Solvent. *Ind. Crops Prod.* 145, 112154. doi:10.1016/j.indcrop.2020.112154
- Li, X., Xu, R., Yang, J., Nie, S., Liu, D., Liu, Y., et al. (2019). Production of 5-hydroxymethylfurfural and Levulinic Acid from Lignocellulosic Biomass and Catalytic Upgradation. *Ind. Crops Prod.* 130, 184–197. doi:10.1016/j.indcrop.2018.12.082
- Lin, W., Chen, D., Yong, Q., Huang, C., and Huang, S. (2019). Improving Enzymatic Hydrolysis of Acid-Pretreated Bamboo Residues Using Amphiphilic Surfactant Derived from Dehydroabietic Acid. *Bioresour. Technology* 293, 122055. doi:10.1016/j.biortech.2019.122055
- Lin, W., Xing, S., Jin, Y., Lu, X., Huang, C., and Yong, Q. (2020). Insight into Understanding the Performance of Deep Eutectic Solvent Pretreatment on Improving Enzymatic Digestibility of Bamboo Residues. *Bioresour. Technology* 306, 123163. doi:10.1016/j.biortech.2020.123163
- Lin, W., Yang, J., Zheng, Y., Huang, C., and Yong, Q. (2021). Understanding the Effects of Different Residual Lignin Fractions in Acid-Pretreated Bamboo Residues on its Enzymatic Digestibility. *Biotechnol. Biofuels* 14, 143. doi:10.1186/s13068-021-01994-y
- Liu, F., Xu, W.-F., Mu, H., Lv, Z.-R., Peng, J., Guo, C., et al. (2020). Inhibition Kinetics of Acetosyringone on Xylanase in Hydrolysis of Hemicellulose. *Biosci. Biotechnol. Biochem.* 84 (9), 1788–1798. doi:10.1080/09168451.2020.1767499
- Liu, H., Du, H., Zheng, T., Liu, K., Ji, X., Xu, T., et al. (2021a). Cellulose Based Composite Foams and Aerogels for Advanced Energy Storage Devices. *Chem. Eng. J.* 426, 130817. doi:10.1016/j.cej.2021.130817
- Liu, H., Xu, T., Liu, K., Zhang, M., Liu, W., Li, H., et al. (2021b). Lignin-based Electrodes for Energy Storage Application. *Ind. Crops Prod.* 165, 113425. doi:10.1016/j.indcrop.2021.113425
- Liu, K., Du, H., Zheng, T., Liu, H., Zhang, M., Zhang, R., et al. (2021c). Recent Advances in Cellulose and its Derivatives for Oilfield Applications. *Carbohydr. Polym.* 259, 117740. doi:10.1016/j.carbpol.2021.117740
- Liu, K., Du, H., Zheng, T., Liu, W., Zhang, M., Liu, H., et al. (2021d). Lignin-containing Cellulose Nanomaterials: Preparation and Applications. *Green. Chem.* doi:10.1039/d1gc02841c
- Liu, S., Du, H., Liu, K., Ma, M.-G., Kwon, Y.-E., Si, C., et al. (2021e). Flexible and Porous Co₃O₄-Carbon Nanofibers as Binder-free Electrodes for Supercapacitors. *Adv. Compos. Hybrid. Mater.* 4. doi:10.1007/s42114-021-00344-8
- Liu, W., Du, H., Liu, H., Xie, H., Xu, T., Zhao, X., et al. (2020a). Highly Efficient and Sustainable Preparation of Carboxylic and Thermostable Cellulose Nanocrystals via FeCl₃-Catalyzed Innocuous Citric Acid Hydrolysis. *ACS Sustainable Chem. Eng.* 8, 16691–16700. doi:10.1021/acssuschemeng.0c06561
- Liu, W., Du, H., Liu, K., Liu, H., Xie, H., Si, C., et al. (2021). Sustainable Preparation of Cellulose Nanofibrils via Choline Chloride-Citric Acid Deep Eutectic Solvent Pretreatment Combined with High-Pressure Homogenization. *Carbohydr. Polym.* 267, 118220. doi:10.1016/j.carbpol.2021.118220
- Liu, W., Du, H., Zhang, M., Liu, K., Liu, H., Xie, H., et al. (2020b). Bacterial Cellulose-Based Composite Scaffolds for Biomedical Applications: A Review. *ACS Sustainable Chem. Eng.* 8, 7536–7562. doi:10.1021/acssuschemeng.0c00125
- Liu, X., Lu, M., Ai, N., Yu, F., and Ji, J. (2012). Kinetic Model Analysis of Dilute Sulfuric Acid-Catalyzed Hemicellulose Hydrolysis in Sweet Sorghum Bagasse for Xylose Production. *Ind. Crops Prod.* 38, 81–86. doi:10.1016/j.indcrop.2012.01.013
- Liu, X., Luan, S., and Li, W. (2019). Utilization of Waste Hemicelluloses Lye for Superabsorbent Hydrogel Synthesis. *Int. J. Biol. Macromolecules* 132, 954–962. doi:10.1016/j.ijbiomac.2019.04.041
- Lloyd, T., and Wyman, C. E. (2003). Application of a Depolymerization Model for Predicting Thermochemical Hydrolysis of Hemicellulose. *Abab* 105, 53–68. doi:10.1385/ABAB:105:1-3:53
- Lu, J., Zhu, W., Dai, L., Si, C., and Ni, Y. (2019). Fabrication of Thermo- and pH-Sensitive Cellulose Nanofibrils-Reinforced Hydrogel with Biomass Nanoparticles. *Carbohydr. Polym.* 215, 289–295. doi:10.1016/j.carbpol.2019.03.100
- Lu, X., Zhang, Y., Liang, Y., Yang, J., Zhang, S., and Suzuki, E. (2008a). Kinetic Studies of Hemicellulose Hydrolysis of Corn stover at Atmospheric Pressure. *Korean J. Chem. Eng.* 25 (2), 302–307. doi:10.1007/s11814-008-0053-y
- Lu, Y., and Mosier, N. S. (2008b). Kinetic Modeling Analysis of Maleic Acid-Catalyzed Hemicellulose Hydrolysis in Corn stover. *Biotechnol. Bioeng.* 101 (6), 1170–1181. doi:10.1002/bit.22008
- Ma, C., Ma, M. G., Si, C., Ji, X. X., and Wan, P. (2021). Flexible MXene-Based Composites for Wearable Devices. *Adv. Funct. Mater.* 31, 2009524. doi:10.1002/adfm.202009524
- Ma, C., Yuan, Q., Du, H., Ma, M.-G., Si, C., and Wan, P. (2020). Multiresponsive MXene (Ti₃C₂T_x)-Decorated Textiles for Wearable Thermal Management and Human Motion Monitoring. *ACS Appl. Mater. Inter.* 12, 34226–34234. doi:10.1021/acsami.0c10750
- Mishra, R. K., and Mohanty, K. (2018). Pyrolysis Kinetics and thermal Behavior of Waste Sawdust Biomass Using Thermogravimetric Analysis. *Bioresour. Technology* 251, 63–74. doi:10.1016/j.biortech.2017.12.029
- Morinelly, J. E., Jensen, J. R., Browne, M., Co, T. B., and Shonnard, D. R. (2009). Kinetic Characterization of Xylose Monomer and Oligomer Concentrations during Dilute Acid Pretreatment of Lignocellulosic Biomass from Forests and Switchgrass. *Ind. Eng. Chem. Res.* 48, 9877–9884. doi:10.1021/ie900793p
- Nabarlatz, D., Farriol, X., and Montané, D. (2004). Kinetic Modeling of the Autohydrolysis of Lignocellulosic Biomass for the Production of Hemicellulose-Derived Oligosaccharides. *Ind. Eng. Chem. Res.* 43, 4124–4131. doi:10.1021/ie034238i
- Negahdar, L., Delidovich, I., and Palkovits, R. (2016). Aqueous-phase Hydrolysis of Cellulose and Hemicelluloses over Molecular Acidic Catalysts: Insights into the Kinetics and Reaction Mechanism. *Appl. Catal. B: Environ.* 184, 285–298. doi:10.1016/j.apcatb.2015.11.039
- Negahdar, L., Oltmanns, J. U., Palkovits, S., and Palkovits, R. (2014). Kinetic Investigation of the Catalytic Conversion of Cellobiose to Sorbitol. *Appl. Catal. B: Environ.* 147, 677–683. doi:10.1016/j.apcatb.2013.09.046
- Ormsby, R., Kastner, J. R., and Miller, J. (2012). Hemicellulose Hydrolysis Using Solid Acid Catalysts Generated from Biochar. *Catal. Today* 190 (1), 89–97. doi:10.1016/j.cattod.2012.02.050
- Ostadjoo, S., Hammerer, F., Dietrich, K., Dumont, M. J., Friščić, T., and Auclair, K. (2019). Efficient Enzymatic Hydrolysis of Biomass Hemicellulose in the Absence of Bulk Water. *Molecules* 24 (23), 4206. doi:10.3390/molecules24234206
- Patwardhan, P. R., Brown, R. C., and Shanks, B. H. (2011). Product Distribution from the Fast Pyrolysis of Hemicellulose. *ChemSusChem* 4 (5), 636–643. doi:10.1002/cssc.201000425
- Pronyk, C., and Mazza, G. (2010). Kinetic Modeling of Hemicellulose Hydrolysis from Triticale Straw in a Pressurized Low Polarity Water Flow-Through Reactor. *Ind. Eng. Chem. Res.* 49, 6367–6375. doi:10.1021/ie1003625
- Qi, C., Hou, S., Lu, J., Xue, W., and Sun, K. (2020). Thermal Characteristics of Birch and its Cellulose and Hemicelluloses Isolated by Alkaline Solution. *Holzforchung* 74 (12), 1099–1112. doi:10.1515/hf-2019-0285

- Rafiqul, I. S. M., and Mimi Sakinah, A. M. (2012). Kinetic Studies on Acid Hydrolysis of Meranti wood Sawdust for Xylose Production. *Chem. Eng. Sci.* 71, 431–437. doi:10.1016/j.ces.2011.11.007
- Ranzi, E., Cuoci, A., Faravelli, T., Frassoldati, A., Migliavacca, G., Pierucci, S., et al. (2008). Chemical Kinetics of Biomass Pyrolysis. *Energy Fuels* 22, 4292–4300. doi:10.1021/ef800551t
- Real, F. J., Benitez, F. J., Acero, J. L., Sagasti, J. J. P., and Casas, F. (2009). Kinetics of the Chemical Oxidation of the Pharmaceuticals Primidone, Ketoprofen, and Diltiazem in Ultrapure and Natural Waters. *Ind. Eng. Chem. Res.* 48 (7), 3380–3388. doi:10.1021/ie801762p
- Relvas, F. M., Morais, A. R. C., and Bogel-Lukasik, R. (2015a). Kinetic Modeling of Hemicellulose-Derived Biomass Hydrolysis under High Pressure CO₂-H₂O Mixture Technology. *J. Supercrit. Fluids* 99, 95–102. doi:10.1016/j.supflu.2015.01.022
- Relvas, F. M., Morais, A. R. C., and Bogel-Lukasik, R. (2015b). Selective Hydrolysis of Wheat Straw Hemicellulose Using High-Pressure CO₂ as Catalyst. *RSC Adv.* 5 (90), 73935–73944. doi:10.1039/c5ra14632a
- Rissanen, J. V., Grénman, H., Willför, S., Murzin, D. Y., and Salmi, T. (2014). Spruce Hemicellulose for Chemicals Using Aqueous Extraction: Kinetics, Mass Transfer, and Modeling. *Ind. Eng. Chem. Res.* 53 (15), 6341–6350. doi:10.1021/ie500234t
- Rissanen, J. V., Murzin, D. Y., Salmi, T., and Grénman, H. (2016). Aqueous Extraction of Hemicelluloses from spruce - from Hot to Warm. *Bioresour. Technology* 199, 279–282. doi:10.1016/j.biortech.2015.08.116
- Rivas, S., González-Muñoz, M. J., Vila, C., Santos, V., and Parajó, J. C. (2013). Manufacture of Levulinic Acid from Pine Wood Hemicelluloses: A Kinetic Assessment. *Ind. Eng. Chem. Res.* 52 (11), 3951–3957. doi:10.1021/ie3018725
- Rivas, S., Vila, C., Santos, V., and Parajó, J. C. (2016). Furfural Production from Birch Hemicelluloses by Two-step Processing: a Potential Technology for Biorefineries. *Holzforschung* 70 (10), 901–910. doi:10.1515/hf-2015-0255
- Saeman, J. F. (1945). Kinetics of Wood Saccharification - Hydrolysis of Cellulose and Decomposition of Sugars in Dilute Acid at High Temperature. *Ind. Eng. Chem.* 37 (1), 43–52. doi:10.1021/ie50421a009
- Salmi, T., Murzin, D. Y., Mäki-Arvela, P., Kusema, B., Holmbom, B., Willför, S., et al. (2014). Kinetic Modeling of Hemicellulose Hydrolysis in the Presence of Homogeneous and Heterogeneous Catalysts. *Aiche J.* 60 (3), 1066–1077. doi:10.1002/aic.14311
- Santos, V. T. d. O., Siqueira, G., Milagres, A. M. F., and Ferraz, A. (2018). Role of Hemicellulose Removal during Dilute Acid Pretreatment on the Cellulose Accessibility and Enzymatic Hydrolysis of Compositionally Diverse Sugarcane Hybrids. *Ind. Crops Prod.* 111, 722–730. doi:10.1016/j.indcrop.2017.11.053
- Santucci, B. S., Maziero, P., Rabelo, S. C., Curvelo, A. A. S., and Pimenta, M. T. B. (2015). Autohydrolysis of Hemicelluloses from Sugarcane Bagasse during Hydrothermal Pretreatment: a Kinetic Assessment. *Bioenerg. Res.* 8 (4), 1778–1787. doi:10.1007/s12155-015-9632-z
- Scheller, H. V., and Ulvskov, P. (2010). Hemicelluloses. *Annu. Rev. Plant Biol.* 61, 263–289. doi:10.1146/annurev-arplant-042809-112315
- Sella Kapu, N., and Trajano, H. L. (2014). Review of Hemicellulose Hydrolysis in Softwoods and Bamboo. *Biofuels, Bioprod. Bioref.* 8 (6), 857–870. doi:10.1002/bbb.1517
- Shatalov, A. A. (2020). Polyoxometalate-catalyzed Hydrolysis of the Hemicelluloses by (Mo-V-P)-Heteropolyacids-Statistical Modeling Using Response Surfaces. *Carbohydr. Polym.* 236, 116091. doi:10.1016/j.carbpol.2020.116091
- Shen, J., and Wyman, C. E. (2011). A Novel Mechanism and Kinetic Model to Explain Enhanced Xylose Yields from Dilute Sulfuric Acid Compared to Hydrothermal Pretreatment of Corn stover. *Bioresour. Technology* 102 (19), 9111–9120. doi:10.1016/j.biortech.2011.04.001
- Shi, S., Guan, W., Kang, L., and Lee, Y. Y. (2017). Reaction Kinetic Model of Dilute Acid-Catalyzed Hemicellulose Hydrolysis of Corn Stover under High-Solid Conditions. *Ind. Eng. Chem. Res.* 56 (39), 10990–10997. doi:10.1021/acs.iecr.7b01768
- Soleimani, M., Tabil, L. G., and Panigrahi, S. (2018). A Kinetic Study of Xylose Recovery from a Hemicellulose-Rich Biomass for Xylitol Fermentative Production. *Chem. Eng. Commun.* 206 (2), 193–206. doi:10.1080/00986445.2018.1478294
- Sun, L., Chen, J. Y., Negulescu, I. I., Moore, M. A., and Collier, B. J. (2011a). Kinetics Modeling of Dynamic Pyrolysis of Bagasse Fibers. *Bioresour. Technology* 102, 1951–1958. doi:10.1016/j.biortech.2010.08.109
- Sun, X.-F., Gan, Z., Jing, Z., Wang, H., Wang, D., and Jin, Y. (2015b). Adsorption of Methylene Blue on Hemicellulose-Based Stimuli-Responsive Porous Hydrogel. *J. Appl. Polym. Sci.* 132 (10), a–n. doi:10.1002/app.41606
- Sun, X.-F., Liu, B., Jing, Z., and Wang, H. (2015a). Preparation and Adsorption Property of Xylan/poly(acrylic Acid) Magnetic Nanocomposite Hydrogel Adsorbent. *Carbohydr. Polym.* 118, 16–23. doi:10.1016/j.carbpol.2014.11.013
- Sun, X.-F., Wang, H.-h., Jing, Z.-x., and Mohanathas, R. (2013). Hemicellulose-based pH-Sensitive and Biodegradable Hydrogel for Controlled Drug Delivery. *Carbohydr. Polym.* 92 (2), 1357–1366. doi:10.1016/j.carbpol.2012.10.032
- Sun, Y., Lu, X., Zhang, S., Zhang, R., and Wang, X. (2011b). Kinetic Study for Fe(NO₃)₃ Catalyzed Hemicellulose Hydrolysis of Different Corn stover Silages. *Bioresour. Technology* 102 (3), 2936–2942. doi:10.1016/j.biortech.2010.11.076
- Tizazu, B. Z., and Moholkar, V. S. (2018). Kinetic and Thermodynamic Analysis of Dilute Acid Hydrolysis of Sugarcane Bagasse. *Bioresour. Technology* 250, 197–203. doi:10.1016/j.biortech.2017.11.032
- Wan, L., Gao, Z., Wu, B., Cao, F., Jiang, M., Wei, P., et al. (2021). Hydrolysis of Corn cob Hemicellulose by Solid Acid Sulfated Zirconia and its Evaluation in Xylitol Production. *Appl. Biochem. Biotechnol.* 193 (1), 205–217. doi:10.1007/s12010-020-03412-9
- Wang, H., Du, H., Liu, K., Liu, H., Xu, T., Zhang, S., et al. (2021). Sustainable Preparation of Bifunctional Cellulose Nanocrystals via Mixed H₂SO₄/formic Acid Hydrolysis. *Carbohydr. Polym.* 266, 118107. doi:10.1016/j.carbpol.2021.118107
- Wang, H., Xie, H., Du, H., Wang, X., Liu, W., Duan, Y., et al. (2020a). Highly Efficient Preparation of Functional and Thermostable Cellulose Nanocrystals via H₂SO₄ Intensified Acetic Acid Hydrolysis. *Carbohydr. Polym.* 239, 116233. doi:10.1016/j.carbpol.2020.116233
- Wang, R., Yue, J., Jiang, J., Li, J., Zhao, J., Xia, H., et al. (2020b). Hydrothermal CO₂-assisted Pretreatment of Wheat Straw for Hemicellulose Degradation Followed with Enzymatic Hydrolysis for Glucose Production. *Waste Biomass Valor.* 12 (3), 1483–1492. doi:10.1007/s12649-020-01103-4
- Wang, X., Hu, M., Hu, W., Chen, Z., Liu, S., Hu, Z., et al. (2016). Thermogravimetric Kinetic Study of Agricultural Residue Biomass Pyrolysis Based on Combined Kinetics. *Bioresour. Technology* 219, 510–520. doi:10.1016/j.biortech.2016.07.136
- Wang, Y., Cao, X., Zhang, R., Xiao, L., Yuan, T., Shi, Q., et al. (2018). Evaluation of Xylooligosaccharide Production from Residual Hemicelluloses of Dissolving Pulp by Acid and Enzymatic Hydrolysis. *RSC Adv.* 8 (61), 35211–35217. doi:10.1039/c8ra07140c
- White, J. E., Catallo, W. J., and Legendre, B. L. (2011). Biomass Pyrolysis Kinetics: A Comparative Critical Review with Relevant Agricultural Residue Case Studies. *J. Anal. Appl. Pyrolysis* 91 (1), 1–33. doi:10.1016/j.jaap.2011.01.004
- Xu, C., Pranovich, A., Vähäsalo, L., Hemming, J., Holmbom, B., Schols, H. A., et al. (2008). Kinetics of Acid Hydrolysis of Water-Soluble Spruce O-Acetyl Galactoglucanmannans. *J. Agric. Food Chem.* 56, 2429–2435. doi:10.1021/jf703702y
- Xu, J., Li, C., Dai, L., Xu, C., Zhong, Y., Yu, F., et al. (2020a). Biomass Fractionation and Lignin Fractionation towards Lignin Valorization. *ChemSusChem* 13, 4284–4295. doi:10.1002/cssc.202001491
- Xu, R., Du, H., Liu, C., Liu, H., Wu, M., Zhang, X., et al. (2021a). An Efficient and Magnetic Adsorbent Prepared in a Dry Process with Enzymatic Hydrolysis Residues for Wastewater Treatment. *J. Clean. Prod.* 313, 127834. doi:10.1016/j.jclepro.2021.127834
- Xu, R., Liu, K., Du, H., Liu, H., Cao, X., Zhao, X., et al. (2020b). Falling Leaves Return to Their Roots: A Review on the Preparation of γ -Valerolactone from Lignocellulose and its Application in the Conversion of Lignocellulose. *ChemSusChem* 13, 6461–6476. doi:10.1002/cssc.202002008
- Xu, T., Du, H., Liu, H., Liu, W., Zhang, X., Si, C., et al. (2021b). Advanced Nanocellulose-Based Composites for Flexible Functional Energy Storage Devices. *Adv. Mater.* 2021, 2101368. doi:10.1002/adma.202101368
- Xu, Y., Wang, P., Xue, S., Kong, F., Ren, H., and Zhai, H. (2020c). Green Biorefinery - the Ultra-high Hydrolysis Rate and Behavior of Populus Tomentosa Hemicellulose Autohydrolysis under Moderate Subcritical Water Conditions. *RSC Adv.* 10 (32), 18908–18917. doi:10.1039/D0RA02350G

- Yáñez, R., Romani, A., Garrote, G., Alonso, J. L., and Parajó, J. C. (2009). Processing of Acacia Dealbata in Aqueous Media: First Step of a Wood Biorefinery. *Ind. Eng. Chem. Res.* 48, 6618–6626. doi:10.1021/ie900233x
- Yang, G. C. C., and Lee, H.-L. (2005). Chemical Reduction of Nitrate by Nanosized Iron: Kinetics and Pathways. *Water Res.* 39 (5), 884–894. doi:10.1016/j.watres.2004.11.030
- Yang, H., Yan, R., Chen, H., Lee, D. H., and Zheng, C. (2007). Characteristics of Hemicellulose, Cellulose and Lignin Pyrolysis. *Fuel* 86 (12–13), 1781–1788. doi:10.1016/j.fuel.2006.12.013
- Yang, X., Xie, H., Du, H., Zhang, X., Zou, Z., Zou, Y., et al. (2019). Facile Extraction of Thermally Stable and Dispersible Cellulose Nanocrystals with High Yield via a green and Recyclable FeCl₃-Catalyzed Deep Eutectic Solvent System. *ACS Sustainable Chem. Eng.* 7, 7200–7208. doi:10.1021/acssuschemeng.9b00209
- Yedro, F. M., Grénman, H., Rissanen, J. V., Salmi, T., García-Serna, J., and Cocero, M. J. (2017). Chemical Composition and Extraction Kinetics of Holm Oak (*Quercus ilex*) Hemicelluloses Using Subcritical Water. *J. Supercrit. Fluids* 129, 56–62. doi:10.1016/j.supflu.2017.01.016
- Yeo, J. Y., Chin, B. L. F., Tan, J. K., and Loh, Y. S. (2019). Comparative Studies on the Pyrolysis of Cellulose, Hemicellulose, and Lignin Based on Combined Kinetics. *J. Energ. Inst.* 92 (1), 27–37. doi:10.1016/j.joei.2017.12.003
- Zaera, F. (2002). Kinetics of Chemical Reactions on Solid Surfaces: Deviations from Conventional Theory. *Acc. Chem. Res.* 35, 129–136. doi:10.1021/ar000193v
- Zazo, J. A., Casas, J. A., Mohedano, A. F., Gilarranz, M. A., and Rodríguez, J. J. (2005). Chemical Pathway and Kinetics of Phenol Oxidation by Fenton's Reagent. *Environ. Sci. Technol.* 39, 9295–9302. doi:10.1021/es050452h
- Zhang, J., Chen, T., Wu, J., and Wu, J. (2014). A Novel Gaussian-DAEM-Reaction Model for the Pyrolysis of Cellulose, Hemicellulose and Lignin. *RSC Adv.* 4, 17513. doi:10.1039/c4ra01445f
- Zhang, M., Du, H., Liu, K., Nie, S., Xu, T., Zhang, X., et al. (2021). Fabrication and Applications of Cellulose-Based Nanogenerators. *Adv. Compos. Hybrid. Mater.* 4. doi:10.1007/s42114-021-00312-2
- Zheng, Y., Yu, Y., Lin, W., Jin, Y., Yong, Q., and Huang, C. (2021). Enhancing the Enzymatic Digestibility of Bamboo Residues by Biphasic Phenoxymethanol-Acid Pretreatment. *Bioresour. Technology* 325, 124691. doi:10.1016/j.biortech.2021.124691
- Zhong, C., Wang, C., Huang, F., Wang, F., Jia, H., Zhou, H., et al. (2015). Selective Hydrolysis of Hemicellulose from Wheat Straw by a Nanoscale Solid Acid Catalyst. *Carbohydr. Polym.* 131, 384–391. doi:10.1016/j.carbpol.2015.05.070
- Zhou, H., Long, Y., Meng, A., Chen, S., Li, Q., and Zhang, Y. (2015). A Novel Method for Kinetics Analysis of Pyrolysis of Hemicellulose, Cellulose, and Lignin in TGA and Macro-TGA. *RSC Adv.* 5 (34), 26509–26516. doi:10.1039/C5RA02715B
- Zhu, L., and Zhong, Z. (2020). Effects of Cellulose, Hemicellulose and Lignin on Biomass Pyrolysis Kinetics. *Korean J. Chem. Eng.* 37 (10), 1660–1668. doi:10.1007/s11814-020-0553-y

Conflict of Interest: The authors declare that the research was conducted in the absence of any commercial or financial relationships that could be construed as a potential conflict of interest.

The reviewer (JX) declared a past co-authorship with one of the authors (MM) to the handling Editor.

Publisher's Note: All claims expressed in this article are solely those of the authors and do not necessarily represent those of their affiliated organizations, or those of the publisher, the editors, and the reviewers. Any product that may be evaluated in this article, or claim that may be made by its manufacturer, is not guaranteed or endorsed by the publisher.

Copyright © 2021 Yuan, Liu, Ma, Ji, Choi and Si. This is an open-access article distributed under the terms of the Creative Commons Attribution License (CC BY). The use, distribution or reproduction in other forums is permitted, provided the original author(s) and the copyright owner(s) are credited and that the original publication in this journal is cited, in accordance with accepted academic practice. No use, distribution or reproduction is permitted which does not comply with these terms.



Using poly(N-Vinylcaprolactam) to Improve the Enzymatic Hydrolysis Efficiency of Phenylsulfonic Acid-Pretreated Bamboo

Xianqing Lv^{1†}, Guangxu Yang^{1†}, Zhenggang Gong¹, Xin Cheng¹, Li Shuai¹, Liulian Huang¹, Lihui Chen¹, Xiaolin Luo^{1,2*} and Jing Liu^{1*}

¹College of Materials Engineering, Fujian Agriculture and Forestry University, Fuzhou, China, ²Jiangsu Provincial Key Laboratory of Pulp and Paper Science and Technology, Nanjing Forestry University, Nanjing, China

OPEN ACCESS

Edited by:

Chao Zhao,
Zhejiang A&F University, China

Reviewed by:

Shuangquan Yao,
Guangxi University, China
Samarthya Bhagia,
Oak Ridge National Laboratory,
United States

*Correspondence:

Xiaolin Luo
xluo@fafu.edu.cn
Jing Liu
jingliu@fafu.edu.cn

[†]These authors have contributed
equally to this work and share first
authorship

Specialty section:

This article was submitted to
Bioprocess Engineering,
a section of the journal
Frontiers in Bioengineering and
Biotechnology

Received: 29 October 2021

Accepted: 18 November 2021

Published: 30 November 2021

Citation:

Lv X, Yang G, Gong Z, Cheng X,
Shuai L, Huang L, Chen L, Luo X and
Liu J (2021) Using poly(N-
Vinylcaprolactam) to Improve the
Enzymatic Hydrolysis Efficiency of
Phenylsulfonic Acid-
Pretreated Bamboo.
Front. Bioeng. Biotechnol. 9:804456.
doi: 10.3389/fbioe.2021.804456

Chemical pretreatment followed by enzymatic hydrolysis has been regarded as a viable way to produce fermentable sugars. Phenylsulfonic acid (PSA) pretreatment could efficiently fractionate the non-cellulosic components (hemicelluloses and lignin) from bamboo and result in increased cellulose accessibility that was 10 times that of untreated bamboo. However, deposited lignin could trigger non-productive adsorption to enzymes, which therefore significantly decreased the enzymatic hydrolysis efficiency of PSA-pretreated bamboo substrates. Herein, poly(N-vinylcaprolactam) (PNVCL), a non-ionic surfactant, was developed as a novel additive for overcoming the non-productive adsorption of lignin during enzymatic hydrolysis. PNVCL was found to be not only more effective than those of commonly used liginosulfonate and polyvinyl alcohol for overcoming the negative effect of lignin, but also comparable to the robust Tween 20 and bovine serum albumin additives. A PNVCL loading at 1.2 g/L during enzymatic hydrolysis of PSA pretreated bamboo substrate could achieve an 80% cellulosic enzymatic conversion and meanwhile reduce the cellulase loading by three times as compared to that without additive. Mechanistic investigations indicated that PNVCL could block lignin residues through hydrophobic interactions and the resultant PNVCL coating resisted the adsorption of cellulase via electrostatic repulsion and/or hydration. This practical method can improve the lignocellulosic enzymatic hydrolysis efficiency and thereby increase the productivity and profitability of biorefinery.

Keywords: lignin, non-productive adsorption, enzymatic hydrolysis, poly(N-vinylcaprolactam), phenylsulfonic acid

INTRODUCTION

Transforming renewable carbohydrates into platform chemicals (such as ethanol and lactic acid) via biochemical conversion (enzymatic hydrolysis and fermentation) methods has become an effective way to reduce the dependence of human society on petrochemical products (Ragauskas et al., 2006). To avoid the competition with humans and poultry for raw materials, the research focus has gradually shifted from edible carbohydrates (e.g., corn starch and sucrose) to inedible lignocelluloses (Shuai et al., 2016a; Luo et al., 2020b; Luo et al., 2022). However, the structurally dense linkages between three macromolecular polymers (i.e., cellulose, hemicellulose and lignin) in lignocelluloses makes the release of sugars from carbohydrates difficult and costly (Himmel et al., 2007).

Compared to five-carbon sugars (e.g. xylose), six-carbon sugars (e.g. glucose) are more easily metabolized by microorganisms into secondary metabolites such as ethanol or lactic acid (Ho Nancy et al., 1998). As such, cellulose that solely polymerized from glucose, has been regarded as an ideal substrate for producing fermentable six-carbon glucose through enzymatic hydrolysis (Pan et al., 2005; Sun and Cheng, 2005). To improve enzymatic accessibility of cellulose to enzymes, different thermochemical pretreatments (e.g., dilute acid, alkaline, organosolv, deep-eutectic solvents and hydrotropic acid) have commonly used to remove non-cellulosic components (e.g., hemicellulose, lignin, or both of them) from lignocelluloses prior to enzymatic hydrolysis (Zhu and Pan, 2010; Shuai et al., 2016b; Liu et al., 2019). Significant removal of non-cellulosic components indeed enables the deconstruction of lignocellulose and therefore improves the accessibility of cellulose in pretreated substrates to enzymes (Yang and Wyman, 2004). However, the accessibility mentioned above can only be termed as “potential accessibility” since it will not necessarily resulted in high cellulose conversion (Liu et al., 2017; Shi et al., 2018). In many cases, high enzyme loadings are still needed because hydrophobic lignin re-distributed or re-deposited on the surface of pretreated substrate would adsorb some of the enzymes (Selig et al., 2007; Donohoe et al., 2008). As lignin has a higher adsorption capacity for cellulase than cellulose (Ko et al., 2015), deposited lignin can competitively adsorbs enzyme molecules with cellulose, resulting in less enzyme molecules that can be used for cellulose hydrolysis (Luo et al., 2019; Luo et al., 2020a; Gong et al., 2021). As a result, more enzymes should be loaded for achieving considerable cellulose conversion, thereby increasing the processing cost of enzymatic hydrolysis.

In addition to chemical or genetic modification of enzymes and lignin (Chen and Dixon, 2007; Brogan et al., 2018), the use of additives for overcoming the lignin's negative effects during enzymatic hydrolysis has been considered as one of the most practical methods (Yang and Wyman, 2006; Li and Zheng, 2017). The reported additives mainly include non-catalytic proteins, metal ions and surfactants (Liu et al., 2016; Saini et al., 2016; Li and Zheng, 2017). Non-catalytic proteins (such as bovine serum protein, casein, soybean protein and peanut protein) can restrain the non-productive adsorption of enzymes via blocking lignin through hydrophobic and/or hydrogen-bonding interactions (Yang and Wyman, 2006; Florencio et al., 2016; Luo et al., 2019). Unfortunately, as a medical material or an edible nutrient, the cost of non-catalytic proteins is still very high (Klein-Marcuschamer et al., 2012). Metal ions are relatively inexpensive, but the accumulated cations will affect the stability of the buffer system and the activity of microbial cells in downstream fermentation (Tejirian and Xu, 2010). Ionic surfactants such as lignosulfonates and cetyltrimethyl ammonium bromide also have inherent defects similar to those of metal ions (Soodma and Nordlie, 1969; Lan et al., 2020; Zheng et al., 2020). Therefore, researchers have done intensive studies on development of inexpensive and biocompatible non-ionic

surfactants (Eriksson et al., 2002). Many non-ionic surfactants such as Tween 80, Tween 20, Triton X-100, polyethylene glycol (PEG) and polyvinyl alcohol (PVA), had been used to improve the enzymatic hydrolysis efficiency of lignocelluloses (Eriksson et al., 2002; Börjesson et al., 2007; Liu et al., 2016; Saini et al., 2016; Li and Zheng, 2017). However, as non-ionic additives containing similar key structure ($-\text{CH}_2\text{CH}_2\text{O}-$), Triton X-100 inhibited the metabolism of glucose to ethanol by microorganisms, while Tween 80 did not exhibit adverse effects (Lee et al., 1996). This indicates that the inhibition mechanism of non-ionic additives to microorganisms is really complex and should be deeply explored in biological research field. Therefore, in addition to revealing the inhibition mechanism towards microorganisms, further development of novel non-ionic surfactants with different structure will be not only benefit to the enzymatic hydrolysis, but also enrich the types of additives compatible to the subsequent fermentation process.

As an additive of enzymatic hydrolysis, it needs not only to block lignin, but also to resist protein adsorption effectively. Developed non-ionic surfactants (e.g., PEG and Tween 20, etc.) commonly possess ($-\text{CH}_2\text{CH}_2\text{O}-$) unit (Eriksson et al., 2002; Börjesson et al., 2007). The foregoing studies (Kristensen et al., 2007; Li and Zheng, 2017) have speculated that effective adsorption could be well formed between carbon skeleton of non-ionic surfactants and lignin through hydrophobic interaction. Residual ether linkages ($-\text{O}-$) tend to hydrate with water molecules, thereby resisting the adsorption of enzymes on the surface of adsorbed non-ionic surfactants. From the perspective of molecular structure, poly(N-vinylcaprolactam) (PNVCL) contains hydrophobic polyethylene chain and hydrophilic amide bonds. Also, PNVCL has been developed as a drug carrier, indicating its biocompatibility to biological system (Vihola et al., 2002). Inspired by the interaction mechanism of developed non-ionic surfactants and lignin and the amphiphilic polymers [e.g. poly(methacrylic acid)] that used for anti-protein fouling (Wang et al., 2020), PNVCL was therefore explored as an additive for improving the enzymatic hydrolysis efficiency of PSA pretreated bamboo substrate in this study. From the perspective of the interactions between lignin, enzyme and additive, the promoting mechanism of PNVCL was also explored, which could be useful for developing advanced additives and improving the economics of lignocellulosic bioconversion process.

MATERIALS AND METHODS

Materials

Moso bamboo chips that provided by Fujian Hibos Chemical Technology Co., Ltd. (Nanping City, China) were air-dried and carefully milled to pass through 40 mesh for subsequent pretreatment. Chemicals including phenylsulfonic acid (PSA), PVA and Tween 20, and dyes (Congo red and Rose Bengal) were purchased from Aladdin® Chemicals (Shanghai, China). PNVCL with molecular weight ranged from 1.3 to 354 kDa and bovine serum albumin (BSA) were obtained from Shanghai Yuanye Bio-

Technology Co., Ltd. (Shanghai City, China) and VWR™ (Shanghai City, China), respectively. Cellulase (Celluclast 1.5 L[®]), β -glucosidase (Novozyme 188), microcrystalline cellulose (Avicel[®] PH-101) and lignosulfonate were ordered from Sigma-Aldrich Company (Shanghai, China). Silicon wafers (boron doping, crystal orientation 100, 5 × 5 mm) used for contact angle measurements were provided by Kaihua Lijing Electronics Co., Ltd. (Zhejiang, China).

Phenylsulfonic Acid Pretreatment and Lignin Isolation

Bamboo particles (< 40 mesh) were pretreated by PSA aqueous solution in a thick-walled glass bottle. Prior to the pretreatment, an 80 wt. % PSA aqueous solution was prepared at 60°C. The prepared PSA aqueous solution was pre-mixed with bamboo particles in the thick-walled glass bottle, while the mass ratio of PSA solution to bamboo particles (o.d.) was kept at 15:1 (w/w). The thick-walled glass bottle was sealed by a Teflon cap and transferred into the oil bath. The mixture in the thick-walled glass bottle was then magnetically stirred at 500 rpm and heated at 95°C for 30 min. Finally, the pretreatment was stopped by cooling the bottle to room temperature with tap water. The slurry was immediately filtered under vacuum to separate the pretreated solid substrate and pretreatment liquor. The separated solid substrate was washed with de-ionic water until obtaining a neutral filtrate. Actually, it is difficult to completely separate PSA from the pretreated solid substrate during scale-up process because of controlling processing cost. Recently, phenol-4-sulfonic acid, a derivative of PSA, was well recovered by using ethanol to washing pretreated solid substrate, which resulted in a high recovery yield (~98.3%) of phenol-4-sulfonic acid and would be a potentially effective way to recover PSA (He et al., 2020). Otherwise, neutralization of residual PSA by weak alkali (e.g. Na₂CO₃) would also be an alternative method to alleviate its negative effects towards enzymes and microorganism. The dissolved lignin was precipitated by diluting pretreatment liquor with 20 times volume of de-ionic water. The precipitated lignin (termed as PSA lignin) was washed with de-ionic water to neutral, vacuum dried and collected for following experiments.

Composition Analysis

After air-dried, the compositions of untreated and PSA pretreated bamboo particles were analyzed by a well-developed method (Sluiter et al., 2008). Based on measured substrate yield (SY) and specific component content, the component (cellulose, hemicellulose or lignin) removal can be calculated as followings:

$$RM = 100 \frac{(W_0 - 0.01W_1 \times SY)}{W_0} \quad (1)$$

where RM is the removal (%) of certain component (cellulose, hemicellulose or lignin) after pretreatment; W_0 and W_1 refer to the mass content (%) of certain component (cellulose, hemicellulose or lignin) in o. d. raw material and pretreated

solid substrate, respectively; SY (%) is the mass yield of solid substrate after pretreatment.

Characterizations of Untreated Bamboo and Pretreated Substrate

Prior to characterization, untreated bamboo particle and pretreated substrate were further vacuum dried for 12 h at 40°C. The dried samples were sputter-coated with gold and imaged by a scanning electron microscopy (SEM, SU8010, Hitachi, Japan). For evaluating the surface diffuse reflectance property, the dried samples without coating gold were further characterized by a UV-Vis-NIR Systems (Agilent Cary 7000, CA, US) at 200–800 nm with a spectral bandwidth of 2 nm. For differentiating the reflection characteristics of the samples especially in UV region (200–350 nm), the measured reflectivity (R_λ) was further converted to its F(R) value based on a well-known Kubelka-Munk function (Klaas et al., 1997).

$$F(R) = \frac{(1 - R_\lambda/100)^2}{2(R_\lambda/100)} \quad (2)$$

where R_λ is the reflectance (%) of sample measured at certain wavelength (nm).

The accessibilities of untreated bamboo particle and pretreated substrate were evaluated by a Congo red staining method (Yu et al., 2020). In general, Congo red dye was pre-dissolved in acetate buffer solution (60 mmol/L and pH 6.0). The solid sample (untreated bamboo particle or pretreated substrate) without additional drying were mixed with a 2 g/L of Congo red buffer solution at a 1% (w/v) concentration in an Erlenmeyer flask. The flask was sealed with a rubber stopper and shaken in an incubator at 50°C and 180 rpm for 24 h. After staining, the solid-liquid mixture was immediately cooled with tap water to room temperature and centrifuged at 740 g for 10 min. The supernatant was filled into a Quartz cuvette and measured by a UV-Vis spectrometer (Agilent 8454, CA, US) at 498 nm. A linear relationship (Absorbance = 19.98 × Congo red concentration + 0.02, $R^2 = 0.99$) was developed between Congo red concentration (0.005–0.1 g/L) and absorbance (0.1–2.0) of UV-Vis spectrometer at 498 nm. The accessibility of sample was referred to the amount of adsorbed Congo red dye (mg/g) that could be calculated based on a pre-established standard curve (dye concentration versus absorbance value).

Similarly, the hydrophobicities of these two samples were measured by Rose Bengal staining method (He et al., 2018). A 40 mg/L of Rose Bengal solution was prepared by dissolving dye in citrate buffer solution (50 mmol/L and pH 4.8). The solid sample without further drying was also directly suspended in Rose Bengal buffer solution with a concentration ranges of 2–10 g/L. The incubation was conducted at 50°C and 150 rpm for 2 h in a shaker. At the end of staining, the concentration of dye in separated supernatant was measured by a UV-Vis spectrometer (Agilent 8454, CA, US) at 543 nm. First, the concentration of Rose Bengal (2.5–25.0 g/L) was linearly plotted against measured absorbance (0.1–1.6) of UV-Vis spectrometer at 543 nm. The residual dye concentration after adsorption could be calculated based on initial dye concentration, measured absorbance and

developed linear relationship (Absorbance = $0.06 \times \text{Rose Bengal concentration} - 0.02$, $R^2 = 0.99$). Another linear relationship was then developed between partition quotients (the mass ratio of adsorbed dye to free dye) and loaded sample concentrations (g/ml). The slope (ml/g) of developed linear curve was thus used to denote the hydrophobicity of sample.

Enzymatic Hydrolysis

The enzymatic hydrolysis of pretreated substrate, microcrystalline cellulose (Avicel) and untreated bamboo were conducted at 50°C and 200 rpm for 72 h in an acetate buffer solution (50 mmol/L). The pH value of buffer solution was adjusted from 4 to 6, while the solid loading in the buffer solution was kept at 2% (w/v). Specifically, about 0.1 g (o.d.) of substrate (PSA-Ba substrate or Avicel) and 5 ml of hydrolysis liquor were performed in a 10-ml centrifuge tube for all hydrolysis experiments. Cellulase and β -glucosidase loadings were 5–20 FPU/g glucan and 7.5–30 CBU/g glucan, respectively. The β -glucosidase loading with a unit of CBU/g glucan was 1.5 times cellulase loading (FPU/g glucan). The concentration of glucose released in the buffer solution was measured by a sugar analyzer (2900D, YSI Inc., Yellow Springs, OH, United States).

To investigate the lignin effect on the enzymatic hydrolysis, PSA-pretreated substrate was soaked in 0.1 mol/L of NaOH or HCl solution at room temperature and 2% (w/v) loading for 2 h and then washed with de-ionic water to neutral before enzymatic hydrolysis. Furthermore, the lignin isolated from the PSA pretreatment liquor was also added into the enzymatic hydrolysis medium of the pretreated substrate or Avicel. The mass ratio of lignin to pretreated substrate or Avicel ranged from 0:1 to 1:1. For overcoming the negative effect of lignin, the additive (PNVCL, Tween 20, BSA, PVA or LS) was pre-mixed with the pretreated substrate in an acetate buffer solution (50 mmol/L, pH 5.0) at 50°C and 200 rpm for 2 h. After that, the enzymes (cellulase and β -glucosidase) were added into the hydrolysis medium and further shaken in the incubator for 72 h at 50°C and 200 rpm.

Based on the measured glucose concentration, the enzymatic conversions (ECs) of glucan in the pretreated substrate or Avicel can be calculated by the following equation.

$$EC = \frac{0.9C_{\text{glucose}} \times V_{\text{buffer}} \times D}{0.01W_{\text{sample}} \times \gamma} \quad (3)$$

where EC refers to the enzymatic conversion (%) of glucan in sample; C_{glucose} and V_{buffer} are the measured glucose concentration (g/ml) of sample and volume (ml) of acetate buffer solution used for the enzymatic hydrolysis; D is the dilution factor for the sample diluted with the fresh acetate buffer solution for glucose concentration measurement; W_{sample} and γ are the o. d. weight (g) of the sample used for enzymatic hydrolysis and corresponding glucan content (%), respectively.

Quartz Crystal Microbalance Measurement

The adsorption properties of cellulase and PNVCL on the PSA lignin film were evaluated by the quartz crystal microbalance (QCM) (Biolin Corp., Gothenburg, Sweden) (Gong et al., 2021; Zheng et al., 2021). Initially, a PSA lignin film was prepared on the surface of the QCM gold sensor according to a reported

spin-coating method (Cai et al., 2017b; Zheng et al., 2021). Sample solution was prepared by dissolving 0.5 g of cellulase or PNVCL in 1 L of acetate buffer solution (50 mmol/L and pH 5.0). After the QCM flow module was thoroughly cleaned by the Milli-Q water, the acetate buffer solution (50 mmol/L and pH 5.0) was imported into the QCM flow module and used to balance the baseline at 23°C and 0.15 ml/min. After that, the sample solution (cellulase or PNVCL, 0.5 g/L) was injected into the QCM flow module at 0.15 ml/min and the corresponding frequency changes (Δf) were immediately monitored. When the adsorption reached an equilibrium, the injection of sample solution was stopped and the fresh acetate buffer solution was re-imported into the flow module for evaluating the desorption properties of cellulase or PNVCL. For PNVCL test, the fresh cellulase buffer solution was further injected into the flow module after the desorption reaching an equilibrium. The third overtone of collected data was used to evaluate the frequency changes (Δf) of the samples. The adsorption capacity of PSA lignin to cellulase or PNVCL was finally estimated by the Sauerbrey equation (Sauerbrey, 1959; Lai et al., 2019).

$$AC = \frac{-\varphi \times \Delta f}{n} \quad (4)$$

where AC (ng/cm²) presents the adsorption capacity of PSA lignin towards enzyme or additive; φ is the QCM constant with a value of 17.7 (ng/cm²/Hz); n is the number of overtone and equals to 3.

Zeta Potential and Contact Angle Analysis

Commercial cellulase or PNVCL was initially dissolved in an acetate buffer solution (50 mmol/L and pH 5.0) for zeta potential analysis. The concentration of the prepared cellulase protein or PNVCL buffer solution was kept at 200 mg/L. To measure the zeta potentials of samples at different pH values, the pH values of the mother acetate buffer solution was adjusted to 3–6 by 1 mol/L of HCl or NaOH aqueous solution. Finally, the zeta potential of the prepared sample was measured by a Malvern Zetasizer (Nano ZS90, Malvern Instruments, Malvern, United Kingdom).

For contact angle measurements, PSA lignin or PNVCL was dissolved in pyridine-acetic acid-water mixture (9:1:4, v/v/v) at a concentration of 2 wt%. The prepared solution was coated on a silicon wafer (boron doping, crystal orientation 100, 5 × 5 mm) via a spin-coating method at 400 rpm for 30 s, 800 rpm for 60 s and 400 rpm for 30 s. The resulted coatings were exposed in HCl steam (37 wt. %) for 30 s and then preserved in de-ionic water. Prior to measurement, the coatings were taken out of the water and thoroughly dried by N₂. The contact angles of dried coatings were finally measured with pure water on a contact angle tester (DSA30S, Krüss GmbH, Germany), when the water droplets stably existed on the silicon wafers.

RESULTS AND DISCUSSION

Effects of Lignin on the Enzymatic Hydrolysis

The aforementioned studies (Chen et al., 2017; Luo et al., 2020a) reported that the aryl sulfonic acid-based hydrotropic medium

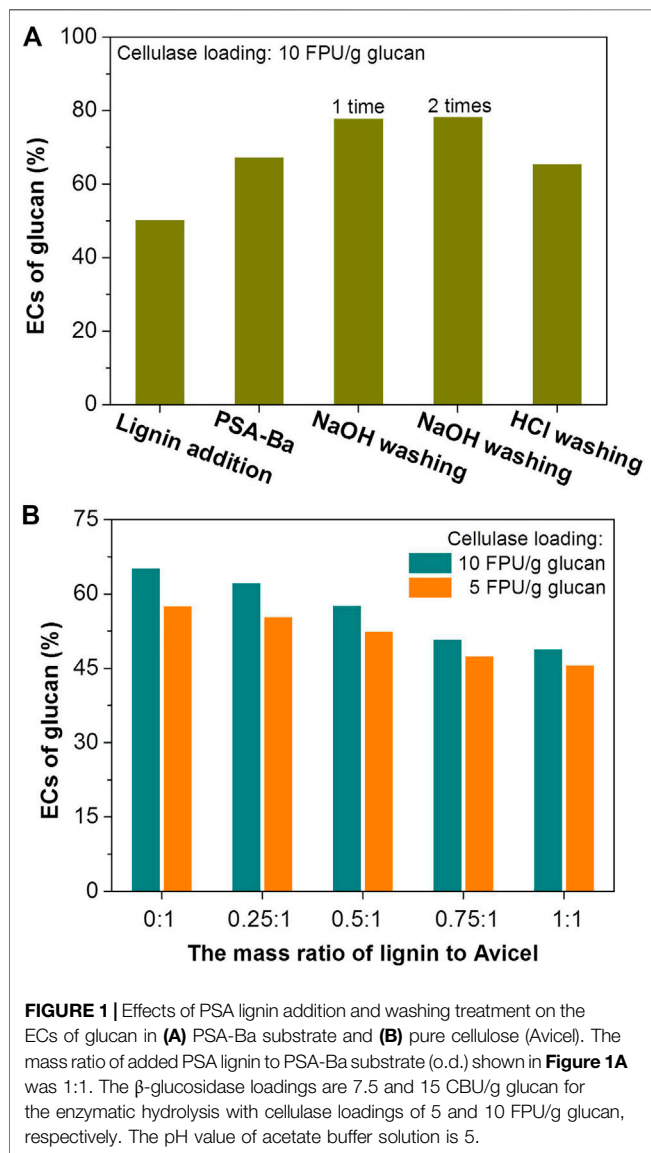
TABLE 1 | The contents and removal of components in untreated bamboo and PSA pretreated solid substrate.

Samples	Temp. (°C)	Time (min)	PSA loading (%)	SY (%) ^a	Components content (%) ^a			Components removal (%) ^b		
					Glucan	Hemi ^c	K. Lignin ^c	Glucan	Hemi	K. Lignin ^c
Un-Ba	—	—	—	—	39.7 ± 1.2	24.0 ± 1.3	26.4 ± 1.5	—	—	—
SA-Ba	95	30	80	43.4 ± 1.6	84.3 ± 0.6	6.0 ± 1.1	6.2 ± 0.7	9.8 ± 2.7	88.9 ± 1.6	90.2 ± 1.5

^aSY, and Components content were calculated based on the o. d. weight of Un-Ba and PSA-Ba substrate.

^bComponents removal was calculated based on the o. d. weight of special component in Un-Ba.

^cHemi. and K. Lignin refer to the abbreviations of hemicellulose and Klason lignin, respectively.



(e.g. *p*-toluenesulfonic acid) could effectively fractionate lignocelluloses. To facilitate the discussion, untreated bamboo and PSA-pretreated bamboo are abbreviated as Un-Ba and PSA-Ba. After the pretreatment, more than 88% of non-cellulosic components (hemicelluloses and lignin) were selectively removed, resulting in a substrate with high glucan content (>84%, **Table 1**). Theoretically, the substantial removal of

non-cellulosic components would be beneficial to improve the accessibility of cellulose in pretreated substrate to enzymes.

Although PSA pretreatment can improve the enzymatic conversion (EC) of glucan in the pretreated substrate, high enzymes loadings are still necessary to afford high cellulose conversion. For example, a cellulosic conversion of 67% was achieved for PSA-Ba substrate (**Figure 1A**), while the EC of glucan in Un-Ba was only 5%. However, such unobtrusive EC was obtained at high cellulase loading (10 FPU/g glucan). Similar phenomena were also reported by previous reports (Chen et al., 2017; Luo et al., 2020a). For PSA-pretreated alkaline peroxide mechanical pulp (APMP), a cellulase loading of 20 FPU/g glucan only resulted in less than 80% of cellulosic EC (Dong et al., 2021). Although the cellulosic EC of poplar wood could reach 90% after *p*-toluenesulfonic acid pretreatment, a cellulase loading as high as 15 FPU/g glucan was still essential (Chen et al., 2017). Some researchers had attributed the need for high cellulase loadings to the lignin deposits (Luo et al., 2020a; Lan et al., 2020), which could significantly adsorb cellulase and reduce the amount of the enzyme molecules involved in cellulose hydrolysis.

Herein, lignin addition and pre-washing were used to verify the above speculation. Under the same enzymatic hydrolysis conditions, adding PSA lignin indeed decreased the EC of glucan in PSA-Ba substrate from 67 to 50% (**Figure 1A**). Pre-washing PSA-Ba substrate prior to enzymatic hydrolysis with 0.1 mol/L of HCl solution resulted in unobvious changes of cellulosic EC (67 versus 65%), presumably due to the insolubility of PSA lignin in acidic aqueous solutions. Under the same washing conditions, pre-washing of the substrate with 0.1 mol/L of NaOH solution once could increase the cellulosic EC from 67 to 78% (**Figure 1A**). However, washing the substrate with NaOH solution twice did not further improve the enzymatic hydrolysis efficiency (**Figure 1A**). This may be due to that washing once would be enough to remove lignin deposits. Increasing the lignin addition also decreased the EC of pure cellulose (Avicel® PH-101) (**Figure 1B**), which directly proved the negative effect of lignin to the cellulose EC. Therefore, to avoid the generation of alkaline waste, developing efficient additives will be an effective way to overcome the negative influence of residual lignin.

Characterizations of Untreated Bamboo and Pretreated Substrate

To verify the speculation mentioned above, the Un-Ba and PSA-Ba substrates were characterized by SEM and other methods. SEM results showed that the surface of Un-Ba was relatively

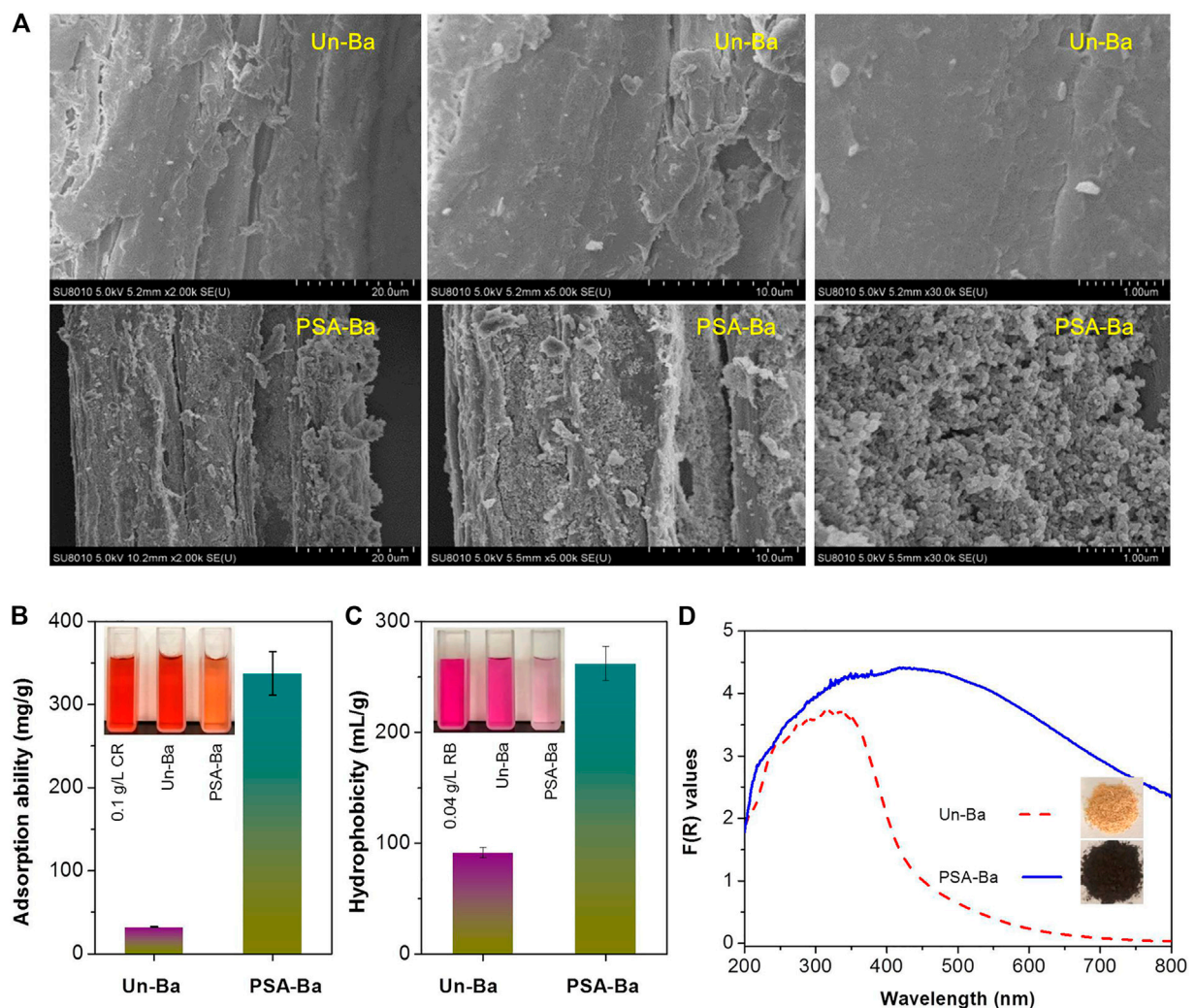
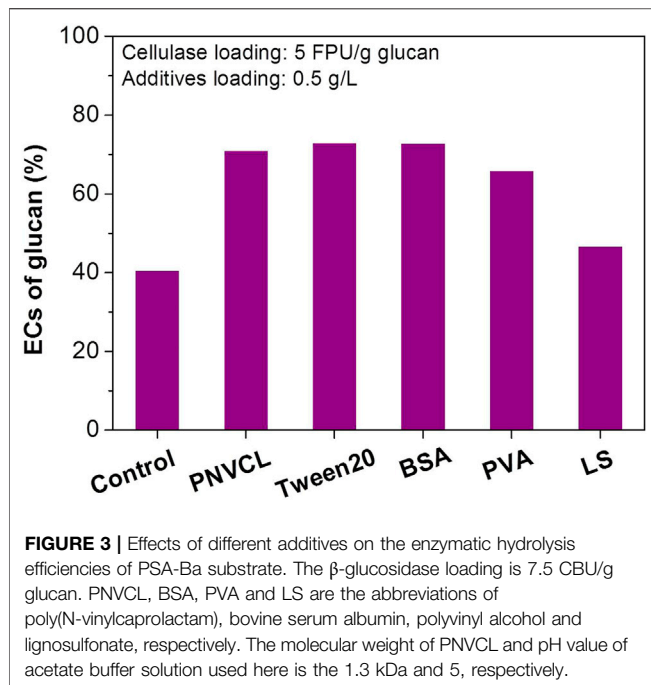


FIGURE 2 | (A) SEM images, **(B)** accessibility, **(C)** hydrophobicity and **(D)** F(R) values of Un-Ba and PSA-Ba substrate. F(R) values were calculated based on the measured sample reflectance (%) and Kubelka-Munk function (Eq. 2). CR and RB shown in **Figure 2B** are the abbreviations of Congo red and Rose Bengal, respectively.

smooth (**Figure 2A**). Without intense mechanical treatments (e.g., stirring or size reduction), the morphology of the PSA-Ba substrate observed by SEM was also relatively complete. However, some small cracks and pores (**Figure 2A**) still appeared on the surface of the PSA-Ba substrate. This may be caused by the removal of non-cellulosic components (hemicellulose and lignin) (Chen et al., 2017; Dong et al., 2021). Based on the results of the compositional analysis (**Table 1**), we speculate that the removal of non-cellulose components will result in exposure of cellulose. Due to the specific adsorption of Congo red dye to cellulose, a well-known Congo red staining method (Yu et al., 2020) was used to semi-quantitatively characterize the accessibilities of Un-Ba and PSA-Ba substrates. As expected, the adsorption capacity of PSA-Ba substrate towards Congo red was 10 times higher than that of Un-Ba (**Figure 2B**), proving the effectiveness of PSA pretreatment for improving substrate accessibility.

However, such considerable substrate accessibility did not yield satisfactory cellulosic EC (<70%) at a relatively high enzyme loading (**Figure 1A**). These seemingly contradictory results promoted us to further characterize Un-Ba and PSA-Ba substrates. In addition to small cracks and pores, many irregular particles could be also observed on the surface of the PSA-Ba substrate (**Figure 2A**). This is probably due to the aggregation and re-deposition of dissolved or relocated hydrophobic lignin fragments in aqueous solution, though sulfonic compounds are actually efficient to catalyze the significant cleavage of the aryl ether bonds of lignin (Bian et al., 2017; Chen et al., 2017). In the pretreatments using polar aqueous solutions (such as liquid hot water and organosolv pretreatments), similar phenomena were also revealed previously (Ko et al., 2015; Liu et al., 2017; Shi et al., 2018; Liu et al., 2019; Luo et al., 2019). For this reason, we further characterized the hydrophobicity of these samples. Although



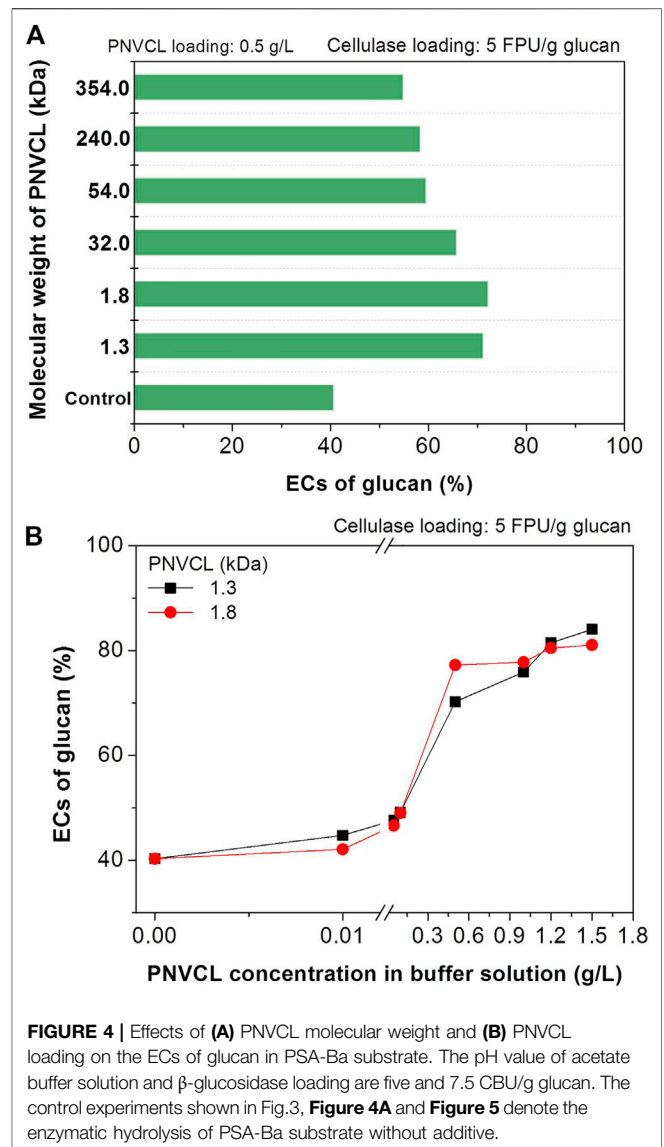
PSA pretreatment removed more than 90% of lignin, we still found that the hydrophobicity of PSA-Ba substrate was about 3 times that of Un-Ba (**Figure 2C**). The F(R) values of the PSA-Ba substrate in UV and Vis regions were also higher than that of Un-Ba (**Figure 2D**), proving that the former possessed higher absorption capacity towards UV and Vis lights. Since cellulose and hemicellulose do not absorb UV and Vis lights under measurement conditions, this result further supports the fact of that more lignin deposits present on the surface of PSA-Ba substrate as compared to the Un-Ba.

The above-mentioned component analysis (**Table 1**), NaOH washing (**Figure 1**), and substrate characterization (**Figure 2**) comprehensively illustrate that although PSA pretreatment can efficiently fractionate bamboo components, lignin deposits can competitively adsorb enzyme molecules from cellulose, which results in reduced enzymatic hydrolysis efficiency.

Comparisons of Different Additives for Enzymatic Hydrolysis

In addition to the complex biochemical modifications of enzyme and lignin (Chen and Dixon, 2007; Brogan et al., 2018), the use of additives is a well-tested method for overcoming the adverse effects of lignin deposits (Eriksson et al., 2002; Yang and Wyman, 2006; Börjesson et al., 2007; Kristensen et al., 2007; Wang et al., 2013). In addition to the poly(N-vinylcaprolactam) (PNVCL) that was explored for improving the enzymatic hydrolysis efficiency of PSA solid substrates, the reported representative additives were also used for comparisons.

At low enzyme loadings, the adverse effect of lignin deposits on the enzymatic hydrolysis becomes more



obvious. When the cellulase loading was reduced from 10 to 5 FPU/g glucan, the EC of glucan in the PSA-Ba substrate rapidly decreased from 67% (**Figure 1A**) to 41% (**Figure 3**). This is most likely caused by the lignin deposits characterized on the surface of PSA-Ba substrate (**Figure 2**), which can result in non-productive adsorption to enzymes. The addition of PNVCL at 0.5 g/L may overcome or at least alleviate such negative effect, which increased the glucan EC from 41% for that without additive to 70% at a cellulase loading of five FPU/g glucan (**Figure 3**). This promotion effect is not only significantly higher than those of PVA and lignosulfonate, but also comparable to Tween 20 and BSA (**Figure 3**), two of the most robust additives reported so far. Considering the inhibition of Tween 20 to *Saccharomyces cerevisiae* (Peng and Chen, 2011) and the high cost of BSA (Klein-Marcuschamer et al., 2012), PNVCL, a non-ionic surfactant that is structurally different from Tween 20 and PEG, would be

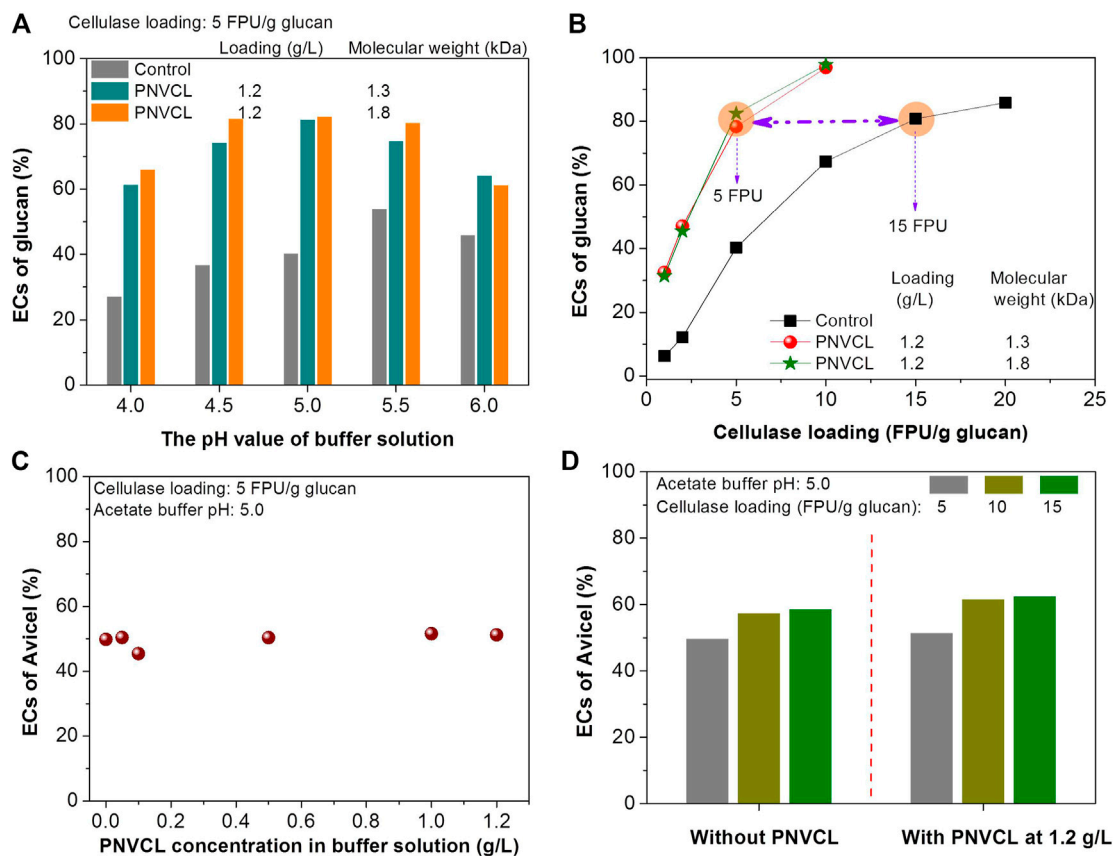


FIGURE 5 | Effects of **(A)** the pH values of acetate buffer solutions and **(B)** cellulase loadings on the ECs of glucan in PSA-Ba substrate; effects of **(C)** and **(D)** PNVC loading on the ECs of Avicel at different cellulase dosage (5–15 FPU/g glucan). The pH values of acetate buffer solution used in **Figure 5B** are 5, and the β -glucosidase loading (CUB/g glucan) for each enzymatic hydrolysis is 1.5 times of cellulase loading (FPU/g glucan).

therefore used as a novel additive for improving the enzymatic hydrolysis efficiency of PSA-Ba substrate.

Improvement of Enzymatic Hydrolysis by PNVC

Herein, the factors that affecting the promoting effect of PNVC to enzymatic hydrolysis will be systematically investigated. With the same enzyme and additive loadings, it can be seen that PNVC (1.3–354 kDa) of different molecular weights had different promoting effects. For example, after adding PNVCs of 1.3 and 1.8 kDa molecular weights into the enzymatic hydrolysis medium, the EC of glucan in the PSA-Ba substrate increased from 41% for the control sample to more than 70% (**Figure 4A**) at a cellulase loading of 5 FPU/g glucan. However, the use of PNVC of a higher molecular weight (32 kDa) led to a slight decrease in the glucan EC (66%). When the molecular weight of PNVC increased to more than 300 kDa (e.g. 354 kDa), the corresponding EC further decreased to 55% (**Figure 4A**). This may be caused by the strengthened inter- and/or intra-molecular aggregations (Maltesh et al., 1992). With polyolefin structure and amide group, increasing molecular weight may facilitate the aggregations of PNVC through hydrophobic and/or

hydrogen-bonding interactions. Therefore, PNVCs with molecular weights of 1.3 and 1.8 kDa were used in other investigations.

By using low-molecular-weight PNVCs as additives, the effect of its addition on the enzymatic hydrolysis efficiency was further investigated at a low cellulase loading (5 FPU/g glucan). When the additive loading was lower than 0.1 g/L, the highest EC did not exceed 50%, despite the ECs of glucan in PSA-Ba substrate increased with the increase in PNVC loading (**Figure 4B**). After increasing the addition of PNVC (1.3 and 1.8 kDa) to 0.5 and 1.2 g/L, the corresponding ECs reached 70 and 80%, respectively. However, further increasing the PNVC loading over 1.2 g/L did not change the enzymatic hydrolysis efficiency of the PSA-Ba substrate (**Figure 4B**). Therefore, a PNVC loading of 1.2 g/L is enough to overcome the adverse effects of PSA lignin on cellulase.

It can be also found that the buffer pH values have different effects on the enzymatic hydrolysis with and without PNVC. The pH value of the acetate buffer was optimized at 5.5 for the enzymatic hydrolysis of PSA-Ba substrate without additive (**Figure 5A**). This is mainly due to that the pH value of the acetate buffer solution not only affects the enzyme activity but also changes the surface charges of enzymes and substrate

(Lan et al., 2013). The high pH value (e.g. 5.5) can make the surface charge of enzymes and substrate more negative, which can trigger the electrostatic repulsion between the enzymes and substrate and thereby reduce the non-productive adsorption of the enzymes on the substrate (Lan et al., 2013; Lou et al., 2013). For the enzymatic hydrolysis using the low-molecular-weight PNVCLs (1.3 and 1.8 kDa) as additives at 1.2 g/L, the highest glucan EC was obtained in the acetate buffer solution at pH 5 (Figure 5A). After blocking the lignin deposits by PNVCL, we speculate the acetate buffer solution with either too high or low pH value would negatively affect the enzyme activity since the robust activity of commercial cellulase preparation from *Trichoderma reesei* was reported at a narrow pH value range (4.8–5) of acetate buffer solution (Lan et al., 2013). However, the ECs of glucan in the PSA-Ba substrate with PNVCL were significantly higher than those without additives at each investigated pH value (4–6), indirectly indicating that lignin deposits rather than the pH value of the buffer solution induced enzyme activity and surface charge would be the key factor governing the enzymatic hydrolysis efficiency.

In addition to the factors discussed above, the effects of cellulase loadings on the enzymatic hydrolysis efficiencies were further investigated. In order to achieve the same level of glucan EC, the cellulase loading required for enzymatic hydrolysis without additives was significantly higher than that with PNVCL. For example, enzymatic hydrolysis without additive required a cellulase loading of 15 FPU/g glucan to achieve an 80% glucan EC, which was three times (Figure 5B) that with the addition of PNVCL at 1.2 g/L and an acetate buffer pH value of 5. These experimental results again indicate that non-productive adsorption of lignin to enzymes would be the key factor affecting the enzymatic hydrolysis efficiency of PSA-Ba substrate.

Although above results verify the validity of low-molecular-weight PNVCL for improving the enzymatic hydrolysis efficiency, its effect on subsequent fermentation of glucose to produce ethanol or other platform chemicals (e.g. lactic acid) would be the on-going experimental focus. Since the molecular weights of PNVCL (1.3–354 kDa) used in this study are far higher than that of glucose, it can be separated from enzymatic hydrolysate by reported membrane technologies (i.e., *in-situ* membrane bioreactor and off-line ultrafiltration) (Toledano et al., 2010; Al-Zuhair et al., 2013), if it presents no positive effect to glucose fermentation. Otherwise, it can also be separated from fermentation broth using similar membrane technologies after fermentation.

Promoting Mechanism of PNVCL Towards Enzymatic Hydrolysis

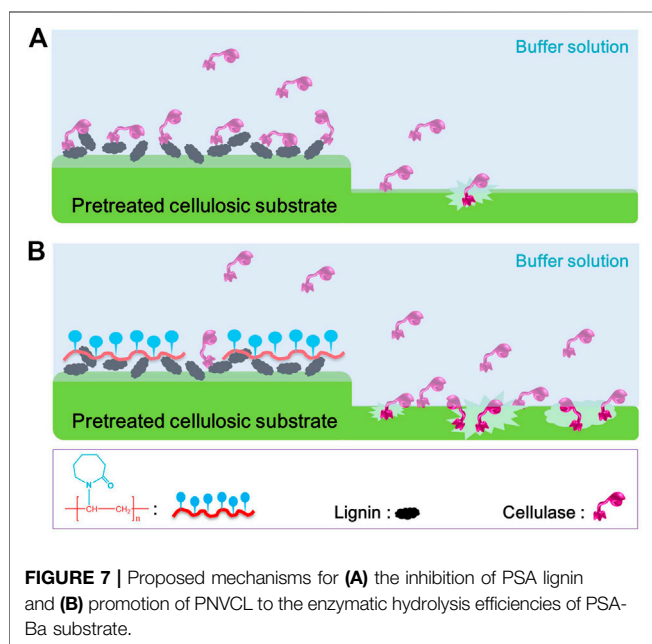
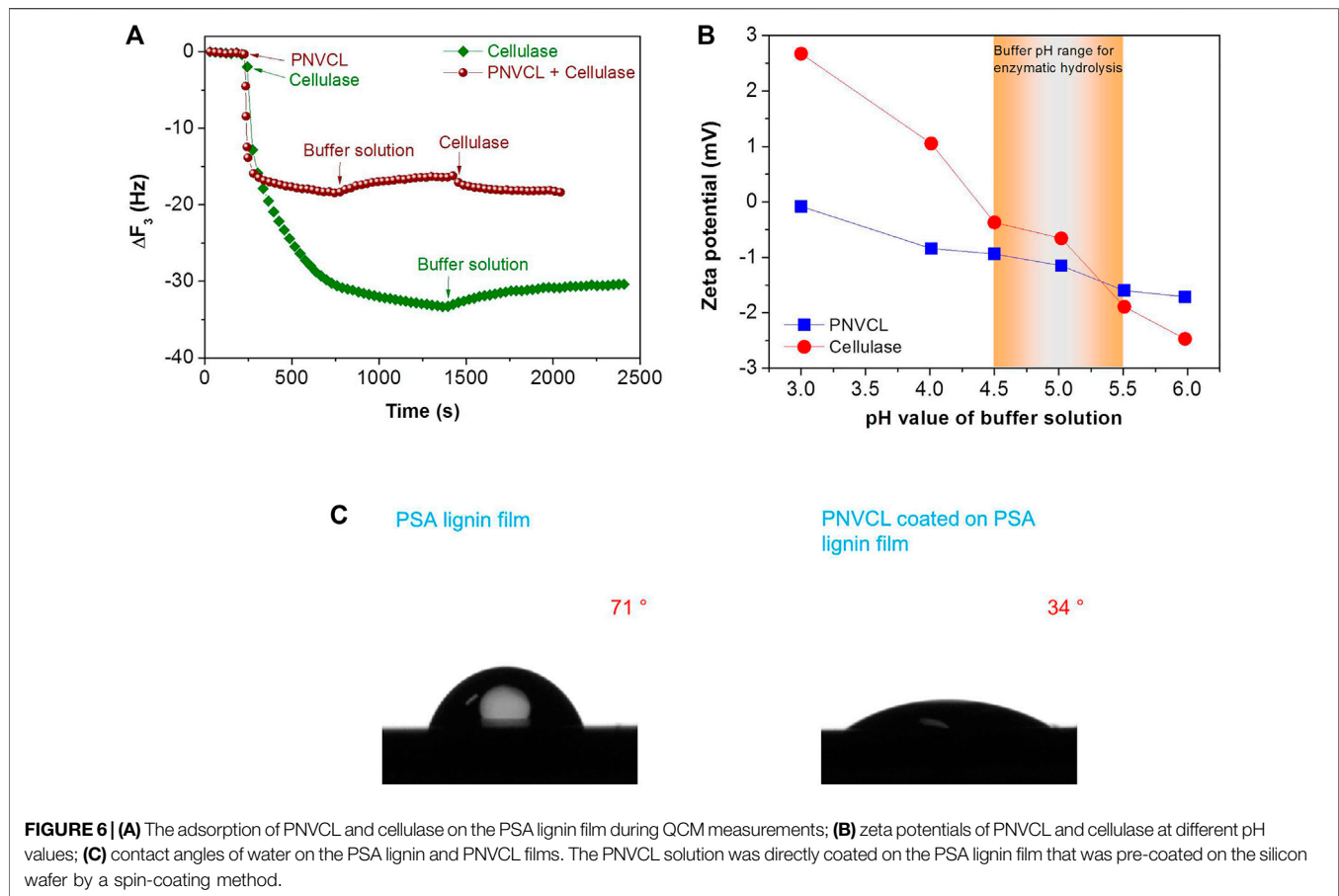
The effectiveness of PNVCL as an enzymatic hydrolysis additive further urged us to explore its promoting mechanism. Previous study (Bhagia et al., 2018) reported that non-ionic surfactants (e.g. Tween 20) could effectively alleviate the inactivation of cellulase at the gas-liquid interface, thus improving the enzymatic hydrolysis efficiency of microcrystalline cellulose (Avicel® PH-101). To validate this effect, enzymatic hydrolysis experiments of Avicel with and without PNVCL were conducted

at a volumetric ratio of 10 ml of reactor (centrifuge tube) to ~5 ml of hydrolysate that used for PSA-Ba substrate. It was found that the ECs of Avicel did not increase with the increase in PNVCL loading (0–1.2 g/L) (Figure 5C) at a cellulase loading of 5 FPU/g cellulose. Moreover, with different cellulase loadings (5, 10, and 15 FPU/g cellulose), there was also no obvious difference in the ECs of Avicel with and without PNVCL (Figure 5D). These results proved that since low volumetric ratio of reactor to hydrolysate (10 vs. 5 ml) used, the role of PNVCL in improving enzymatic hydrolysis efficiency of PSA-Ba substrate would mainly contribute from inhibiting cellulase non-productive adsorption through blocking lignin.

To reveal the blocking performance of PNVCL towards lignin, adsorption properties of cellulase and PNVCL on lignin film were investigated by QCM analysis. In the process of QCM analysis, enzymes were quickly absorbed on the PSA lignin film and resulted in a significant frequency changes (Δf , 33.3 Hz) (Figure 6A). After fresh buffer solution was injected into the QCM flow module, only 10% of the cellulase (Δf , 33.3 to 30.4 Hz) was desorbed, indicating the stable adsorption of cellulases on the PSA lignin film. When the adsorption of PNVCL on PSA lignin film reached equilibrium, introducing fresh acetate buffer solution also resulted in only 2.2 Hz of frequency change (Δf , 18.4–16.2 Hz), i.e. only 12% desorption of PNVCL from PSA lignin film. Another 2.1 Hz of frequency change (Figure 6A) was observed for further switching the fresh buffer solution in flow module to the cellulase solution, indicating that only few PSA lignin sites (12%) released by the desorption of PNVCL could be re-adsorbed by cellulase molecules. Overall, these QCM adsorption-desorption results illustrate that PNVCL can not only block lignin firmly, but also effectively restrain cellulase adsorption. As a result, even though the adsorption capacity of PSA lignin towards cellulase (197 ng/cm²) was higher than that toward PNVCL (109 ng/cm²), PSA lignin-induced non-productive adsorption during enzymatic hydrolysis could be effectively overcome if PNVCL was pre-mixed with the solid substrate in an acetate buffer solution.

In addition to adsorption capacity, the interactions among PNVCL, lignin and cellulase molecules were further analyzed. First, it was found that the surface electronegativity of the PNVCL and cellulase increased with the increase in the pH values of the acetate buffer. The zeta potentials (Figure 6B) were measured as –0.9 to –1.6 for PNVCL and –0.4 to –1.9 for cellulase in the pH range (4.5–5.0) commonly used for enzymatic hydrolysis. In this pH range, the net surface charge of PSA lignin was also reported to be negative (Chen et al., 2017; Luo et al., 2020a). Therefore, we infer that electrostatic attraction (Wang et al., 2013) and cation- π interaction (Zheng et al., 2021) would be not the main factors governing the efficient blocking of PNVCL towards PSA lignin. Because of the negative surface charge, the PNVCL coating formed on the surface of PSA lignin may further inhibit the adsorption of cellulase via electrostatic repulsion.

In addition to electrostatic and cation- π interactions, the hydrophobicities of PSA lignin and PNVCL were further investigated. When PSA lignin was adsorbed on the surface of relatively hydrophobic silicon wafer, the surface of PSA lignin film was still hydrophobic (71°) (Figure 6C). However, the continued spin-coating of PNVCL on the surface of the



hydrophobic PSA lignin film contrarily reduced the contact angle of water on the new coating to 34° (Figure 6C). This indicates that PNVL can not only be adsorbed on the surface of the hydrophobic PSA lignin film, but also form a hydrophilic coating after shielding the PSA lignin. Previous studies have found that hydrophilic surfaces could be easily hydrated, which would facilitate the inhibition of protein fouling induced by the hydrophobic interaction (Cai et al., 2017a; Cai et al., 2017b; Wang et al., 2020; Zheng et al., 2021).

Based on these results, we speculate that the non-productive adsorption of PSA lignin to cellulase is mainly driven by the hydrophobic interaction, which inevitably decreased the enzymatic hydrolysis efficiency of PSA-Ba substrate (Figure 7A). Moreover, the mechanisms of PNVL for shielding lignin and inhibiting enzyme adsorption (Figure 7B) can be also reasonably proposed as: (1) the hydrophobic polyolefin chains of PNVL facilitate efficient blocking of PSA lignin through hydrophobic interactions; (2) PNVL adsorbed on the surface of lignin can further inhibit the non-productive adsorption of cellulase via electrostatic repulsion and/or hydration; (3) more free enzyme molecules will be available to hydrolyze cellulose, thereby improving its enzymatic hydrolysis efficiency.

CONCLUSION

PSA pretreatment can effectively improve the accessibility of bamboo substrate to enzymes through removing non-cellulosic components (hemicellulose and lignin). However, the lignin residues deposited on the surface of the PSA-Ba substrate caused serious non-productive adsorption to enzymes, which significantly reduced enzymatic hydrolysis efficiency. PNVCL, a non-ionic surfactant, was developed as a novel additive for enzymatic hydrolysis. Similar to intensively-studied tween 20 and BSA additives, the addition of PNVCL during enzymatic hydrolysis of cellulose could substantially reduce cellulase loadings as compared to that without additive for achieving remarkable cellulose EC. In general, PNVCL could effectively block PSA lignin and prevent non-productive adsorption of enzymes through intermolecular non-covalent interactions, which would reduce the loading of enzymes and therefore facilitate the economics of PSA pretreatment-based biorefinery.

DATA AVAILABILITY STATEMENT

The original contributions presented in the study are included in the article/supplementary material, further inquiries can be directed to the corresponding authors.

REFERENCES

- Al-Zuhair, S., Al-Hosany, M., Zooba, Y., Al-Hammadi, A., and Al-Kaabi, S. (2013). Development of a Membrane Bioreactor for Enzymatic Hydrolysis of Cellulose. *Renew. Energ.* 56, 85–89. doi:10.1016/j.renene.2012.09.044
- Bhagia, S., Dhir, R., Kumar, R., and Wyman, C. E. (2018). Deactivation of Cellulase at the Air-Liquid Interface Is the Main Cause of Incomplete Cellulose Conversion at Low Enzyme Loadings. *Sci. Rep.* 8 (1), 1350. doi:10.1038/s41598-018-19848-3
- Bian, H., Chen, L., Gleisner, R., Dai, H., and Zhu, J. Y. (2017). Producing wood-based Nanomaterials by Rapid Fractionation of wood at 80 °C Using a Recyclable Acid Hydrotrope. *Green. Chem.* 19 (14), 3370–3379. doi:10.1039/C7GC00669A
- Börjesson, J., Engqvist, M., Sipos, B., and Tjerneld, F. (2007). Effect of Poly(ethylene Glycol) on Enzymatic Hydrolysis and Adsorption of Cellulase Enzymes to Pretreated Lignocellulose. *Enzyme Microb. Techn.* 41 (1), 186–195. doi:10.1016/j.enzymictec.2007.01.003
- Brogan, A. P. S., Bui-Le, L., and Hallett, J. P. (2018). Non-aqueous Homogenous Biocatalytic Conversion of Polysaccharides in Ionic Liquids Using Chemically Modified Glucosidase. *Nat. Chem.* 10 (8), 859–865. doi:10.1038/s41557-018-0088-6
- Cai, C., Qiu, X., Zeng, M., Lin, M., Lin, X., Lou, H., et al. (2017a). Using Polyvinylpyrrolidone to Enhance the Enzymatic Hydrolysis of Lignocelluloses by Reducing the Cellulase Non-productive Adsorption on Lignin. *Bioresour. Techn.* 227, 74–81. doi:10.1016/j.biortech.2016.12.002
- Cai, C., Zhan, X., Zeng, M., Lou, H., Pang, Y., Yang, J., et al. (2017b). Using Recyclable pH-Responsive Lignin Amphoteric Surfactant to Enhance the Enzymatic Hydrolysis of Lignocelluloses. *Green. Chem.* 19 (22), 5479–5487. doi:10.1039/C7GC02571H
- Chen, F., and Dixon, R. A. (2007). Lignin Modification Improves Fermentable Sugar Yields for Biofuel Production. *Nat. Biotechnol.* 25 (7), 759–761. doi:10.1038/nbt1316
- Chen, L., Dou, J., Ma, Q., Li, N., Wu, R., Bian, H., et al. (2017). Rapid and Near-Complete Dissolution of wood Lignin at ≤80°C by a Recyclable Acid Hydrotrope. *Sci. Adv.* 3 (9), e1701735. doi:10.1126/sciadv.1701735

AUTHOR CONTRIBUTIONS

XLL and JL proposed the concept, designed the experiments, analyzed the data and wrote the manuscript; XQL, GXY, ZGG, and XC carried out the experiments and analyzed the data; XLL, JL, LS, LLH, and LHC supervised the experiments, reviewed and revised the manuscript. All authors read and approved the final manuscript.

FUNDING

This work was supported by National Key R&D Program Project of China (2019YFC1905903), National Natural Science Foundation of China (31870559, 31901262 and 32071716), Fujian Provincial Department of Science and Technology (2018J01590 and 2019J01387), Outstanding Youth Funding (xjq201923) of Fujian Agriculture and Forestry University. We also thank the financial support from the Jiangsu Provincial Key Laboratory of Pulp and Paper Science and Technology (KL201911).

ACKNOWLEDGMENTS

The authors gratefully acknowledge Fujian Hibos Chemical Technology Co., Ltd. for providing bamboo raw materials.

- Dong, M., Wu, C., Chen, L., Zhou, X., Yang, W., Xiao, H., et al. (2021). Benzenesulfonic Acid-Based Hydrotropic System for Achieving Lignocellulose Separation and Utilization under Mild Conditions. *Bioresour. Techn.* 337, 125379. doi:10.1016/j.biortech.2021.125379
- Donohoe, B. S., Decker, S. R., Tucker, M. P., Himmel, M. E., and Vinzant, T. B. (2008). Visualizing Lignin Coalescence and Migration through maize Cell walls Following Thermochemical Pretreatment. *Biotechnol. Bioeng.* 101 (5), 913–925. doi:10.1002/bit.21959
- Eriksson, T., Börjesson, J., and Tjerneld, F. (2002). Mechanism of Surfactant Effect in Enzymatic Hydrolysis of Lignocellulose. *Enzyme Microb. Techn.* 31 (3), 353–364. doi:10.1016/S0141-0229(02)00134-5
- Florencio, C., Badino, A. C., and Farinas, C. S. (2016). Soybean Protein as a Cost-Effective Lignin-Blocking Additive for the Saccharification of Sugarcane Bagasse. *Bioresour. Techn.* 221, 172–180. doi:10.1016/j.biortech.2016.09.039
- Gong, Z., Yang, G., Song, J., Zheng, P., Liu, J., Zhu, W., et al. (2021). Understanding the Promoting Effect of Non-catalytic Protein on Enzymatic Hydrolysis Efficiency of Lignocelluloses. *Bioresour. Bioproc.* 8 (1), 9. doi:10.1186/s40643-021-00363-9
- He, D., Wang, Y., Yoo, C. G., Chen, Q.-J., and Yang, Q. (2020). The Fractionation of Woody Biomass under Mild Conditions Using Bifunctional Phenol-4-Sulfonic Acid as a Catalyst and Lignin Solvent. *Green. Chem.* 22 (16), 5414–5422. doi:10.1039/D0GC01722A
- He, J., Huang, C., Lai, C., Huang, C., Li, X., and Yong, Q. (2018). Elucidation of Structure-Inhibition Relationship of Monosaccharides Derived Pseudo-lignin in Enzymatic Hydrolysis. *Ind. Crops Prod.* 113, 368–375. doi:10.1016/j.indcrop.2018.01.046
- Himmel, M. E., Ding, S.-Y., Johnson, D. K., Adney, W. S., Nimlos, M. R., Brady, J. W., et al. (2007). Biomass Recalcitrance: Engineering Plants and Enzymes for Biofuels Production. *Science* 315 (5813), 804–807. doi:10.1126/science.1137016
- Ho, N. W. Y., Chen, Z., and Brainard, A. P. (1998). Genetically Engineered Saccharomyces Yeast Capable of Effective Cofermentation of Glucose and Xylose. *Appl. Environ. Microbiol.* 64 (5), 1852–1859. doi:10.1128/AEM.64.5.1852-1859.1998
- Klaas, J., Schulz-Ekloff, G., and Jaeger, N. I. (1997). UV-Visible Diffuse Reflectance Spectroscopy of Zeolite-Hosted Mononuclear Titanium Oxide Species. *J. Phys. Chem. B* 101 (8), 1305–1311. doi:10.1021/jp9627133

- Klein-Marcuschamer, D., Oleskiewicz-Popiel, P., Simmons, B. A., and Blanch, H. W. (2012). The challenge of Enzyme Cost in the Production of Lignocellulosic Biofuels. *Biotechnol. Bioeng.* 109 (4), 1083–1087. doi:10.1002/bit.24370
- Ko, J. K., Kim, Y., Ximenes, E., and Ladisch, M. R. (2015). Effect of Liquid Hot Water Pretreatment Severity on Properties of Hardwood Lignin and Enzymatic Hydrolysis of Cellulose. *Biotechnol. Bioeng.* 112 (2), 252–262. doi:10.1002/bit.25349
- Kristensen, J. B., Börjesson, J., Bruun, M. H., Tjerneld, F., and Jørgensen, H. (2007). Use of Surface Active Additives in Enzymatic Hydrolysis of Wheat Straw Lignocellulose. *Enzyme Microb. Techn.* 40 (4), 888–895. doi:10.1016/j.enzmictec.2006.07.014
- Lai, C., Yang, B., Lin, Z., Jia, Y., Huang, C., Li, X., et al. (2019). New Strategy to Elucidate the Positive Effects of Extractable Lignin on Enzymatic Hydrolysis by Quartz crystal Microbalance with Dissipation. *Biotechnol. Biofuels* 12 (1), 57. doi:10.1186/s13068-019-1402-2
- Lan, T. Q., Lou, H., and Zhu, J. Y. (2013). Enzymatic Saccharification of Lignocelluloses Should Be Conducted at Elevated pH 5.2–6.2. *Bioenerg. Res.* 6 (2), 476–485. doi:10.1007/s12155-012-9273-4
- Lan, T. Q., Wang, S. R., Li, H., Qin, Y. Y., and Yue, G. J. (2020). Effect of Lignin Isolated from P-Toluenesulfonic Acid Pretreatment Liquid of Sugarcane Bagasse on Enzymatic Hydrolysis of Cellulose and Cellulase Adsorption. *Ind. Crops Prod.* 155, 112768. doi:10.1016/j.indcrop.2020.112768
- Lee, W. G., Lee, J. S., Lee, J. P., Shin, C. S., Kim, M. S., and Park, S. C. (1996). Effect of Surfactants on Ethanol Fermentation Using Glucose and Cellulosic Hydrolyzates. *Biotechnol. Lett.* 18 (3), 299–304. doi:10.1007/BF00142948
- Li, X., and Zheng, Y. (2017). Lignin-enzyme Interaction: Mechanism, Mitigation Approach, Modeling, and Research Prospects. *Biotechnol. Adv.* 35 (4), 466–489. doi:10.1016/j.biotechadv.2017.03.010
- Liu, H., Sun, J., Leu, S.-Y., and Chen, S. (2016). Toward a Fundamental Understanding of Cellulase-Lignin Interactions in the Whole Slurry Enzymatic Saccharification Process. *Biofuels, Bioprod. Bioref* 10 (5), 648–663. doi:10.1002/bbb.1670
- Liu, J., Hu, H., Gong, Z., Yang, G., Li, R., Chen, L., et al. (2019). Near-complete Removal of Non-cellulosic Components from Bamboo by 1-pentanol Induced Organosolv Pretreatment under Mild Conditions for Robust Cellulose Enzymatic Hydrolysis. *Cellulose* 26 (6), 3801–3814. doi:10.1007/s10570-019-02334-y
- Liu, J., Li, R., Shuai, L., You, J., Zhao, Y., Chen, L., et al. (2017). Comparison of Liquid Hot Water (LHW) and High Boiling Alcohol/water (HBAW) Pretreatments for Improving Enzymatic Saccharification of Cellulose in Bamboo. *Ind. Crops Prod.* 107, 139–148. doi:10.1016/j.indcrop.2017.05.035
- Lou, H., Zhu, J. Y., Lan, T. Q., Lai, H., and Qiu, X. (2013). pH-Induced Lignin Surface Modification to Reduce Nonspecific Cellulase Binding and Enhance Enzymatic Saccharification of Lignocelluloses. *ChemSusChem* 6 (5), 919–927. doi:10.1002/cssc.201200859
- Luo, X., Gong, Z., Shi, J., Chen, L., Zhu, W., Zhou, Y., et al. (2020a). Integrating Benzenesulfonic Acid Pretreatment and Bio-Based Lignin-Shielding Agent for Robust Enzymatic Conversion of Cellulose in Bamboo. *Polymers* 12 (1), 191. doi:10.3390/polym12010191
- Luo, X., Gong, Z., Yang, G., Huang, L., Chen, L., and Shuai, L. (2022). In-situ Oxidation/reduction Facilitates One-Pot Conversion of Lignocellulosic Biomass to Bulk Chemicals in Alkaline Solution. *Chem. Eng. J.* 429, 132365. doi:10.1016/j.cej.2021.132365
- Luo, X., Li, Y., Gupta, N. K., Sels, B., Ralph, J., and Shuai, L. (2020b). Protection Strategies Enable Selective Conversion of Biomass. *Angew. Chem. Int. Ed.* 59 (29), 11704–11716. doi:10.1002/anie.201914703
- Luo, X., Liu, J., Zheng, P., Li, M., Zhou, Y., Huang, L., et al. (2019). Promoting Enzymatic Hydrolysis of Lignocellulosic Biomass by Inexpensive Soy Protein. *Biotechnol. Biofuels* 12 (1), 51. doi:10.1186/s13068-019-1387-x
- Maltesh, C., Xu, Q., Somasundaran, P., Benton, W. J., and Nguyen Hung, H. (1992). Aggregation Behavior of and Surface Tension Reduction by Comblike Amphiphilic Polymers. *Langmuir* 8 (6), 1511–1513. doi:10.1021/la00042a004
- Pan, X., Arato, C., Gilkes, N., Gregg, D., Mabey, W., Pye, K., et al. (2005). Biorefining of Softwoods Using Ethanol Organosolv Pulping: Preliminary Evaluation of Process Streams for Manufacture of Fuel-Grade Ethanol and Co-products. *Biotechnol. Bioeng.* 90 (4), 473–481. doi:10.1002/bit.20453
- Peng, L., and Chen, Y. (2011). Conversion of Paper Sludge to Ethanol by Separate Hydrolysis and Fermentation (SHF) Using *Saccharomyces cerevisiae*. *Biomass and Bioenergy* 35 (4), 1600–1606. doi:10.1016/j.biombioe.2011.01.059
- Ragauskas, A. J., Williams, C. K., Davison, B. H., Britovsek, G., Cairney, J., Eckert, C. A., et al. (2006). The Path Forward for Biofuels and Biomaterials. *Science* 311 (5760), 484–489. doi:10.1126/science.1114736
- Saini, J. K., Patel, A. K., Adsul, M., and Singhania, R. R. (2016). Cellulase Adsorption on Lignin: A Roadblock for Economic Hydrolysis of Biomass. *Renew. Energ.* 98, 29–42. doi:10.1016/j.renene.2016.03.089
- Sauerbrey, G. n. (1959). Verwendung von Schwingquarzen zur Wägung dünner Schichten und zur Mikrowägung. *Z. Physik* 155 (2), 206–222. doi:10.1007/BF01337937
- Selig, M. J., Viamajala, S., Decker, S. R., Tucker, M. P., Himmel, M. E., and Vinzant, T. B. (2007). Deposition of Lignin Droplets Produced during Dilute Acid Pretreatment of maize Stems Retards Enzymatic Hydrolysis of Cellulose. *Biotechnol. Prog.* 23 (6), 1333–1339. doi:10.1021/bp0702018
- Shi, J., Liu, J., Li, M., Huang, L., Chen, L., and Luo, X. (2018). Acid-Free Ethanol-Water Pretreatment with Low Ethanol Concentration for Robust Enzymatic Saccharification of Cellulose in Bamboo. *Bioenerg. Res.* 11 (3), 665–676. doi:10.1007/s12155-018-9928-x
- Shuai, L., Amiri, M. T., Questell-Santiago, Y. M., Héroguel, F., Li, Y., Kim, H., et al. (2016a). Formaldehyde Stabilization Facilitates Lignin Monomer Production during Biomass Depolymerization. *Science* 354 (6310), 329–333. doi:10.1126/science.aaf7810
- Shuai, L., Questell-Santiago, Y. M., and Luterbacher, J. S. (2016b). A Mild Biomass Pretreatment Using γ -valerolactone for Concentrated Sugar Production. *Green. Chem.* 18 (4), 937–943. doi:10.1039/C5GC02489G
- Sluiter, A., Hames, B., Ruiz, R., Scarlata, C., Sluiter, J., Templeton, D., et al. (2008). "Determination of Structural Carbohydrates and Lignin in Biomass," in *Laboratory Analytical Procedure (LAP)* (Golden, CO, United States: National Renewable Energy Laboratory).
- Soodsma, J. F., and Nordlie, R. C. (1969). Effects of Cetyltrimethylammonium Bromide on Catalytic Properties of Kidney Microsomal Glucose-6-Phosphatase, Inorganic Pyrophosphate-Glucose Phosphotransferase and Inorganic Pyrophosphatase Activities. *Biochim. Biophys. Acta (Bba) - Enzymol.* 191 (3), 636–643. doi:10.1016/0005-2744(69)90356-8
- Sun, Y., and Cheng, J. (2005). Dilute Acid Pretreatment of rye Straw and Bermudagrass for Ethanol Production. *Bioresour. Techn.* 96 (14), 1599–1606. doi:10.1016/j.biortech.2004.12.022
- Tejirian, A., and Xu, F. (2010). Inhibition of Cellulase-Catalyzed Lignocellulosic Hydrolysis by Iron and Oxidative Metal Ions and Complexes. *Appl. Environ. Microbiol.* 76 (23), 7673–7682. doi:10.1128/AEM.01376-10
- Toledano, A., García, A., Mondragon, I., and Labidi, J. (2010). Lignin Separation and Fractionation by Ultrafiltration. *Sep. Purif. Techn.* 71 (1), 38–43. doi:10.1016/j.seppur.2009.10.024
- Vihola, H., Laukkanen, A., Hirvonen, J., and Tenhu, H. (2002). Binding and Release of Drugs into and from Thermosensitive poly(N-Vinyl Caprolactam) Nanoparticles. *Eur. J. Pharm. Sci.* 16 (1), 69–74. doi:10.1016/S0928-0987(02)00076-3
- Wang, F., Zhang, H., Yu, B., Wang, S., Shen, Y., and Cong, H. (2020). Review of the Research on Anti-protein Fouling Coatings Materials. *Prog. Org. Coat.* 147, 105860. doi:10.1016/j.porgcoat.2020.105860
- Wang, Z., Zhu, J., Fu, Y., Qin, M., Shao, Z., Jiang, J., et al. (2013). Lignosulfonate-mediated Cellulase Adsorption: Enhanced Enzymatic Saccharification of Lignocellulose through Weakening Nonproductive Binding to Lignin. *Biotechnol. Biofuels* 6 (1), 156. doi:10.1186/1754-6834-6-156
- Yang, B., and Wyman, C. E. (2006). BSA Treatment to Enhance Enzymatic Hydrolysis of Cellulose in Lignin Containing Substrates. *Biotechnol. Bioeng.* 94 (4), 611–617. doi:10.1002/bit.20750
- Yang, B., and Wyman, C. E. (2004). Effect of Xylan and Lignin Removal by Batch and Flowthrough Pretreatment on the Enzymatic Digestibility of Corn stover Cellulose. *Biotechnol. Bioeng.* 86 (1), 88–98. doi:10.1002/bit.20043

- Yu, H., Xu, Y., Hou, J., Nie, S., Liu, S., Wu, Q., et al. (2020). Fractionation of Corn stover for Efficient Enzymatic Hydrolysis and Producing Platform Chemical Using P-Toluenesulfonic Acid/water Pretreatment. *Ind. Crops Prod.* 145, 111961. doi:10.1016/j.indcrop.2019.111961
- Zheng, P., Xiang, L., Chang, J., Lin, Q., Xie, L., Lan, T., et al. (2021). Nanomechanics of Lignin-Cellulase Interactions in Aqueous Solutions. *Biomacromolecules* 22 (5), 2033–2042. doi:10.1021/acs.biomac.1c00140
- Zheng, W., Lan, T., Li, H., Yue, G., and Zhou, H. (2020). Exploring Why Sodium Lignosulfonate Influenced Enzymatic Hydrolysis Efficiency of Cellulose from the Perspective of Substrate-Enzyme Adsorption. *Biotechnol. Biofuels* 13 (1), 19. doi:10.1186/s13068-020-1659-5
- Zhu, J. Y., and Pan, X. J. (2010). Woody Biomass Pretreatment for Cellulosic Ethanol Production: Technology and Energy Consumption Evaluation☆. *Bioresour. Techn.* 101 (13), 4992–5002. doi:10.1016/j.biortech.2009.11.007

Conflict of Interest: The authors declare that the research was conducted in the absence of any commercial or financial relationships that could be construed as a potential conflict of interest.

Publisher's Note: All claims expressed in this article are solely those of the authors and do not necessarily represent those of their affiliated organizations, or those of the publisher, the editors and the reviewers. Any product that may be evaluated in this article, or claim that may be made by its manufacturer, is not guaranteed or endorsed by the publisher.

Copyright © 2021 Lv, Yang, Gong, Cheng, Shuai, Huang, Chen, Luo and Liu. This is an open-access article distributed under the terms of the Creative Commons Attribution License (CC BY). The use, distribution or reproduction in other forums is permitted, provided the original author(s) and the copyright owner(s) are credited and that the original publication in this journal is cited, in accordance with accepted academic practice. No use, distribution or reproduction is permitted which does not comply with these terms.



Isolation and Fractionation of the Tobacco Stalk Lignin for Customized Value-Added Utilization

Zhi Chang Liu^{1,2,3}, Zi Wei Wang^{1,2,3}, Song Gao^{1,2,3}, Yu Xing Tong^{1,2,3}, Xi Le^{1,2,3}, Nian Wu Hu^{1,2,3}, Qun Shan Yan^{1,2,3}, Xian Gang Zhou^{1,2,3}, Yan Rong He^{4*} and Lei Wang^{4*}

¹China Tobacco Hubei Industrial Co., Ltd., Wuhan, China, ²Hubei Xinye Reconstituted Tobacco Development Co., Ltd, Wuhan, China, ³Applied Technology Research of Reconstituted Tobacco Hubei Province Key Laboratory, Wuhan, China, ⁴Hubei Provincial Key Laboratory of Green Materials for Light Industry, Hubei University of Technology, Wuhan, China

OPEN ACCESS

Edited by:

Jia-Long Wen,
Beijing Forestry University, China

Reviewed by:

Han-Min Wang,
Tianjin University of Science and
Technology, China
Ran Zhang,
Wuhan Textile University, China

*Correspondence:

Yan Rong He
heyarong1247@163.com
Lei Wang
wanglei820117@163.com

Specialty section:

This article was submitted to
Bioprocess Engineering,
a section of the journal
Frontiers in Bioengineering and
Biotechnology

Received: 08 November 2021

Accepted: 22 November 2021

Published: 06 December 2021

Citation:

Liu ZC, Wang ZW, Gao S, Tong YX,
Le X, Hu NW, Yan QS, Zhou XG, He YR
and Wang L (2021) Isolation and
Fractionation of the Tobacco Stalk
Lignin for Customized Value-
Added Utilization.
Front. Bioeng. Biotechnol. 9:811287.
doi: 10.3389/fbioe.2021.811287

The value-added utilization of tobacco stalk lignin is the key to the development of tobacco stalk resources. However, the serious heterogeneity is the bottleneck for making full use of tobacco stalk lignin. Based on this, lignin was separated from tobacco stalk through hydrothermal assisted dilute alkali pretreatment. Subsequently, the tobacco stalk alkaline lignin was fractionated into five uniform lignin components by sequential solvent fractionation. Advanced spectral technologies (FT-IR, NMR, and GPC) were used to reveal the effects of hydrothermal assisted dilute alkali pretreatment and solvent fractionation on the structural features of tobacco stalk lignin. The lignin fractions extracted with *n*-butanol and ethanol had low molecular weight and high phenolic hydroxyl content, thus exhibiting superior chemical reactivity and antioxidant capacity. By contrast, the lignin fraction extracted with dioxane had high molecular weight and low reactivity, nevertheless, the high residual carbon rate made it suitable as a precursor for preparing carbon materials. In general, hydrothermal assisted dilute alkali pretreatment was proved to be an efficient method to separate lignin from tobacco stalk, and the application of sequential solvent fractionation to prepare lignin fractions with homogeneous structural features has specific application prospect.

Keywords: tobacco stalk, lignin, pretreatment, fractionation, structural interpretation

INTRODUCTION

Lignin is generally considered to be a polymer formed by free radical coupling dehydrogenation of three hydroxycinnamyl alcohols (*p*-coumaryl, coniferyl, and sinapyl alcohols), and it is the second most renewable natural terrestrial polymer (Huang et al., 2008; Mahmood et al., 2016). However, lignin is often defined as a by-product of the pulping and biorefinery industries due to its complex structural (Wen et al., 2013b; Han et al., 2021a). The annual production of industrial lignin is up to 60 million tons, but it is often used for low-value thermal energy conversion, and the high value utilization rate is less than 2% (Aro and Fatehi, 2017). In addition, lignin is gradually being regarded as inferior raw material for obtaining heat energy due to its high carbon dioxide emissions during combustion (Ogunkoya et al., 2015). Therefore, the inefficient use of lignin not only wastes valuable resources, but also brings an inevitable burden to the natural environment.

The development of high-value commercial products with lignin as raw materials is the key to the sustainable development of lignocellulosic resources, which has tremendous economic and environmental benefits (Ma et al., 2021a; Han et al., 2021b). Lignin is the unique non-petroleum

resource that can provide renewable aromatic compounds, and it has various active functional groups such as hydroxyl, methoxy and carboxyl groups (Lee et al., 2019). Therefore, lignin is considered to be an excellent raw material to replace petroleum-based polymers to commercial products. For example, it has been used in dispersants (Xiao et al., 2021), biofuels (Beauchet et al., 2012), adhesives (Ghaffar and Fan, 2014), flocculants (Wang et al., 2020a), phenolic resins (Lupoi et al., 2015), composite film material (Wang et al., 2021b), carbon fibers (Kadla et al., 2002), polyurethane foams (Cinelli et al., 2013), hydrogels and many other fields (Wang et al., 2020b; Ma et al., 2021b). However, most of the research on the preparation of commercial products using lignin is still in the laboratory stage, and a large-scale industrial breakthrough in lignin-based polymer materials has not yet been achieved. The main reason is the structure complexity and heterogeneity of industrial lignin, which is affected by source, processing, extraction and post-treatments (Gioia et al., 2018). The heterogeneity of lignin makes it difficult to prepare the lignin-based product with stable performance. Therefore, refining industrial lignin into components with homogeneous structure and outstanding functional property is essential for the commercial use of lignin.

In order to obtain more uniform industrial lignin, several fractionation methods have been developed in recent years, including membrane separation, pH acid precipitation, gel permeation chromatography, and organic solvent fractionation (Sadeghifar and Ragauskas, 2020). Among them, the fractionation of lignin by membrane separation method requires a large number of filtration membranes, causing high separation cost (Toledano et al., 2010). The efficiency of lignin fractionation by pH acid precipitation method is quite low. Generally, the yield of lignin components is high at a certain pH value, while the yields of lignin components were lower at other pH values (Gigli and Crestini, 2020). The lignin fractionation by gel permeation chromatography requires complicated equipment and operations (Kirk et al., 1969). Fortunately, sequential solvent fractionation of industrial lignin has received more and more attention due to the advantages of simple operation, low cost, solvent recovery, and low energy consumption (Yuan et al., 2009). The procedure of sequential solvent fractionation is based on the order from low to high solubility of lignin, which mainly depends on the cohesive energy and hydrogen-bonding capacity of the solvent (Schuerch, 1952). It can fractionate industrial lignin into more uniform multiple components according to the structural characteristics and physico-chemical properties, which is an attractive method for the refining of lignin. Moreover, the structure of fractionated lignin is fully interpreted through a variety of advanced characterization techniques to establish a reliable relationship between the lignin structure, lignin reactivity, and specific functionalization requirements, which greatly promotes the diversity and customization of industrial lignin utilization.

Tobacco is widely grown throughout the world, and the output of tobacco stalk left after the leafage production is huge, which is often discarded or used for low-value thermal energy conversion (Meng et al., 2015). The recycling of agricultural waste tobacco stalks has important environmental and economic benefits (Wang et al., 2020c;

Jiang et al., 2020). Among them, the high-value utilization of lignin is the top priority. Recently, it was reported that hydrothermal-assisted pretreatment is a good approach to prepare homogeneous hemicelluloses or xylooligosaccharide (XOS) from different lignocellulosic biomass (Ma et al., 2021b). In addition, autohydrolysis can facilitate the subsequent delignification process (Wen et al., 2013d; Chen et al., 2017). Based on these investigations, we firstly separated and obtained lignin from tobacco stem by hydrothermal assisted dilute alkali pretreatment. Subsequently, an economical, easy-to-operate and commercially feasible sequential solvent fractionation process was designed and implemented by using cheap and easy-to-recover organic solvents, such as n-butanol, ethanol, methanol, dioxane. The tobacco stalk lignin was successfully separated into five lignin fractions with lower dispersion and more uniform functional groups. Thereafter, the lignin was comprehensively characterized by a variety of characterization techniques, such as FT-IR, GPC, and 2D-HSQC and ^{31}P NMR. Furthermore, the antioxidant activity and thermostability of lignin samples were also studied to provide a theoretical basis for their customized high-value utilization.

MATERIALS AND METHODS

Materials

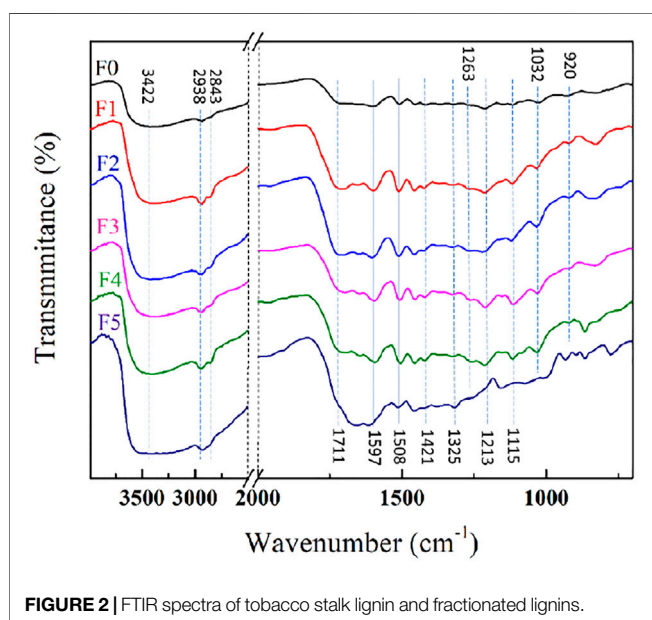
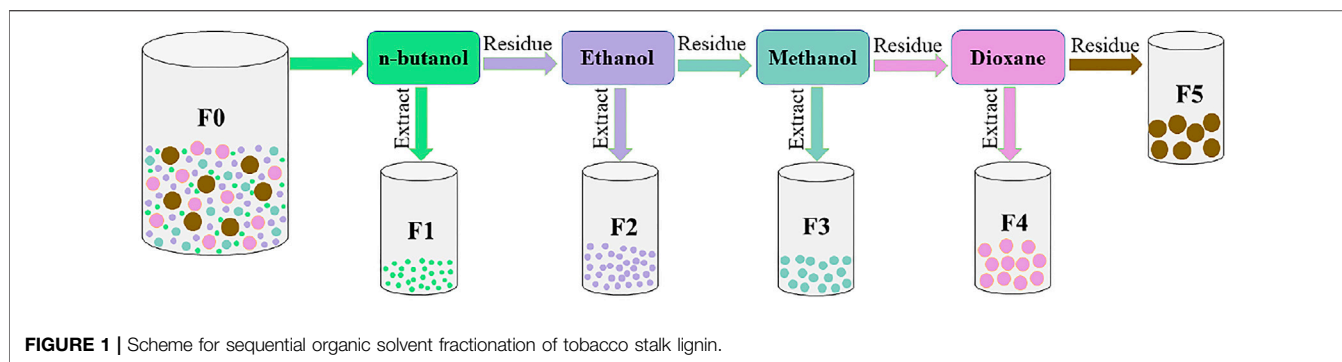
The tobacco stalk was provided by China Tobacco Hubei Industrial Co., Ltd., Wuhan, China. Before use, tobacco stalk was grinded into fine powders (60–80 mesh) and extracted using the mixture of ethanol/toluene for 12 h in order to remove extractives. The other reagents were purchased from Macklin Biochemical Co., Ltd., China.

Isolation of Lignin

The lignin was isolated from tobacco stalk by combining hydrothermal pre-treatment with alkali post-treatment. In simple terms, tobacco stalk lignin and distilled water were mixed at a solid-liquid ratio of 10 to 1, and then poured into an autoclave for hydrothermal pre-treatment at 170°C for 30 min in order to remove a portion of hemicellulose and improve the subsequent delignification efficiency. The residue obtained from the hydrothermal process was added to a 2% NaOH alkaline solution at a solid-to-liquid ratio of 1–20 and reacted at 100°C for 3 h. Subsequently, the supernatant containing lignin was obtained through filtration, and added to 6 times the volume of acid water (pH = 2). The solid matter was recovered by filtration and washed three times with acid water. Finally, tobacco stalk lignin was obtained by freeze-drying the solid matter.

Sequential Solvent Fractionation

The tobacco stalk lignin was fractionated using organic solvents with lignin dissolution capacity from low to high, which were n-butanol, ethanol, methanol, and dioxane in turn, as shown in **Figure 1**. First, 50 g tobacco stalk lignin and 500 ml n-butanol were added to a 1,000 ml volumetric flask, and the mixture was stirred at a uniform speed (100 rpm) for 3 h. Subsequently, the solution obtained by filtration was evaporated under reduced pressure and dried to obtain a lignin component soluble in



n-butanol, which was noted as F1. The obtained residue was fractionated using ethanol, methanol and dioxane in sequence according to the above steps, and the obtained lignin fractions were F2, F3, and F4, respectively. The resulting insoluble residue was named F5.

Structural Characterization

The FT-IR spectra, NMR spectra (^2D -HSQC, and ^{31}P NMR spectra), thermogravimetric analysis (TGA) of lignin samples were recorded by Bruker Tensor II spectrometer, Bruker AVIII (400 M), and NETZSCH TG 209 F1 Libra, respectively. The detailed running program and analysis methods of NMR spectra were adopted the procedures and description in the previous literatures (Wang et al., 2017; Ma et al., 2021a). The Mw, Mn, and PDI were measured using the Agilent 1200 GPC system (Ma et al., 2020).

Thermogravimetric Analysis

The thermal decomposition behavior of lignin was recorded using a thermal analyzer (NETZSCH TG 209 F1 Libra). The

TABLE 1 | Yields and molecular weight distributions of lignin samples.

Lignin sample	Yield (%)	Mn (g/mol)	Mw (g/mol)	PDI
F0	—	1,066	3,155	2.96
F1	14.59	1,005	1,256	1.25
F2	15.40	2,511	2,988	1.19
F3	35.49	3,085	4,196	1.36
F4	23.18	5,611	6,845	1.22
F5	11.35	5,095	9,783	1.92

tobacco stalk lignin was heated under N_2 atmosphere with a heating rate of $10^\circ\text{C}/\text{min}$ from room temperature to 800°C .

Antioxidant Activity Analysis

The detailed operation steps refer to previous research (Pan et al., 2006). The radical scavenging activity of 1,1-Diphenyl-2-picrylhydrazyl (DPPH) was recorded using UV-2450 spectrophotometer. Briefly, 0.18 ml of lignin solution (0.01–3 g/L) in 90% aqueous dioxane was added into 0.72 ml of a 25 mg/L DPPH methanol solution at room temperature for 16 min. The concentrations of DPPH radicals at 0 and 16 min were monitored at 515 nm (λ_{max}) using UV-2450 spectrophotometer.

RESULTS AND DISCUSSION

Yields and Molecular Weight Distributions of Lignin Fractions

Regarding the sequential solvent fractionation, the ability of solvent to dissolve lignin is the first consideration when selecting solvents and arranging the extraction order, which is affected by the hydrogen-bonding capacity and the cohesive energy of the solvent. The solubility parameter of solvent can be calculated from the square root of the cohesive energy density, and the shift in wave length can be obtained according to the hydrogen bonding ability (Li et al., 2012). Under the synergistic assistance of solubility parameters with the shift in wave length, coupled with preliminary experimental verification, four organic solvents with increasing ability to dissolve lignin, namely n-butanol, ethanol, methanol, and dioxane, were applied to the sequential solvent fractionation of tobacco stalk lignin.

The yield of the five lignin fractions is shown in **Table 1**. The yield of lignin fraction dissolved in n-butanol and ethanol (F1 and F2) was 14.59 and 15.4%, respectively. The yield of the lignin fraction dissolved in methanol (F3) was the highest 35.49%, while the yield of the lignin fraction dissolved in dioxane (F4) was 23.18%. The yield of final insoluble residue (F5) was 11.35%. The effect of sequential solvent fractionation on the molecular weight of lignin was explored by GPC technology. The weight-average molecular weight (M_w), number-average molecular weight (M_n) and polydispersity (PDI) of all lignin samples can be seen in **Table 1**. The weight-average molecular weight of unfractionated tobacco stalk lignin (F0) was 3,155 g/mol, which was much lower than that of natural tobacco stalk lignin. This was because the lignin was degraded and some of the chemical bonds were broken during the hydrothermal-assisted alkaline pretreatment process (Wang et al., 2017a). In addition, the PDI of F0 was as high as 2.96, showing serious heterogeneity, which severely hindered its subsequent high-value applications. After fractionation, the weight-average molecular weights of F1, F2, F3, F4, and F5 were 1,256, 2,988, 4,196, 6,845, and 9,783 g/mol, respectively. It could be found that the molecular weight gradually increased from F1 to F5, which proved that the lignin with small molecular weight had better solubility and was extracted first during the sequential solvent fractionation. The small molecular weight of F1 indicated that it was seriously degraded and the chemical bonds between structural units were destroyed. The excessively high molecular weight of F5 might be due to the severe condensation and the presence of carbohydrates, which would be proved in subsequent analyses (Zhao et al., 2018). In addition, it could be observed that the dispersibility of the fractionated lignin fraction had been greatly improved as compared with F0, which had a positive effect on the high-value utilization (Wang et al., 2021a). In general, the solvent selected and the specified extraction sequence could selectively fractionate tobacco stalk lignin and improve the dispersibility.

Spectral Analysis

The alkaline extraction is an efficient method for removing lignin from gramineous plant (Al Arni, 2018). Moreover, the hydronium ion (H_3O^+) can be released through the autohydrolysis of water in the hydrothermal pre-treatment process, which could dissolve hemicellulose by breaking the lignin-carbohydrate complexes network and promote follow-up delignification (Garrote et al., 2001; Wen et al., 2013d; Chen et al., 2017). In order to understand the structural evolution of tobacco stalk lignin during the pretreatment process and the effect of the fractionation process on its structure, the FT-IR spectra of the tobacco stalk lignin before and after fractionation were recorded in **Figure 2**. Previous studies reported that the residue insoluble in dioxane was mainly composed of severely condensed lignin, carbohydrates and ash, and it did not have the potential to produce commercial products (Guo et al., 2013). Except for the final residue insoluble in dioxane (F5), the structure of fractionated lignin was similar to that of unfractionated lignin, but some corresponding signal strengths were slightly different.

The signals at 1,597, 1,508, and $1,421\text{ cm}^{-1}$ are attributable to the aromatic skeleton vibrations, which are signal peaks unique to lignin (Ma et al., 2021c; Xu et al., 2021). This result proved that although the bonds between the structural units would be broken during the hydrothermal assisted dilute alkali pretreatment, the basic skeleton of lignin was not destroyed. The corresponding signals for the vibration of OH groups, the C-H stretch in CH_2 and CH_3 groups appeared at 3,422, 2,938 and $2,843\text{ cm}^{-1}$, which were similar in all lignin samples. However, there was a difference in the relative intensities of non-conjugated carbonyl stretching assigned at 1711 cm^{-1} . It could be clearly observed that the lignin components with lower molecular weight had a stronger absorption peak at 1711 cm^{-1} as compared to the lignin components with higher molecular weight. This preliminarily proved that lignin components with lower molecular weight had more carboxyl groups, which would be proved in the subsequent characterization. Moreover, the signals at 1,325, 1,213, and $1,115\text{ cm}^{-1}$ belong to S unit, which could be seen in all lignin samples. However, the G unit signals for aromatic ring distributed in at 1,267, 1,029, and 917 cm^{-1} could only be observed in F1-F4, but not in F5. This proved that the lignin component containing more G-type units had better solubility and was fractionated earlier.

The comprehensive structural information of lignin can be understood *via* NMR techniques (^{31}P and 2D-HSQC), which facilitate the understanding of the structural evolution of lignin in the pretreatment process and the effects of the fractionation process on the structural changes of lignin. The side-chain HSQC spectra (δ_C/δ_H 50–90/2.1–5.7 ppm) of lignin sample was shown in **Figure 3**. The main cross-signal assignments referred to previous studies regarding to structural characterization of lignin (Wen et al., 2013a; Wang et al., 2017b). In addition to the main C-H correlations of inter-coupling bonds of lignin, such as the methoxyl groups (OCH_3), β -O-4 aryl ethers (A), resinols (β - β , B), and phenylcoumarans (β -5, C), and *p*-hydroxycinnamyl alcohol end-groups (I), there were β -D-xylopyranosyl signals (X2, X3, and X4) in F0 (Sun et al., 2019). The lignin-carbohydrate complex was formed by combining the lignin at the α - α - γ position and the polysaccharide in substructures *p*-hydroxycinnamyl alcohol end-groups through ether bond. By comparing the spectra of the side chain region of different lignin fractions, it could be found that the carbohydrate signal did not appear in the earlier extracted lignin fractions (F1, F2, and F3), which proved that the purity of these fractions was quite high (Wang et al., 2019). The corresponding signal of carbohydrates could be significantly observed on F5. This proved that F5 contained a lot of carbohydrates, which was one of the reasons for the higher molecular weight.

According to the aromatic region (δ_C/δ_H 100–140/5.5–8.5 ppm) in **Figure 4**, cross-signals from guaiacyl (G), syringyl (S), *p*-hydroxyphenyl (H) units were clearly observed (Wen et al., 2013a; Sun et al., 2019), but their signal intensities in each lignin sample were quite different. The normal and α -oxidized S units showed obvious signals for the $C_{2,6}$ - $H_{2,6}$ correlations at δ_C/δ_H 103.8/6.68 and 86.8/3.96 ppm, respectively. It was worth noting that the trailing of $S_{2,6}$ signal

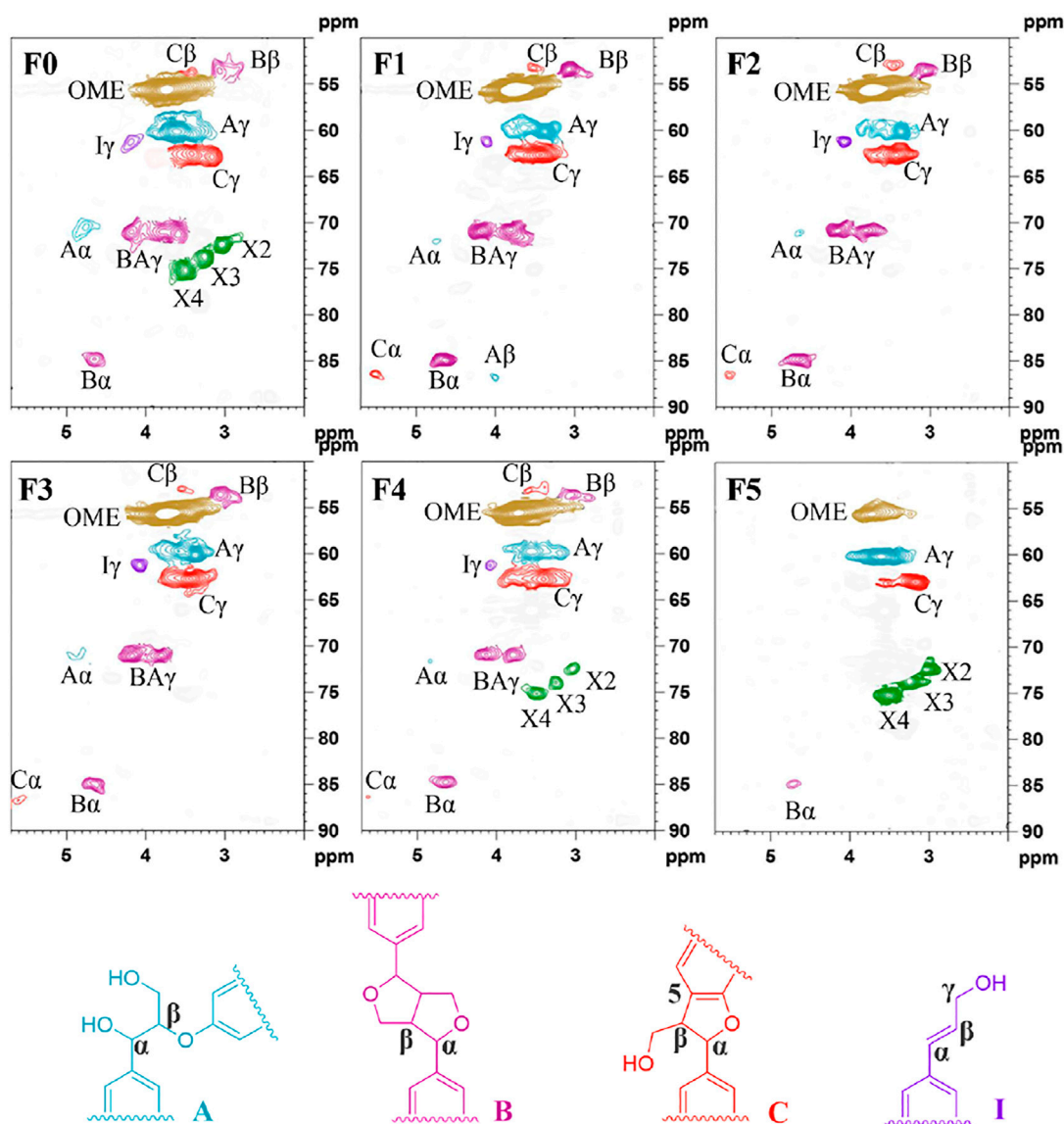


FIGURE 3 | The side-chain of lignin samples in the 2D HSQC NMR spectra.

in F0 reflected the condensation of lignin, which was caused by the high temperature during the hydrothermal process. The G units showed three correlations for G6, G5, and G2. Among them, the reason for the double signals on G2 was the serious heterogeneity, which was affected by the substituent group at C4 position of G unit (Shen et al., 2016). Moreover, the structural units of different lignin fractions were different. The lignin fractions (F1, F2, and F3) with more H and G type units had better solubility and could be extracted earlier. Only the weak signal attributed to the S unit could be observed in the F5 spectrum. These results were consistent with the above FT-IR analysis results. In terms of structure, lignin components with more H and G units had better reactivity due to more active sites and smaller steric hindrance (Yang et al., 2015), which was more

conductive to the preparation of high value-added products through chemistry reaction.

The quantitative ^{31}P NMR spectra of lignin samples were recorded to determine the hydroxyl content of lignin. The corresponding quantitative results were listed in **Table 2**. Phenolic hydroxyl group is decisive factors for the reactivity and the prospects for commercial application of lignin. Because of the cleavage of β -O-4 linkages and release of more phenolic OH groups, the tobacco stalk lignin F0 obtained by hydrothermal assisted dilute alkali pretreatment has a high phenolic hydroxyl content (2.41 mmol/g). In addition, it could be found that the phenolic hydroxyl content of lignin was negatively correlated with its molecular weight. The lignin component

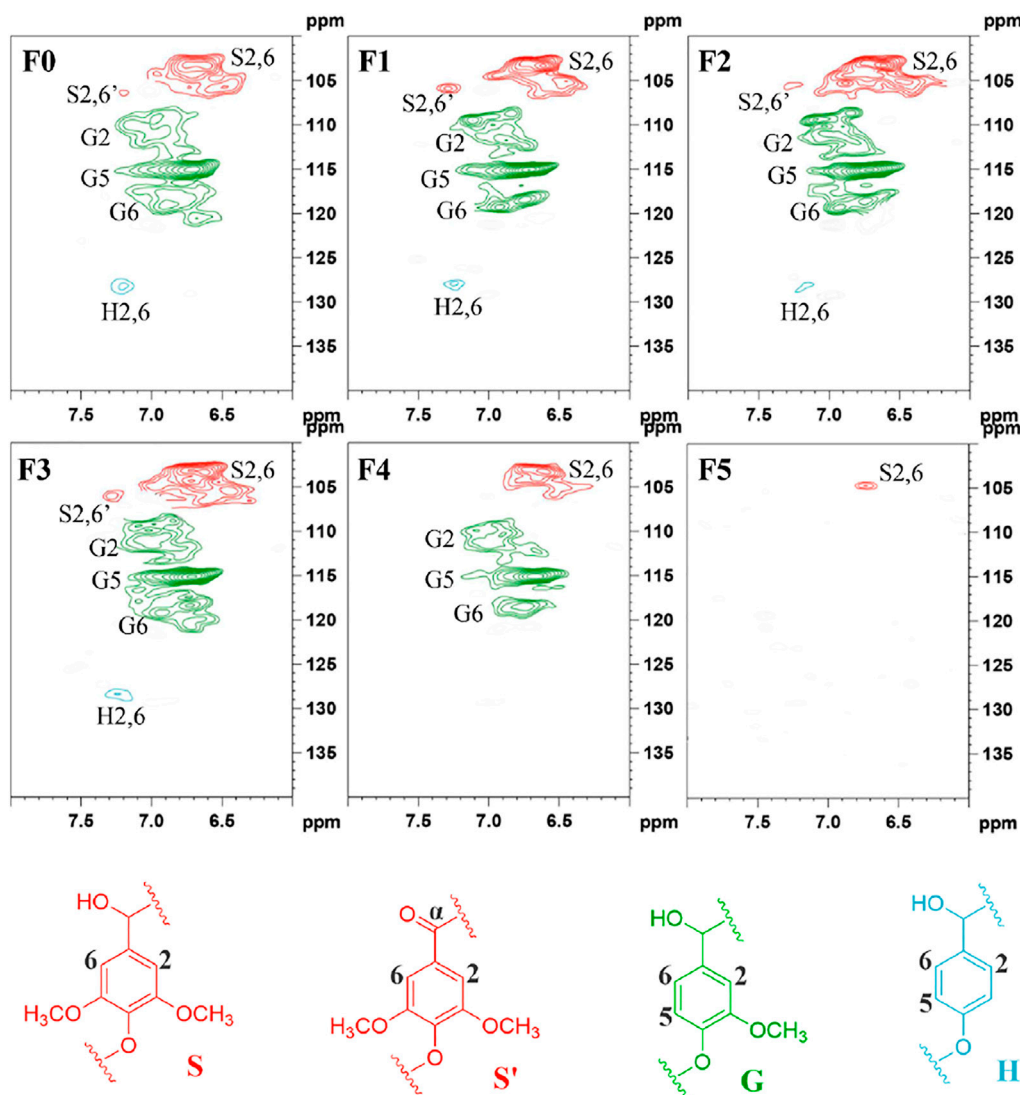


FIGURE 4 | The aromatic ring of lignin samples in the 2D HSQC NMR spectra.

TABLE 2 | Quantification of the lignin samples by quantitative ³¹P-NMR Method (mmol/g).

Lignin sample	AL-OH	S-OH	CG-OH	G-OH	H-OH	Total phenolic-OH	COOH
F0	2.52	0.85	0.19	0.81	0.56	2.41	0.75
F1	1.94	0.92	0.20	1.29	0.68	3.09	1.23
F2	2.59	0.88	0.21	0.98	0.43	2.50	0.85
F3	2.26	0.80	0.15	0.76	0.23	1.94	0.56
F4	2.04	0.69	0.13	0.56	0.24	1.62	0.43
F5	2.68	0.61	0.08	0.38	0.15	1.22	0.15

with a lower molecular weight had more phenolic hydroxyl groups and better reactivity. Among them, the phenolic hydroxyl content of F1 obtained by *n*-butanol fractionation was as high as 3.09 mmol/g. Coupled with the above analysis that F1 has more H and G units, F1 had obvious advantages as a raw material for preparing high value-added products.

Antioxidant Capacity

Lignin is rich in phenolic structure and has antioxidant effect (Dong et al., 2011). To explore the antioxidant capacity, the antioxidant test of lignin samples was performed using DPPH as the radical generator. EC₅₀ is the concentration of lignin when the free radical inhibition rate is 50%. The reciprocal of EC₅₀ can be

TABLE 3 | The free radical scavenging index (RSI) of the lignin samples.

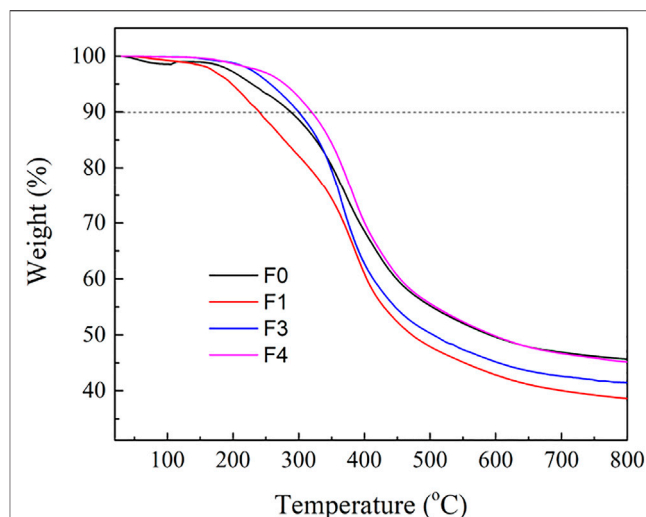
Lignin sample	EC50 ($\mu\text{g/ml}$)	RSI
F0	35.06	28.52
F1	28.07	35.63
F2	32.72	30.56
F3	46.69	21.42
F4	54.44	18.37
F5	65.70	15.22

used to calculate the free radical scavenging index (RSI), indicating that the EC50 and RSI values have a negative correlation. In general, the inhibitory effect of lignin increased with the increase of concentration. The RSI values of F0-F5 were 28.52, 35.63, 30.56, 21.42, 18.37, and 15.22, respectively (Table 3). It was obvious that the antioxidant capacity of lignin was negatively correlated with its molecular weight. Previous studies have demonstrated that the antioxidant capacity of lignin depends mainly on the content of free phenolic hydroxyl groups, followed by other groups such as aliphatic hydroxyl groups and methoxyl groups (Pan et al., 2006; Ma et al., 2021d). Therefore, F1 with the highest phenolic hydroxyl content had the strongest antioxidant capacity, and F1 was an excellent raw material for preparing green antioxidants.

Thermal Stability

The thermal behavior of lignin plays a crucial role in the preparation of carbon materials, thermoplastic materials and phenol-rich bio-oils (Sen et al., 2015). In this study, the thermogravimetric analysis (TG) of lignin was used to explore the relationship between thermal stability and structure. The thermal degradation process of lignin is very complex, which is affected by various factors, such as the breakage of internal chemical bonds, the types of functional groups, and the degree of condensation (Xu et al., 2021). Lignin has outstanding thermostability, and its thermal decomposition process can be roughly divided into four stages. In addition, the different thermal stabilities are not only influenced by inherent structure and various functional groups of lignin polymers, degree of branching, and condensation of the lignin macromolecule but also related to specific chemical structures (Wen et al., 2013c). For example, it was reported that the maximum decomposition temperature (TM) was related to the corresponding β -O-4 ether linkage content and molecular weight (Mw) (Wen et al., 2013c). As shown in Figure 5, the first stage was below 200°C. Dehydration and deformation of weak chemical linkages in the β -O-4 structure were responsible for the weight loss in this stage (Faravelli et al., 2010). The second stage at 200–350°C was due to the decomposition of ether bonds (mainly β -O-4 linkages). The subsequent third stage (350–400°C) mainly involved side chain oxidation, such as side chain dehydrogenation, carboxylation of aliphatic hydroxyl group (Ke et al., 2011). The cleavage C-C bond (5-5) and aromatic ring of the lignin caused the fourth stage weight loss at temperatures above 400°C (Yang et al., 2007). Finally, the residue obtained after pyrolysis was mainly composed of inorganic salts and ash.

By comparing the thermal decomposition behavior of each lignin fraction, it could be found that the thermal decomposition behavior of lignin had an excellent correlation with its molecular weight. The

**FIGURE 5** | TG curves of tobacco stalk lignin and fractionated lignins.

decomposition temperatures (10% weight loss) of F1, F3, and F4 were 240, 300, and 320°C respectively, indicating that lignin fraction with low molecular weight was easier to be pyrolyzed. However, the unfractionated F0 (288°C) did not meet this result, which indicated that the thermal decomposition behavior of lignin was not only related to molecular weight, but also affected by many factors, such as heterogeneity, functional groups, and degree of condensation (Gioia et al., 2018). Similarly, the residue weights at 800°C of F1, F3, and F4 were 38.4, 41.4, and 45.9% respectively, which had an excellent positive correlation with molecular weight. However, F0 with lower molecular weight had the highest residual carbon rate of 45.5%. The main reason was the serious heterogeneity of F0 and the existence of ash, making it difficult to use F0 as a promising carbon material precursor. In general, although F4 had inferior reactivity and was difficult to prepare high value-added products through chemical modification, its high carbon residue rate contributed to its application in preparing carbon materials.

CONCLUSION

The tobacco stalk lignin was obtained by hydrothermal assisted dilute alkali pretreatment, and the structural features of the lignin were characterized by modern characterization techniques. Subsequently, the tobacco stalk lignin (F0) was divided into five lignin components by sequential solvent fractionation with *n*-butanol (F1), ethanol (F2), methanol (F3), and dioxane (F4). The molecular weight of the lignin elevated with the increase in the solubility of the solvent, and the polydispersity was greatly improved after fractionation process. In addition, the phenolic hydroxyl content in lignin was negatively related to its molecular weight, and the high phenolic hydroxyl content could improve the reactivity and antioxidant capacity. Therefore, lignin components with lower molecular weight (F1 and F2) showed great potentials in the preparation of green antioxidants and high value-added chemical products. By contrast, lignin fraction with high molecular weight was

more suitable for preparing carbon materials due to its high residual carbon rate. In short, the full utilization of lignin is the key to tobacco stalk resource recovery. The sequential solvent fractionation can promote the customized utilization of tobacco stalk lignin according to the structural advantage of different lignin fractions.

DATA AVAILABILITY STATEMENT

The original contributions presented in the study are included in the article/Supplementary Material, further inquiries can be directed to the corresponding authors.

REFERENCES

- Al Arni, S. (2018). Extraction and Isolation Methods for Lignin Separation from Sugarcane Bagasse: A Review. *Ind. Crops Prod.* 115, 330–339. doi:10.1016/j.indcrop.2018.02.012
- Aro, T., and Fatehi, P. (2017). Production and Application of Lignosulfonates and Sulfonated Lignin. *ChemSusChem* 10, 1861–1877. doi:10.1002/cssc.201700082
- Beauchet, R., Monteil-Rivera, F., and Lavoie, J. M. (2012). Conversion of Lignin to Aromatic-Based Chemicals (L-Chems) and Biofuels (L-Fuels). *Bioresour. Technol.* 121, 328–334. doi:10.1016/j.biortech.2012.06.061
- Chen, T.-Y., Wen, J.-L., Wang, B., Wang, H.-M., Liu, C.-F., and Sun, R.-C. (2017). Assessment of Integrated Process Based on Autohydrolysis and Robust Delignification Process for Enzymatic Saccharification of Bamboo. *Bioresour. Technol.* 244, 717–725. doi:10.1016/j.biortech.2017.08.032
- Cinelli, P., Anguillesi, I., and Lazzeri, A. (2013). Green Synthesis of Flexible Polyurethane Foams from Liquefied Lignin. *Eur. Polym. J.* 49, 1174–1184. doi:10.1016/j.eurpolymj.2013.04.005
- Dong, X., Dong, M., Lu, Y., Turley, A., Jin, T., and Wu, C. (2011). Antimicrobial and Antioxidant Activities of Lignin from Residue of Corn stover to Ethanol Production. *Ind. Crops Prod.* 34, 1629–1634. doi:10.1016/j.indcrop.2011.06.002
- Faravelli, T., Frassoldati, A., Migliavacca, G., and Ranzi, E. (2010). Detailed Kinetic Modeling of the thermal Degradation of Lignins. *Biomass and Bioenergy* 34, 290–301. doi:10.1016/j.biombioe.2009.10.018
- Garrote, G., Domínguez, H., and Parajó, J. C. (2001). Study on the Deacetylation of Hemicelluloses during the Hydrothermal Processing of Eucalyptus wood. *Holz als Roh- und Werkstoff* 59, 53–59. doi:10.1007/s001070050473
- Ghaffar, S. H., and Fan, M. (2014). Lignin in Straw and its Applications as an Adhesive. *Int. J. Adhes. Adhesives* 48, 92–101. doi:10.1016/j.jadhadh.2013.09.001
- Gigli, M., and Crestini, C. (2020). Fractionation of Industrial Lignins: Opportunities and Challenges. *Green. Chem.* 22, 4722–4746. doi:10.1039/d0gc01606c
- Gioia, C., Lo Re, G., Lawoko, M., and Berglund, L. (2018). Tunable Thermosetting Epoxies Based on Fractionated and Well-Characterized Lignins. *J. Am. Chem. Soc.* 140, 4054–4061. doi:10.1021/jacs.7b13620
- Guo, G., Li, S., Wang, L., Ren, S., and Fang, G. (2013). Separation and Characterization of Lignin from Bio-Ethanol Production Residue. *Bioresour. Technol.* 135, 738–741. doi:10.1016/j.biortech.2012.10.041
- Han, X., Ding, L., Tian, Z., Wu, W., and Jiang, S. (2021a). Extraction and Characterization of Novel Ultrastrong and Tough Natural Cellulosic Fiber Bundles from Manau rattan (Calamus Manan). *Ind. Crops Prod.* 173, 114103. doi:10.1016/j.indcrop.2021.114103
- Han, X., Wu, W., Wang, J., Tian, Z., and Jiang, S. (2021b). Hydrogen-Bonding-Aided Fabrication of wood Derived Cellulose Scaffold/Aramid Nanofiber into High-Performance Bulk Material. *Materials* 14, 5444. doi:10.3390/ma14185444
- Huang, H.-J., Ramaswamy, S., Tschirner, U. W., and Ramarao, B. V. (2008). A Review of Separation Technologies in Current and Future Biorefineries. *Separat. Purif. Technol.* 62, 1–21. doi:10.1016/j.seppur.2007.12.011
- Jiang, J., Carrillo-Enriquez, N. C., Ogunzulu, H., Han, X., Bi, R., Song, M., et al. (2020). High Production Yield and More Thermally Stable Lignin-Containing Cellulose Nanocrystals Isolated Using a Ternary Acidic Deep Eutectic Solvent. *ACS Sustain. Chem. Eng.* 8, 7182–7191. doi:10.1021/acssuschemeng.0c01724
- Kadla, J. F., Kubo, S., Venditti, R. A., Gilbert, R. D., Compere, A. L., and Griffith, W. (2002). Lignin-based Carbon Fibers for Composite Fiber Applications. *Carbon* 40, 2913–2920. doi:10.1016/s0008-6223(02)00248-8
- Ke, J., Singh, D., Yang, X., and Chen, S. (2011). Thermal Characterization of Softwood Lignin Modification by Termite *Coptotermes Formosanus* (Shiraki). *Biomass and Bioenergy* 35, 3617–3626. doi:10.1016/j.biombioe.2011.05.010
- Kirk, T. K., Brown, W., and Cowling, E. B. (1969). Preparative Fractionation of Lignin by Gel-Permeation Chromatography. *Biopolymers* 7, 135–153. doi:10.1002/bip.1969.360070202
- Lee, S., Kang, M., Bae, J.-H., Sohn, J.-H., and Sung, B. H. (2019). Bacterial Valorization of Lignin: Strains, Enzymes, Conversion Pathways, Biosensors, and Perspectives. *Front. Bioeng. Biotechnol.* 7, 209. doi:10.3389/fbioe.2019.00209
- Li, M.-F., Sun, S.-N., Xu, F., and Sun, R.-C. (2012). Sequential Solvent Fractionation of Heterogeneous Bamboo Organosolv Lignin for Value-Added Application. *Separat. Purif. Technol.* 101, 18–25. doi:10.1016/j.seppur.2012.09.013
- Lupoi, J. S., Gjersing, E., and Davis, M. F. (2015). Evaluating Lignocellulosic Biomass, its Derivatives, and Downstream Products with Raman Spectroscopy. *Front. Bioeng. Biotechnol.* 3, 50. doi:10.3389/fbioe.2015.00050
- Ma, C.-Y., Wang, H.-M., Wen, J.-L., Shi, Q., Wang, S.-F., Yuan, T.-Q., et al. (2020). Structural Elucidation of Lignin Macromolecule from Abaca during Alkaline Hydrogen Peroxide Delignification. *Int. J. Biol. Macromolecules* 144, 596–602. doi:10.1016/j.ijbiomac.2019.12.080
- Ma, C.-Y., Gao, X., Peng, X.-P., Gao, Y.-F., Liu, J., Wen, J.-L., et al. (2021a). Microwave-Assisted Deep Eutectic Solvents (DES) Pretreatment of Control and Transgenic Poplars for Boosting the Lignin Valorization and Cellulose Bioconversion. *Ind. Crops Prod.* 164, 113415. doi:10.1016/j.indcrop.2021.113415
- Ma, C., Kim, T., Liu, K., Ma, M., Choi, S., and Si, C. (2021b). Multifunctional Lignin-Based Composite Materials for Emerging Applications. *Front. Bioeng. Biotechnol.* 9, 511. doi:10.3389/fbioe.2021.708976
- Ma, C.-Y., Peng, X.-P., Sun, S., Wen, J.-L., and Yuan, T.-Q. (2021c). Short-Time Deep Eutectic Solvents Pretreatment Enhanced Production of Fermentable Sugars and Tailored Lignin Nanoparticles from Abaca. *Int. J. Biol. Macromolecules* 192, 417–425. doi:10.1016/j.ijbiomac.2021.09.140
- Ma, C.-Y., Xu, L.-H., Zhang, C., Guo, K.-N., Yuan, T.-Q., and Wen, J.-L. (2021d). A Synergistic Hydrothermal-Deep Eutectic Solvent (DES) Pretreatment for Rapid Fractionation and Targeted Valorization of Hemicelluloses and Cellulose from poplar wood. *Bioresour. Technol.* 341, 125828. doi:10.1016/j.biortech.2021.125828
- Mahmood, N., Yuan, Z., Schmidt, J., and Xu, C. (2016). Depolymerization of Lignins and Their Applications for the Preparation of Polyols and Rigid Polyurethane Foams: A Review. *Renew. Sustain. Energy Rev.* 60, 317–329. doi:10.1016/j.rser.2016.01.037
- Meng, A., Zhang, Y., Zhuo, J., Li, Q., and Qin, L. (2015). Investigation on Pyrolysis and Carbonization of Eupatorium Adenophorum Spreng and Tobacco Stem. *J. Energy Inst.* 88, 480–489. doi:10.1016/j.joei.2014.10.003
- Ogunkoya, D., Li, S., Rojas, O. J., and Fang, T. (2015). Performance, Combustion, and Emissions in a Diesel Engine Operated with Fuel-In-Water Emulsions Based on Lignin. *Appl. Energy* 154, 851–861. doi:10.1016/j.apenergy.2015.05.036

AUTHOR CONTRIBUTIONS

ZL: Conceptualization, Methodology, Investigation, Validation, Writing—original draft. ZW: Software, Visualization, Validation. SG: Software, Visualization. YT: Formal analysis, Data curation, Project administration. XL: Formal analysis, Data curation, Project administration. NH: Resources, Project administration. QY: Resources, Project administration. XZ: Resources, Project administration. YH: Conceptualization, Methodology, Writing—original draft, Writing—review and editing, Supervision. LW: Conceptualization, Methodology, Writing—review and editing, Supervision, Funding acquisition.

- Pan, X., Kadla, J. F., Ehara, K., Gilkes, N., and Saddler, J. N. (2006). Organosolv Ethanol Lignin from Hybrid poplar as a Radical Scavenger: Relationship between Lignin Structure, Extraction Conditions, and Antioxidant Activity. *J. Agric. Food Chem.* 54, 5806–5813. doi:10.1021/jf0605392
- Sadeghifar, H., and Ragauskas, A. (2020). Perspective on Technical Lignin Fractionation. *ACS Sustain. Chem. Eng.* 8, 8086–8101. doi:10.1021/acssuschemeng.0c01348
- Schuerch, C. (1952). The Solvent Properties of Liquids and Their Relation to the Solubility, Swelling, Isolation and Fractionation of Lignin. *J. Am. Chem. Soc.* 74, 5061–5067. doi:10.1021/ja01140a020
- Sen, S., Patil, S., and Argyropoulos, D. S. (2015). Thermal Properties of Lignin in Copolymers, Blends, and Composites: A Review. *Green. Chem.* 17, 4862–4887. doi:10.1039/c5gc01066g
- Shen, X.-J., Wang, B., Pan-Li, H., Wen, J.-L., and Sun, R.-C. (2016). Understanding the Structural Changes and Depolymerization of Eucalyptus Lignin under Mild Conditions in Aqueous AlCl₃. *RSC Adv.* 6, 45315–45325. doi:10.1039/c6ra08945c
- Sun, D., Wang, B., Wang, H.-M., Li, M.-F., Shi, Q., Zheng, L., et al. (2019). Structural Elucidation of Tobacco Stalk Lignin Isolated by Different Integrated Processes. *Ind. Crops Prod.* 140, 111631. doi:10.1016/j.indcrop.2019.111631
- Toledano, A., García, A., Mondragon, I., and Labidi, J. (2010). Lignin Separation and Fractionation by Ultrafiltration. *Separat. Purif. Technol.* 71, 38–43. doi:10.1016/j.seppur.2009.10.024
- Wang, C., Li, H., Li, M., Bian, J., and Sun, R. (2017a). Revealing the Structure and Distribution Changes of Eucalyptus Lignin during the Hydrothermal and Alkaline Pretreatments. *Sci. Rep.* 7, 1–10. doi:10.1038/s41598-017-00711-w
- Wang, H.-M., Wang, B., Wen, J.-L., Yuan, T.-Q., and Sun, R.-C. (2017b). Structural Characteristics of Lignin Macromolecules from Different Eucalyptus Species. *ACS Sustain. Chem. Eng.* 5, 11618–11627. doi:10.1021/acssuschemeng.7b02970
- Wang, H.-M., Sun, Y.-C., Wang, B., Sun, D., Shi, Q., Zheng, L., et al. (2019). Insights into the Structural Changes and Potentials of Lignin from Bagasse during the Integrated Delignification Process. *ACS Sustain. Chem. Eng.* 7, 13886–13897. doi:10.1021/acssuschemeng.9b02071
- Wang, B., Wang, H.-M., Sun, D., Yuan, T.-Q., Song, G.-Y., Shi, Q., et al. (2020a). Chemosynthesis, Characterization and Application of Lignin-Based Flocculants with Tunable Performance Prepared by Short-Wavelength Ultraviolet Initiation. *Ind. Crops Prod.* 157, 112897. doi:10.1016/j.indcrop.2020.112897
- Wang, B., Wang, S.-F., Lam, S. S., Sonne, C., Yuan, T.-Q., Song, G.-Y., et al. (2020b). A Review on Production of Lignin-Based Flocculants: Sustainable Feedstock and Low Carbon Footprint Applications. *Renew. Sustain. Energ. Rev.* 134, 110384. doi:10.1016/j.rser.2020.110384
- Wang, H.-M., Wang, B., Yuan, T.-Q., Zheng, L., Shi, Q., Wang, S.-F., et al. (2020c). Tunable, UV-Shielding and Biodegradable Composites Based on Well-Characterized Lignins and Poly(butylene Adipate-Co-Terephthalate). *Green. Chem.* 22, 8623–8632. doi:10.1039/d0gc03284k
- Wang, B., Sun, D., Yuan, T.-Q., Song, G., and Sun, R.-C. (2021a). “Recent Advances in Lignin Modification and its Application in Wastewater Treatment,” in *Lignin Utilization Strategies: From Processing to Applications*. New York: American Chemical Society, 143–173. doi:10.1021/bk-2021-1377.ch007
- Wang, H.-M., Yuan, T.-Q., Song, G.-Y., and Sun, R.-C. (2021b). Advanced and Versatile Lignin-Derived Biodegradable Composite Film Materials toward a Sustainable World. *Green. Chem.* 23, 3790–3817. doi:10.1039/d1gc00790d
- Wen, J.-L., Sun, S.-L., Xue, B.-L., and Sun, R.-C. (2013a). Recent Advances in Characterization of Lignin Polymer by Solution-State Nuclear Magnetic Resonance (NMR) Methodology. *Materials* 6, 359–391. doi:10.3390/ma6010359
- Wen, J.-L., Xue, B.-L., Xu, F., Sun, R.-C., and Pinkert, A. (2013b). Unmasking the Structural Features and Property of Lignin from Bamboo. *Ind. Crops Prod.* 42, 332–343. doi:10.1016/j.indcrop.2012.05.041
- Wen, J.-L., Sun, S.-L., Xue, B.-L., and Sun, R.-C. (2013c). Quantitative Structures and thermal Properties of Birch Lignins after Ionic Liquid Pretreatment. *J. Agric. Food Chem.* 61, 635–645. doi:10.1021/jf3051939
- Wen, J.-L., Sun, S.-N., Yuan, T.-Q., Xu, F., and Sun, R.-C. (2013d). Fractionation of Bamboo Culms by Autohydrolysis, Organosolv Delignification and Extended Delignification: Understanding the Fundamental Chemistry of the Lignin during the Integrated Process. *Bioresour. Technol.* 150, 278–286. doi:10.1016/j.biortech.2013.10.015
- Xiao, X., Jiang, J., Wang, Y., Wang, B., Yuan, T.-Q., Shi, Q., et al. (2021). Microwave-Assisted Sulfonation of Lignin for the Fabrication of a High-Performance Dye Dispersant. *ACS Sustain. Chem. Eng.* 9, 9053–9061. doi:10.1021/acssuschemeng.1c02148
- Xu, R., Du, H., Wang, H., Zhang, M., Wu, M., Liu, C., et al. (2021). Valorization of Enzymatic Hydrolysis Residues from Corn cob into Lignin-Containing Cellulose Nanofibrils and Lignin Nanoparticles. *Front. Bioeng. Biotechnol.* 9, 252. doi:10.3389/fbioe.2021.677963
- Yang, H., Yan, R., Chen, H., Lee, D. H., and Zheng, C. (2007). Characteristics of Hemicellulose, Cellulose and Lignin Pyrolysis. *Fuel* 86, 1781–1788. doi:10.1016/j.fuel.2006.12.013
- Yang, S., Wu, J.-Q., Zhang, Y., Yuan, T.-Q., and Sun, R.-C. (2015). Preparation of Lignin-Phenol-Formaldehyde Resin Adhesive Based on Active Sites of Technical Lignin. *J. Biobased Mat Bioenergy* 9, 266–272. doi:10.1166/jbmb.2015.1514
- Yuan, T.-Q., He, J., Xu, F., and Sun, R.-C. (2009). Fractionation and Physico-Chemical Analysis of Degraded Lignins from the Black Liquor of Eucalyptus Pellita KP-AQ Pulping. *Polym. Degrad. Stab.* 94, 1142–1150. doi:10.1016/j.polymdegradstab.2009.03.019
- Zhao, B.-C., Xu, J.-D., Chen, B.-Y., Cao, X.-F., Yuan, T.-Q., Wang, S.-F., et al. (2018). Selective Precipitation and Characterization of Lignin-Carbohydrate Complexes (LCCs) from Eucalyptus. *Planta* 247, 1077–1087. doi:10.1007/s00425-018-2842-9

Conflict of Interest: ZL, ZW, SG, YT, XL, NH, QY, and XZ were employed by the companies China Tobacco Hubei Industrial Co., Ltd. and Hubei Xinye Reconstituted Tobacco Development Co., Ltd.

The remaining authors declare that the research was conducted in the absence of any commercial or financial relationships that could be construed as a potential conflict of interest.

Publisher's Note: All claims expressed in this article are solely those of the authors and do not necessarily represent those of their affiliated organizations, or those of the publisher, the editors and the reviewers. Any product that may be evaluated in this article, or claim that may be made by its manufacturer, is not guaranteed or endorsed by the publisher.

Copyright © 2021 Liu, Wang, Gao, Tong, Le, Hu, Yan, Zhou, He and Wang. This is an open-access article distributed under the terms of the Creative Commons Attribution License (CC BY). The use, distribution or reproduction in other forums is permitted, provided the original author(s) and the copyright owner(s) are credited and that the original publication in this journal is cited, in accordance with accepted academic practice. No use, distribution or reproduction is permitted which does not comply with these terms.



Salix spp. Bark Hot Water Extracts Show Antiviral, Antibacterial, and Antioxidant Activities—The Bioactive Properties of 16 Clones

Jenni Tienaho^{1*}, Dhanik Reshamwala², Tytti Sarjala¹, Petri Kilpeläinen¹, Jaana Liimatainen¹, Jinze Dou³, Anneli Viherä-Aarnio¹, Riikka Linnakoski⁴, Varpu Marjomäki² and Tuula Jyske¹

¹Production Systems, Natural Resources Institute Finland (Luke), Helsinki, Finland, ²Department of Biological and Environmental Science, Nanoscience Center, University of Jyväskylä, Jyväskylä, Finland, ³Department of Bioproducts and Biosystems, School of Chemical Engineering, Aalto University, Espoo, Finland, ⁴Natural Resources, Natural Resources Institute Finland (Luke), Helsinki, Finland

OPEN ACCESS

Edited by:

Caoxing Huang,
Nanjing Forestry University, China

Reviewed by:

Chuan-Ling Si,
Tianjin University of Science and
Technology, China
Hayssam M. Ali,
King Saud University, Saudi Arabia

*Correspondence:

Jenni Tienaho
jenni.tienaho@luke.fi

Specialty section:

This article was submitted to
Bioprocess Engineering,
a section of the journal
Frontiers in Bioengineering and
Biotechnology

Received: 19 October 2021

Accepted: 15 November 2021

Published: 16 December 2021

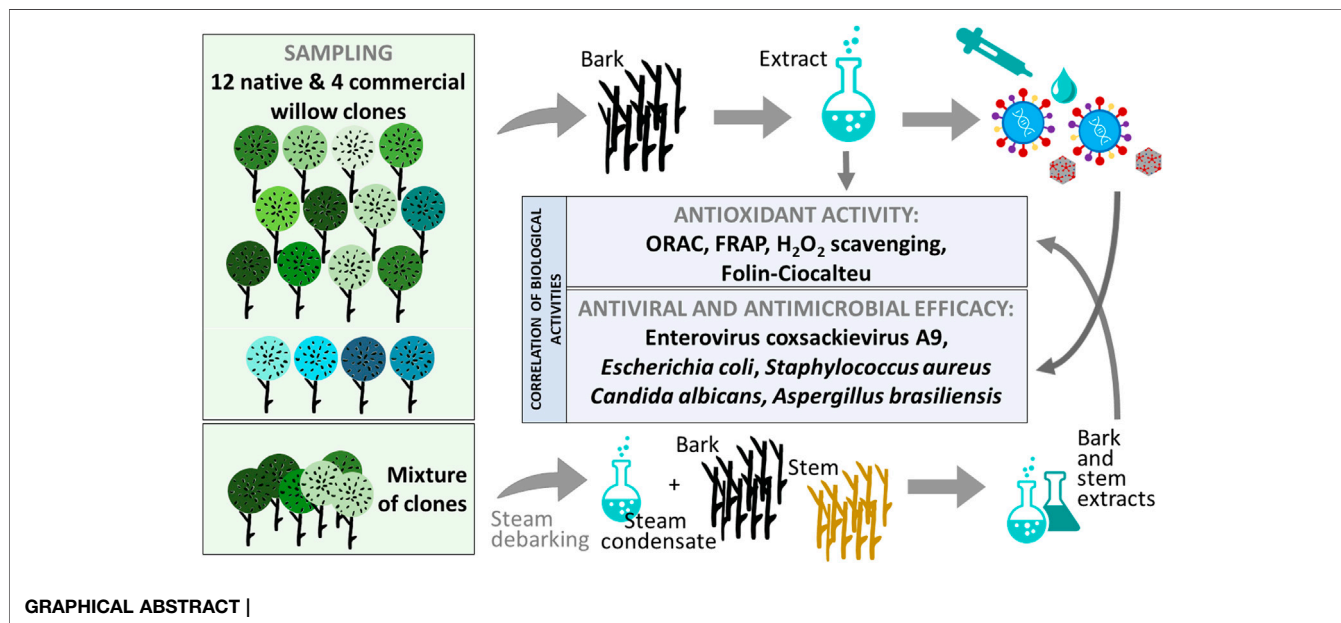
Citation:

Tienaho J, Reshamwala D, Sarjala T, Kilpeläinen P, Liimatainen J, Dou J, Viherä-Aarnio A, Linnakoski R, Marjomäki V and Jyske T (2021) Salix spp. Bark Hot Water Extracts Show Antiviral, Antibacterial, and Antioxidant Activities—The Bioactive Properties of 16 Clones. Front. Bioeng. Biotechnol. 9:797939. doi: 10.3389/fbioe.2021.797939

Earlier studies have shown that the bark of *Salix* L. species (Salicaceae family) is rich in extractives, such as diverse bioactive phenolic compounds. However, we lack knowledge on the bioactive properties of the bark of willow species and clones adapted to the harsh climate conditions of the cool temperate zone. Therefore, the present study aimed to obtain information on the functional profiles of northern willow clones for the use of value-added bioactive solutions. Of the 16 willow clones studied here, 12 were examples of widely distributed native Finnish willow species, including dark-leaved willow (*S. myrsinifolia* Salisb.) and tea-leaved willow (*S. phylicifolia* L.) (3 + 4 clones, respectively) and their natural and artificial hybrids (3 + 2 clones, respectively). The four remaining clones were commercial willow varieties from the Swedish willow breeding program. Hot water extraction of bark under mild conditions was carried out. Bioactivity assays were used to screen antiviral, antibacterial, antifungal, yeasticidal, and antioxidant activities, as well as the total phenolic content of the extracts. Additionally, we introduce a fast and less labor-intensive steam-debarking method for *Salix* spp. feedstocks. Clonal variation was observed in the antioxidant properties of the bark extracts of the 16 *Salix* spp. clones. High antiviral activity against a non-enveloped enterovirus, coxsackievirus A9, was found, with no marked differences in efficacy between the native clones. All the clones also showed antibacterial activity against *Staphylococcus aureus* and *Escherichia coli*, whereas no antifungal (*Aspergillus brasiliensis*) or yeasticidal (*Candida albicans*) efficacy was detected. When grouping the clone extract results into *Salix myrsinifolia*, *Salix phylicifolia*, native hybrid, artificial hybrid, and commercial clones, there was a significant difference in the activities between *S. phylicifolia* clone extracts and commercial clone extracts in the favor of *S. phylicifolia* in the antibacterial and antioxidant tests. In some antioxidant tests, *S. phylicifolia* clone extracts were also significantly more active than artificial clone extracts. Additionally, *S. myrsinifolia* clone extracts showed significantly higher activities in some antioxidant tests than commercial clone extracts and artificial clone extracts. Nevertheless, the bark extracts of native Finnish willow clones showed high bioactivity. The obtained knowledge paves the way towards

developing high value-added biochemicals and other functional solutions based on willow biorefinery approaches.

Keywords: antimicrobial, antioxidant, antiviral, bark, debarking, *Salix* spp., water-extracts



1 INTRODUCTION

Willows (genus *Salix* L.) correspond to approximately 450 species of deciduous trees and shrubs, which are mostly found in moist soils of the Northern Hemisphere (Christenhusz et al., 2017). In general, the major components of willows' biomass are cellulose, hemicellulose, and lignin, while various minor constituents include flavonoids and other polyphenols (Yan et al., 2021). Willow leaves and bark have long been known as herbal medicines because of their ability to relieve fever and aches. These properties have been attributed to compounds identified from willow species, such as salicinoids and various polyphenols. Salicinoids (syn. salicylates) are phenolic glucosides, which are derivatives of salicyl alcohol, and are commonly found at high levels in the bark and leaves of willows. Most of the salicinoids are signature compounds of *Salix* and *Populus* L. species, and over 20 individual salicinoids have been characterized. Whereas salicylic acid is a ubiquitous plant hormone. Salicin is the simplest and most common salicinoid compound; however, it is often found at low quantities depending on the willow hybrid. Other salicinoids in willows are formed by the esterification of one or more hydroxyl groups of salicin with organic acids, such as benzoic acid in populin and 1-hydroxy-6-oxocyclohex-2-en-1-carboxylic acid in salicortin (Boeckler et al., 2011; Julkunen-Tiitto and Virjamo, 2017). Other small phenolic glycosides common in willow bark are picein, a glucoside of hydroxyacetophenone, salidroside, a glucoside of phenylethanoid, and derivatives of

cinnamic alcohols such as triandrin and vimalin (Julkunen-Tiitto, 1985; Kammerer et al., 2005; Dou et al., 2018). Proanthocyanidins up to 20% of bark dry weight (Heiska et al., 2007) and several flavonoids belonging to flavan-3-ols, flavonols, flavanones, and chalcones have also been characterized. A comprehensive review of the phytochemistry and pharmacological activities of *Salix* spp. was recently published by Tawfeek et al. (2021).

Salicinoids of willow bark can decompose into salicylic acid, which has been found to possess anti-inflammatory and antiviral properties (Singh et al., 2004; Wood, 2015). Highly purified proanthocyanidin fractions of *Salix* spp. extract have also been reported to have antiviral and antibacterial activities (Quosdorf et al., 2017). Overall, proanthocyanidins, or condensed tannins, have been characterized by many biological effects, including antioxidant, antibacterial, antitumor, anticancer, neuroprotective, hypoglycemic, and lipid-lowering activities with a comprehensive positive impact on gastrointestinal health (Yan et al., 2021). Saracila et al. (2018) observed that by feeding the bark extract of *Salix alba* L. to broilers, the number of pathogenic bacteria (Enterobacteriaceae, *Escherichia coli*) on the cecal microbial population decreased while the number of beneficial lactobacilli increased. Three *Salix* spp. bark extracts were also found to have bactericidal effects against *Staphylococcus aureus*, with no significant differences between these species (Ramos et al., 2019). Polyphenols from *Salix tetrasperma* Roxb. stem bark extract were also found to be effective in inhibiting the quorum sensing and virulence of *Pseudomonas*

aeruginosa (Mostafa et al., 2020). Malterud et al. (1985) showed that the flavonoid composition from *Salix caprea* L. wood was able to inhibit rot producing wood-destroying fungi *Caniophora puteana*, *Sporotrichum pulverulentum*, and *Trichoderma viride*. Furthermore, willow bark extracts are known to have strong antioxidant and radical scavenging properties (Durak and Gawlik-Dziki, 2014; Bounaama et al., 2016; Ramos et al., 2019). Pharmacological studies have revealed interesting aspects of antitumor and anticancer therapy, including the discovery of a novel cyclodimeric salicinoid, miyabeacin, from *Salix miyabeana* Seemen. and *Salix dasyclados* Wimm. (El-Shemy et al., 2007; Ward et al., 2020). Willow extracts can also be used to relieve pain, inflammation, and fever in a wide variety of conditions with minor adverse effects (Chrubasik et al., 2000; Vlachojannis et al., 2009; Shara and Stohs, 2015). As only mild cytotoxicity has been discovered in willow bark extracts, willows are a promising biomass for various health applications (Ramos et al., 2019). However, because of the vast number of different willow species and their widespread ability to form hybrids, as well as recently identified compounds (e.g., Wu et al., 2016; Noletto-Dias et al., 2018; Noletto-Dias et al. 2019; Noletto-Dias et al. 2020; Ward et al., 2020), there is still much to explore regarding *Salix* spp. and their metabolites.

The biomass of fast-growing willows is recognized as a suitable raw material for biorefineries (Parajuli et al., 2015). Willows can be grown in low-quality agricultural land that cannot be used for food production, thereby reducing competition between food and biomass production (Krzyżaniak et al., 2016). Also, short-rotation woody crop management is less energy consuming than that required for food crops (Djomo et al., 2011). In addition to its potential as a lignocellulosic option for biofuels and bioenergy, willows can be exploited as a renewable source of biochemicals (Brereton et al., 2017). To fully utilize willows' biomass, both bark and stem wood must be separately valorized (Dou et al., 2016). Carbonized willow bark and wood can be used in supercapacitors (Phiri et al., 2019; Hobisch et al., 2020) and fiber composites (Dou et al., 2019). The cascading use of biomass would be preferential. Isolated biomass fractions should be used as reusable products as much as possible and, finally, after a cycle of reasonable use, compounds and materials should be used as energy after their combustion or anaerobic digestion. For example, the polyphenol containing fraction can be extracted first with hot water, and then the remaining material could be pyrolyzed and anaerobically gasified (Rasi et al., 2019) or used in the production of biochar by slow pyrolysis technology (Rasa et al., 2021). Hot water extraction has been shown to be able to achieve the maximal extract yield from willow bark at 80°C for 20 min (Dou et al., 2018).

Extensive characterization and quantification have been conducted on the components of pharmaceutical preparations from *Salix* spp. (Kammerer et al., 2005) and willow species' phytochemicals extracted from the bark (Julkunen-Tiitto, 1985; Heiska et al., 2007; Lavola et al., 2018), leaves (Ikonen et al., 2002; Lavola et al., 2018), and whole twigs/biomass (Julkunen-Tiitto, 1985; Brereton et al., 2017). Willow bark is one of the most bioactive compound-rich plant parts (Lavola et al., 2018; Tyśkiewicz et al., 2019), but leaves are also a promising source of polyphenols and

antioxidants (Piatczak et al., 2020). However, the content of bark phytochemicals is known to vary among *Salix* spp. (Julkunen-Tiitto, 1985) because of seasonal and environmental factors (Förster et al., 2008), as well as among genotypes and developmental stages of the plant (Lavola et al., 2018). Although the variation of phytochemicals between *Salix* spp. genotypes is mainly quantitative, there can be large differences in compound composition between species and hybrids, which could be a result of the effortless hybridization of *Salix* spp. (Julkunen-Tiitto and Virjamo, 2017). Nevertheless, we lack knowledge on the bark bioactive properties of willow species and/or clones that are well adapted to the northern areas of the cool temperate zone. Therefore, the present study focused on the bark extracts of Finnish willows by screening their antioxidant, antiviral, antibacterial, and antifungal properties.

First, we screened the bioactive properties, i.e., the antioxidant, antiviral (enterovirus strain coxsackievirus A9), antibacterial [*E. coli* (Gram-negative) and *S. aureus* (Gram-positive)], antifungal (*Aspergillus brasiliensis*), and yeasticidal (*Candida albicans*) activities of 16 aqueous bark extracts to the potential of willow materials for various biochemicals and functional products. Additionally, we tested steam-debarking at the 300-L scale as a potentially less-laborious debarking method for northern cultivated willows. We hypothesized that (1) the bark extracts of native willows of local origin have higher biological activity than those of commercial willows due to higher resource allocation to secondary metabolites in native willows; (2) between-species variation in the biological activity of bark extracts offsets the variation among clones; (3) the biological activities of bark extracts are highly intercorrelated; for example, antiviral efficacy can be predicted by the total phenolic content and antibacterial power; (4) individual compounds do not explain the biological activities of crude bark extracts but the extract antioxidant activity and efficacies against viruses and bacteria are due to the synergistic effects of several compounds together—to challenge this pure commercial compounds were also tested; (5) when grouping the clones into *S. phylicifolia*, *S. myrsinifolia*, native hybrid, artificial hybrid, and commercial clones, significant differences can be detected; and (6) when compared to conventional debarking methods, steam-aided debarking is an efficient and less laborious process resulting in *Salix* spp. products with high bioactive potential.

2 MATERIALS AND METHODS

2.1 *Salix* spp. Sample Collection

The study materials consisted of 16 willow clones. Of these, 12 clones originated from two common and widely distributed native willow species, dark-leaved willow (*S. myrsinifolia* Salisb.) and tea-leaved willow (*S. phylicifolia* L.) (Väre et al., 2021), as well as from their natural and artificial hybrids. The other four clones were commercial willow varieties from the Swedish willow breeding program (Table 1). Herbarium specimens of the native materials were collected, the identification of the willow species was verified, and the plant specimens were deposited at the Finnish Museum of Natural History, Botanical Museum (H).

TABLE 1 | Willow clones used for the screening of biological activities.

Sample number	Clone	Species	Type
1	E6682	<i>S. myrsinifolia</i>	Native
2	E6771	<i>S. myrsinifolia</i>	Native
3	E6948	<i>S. myrsinifolia</i>	Native
4	E6666	<i>S. phylicifolia</i>	Native
5	K2191	<i>S. phylicifolia</i>	Native
6	K2218	<i>S. phylicifolia</i>	Native
7	K2277	<i>S. phylicifolia</i>	Native
8	K2183	<i>S. myrsinifolia</i> × <i>phylicifolia</i>	Native hybrid
9	K2269	<i>S. myrsinifolia</i> × <i>phylicifolia</i>	Native hybrid
10	K2341	<i>S. myrsinifolia</i> × <i>phylicifolia</i>	Native hybrid
11	V7545	(K2183 <i>S. myrs.</i> × <i>phyl.</i>) × S15136 <i>S. gmelinii</i> ^a	Artificial hybrid
12	V7546	(K2183 <i>S. myrs.</i> × <i>phyl.</i>) × P6011 <i>S. gmelinii</i> ^a	Artificial hybrid
13	Scherenee		Commercial clone
14	Tordis		Commercial clone
15	Tora		Commercial clone
16	Klara		Commercial clone

^a*Salix gmelinii* Pall. is former *S. dasyclados* Wimm. (Väre et al., 2021).

The native willow clones and artificial hybrids (sample numbers 1–12) were rooted in 20-cm-long cuttings in polystyrene containers (TA913) in a greenhouse at the Haapastensyrjä field station (N60°43'0.01" E24°26'60.00"), Natural Resources Institute Finland, in the spring of 2017. The growing medium used was a mixture of 2/3 Kekkila FPM 420 F6 HS *Sphagnum* peat and 1/3 perlite (size 2–6 mm). The containerized plants were moved to the nursery of the Piikkiö field station (N60°25'29.32" E22°30'57.64"), Natural Resources Institute Finland, in June 2017, where they were grown for the next 2 years. The plants were watered and fertilized according to the normal nursery practices. On May 7, 2019, the 2-year-old willow plants were cut down and the harvested shoots of each clone were packed separately in plastic bags and immediately frozen at –20°C. The harvested willow coppice varied between 1 and 1.5 m in length and 0.5–2 cm diameter at the base.

Commercial willow clones (sample numbers 13–16) were grown by Carbons Finland Ltd. in a peat field at Aitomäki, Kouvola south-eastern Finland (N60°52'0.01" E26°41'60.00") from 2016 to March 2019, when the 3-year-old coppice was cut down on March 30 and taken for the study. The 3-m-long sample shoots were cut to shorter, ca. 40-cm-long, pieces and frozen (–20°C) until further treatment.

Two shoots of each willow clone were debarked 50 cm from the base and pooled. The bark was cut into small pieces, frozen at –80°C, and finally freeze-dried. The freeze-dried material was ground with a Moulinex grinder to 1- to 2-mm pieces and kept frozen at –80°C until water extraction.

In addition, *Salix Klara* for the 2-L stirring reactor extraction was provided by Carbons Finland Ltd. from the same growth environment and site, except from spring 2017 to 2020. The willow banks were partly cut down in spring 2018 and 2019 and, for the present study, were cut and gathered on October 24, 2020. The material was then debarked and immediately placed in a freezer (–20°C). The bark was ground with a Kamas cutting mill with a 2-cm sieve.

The material for the pilot-scale bark removal by steaming was collected from a willow clone bank growing at the Piikkiö field

station, Finland. The clone bank was established in the summer of 2007. Part of it was cut down in 2013, and all the clones were cut down again on April 4–5, 2019. Material for the steaming experiment was collected as two sample lots, the first containing a mixture of five 6-year-old *Salix purpurea* L. clones. The second sample included a 12-year-old mixture of five *Salix daphnoides* Vill. clones, one *S. purpurea* clone, and two unknown clones. Finally, these two samples were combined, and a bulk sample was used for the steam debarking experiment to ensure the material availability for testing the suitability of the method in general. Detailed information about the samples and their origin can be found in the **Supplementary Appendix Table SA1**.

2.2 *Salix* spp. Clone Extractions

Salix spp. samples were freeze-dried before the extraction. Bark was extracted using an ASE-350 accelerated solvent extractor (Dionex, Sunnyvale, CA, United States). The bark sample (1 g) was placed in a stainless-steel extraction vessel (22 ml). The sample was then extracted three times for 15 min with hot water (1:66, w/v) at 90°C, and the extract was stored at –20°C before further analyses.

2.2.1 *Salix Klara* 2-L Stirring Reactor Extractions

Klara bark was extracted using a 2-L stirring reactor (Polyclave, Büchi, Switzerland). The fresh willow bark sample (358 g, corresponding to 150 g dry weight) was placed in the reactor and extracted in a 1:10 bark dry weight/water ratio. The extraction temperature was 80°C, and there was constant stirring (60 rpm) during the 60-min extraction. Solids were separated by collecting liquid through a 50-µm sintered metal filter at the bottom of the reactor. The extract was cooled to room temperature using a heat exchanger. In total, four extractions were carried out under the same conditions, and the average measured total dissolved solids of the extracts was 13.7 ± 0.2 wt% of the dry weight of the original bark. After extraction, the bark extracts were combined into one sample. The extract was

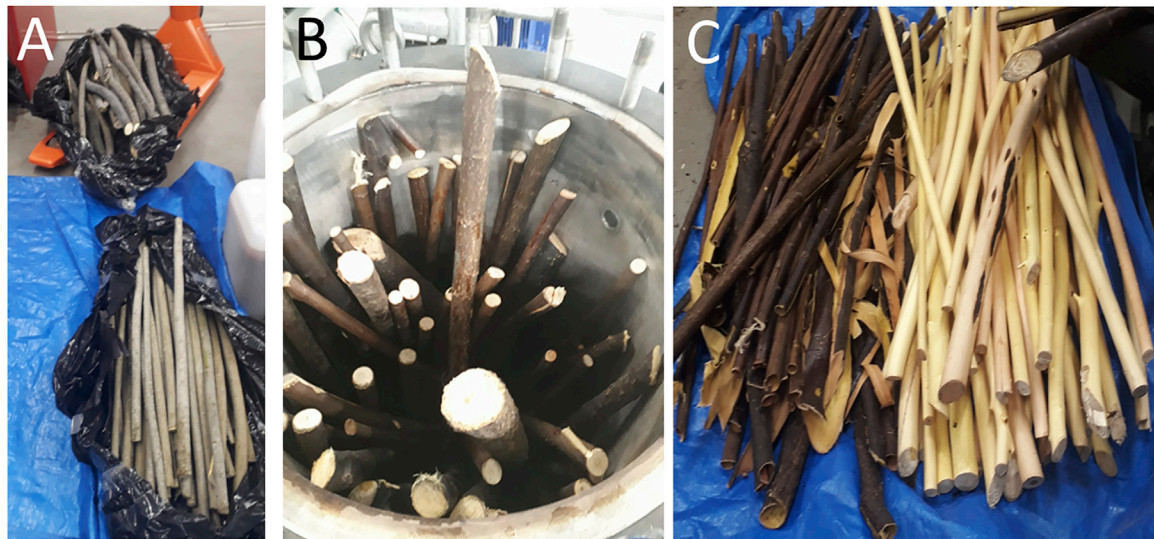


FIGURE 1 | Original willow samples (A), combined willow sticks in reactor (B), and steam-treated bark and woody material (C).

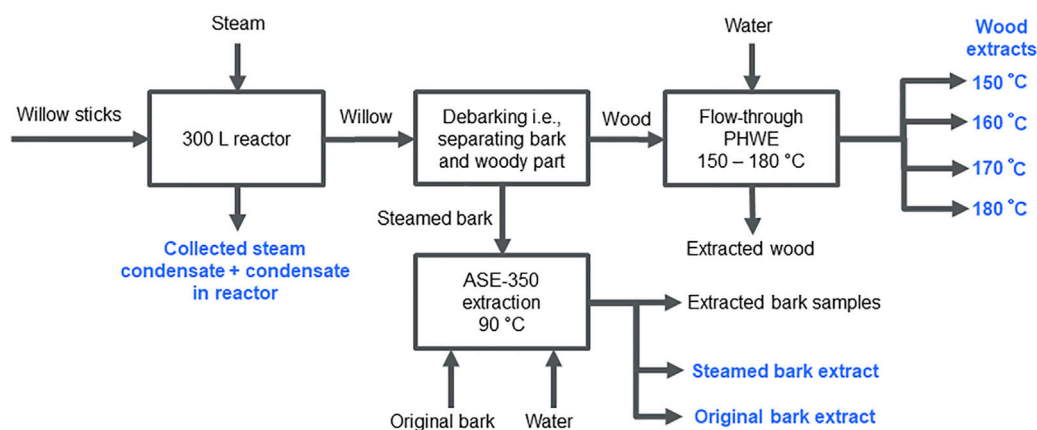


FIGURE 2 | Willow steam treatment, debarking, and extractions. Willow steam treatment condensate, original willow bark ASE-350 extract, and steam-treated bark ASE-350 extract contained polyphenols. Carbohydrates were extracted from woody samples at temperatures from 150 to 180°C after debarking. Collected samples are indicated with blue color.

concentrated using a rotary evaporator at 60°C, freeze-dried, and the dried extract was ground into powder with a mortar and pestle.

2.2.2 Willow Steam Debarking and Extractions

A batch of the combined samples of willow sticks was first steam-treated in a 300-L reactor to remove bark (Figure 1). Samples of steam-treated bark and wood were then extracted at small scale to isolate polyphenol- and carbohydrate-containing fractions. Bark samples were extracted in hot water (90°C) with ASE-350 to isolate polyphenols and wood samples were extracted with a pressurized hot water flow-through extraction system with a 50-ml extraction vessel at 150–180°C to extract carbohydrates. Details of the flow-through extraction system can be found in Kilpeläinen et al. (2014).

Fresh willow sticks (42.2 ± 0.2 kg) were loaded inside the 300-L extraction system that was used in the experiments (Kilpeläinen et al., 2014). For steam collection, 30 L of water was weighed into a tub, and steam was directed to water in the tub with a hose from the extraction system. The temperature inside the vessel was measured during the treatment. Continuous steam flow of 1.6 kg/min (214°C) was passed into the vessel containing willow samples for 20 min. The temperature inside the reactor increased to 100°C after 5–6 min. After 7.5 min, steam started to come out of the vessel, and it was collected into the water-filled tub. When steaming ended after 20 min, the temperature increased to 130°C and the pressure increased to 1.7 bar with a fully open exhaust line.

Steam (3.6 ± 0.2 kg) was collected by the steam collection tub. The condensate was removed *via* the reactor's drain valve and weighed (19.2 ± 0.2 kg). The steam-treated willow sticks could be

easily debarked by hand, as the bark was barely attached to the wood. Samples of the steam condensates, steam-treated bark, and wood were collected and frozen (-20°C) before further analysis.

After the willow steam treatment, the woody material was extracted with a pressurized hot water flow-through system (Kilpeläinen et al., 2012) to isolate fractions with the willow hemicelluloses. Pressurized hot water flow-through extraction has been used to extract hemicelluloses from woody materials (Kilpeläinen et al., 2012; Kilpeläinen et al., 2014). Before extraction, the sample was pre-steamed at 100°C to prevent water channeling through the sample during extraction. Samples (10 g o.d.) were extracted at $150\text{--}180^{\circ}\text{C}$ with a flow rate of 4 ml/min for 60 min. The extract was collected, diluted to 250 ml, and stored in a freezer (-20°C) before analysis.

Steamed bark was extracted with hot water using ASE-350 under the same conditions as the *Salix* spp. clones. Willow samples and treatment techniques used are shown in **Figure 2**.

2.3 Commercial Substances and Samples

Commercial substances were used as references in the antibacterial and antiviral measurements. Salicin and picein (purity $>98\%$) were purchased from Merck Life Science Oy. Salicylic acid (purity $>99\%$) was obtained from VWR Chemicals and triandrin (purity 85%) was obtained from Molport EU. Additionally, Salixin Organic Powder (48^{TM}) and Salixin Organic Extract (800NP^{TM}) were supplied by Søren Fisker (Salixin A/S) and Pia Wikström (OY CELEGO AB) and were tested for their antibacterial and antiviral efficacy along with the reference substances.

2.4 Bioactive Efficacy

2.4.1 Antioxidant Properties

The antioxidant properties of the *Salix* spp. clone bark extracts were tested using the oxygen radical absorbance capacity (ORAC) assay, ferric reducing antioxidant power (FRAP), H_2O_2 scavenging test, and Folin-Ciocalteu assay for total phenolic content. All antioxidant assays were carried out using a Varioskan Flash multimode reader (Thermo Scientific) in a 96-well format. The tests covered different antioxidant mechanisms: hydrogen atom transfer (ORAC), single electron transfer (FRAP), and radical scavenging (H_2O_2 scavenging). All tests were performed using internal standards with which the sample results were compared.

Oxygen Radical Absorbance Capacity

This assay is based on hydrogen atom transfer (HAT) and measures the reduction in fluorescence signal caused by the oxidative dissociation of fluorescein in the presence of peroxy radicals ($\text{R-O-O}\bullet$) (Huang et al., 2002; Prior et al., 2003). The inhibition of fluorescein breakdown indicates the antioxidant's protective ability. The experimental setup is described in detail by Tienaho et al. (2020). Briefly, the assay was carried out using four dilutions of each sample, with two technical replicates, by mixing the sample in 0.075 M phosphate buffer pH 7.5 (Merck) with 8.16×10^{-5} mM fluorescein (Sigma-Aldrich Chemie GmbH, Steinheim, Germany) and 2,2'-azobis(2-methylpropionamidine) dihydrochloride (Sigma-Aldrich Chemie GmbH, Steinheim, Germany). Trolox (vitamin E analog) ((\pm)-6-Hydroxy-2,5,7,8-tetramethylchromane-2-

carboxylic acid) (Sigma-Aldrich Chemie GmbH, Steinheim, Germany) was used as the standard, and the results are expressed as Trolox equivalents ($\mu\text{mol TE per } 100 \text{ g}$).

Ferric Reducing Antioxidant Power

This assay is based on single electron transfer (SET) and measures the ability of an antioxidant to reduce ferric (Fe^{III}) to ferrous (Fe^{II}) ions (Benzie and Strain, 1996). The test protocol was described by Tienaho et al. (2021). In brief, a series of four dilutions of each sample, with three technical replicates, in a 96-well format were used in the assay. The samples were mixed with 20 mM $\text{FeCl}_3 \bullet 6\text{H}_2\text{O}$ (Sigma-Aldrich Chemie GmbH, Steinheim, Germany) and 10 mM 2,4,6-tris-(2-pyridyl)-s-triazine (TPTZ) (Sigma-Aldrich Chemie GmbH, Steinheim, Germany) in 300 mM acetate buffer (pH 3.6). The absorbance was measured at 594 nm with a microplate fluorescence reader (Varioskan Flash, Thermo Scientific) after the formation of the ferrous-tripyridyltriazine complex in the reaction mixture. $\text{FeSO}_4 \bullet 7\text{H}_2\text{O}$ (Sigma-Aldrich Chemie GmbH, Steinheim, Germany) was used as the standard and L(+)-ascorbic acid (150 and 800 μM) (VWR Chemicals) as the control. The results are expressed as $\mu\text{mol/L Fe(II)}$ equivalents.

The Hydrogen Peroxide (H_2O_2) Scavenging

Activity was determined using a method modified from Hazra et al. (2008) and Jiang et al. (1990). The experimental setup has been described in detail by Tienaho et al. (2020). In brief, an aliquot of 2 mM H_2O_2 (Merck KGaA, Darmstadt, Germany) was added to the reaction mixture with the sample and a mixture containing 2.56 mM ammonium ferrous (II) sulfate (BDH Prolabo) in 0.25 mM H_2SO_4 (Merck KGaA) and 27.8 μM xylenol orange disodium salt (Sigma-Aldrich Chemie GmbH, Steinheim, Germany) in 4.4 mM sorbitol (D(-)-sorbitol, AppliChem GmbH). After 30 min of incubation, the absorbance of violet-colored ferric-xylenol orange complexes at 560 nm was measured. The assay measures the ability of the sample to scavenge H_2O_2 and prevent the oxidation of Fe(II) to Fe(III), which is indicated by the formation of the ferric-xylenol orange complex. The inhibition of oxidation is expressed as the inhibition (%) of the reaction, and the samples with 100% inhibition activity will remain yellowish. Sodium pyruvate (Sigma-Aldrich) was used as a reference compound.

Folin-Ciocalteu Assay

The Folin-Ciocalteu method (Singleton and Rossi, 1965; Singleton et al., 1999; Ainsworth and Gillespie, 2007) was used to analyze the total phenolic content, which is known to reflect antioxidant capacity. The test protocol was described by Tienaho et al. (2021). In brief, the samples were mixed with Folin-Ciocalteu reagent (Merck KGaA, Darmstadt, Germany) and 20% Na_2CO_3 (Merck KGaA, Darmstadt, Germany), and absorbance was measured at 750 nm with gallic acid (Sigma-Aldrich Chemie GmbH, Steinheim, Germany) as a reference compound. The results are expressed as gallic acid equivalents per gram (GAE/g).

2.4.2 Antibacterial Properties

Two constitutively light-emitting bacterial biosensor strains, *E. coli* K12 + pCGLS11 and *S. aureus* RN4220 + pAT19,

described by Vesterlund et al. (2004), were used in the present study. Bacterial cultivation and stocks were grown as previously described (Välimaa et al., 2020). Briefly, the bacteria were stored at -80°C and cultivated for approximately 16 h at 30°C (*E. coli*) and 37°C (*S. aureus*) on lysogeny agar (LA) plates (tryptone 10 g/L; yeast extract 5 g/L; NaCl 10 g/L; and agar 15 g/L). The LA plates were supplemented with 10% (v/v) sterile filtered phosphate buffer (PB) (1 M, pH 7.0) and 100 $\mu\text{g/ml}$ of ampicillin (*E. coli*) or 5 $\mu\text{g/ml}$ erythromycin (*S. aureus*). Biosensor stocks were prepared by inoculating a single colony of bacteria in lysogeny broth supplemented with 10% (v/v) of sterile filtered PB 1 M (pH 7.0), 100 $\mu\text{g/ml}$ ampicillin (*E. coli*), or 5 $\mu\text{g/ml}$ erythromycin (*S. aureus*). Stocks were cultivated for approximately 16 h at 300 rpm shaking at 30°C (*E. coli*) and 37°C (*S. aureus*). Extractions of all the willow clones in **Table 1** were diluted in double-distilled water to achieve a 5% v/v concentration per microplate well. Ethanol 35% per microplate well was used as a positive control, and double-distilled water was used as a negative control. The reference substances, picein, triandrin, salicin, salicylic acid, and Salixin Organic Powder were diluted in double-distilled water to achieve concentrations of 250 $\mu\text{g/ml}$ and 125 $\mu\text{g/ml}$ per microplate well, whereas Salixin Organic Extract was used in 2.5% and 1.25% v/v per microplate well. Aliquots of 50 μl of samples and controls were pipetted in triplicate into opaque white polystyrene microplates, and 50 μl of bacterial culture was pipetted into the same wells. The luminescence was then measured using a Varioskan Flash Multilabel device (Thermo Scientific) once every 5 min for 95 min at room temperature, and the plate was briefly shaken before every measurement. The results are expressed as relative light units (RLUs) drawn at a time point of 40 min of measurement. Error bars represent the standard deviations between the sample triplicates.

2.4.3 Antiviral Activity

Enterovirus coxsackievirus A9 (CVA9; Griggs strain, ATCC) was used to assess the antiviral efficacy of the *Salix* spp. clone extracts. CVA9 was produced and purified using a sucrose gradient, as previously described (Ruokolainen et al., 2019). Pretreatment of CVA9 [2×10^6 plaque-forming unit (PFU) per ml] was performed with different amounts of *Salix* spp. extract (0.1%, 1%, and 10% v/v). After 1 h incubation at 37°C , the virus-*Salix* spp. mix was diluted 10-fold in 10% Dulbecco's Modified Eagle Medium (DMEM). The mixture was added to the lung carcinoma cell line A549 (ATCC) containing 96-well plates with 12,000 cells/well density, plated on the previous day. After 48 h, the wells were washed twice with phosphate-buffered saline (PBS) and stained with crystal violet solution (0.03% crystal violet, 2% ethanol, and 36.5% formaldehyde) for 10 min, as described previously (Ruokolainen et al., 2019). The color was left in the wells because the remaining surviving cells were dissolved in a homogenization solution (0.8979 g of sodium citrate and 1 N HCl in 47.5% ethanol). The absorbance was measured spectrophotometrically at 570 nm using a PerkinElmer VICTORTM X4 multilabel reader. Cytotoxicity of the *Salix* spp. preparations was evaluated using the crystal violet solution mentioned above (Ruokolainen et al., 2019).

2.4.4 Antifungal Activity

Quantitative suspension tests for the evaluation of basic fungicidal and basic yeasticidal activity of the *Salix* spp. samples were performed according to DIN EN 1275 (2006) and European Standard (2006). The fungicidal activity was evaluated using *A. brasiliensis* (strain ATCC 16404) and the yeasticidal activity using *C. albicans* (ATCC 10231) as a test organism. The microorganism suspension used ranged between 1.5×10^7 colony forming units (CFU)/ml to 5.0×10^7 CFU/ml for *A. brasiliensis* and *C. albicans*. For both organisms, the choice of the test method was the dilution-neutralization method using Tween80 + lecithin (30 g/L polysorbate 80 and lecithin 3 g/L) as a neutralizer. Sterile double-distilled water was used as the diluent during the test. The test concentrations for the samples Salixin Organic Extract 800NP, Salixin Organic Powder, and Klara (2-L scale sample P-16) were 10, 2.5, 1.25, 0.625, 0.3125, 0.156, 0.078, and 0.039 mg/ml. Unlike that described for EN 1275, in some cases, total test volume of 5 ml was used in the experiments instead of 10 ml. The contact time and test temperature were 15 min (± 10 s) and 20°C ($\pm 1^{\circ}\text{C}$), respectively. In addition, the following higher test concentrations were evaluated for the samples: Klara P-16 100 mg/ml, Salixin Organic Powder 100 mg/ml, Salixin Organic Extract 100%, 50%, 25%, 10%, and 5% (v/v), and lyophilized Salixin Organic Extract 50% and 100%.

The number of viable spores was assessed on malt extract agar (four replicates). Plates were incubated for 42–48 h at 30°C , *A. brasiliensis* for a further 20–24 h, and viable spores were determined by counting the colonies (colony counts less than 300 CFU/plate). The reduction in viability is the ratio N/N_0 , where N_0 is the number of CFU/ml in the fungal spore test suspension and N is the number of CFU/ml after the test procedure for the fungicidal activity of the product. The sample is fungicidal or yeasticidal if it produces at least a 10^4 reduction in the number of viable vegetative yeast cells and mold spores under conditions defined by EN 1275 (2006).

2.5 Statistical Methods

Relationships among *Salix* spp. clone extract bioactivities were evaluated by Pearson's correlation coefficients (in absolute values), and the differences between mean values were assessed using a two-tailed *t*-test with a significance level of 0.05 ($n = 16$ for ORAC, FRAP, and Folin-Ciocalteu tests; $n = 17$ for the *E. coli*, *S. aureus*, and Enterovirus test). Statistical differences between the grouped clones were determined by one-way ANOVA and Tukey post-hoc test, where results were determined to be statistically significantly different if *p*-values were below 0.05. All statistical analyses were performed using IBM SPSS Statistics (v. 26.0) (IBM, Armonk, NY, United States).

3 RESULTS

3.1 Antioxidant Properties

The steam treatment results in **Figure 3** show that the highest antioxidant potential and phenolic content (Folin-Ciocalteu) were found in the original willow bark ASE-350 extract. The steamed bark extract also showed elevated antioxidant activity, while the different hot water flow-through extracted wood

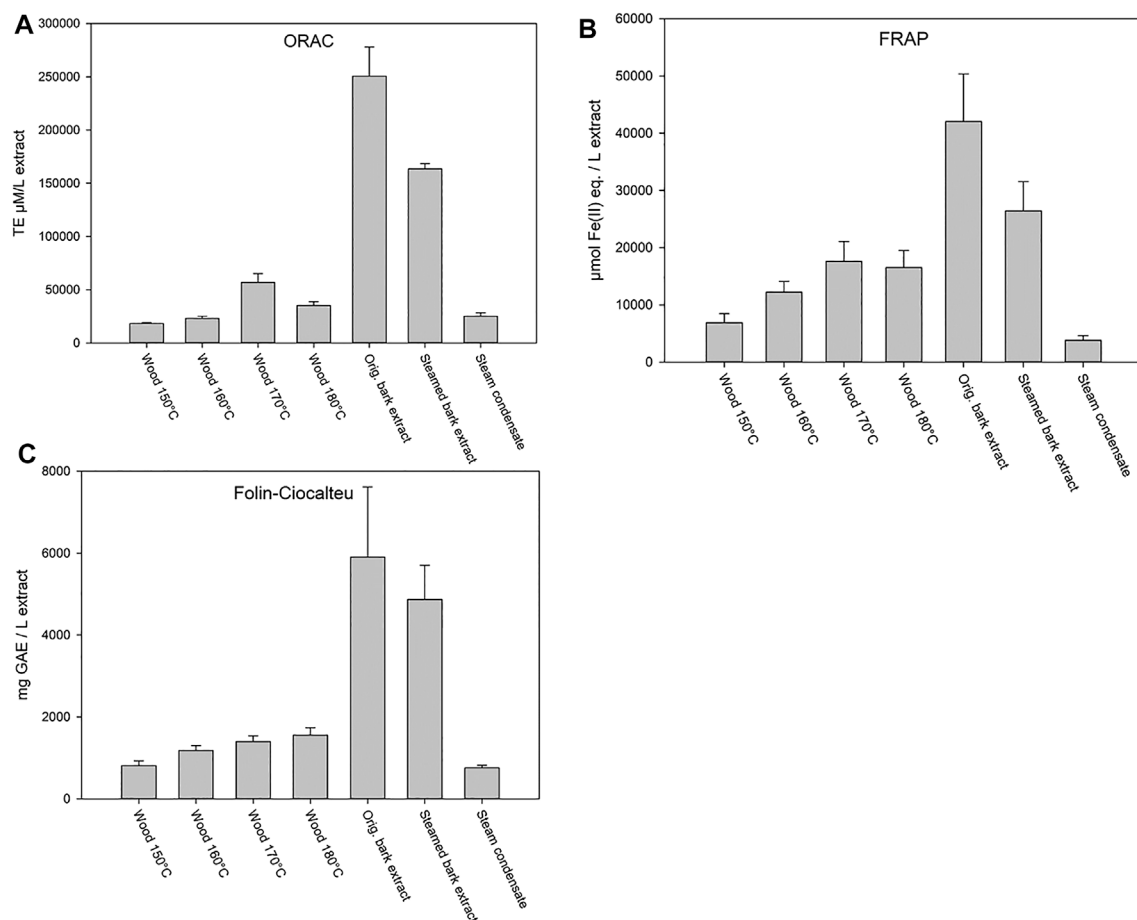


FIGURE 3 | ORAC (A) and FRAP (B) activities, and total phenolic content (Folin-Ciocalteu) (C) of willow wood after debarking extracted at different temperatures (150, 160, 170, and 180°C) and bark extracts (original bark extract, steam-treated bark extract, and steam condensate). Error bars present the standard deviations of the sample triplicates in a microplate. ORAC test results are expressed as Trolox equivalents (TE), FRAP results are expressed as ferrous ion equivalents (Fe(II) eq.), and Folin-Ciocalteu test results are expressed as gallic acid equivalents (GAE).

samples at temperatures of 150–180°C, high in carbohydrates and hemicelluloses, showed much lower antioxidant potential. Reductions in both antioxidant activities (FRAP and ORAC) and total phenolic content were observed when compared to that of original bark extract (Figure 3), indicating that some phytochemicals are leached away. In addition, steam condensate showed some activity, which further supported the partial loss of compounds.

The *Salix* spp. clone extract results (Figure 4) showed that the highest ORAC activity (μmol TE/100 g) was obtained with clone number 5, while clones 3, 6, and 10 also showed high ORAC activity. Clone extract 6 showed the highest FRAP efficiency, while clone extracts 3, 4, and 5 also showed high activity. All clone extracts except 7, 13, 15, and 16 showed high activity in the hydrogen peroxide scavenging test. The highest total phenolic content was found in the clone extract 6. Commercial clone extracts 13, 15, and 16 showed very low hydrogen peroxide scavenging activity (Figure 4D).

When grouping the clone extract antioxidant results into *S. myrsinifolia* (clones 1–3), *S. phylicifolia* (4–7), native hybrid

(8–10), artificial hybrid (11–12), and commercial clones (13–16), there was a significant difference between the groups as determined by one-way ANOVA [ORAC: $F(4,11) = 4.012$, $p = 0.030$; FRAP: $F(4,11) = 10.102$, $p = 0.001$; Folin-Ciocalteu: $F(4,11) = 7.552$, $p = 0.004$; and H_2O_2 scavenging with clones 7 and 14 emitted: $F(4,9) = 14065.006$, $p < 0.001$]. A Tukey post-hoc test revealed that *S. phylicifolia* clone extracts showed significantly higher activity in the ORAC test than the commercial clone extracts ($p = 0.045$) (Figure 5A), and significantly higher FRAP activity than the artificial hybrid extracts ($p = 0.003$) and commercial clone extracts ($p = 0.002$) (Figure 5B). In addition, *S. myrsinifolia* clone extracts showed significantly higher FRAP activity than the artificial hybrid extracts ($p = 0.036$) and commercial clone extracts ($p = 0.041$) (Figure 5B). *S. phylicifolia* clone extracts also showed statistically significantly higher total phenolic compound capacity in the Folin-Ciocalteu test than artificial hybrid extracts ($p = 0.009$) and commercial clone extracts ($p = 0.006$). In the H_2O_2 scavenging test, clone 7 gave inconsistently lower results than the other *S. phylicifolia* clone extracts, and clone 14 gave inconsistently high results when

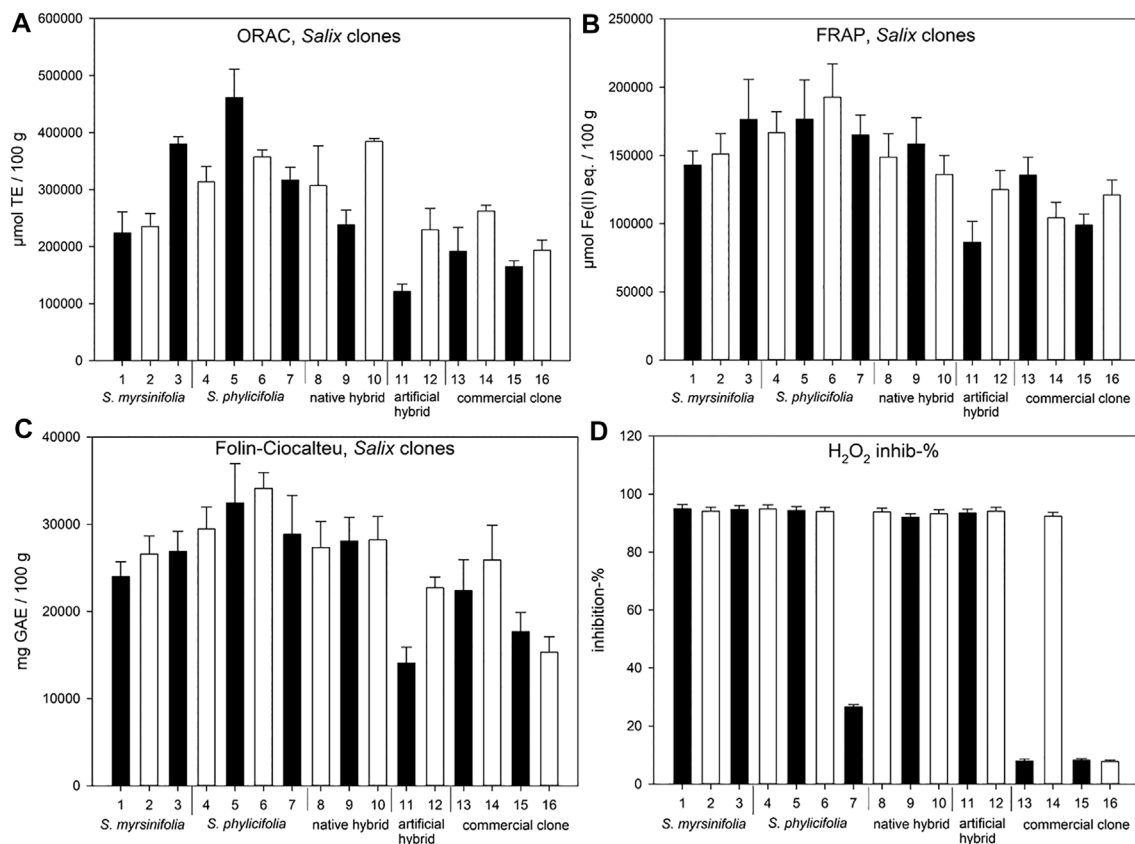


FIGURE 4 | ORAC (A), FRAP (B), and H₂O₂ scavenging (D) activities, as well as total phenolic content (Folin-Ciocalteu) (C) of the *Salix* spp. clone extracts. Error bars present the standard deviations of the sample triplicates in a microplate. The clones are numbered 1–16 (see Table 1) and 13–16 are commercial clones. ORAC test results are expressed as Trolox equivalents (TE), FRAP results are expressed as ferrous ion equivalents (Fe(II) eq.), Folin-Ciocalteu test results are expressed as gallic acid equivalents (GAE), and hydrogen peroxide scavenging test results are expressed as the percentage of H₂O₂ inhibition.

compared to the other commercial clone extracts. In dioecious plant species such as *Salix* spp., gender can be the reason for clonal differences in growth and wood quality, as shown by Hou et al. (2017). In this case, gender may not explain the differences in the activity, because all of the commercial clones included, also clone 14, were known to be female. However, when the outlier clones 7 and 14 were removed from the groups, *S. myrsinifolia* ($p < 0.001$), *S. phylicifolia* ($p < 0.001$), native hybrid ($p < 0.001$), and artificial hybrid ($p < 0.001$) clone extracts showed significantly higher antioxidant activity in the H₂O₂ scavenging test than commercial clone extracts (Figure 5D). In addition, *S. myrsinifolia* clone extracts showed significantly higher activity ($p = 0.049$) than native clone extracts (Figure 5D).

3.2 Biosensor Analysis and Antibacterial Activity

The antibacterial activity was evaluated using recombinant constitutively bioluminescent strains of the leading bacterial pathogens of healthcare-associated infections and bacteremia: *E. coli* and *S. aureus* (Poolman and Anderson, 2018). The results are shown in Figure 6. Tienaho et al. (2015) showed that when

using whole-cell bacterial biosensors, the empirical conditions could take from 10 to 15 min of incubation to stabilize. As shown in Figure 6, all the *Salix* spp. clone extracts had antibacterial activity, as evidenced by the lower RLU values than the negative control (water) with both bacterial strains after 10 min of incubation. The lower RLU values imply an inhibition of bacterial luminescence production and, thus, interference with bacterial metabolism. The highest inhibition effect after 40 min incubation was achieved by clone extract 4 in *E. coli* and clone extract 10 in *S. aureus*. However, the differences between the clones were small, with the exceptions of commercial clone extracts 14–16 and clone extract number 14, which had a somewhat lower effect on *E. coli* and *S. aureus*, respectively. For both bacterial strains, all the clone extracts exhibited stronger antibacterial activity than the control substances, salicin, salicylic acid, picein, and triandrin. The lowest inhibition seemed to be achieved with the 2-L stirring reactor extracted clone 16 (P-16); however, it still had lower luminescence production (in RLU) than the water control. The commercial reference substances showed lower antibacterial activity against both bacterial strains, except for the Salixin Organic Extract, which was equally active as the willow clone extracts with *E. coli* and showed almost as high antibacterial activity as ethanol (35%) with *S.*

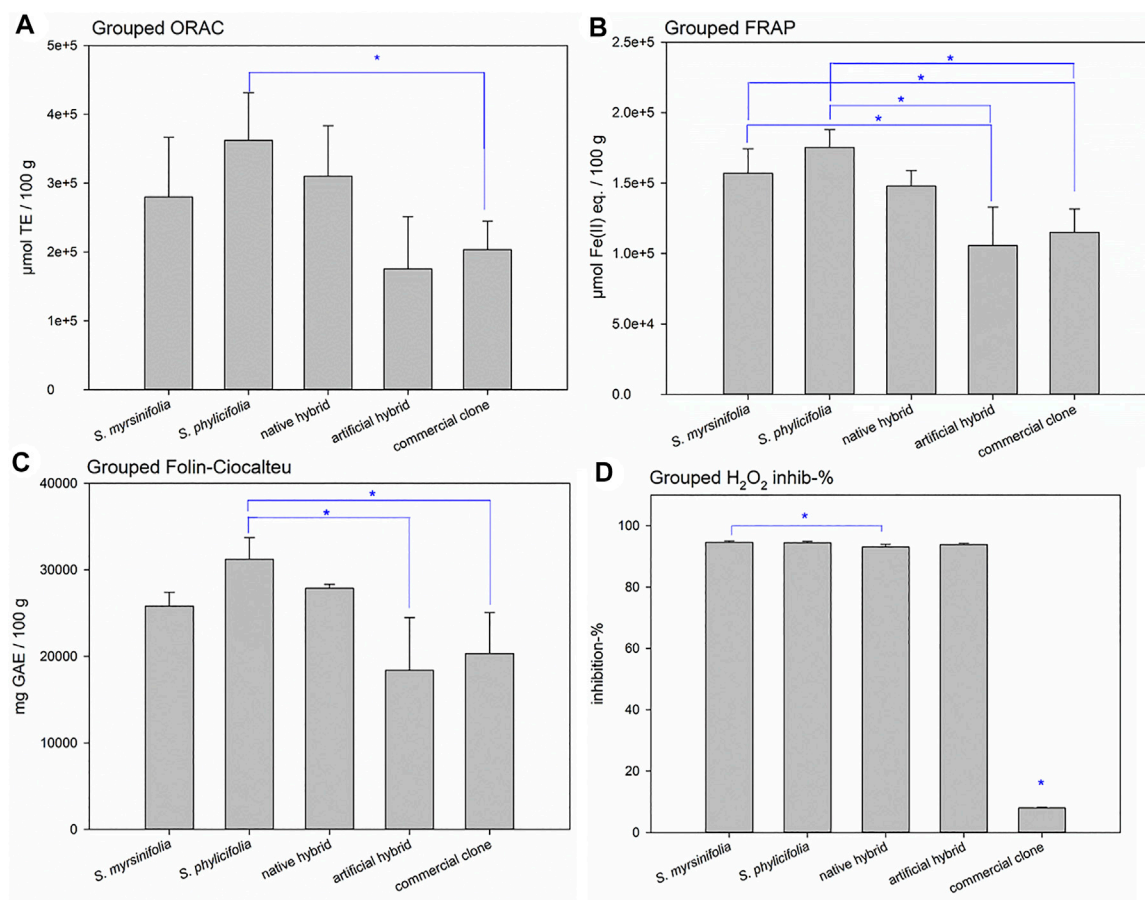


FIGURE 5 | Grouped ORAC (A), FRAP (B), and H_2O_2 scavenging (D) activities, as well as total phenolic content (Folin-Ciocalteu) (C) of the *Salix* spp. clone extracts. Error bars show the standard deviation between the grouped clones. Significant differences are expressed with a blue asterisk. ORAC test results are expressed as Trolox equivalents (TE), FRAP results are expressed as ferrous ion equivalents (Fe(II) eq.), Folin-Ciocalteu test results are expressed as gallic acid equivalents (GAE), and hydrogen peroxide scavenging test results are expressed as the percentage of H_2O_2 inhibition.

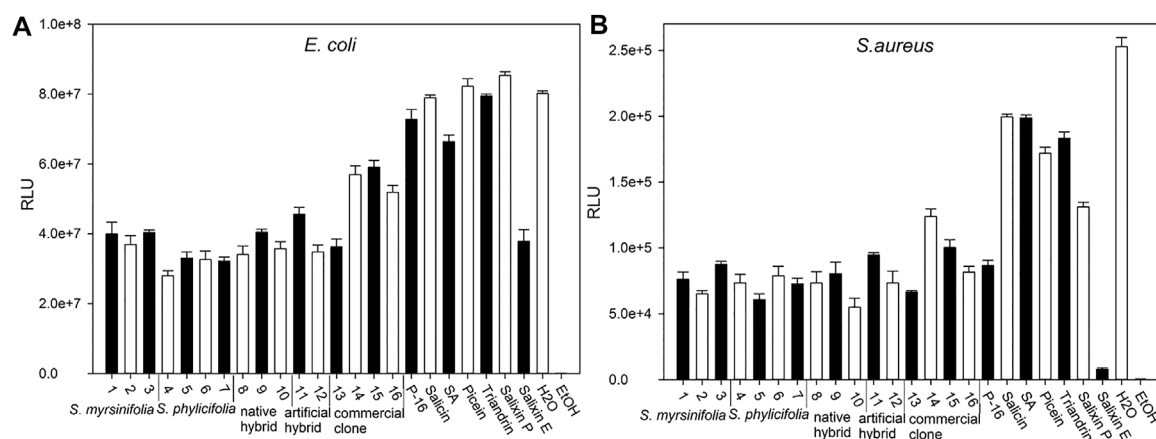


FIGURE 6 | The bacterial biosensor results. Efficacy against *E. coli* (A) and *S. aureus* (B) after 40 min incubation time. The *Salix* spp. clones (Table 1) of 5% v/v concentration per a microplate well are indicated with numbers 1–16. P-16 = 2-L scale clone 16; commercial substances Salicin P = Salicin Organic Powder 48™ (250 $\mu\text{g}/\text{ml}$) and Salicin E = Salicin Organic Extract 800NP™ (1.25% v/v); SA = salicylic acid (250 $\mu\text{g}/\text{ml}$). Results obtained for salicin, triandrin, and picein are also shown at the concentration of 250 $\mu\text{g}/\text{ml}$ per microplate well. Error bars indicate the standard deviation between the sample triplicates in the microplate. Lower RLU values indicate stronger antibacterial activity.

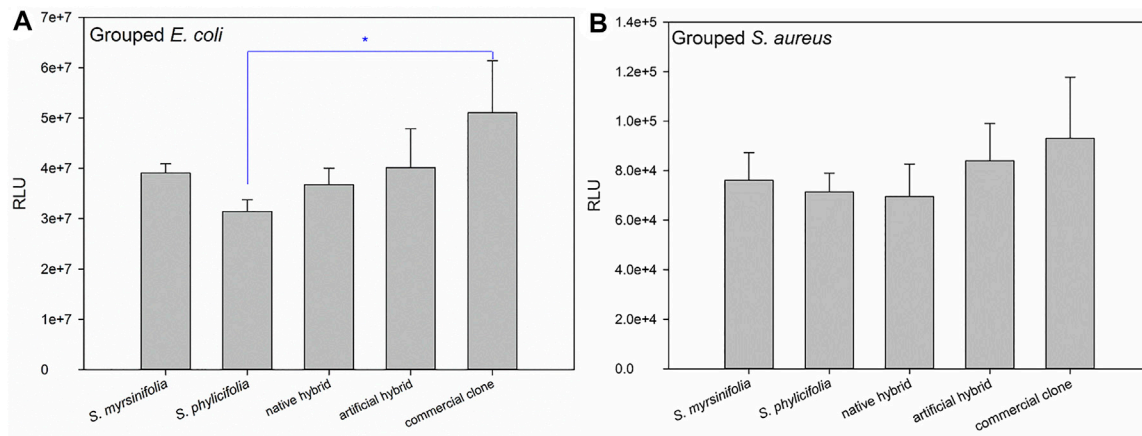


FIGURE 7 | The grouped antibacterial results against *E. coli* (A) and *S. aureus* (B). Error bars show the standard deviation between the grouped clones. Significant differences are indicated with a blue asterisk.

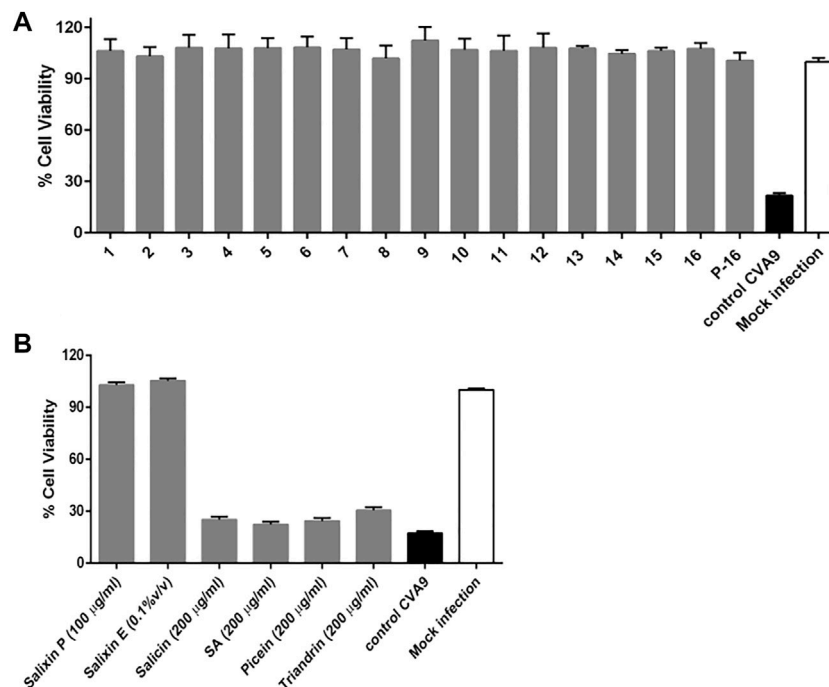
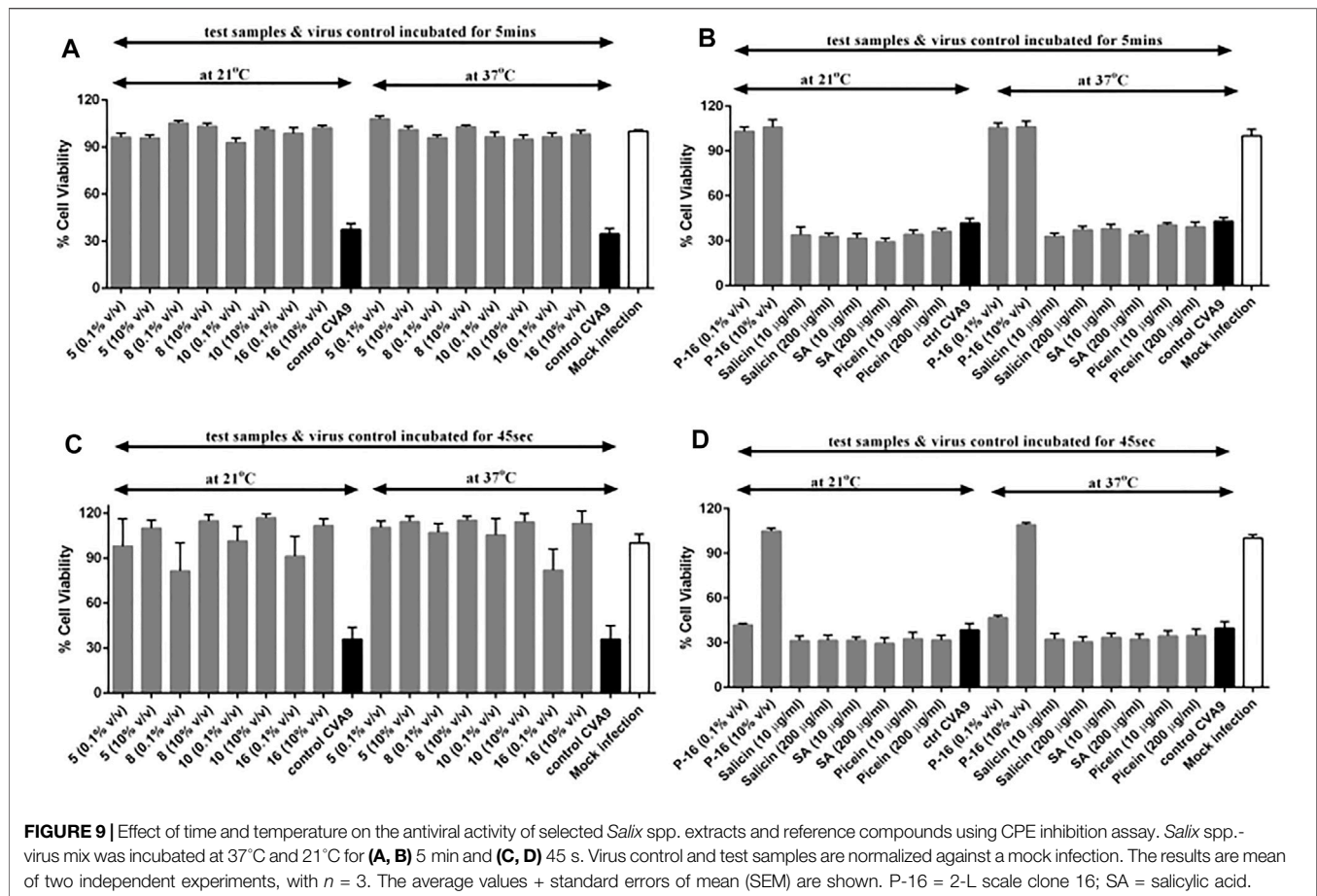


FIGURE 8 | Testing the antiviral activity of (A) *Salix* spp. extracts (0.1% v/v) and (B) reference compounds (salicin, salicylic acid, picein, and triandrin) and Salixin Organic Powder and Extract against CVA9 using CPE inhibition assay. Virus control and test samples are normalized against a mock infection. The results are mean of two independent experiments with $n = 3$. The average values + standard errors of mean (SEM) are shown. P-16 = 2-L scale clone 16; Salixin P = Salixin Organic Powder 48TM; Salixin E = Salixin Organic Extract 800NPTM; SA = salicylic acid.

aureus. However, Salixin Organic Extract was considerably darker than the other samples, and this could have an effect on light reduction. The disadvantages of this method have been minimized by using small concentrations of dark-colored samples to reduce the effect of color and by repeating the measurement three times to ensure comparability between measurements (Tienaho, 2020).

When grouping the clone extract results into *S. myrsinifolia* (clones 1–3), *S. phylicifolia* (4–7), native hybrid (8–10), artificial hybrid

(11–12), and commercial clones (13–16), there was a significant difference between the groups as determined by one-way ANOVA in the *E. coli* biosensor results [$F(4,9) = 5.266, p = 0.013$], whereas the differences in the *S. aureus* results were statistically insignificant (Figure 7B). A Tukey post-hoc test revealed that *S. phylicifolia* clone extracts had significantly higher antibacterial activity against *E. coli* than the commercial clone extracts ($p = 0.007$) (Figure 7A). Other results were statistically similar.



3.3 Antiviral Activity

The antiviral activity was evaluated using the highly stable non-enveloped enterovirus CVA9. There are more than 100 serotypes of enteroviruses with very similar structures and functions (Marjomäki et al., 2015). To date, there are no clinically approved antivirals against enteroviruses or any non-toxic natural compounds that can safely disinfect enteroviruses or other non-enveloped viruses from surfaces. Here, the tested *Salix* spp. preparations proved to be very efficient against CVA9 (Figure 8A). Pre-incubation of the virus with *Salix* spp. extracts fully rescued the A549 cells from infection, proving that the extracts directly bound to the capsid. *Salix* spp. samples did not show any cytotoxicity (data not shown). We also tested Salixin Organic Extract and Powder along with the reference compounds (salicin, salicylic acid, picein, and triandrin). Similar to *Salix* spp. samples, Salixin Organic Powder and Extract also showed antiviral activity and protected the cells against CVA9 infection, whereas none of the reference compounds were effective in stopping the viral infection (Figure 8B).

To study the impact of time and temperature on the antiviral activity of *Salix* spp. extracts in further detail, we incubated selected *Salix* spp. samples with CVA9 for a shorter time interval (5 min) and at lower temperatures (21°C vs. 37°C). The selected *Salix* spp. extracts retained their antiviral efficacy even at room temperature (21°C) and were able to stop CVA9 infection within 5 min of incubation at both

temperatures tested (Figures 9A,B). None of the reference compounds tested showed antiviral activity (Figure 9B). We tested an even shorter incubation time (45 s) to further determine the efficacy of the *Salix* spp. extracts. Interestingly, this short pre-treatment with the *Salix* spp. extracts was sufficient for the samples to exert their antiviral efficacy and protect the cells from CVA9 infection (Figures 9C,D). However, the 2-L stirring reactor extracted clone 16, sample P-16, did not show antiviral activity at lower concentrations (0.1% v/v) when incubated with CVA9 for 45 s at 21°C or 37°C. Nevertheless, it completely protected the cells when tested at higher concentrations (10% v/v) (Figure 9D). These results indicate that the *Salix* spp. extracts can effectively block CVA9 infection within a few seconds of interacting with the virus at room temperature by acting directly on the virus capsid.

When grouping the clone extract results from Figure 8 into *S. myrsinifolia* (clones 1–3), *S. phylicifolia* (4–7), native hybrid (8–10), artificial hybrid (11–12), and commercial clones (13–16), there were no statistical differences between the groups as determined by one-way ANOVA [$F(4,11) = 0.276$, $p = 0.887$].

3.4 Antifungal Activity

The tested concentrations of *Salix* extract Klara (the 2-L scale sample) and Salixin Organic Extract and Powder were not

effective against fungi (*A. brasiliensis*) and yeast (*C. albicans*). A reduction in viability higher than 4 log units, as required by the EN 1275 norms to qualify the product with fungicidal or yeasticidal efficiency, was not detected. However, higher concentrations of the commercial Salixin Organic Extract (50 and 100% v/v) showed minor inhibition against both *C. albicans* and *A. brasiliensis*.

4 DISCUSSION

In the present study, we introduced a steam debarking method, which loosens the bark and allows its efficient removal; therefore, this method has the potential to decrease the costs of willow debarking. However, our results showed that some antioxidant activity was lost in the steam-treated bark samples. The original bark extract had higher polyphenol content and antioxidant capacity than the steam-treated bark extract, indicating that some phytochemicals were leached away in the process. One of the major constituents of various biomasses is lignin, which has been found to possess anti-inflammatory and antioxidant activities, and it has been found to degrade at high temperatures (Gu et al., 2021; Wang et al., 2021; Zheng et al., 2021). However, the steam-treatment temperatures did not rise above 180°C, and the decomposition of lignin, which is rather slow, has been considered to start at temperatures over 180°C (Nassar and MacKay, 1984; Brebu and Vasile, 2010). In the hydrothermal steam treatment of *Populus deltoides* (W. Bartram ex Marshall, Salicaceae), lignin content was only slightly decreased (Bobleter, 1994). Therefore, it is more likely that the degradation of other extractives, such as salicinoid or polyphenol structures, caused the decrease in the antioxidant capacity after steam treatment, especially if salicinoid structures were unstable (Julkunen-Tiitto and Sorsa, 2001; Ruuhola and Julkunen-Tiitto, 2003). Additionally, a substantial degradation of acetyl groups in hemicellulose can be expected at the temperature of 180°C (Steinbach et al., 2017). Antioxidant activity has been reported at least for xylo-oligosaccharide (hemicellulose model compounds) (Wu et al., 2019) and corn bran hemicellulose fragments (Ohta et al., 1994). However, without further structural characterization, any certainty is difficult to accomplish, and this poses a great opportunity for subsequent experimental studies.

All the tested concentrations of *Salix* spp. extracts and the commercial Salixin Organic Extract and Powder were effective against the non-enveloped CVA9. Enteroviruses such as CVA9 cause many acute and chronic infections on a yearly basis (Marjomäki et al., 2015). To the best of our knowledge, no previous studies have investigated the effectiveness of willow extracts directly against non-enveloped enteroviruses. However, effectiveness of natural compounds found in *Salix* spp. has been established for viruses sealed with lipid envelopes. For example, a review by Grienke et al. (2012) covered several studies performed between 2000 and 2011 on natural products specifically targeting the viral surface protein neuraminidase of influenza virus. They showed that the majority of the active natural products with the desired activity belonged to

flavonoids, while (oligo)stilbenes, coumarins, and diarylheptanoids exhibited lower activity (Grienke et al., 2012). Liu et al. (2008) found that the activity for flavonoids was highest in auronones followed by flavon(ol)es, isoflavones, and flavan(ol)es and flavan(ol)es, in this order, and that the C4'-OH, C7-OH, C4-O double bond, and C2-C3 double bond functionalities were essential for the inhibitory activity of these compounds.

Here, we showed that salicin, picein, salicylic acid, and triandrin were not responsible for the antibacterial and antiviral activities detected, at least not alone. *Salix* spp. clone extracts are highly antibacterial even at low concentrations and show similar luminescence light reduction as the bark extracts from Norway spruce [*Picea abies* (L.) H. Karst] found in Välimaa et al. (2020). Salicinoids are not present in spruce, and they are unstable and prone to decomposition especially with higher molecular masses (Julkunen-Tiitto and Sorsa, 2001; Ruuhola and Julkunen-Tiitto, 2003). This could indicate that other secondary metabolites, such as tannins, could affect bactericidal efficacy. In addition, none of the reference compounds showed antiviral activity against non-enveloped CVA9. This indicated that the presence of bioactive compounds other than the reference compounds tested here (e.g., picein and triandrin) is responsible for the antiviral activity of the *Salix* spp. extracts (cf. Dou et al., 2021). One interesting option for future studies is the tannins, which are likely to be found in the willow bark water extracts and have recently been associated with antiviral efficacies (e.g., Vilhelmova-Ilieva et al., 2019; Fraga-Corral et al., 2021). Contradictory results and hypotheses exist on whether polyphenols influence the overall bioactive efficacy of willow extracts (Khayyal et al., 2005; Nahrstedt et al., 2007; Antoniadou et al., 2021). Therefore, more research is needed to achieve any certainty regarding their effects on the bioactivities of willow extracts. However, extracts containing a mixture of willow compounds could also have synergistic effects. Similar observations were made by Shara and Stohs (2015), who concluded that the typical effective dosage of aspirin is twice that of salicin needed in willow bark extract, probably because of the presence of beneficial polyphenols and flavonoids in the bark extract.

The results obtained in the present study demonstrate the excellent antiviral, antioxidant, and antibacterial effects of *Salix* spp. bark extracts. Pearson's linear correlation coefficient absolute values (Table 2) indicated either a strong or moderate relationship between *E. coli* and *S. aureus* antibacterial test results (60%) for the *Salix* clones, both bacteria with enterovirus results (*E. coli* vs. entero: 67%; *S. aureus* vs. entero: 28%), ORAC and FRAP values (76%), ORAC and total phenol content (84%), FRAP and total phenol content (85%), and *E. coli* and FRAP test results (75%). A strong relationship was obtained between *E. coli* and ORAC test values (61%), *E. coli* and total phenol results (67%), *S. aureus* and ORAC values (41%), and *S. aureus* and FRAP values (53%). A moderate relationship was obtained for *S. aureus* and total phenol content (38%) and for enterovirus results and FRAP values (47%) as well as enterovirus and total phenol content results (45%), and enterovirus and ORAC results (36%).

TABLE 2 | Pearson's correlation coefficients for the different bioactivity tests. Values 0.70–0.99 indicate a very strong relationship, values 0.40–0.69 indicate a strong relationship, values 0.30–0.39 indicate a mediocre relationship, values 0.20–0.29 indicate a weak relationship, and values 0.01–0.19 indicate no or negligible relationship. The upper part of the matrix indicates the *p*-values for the data determined by a two-tailed *t*-test (*n* = 16 for ORAC, FRAP, and Phenols tests, *n* = 17 for the *E. coli*, *S. aureus*, and Enterovirus test). Most of the *p*-values are below 0.05, which indicates significant differences.

	ORAC	<i>E. coli</i>	FRAP	Phenols	<i>S. aureus</i>	Enterovirus
ORAC	1	<0.05	<0.001	<0.001	0.113	0.167
<i>E. coli</i>	0.61	1	<0.001	<0.05	<0.05	<0.05
FRAP	0.76	0.75	1	<0.001	<0.05	0.065
Phenols	0.84	0.67	0.85	1	0.146	<0.01
<i>S. aureus</i>	0.41	0.60	0.53	0.38	1	0.28
Enterovirus	0.36	0.67	0.47	0.45	0.28	1

Fungal infections and fungal resistance to currently available antifungal drugs are increasing globally. Fungal infections, as well as their prevention and treatment, also remain largely understudied compared to other infectious diseases (Brown et al., 2012). Novel and safe antifungal drugs and agents are needed for currently less common fungi, such as the recently reported Zygomycetes causing rare and life-threatening mucormycosis infection in patients with COVID-19 (do Monte Junior et al., 2020). For long, Amphotericin B was the only antifungal medication available, and only during the past three decades has a wider spectrum of antifungal agents (e.g., triazoles and echinocandin antifungals) become available (Spanakis et al., 2006). Promising antifungal compounds, including phenolic compounds, have been found in plants (Arif et al., 2008). To the best of our knowledge, no previous studies have investigated the efficacy of willow extracts against fungi and yeasts. Unfortunately, the *Salix* spp. bark extracts tested here showed no antifungal or yeastcidal activity. The only sample with putative mild activity was the commercial Salixin Organic Extract, which showed a minor inhibition of both *C. albicans* and *A. brasiliensis* when considerably concentrated.

The bioactivities of the domestic (1–12) and commercial clone extracts (13–16) were surprisingly similar despite the differences in harvesting time, age, and growing conditions of these two groups. However, the grouped commercial clone extracts showed significantly lower antioxidant (in ORAC and FRAP) and antimicrobial (*E. coli*) activities, as well as lower total phenolic capacity (Folin-Ciocalteu), than *S. phylicifolia*. In the H₂O₂ scavenging tests, the commercial clones showed significantly lower activities than all the other groups, and the FRAP test evidenced lower activity than that of *S. myrsinifolia*. The native clones had already reached the stage of vegetative bud burst, whereas the commercial clones had no visible signs of vegetative growth, indicating that they were in a state of dormancy (Saska and Kuzovkina 2010). According to Förster et al. (2008), the number of secondary metabolites in the bark of willow clones decreased during the vegetative season from March to July. The domestic clones were 1 year younger than the commercial clones. Nissinen et al. (2018) found only a minor decrease in the stem phenolic concentrations of *S. myrsinifolia* during a 7-year study period. Instead, Tahvanainen et al. (1985a) showed a significantly higher concentration of phenolic glycosides in juvenile willow twigs than in mature twigs. In the present study, the domestic clones grew in small polystyrene containers and restricted

conditions, which could have resulted in higher amounts of polyphenolic defense and resistance compounds. According to Paunonen et al. (2009), polythene mulching and fertilization increased the yield of foliar salicylates because of the enhanced leaf biomass, but not the salicylate concentration in *S. myrsinifolia* clones. Furthermore, they noted that the yields and concentrations of leaf phenolics seemed to be more influenced by the clone than by the cultivation method. According to Glynn et al. (2004), drought treatment did not affect the foliar phenolic concentrations of willow genotypes.

Small differences were observed in the antibacterial tests, where commercial clones 14–16 seemed to have a somewhat lower effect in *E. coli* and commercial clone 14 seemed to have a lower effect in *S. aureus*. The commercial clones 13, 15, and 16 also showed almost no H₂O₂ scavenging activity in the antioxidant tests. The total phenol content and the composition of phenolic compounds vary widely among willow species, and the composition of leaf phenolic glycosides is species-specific (Julkunen-Tiitto, 1986). *S. myrsinifolia* (former *Salix nigricans* Sm.) clearly differed from other native species in terms of high phenolic glycoside content in leaves, mostly due to salicortin (Tahvanainen et al., 1985b), and so did the introduced species *S. dasyclados*. According to Julkunen-Tiitto (1986), *S. phylicifolia* leaves contained the highest total phenolic content among the 15 Salicaceae species studied, with more than 15% of dry weight, whereas *S. myrsinifolia* leaves had the lowest total phenolic content. In the present study, four clones (clones 4–7) with the highest total phenol content in the bark extracts were identified as *S. phylicifolia*. In contrast, *S. myrsinifolia* bark and leaves were characterized by higher amounts of phenolic glycosides such as salicylates (Julkunen-Tiitto, 1985, 1986), whereas the low content of phenolic glycosides was typical of *S. phylicifolia* and *S. viminalis* L. The latter is the main species in the ancestry of the commercial clones examined here, showing slightly lower antibacterial effects. Clonal variation exists within species; for example, Paunonen et al. (2009) showed highly variable responses of *S. myrsinifolia* clones to fertilization and mulching treatments, and thus to the yield of foliar phenolics, and they concluded that willow cultivation for the herbal industry should be based on correct clone selection.

Bark extracts of *S. myrsinifolia* × *phylicifolia* hybrids (clones 8–10) did not statistically differ from other native clones in terms of bioactivity, except in the H₂O₂ scavenging antioxidant test, when clones 7 and 14 were removed. There was also a statistically

significant difference between the higher inhibition-% values of *S. myrsinifolia* clone extracts compared to native hybrid extract values ($p = 0.049$). According to Julkunen-Tiitto (1986), these native hybrids resemble *S. phylicifolia* on the basis of total phenolics in leaves, but *S. myrsinifolia* by their foliar glycosidic composition (Julkunen-Tiitto, 1986). In Hallgren et al. (2003), F1-hybrids of *S. caprea* L. and *S. repens* L. were intermediate between their parental species in terms of foliar secondary metabolites and herbivore resistance but increased hybridization decreased this resistance. In the present study, clones 11 and 12 were hybrids of three species from controlled crossings, i.e., female (*S. myrsinifolia* \times *phylicifolia*) \times male *S. dasyclados*. In particular, the bark extract of clone 11 showed a somewhat lower total phenolic content and weaker antibacterial activity than the bark extracts of native species. In fact, all commercial clones are also outcomes of multiple crossings between different willow species, with *S. viminalis* being the most used ancestor, and characterized by low content of phenolic glycosides (Julkunen-Tiitto, 1985, 1986). Thus, both of these reasons may explain the significantly lower antibacterial effects of the commercial clones. Another possible cause of the difference in the activities of artificial hybrids and commercial clones could be the difference in the bioactive polyphenol compound composition or quantity, which would be interesting to study in the future. Further interesting questions arise, whether the beneficial antioxidant and antimicrobial activities and total phenolic capacity of *S. phylicifolia* could be increased by intraspecific crossings, or whether they are inevitably decreased by repeated species hybridization when, for instance, breeding for higher yield.

This study verified the antimicrobial potential of the willow bark biomass extracts. Antimicrobial and antiviral protection are required for a variety of industrial applications. For example, it has been estimated that by the year 2027, the antimicrobial packaging market would globally reach the value of 13.28 billion pounds (VMR Verified Market Research, 2020). It is noteworthy that viruses such as noroviruses, which cause the nasty outbreaks of stomach infection, are non-enveloped viruses such as the enterovirus CVA9 studied here. Non-enveloped viruses are much more difficult to decontaminate than enveloped viruses because of the tight protein package around the virus genome instead of the lipid envelope, which is more vulnerable to breakage. In addition to noroviruses, enteroviruses transmit easily through surfaces and cause acute and chronic infections. Currently, there are no effective and safe antivirals that directly act on virus particles. *Salix* spp. extracts offer a safe and affordable solution to combat these stable viruses. Antiviral and antimicrobial compounds from renewable willow could also replace products that may not be readily biodegradable.

For obtaining valuable phenolic compounds from willow bark, one of the limiting factors has been laborious debarking. In the present study, we showed that steaming can be used for fast and efficient debarking, while only some antioxidant potential is lost in the process. Thus, this method has potential at industrial scale.

In the European Union, plantations of short rotation coppice (SRC) willows have been established in the past, primarily for energy use purposes. Willows could offer advantages over

mainstream commercial conifers owing to their fast growth and high productivity. SRC willows may also provide environmental benefits in terms of carbon sequestration when grown on marginal land, such as abandoned agricultural land or peatland (Rytter et al., 2015). For well-managed willows growing at the underappreciated peatland, the annual yield can reach up to >12.3 oven dry ton (odt)/ha, which exceeds about 8%–30% of the yield obtained with the domestic natural forest species (i.e., birch and grey alder) on the same land (Hytönen and Saarsalmi, 2009). In Finland, bioenergy-targeted projects in the 1980s produced knowledge on the hybridization, cultivation, and management of SRC willows for energy use. High biomass yields are achievable if cultivation is based on well-adapted, selected clones, and biotic and abiotic damages are avoided (Volk et al., 2004; Verwijst et al., 2013). This knowledge is a valuable foundation for creating willow biorefinery approaches for high added value. The comprehensive and optimized utilization of willow lignocellulosic biomass will promote sustainability and carbon neutrality, but requires further research, for example, on the life-cycle assessment of the production and processing value chain (cf. Rasi et al., 2019).

In conclusion, the present study provides novel information on the antioxidant, antibacterial, and antiviral properties of polyphenolic bark extracts of SRC willows well adapted to the Finnish growing environment, by using scalable green extraction techniques. We found that all the tested concentrations of *Salix* spp. extracts were effective against the non-enveloped enterovirus CVA9 as well as *E. coli* and *S. aureus* strains. However, there seemed to be more variation between the clones in their antioxidant activities determined by ORAC, FRAP, and H_2O_2 scavenging abilities. No marked efficacy was detected in the antifungal or yeasticidal tests. When clone extracts were grouped, *S. phylicifolia* clones showed the most promising antioxidant and antibacterial activities with significant differences when compared to commercial and artificial clones. This can partly be caused by the effect of stronger hybridization; however, more studies are needed to examine the possible effects of compound composition and content of the extracts. We also showed that salicin, picein, salicylic acid, and triandrin are not responsible for the antibacterial and antiviral activities detected here, at least not alone. Instead, other compounds of interest, such as polyphenols, or synergistic effects between the compounds, are likely to cause the detected efficacies. We also demonstrated for the first time that steam debarking is a promising, less-laborious method for the efficient separation of bark from wood (harvested in the spring season), with only minor effects on the antioxidant properties of bark. This method promotes the cascade use of willow biomass, where the debarked wood can be used for other purposes. Our findings will potentially lead to scientific breakthroughs given that the studied crude extracts with promising mixtures of components are highly effective against the stable non-enveloped viruses that cause nasty acute and chronic infections. Further investigations and development of such antiviral solutions for enveloped viruses are topics for our next studies. Biochemicals obtained from tree bark biomass and side products of biorefinery approaches have potential for various

applications (e.g., health promotion, cosmetics, pharmaceuticals, packaging, coatings, other functional materials, and surfaces). Willow, as a short-rotation coppice species with a fast growth rate and high yield on marginal lands, presents a promising alternative for the currently most common commercial tree species in Finland.

DATA AVAILABILITY STATEMENT

The original contributions presented in the study are included in the article/**Supplementary Material**. Further inquiries can be directed to the corresponding author.

AUTHOR CONTRIBUTIONS

Conceptualization: AV-A, PK, TJ, and VM; Data curation: DR, JL, JT, PK, RL, and TS; Formal analysis: AV-A, DR, JD, JT, PK, and RL; Funding acquisition and Resources: TJ and VM; Investigation: DR, JD, JT, and PK; Methodology: JD, JT, PK, RL, TS, and VM; Project administration and Supervision: TJ and VM; Validation: AV-A, DR, JT, PK, RL, and TS; Visualization: DR, JT, PK, and TS; Writing—original draft: AV-A, DR, JL, JT, PK, RL, TJ, and VM; Writing—review and editing: all authors.

FUNDING

This work was supported by Business Finland corona-co-creation funding for the project Antiviral Fibers—pilot with extracts from Finnish forests (grant: 40699/31/2020). This study was also

funded by the Natural Resources Institute Finland's strategic research funding to the projects "More, faster, higher quality: potential of short-rotation aspen and willow biomass for novel products in bioeconomy" (AspenWill) and "Added value potential of new and under-utilized fibre sources in Finnish value networks of green bioeconomy: prefeasibility, prototyping, and market acceptance" (VALUEPOT). In addition, Academy of Finland has supported this study *via* the project "Antivirals from Forest Biomasses: Structure, Function, and Applicability" (grant: 342250). Work was also funded by Jane and Aatos Erkko Foundation: Novel probes for discovering antivirals.

ACKNOWLEDGMENTS

We thank Elvi Pääkkönen, Esa Ek, Pauli Karppinen, Kalle Kaipainen, Carita Karenius, Katri Leino, Tuija Hytönen, Hanna Leppälamm, Anneli Käenmäki, and Eeva Pihlajaviita for skillful laboratory and field work. Markku Suutari (Carbons Finland Oy) is acknowledged for providing the research with Swedish commercial willow materials. Senior Curator Henry Väre is warmly acknowledged for the help with the willow identifications. The authors also thank Janne Kaseva for proficient help with the statistical analysis.

SUPPLEMENTARY MATERIAL

The Supplementary Material for this article can be found online at: <https://www.frontiersin.org/articles/10.3389/fbioe.2021.797939/full#supplementary-material>

REFERENCES

- Ainsworth, E. A., and Gillespie, K. M. (2007). Estimation of Total Phenolic Content and Other Oxidation Substrates in Plant Tissues Using Folin-Ciocalteu Reagent. *Nat. Protoc.* 2, 875–877. doi:10.1038/nprot.2007.102
- Antoniadou, K., Herz, C., Le, N. P. K., Mittermeier-Kleßinger, V. K., Förster, N., Zander, M., et al. (2021). Identification of Salicylates in Willow Bark (*Salix Cortex*) for Targeting Peripheral Inflammation. *Ijms* 22, 11138. doi:10.3390/ijms222011138
- Arif, T., Bhosale, J. D., Kumar, N., Mandal, T. K., Bendre, R. S., Lavekar, G. S., et al. (2009). Natural Products - Antifungal Agents Derived from Plants. *J. Asian Nat. Prod. Res.* 11, 621–638. doi:10.1080/10286020902942350
- Benzie, I. F. F., and Strain, J. J. (1996). The Ferric Reducing Ability of Plasma (FRAP) as a Measure of "Antioxidant Power": The FRAP Assay. *Anal. Biochem.* 239, 70–76. doi:10.1006/abio.1996.0292
- Bobleter, O. (1994). Hydrothermal Degradation of Polymers Derived from Plants. *Prog. Polym. Sci.* 19, 797–841. doi:10.1016/0079-6700(94)90033-7
- Boeckler, G. A., Gershenzon, J., and Unsicker, S. B. (2011). Phenolic Glycosides of the Salicaceae and Their Role as Anti-herbivore Defenses. *Phytochemistry* 72, 1497–1509. doi:10.1016/j.phytochem.2011.01.038
- Bounaama, A., Enayat, S., Ceyhan, M. S., Moulahoum, H., Djerdjouri, B., and Banerjee, S. (2016). Ethanolic Extract of Bark from *Salix aegyptiaca* Ameliorates 1,2-Dimethylhydrazine-Induced Colon Carcinogenesis in Mice by Reducing Oxidative Stress. *Nutr. Cancer* 68, 495–506. doi:10.1080/01635581.2016.1152379
- Brebu, M., and Vasile, C. (2010). Thermal Degradation of Lignin—A Review. *Cellul. Chem. Technol.* 44, 353.
- Brereton, N. J. B., Berthod, N., Lafleur, B., Pedneault, K., Pitre, F. E., and Labrecque, M. (2017). Extractable Phenolic Yield Variation in Five Cultivars of Mature Short Rotation Coppice Willow from Four Plantations in Quebec. *Ind. Crops Prod.* 97, 525–535. doi:10.1016/j.indcrop.2016.12.049
- Brown, G. D., Denning, D. W., and Levitz, S. M. (2012). Tackling Human Fungal Infections. *Science* 336, 647. doi:10.1126/science.1222236
- Christenhusz, M. J. M., Fay, M. F., and Chase, M. W. (2017). *Plants of the World*. KewChina: Kew Publishing Royal Botanic GardensThe University of Chicago Press.
- Chrubasik, S., Eisenberg, E., Balan, E., Weinberger, T., Luzzati, R., and Conrad, C. (2000). Treatment of Low Back Pain Exacerbations with Willow Bark Extract: a Randomized Double-Blind Study. *Am. J. Med.* 109, 9–14. doi:10.1016/S0002-9343(00)00442-3
- DIN EN 1275 (2006). *Chemical Disinfectants and Antiseptics - Quantitative Suspension Test for the Evaluation of Basic Fungicidal or Basic Yeastcidal Activity of Chemical Disinfectants and Antiseptics - Test Method and Requirements*. (phase 1).
- Djomo, S. N., Kasmioui, O. E., and Ceulemans, R. (2011). Energy and Greenhouse Gas Balance of Bioenergy Production from poplar and Willow: a Review. *Glob. Change Biol. Bioenergy* 3, 181–197. doi:10.1111/j.1757-1707.2010.01073.x
- Dou, J., Galvis, L., Holopainen-Mantila, U., Reza, M., Tamminen, T., and Vuorinen, T. (2016). Morphology and Overall Chemical Characterization of Willow (*Salix* sp.) Inner Bark and Wood: Toward Controlled Deconstruction of Willow Biomass. *ACS Sustainable Chem. Eng.* 4, 3871–3876. doi:10.1021/acssuschemeng.6b00641
- Dou, J., Heinonen, J., Vuorinen, T., Xu, C., and Sainio, T. (2021). Chromatographic Recovery and Purification of Natural Phytochemicals from Underappreciated

- Willow Bark Water Extracts. *Separation Purif. Technology* 261, 118247. doi:10.1016/j.seppur.2020.118247
- Dou, J., Paltakari, J., Johansson, L.-S., and Vuorinen, T. (2019). Novel Insight into the Separation and Composite Utilization of Sclerenchyma Fiber Bundles of Willow Bark. *ACS Sustainable Chem. Eng.* 7, 2964–2970. doi:10.1021/acssuschemeng.8b04001
- Dou, J., Xu, W., Koivisto, J. J., Mobley, J. K., Padmakshan, D., Kögler, M., et al. (2018). Characteristics of Hot Water Extracts from the Bark of Cultivated Willow (*Salix* sp.). *ACS Sustainable Chem. Eng.* 6, 5566–5573. doi:10.1021/acssuschemeng.8b00498
- Durak, A., and Gawlik-Dziki, U. (2014). The Study of Interactions between Active Compounds of Coffee and Willow (*Salix*sp.) Bark Water Extract. *Biomed. Res. Int.* 2014, 1–11. doi:10.1155/2014/386953
- El-Shemy, H. A., Aboul-Enein, A. M., Aboul-Enein, K. M., and Fujita, K. (2007). Willow Leaves' Extracts Contain Anti-tumor Agents Effective against Three Cell Types. *PLoS One* 2 (1), e178. doi:10.1371/journal.pone.0000178
- Förster, N., Ulrichs, C., Zander, M., Kätzel, R., and Mewis, I. (2008). Influence of the Season on the Salicylate and Phenolic Glycoside Contents in the Bark of *Salix Daphnoides*, *Salix Pentandra*, and *Salix Purpurea*. *J. Appl. Bot. Food Qual.* 82, 99–102.
- Fraga-Corral, M., Otero, P., Echave, J., Garcia-Oliveira, P., Carpena, M., Jarboui, A., et al. (2021). By-Products of Agri-Food Industry as Tannin-Rich Sources: A Review of Tannins' Biological Activities and Their Potential for Valorization. *Foods* 10, 137. doi:10.3390/foods10010137
- Glynn, C., Rönnerberg-Wästljung, A.-C., Julkunen-Tiitto, R., and Weih, M. (2004). Willow Genotype, but Not Drought Treatment, Affects Foliar Phenolic Concentrations and Leaf-Beetle Resistance. *Entomologia Experimentalis et Applicata* 113, 1–14. doi:10.1111/j.0013-8703.2004.00199.x
- Grienke, U., Schmidtke, M., von Grafenstein, S., Kirchmair, J., Liedl, K. R., and Rollinger, J. M. (2012). Influenza Neuraminidase: a Druggable Target for Natural Products. *Nat. Prod. Rep.* 29, 11–36. doi:10.1039/C1NP00053E
- Gu, J., Guo, M., Zheng, L., Yin, X., Zhou, L., Fan, D., et al. (2021). Protective Effects of Lignin-Carbohydrate Complexes from Wheat Stalk against Bisphenol A Neurotoxicity in Zebrafish via Oxidative Stress. *Antioxidants* 10, 1640. doi:10.3390/antiox10101640
- Hallgren, P., Ikonen, A., Hjalten, J., and Roininen, H. (2003). Inheritance Patterns of Phenolics in F1, F2, and Back-Cross Hybrids of willows: Implications for Herbivore Responses to Hybrid Plants. *J. Chem. Ecol.* 29, 1143–1158. doi:10.1023/A:1023829506473
- Hazra, B., Biswas, S., and Mandal, N. (2008). Antioxidant and Free Radical Scavenging Activity of *Spondias Pinnata*. *BMC Complement. Altern. Med.* 8, 63. doi:10.1186/1472-6882-8-63
- Heiska, S., Tikkanen, O.-P., Rousi, M., and Julkunen-Tiitto, R. (2007). Bark Salicylates and Condensed Tannins Reduce Vole Browsing Amongst Cultivated Dark-Leaved willows (*Salix Myrsinifolia*). *Chemoecology* 17, 245–253. doi:10.1007/s00049-007-0385-9
- Hobisch, M. A., Phiri, J., Dou, J., Gane, P., Vuorinen, T., Bauer, W., et al. (2020). Willow Bark for Sustainable Energy Storage Systems. *Materials* 13, 1016. doi:10.3390/ma13041016
- Hou, J., Guo, Z., Liu, H., and Yin, T. (2017). Gender Effects on *Salix Suchowensis* Growth and wood Properties as Revealed by a Full-Sib Pedigree. *Can. J. Plant Sci.* 97, 594–600. doi:10.1139/cjps-2016-0153
- Huang, D., Ou, B., Hampsch-Woodill, M., Flanagan, J. A., and Prior, R. L. (2002). High-throughput Assay of Oxygen Radical Absorbance Capacity (ORAC) Using a Multichannel Liquid Handling System Coupled with a Microplate Fluorescence Reader in 96-well Format. *J. Agric. Food Chem.* 50, 4437–4444. doi:10.1021/jf0201529
- H. Väre, J. Saarinen, A. Kurtto, and L. Hämet-Ahti (Editors) (2021). *Suomen Puu-Ja Pensaskasvio [Woody Flora of Finland]*. third ed. (Helsinki: Publications of the Finnish Dendrological Society), 10.
- Hytönen, J., and Saarsalmi, A. (2009). Long-term Biomass Production and Nutrient Uptake of Birch, Alder and Willow Plantations on Cut-Away Peatland. *Biomass and Bioenergy* 33, 1197–1211. doi:10.1016/j.biombioe.2009.05.014
- Ikonen, A., Tahvanainen, J., and Roininen, H. (2002). Phenolic Secondary Compounds as Determinants of the Host Plant Preferences of the Leaf Beetle *Agelastica Alni*. *Chemoecology* 12, 125–131. doi:10.1007/s00012-002-8337-2
- Jiang, Z.-Y., Woollard, A. C. S., and Wolff, S. P. (1990). Hydrogen Peroxide Production during Experimental Protein Glycation. *FEBS Lett.* 268, 69–71. doi:10.1016/0014-5793(90)80974-N
- Julkunen-Tiitto, R. (1986). A Chemotaxonomic Survey of Phenolics in Leaves of Northern Salicaceae Species. *Phytochemistry* 25, 663–667. doi:10.1016/0031-9422(86)88020-7
- Julkunen-Tiitto, R. (1985). Chemotaxonomical Screening of Phenolic Glycosides in Northern Willow Twigs by Capillary Gas Chromatography. *J. Chromatogr. A* 324, 129–139. doi:10.1016/S0021-9673(01)81312-1
- Julkunen-Tiitto, R., and Sorsa, S. (2001). Testing the Effect of Drying Methods on Willow Flavonoids, Tannins and Salicylates. *J. Chem. Ecol.* 27, 779–789. doi:10.1023/A:1010358120482
- Julkunen-Tiitto, R., and Virjamo, V. (2017). "Biosynthesis and Roles of Salicaceae Salicylates," in *Plant Specialized Metabolism: Genomics, Biochemistry, and Biological Functions*. Editors G. Arimura and M. Maffei (Boca Raton: CRC Press), 65–83.
- Kammerer, B., Kahlich, R., Biegert, C., Gleiter, C. H., and Heide, L. (2005). HPLC-MS/MS Analysis of Willow Bark Extracts Contained in Pharmaceutical Preparations. *Phytochem. Anal.* 16, 470–478. doi:10.1002/pca.873
- Khayyal, M., El-Ghazaly, M., Abdallah, D., Okpanyi, S., Kelber, O., and Weiser, D. (2005). Mechanisms Involved in the Anti-inflammatory Effect of a Standardized Willow Bark Extract. *Arzneimittelforschung* 55, 677–687. doi:10.1055/s-0031-1296917
- Kilpeläinen, P., Leppänen, K., Spetz, P., Kitunen, V., Ilvesniemi, H., Pranovich, A., et al. (2012). BIOREFINERY. Pressurised Hot Water Extraction of Acetylated Xylan from Birch Sawdust. *Pulp Pap. Res. J.* 27, 680–688. doi:10.3183/npprj-2012-27-04-p680-688
- Kilpeläinen, P. O., Hautala, S. S., Byman, O. O., Tanner, L. J., Korpinen, R. I., Lillandt, M. K.-J., et al. (2014). Pressurized Hot Water Flow-Through Extraction System Scale up from the Laboratory to the Pilot Scale. *Green. Chem.* 16, 3186–3194. doi:10.1039/C4GC00274A
- Krzyżaniak, M., Stolarski, M. J., Szczukowski, S., and Tworowski, J. (2016). Life Cycle Assessment of New Willow Cultivars Grown as Feedstock for Integrated Biorefineries. *Bioenerg. Res.* 9, 224–238. doi:10.1007/s12155-015-9681-3
- Lavola, A., Maukonen, M., and Julkunen-Tiitto, R. (2018). Variability in the Composition of Phenolic Compounds in winter-dormant *Salix Pyrolifolia* in Relation to Plant Part and Age. *Phytochemistry* 153, 102–110. doi:10.1016/j.phytochem.2018.05.021
- Liu, A.-L., Wang, H.-D., Lee, S. M., Wang, Y.-T., and Du, G.-H. (2008). Structure-activity Relationship of Flavonoids as Influenza Virus Neuraminidase Inhibitors and Their *In Vitro* Anti-viral Activities. *Bioorg. Med. Chem.* 16, 7141–7147. doi:10.1016/j.bmc.2008.06.049
- Malterud, K. E., Bremnes, T. E., Faegri, A., Moe, T., Dugstad, E. K. S., Anthonsen, T., et al. (1985). Flavonoids from the wood of *Salix Caprea* as Inhibitors of wood-destroying Fungi. *J. Nat. Prod.* 48, 559–563. doi:10.1021/np50040a007
- Marjomäki, V., Turkki, P., and Huttunen, M. (2015). Infectious Entry Pathway of Enterovirus B Species. *Viruses* 7, 6387–6399. doi:10.3390/v7122945
- Monte Junior, E. S. d., Santos, M. E. L. d., Ribeiro, I. B., Luz, G. d. O., Baba, E. R., Hirsch, B. S., et al. (2020). Rare and Fatal Gastrointestinal Mucormycosis (Zygomycosis) in a COVID-19 Patient: a Case Report. *Clin. Endosc.* 53, 746–749. doi:10.5946/ce.2020.180
- Mostafa, I., Abbas, H. A., Ashour, M. L., Yasri, A., El-Shazly, A. M., Wink, M., et al. (2020). Polyphenols from *Salix Tetrasperma* Impair Virulence and Inhibit Quorum Sensing of *Pseudomonas aeruginosa*. *Molecules* 25, 1341. doi:10.3390/molecules25061341
- Nährstedt, A., Schmidt, M., Jäggi, R., Metz, J., and Khayyal, M. T. (2007). Willow Bark Extract: the Contribution of Polyphenols to the Overall Effect. *Wien. Med. Wochenschr.* 157, 348–351. doi:10.1007/s10354-007-0437-3
- Nassar, M. M., and MacKay, G. D. M. (1984). Mechanism of thermal Decomposition of Lignin. *Wood Fiber Sci.* 16, 441–453.
- Nissinen, K., Virjamo, V., Mehtätalo, L., Lavola, A., Valtonen, A., Nybakken, L., et al. (2018). A Seven-Year Study of Phenolic Concentrations of the Dioecious *Salix Myrsinifolia*. *J. Chem. Ecol.* 44, 416–430. doi:10.1007/s10886-018-0942-4
- Noletto-Dias, C., Harflett, C., Beale, M. H., and Ward, J. L. (2020). Sulfated Flavanones and Dihydroflavonols from Willow. *Phytochemistry Lett.* 35, 88–93. doi:10.1016/j.phytol.2019.11.008

- Noleto-Dias, C., Ward, J. L., Bellisai, A., Lomax, C., and Beale, M. H. (2018). Salicin-7-sulfate: A New Salicinoid from Willow and Implications for Herbal Medicine. *Fitoterapia* 127, 166–172. doi:10.1016/j.fitote.2018.02.009
- Noleto-Dias, C., Wu, Y., Bellisai, A., Macalpine, W., Beale, M., and Ward, J. (2019). Phenylalkanoic Glycosides (Non-salicinoids) from Wood Chips of *Salix Triandra* × *Dasyclados* Hybrid Willow. *Molecules* 24, 1152. doi:10.3390/molecules24061152
- Ohta, T., Yamasaki, S., Egashira, Y., and Sanada, H. (1994). Antioxidative Activity of Corn Bran Hemicellulose Fragments. *J. Agric. Food Chem.* 42, 653–656. doi:10.1021/jf00039a010
- Parajuli, R., Knudsen, M. T., and Dalgaard, T. (2015). Multi-criteria Assessment of Yellow, green, and Woody Biomasses: Pre-screening of Potential Biomasses as Feedstocks for Biorefineries. *Biofuels, Bioprod. Bioref.* 9, 545–566. doi:10.1002/bbb.1567
- Paunonen, R., Julkunen-Tiitto, R., Tegelberg, R., Rousi, M., and Heiska, S. (2009). Salicylate and Biomass Yield, and Leaf Phenolics of Dark-Leaved Willow (*Salix Myrsinifolia* Salisb.) Clones under Different Cultivation Methods after the Second Cultivation Cycle. *Ind. Crops Prod.* 29, 261–268. doi:10.1016/j.indcrop.2008.05.009
- Phiri, J., Dou, J., Vuorinen, T., Gane, P. A. C., and Maloney, T. C. (2019). Highly Porous Willow Wood-Derived Activated Carbon for High-Performance Supercapacitor Electrodes. *ACS Omega* 4, 18108–18117. doi:10.1021/acsomega.9b01977
- Piątczak, E., Dybowska, M., Pluciennik, E., Kośla, K., Kolniak-Ostek, J., and Kalinowska-Lis, U. (2020). Identification and Accumulation of Phenolic Compounds in the Leaves and Bark of *Salix alba* (L.) and Their Biological Potential. *Biomolecules* 10, 1391. doi:10.3390/biom10101391
- Poolman, J. T., and Anderson, A. S. (2018). *Escherichia coli* and *Staphylococcus Aureus*: Leading Bacterial Pathogens of Healthcare Associated Infections and Bacteremia in Older-Age Populations. *Expert Rev. Vaccin.* 17, 607–618. doi:10.1080/14760584.2018.1488590
- Prior, R. L., Hoang, H., Gu, L., Wu, X., Bacchiocca, M., Howard, L., et al. (2003). Assays for Hydrophilic and Lipophilic Antioxidant Capacity (Oxygen Radical Absorbance Capacity (ORACFL)) of Plasma and Other Biological and Food Samples. *J. Agric. Food Chem.* 51, 3273–3279. doi:10.1021/jf0262256
- Quosdorf, S., Schuetz, A., and Kolodziej, H. (2017). Different Inhibitory Potencies of Osetamivir Carboxylate, Zanamivir, and Several Tannins on Bacterial and Viral Neuraminidases as Assessed in a Cell-free Fluorescence-Based Enzyme Inhibition Assay. *Molecules* 22, 1989. doi:10.3390/molecules22111989
- Ramos, P. A. B., Moreirinha, C., Silva, S., Costa, E. M., Veiga, M., Coscueta, E., et al. (2019). The Health-Promoting Potential of *Salix* Spp. Bark Polar Extracts: Key Insights on Phenolic Composition and *In Vitro* Bioactivity and Biocompatibility. *Antioxidants* 8, 609. doi:10.3390/antiox8120609
- Rasa, K., Viherä-Aarnio, A., Rytönen, P., Hyväluoma, J., Kaseva, J., Suhonen, H., et al. (2021). Quantitative Analysis of Feedstock Structural Properties Can Help to Produce Willow Biochar with Homogeneous Pore System. *Ind. Crops Prod.* 166, 113475. doi:10.1016/j.indcrop.2021.113475
- Rasi, S., Kilpeläinen, P., Rasa, K., Korpinen, R., Raitanen, J.-E., Vainio, M., et al. (2019). Cascade Processing of Softwood Bark with Hot Water Extraction, Pyrolysis and Anaerobic Digestion. *Bioresour. Technology* 292, 121893. doi:10.1016/j.biortech.2019.121893
- Ruokolainen, V., Domanska, A., Laajala, M., Pelliccia, M., Butcher, S. J., and Marjomäki, V. (2019). Extracellular Albumin and Endosomal Ions Prime Enterovirus Particles for Uncoating that Can Be Prevented by Fatty Acid Saturation. *J. Virol.* 93, e00599–19. doi:10.1128/JVI.00599-19
- Ruuhola, T., and Julkunen-Tiitto, R. (2003). Trade-off between Synthesis of Salicylates and Growth of Micropropagated *Salix Pentandra*. *J. Chem. Ecol.* 29, 1565–1588. doi:10.1023/A:1024266612585
- Rytter, R.-M., Rytter, L., and Högbom, L. (2015). Carbon Sequestration in Willow (*Salix* spp.) Plantations on Former Arable Land Estimated by Repeated Field Sampling and C Budget Calculation. *Biomass and Bioenergy* 83, 483–492. doi:10.1016/j.biombioe.2015.10.009
- Saracila, M., Tabuc, C., Panaite, T. D., Papuc, C. P., Olteanu, M., and Criste, R. D. (2018). Effect of the Dietary Willow Bark Extract (*Salix Alba*) on the Caecal Microbial Population of Broilers (14-28 Days) Reared at 32°C. *Life Agriculture* Conf. Proc. 1 (1), 155–161. doi:10.2478/alife-2018-0023
- Saska, M. M., and Kuzovkina, Y. A. (2010). Phenological Stages of Willow (*Salix*). *Ann. Appl. Biol.* 156, 431–437. doi:10.1111/j.1744-7348.2010.00400.x
- Shara, M., and Stohs, S. J. (2015). Efficacy and Safety of White Willow Bark (*Salix alba*) Extracts. *Phytother. Res.* 29, 1112–1116. doi:10.1002/ptr.5377
- Singh, D. P., Moore, C. A., Gilliland, A., and Carr, J. P. (2004). Activation of Multiple Antiviral Defence Mechanisms by Salicylic Acid. *Mol. Plant Pathol.* 5, 57–63. doi:10.1111/j.1364-3703.2004.00203.x
- Singleton, V. L., Orthofer, R., and Lamuela-Raventós, R. M. (1999). [14] Analysis of Total Phenols and Other Oxidation Substrates and Antioxidants by Means of Folin-Ciocalteu Reagent. *Meth. Enzymol.* 299, 152–178. doi:10.1016/S0076-6879(99)90017-1
- Singleton, V. L., and Rossi, J. A., Jr. (1965). Colorimetry of Total Phenolics with Phosphomolybdic-Phosphotungstic Acid Reagents. *Am. J. Enol. Vitic.* 16, 144–158. doi:10.2307/3006717
- Spanakis, E. K., Aperis, G., and Mylonakis, E. (2006). Reviews of Anti-infective Agents: New Agents for the Treatment of Fungal Infections: Clinical Efficacy and Gaps in Coverage. *Clin. Infect. Dis.* 43, 1060–1068. doi:10.1086/507891
- Steinbach, D., Kruse, A., and Sauer, J. (2017). Pretreatment Technologies of Lignocellulosic Biomass in Water in View of Furfural and 5-hydroxymethylfurfural Production- A Review. *Biomass Conv. Bioref.* 7, 247–274. doi:10.1007/s13399-017-0243-0
- Tahvanainen, J., Helle, E., Julkunen-Tiitto, R., and Lavola, A. (1985a). Phenolic Compounds of Willow Bark as Deterrents against Feeding by Mountain Hare. *Oecologia* 65, 319–323. doi:10.1007/bf00378905
- Tahvanainen, J., Julkunen-Tiitto, R., Kettunen, J., and Lavola, A. (1985b). Phenolic Glycosides Govern the Food Selection Pattern of Willow Feeding Leaf Beetles. *Oecologia* 67, 52–56. doi:10.1007/bf00378451
- Tawfeek, N., Mahmoud, M. F., Hamdan, D. I., Sobeh, M., Farrag, N., Wink, M., et al. (2021). Phytochemistry, Pharmacology and Medicinal Uses of Plants of the Genus *Salix*: An Updated Review. *Front. Pharmacol.* 12, 50. doi:10.3389/fphar.2021.593856
- Tienaho, J., Karonen, M., Muilu-Mäkelä, R., Kaseva, J., De Pedro, N., Vicente, F., et al. (2020). Bioactive Properties of the Aqueous Extracts of Endophytic Fungi Associated with Scots Pine (*Pinus Sylvestris*) Roots. *Planta Med.* 86, 1009–1024. doi:10.1055/a-1185-4437
- Tienaho, J., Sarjala, T., Franzén, R., and Karp, M. (2015). Method with High-Throughput Screening Potential for Antioxidative Substances Using *Escherichia coli* Biosensor katG⁺lux. *J. Microbiol. Methods* 118, 78–80. doi:10.1016/j.mimet.2015.08.018
- Tienaho, J., Silvan, N., Muilu-Mäkelä, R., Kilpeläinen, P., Poikulainen, E., and Sarjala, T. (2021). Ultraviolet Absorbance of *Sphagnum Magellanicum*, *S. Fallax* and *S. Fuscum* Extracts with Seasonal and Species-specific Variation. *Photochem. Photobiol. Sci.* 20, 379–389. doi:10.1007/s43630-021-00026-w
- Tienaho, J. (2020). Utilizing Nordic Forest Plant and Fungi Extracts: Bioactivity Assessment with Bacterial Whole-Cell Biosensors. Academic dissertation. . <https://trepo.tuni.fi/handle/10024/120296>.
- Tyskiewicz, K., Konkol, M., Kowalski, R., Rój, E., Warmiński, K., Krzyżaniak, M., et al. (2019). Characterization of Bioactive Compounds in the Biomass of Black Locust, poplar and Willow. *Trees* 33, 1235–1263. doi:10.1007/s00468-019-01837-2
- Välilä, A.-L., Raitanen, J.-E., Tienaho, J., Sarjala, T., Nakayama, E., Korpinen, R., et al. (2020). Enhancement of Norway spruce Bark Side-Streams: Modification of Bioactive and Protective Properties of Stilbenoid-Rich Extracts by UVA-Irradiation. *Ind. Crops Prod.* 145, 112150. doi:10.1016/j.indcrop.2020.112150
- Verwijst, T., Lundkvist, A., Edelfeldt, S., and Albertsson, J. (2013). “Development of Sustainable Willow Short Rotation Forestry in Northern Europe,” in *Biomass Now-Sustainable Growth and Use*. Editor M. D. Matovic (London: IntechOpen), 479–502. doi:10.5772/55072
- Vesterlund, S., Paltta, J., Lauková, A., Karp, M., and Ouwehand, A. C. (2004). Rapid Screening Method for the Detection of Antimicrobial Substances. *J. Microbiol. Methods* 57, 23–31. doi:10.1016/j.mimet.2003.11.01410.1016/j.mimet.2003.11.014
- Vilhelmova-Ilieva, N., S. Galabov, A., and Mileva, M. (2019). “Tannins as Antiviral Agents,” in *Tannins-Structural Properties, Biological Properties and Current Knowledge*. Editor A. Aires (London: IntechOpen Limited). doi:10.5772/intechopen.86490
- Vlachojannis, J. E., Cameron, M., and Chrubasik, S. (2009). A Systematic Review on the Effectiveness of Willow Bark for Musculoskeletal Pain. *Phytother. Res.* 23, 897–900. doi:10.1002/ptr.2747

- VMR, Verified Market Research (2020). Global Antimicrobial Packaging Market. <https://www.verifiedmarketresearch.com/product/antimicrobial-packaging-market/> (accessed May 19, 2021).
- Volk, T. A., Verwijst, T., Tharakan, P. J., Abrahamson, L. P., and White, E. H. (2004). Growing Fuel: a Sustainability Assessment of Willow Biomass Crops. *Front. Ecol. Environ.* 2, 411–418. doi:10.1890/1540-9295(2004)002[0411: gfasao]2.0.co;2
- Wang, R., Zheng, L., Xu, Q., Xu, L., Wang, D., Li, J., et al. (2021). Unveiling the Structural Properties of Water-Soluble Lignin from Gramineous Biomass by Autohydrolysis and its Functionality as a Bioactivator (Anti-inflammatory and Antioxidative). *Int. J. Biol. Macromolecules* 191, 1087–1095. doi:10.1016/j.ijbiomac.2021.09.124
- Ward, J. L., Wu, Y., Harflett, C., Onafuye, H., Corol, D., Lomax, C., et al. (2020). Miyabeacin: A New Cyclodimer Presents a Potential Role for Willow in Cancer Therapy. *Sci. Rep.* 10, 6477. doi:10.1038/s41598-020-63349-1
- Wood, J. N. (2015). From Plant Extract to Molecular Panacea: a Commentary on Stone (1763) 'An Account of the success of the Bark of the Willow in the Cure of the Agues'. *Phil. Trans. R. Soc. B* 370, 20140317. doi:10.1098/rstb.2014.0317
- Wu, F., Jia, X., Yin, L., Cheng, Y., Miao, Y., and Zhang, X. (2019). The Effect of Hemicellulose and Lignin on Properties of Polysaccharides in *Lentinus Edodes* and Their Antioxidant Evaluation. *Molecules* 24, 1834. doi:10.3390/molecules24091834
- Wu, Y., Dobermann, D., Beale, M. H., and Ward, J. L. (2016). Acutifoliside, a Novel Benzoic Acid Glycoside from *Salix Acutifolia*. *Nat. Product. Res.* 30, 1731–1739. doi:10.1080/14786419.2015.1137571
- Yan, B., Chen, Z. S., Hu, Y., and Yong, Q. (2021). Insight in the Recent Application of Polyphenols from Biomass. *Front. Bioeng. Biotechnol.* 9. doi:10.3389/fbioe.2021.753898
- Zheng, L., Lu, G., Pei, W., Yan, W., Li, Y., Zhang, L., et al. (2021). Understanding the Relationship between the Structural Properties of Lignin and Their Biological Activities. *Int. J. Biol. Macromolecules* 190, 291–300. doi:10.1016/j.ijbiomac.2021.08.168

Conflict of Interest: The authors declare that the research was conducted in the absence of any commercial or financial relationships that could be construed as a potential conflict of interest.

Publisher's Note: All claims expressed in this article are solely those of the authors and do not necessarily represent those of their affiliated organizations, or those of the publisher, the editors, and the reviewers. Any product that may be evaluated in this article, or claim that may be made by its manufacturer, is not guaranteed or endorsed by the publisher.

Copyright © 2021 Tienaho, Reshamwala, Sarjala, Kilpeläinen, Liimatainen, Dou, Viherä-Aarnio, Linnakoski, Marjomäki and Jyske. This is an open-access article distributed under the terms of the Creative Commons Attribution License (CC BY). The use, distribution or reproduction in other forums is permitted, provided the original author(s) and the copyright owner(s) are credited and that the original publication in this journal is cited, in accordance with accepted academic practice. No use, distribution or reproduction is permitted which does not comply with these terms.



The Biodegradation of Soil Organic Matter in Soil-Dwelling Humivorous Fauna

Xuliang Lou¹, Jianming Zhao¹, Xiangyang Lou¹, Xiejiang Xia², Yilu Feng² and Hongjie Li^{2*}

¹Zhuji Real Estate Management Service Center, Shaoxing, China, ²State Key Laboratory for Managing Biotic and Chemical Threats to the Quality and Safety of Agro-products, Key Laboratory of Biotechnology in Plant Protection of Ministry of Agriculture and Zhejiang Province, Institute of Plant Virology, Ningbo University, Ningbo, China

OPEN ACCESS

Edited by:

Jia-Long Wen,
Beijing Forestry University, China

Reviewed by:

Baoku Shi,
Northeast Normal University, China
Chengyuan Pan,
Zhejiang Agriculture and Forestry
University, China

*Correspondence:

Hongjie Li
lihongjie@nbu.edu.cn

Specialty section:

This article was submitted to
Bioprocess Engineering,
a section of the journal
Frontiers in Bioengineering and
Biotechnology

Received: 03 November 2021

Accepted: 13 December 2021

Published: 10 January 2022

Citation:

Lou X, Zhao J, Lou X, Xia X, Feng Y and
Li H (2022) The Biodegradation of Soil
Organic Matter in Soil-Dwelling
Humivorous Fauna.
Front. Bioeng. Biotechnol. 9:808075.
doi: 10.3389/fbioe.2021.808075

Soil organic matter contains more carbon than global vegetation and the atmosphere combined. Gaining access to this source of organic carbon is challenging and requires at least partial removal of polyphenolic and/or soil mineral protections, followed by subsequent enzymatic or chemical cleavage of diverse plant polysaccharides. Soil-feeding animals make significant contributions to the recycling of terrestrial organic matter. Some humivorous earthworms, beetles, and termites, among others, have evolved the ability to mineralize recalcitrant soil organic matter, thereby leading to their tremendous ecological success in the (sub)tropical areas. This ability largely relies on their symbiotic associations with a diverse community of gut microbes. Recent integrative omics studies, including genomics, metagenomics, and proteomics, provide deeper insights into the functions of gut symbionts. In reviewing this literature, we emphasized that understanding how these soil-feeding fauna catabolize soil organic substrates not only reveals the key microbes in the intestinal processes but also uncovers the potential novel enzymes with considerable biotechnological interests.

Keywords: soil organic matter, biodegradation, humivorous, biotechnology, enzyme

INTRODUCTION

Soil organic matter (SOM) is massive and representative of a major organic carbon pool on the planet, which is considered as an essential agent in maintaining ecosystem productivity and sustainability through its physical, chemical, and biological properties. More specifically, soil organic matter not only retains nutrients that improve plant growth but also contributes soil physicochemical property enhancements such as infiltration, water-holding capacity, and aggregates (Lehmann and Kleber, 2015). To date, researchers estimate SOM approximately makes up less than 5% of the global dry weight soil (Stevenson, 1972; Liang et al., 2017). Soils also contribute an important source of aquatic and atmospheric carbon; moreover, diverse living organisms within the soils are considered as the most driving force of carbon cycling in biogeochemical processes. Collectively, organic matter in the soil represents the most abundant source of organic carbon and has unparalleled ecological and economic impacts on the Earth (Bolan et al., 2011).

The formation and turnover of soil organic matter is a continuum of progressively decomposing processes. Biological, physical, and chemical transformation processes convert dead plant material into organic products that form intimate associations with soil minerals (Lehmann and Kleber, 2015). The fragments of plants are often first broken up into small pieces at the beginning of decomposition by soil fauna. The plant residues are further degraded by subsequent exo-enzymes

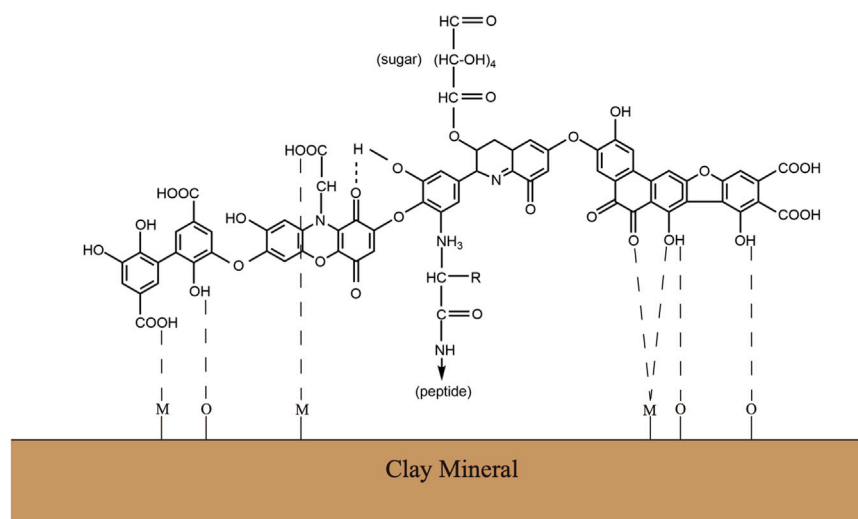


FIGURE 1 | Traditional view of the chemical complex of soil organic matters or humus substance. Modified from Wagner and Wolf (1998).

derived from surrounding microorganisms, where they are broken down to a relatively small size. The generated organic compounds at various stages of decay not only represent energy-rich spots in the soils but also relatively recalcitrant components. For instance, polyphenols in soils exist either in a dissolved form that moves freely in the soil solution, in a sorbed form that reversibly binds to the soil particle or proteins, or in a polymerized form that consists of humic substances (Min et al., 2015). Among them, lignin is one of the most recalcitrant carbon compounds and can bind with proteins, thereby immobilizing nitrogen (Gentile et al., 2011). Increasing evidence shows that soil-dwelling fauna and their gut microbial symbionts have the ability to decompose these persistent materials even more quickly than previously recognized (Coleman and Wall, 2015). In this review, we provide an overview of the recent omics-based research, including soil-dwelling fauna and their associated gut bacterial genomic and metagenomic studies, which have led to a deeper understanding of soil organic matter degradation processes and uncovered the presence of only recently recognized microbial symbionts and relevant degradative enzymes.

THE CHEMICAL COMPLEXITY AND RECALCITRANCE OF SOIL ORGANIC MATTER

Soil organic matter is heterogeneous complexes with a variety of chemical components. Although the definite chemical structures have remained contentious, it is generally accepted that humic substances consist of polyphenols, peptides, lipids, and polysaccharides (Figure 1) (Gerke, 2018). This supramolecular network formed by complex carbohydrates and aromatic polymers provides the SOM complexes with sufficient stability, but it also makes the SOM a major barrier to gain access to the

stored hydrolysable aliphatic components (Horwath and Paul, 2015). The substantial ether- and carbon-carbon interunit linkages between aromatic units possess an inherent chemical recalcitrance. At the same time, the SOM often has chemical interaction with inorganic soil colloids, including mineral or clay particles, to form dense aggregates, which further provides the physical protections against decomposition (Oades and Waters, 1991). Specifically, owing to the stimulation of microbial activity and microbe-derived carbon, plant residue starts to form aggregates when it enters the soil. Along with the decomposition processing, plant residues or other particulate organic matter gradually encrusted with clay particles and microbial byproducts to form the core of stable microaggregates. Consequently, the mineral crusts interacting with microbial byproducts managed to form recalcitrant organo-mineral complexes (Six et al., 2004).

The stability of soil organic matter including peptides, amino acids, and polysaccharides is strongly related to the presence of humic substances, which is largely owing to the polymerization of aromatic units during the humification (Shan et al., 2010). Modern analytical approaches for characterization of biomolecules in microbial cells and soils now suggest a direct and rapid contribution of microbial cell walls to soil organic matter protections when associated with model polyphenolic components. The emergent concept of soil organic matter as a continuum spanning the full range from intact plant material to highly oxidized carbon in carboxylic acids represents the more common view among the public (Lehmann and Kleber, 2015).

BIODEGRADATION MECHANISM OF SOIL ORGANIC MATTER

Soil organic matter degradation mechanisms in natural systems have remained less known since their structural complexes and therefore a suite of ligninolytic enzymes are likely engaged in the

degradation of humic substances, such as lignin peroxidase (LiP), manganese peroxidase (MnP), versatile peroxidase (VP), and laccase (Abdel-Hamid et al., 2013).

Among organisms, actinobacteria and fungi are most well known to be capable of degrading humic substances. The fungi involved in humic acid degradation are usually known as white-rot fungi capable of lignin degradation (Dashtban et al., 2010; Datta et al., 2017). Extracellular enzymes including laccase and ligninolytic peroxidase are involved in the cleavage of aromatic rings; among them, manganese peroxidase is the most investigated (Nousiainen et al., 2014). Also, protease, lipase, and various carbohydrases may be involved in the degradation of aliphatic structural components (peptides, lipids, polysaccharides, etc.) (Holtorf et al., 2019). Enzymatic degradation of protein from humic acids has been demonstrated. Meanwhile, the release of amino acids from humic substances by chemical autooxidation has also been observed (Kappler and Brune, 1999).

THE MECHANISM AND PROCESS OF SOIL-DWELLING MACROFAUNA BREAKING DOWN THE SOIL ORGANIC MATTER

Some soil fauna feed on soil organic matter, exclusively relying on soil organic matter in an advanced stage of humification (Briones, 2014). In fact, Donovan et al. (2001) defined four feeding groups of soil faunas based on the humification stages of their gut content: 1) feeding on wood, litter, and grass; 2) feeding on very decayed wood and/or high organic content soil; and 3) feeding on only organic soil (so-called true soil feeders) (Donovan et al., 2001). The mineralization of SOM components throughout the guts of soil-feeding fauna has a significant impact on carbon-cycling globally. Indeed, several soil-dwelling fauna evolved the capacity to efficiently utilize the stored organic carbon within the soil organic matter (Jiang et al., 2018). Given the independent evolution of different soil-dwelling fauna, diverse bioprocessing mechanisms of the soil organic matter-based diet across these organisms have been established. The major innovation in soil fauna is a variety of microbes and their relevant enzymes engaged in these biodegradation processes, which either hydrolyze residual polysaccharides or degrade polyphenolic components of soil organic matter.

In the natural ecosystem, there is a diverse population of soil-dwelling fauna; among them, most research concentrates on earthworms, beetles, and termites (Swift et al., 1979; Li et al., 2021). Organic matter transformation is directly affected by soil macrofauna through the incorporation and redistribution of various materials and indirectly by making use of the microbial community with both constructive and destructive means (Wolters, 2000; Lavelle et al., 2001; Liu et al., 2019). More current research studies concentrate on the representative soil organisms including earthworms, beetles, and termites, which ingest a mixture of organic matter, soil components, and microorganisms adhering to mineral

particles (Mcquillan and Webb, 1994; Lavelle et al., 1997; Brauman et al., 2000). Highly compartmentalized gut structure, extremely alkaline gut microenvironment, hydrolytic enzymes, and specialized microbiota in the gut of soil-dwelling fauna are the key points in the digestion of organic matter.

THE CONVERSION OF SOIL ORGANIC MATTER IN EARTHWORMS

Earthworms live in diverse types of soil, ranging from the top of soil in the surface litter, rotting logs, and the axils of tree branches, to the moist soil surrounding natural freshwater bodies (Reynolds, 1994). Earthworms contribute huge ecological impacts by modifying the soil structure. For example, the tropical earthworm *Reginaldia omodei* can take up to 30 times its own biomass of soil per day through its simple and tubular gut (Figure 2A) (Blouin et al., 2013). In temperate ecosystems, earthworms also ingest large amounts of material, with approximately 2–15% of organic matter inputs (Whalen and Parmelee, 2000). Earthworms live in the soil and ingest a mixture of soil and organic matter and finally excrete organo-mineral feces. Some species are dwellers and transformers of litter, living in organic soil horizons in or near the surface litter, with a diet of coarse particulate organic matter. This species takes large amounts of undecomposed litter and excretes holorganic fecal pellets (Dominguez and Edwards, 2010). Consequently, incorporation of organic matter into soil and the formation of macroaggregates are finished through burrowing, consumption, and egestion activities of earthworms (Guggenberger et al., 1996; Blanchart et al., 1997). After digestion, nitrogen is also reused by plants so that in the presence of earthworms, nitrogen mineralization increases either directly through the release of nitrogen by their metabolic products and dead tissues or indirectly through changes in soil physical properties and fragmentation of organic material and through interactions with other soil organisms (Lee, 1985; Bityutskii et al., 2002).

Research studies about degradation of soil organic matter by earthworms are currently focused on the degradation and transformation of plant-derived materials, such as cellulose, lignin, and other components of plant litter (Angst et al., 2021). Early feeding experiments on earthworms by using ¹⁴C-labeled lignin substrates indicate that the effect of earthworms on the degradation of cellulose and lignin has two distinct aspects: promotion of initial biodegradation and inhibitory effect of lateral biodegradation (Scheu, 1993). In holocellulose mineralization, earthworm processing causes a two-phase alteration: mineralization rates were initially increased for 6–15 weeks but decreased later in the experiment. Overall holocellulose mineralization in the soil of the 6- and 13-year-old fallows was increased by factors of 1.5 and 1.4 due to earthworm processing, respectively, whereas in wheatfield and beechwood soil, the effects are only slight. In the case of wheatfield soil, the earthworm processing causes a two-phase alteration in the context of the rate of lignin mineralization: mineralization rates were increased for about 10 weeks but decreased afterward in the experiment.

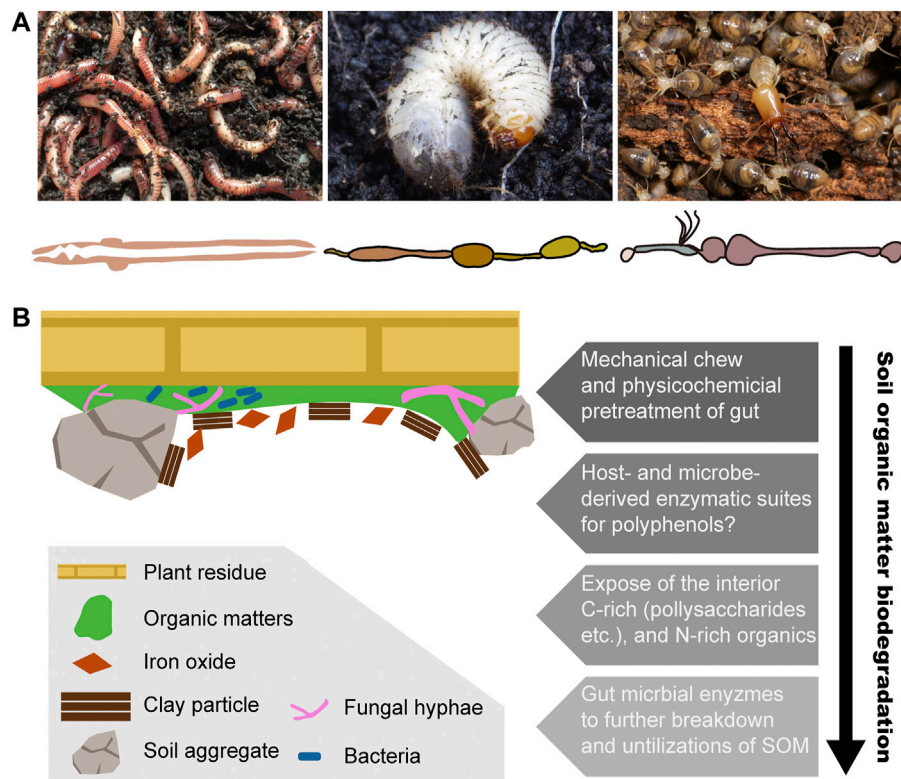


FIGURE 2 | Biodegradation process of soil organic matter in three representative humivorous fauna. **(A)** Humivorous earthworm, beetle larva, and higher termites, as well as their gut morphology. Termite photo image courtesy of Jan Šobotník. **(B)** Structural complex and heterogeneity of soil organic matter and the hypothetical biodegradation mechanism among soil-feeding macrofauna.

Moreover, these earthworms have much a higher degradation capacity on cellulose than on lignin (Scheu, 1993).

In earthworms, the gut community is dominated by the Proteobacteria, Acidobacteria, Actinobacteria, Firmicutes and Verrucomicrobia taxa within three genera of earthworms, *Aporrectodea*, *Allolobophora*, and *Lumbricus* (Sapkota et al., 2020). Several microbiome analysis results of different earthworms indicate that Proteobacteria is likely the most abundant in the gut microbiota (Knapp et al., 2009; Liu et al., 2011; Liu et al., 2018), which is consistent with early reports that Proteobacteria might be involved in the fermentation, digestion, and absorption of food for the earthworm host (Flint et al., 2012).

SELECTIVE DIGESTION OF POLYSACCHARIDES OF SOM IN HUMIVOROUS LARVA OF BEETLES

Among beetles, most larvae feed on fresh or decomposing vegetable materials (Wolters, 2000). In the case of the Scarabaeidae beetle *Pachnoda ephippiata*, the larvae are considered almost entirely herbivorous or saprophagous (Crowson, 2013). The intestinal tract of Scarabaeid beetle larvae is mainly composed of two enlarged components, the long tubular midgut and a paunch hindgut, but also a poorly

developed foregut (Figure 2A) (Cazemier, 1999). It has been observed that in saprophagous beetle larvae, the gut contains not only a large amount of humic material and plant residues but also fungal hyphae and other microbes (Bauchop and Clarke, 1977; Crowson, 2013). In Scarabaeidae families, similar to many soil-feeders, alkaline pH (>10) is always found in the midgut. The recalcitrant chitin and peptidoglycan, also the major structural polymers in the soil organic matter, are co-polymerized with polyphenols and thereby more likely to be against the soil microbial degradation. Early feeding experiments reveal that *P. ephippiata* larvae enable the selective digestion of those two polysaccharides over the protections from the polyphenols (Li and Brune, 2005).

The bacterial community structure study of the *P. ephippiata* larvae gut indicates the presence of dense and diverse microbiota, which is considerably different to the surrounding soils (Egert et al., 2003; Lemke et al., 2003). One of the dominant bacterial species isolated from the hindgut of the larvae, *Promicromonospora pachnodae*, is capable of reducing iron and degrading (hemi)cellulose (probably simultaneously), which indicates that dissimilatory iron reduction is involved in the degradation of organic matter in the intestinal tract. Also, other substantial cellulolytic bacteria, hemicellulolytic bacteria, and methanogenic archaea have been found in the intestinal tract (Bayon and Mathelin, 1980).

In some dung beetles, microbiome research studies of *Onthophagus* beetles reveal that *Enterobacter* and *Serratia* are the dominant genera in the adults, while *Dysgonomonas* and *Parabacteroides* dominate in larval and pupal stages (Suárez-Moo et al., 2020). Nevertheless, the genus *Dysgonomonas* is more abundant in the larval stage of *E. intermedius* and *E. triangulatus* (Shukla et al., 2016) and the gut microbiota of two *Pachysoma MacLeay* desert dung beetle species (Franzini et al., 2016).

MOBILIZATION AND TRANSFORMATION OF NITROGENOUS COMPONENTS WITHIN SOM IN HUMIVOROUS HIGHER TERMITES

Termites consist of seven families and are phylogenetically classified into lower termites with six families and higher termites with just one family (Noirot, 1992). For the wood-feeding “lower” termites, cellulolytic protozoa and bacteria attribute the plant biomass digestions. Evolutionarily derived “higher” termites, which are completely lacking in protozoa, have an extensive diet diversity ranging from wood, grass, bark, lichen, and decayed litter to organic soil (Wood, 1978). Among them, soil-feeding species are found in three subfamilies of higher termites and constitute approximately 67% of all genera (Brauman et al., 2000). Soil-feeding termites have been considered as important contributors to biogeochemical cycles, especially in carbon, methane, and nitrogen (Sugimoto et al., 2000; Ji and Brune, 2006). In the tropical savanna, termites have been estimated to be directly responsible for up to 20% of total carbon mineralization (Lavelle et al., 1997).

In soil-feeding termites, the hindgut is highly compartmentalized and longer, which is classified in five sections, from P1 to P5 (Figure 2A) (Brune and Kühl, 1996). It is observed that in comparison with the generally tubular compartments of wood feeders, humivorous higher termites are characterized by dilated P1 compartments, which is characterized by an increase in the length and volume, so that it allows a sequential transit of long duration. Notably, the pH sharply increases in the mixed segment and results in the alkalinity in the anterior hindgut of soil feeders being the highest values that have been reported for biological systems (Wang, 2018).

Early studies have already estimated the strong mineralization of carbon and nitrogen in the gut of soil-feeding termites, even though the overall information on humivorous termites is still limited. Ji and Brune (2005) found that soil-feeding termites, *Cubitermes orthognathus*, enable the efficient mobilization and digestion of the peptidic components within the soil organic matter by a combination of proteolytic activities and extreme alkalinity in their intestinal tract (Ji and Brune, 2005). By using pyrolysis-GC-MS, Griffiths et al. (2013) further confirms that in comparison to the wood-feeding termites, the soil-feeder *Cubitermes* termites efficiently digested peptides and other nitrogenous residues such as chitin and peptidoglycan of soil organic carbon, rather than polyphenols (Griffiths et al., 2013). Interestingly, nitrogenous components are derived from

microbial biomass, which are generally protected from degradation by covalent linkage to polyphenols and an intimate association with clay minerals. The ability to mobilize such recalcitrant humus constituents is accompanied by an even more pronounced elongation and extreme alkalization (to >pH 12) of the anterior hindgut, which remains a mystery.

Diverse and unique microbial populations exist in the hindgut of soil-feeding termites. Termites largely depend on these complex microbial communities to digest and utilize soil organic matter, including highly recalcitrant lignocellulose and other organic matters in advanced stages of humification (Ohkuma and Brune, 2011). It has been demonstrated that the relative increase in alkali-active proteases in the P1 section and ammonia accumulates to high concentrations in the posterior hindgut. The magnified abundance of these alkali-adapted Firmicutes belongs to clostridia in their hindguts may satisfy the metabolic requirement (Mikaelyan et al., 2015). However, the concrete roles played by intestinal microbiota in the digestive process are still unclear.

To date, there are numerous gut microbiome studies across feeding groups of termites. The overall pattern indicates a prevalence of Fibrobacteres and Spirochaetes bacteria in the wood feeders, whereas humus feeders, soil feeders, and fungus feeders shared similarities in community structure, with large proportions of Firmicutes, Bacteroidetes, and Proteobacteria. Furthermore, the soil feeders also harbored a larger proportion of actinobacteria (Schloss et al., 2006; Dietrich et al., 2014; Su et al., 2016; Bucek et al., 2019; Hu et al., 2019). The latest work on the large-scale metagenomic analysis of 145 termite species revealed the correlation between host phylogeny and the functionalities of their microbiota (Arora et al., 2021).

MICROBIOME OF SOIL-DWELLING HUMIVOROUS FAUNA AND BIOENERGY APPLICATIONS

As one of the largest carbon pools, soil organic matter represents a complex and recalcitrant carbon that has an inherent resistance to decomposition, which is largely owing to the protection provided by soil minerals and a variety of aromatic biopolymers (Kleber, 2010). The ability of decomposer soil fauna to access the stored carbon of soil organic matter at an incredibly efficient level has fascinated biologists for more than a century. In parallel to the current industrial saccharification, the breakdown of complex polysaccharides into monosaccharides employs strategies involving a combination of chemical pretreatment and enzymatic hydrolysis to obtain simple sugar for subsequent fermentation (Hafid et al., 2017). The depolymerization processing is still not economically viable and is even challenging.

Notably, soil-dwelling fauna is widespread on Earth, for example, soil-feeding termites inhabit approximately 75% of the terrestrial soil surface and consume wood and litter in different stages of decay and humification (Noirot, 1992; Li et al., 2017). The microbiome of soil-dwelling humivorous fauna represents a particularly vast and promising source of

novel cellulolytic enzymes, or enzyme cocktails, for industrial cellulosic biofuel production. Yet, we have only begun to understand the ecologic impacts. Work on the core and functional bacterial lineages and their related microbial enzymes and genomic investigations have led to discoveries of novel and diverse microbe-derived enzymes. To further explore these biological systems, it is essential to proceed beyond a full understanding of the chemistry of the nature of all organic matter in soil. An integrative analysis of chemically tracking the fate of soil organic matter throughout soil-dwelling humivorous fauna is urgently necessary.

REFERENCES

- Abdel-Hamid, A. M., Solbiati, J. O., and Cann, I. K. O. (2013). "Insights into Lignin Degradation and its Potential Industrial Applications," in *Advances in Applied Microbiology*. Editors S. Sariaslani, and G. M. Gadd (Amsterdam: Elsevier), 1–28. doi:10.1016/b978-0-12-407679-2.00001-6
- Angst, G., Mueller, K. E., Nierop, K. G. J., and Simpson, M. J. (2021). Plant- or Microbial-Derived? A Review on the Molecular Composition of Stabilized Soil Organic Matter. *Soil Biol. Biochem.* 156, 108189. doi:10.1016/j.soilbio.2021.108189
- Arora, J., Kinjo, Y., Šobotník, J., Buček, A., Clitheroe, C., Stiblik, P., et al. (2021). The Functional Evolution of Termite Gut Microbiota. *bioRxiv*. doi:10.1101/2021.12.01.470864
- Bauchop, T., and Clarke, R. T. J. (1977). Degree of Plant Root Digestion by the Larva of the Beetle, *Costelytra Zealandica*. *J. Insect Physiol.* 23 (1), 65–71. doi:10.1016/0022-1910(77)90110-X
- Bayon, C., and Mathelin, J. (1980). Carbohydrate Fermentation and By-Product Absorption Studied with Labelled Cellulose in *Oryctes Nasicornis* Larvae (Coleoptera:Scarabaeidae). *J. Insect Physiol.* 26 (12), 833–840. doi:10.1016/0022-1910(80)90100-6
- Bityutskii, N. P., Lapshina, I. N., Lukina, E. I., Solov'eva, A. N., Patsevich, V. G., and Vygovskaya, A. A. (2002). Role of Earthworms in Mineralization of Organic Nitrogen Compounds in Soil. *Eurasian Soil Sci.* 35 (10), 1100–1107. doi:10.1346/000986002320679549
- Blanchart, E., Lavelle, P., Braudeau, E., Le Bissonnais, Y., and Valentin, C. (1997). Regulation of Cote Structure by Geophagous Earthworm Activities in Humid Savannas of Côte d'Ivoire. *Soil Biol. Biochem.* 29 (3), 431–439. doi:10.1016/S0038-0717(96)00042-9
- Blouin, M., Hodson, M. E., Delgado, E. A., Baker, G., Brussaard, L., Butt, K. R., et al. (2013). A Review of Earthworm Impact on Soil Function and Ecosystem Services. *Eur. J. Soil Sci.* 64 (2), 161–182. doi:10.1111/ejss.12025
- Bolan, N. S., Adriano, D. C., Kunhikrishnan, A., James, T., McDowell, R., and Senesi, N. (2011). "Dissolved Organic Matter," in *Dissolved Organic Matter: Biogeochemistry, Dynamics, and Environmental Significance in Soils*, in *Advances in Agronomy*. Editor D. L. Sparks (Amsterdam: Elsevier), 1–75. doi:10.1016/b978-0-12-385531-2.00001-3
- Brauman, A., Bignell, D. E., and Tayasu, I. (2000). "Soil-feeding Termites: Biology, Microbial Associations and Digestive Mechanisms," in *Termites: Evolution, Sociality, Symbioses, Ecology*. Editors T. Abe, D. E. Bignell, M. Higashi, T. Higashi, and Y. Abe (Dordrecht: Springer), 233–259. doi:10.1007/978-94-017-3223-9_11
- Briones, M. a. J. I. (2014). Soil Fauna and Soil Functions: a Jigsaw Puzzle. *Front. Environ. Sci.* 2, 7. doi:10.3389/fenvs.2014.00007
- Brune, A., and Kühl, M. (1996). pH Profiles of the Extremely Alkaline Hindguts of Soil-Feeding Termites (Isoptera: Termitidae) Determined with Microelectrodes. *J. Insect Physiol.* 42 (11), 1121–1127. doi:10.1016/S0022-1910(96)00036-4
- Bucek, A., Šobotník, J., He, S., Shi, M., McMahon, D. P., Holmes, E. C., et al. (2019). Evolution of Termite Symbiosis Informed by Transcriptome-Based Phylogenies. *Curr. Biol.* 29 (21), 3728–3734. doi:10.1016/j.cub.2019.08.076
- Cazemier, A. E. (1999). *(Hemi)cellulose Degradation by Microorganisms from the Intestinal Tract of Arthropods*. [dissertation]. [Nijmegen (Nederland)]: Radboud University.
- Coleman, D. C., and Wall, D. H. (2015). "Soil Fauna," in *Soil Microbiology, Ecology and Biochemistry*. Editor E. Paul (Cambridge, MA: Academic Press), 111–149. doi:10.1016/b978-0-12-415955-6.00005-0
- Crowson, R. A. (2013). *The Biology of the Coleoptera*. Massachusetts: Academic Press.
- Dashtban, M., Schraft, H., Syed, T. A., and Qin, W. (2010). Fungal Biodegradation and Enzymatic Modification of Lignin. *Int. J. Biochem. Mol. Biol.* 1 (1), 36–50. doi:10.1111/j.1432-1033.1987.tb11073.x
- Datta, R., Kelkar, A., Baraniya, D., Molaei, A., Moulick, A., Meena, R., et al. (2017). Enzymatic Degradation of Lignin in Soil: a Review. *Sustainability* 9 (7), 1163. doi:10.3390/su9071163
- Dietrich, C., Köhler, T., and Brune, A. (2014). The Cockroach Origin of the Termite Gut Microbiota: Patterns in Bacterial Community Structure Reflect Major Evolutionary Events. *Appl. Environ. Microbiol.* 80 (7), 2261–2269. doi:10.1128/AEM.04206-13
- Dominguez, J., and Edwards, C. (2010). "Biology and Ecology of Earthworm Species Used for Vermicomposting," in *Biology and Ecology of Earthworm Species Used for Vermicomposting*, in *Vermiculture Technology*. Editors C. A. Edwards, N. Q. Arancon, and R. L. Sherman (Boca Raton, FL: CRC Press), 27–40. doi:10.1201/b10453-4
- Donovan, S. E., Eggleton, P., and Bignell, D. E. (2001). Gut Content Analysis and a New Feeding Group Classification of Termites. *Ecol. Entomol.* 26 (4), 356–366. doi:10.1046/j.1365-2311.2001.00342.x
- Egert, M., Wagner, B., Lemke, T., Brune, A., and Friedrich, M. W. (2003). Microbial Community Structure in Midgut and Hindgut of the Humus-Feeding Larva of *Pachnoda ephippiata* (Coleoptera: Scarabaeidae). *Appl. Environ. Microbiol.* 69 (11), 6659–6668. doi:10.1128/AEM.69.11.6659-6668.2003
- Flint, H. J., Scott, K. P., Louis, P., and Duncan, S. H. (2012). The Role of the Gut Microbiota in Nutrition and Health. *Nat. Rev. Gastroenterol. Hepatol.* 9 (10), 577–589. doi:10.1038/nrgastro.2012.156
- Franzini, P. Z. N., Ramond, J.-B., Scholtz, C. H., Sole, C. L., Ronca, S., and Cowan, D. A. (2016). The Gut Microbiomes of Two *Pachysoma* Macleay Desert Dung Beetle Species (Coleoptera: Scarabaeidae: Scarabaeinae) Feeding on Different Diets. *PLoS One* 11 (8), e0161118. doi:10.1371/journal.pone.0161118
- Gentile, R., Vanlauwe, B., and Six, J. (2011). Litter Quality Impacts Short- but Not Long-Term Soil Carbon Dynamics in Soil Aggregate Fractions. *Ecol. Appl.* 21 (3), 695–703. doi:10.1890/09-2325.1
- Gerke, J. (2018). Concepts and Misconceptions of Humic Substances as the Stable Part of Soil Organic Matter: a Review. *Agronomy* 8 (5), 76. doi:10.3390/agronomy8050076
- Griffiths, B. S., Bracewell, J. M., Robertson, G. W., and Bignell, D. E. (2013). Pyrolysis-mass Spectrometry Confirms Enrichment of Lignin in the Faeces of a wood-feeding Termite, *Zootermopsis Nevadaensis* and Depletion of Peptides in a Soil-Feeder, *Cubitermes Ugandensis*. *Soil Biol. Biochem.* 57, 957–959. doi:10.1016/j.soilbio.2012.08.012
- Guggenberger, G., Thomas, R. J., and Zech, W. (1996). Soil Organic Matter within Earthworm Casts of an Anecic-Endogeic Tropical Pasture

AUTHOR CONTRIBUTIONS

All the authors drafted the outline of this review; XuL and HL wrote the manuscript.

FUNDING

This study was funded by the Zhejiang Provincial Natural Science Foundation Project (LR21C160001) and the National Natural Science Foundation of China (Grant Project 32171796 and 31500528).

- Community, Colombia. *Appl. Soil Ecol.* 3 (3), 263–274. doi:10.1016/0929-1393(95)00081-X
- Hafid, H. S., Rahman, N. A. A., Shah, U. K. M., Baharuddin, A. S., and Ariff, A. B. (2017). Feasibility of Using Kitchen Waste as Future Substrate for Bioethanol Production: a Review. *Renew. Sustainable Energ. Rev.* 74, 671–686. doi:10.1016/j.rser.2017.02.071
- Holtot, M., Lenaerts, C., Cullen, D., and Vanden Broeck, J. (2019). Extracellular Nutrient Digestion and Absorption in the Insect Gut. *Cell Tissue Res* 377 (3), 397–414. doi:10.1007/s00441-019-03031-9
- Horwath, W., and Paul, E. A. (2015). “Carbon Cycling,” in *Soil Microbiology, Ecology and Biochemistry*. Editor E. Paul (Cambridge, MA: Academic Press), 339–382. doi:10.1016/B978-0-12-415955-6.00012-8
- Hu, H., da Costa, R. R., Pilgaard, B., Schiøtt, M., Lange, L., Poulsen, M., et al. (2019). Fungiculture in Termites Is Associated with a Mycolytic Gut Bacterial Community. *MSphere* 4 (3), e00165–00119. doi:10.1128/mSphere.00165-19
- Ji, R., and Brune, A. (2005). Digestion of Peptidic Residues in Humic Substances by an Alkali-Stable and Humic-Acid-Tolerant Proteolytic Activity in the Gut of Soil-Feeding Termites. *Soil Biol. Biochem.* 37 (9), 1648–1655. doi:10.1016/j.soilbio.2005.01.026
- Ji, R., and Brune, A. (2006). Nitrogen Mineralization, Ammonia Accumulation, and Emission of Gaseous NH₃ by Soil-Feeding Termites. *Biogeochemistry* 78 (3), 267–283. doi:10.1007/s10533-005-4279-z
- Jiang, Y., Qian, H., Wang, X., Chen, L., Liu, M., Li, H., et al. (2018). Nematodes and Microbial Community Affect the Sizes and Turnover Rates of Organic Carbon Pools in Soil Aggregates. *Soil Biol. Biochem.* 119, 22–31. doi:10.1016/j.soilbio.2018.01.001
- Kappler, A., and Brune, A. (1999). Influence of Gut Alkalinity and Oxygen Status on Mobilization and Size-Class Distribution of Humic Acids in the Hindgut of Soil-Feeding Termites. *Appl. Soil Ecol.* 13 (3), 219–229. doi:10.1016/S0929-1393(99)00035-9
- Kleber, M. (2010). What Is Recalcitrant Soil Organic Matter? *Environ. Chem.* 7 (4), 320–332. doi:10.1071/EN10006
- Knapp, B. A., Podmirseg, S. M., Seeber, J., Meyer, E., and Insam, H. (2009). Diet-related Composition of the Gut Microbiota of *Lumbricus Rubellus* as Revealed by a Molecular Fingerprinting Technique and Cloning. *Soil Biol. Biochem.* 41 (11), 2299–2307. doi:10.1016/j.soilbio.2009.08.011
- Lavelle, P., Barros, E., Blanchart, E., Brown, G., Desjardins, T., Mariani, L., et al. (2001). SOM Management in the Tropics: Why Feeding the Soil Macrofauna? *Nutr. Cycl. Agroecosys.* 61, 53–61. doi:10.1023/A:101336871574210.1007/978-94-017-2172-1_6
- Lavelle, P., Bignell, D., Lepage, M., Wolters, V., Roger, P., Ineson, P., et al. (1997). Soil Function in a Changing World: the Role of Invertebrate Ecosystem Engineers. *Eur. J. Soil Biol.* 33 (4), 159–193. doi:10.1023/A:1007339916013
- Lee, K. E. (1985). *Earthworms, Their Ecology and Relationships with Soils and Land Use*. Massachusetts: Academic Press. doi:10.1016/0143-1471(86)90050-4
- Lehmann, J., and Kleber, M. (2015). The Contentious Nature of Soil Organic Matter. *Nature* 528 (7580), 60–68. doi:10.1038/nature16069
- Lemke, T., Stingl, U., Egert, M., Friedrich, M. W., and Brune, A. (2003). Physicochemical Conditions and Microbial Activities in the Highly Alkaline Gut of the Humus-Feeding Larva of *Pachnoda ephippiata* (Coleoptera: Scarabaeidae). *Appl. Environ. Microbiol.* 69 (11), 6650–6658. doi:10.1128/AEM.69.11.6650-6658.2003
- Li, H., Yelle, D. J., Li, C., Yang, M., Ke, J., Zhang, R., et al. (2017). Lignocellulose Pretreatment in a Fungus-Cultivating Termite. *Proc. Natl. Acad. Sci. U.S.A.* 114 (18), 4709–4714. doi:10.1073/pnas.1618360114
- Li, H., Young, S. E., Poulsen, M., and Currie, C. R. (2021). Symbiont-mediated Digestion of Plant Biomass in Fungus-Farming Insects. *Annu. Rev. Entomol.* 66, 297–316. doi:10.1146/annurev-ento-040920-061140
- Li, X., and Brune, A. (2005). Selective Digestion of the Peptide and Polysaccharide Components of Synthetic Humic Acids by the Humivorous Larva of *Pachnoda ephippiata* (Coleoptera: Scarabaeidae). *Soil Biol. Biochem.* 37 (8), 1476–1483. doi:10.1016/j.soilbio.2005.01.004
- Liang, C., Schimel, J. P., and Jastrow, J. D. (2017). The Importance of Anabolism in Microbial Control over Soil Carbon Storage. *Nat. Microbiol.* 2 (8), 17105. doi:10.1038/nmicrobiol.2017.105
- Liu, D., Lian, B., Wang, B., and Jiang, G. (2011). Degradation of Potassium Rock by Earthworms and Responses of Bacterial Communities in its Gut and Surrounding Substrates after Being Fed with mineral. *PLoS One* 6 (12), e28803. doi:10.1371/journal.pone.0028803
- Liu, D., Lian, B., Wu, C., and Guo, P. (2018). A Comparative Study of Gut Microbiota Profiles of Earthworms Fed in Three Different Substrates. *Symbiosis* 74 (1), 21–29. doi:10.1007/s13199-017-0491-6
- Liu, N., Li, H., Chevrette, M. G., Zhang, L., Cao, L., Zhou, H., et al. (2019). Functional Metagenomics Reveals Abundant Polysaccharide-Degrading Gene Clusters and Cellobiose Utilization Pathways within Gut Microbiota of a wood-feeding Higher Termite. *ISME J.* 13 (1), 104–117. doi:10.1038/s41396-018-0255-1
- Mcquillan, P. B., and Webb, W. R. (1994). Selective Soil Organic Matter Consumption by Larvae of *Adoryphorus Couloni* (Burmeister) (Coleoptera: Scarabaeidae). *Aust. J. ENTOMOL.* 33 (1), 49–50. doi:10.1111/j.1440-6055.1994.tb00918.x
- Mikaelyan, A., Dietrich, C., Köhler, T., Poulsen, M., Sillam-Dussès, D., and Brune, A. (2015). Diet Is the Primary Determinant of Bacterial Community Structure in the Guts of Higher Termites. *Mol. Ecol.* 24 (20), 5284–5295. doi:10.1111/mec.13376
- Min, K., Freeman, C., Kang, H., and Choi, S.-U. (2015). The Regulation by Phenolic Compounds of Soil Organic Matter Dynamics under a Changing Environment. *Biomed. Res. Int.* 2015, 1–11. doi:10.1155/2015/825098
- Noirot, C. (1992). “From wood- to Humus-Feeding: an Important Trend in Termite Evolution,” in *Biology and Evolution of Social Insects*. Editor J. Billen (Leuven, Belgium: Leuven University Press), 107–119.
- Nousiainen, P., Kontro, J., Manner, H., Hatakka, A., and Sipilä, J. (2014). Phenolic Mediators Enhance the Manganese Peroxidase Catalyzed Oxidation of Recalcitrant Lignin Model Compounds and Synthetic Lignin. *Fungal Genet. Biol.* 72, 137–149. doi:10.1016/j.fgb.2014.07.008
- Oades, J., and Waters, A. (1991). Aggregate Hierarchy in Soils. *Soil Res.* 29 (6), 815–828. doi:10.1071/SR9910815
- Ohkuma, M., and Brune, A. (2011). “Diversity, Structure, and Evolution of the Termite Gut Microbial Community,” in *Biology of Termites: A Modern Synthesis*. Editors D. E. Bignell, Y. Roisin, and N. Lo (Dordrecht: Springer), 413–438.
- Reynolds, J. (1994). Earthworms of the World. *Glob. Biodivers.* 4 (1), 11–16.
- Sapkota, R., Santos, S., Farias, P., Krogh, P. H., and Winding, A. (2020). Insights into the Earthworm Gut Multi-Kingdom Microbial Communities. *Sci. Total Environ.* 727, 138301. doi:10.1016/j.scitotenv.2020.138301
- Scheu, S. (1993). Cellulose and Lignin Decomposition in Soils from Different Ecosystems on limestone as Affected by Earthworm Processing. *Pedobiologia* 37, 167–177.
- Schloss, P. D., Delalibera, I., Jr, Handelsman, J., and Raffa, K. F. (2006). Bacteria Associated with the Guts of Two wood-boring Beetles: *Anoplophora glabripennis* and *Saperda vestita* (Cerambycidae). *Environ. Entomol.* 35 (3), 625–629. doi:10.1603/0046-225X-35.3.625
- Shan, J., Brune, A., and Ji, R. (2010). Selective Digestion of the Proteinaceous Component of Humic Substances by the Geophagous Earthworms *Metaphire guillelmi* and *Amyntas corrugatus*. *Soil Biol. Biochem.* 42 (9), 1455–1462. doi:10.1016/j.soilbio.2010.05.008
- Shukla, S. P., Sanders, J. G., Byrne, M. J., and Pierce, N. E. (2016). Gut Microbiota of Dung Beetles Correspond to Dietary Specializations of Adults and Larvae. *Mol. Ecol.* 25 (24), 6092–6106. doi:10.1111/mec.13901
- Six, J., Bossuyt, H., Degryze, S., and Denef, K. (2004). A History of Research on the Link between (Micro)aggregates, Soil Biota, and Soil Organic Matter Dynamics. *Soil Tillage Res.* 79 (1), 7–31. doi:10.1016/j.still.2004.03.008
- Stevenson, F. J. (1972). Role and Function of Humus in Soil with Emphasis on Adsorption of Herbicides and Chelation of Micronutrients. *BioScience* 22 (11), 643–650. doi:10.2307/1296265
- Su, L., Yang, L., Huang, S., Su, X., Li, Y., Wang, F., et al. (2016). Comparative Gut Microbiomes of Four Species Representing the Higher and the Lower Termites. *J. Insect Sci.* 16 (1), 97. doi:10.1093/jisesa/iew081
- Suárez-Moo, P., Cruz-Rosales, M., Ibarra-Laclette, E., Desgarenes, D., Huerta, C., and Lamelas, A. (2020). Diversity and Composition of the Gut Microbiota in the Developmental Stages of the Dung Beetle *Copris*

- Incertus* Say (Coleoptera, Scarabaeidae). *Front. Microbiol.* 11, 1698. doi:10.3389/fmicb.2020.01698
- Sugimoto, A., Bignell, D. E., and MacDonald, J. A. (2000). "Global Impact of Termites on the Carbon Cycle and Atmospheric Trace Gases," in *Termites: Evolution, Sociality, Symbioses, Ecology*. Editors T. Abe, D. E. Bignell, M. Higashi, T. Higashi, and Y. Abe (Dordrecht: Springer), 409–435. doi:10.1007/978-94-017-3223-9_19
- Swift, M. J., Heal, O. W., Anderson, J. M., and Anderson, J. M. (1979). *Decomposition in Terrestrial Ecosystems*. California: University of California Press.
- Wang, W. (2018). *The Bacterial Gut Microbiota of wood-and Humus-Feeding Termites: Diazotrophic Populations and Compartment-specific Response of Bacterial Communities to Environmental Factors*. [dissertation]. [Marburg (HE)]. Marburg city: Philipps-Universität Marburg.
- Wagner, G. H., and Wolf, D. C. (1998). "Carbon transformations and soil organic matter formation," in *Principles and applications of soil microbiology*. Editors D. M. Sylvia, J. J. Fuhrmann, P. Hartel, and D. Zuberer (NJ: Prentice Hall), 218–258.
- Whalen, J. K., and Parmelee, R. W. (2000). Earthworm Secondary Production and N Flux in Agroecosystems: a Comparison of Two Approaches. *Oecologia* 124 (4), 561–573. doi:10.1007/s004420000413
- Wolters, V. (2000). Invertebrate Control of Soil Organic Matter Stability. *Biol. Fertil. Soils* 31 (1), 1–19. doi:10.1007/s003740050618
- Wood, T. G. (1978). "The Role of Termites (Isoptera) in Decomposition Processes," in *The Role of Terrestrial and Aquatic Organisms in Decomposition Processes*. Editors J. M. Anderson, and A. Macfadyen (Osney Mead, Oxford: Blackwell Science), 145–168.

Conflict of Interest: The authors declare that the research was conducted in the absence of any commercial or financial relationships that could be construed as a potential conflict of interest.

Publisher's Note: All claims expressed in this article are solely those of the authors and do not necessarily represent those of their affiliated organizations, or those of the publisher, the editors, and the reviewers. Any product that may be evaluated in this article, or claim that may be made by its manufacturer, is not guaranteed or endorsed by the publisher.

Copyright © 2022 Lou, Zhao, Lou, Xia, Feng and Li. This is an open-access article distributed under the terms of the Creative Commons Attribution License (CC BY). The use, distribution or reproduction in other forums is permitted, provided the original author(s) and the copyright owner(s) are credited and that the original publication in this journal is cited, in accordance with accepted academic practice. No use, distribution or reproduction is permitted which does not comply with these terms.



Lignin-Based/Polypyrrole Carbon Nanofiber Electrode With Enhanced Electrochemical Properties by Electrospun Method

Zhou-Rui Hu^{1†}, Dan-Dan Li^{1†}, Tae-Hee Kim², Min-Seok Kim², Ting Xu³, Ming-Guo Ma^{1*}, Sun-Eun Choi^{2*} and Chuanling Si^{3*}

¹Beijing Key Laboratory of Lignocellulosic Chemistry, Engineering Research Center of Forestry Biomass Materials and Bioenergy, Research Center of Biomass Clean Utilization, College of Materials Science and Technology, Beijing Forestry University, Beijing, China, ²Department of Forest Biomaterials Engineering, College of Forest and Environmental Sciences, Kangwon National University, Chuncheon, South Korea, ³Tianjin Key Laboratory of Pulp and Paper, Tianjin University of Science and Technology, Tianjin, China

OPEN ACCESS

Edited by:

Zhongqing Ma,
Zhejiang Agriculture and Forestry
University, China

Reviewed by:

Lian-Hua Fu,
Shenzhen University, China
Jiefang Zhu,
Uppsala University, Sweden

*Correspondence:

Ming-Guo Ma
mg_ma@bjfu.edu.cn
Sun-Eun Choi
oregonin@kangwon.ac.kr
Chuanling Si
sichl@tust.edu.cn

[†]These authors have contributed
equally to this work

Specialty section:

This article was submitted to
Green and Sustainable Chemistry,
a section of the journal
Frontiers in Chemistry

Received: 27 December 2021

Accepted: 11 January 2022

Published: 08 February 2022

Citation:

Hu Z-R, Li D-D, Kim T-H, Kim M-S,
Xu T, Ma M-G, Choi S-E and Si C
(2022) Lignin-Based/Polypyrrole
Carbon Nanofiber Electrode With
Enhanced Electrochemical Properties
by Electrospun Method.
Front. Chem. 10:841956.
doi: 10.3389/fchem.2022.841956

Tailoring the structure and properties of lignin is an important step toward electrochemical applications. In this study, lignin/polypyrrole (PPy) composite electrode films with microporous and mesoporous structures were designed effectively by electrostatic spinning, carbonization, and *in situ* polymerization methods. The lignin can not only reduce the cost of carbon fiber but also increase the specific surface area of composite films due to the removal of carbonyl and phenolic functional groups of lignin during carbonization. Besides, the compact three-dimensional (3D) conductive network structures were constructed with PPy particles densely coated on the lignin nanofibers, which was helpful to improve the conductivity and fast electron transfer during the charging and discharging processes. The synthesized lignin carbon fibers/PPy anode materials had good electrochemical performance in 1 M H₂SO₄ electrolyte. The results showed that, at a current density of 1 A g⁻¹, the lignin carbon nanofibers/PPy (LCNFs/PPy) had a larger specific capacitance of 213.7 F g⁻¹ than carbon nanofibers (CNFs), lignin carbon nanofibers (LCNFs), and lignin/PPy fiber (LPAN/PPy). In addition, the specific surface area of LCNFs/PPy reached 872.60 m² g⁻¹ and the average pore size decreased to 2.50 nm after being coated by PPy. Therefore, the independent non-binder and self-supporting conductive film is expected to be a promising electrode material for supercapacitors with high performance.

Keywords: supercapacitors, lignin, electrostatic spinning, polypyrrole, film

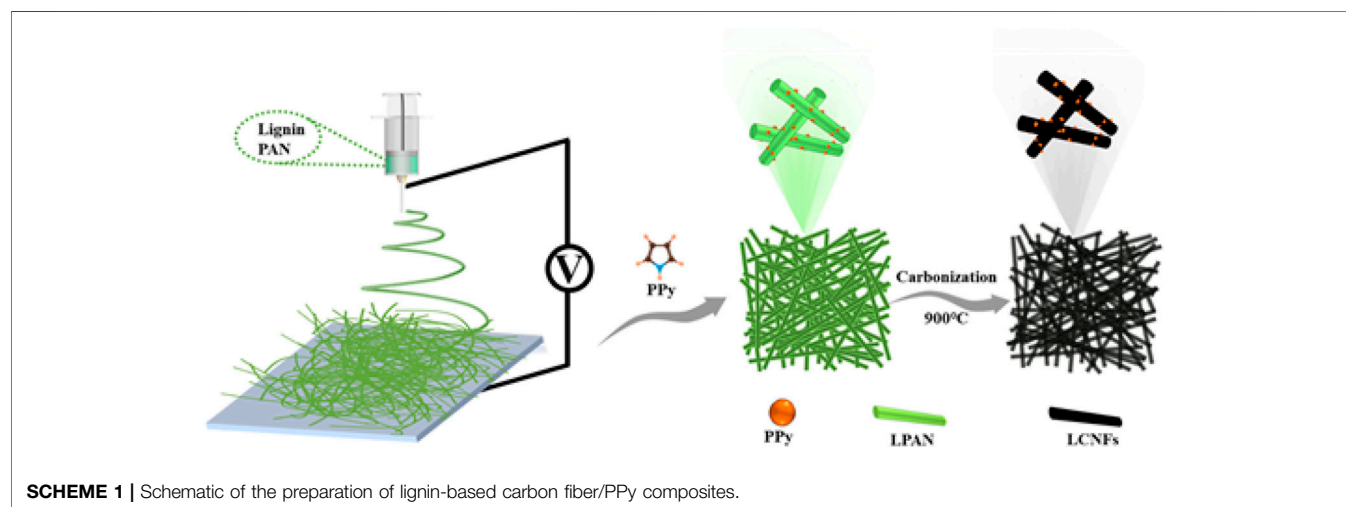
INTRODUCTION

Supercapacitors rely on electrode materials for charge storage, so electrode materials are the key part of the performance of supercapacitors (Choi et al., 2020; WulanSeptiani et al., 2020; Fu et al., 2021; Xu et al., 2021b; Liu et al., 2021a; Liu et al., 2021b; Du et al., 2022). Carbon materials, such as porous carbon (Li et al., 2019a), graphene (Zhou et al., 2020), carbon nanotubes (Fan et al., 2020), and ordered mesoporous carbon (Wang et al., 2018), are considered the most suitable electrode materials for supercapacitors due to their high specific surface area, developed pore structure, high electronic conductivity, and excellent stability (Chen et al., 2020a; Shang et al., 2020; Xu et al., 2020c). Unfortunately, strong van der Waals forces between graphene sheets tend to cause graphene sheets to accumulate and agglomerate (Xiong

et al., 2020). And the biggest problem in the preparation of carbon nanotube composites is that carbon nanotubes are difficult to disperse effectively into the polymer matrix (Sahoo et al., 2010). Also, the process of ordered mesoporous carbon is complicated due to the use of various templates (Lin et al., 2015). However, porous carbon has gained wide raw material sources, low cost, well-developed pores, and an easy-to-control structure (Li et al., 2020). Moreover, the large amount of oxygen functional groups such as -OH and -COOH in these materials as another advantage provided interesting attention for better superior charge storage (Ding et al., 2021). Like the latest report, Xu et al. (2022) prepared dung beetle forewing carbon materials with a hierarchical porous structure, self-doped nitrogen, oxygen, and a large specific surface area, which obtained a specific capacitance of 348 F g^{-1} . Wang et al. (2022) converted waste peach gum as a raw material into layered porous carbon doped with N, P, and O through impregnation and carbonization. The electrode exhibited excellent electrochemical performance (490 F g^{-1} under 1 A g^{-1}) due to the synergistic effects of high specific surface area and multiple heteroatomic co-doping amounts.

Therefore, more and more attention has been paid to the preparation of porous carbon electrode materials for supercapacitors using biomass as precursors (Lian et al., 2018; Zhu et al., 2018; Yang et al., 2019; Liu et al., 2021g). Lignocellulosic biomass is one of the most abundant resources, which is a promising source of renewable energy (Du et al., 2019; Liu et al., 2020a; Liu et al., 2020b; Wang et al., 2020; Liu et al., 2021d; Xu et al., 2021a; Zhang et al., 2021a). Lignocellulosic biomass is mainly composed of cellulose, hemicelluloses, and lignin (Liu et al., 2021e; Liu et al., 2021f; Xu et al., 2020b; Liu et al., 2021h; Wang et al., 2021a). Among them, lignin as a kind of biomass carbon precursor is considered with broad application prospects due to its high carbon yield, large space for molecular structure modification, and abundant industrial sources (Dai et al., 2019; Li et al., 2019b; Chen et al., 2020b; Chen et al., 2020c; Dai et al., 2020; Xu et al., 2020a; Zhou et al., 2021; Park et al., 2022). In addition, researchers are committed to designing and manufacturing advanced lignin carbon fibers with high specific surface area, controllable porosity, and appropriate pore size using electrostatic spinning technology, and

this technique has obvious advantages over other preparation methods in controlling the fiber inner diameter, surface morphology, and orientation degree (Qu et al., 2021; Thongsai et al., 2021). However, pure lignin has a low molecular weight and is not easily spinnable into fibers in practical applications (An et al., 2019). Therefore, high-molecular-weight polymers such as polyacrylonitrile (Szabó et al., 2021), poly(vinyl pyrrolidone) (Cao et al., 2020a), polyethylene oxide (Dallmeyer et al., 2010), and polyvinyl alcohol (Camiré et al., 2020) need to be added to the lignin solution to improve the viscosity and spinnability of the fiber preparation spinning solution. Furthermore, the mechanical strength of spun fibers can be improved by using high-molecular-weight polymers. Meanwhile, the introduction of conductive polymer into carbon fiber can generate more electrochemical active sites for a rapid charge-discharge conversion reaction, thus further improving the electrochemical performance (Zhang et al., 2017). Polypyrrole (PPy) is one of the most widely studied conductive polymers, which has a broad application prospect in supercapacitors due to its excellent energy storage capacity, easy synthesis, and high conductivity (Tian et al., 2019; Du et al., 2021; Yuan and Ma, 2021). Unfortunately, PPy as a supercapacitor electrode undergoes continuous expansion and contraction during the doping/de-doping process, which reduces its cyclic stability and electrochemical performance (Tian et al., 2021). Therefore, researchers used the strategy of depositing PPy on carbon-based materials to obtain enhanced capacitance performance in practical applications (Fan et al., 2014). For example, Li et al. (He et al., 2021) fabricated graphene/graphite/PPy composite fibers using a vertical alignment method, and the 3D microelectrode was helpful to improve electrochemical performance. Zhan et al. (2021) developed electrode materials with high capacitance ($5,299 \text{ mF cm}^{-2}$) and mechanical flexibility by synthesizing PPy *in situ* in cellulose nanofiber/sulfonated carbon nanotube composite hydrogel. In the literature, our group reviewed multifunctional lignin-based composite materials and nano-lignin materials for emerging applications (Deng et al., 2021; Ma et al., 2021a). Moreover, we prepared the flexible N-doped carbon nanotubes/MXene/PAN nanocomposite films with improved electrochemical properties via the electrostatic spinning method (Li et al., 2021).



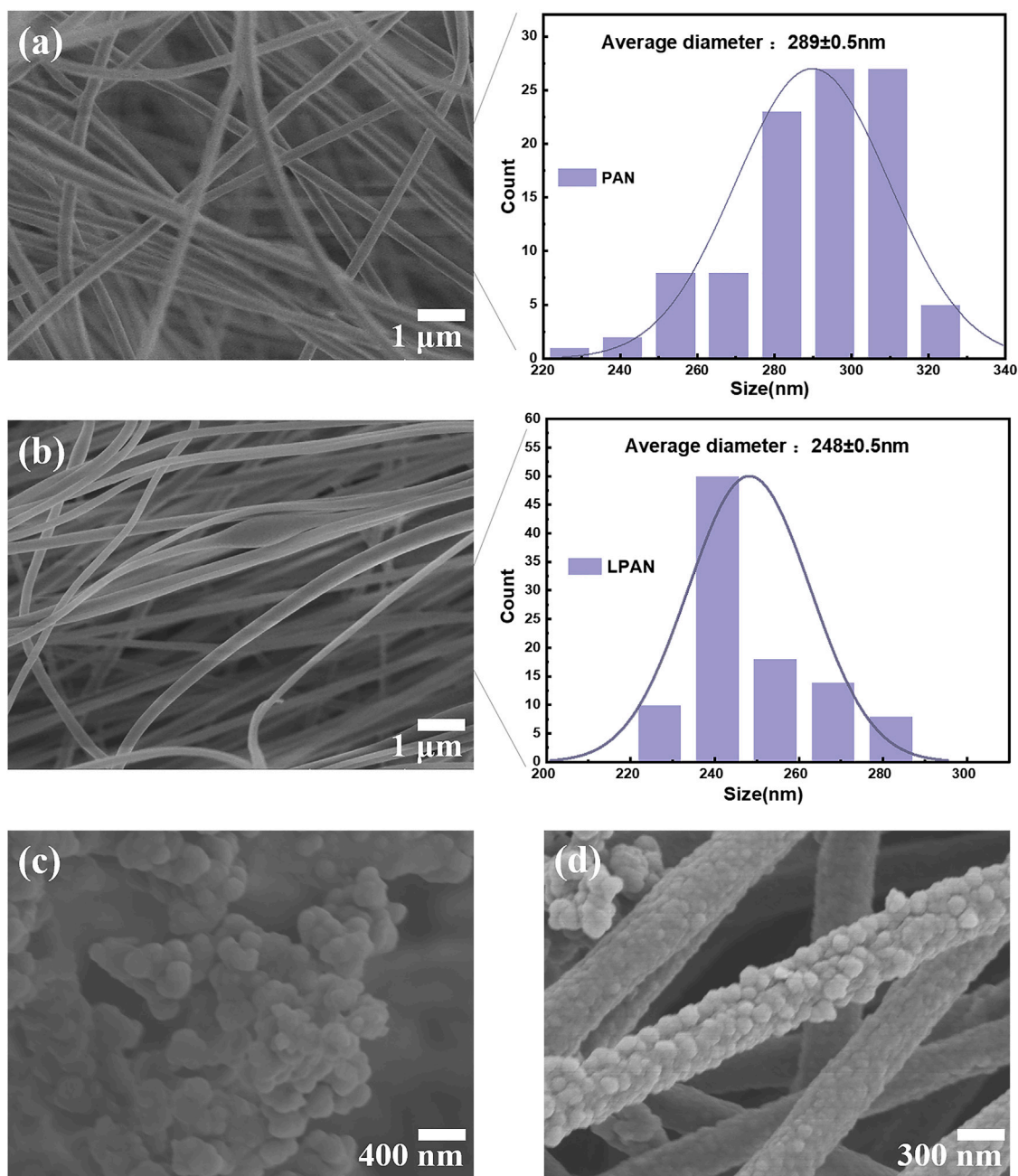


FIGURE 1 | SEM images of electrospun fibers after thermal stabilization with fiber diameter distribution graphs: **(A)** stabilized PAN fibers; **(B)** stabilized LPAN fibers; **(C)** PPy; **(D)** LPAN/PPy.

In this paper, the method of preparing PPy-coated lignin carbon fiber composite films by electrostatic spinning, *in situ* chemical polymerization, and carbonization was proposed. Electrostatic spinning combining carbonization has the advantages of large specific surface area, uniform pore distribution, and low density, compared with the vacuum filtration method. In a three-electrode system, the high capacitance of the composite films electrode was 213.7 F g^{-1} at a current density of 1 A g^{-1} . More importantly, biomass lignin

provided a possibility as a low-cost self-supporting electrode material for energy storage devices.

EXPERIMENTAL SECTION

Materials

Lignin was purchased from Shandong Longli Biotechnology Co., Ltd. Pyrrole, polyacrylonitrile (PAN) ($M_w = 150,000$), and

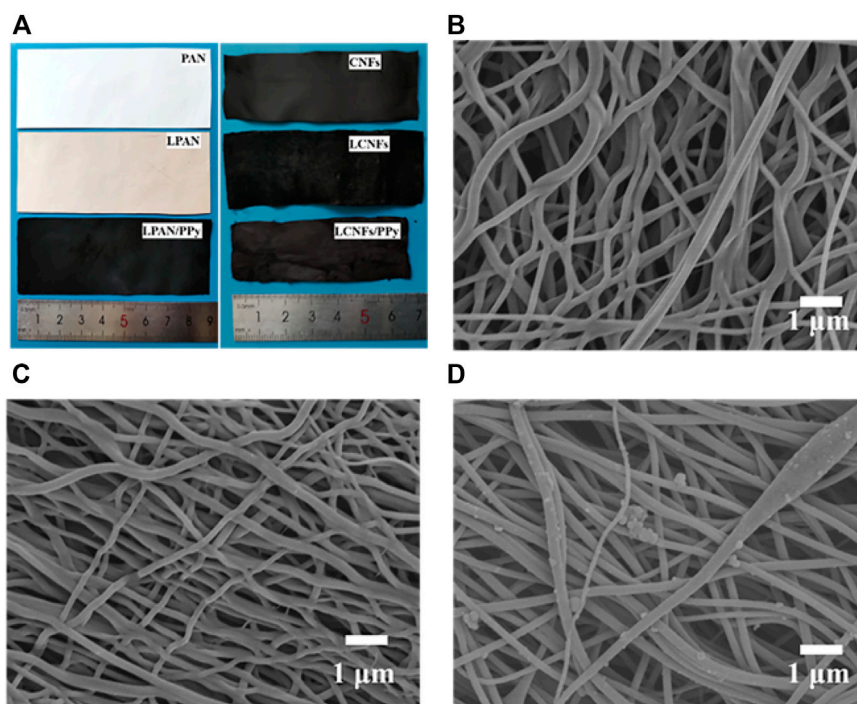


FIGURE 2 | (A) Photographic image of the prepared samples. SEM micrographs of fibers after carbonization graphs: (B) CNFs; (C) LCNFs; (D) LCNFs/PPy.

N,N-dimethylformamide (DMF) were purchased from Shanghai Macklin Biochemical Co., Ltd. Ammonium persulfate ($(\text{NH}_4)_2\text{S}_2\text{O}_8$) and urea ($\text{CH}_4\text{N}_2\text{O}$) were purchased from Beijing Chemical Plant Co., Ltd. All other chemicals were of analytical grade.

Preparation of Electrospinning Solution

The spinning solution was obtained by stirring lignin and PAN (ratio: 0:1 and 1:4) in DMF solvent for 24 h at room temperature until completely dissolved. The precursory solution was transferred into a 5 ml syringe for electrospinning by using a voltage in the range of 15–17 kV and a distance of 13–15 cm from the needle tip to the aluminum foil collector. After spinning, the fibers were collected, and the two kinds of electrospun fiber membranes were named “PAN” and “LPAN,” respectively.

Preparation of Lignin/PPy Filament Fiber

The PPy-coated nanofiber films were prepared using a simple *in situ* chemical polymerization. The above electrospun nanofiber LPAN film was dipped into a beaker containing an aqueous solution of 25 ml pyrrole (5 g L^{-1}), which had been stirred for several minutes in advance. Then, after soaking for 3 h, 25 ml of $(\text{NH}_4)_2\text{S}_2\text{O}_8$ (0.2 mol L^{-1}) solution was added dropwise, and holding at 0°C for 4 h. The sample was removed from the solution and rinsed with deionized water to remove PPy particles and residual reactants and dried in an oven for 4 h. The film containing PPy was named “LPAN/PPy.”

Preparation of Lignin-Based Carbon Fiber/PPy Composites

The freestanding carbonized composites were fabricated as follows. Pyrolysis of polymer fibers was performed in a tubular furnace under the following condition: The heating rate was 1°C min^{-1} from room temperature to 250°C . The temperature was set constant at 250°C for 1 h and from 250 to 900°C with 5°C min^{-1} by blowing N_2 gas. Then, the setup was maintained at that temperature for 2 h and cooled to room temperature. The preparation of lignin-based carbon fiber/PPy composites is shown in **Scheme 1**, which are named “LCNFs/PPy.” For comparison, the electrospun lignin-free carbon fiber film was prepared and marked as CNFs. In addition, the composites without adding PPy were prepared and marked as LCNFs.

Material Characterization

The morphologies of the electrospun fiber membranes, lignin/PPy filament fibers, and lignin-based carbon fiber/PPy composites were characterized via scanning electron microscopy (SEM, SU8010, Hitachi, Japan). X-ray diffractometry (XRD, Ultima IV, Rigaku, Japan) was carried out to study the crystallographic information of the sample. TG-DTA (TG209F3, Netzsch, Germany) was tested under air to analyze the composition ration of the samples. The chemical groups were characterized with a PerkinElmer Frontier Fourier transform infrared (FT-IR) spectrometer.

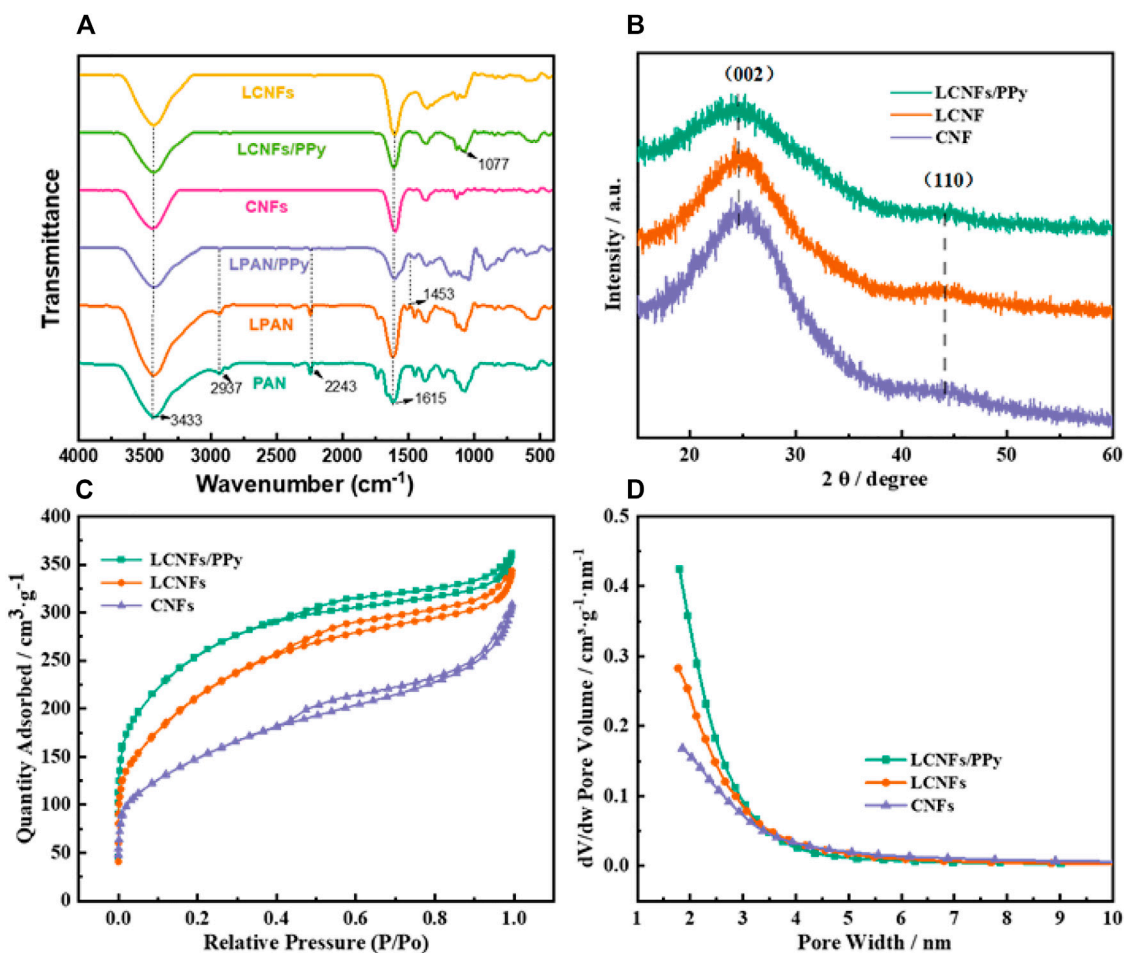


FIGURE 3 | FT-IR spectra (A) of protofilament fibers and carbon fibers, XRD patterns (B), N_2 adsorption–desorption isotherms (C), and pore-size distribution (D) of the carbon fiber composite electrodes.

Electrochemical Measurements

All electrochemical tests were performed on an electrochemical workstation (CHI 660D) using a three-electrode configuration using a 1 M H_2SO_4 aqueous solution as the electrolyte at room temperature. A Pt mesh electrode and an $Hg/HgCl_2$ electrode were used as the counter and reference electrodes, respectively. The cyclic voltammetry (CV) curves were plotted in a potential range between 0 and 1 V at different scan rates from 5 to 500 mV s^{-1} . The EIS experiments in the frequency range of 1 MHz–0.01 Hz were executed at 5 mV AC amplitude. And the specific capacitance was calculated from galvanostatic charge/discharge (GCD) curves according to the following equation (Liu et al., 2021c):

$$C_s = \frac{I \times \Delta t}{m \times \Delta U}, \quad (1)$$

where C_s ($F\text{ g}^{-1}$) is the specific capacitance, I ($A\text{ g}^{-1}$) is the discharge current, Δt (s) is the discharge time, ΔU (V) represents the potential window, and m (g) is the electrode material mass.

RESULTS AND DISCUSSION

Figure 1 shows the SEM images of the PAN, LPAN, PPy, and LPAN/PPy films prepared by electrostatic spinning and *in situ* chemical polymerization, which could intuitively reflect the microscopic morphology and structural differences of the precursor fibers. As shown in Figure 1A, the pure PAN fiber morphology was regular without beading or bending, which had uniform thickness and a diameter of about 289 nm. When the lignin:PAN ratio was 1:4, part of the fiber beaded and fractured (Figure 1B), and the fiber diameter was within the range of 248 nm. The interaction between lignin and PAN may contribute to the agglomerated, beading, and defective fibers. In addition, some lignin groups changed the polarity of the spinning solution, inducing the phenomenon of large fluctuation in the process of high-pressure spinning, which further affected the regularity of fiber diameter (Wang et al., 2013). Figure 1C shows the SEM image of PPy particles prepared by the chemical oxidation method. Besides, as shown in Figure 1D, the electrospinning fibers were coated

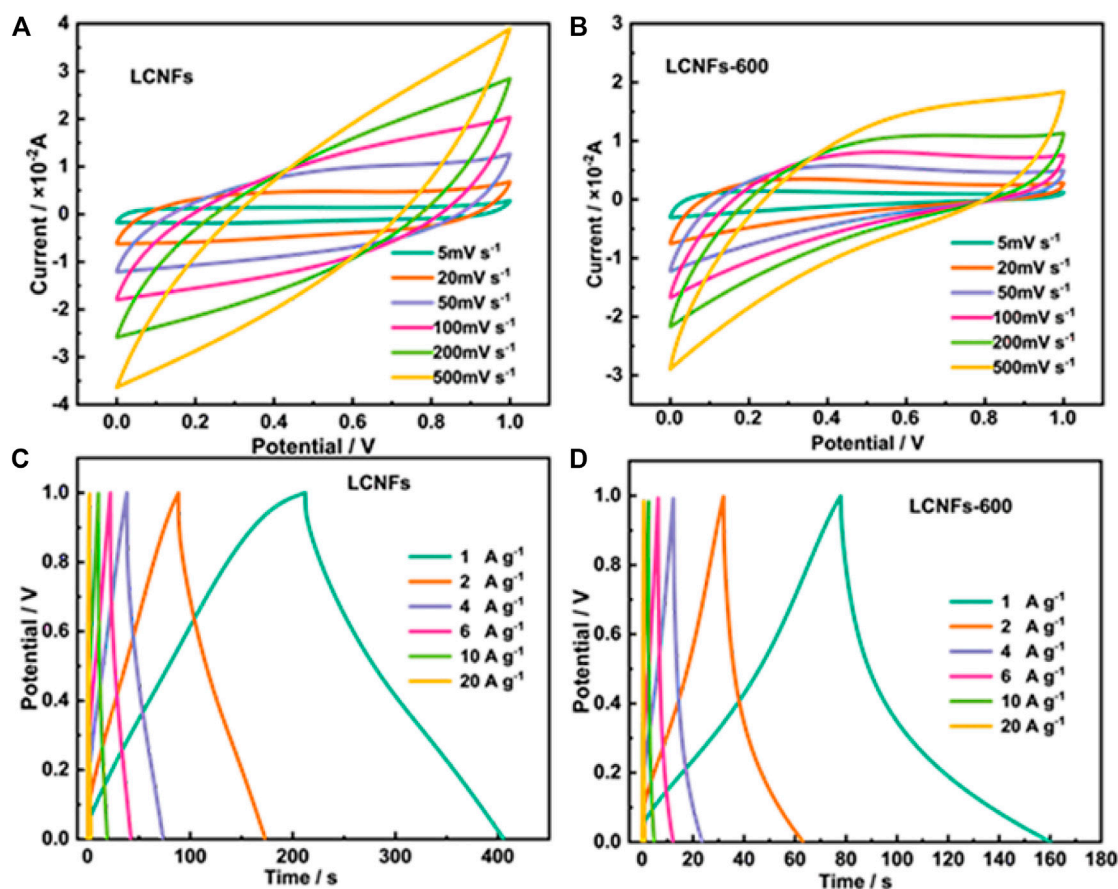


FIGURE 4 | CV curves of LCNFs (A) and LCNFs-600 (B) at different scan rates with a potential range of 0–1 V. GCD cycle curves of LCNFs (C) and LCNFs-600 (D) with different charge densities.

with PPy evenly, and the diameter was mainly distributed at about 200–300 nm.

Compared with lignin-based filament fibers prepared by the electrospinning method, the diameter of carbon fibers after pre-oxidation and high-temperature carbonization was significantly smaller, and part of the fiber showed a state of curvature and connection. It could be more intuitively observed from the digital image in **Figure 2A** that the sample area had a certain contraction after carbonization at 900°C. This could be attributed to the fracture, removal, and cyclization of lignin groups in the fiber (Ding et al., 2016; Ma et al., 2020). The LCNFs (**Figure 2C**) exhibited a smaller diameter than CNFs (**Figure 2B**), which increased the specific surface area and porosity, thereby improving the cyclic stability and specific capacitance. On the contrary, the carbon nanofibers connect and bridge with each other to form a highly conductive network structure that facilitated rapid electron transfer during charging and discharging processes, thus improving the rate capacity. In addition, PPy on the surface of carbon fiber was closely attached (**Figure 2D**), which also contributed to the improvement of electrochemical properties.

FT-IR was performed to determine the chemical structure of the prepared samples (**Figure 3A**). The peak at 3,433 cm^{-1} was

attributed to N-H in PAN, and O-H in the aromatic ring of lignin. In addition, the peaks of PAN at 2,937 and 2,243 cm^{-1} were attributed to C-H and C≡N, respectively (Si et al., 2009; Xu et al., 2021c). It was noted that the O-H peak increased with the increase of lignin content and had a trend of low-wavelength shift, and C≡N cyanine peaks gradually weakened. And the peaks at 1,183 and 1,077 cm^{-1} were C-N and C-H in a PPy long chain, respectively (Si et al., 2008; Wang et al., 2015). The results showed that the pyrrole rings were mainly connected by an α - α bond after the composite PPy on the surface of the filament. The FT-IR spectra of carbon fibers displayed three emblematic bands at 3,430 (N-H stretching), 1,610 (C=C stretching), and 1,370 cm^{-1} ($-\text{CH}_3$ bending), respectively (Si et al., 2013; Ma et al., 2021b). After calcination at 900°C, the groups (cyanogenic C≡N in PAN) of the filament basically disappear, which was due to the decomposition of organic compounds at high temperature and the formation of amorphous carbon. The XRD patterns of carbon fibers are demonstrated in **Figure 3B**. The carbon peak position had been located at 26.6° and 44°, which corresponded to the (002) and (100) diffraction planes of disordered stacking of graphite structures (Jayachandran et al., 2021). It was also confirmed that the linear structure of the fiber was transformed into a heat-resistant trapezoidal structure during

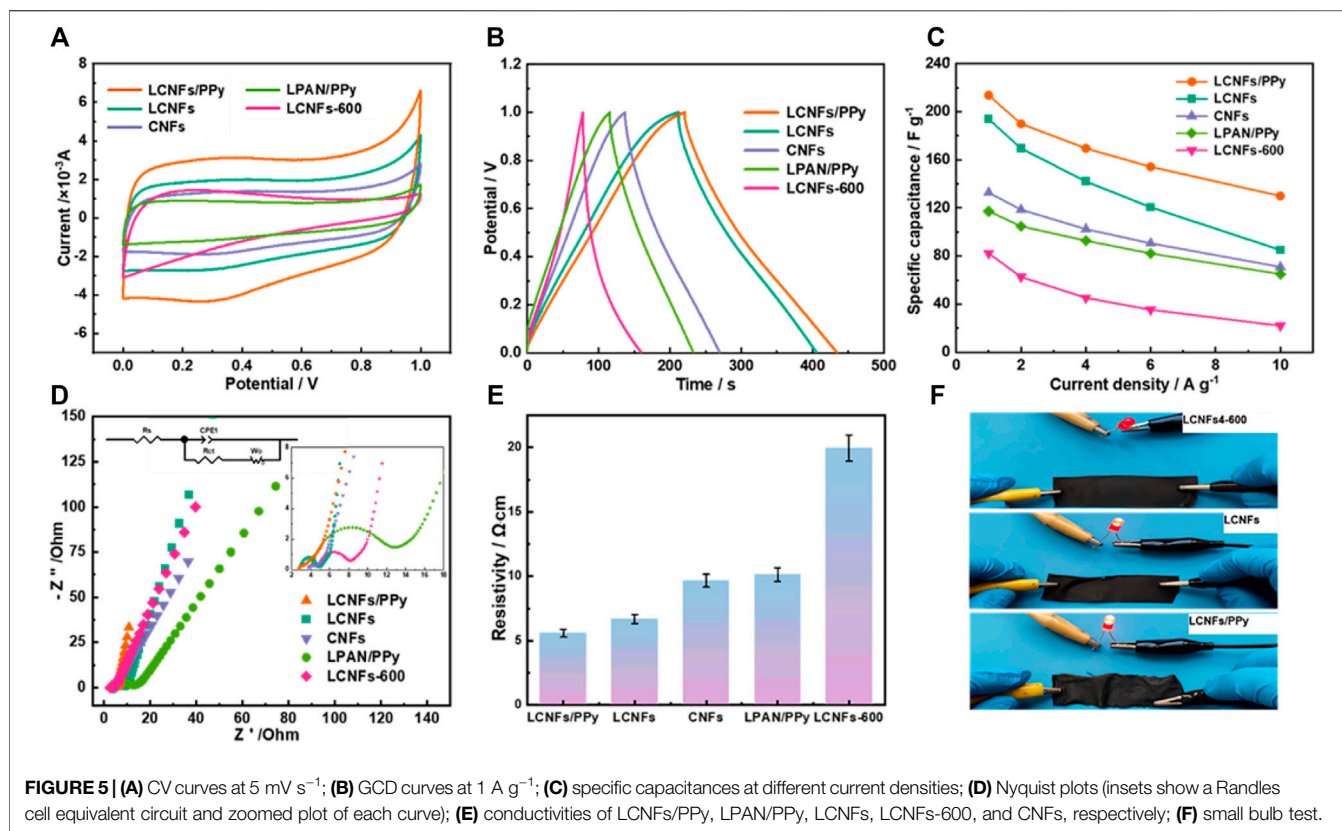
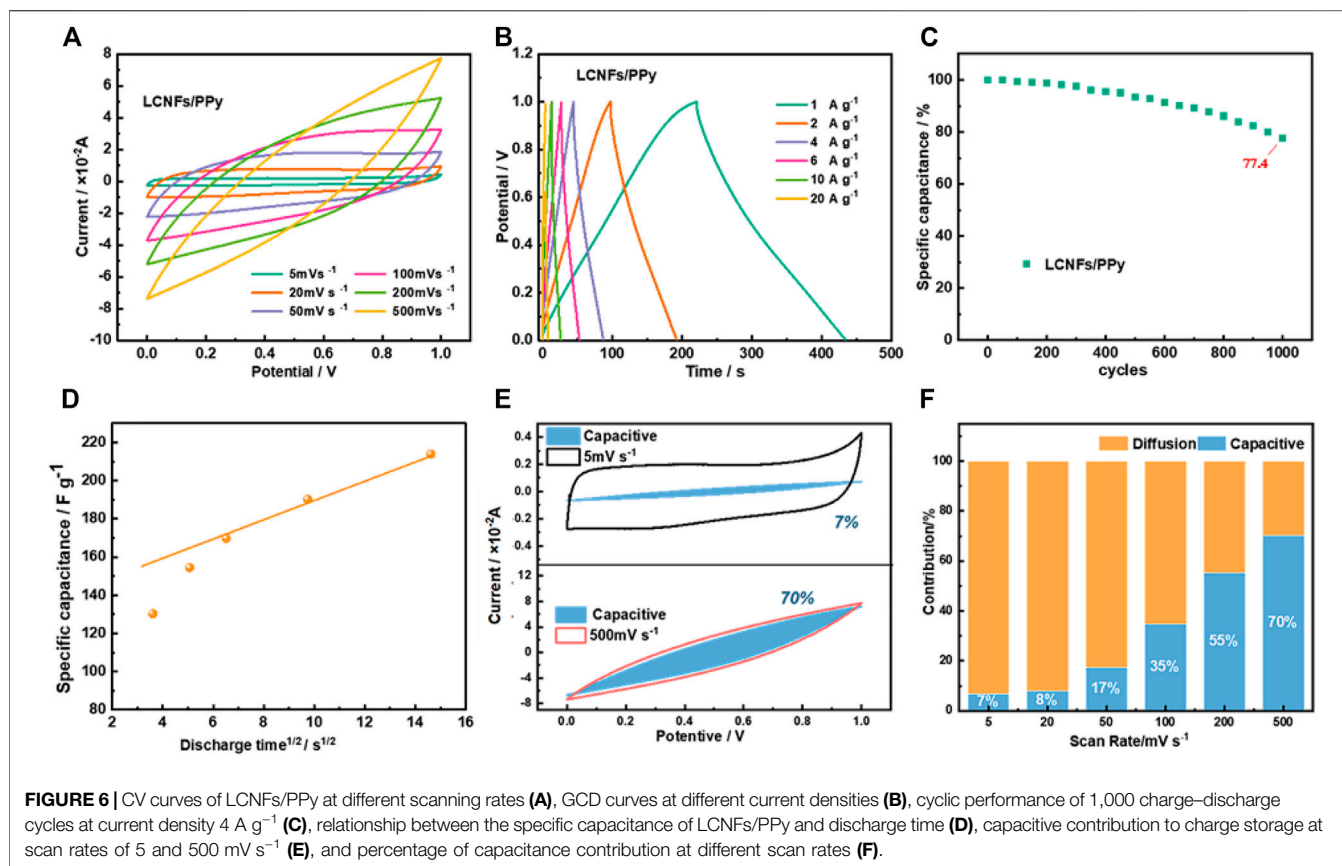


TABLE 1 | Comparison of supercapacitive performance of recently reported lignin-based and PPy-based composite electrodes.

Electrode material	Specific capacitance	Electrolyte	Refs.
Lignin/PAN	148.0 F g ⁻¹ (50 mV s ⁻¹)	0.5 M KOH	Thongsai et al. (2021)
Lignin/LaMnO ₃	95.2 F g ⁻¹ (1 A g ⁻¹)	6 M KOH	Gang et al. (2021)
Lignin/KHCO ₃	114.0 F g ⁻¹ (0.5 A g ⁻¹)	2.5 M KNO ₃	Mutuma et al. (2021)
Lignin	197.3 F g ⁻¹ (0.2 A g ⁻¹)	6 M KOH	Sima et al. (2021)
Lignin	155.0 F g ⁻¹ (0.5 A g ⁻¹)	6 M KOH	Rong et al. (2021)
Alkali lignin	168.3 F g ⁻¹ (10 mV s ⁻¹)	3 M KCl	Rois et al. (2021)
PPy-thieno[3,4-b]thiophene	28.1 F g ⁻¹ (0.1 mA cm ⁻²)	2 M LiCl	Wang et al. (2021b)
N,B-codoped graphene/PPy	160.3 F g ⁻¹ (0.5 A g ⁻¹)	1 M H ₂ SO ₄	Xin et al. (2021)
PPy/birnessite	183.0 F g ⁻¹ (0.5 A g ⁻¹)	1 M Na ₂ SO ₄	Zhuang et al. (2021)
Lignin/PPy	213.7 F g ⁻¹ (1 A g ⁻¹)	1 M H ₂ SO ₄	This work

the pre-oxidation process, and the graphitization crystal structure could provide good structural stability, which was advantageous to improve the capacitive performance. In addition, a large specific surface area provided more active sites for charge storage, which improved the electrochemical performance of supercapacitors. The N₂ adsorption-desorption isotherms and pore-size distribution of composite carbon fibers are illustrated in **Figures 3C,D**, respectively. According to IUPAC classification, the N₂ adsorption-desorption isotherms of the three samples all exhibited a mixed type I curve and type IV curve with a steep increase of N₂ adsorbed at low pressure and a distinct hysteresis loop at high-pressure regions (0.4 < P/P₀ < 1.0), indicating the coexistence of microporous and mesoporous structures

(Schneidermann et al., 2017; Bai et al., 2020). The micropores increased the specific surface area of the material, increasing the active site of pseudo-capacitance reaction, and the mesopores provided a smooth channel to help electrolyte ions quickly enter the reaction interface of the material bulk phase. Therefore, the existence of these pores directly affected the specific capacity of the electrode material. Compared to CNFs (519.81 m² g⁻¹ and 3.55 nm), the BET surface area and pore diameter of LCNFs were 746.37 m² g⁻¹ and 2.76 nm, respectively. It was noted that the specific surface area of LCNFs/PPy reached 872.60 m² g⁻¹ and the average pore size decreased to 2.50 nm after the composite by PPy, which may be caused by the filling of the fiber gap with PPy to form smaller pores.



To explore the electrochemical capacitive properties of carbon fibers at different temperatures, after that, the stabilized lignin/PAN fiber film was carbonized by heating to 600°C as the control sample, denoted as LCNFs-600. The capacitive properties of LCNF and LCNF-600 electrodes were measured in $1 \text{ M H}_2\text{SO}_4$ using a three-electrode system. From the electrode under different scan rate cyclic voltammetry (CV) curves, it is found that the curve area of the LCNFs (Figure 4A) was larger than that of the LCNFs-600 (Figure 4B). And at low scanning rates, the CV curves of LCNFs were closer to rectangles. These results clearly showed that the calcination temperature was 900°C and the graphitization and amorphous area of carbon fibers increased, further improving the specific surface area for better permeation H^+ to access more active sites. Furthermore, at different current densities of $1\text{--}20 \text{ A g}^{-1}$, the GCD curves of the LCNFs were near the isosceles triangle shapes (Figure 4C). Compared to LCNFs-600, the LCNF electrode had an ideal capacitance and ion adsorption/desorption mode during the energy storage process (Figure 4D).

Figure 5A shows the CV curves of composite electrode materials at 5 mV s^{-1} . It was evident that the LCNF/PPy composite films approximated rectangles, which showed good electrochemical reversibility. Compared with LCNF composite films without PPy composite, the area was larger and the specific capacitance was higher, indicating that the addition of conductive polymer PPy could improve the specific capacitance of carbon fibers. In addition, with the addition of lignin, the charge storage

capacity of the material significantly enhanced. This was attributed to the natural pore structure and complex functional groups of lignin, which enhanced the specific surface area and electrochemical reversibility of carbon fibers after calcination (Cao et al., 2020b). In order to better compare the electrochemical performance, chronopotentiograms are drawn for the samples at a constant current density of 1 A g^{-1} in Figure 5B. It could be observed that the LCNF/PPy composite film had a visibly larger discharging time (Δt) than the other samples. The relationships between specific capacitances and current densities of these five samples are shown in Figure 5C. The highest specific capacitance of 213.7 F g^{-1} was obtained for the LCNF/PPy electrode at a current density of 1 A g^{-1} , compared with specific capacitances of 193.8 F g^{-1} , 132.8 F g^{-1} , 117.3 F g^{-1} , and 82.3 F g^{-1} for LCNFs, CNFs, LPAN/PPy, and LCNFs-600, respectively. And the LCNF/PPy electrode also showed a higher specific capacitance, compared with other recently reported lignin and PPy composite electrodes (Table 1). To further verify the excellent properties, EIS measurements were performed in the frequency range from 1 MHz to 0.01 Hz , as shown in Figure 5D. The series resistance of the LCNFs/PPy was only 2.7Ω , and the small semicircle reveals the low charge transfer resistance (R_{ct}). Moreover, it showed a high slope in the high-frequency region, which indicated good ion diffusion process and double-layer behavior in the electrochemical reaction process. Furthermore, the four-probe method was used to

test the conductivity of the composite films, and the results are shown in **Figure 5E**. The addition of PPy into LCNFs has been demonstrated to be an effective strategy to reduce resistivity. The low resistivity of LCNFs/PPy ($5.58 \Omega \text{ cm}^{-1}$) is also demonstrated in the small bulb test in **Figure 5F**. Moreover, the poor conductivity of the calcined sample at 600°C should be caused by its low graphitization degree and long charge diffusion path.

To further clarify the electrochemical behavior of LCNF/PPy films, the complete CV curves and GCD curves of the SCs are plotted in **Figures 6A,B**, respectively. The results in **Figure 6A** showed that all CV curves maintain the similar shape at different scanning rates, demonstrating well capacitance performance and relatively good rate capability. Subsequently, the GCD curves of the LCNFs/PPy are displayed in **Figure 6B**. The curves had a shape of a symmetrical triangle that showed good capacitive behavior. It was important to assess the long-cycle stability of LCNF/PPy positive material by repeating the GCD test at 4 A g^{-1} . **Figure 6C** shows a well stability of about 77% after 1,000 cycles. For further understanding the charge storage process of LCNFs/PPy, the electrochemical dynamics of electrode composite films were studied. The capacitance C could be calculated by (Lin et al., 2015)

$$C = K_1 + K_2 T^{1/2}, \quad (2)$$

where T is the discharge time of the GCD test, k_1 corresponds to the surface capacitance effect (usually from the double-layer capacitance, $T \rightarrow 0$), and $k_2 T^{1/2}$ corresponds to the capacitance effect of diffusion control (affected by the charge and discharge rates, $T \rightarrow \infty$). **Figure 6D** shows the relationship between specific capacitance and discharge time of LCNFs/PPy. When $T \rightarrow 0$, the intercept was k_1 , representing the specific capacitance contributed by the double-layer effect. The double-layer capacitance of LCNFs/PPy reached 148.7 F g^{-1} , accounting for 69.6% of the total capacitance, which showed that the capacitance effect mainly came from double-layer adsorption (Chen et al., 2021a). In addition, the capacitance control and diffusion control in total charge storage could be further calculated and quantified by (Zhang et al., 2021b)

$$i = k_1 v + k_2 v^{1/2}. \quad (3)$$

In short, at a certain voltage (v), the current response (i) consisted of two parts, wherein $k_1 v$ and $k_2 v^{1/2}$ corresponded to the surface control process (pseudo-capacitance and double-layer capacitance) and the diffusion control process, respectively (Chen et al., 2021b). As could be seen from **Figures 6E,F**, the capacitance contribution of

the LCNF/PPy positive electrode film enlarged from 7 to 70% with the increase of scanning rate, which was caused by the relatively low ion diffusion rate at large scanning rates.

CONCLUSION

In summary, carbon fiber precursors with lignin and PAN (ratio 1:4) were prepared by the electrostatic spinning method, and PPy was *in situ* polymerized to improve electrochemical performance. In addition, lignin/PPy composite films were produced without the use of any crosslinking agents and physical/chemical activation during thermal stabilization and carbonization. Lignin/PPy composite films with microporous and mesoporous structures were designed as the positive materials of the supercapacitor. Among them, the LCNF/PPy electrode had a large specific surface area, high pore volume, and the specific capacitance of 213.7 F g^{-1} at the current density of 1 A g^{-1} . This work has the potential to use lignin to produce carbon fibers as a low-cost electrode material for high-performance supercapacitors.

DATA AVAILABILITY STATEMENT

The original contributions presented in the study are included in the article/Supplementary Material, and further inquiries can be directed to the corresponding authors.

AUTHOR CONTRIBUTIONS

Z-RH, D-DL, and M-GM investigated the data and wrote the original draft. T-HK, M-SK, TX, M-GM, S-EC, and CS supervised the work and reviewed and edited the paper.

FUNDING

The financial support from the Innovation and Entrepreneurship Training Program for College Students (No. G201910022053) is gratefully acknowledged, and this work was also partially supported by the R&D Program for Forest Science Technology (2019151D10-2223-0301) provided by the Korea Forest Service (Korea Forestry Promotion Institute) and Technology Development Program (S3030198) funded by the Ministry of SMEs and Startups (MSS, South Korea) to S-EC.

REFERENCES

- An, L., Si, C., Wang, G., Sui, W., and Tao, Z. (2019). Enhancing the Solubility and Antioxidant Activity of High-Molecular-Weight Lignin by Moderate Depolymerization via In Situ Ethanol/acid Catalysis. *Ind. Crops Prod.* 128, 177–185. doi:10.1016/j.indcrop.2018.11.009
- Bai, Z., Liu, S., Chen, P., Cheng, G., Wu, G., Li, H., et al. (2020). Nickel Nanoparticles Embedded in Porous Carbon Nanofibers and its Electrochemical Properties. *Nanotechnology* 31, 305705. doi:10.1088/1361-6528/ab8594

- Camiré, A., Espinasse, J., Chabot, B., and Lajeunesse, A. (2020). Development of Electrospun Lignin Nanofibers for the Adsorption of Pharmaceutical Contaminants in Wastewater. *Environ. Sci. Pollut. Res.* 27, 3560–3573. doi:10.1007/s11356-018-3333-z
- Cao, M., Cheng, W., Ni, X., Hu, Y., and Han, G. (2020). Lignin-based Multi-Channels Carbon Nanofibers @ SnO₂ Nanocomposites for High-Performance Supercapacitors. *Electrochimica Acta* 345, 136172. doi:10.1016/j.electacta.2020.136172
- Cao, Q., Zhu, M., Chen, J., Song, Y., Li, Y., and Zhou, J. (2020). Novel Lignin-Cellulose-Based Carbon Nanofibers as High-Performance Supercapacitors. *ACS Appl. Mater. Inter.* 12, 1210–1221. doi:10.1021/acsami.9b14727

- Chen, L., Yu, H., Li, Z., Chen, X., and Zhou, W. (2021a). Cellulose Nanofiber Derived Carbon Aerogel with 3D Multiscale Pore Architecture for High-Performance Supercapacitors. *Nanoscale* 13, 17837–17845. doi:10.1039/d1nr04838d
- Chen, Q., Jin, J., Song, M., Zhang, X., Li, H., Zhang, J., et al. (2021b). High-energy Aqueous Ammonium-Ion Hybrid Supercapacitors. *Adv. Mater.*, e2107992. doi:10.1002/adma.202107992
- Chen, S., Qiu, L., and Cheng, H.-M. (2020a). Carbon-based Fibers for Advanced Electrochemical Energy Storage Devices. *Chem. Rev.* 120, 2811–2878. doi:10.1021/acs.chemrev.9b00466
- Chen, S., Wang, G., Sui, W., Parvez, A. M., Dai, L., and Si, C. (2020b). Novel Lignin-Based Phenolic Nanosphere Supported Palladium Nanoparticles with Highly Efficient Catalytic Performance and Good Reusability. *Ind. Crops Prod.* 145, 112164. doi:10.1016/j.indcrop.2020.112164
- Chen, S., Wang, G., Sui, W., Parvez, A. M., and Si, C. (2020c). Synthesis of Lignin-Functionalized Phenolic Nanosphere Supported Ag Nanoparticles with Excellent Dispersion Stability and Catalytic Performance. *Green. Chem.* 22, 2879–2888. doi:10.1039/c9gc04311j
- Choi, C., Ashby, D. S., Butts, D. M., DeBlock, R. H., Wei, Q., Lau, J., et al. (2020). Achieving High Energy Density and High Power Density with Pseudocapacitive Materials. *Nat. Rev. Mater.* 5, 5–19. doi:10.1038/s41578-019-0142-z
- Dai, L., Ma, M., Xu, J., Si, C., Wang, X., Liu, Z., et al. (2020). All-Lignin-Based Hydrogel with Fast pH-Stimuli Responsiveness for Mechanical Switching and Actuation. *Chem. Mater.* 32, 4324–4330. doi:10.1038/s41578-019-0142-z
- Dai, L., Zhu, W., Lu, J., Kong, F., Si, C., Ni, Y., et al. (2019). A Lignin-Containing Cellulose Hydrogel for Lignin Fractionation. *Green. Chem.* 21, 5222–5230. doi:10.1039/c9gc01975h
- Dallmeyer, I., Ko, F., and Kadla, J. F. (2010). Electrospinning of Technical Lignins for the Production of Fibrous Networks. *J. Wood Chem. Tech.* 30, 315–329. doi:10.1080/02773813.2010.527782
- Deng, J., Sun, S.-F., Zhu, E.-Q., Yang, J., Yang, H.-Y., Wang, D.-W., et al. (2021). Sub-micro and Nano-Lignin Materials: Small Size and Rapid Progress. *Ind. Crops Prod.* 164, 113412. doi:10.1016/j.indcrop.2021.113412
- Ding, R., Wu, H., Thunga, M., Bowler, N., and Kessler, M. R. (2016). Processing and Characterization of Low-Cost Electrospun Carbon Fibers from Organosolv Lignin/polyacrylonitrile Blends. *Carbon* 100, 126–136. doi:10.1016/j.carbon.2015.12.078
- Ding, Y., Huang, S., Sun, Y., Li, Y., Zhu, L., and Wang, S. (2021). Preparation of Nitrogen and Sulfur Co-doped and Interconnected Hierarchical Porous Biochar by Pyrolysis of Mantis Shrimp in CO₂ Atmosphere for Symmetric Supercapacitors. *ChemElectroChem* 8, 3745–3754. doi:10.1002/celec.202101151
- Du, H., Liu, W., Zhang, M., Si, C., Zhang, X., and Li, B. (2019). Cellulose Nanocrystals and Cellulose Nanofibrils Based Hydrogels for Biomedical Applications. *Carbohydr. Polym.* 209, 130–144. doi:10.1016/j.carbpol.2019.01.020
- Du, H., Parit, M., Liu, K., Zhang, M., Jiang, Z., Li, T.-S., et al. (2021). Multifunctional Cellulose Nanopaper with superior Water-Resistant, Conductive, and Antibacterial Properties Functionalized with Chitosan and Polypyrrole. *ACS Appl. Mater. Inter.* 13, 32115–32125. doi:10.1021/acsami.1c06647
- Du, H., Zhang, M., Liu, K., Parit, M., Jiang, Z., Zhang, X., et al. (2022). Conductive PEDOT:PSS/cellulose Nanofibril Paper Electrodes for Flexible Supercapacitors with superior Areal Capacitance and Cycling Stability. *Chem. Eng. J.* 428, 131994. doi:10.1016/j.cej.2021.131994
- Fan, L.-Q., Liu, G.-J., Wu, J.-H., Liu, L., Lin, J.-M., and Wei, Y.-L. (2014). Asymmetric Supercapacitor Based on Graphene Oxide/polypyrrole Composite and Activated Carbon Electrodes. *Electrochimica Acta* 137, 26–33. doi:10.1016/j.electacta.2014.05.137
- Fan, L.-Q., Tu, Q.-M., Geng, C.-L., Huang, J.-L., Gu, Y., Lin, J.-M., et al. (2020). High Energy Density and Low Self-Discharge of a Quasi-Solid-State Supercapacitor with Carbon Nanotubes Incorporated Redox-Active Ionic Liquid-Based Gel Polymer Electrolyte. *Electrochimica Acta* 331, 135425. doi:10.1016/j.electacta.2019.135425
- Fu, Q., Hao, S., Meng, L., Xu, F., and Yang, J. (2021). Engineering Self-Adhesive Polyzwitterionic Hydrogel Electrolytes for Flexible Zinc-Ion Hybrid Capacitors with superior Low-Temperature Adaptability. *ACS Nano* 15, 18469–18482. doi:10.1021/acsnano.1c08193
- Gang, H.-E., Park, G.-T., Jeon, H.-B., Kim, S.-Y., and Jeong, Y. G. (2021). PAN/lignin and LaMnO₃-Derived Hybrid Nanofibers for Self-Standing High-Performance Energy Storage Electrode Materials. *J. Mater. Sci.* 56, 19636–19650. doi:10.1007/s10853-021-06528-3
- He, D., Tang, F., Jiang, H., Hirunpinyopas, W., Cetinkaya, T., and Li, Z. (2021). The Vertically Aligned graphene/graphite/PPy Composites Electrode and its PPy Thickness-dependent Electrochemical Performance. *Electrochimica Acta* 399, 139426. doi:10.1016/j.electacta.2021.139426
- Jayachandran, M., Kishore Babu, S., Maiyalagan, T., Rajadurai, N., and Vijayakumar, T. (2021). Activated Carbon Derived from Bamboo-Leaf with Effect of Various Aqueous Electrolytes as Electrode Material for Supercapacitor Applications. *Mater. Lett.* 301, 130335. doi:10.1016/j.matlet.2021.130335
- Li, D.-D., Yuan, Q., Huang, L.-Z., Zhang, W., Guo, W.-Y., and Ma, M.-G. (2021). Preparation of Flexible N-Doped Carbon Nanotube/MXene/PAN Nanocomposite Films with Improved Electrochemical Properties. *Ind. Eng. Chem. Res.* 60, 15352–15363. doi:10.1021/acs.iecr.1c03182
- Li, J., Wang, Y., Xu, W., Wang, Y., Zhang, B., Luo, S., et al. (2019a). Porous Fe₂O₃ Nanospheres Anchored on Activated Carbon Cloth for High-Performance Symmetric Supercapacitors. *Nano Energy* 57, 379–387. doi:10.1016/j.nanoen.2018.12.061
- Li, X., Xu, R., Yang, J., Nie, S., Liu, D., Liu, Y., et al. (2019b). Production of 5-hydroxymethylfurfural and Levulinic Acid from Lignocellulosic Biomass and Catalytic Upgradation. *Ind. Crops Prod.* 130, 184–197. doi:10.1016/j.indcrop.2018.12.082
- Li, Z., Hanafy, H., Zhang, L., Sellaoui, L., Schadeck Netto, M., Oliveira, M. L. S., et al. (2020). Adsorption of Congo Red and Methylene Blue Dyes on an Ashitaba Waste and a Walnut Shell-Based Activated Carbon from Aqueous Solutions: Experiments, Characterization and Physical Interpretations. *Chem. Eng. J.* 388, 124263. doi:10.1016/j.cej.2020.124263
- Lian, Y. M., Ni, M., Zhou, L., Chen, R. J., and Yang, W. (2018). Synthesis of Biomass-Derived Carbon Induced by Cellular Respiration in Yeast for Supercapacitor Applications. *Chem. Eur. J.* 24, 18068–18074. doi:10.1002/chem.201803836
- Lin, T., Chen, I.-W., Liu, F., Yang, C., Bi, H., Xu, F., et al. (2015). Nitrogen-doped Mesoporous Carbon of Extraordinary Capacitance for Electrochemical Energy Storage. *Science* 350, 1508–1513. doi:10.1126/science.aab3798
- Liu, H., Du, H., Zheng, T., Liu, K., Ji, X., Xu, T., et al. (2021a). Cellulose Based Composite Foams and Aerogels for Advanced Energy Storage Devices. *Chem. Eng. J.* 426, 130817. doi:10.1016/j.cej.2021.130817
- Liu, H., Xu, T., Liu, K., Zhang, M., Liu, W., Li, H., et al. (2021b). Lignin-based Electrodes for Energy Storage Application. *Ind. Crops Prod.* 165, 113425. doi:10.1016/j.indcrop.2021.113425
- Liu, H., Zhu, J., Li, Z., Shi, Z., Zhu, J., and Mei, H. (2021c). Fe₂O₃/N Doped rGO Anode Hybridized with NiCo LDH/Co(OH)₂ Cathode for Battery-like Supercapacitor. *Chem. Eng. J.* 403, 126325. doi:10.1016/j.cej.2020.126325
- Liu, K., Du, H., Liu, W., Liu, H., Zhang, M., Xu, T., et al. (2021d). Cellulose Nanomaterials for Oil Exploration Applications. *Polym. Rev.* doi:10.1080/15583724.2021.2007121
- Liu, K., Du, H., Zheng, T., Liu, H., Zhang, M., Zhang, R., et al. (2021e). Recent Advances in Cellulose and its Derivatives for Oilfield Applications. *Carbohydr. Polym.* 259, 117740. doi:10.1016/j.carbpol.2021.117740
- Liu, K., Du, H., Zheng, T., Liu, W., Zhang, M., Liu, H., et al. (2021f). Lignin-containing Cellulose Nanomaterials: Preparation and Applications. *Green Chem.* 23, 9723–9746. doi:10.1039/d1gc02841c
- Liu, S., Du, H., Liu, K., Ma, M., Kwon, Y.-E., Si, C., et al. (2021g). Flexible and Porous Co₃O₄-Carbon Nanofibers as Binder-free Electrodes for Supercapacitors. *Adv. Compos. Hybrid. Mater.* 4, 1367–1383. doi:10.1007/s42114-021-00344-8
- Liu, W., Du, H., Liu, H., Xie, H., Xu, T., Zhao, X., et al. (2020a). Highly Efficient and Sustainable Preparation of Carboxylic and Thermostable Cellulose Nanocrystals via FeCl₃-Catalyzed Innocuous Citric Acid Hydrolysis. *ACS Sustain. Chem. Eng.* 8, 16691–16700. doi:10.1021/acssuschemeng.0c06561
- Liu, W., Du, H., Liu, K., Liu, H., Xie, H., Si, C., et al. (2021h). Sustainable Preparation of Cellulose Nanofibrils via Choline Chloride-Citric Acid Deep Eutectic Solvent Pretreatment Combined with High-Pressure Homogenization. *Carbohydr. Polym.* 267, 118220. doi:10.1016/j.carbpol.2021.118220

- Liu, W., Du, H., Zhang, M., Liu, K., Liu, H., Xie, H., et al. (2020b). Bacterial Cellulose-Based Composite Scaffolds for Biomedical Applications: A Review. *ACS Sustain. Chem. Eng.* 8, 7536–7562. doi:10.1021/acssuschemeng.0c00125
- Ma, C., Kim, T.-H., Liu, K., Ma, M.-G., Choi, S.-E., and Si, C. (2021a). Multifunctional Lignin-Based Composite Materials for Emerging Applications. *Front. Bioeng. Biotechnol.* 9, 708976. doi:10.3389/fbioe.2021.708976
- Ma, C., Ma, M., Si, C., Ji, X., and Wan, P. (2021b). Flexible MXene-Based Composites for Wearable Devices. *Adv. Funct. Mater.* 31, 2009524. doi:10.1002/adfm.202009524
- Ma, C., Yuan, Q., Du, H., Ma, M., Si, C., and Wan, P. (2020). Multiresponsive MXene ($\text{Ti}_3\text{C}_2\text{T}_x$)-Decorated Textiles for Wearable Thermal Management and Human Motion Monitoring. *ACS Appl. Mater. Inter.* 12, 34226–34234. doi:10.1021/acsaami.0c10750
- Mutuma, B. K., Sylla, N. F., Bubu, A., Ndiaye, N. M., Santoro, C., Brilloni, A., et al. (2021). Valorization of Biodigester Plant Waste in Electrodes for Supercapacitors and Microbial Fuel Cells. *Electrochimica Acta* 391, 138960. doi:10.1016/j.electacta.2021.138960
- Park, G.-T., Jeon, H.-B., Kim, S.-Y., Gang, H.-E., and Jeong, Y. G. (2022). Flexible and Self-Standing Polyimide/lignin-Derived Carbon Nanofibers for High-Performance Supercapacitor Electrode Material Applications. *Mater. Sci. Eng. B* 275, 115530. doi:10.1016/j.mseb.2021.115530
- Qu, W., Yang, J., Sun, X., Bai, X., Jin, H., and Zhang, M. (2021). Towards Producing High-Quality Lignin-Based Carbon Fibers: A Review of Crucial Factors Affecting Lignin Properties and Conversion Techniques. *Int. J. Biol. Macromolecules* 189, 768–784. doi:10.1016/j.ijbiomac.2021.08.187
- Rois, M. F., Widiyastuti, W., Setyawan, H., Rahmatika, A. M., and Ogi, T. (2021). Preparation of Activated Carbon from Alkali Lignin Using Novel One-step Process for High Electrochemical Performance Application. *Arabian J. Chem.* 14, 103162. doi:10.1016/j.arabj.2021.103162
- Rong, K., Wei, J., Wang, Y., Liu, J., Qiao, Z.-A., Fang, Y., et al. (2021). Deep Eutectic Solvent Assisted Zero-Waste Electrospinning of Lignin Fiber Aerogels. *Green. Chem.* 23, 6065–6075. doi:10.1039/d1gc01872h
- Sahoo, N. G., Rana, S., Cho, J. W., Li, L., and Chan, S. H. (2010). Polymer Nanocomposites Based on Functionalized Carbon Nanotubes. *Prog. Polym. Sci.* 35, 837–867. doi:10.1016/j.progpolymsci.2010.03.002
- Schneidermann, C., Jäckel, N., Oswald, S., Giebler, L., Presser, V., and Borchardt, L. (2017). Solvent-free Mechanochemical Synthesis of Nitrogen-Doped Nanoporous Carbon for Electrochemical Energy Storage. *ChemSusChem* 10, 2416–2424. doi:10.1002/cssc.201700459
- Shang, Z., An, X., Zhang, H., Shen, M., Baker, F., Liu, Y., et al. (2020). Houttuynia-derived Nitrogen-Doped Hierarchically Porous Carbon for High-Performance Supercapacitor. *Carbon* 161, 62–70. doi:10.1016/j.carbon.2020.01.020
- Si, C., Jiang, J., Liu, S., Hu, H., Ren, X., Yu, G., et al. (2013). A new lignan glycoside and phenolics from the branch wood of *Pinus banksiana* Lambert. *Holzforchung* 67, 357–363. doi:10.1515/hf-2012-0137
- Si, C., Kim, J. K., Bae, Y. S., and Li, S. M. (2009). Phenolic compounds in the leaves of *Populus ussuriensis* and their antioxidant activities. *Planta Med.* 75, 1165–1167. doi:10.1055/s-0029-1185476
- Si, C., Liu, Z., Kim, J. K., and Bae, Y. S. (2008). Structure elucidation of phenylethanoid glycosides from *Paulownia tomentosa* Steud. var. *tomentosa* wood. *Holzforchung* 62, 197–200. doi:10.1515/HF.2008.047
- Sima, G., Gan, L. H., Chang, L. J., Cui, Y., and Kankala, R. K. (2021). Efficient Fabrication of Ordered Mesoporous Carbon Derived from Lignin via Deep Eutectic Solvent Pretreatment for Supercapacitors. *Microp. Mesop. Mater.* doi:10.1016/j.micromeso.2021.111192
- Szabó, L., Milotskyi, R., Ueda, H., Tsukegi, T., Wada, N., and Takahashi, K. (2021). Controlled Acetylation of Kraft Lignin for Tailoring Polyacrylonitrile-Kraft Lignin Interactions towards the Production of Quality Carbon Nanofibers. *Chem. Eng. J.* 405, 126640. doi:10.1016/j.cej.2020.126640
- Thongsai, N., Hrimchum, K., and Aussawasathien, D. (2021). Carbon Fiber Mat from palm-kernel-shell Lignin/polyacrylonitrile as Intrinsic-Doping Electrode in Supercapacitor. *Sust. Mater. Tech.* 30, e00341. doi:10.1016/j.susmat.2021.e00341
- Tian, W., Li, Y., Zhou, J., Wang, T., Zhang, R., Cao, J., et al. (2021). Implantable and Biodegradable Micro-supercapacitor Based on a Superassembled Three-Dimensional Network Zn@PPy Hybrid Electrode. *ACS Appl. Mater. Inter.* 13, 8285–8293. doi:10.1021/acsaami.0c19740
- Tian, Y., Yang, C., Song, X., Liu, J., Zhao, L., Zhang, P., et al. (2019). Engineering the Volumetric Effect of Polypyrrole for Auto-Deformable Supercapacitor. *Chem. Eng. J.* 374, 59–67. doi:10.1016/j.cej.2019.05.153
- Wang, H., Du, H., Liu, K., Liu, H., Xu, T., Zhang, S., et al. (2021a). Sustainable Preparation of Bifunctional Cellulose Nanocrystals via Mixed H_2SO_4 /formic Acid Hydrolysis. *Carbohydr. Polym.* 266, 118107. doi:10.1016/j.carbpol.2021.118107
- Wang, H., Xie, H., Du, H., Wang, X., Liu, W., Duan, Y., et al. (2020). Highly Efficient Preparation of Functional and Thermostable Cellulose Nanocrystals via H_2SO_4 Intensified Acetic Acid Hydrolysis. *Carbohydr. Polym.* 239, 116233. doi:10.1016/j.carbpol.2020.116233
- Wang, J.-G., Liu, H., Sun, H., Hua, W., Wang, H., Liu, X., et al. (2018). One-pot Synthesis of Nitrogen-Doped Ordered Mesoporous Carbon Spheres for High-Rate and Long-Cycle Life Supercapacitors. *Carbon* 127, 85–92. doi:10.1016/j.carbon.2017.10.084
- Wang, L. L., Li, X. J., Huang, X., Han, S., and Jiang, J. B. (2022). Activated green Resources to Synthesize N, P Co-doped O-Rich Hierarchical Interconnected Porous Carbon for High-Performance Supercapacitors. *J. All. Comp.* doi:10.1016/j.jallcom.2021.161908
- Wang, M., Meng, Y., Sun, G., Ma, S., Qian, M., and Duan, M. (2021b). Designing Cross-linked Pyrrole-thieno [3,4- B] Thiophene Copolymer to Push Forward Electrochemical Performance and Access Flexible Micro-supercapacitor with Ultra-long Cycling Stability. *Int. J. Energy. Res.* 45, 20878–20890. doi:10.1002/er.7144
- Wang, N., Li, G., Yu, Z., Zhang, X., and Qi, X. (2015). Conductive Polypyrrole/viscose Fiber Composites. *Carbohydr. Polym.* 127, 332–339. doi:10.1016/j.carbpol.2015.03.076
- Wang, S.-X., Yang, L., Stubbs, L. P., Li, X., and He, C. (2013). Lignin-derived Fused Electrospun Carbon Fibrous Mats as High Performance Anode Materials for Lithium Ion Batteries. *ACS Appl. Mater. Inter.* 5, 12275–12282. doi:10.1021/am4043867
- Wulan Septiani, N. L., Kaneti, Y. V., Fathoni, K. B., Wang, J., Ide, Y., Yuliarto, B., et al. (2020). Self-assembly of Nickel Phosphate-Based Nanotubes into Two-Dimensional Crumpled Sheet-like Architectures for High-Performance Asymmetric Supercapacitors. *Nano Energy* 67, 104270. doi:10.1016/j.nanoen.2019.104270
- Xin, Q., Yu, J., Lin, J., and Zang, Y. (2021). Fabrication of N,B-codoped Graphene Aerogel/PPy Composites for Asymmetric Supercapacitor. *Chemistryselect* 6, 11569–11576. doi:10.1002/slct.202102995
- Xiong, C., Li, M., Zhao, W., Duan, C., and Ni, Y. (2020). Flexible N-Doped Reduced Graphene Oxide/carbon Nanotube-MnO₂ Film as a Multifunctional Material for High-Performance Supercapacitors, Catalysts and Sensors. *J. Materiomics* 6, 523–531. doi:10.1016/j.jmat.2020.03.008
- Xu, J., Li, C., Dai, L., Xu, C., Zhong, Y., Yu, F., et al. (2020a). Biomass Fractionation and Lignin Fractionation towards Lignin Valorization. *ChemSusChem* 16, 4284–4295. doi:10.1002/cssc.202001491
- Xu, P., Tong, J., Zhang, L., Yang, Y., Chen, X., Wang, J., et al. (2022). Dung Beetle Forewing-Derived Nitrogen and Oxygen Self-Doped Porous Carbon for High Performance Solid-State Supercapacitors. *J. Alloys Comp.* 892, 162129. doi:10.1016/j.jallcom.2021.162129
- Xu, R., Du, H., Liu, C., Liu, H., Wu, M., Zhang, X., et al. (2021a). An Efficient and Magnetic Adsorbent Prepared in a Dry Process with Enzymatic Hydrolysis Residues for Wastewater Treatment. *J. Clean. Prod.* 313, 127834. doi:10.1016/j.jclepro.2021.127834
- Xu, R., Liu, K., Du, H., Liu, H., Cao, X., Zhao, X., et al. (2020b). Falling Leaves Return to Their Roots: A Review on the Preparation of γ -Valerolactone from Lignocellulose and its Application in the Conversion of Lignocellulose. *ChemSusChem* 13, 6461–6476. doi:10.1002/cssc.202002008
- Xu, T., Du, H., Liu, H., Liu, W., Zhang, X., Si, C., et al. (2021b). Advanced Nanocellulose-Based Composites for Flexible Functional Energy Storage Devices. *Adv. Mater.* 2021, 2101368. doi:10.1002/adma.202101368
- Xu, X., Yang, T., Zhang, Q., Xia, W., Ding, Z., Eid, K., et al. (2020c). Ultrahigh Capacitive Deionization Performance by 3D Interconnected MOF-Derived Nitrogen-Doped Carbon Tubes. *Chem. Eng. J.* 390, 124493. doi:10.1016/j.cej.2020.124493
- Xu, Y., Chen, S., Zhu, M., and Liu, Y. (2021c). Novel Silicon-contained Lignin-based Carbon Fibers Derived from Bamboo Pulping Black Liquor with Improved Electrochemical Performance for Supercapacitors. *J. Appl. Polym. Sci.* 138, 51321. doi:10.1002/app.51321

- Yang, H., Ye, S., Zhou, J., and Liang, T. (2019). Biomass-derived Porous Carbon Materials for Supercapacitor. *Front. Chem.* 7. doi:10.3389/fchem.2019.00274
- Yuan, Q., and Ma, M.-G. (2021). Conductive Polypyrrole Incorporated nanocellulose/MoS₂ Film for Preparing Flexible Supercapacitor Electrodes. *Front. Mater. Sci.* 15, 227–240. doi:10.1007/s11706-021-0549-5
- Zhan, Y., Hu, Y., Chen, Y., Yang, Q., Shi, Z., and Xiong, C. (2021). In-situ Synthesis of Flexible Nanocellulose/carbon Nanotube/polypyrrole Hydrogels for High-Performance Solid-State Supercapacitors. *Cellulose* 28, 7097–7108. doi:10.1007/s10570-021-03998-1
- Zhang, J., Su, L., Ma, L., Zhao, D., Qin, C., Jin, Z., et al. (2017). Preparation of Inflorescence-like ACNF/PANI/NiO Composite with Three-Dimension Nanostructure for High Performance Supercapacitors. *J. Electroanalytical Chem.* 790, 40–49. doi:10.1016/j.jelechem.2017.02.047
- Zhang, P., Du, H., Liu, K., Nie, S., Xu, T., Zhang, X., et al. (2021a). Fabrication and Applications of Cellulose-Based Nanogenerators. *Adv. Compos. Hybrid. Mater.* 4, 865–884. doi:10.1007/s42114-021-00312-2
- Zhang, P., Wang, M., Liu, Y., Yang, S., Wang, F., Li, Y., et al. (2021b). Dual-redox-sites Enable Two-Dimensional Conjugated Metal-Organic Frameworks with Large Pseudocapacitance and Wide Potential Window. *J. Am. Chem. Soc.* 143, 10168–10176. doi:10.1021/jacs.1c03039
- Zhou, B., Li, Z., Liu, W., Shao, Y., Ren, X., Lv, C., et al. (2021). Hierarchical Porous Carbon/kraft Lignin Composite with Significantly Improved superior Pseudocapacitive Behavior. *Electrochimica Acta* 398, 139307. doi:10.1016/j.electacta.2021.139307
- Zhou, Y., Maleski, K., Anasori, B., Thostenson, J. O., Pang, Y., Feng, Y., et al. (2020). Ti₃C₂T_x MXene-Reduced Graphene Oxide Composite Electrodes for Stretchable Supercapacitors. *ACS Nano* 14, 3576–3586. doi:10.1021/acsnano.9b10066
- Zhu, Y., Chen, M., Zhang, Y., Zhao, W., and Wang, C. (2018). A Biomass-Derived Nitrogen-Doped Porous Carbon for High-Energy Supercapacitor. *Carbon* 140, 404–412. doi:10.1016/j.carbon.2018.09.009
- Zhuang, Y., Niu, Q. Q., Wu, W. J., Yan, D., Huang, J. J., Peng, S. L., et al. (2021). Enhanced Supercapacitive Properties of Hydrohausmannite by In-Situ Polymerization of Polypyrrole. *Electrochim. Acta*. doi:10.1016/j.electacta.2021.137989

Conflict of Interest: The authors declare that the research was conducted in the absence of any commercial or financial relationships that could be construed as a potential conflict of interest.

Publisher's Note: All claims expressed in this article are solely those of the authors and do not necessarily represent those of their affiliated organizations, or those of the publisher, the editors, and the reviewers. Any product that may be evaluated in this article, or claim that may be made by its manufacturer, is not guaranteed or endorsed by the publisher.

Copyright © 2022 Hu, Li, Kim, Kim, Xu, Ma, Choi and Si. This is an open-access article distributed under the terms of the Creative Commons Attribution License (CC BY). The use, distribution or reproduction in other forums is permitted, provided the original author(s) and the copyright owner(s) are credited and that the original publication in this journal is cited, in accordance with accepted academic practice. No use, distribution or reproduction is permitted which does not comply with these terms.



Pyroligneous Acids of Differently Pretreated Hybrid Aspen Biomass: Herbicide and Fungicide Performance

Pasi Korkalo^{1*}, Marleena Hagner^{2,3}, Janne Jänis⁴, Marko Mäkinen⁴, Janne Kaseva², Ulla Lassi⁵, Kimmo Rasa⁶ and Tuula Jyske⁷

¹Production Systems, Natural Resources Institute Finland (Luke), Rovaniemi, Finland, ²Natural Resources, Natural Resources Institute Finland (Luke), Jokioinen, Finland, ³Ecosystems and Environment Research Programme, University of Helsinki, Helsinki, Finland, ⁴Department of Chemistry, University of Eastern Finland, Joensuu, Finland, ⁵Research Unit of Sustainable Chemistry, University of Oulu, Oulu, Finland, ⁶Production Systems, Natural Resources Institute Finland (Luke), Jokioinen, Finland, ⁷Production Systems, Natural Resources Institute Finland (Luke), Espoo, Finland

OPEN ACCESS

Edited by:

Zhongqing Ma,
Zhejiang Agriculture and Forestry
University, China

Reviewed by:

Mattia Bartoli,
Politecnico di Torino, Italy
Zhuohua Sun,
Beijing Forestry University, China

*Correspondence:

Pasi Korkalo
pasi.korkalo@luke.fi

Specialty section:

This article was submitted to
Green and Sustainable Chemistry,
a section of the journal
Frontiers in Chemistry

Received: 24 November 2021

Accepted: 23 December 2021

Published: 08 February 2022

Citation:

Korkalo P, Hagner M, Jänis J, Mäkinen M, Kaseva J, Lassi U, Rasa K and Jyske T (2022) Pyroligneous Acids of Differently Pretreated Hybrid Aspen Biomass: Herbicide and Fungicide Performance. *Front. Chem.* 9:821806. doi: 10.3389/fchem.2021.821806

The pyroligneous acids (PAs) of woody biomass produced by torrefaction have pesticidal properties. Thus, PAs are potential alternatives to synthetic plant protection chemicals. Although woody biomass is a renewable feedstock, its use must be efficient. The efficiency of biomass utilization can be improved by applying a cascading use principle. This study is novel because we evaluate for the first time the pesticidal potential of PAs derived from the bark of hybrid aspen (*Populus tremula* L. × *Populus tremuloides* Michx.) and examine simultaneously how the production of the PAs can be interlinked with the cascade processing of hybrid aspen biomass. Hybrid aspen bark contains valuable extractives that can be separated before the hemicellulose is thermochemically converted into plant protection chemicals. We developed a cascade processing scheme, where these extractives were first extracted from the bark with hot water (HWE) or with hot water and alkaline alcohol (HWE+AAE) prior to their conversion into PAs by torrefaction. The herbicidal performance of PAs was tested using *Brassica rapa* as the test species, and the fungicidal performance was proven using *Fusarium culmorum*. The pesticidal activities were compared to those of the PAs of debarked wood and of commercial pesticides. According to the results, extractives can be separated from the bark without overtly diminishing the weed and fungal growth inhibitor performance of the produced PAs. The HWE of the bark before its conversion into PAs appeared to have an enhancing effect on the herbicidal activity. In contrast, HWE+AAE lowered the growth inhibition performance of PAs against both the weeds and fungi. This study shows that hybrid aspen is a viable feedstock for the production of herbicidal and fungicidal active chemicals, and it is possible to utilize biomass according to the cascading use principle.

Keywords: pyroligneous acid, hybrid aspen, biomass, torrefaction, biopesticide, herbicide, fungicide, cascade utilization

INTRODUCTION

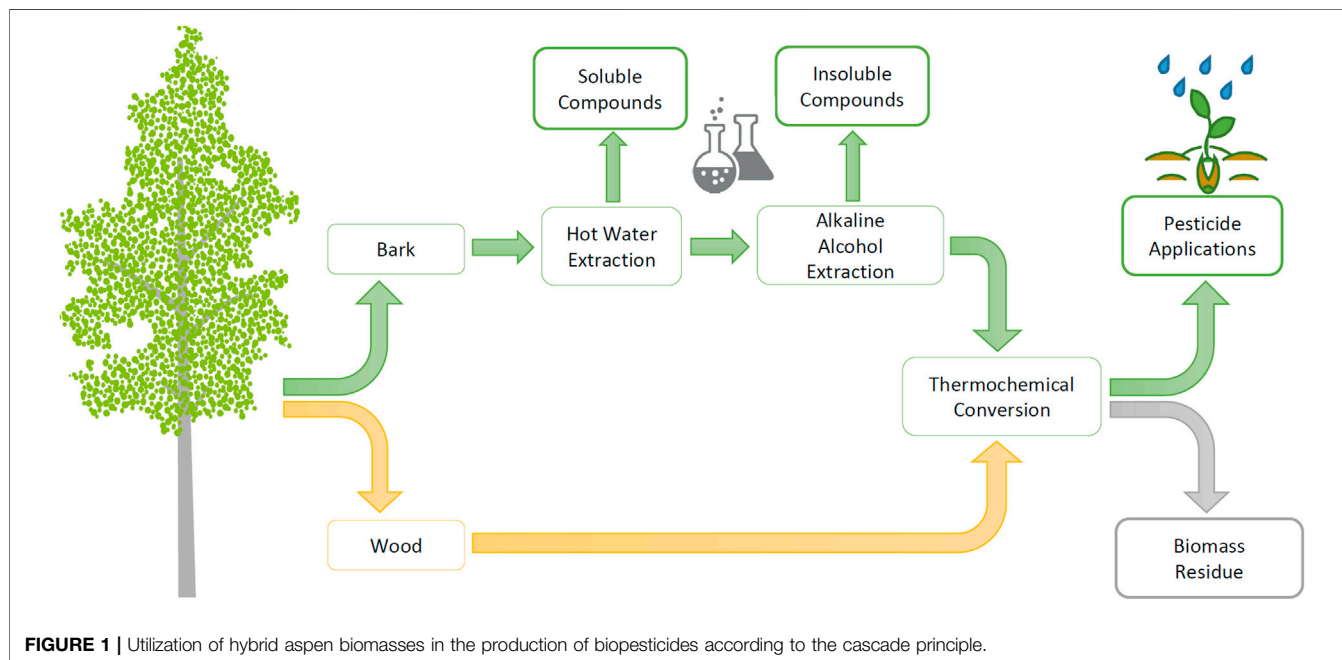
One possible way to produce acidic chemical products from biomass is thermochemical conversion, e.g., torrefaction (Fagernäs et al., 2015; Grewal et al., 2018). Typically, the technique is used as a biomass pretreatment process, such as for gasification or combustion (Van der Stelt et al., 2011; Cahyanti et al., 2020). Torrefaction is a technique similar to slow pyrolysis, where conversion is performed at a slow heating rate under anaerobic conditions, but is conducted at lower temperatures. When using lower process temperatures, the hemicelluloses of lignocellulosic biomass are the most essential precursors to produce pyroligneous acids (PAs) (Collard and Blin, 2014; Chen et al., 2019). PAs are known to have pesticidal activity (Oramahi and Yoshimura, 2013; Theapparatt et al., 2015; Oramahi et al., 2018; Hagner et al., 2020); therefore, the method appears to be a viable way to produce bio-based pesticides as a substitute for synthetic chemicals (Tiilikkala et al., 2010). Wood material is a potential and renewable natural resource for the production of pesticide-active chemicals, but the sustainable use of forest resources must be taken into account (Cambero and Sowlati, 2014). This can be promoted by studying the use of raw materials according to the cascade principle and by investigating the effects of the processes on the chemical products.

In recent years, the utilization of biomass in chemical production has increased. Recovery techniques are mainly conversion processes, such as catalytic, biological, and thermochemical processes. So far, the sources of bio-based raw materials for biochemical production are largely those that compete with other sectors, such as the food industry. In the cultivation of forest as a feedstock source, such a competitive situation is more easily evaded (Cherubini, 2010). Currently, the

high market potential for bio-based chemicals includes biofuels, biomaterials such as degradable plastics, and a variety of biochemical applications such as adhesives and packaging coatings (Cherubini, 2010; Hassan et al., 2019). The number of bio-based products on the market is clearly growing, but the utilization of by-products is still low (Cherubini, 2010). As the chemical industry aims to electrify processes with renewable energy, produce biochemicals by converting from forest biomass, and reduce the need for fossil-derived reagents in biochemical production (Toivanen et al., 2021), pyrolysis techniques such as torrefaction are essential methods to be explored. The method also has the advantage of being able to generate side streams for recovery (Figure 1).

There are still numerous encounters with the enhanced use of forest biomass, such as availability, price, and sustainability (Toivanen et al., 2021). One possible solution could be to cultivate fast-growing tree species as a source of raw materials for chemical production. By cultivating clonal trees, the raw material can be tailored (Korkalo et al., 2020) to serve better the needs of the chemical industry, locate the biomass source closer to chemical production, and accelerate biomass production (Beuker et al., 2016).

At the same time, as the goal is to increase the utilization of forest biomass in the chemical industry, the adequacy and sustainable consumption of forest resources must be taken into account (Azapagic, 2014). This means more efficient and versatile use of raw materials, where cascade utilization plays a key role. The term “cascade utilization” describes an enhanced use of biomass that produces multiple products before the biomass ends up as a waste residue, energy production, or other end-products. There is no consistent description of the concept of the cascade principle, but the definition of the term is met if the utilization of biomass involves linear utilization,



product side streams, recycling, and other activities that increase the life cycle of biomass or maximizes its value in use (Keegan et al., 2013; Sokka et al., 2015).

Cultivated hybrid aspen is an interesting raw material alternative for various bio-based conversion products due to its rapid biomass yield potential. In Finland, the tree species reaches its felling age in the first growth cycle in 20–25 years and in the second growth cycle in 15 years. In northern growth areas, the growth rate compared to other commercially important tree species can be 40% faster than birch and 50% faster than spruce. Thanks to its rapid growth, the biomass yield of cultured hybrid aspen can reach up to 20 m³ ha⁻¹ year⁻¹ in 25-year cycles (Beuker et al., 2016).

This study investigated the use of hybrid aspen (*Populus tremula* L. × *Populus tremuloides* Michx.) as a feedstock and the cascade utilization of the biomass in the production of herbicidal and fungicidal active chemicals (Figure 1). Due to the low extractive content of the debarked wood, the wood biomass is led directly to thermochemical conversion. However, the bark is known to be rich in extractives (Korkalo et al., 2020), so the effects of bark raw material pre-extraction on the pesticidal activity of PAs were studied.

Hot water extraction (HWE) was chosen as the first pre-extraction step for bark cascade processing (Figure 1) since the method can be used to separate soluble hydrophilic extractives into value-added products (Rasi et al., 2019). Moreover, HWE at moderate temperature and normal atmospheric pressure is not expected to significantly affect bark hemicellulose contents. The soluble hydrophilic compounds consist of tannins and strongly antioxidant phenolic substances (Korkalo et al., 2020). These groups of compounds are of interest for several practical applications, e.g., tannins in rigid foam forming (Tondi and Pizzi, 2009; Varila et al., 2020) and phenolic compounds as antioxidants in various end uses (Reuter et al., 2010).

Alkaline alcohol extraction (AAE), which can be used to separate insoluble bark compounds such as suberinic acids, was chosen as the second pre-extraction step to be tested (Figure 1). Suberin-derived fatty acids have been found to have promising properties to act, e.g., as a coating material for paper, fabrics, and packaging (Korpinen et al., 2019). The pretreatment of the bark with AAE prior to conversion to the biopesticide has been considered, even though hemicellulose structures are known to be soluble under alkaline conditions (Stoklosa and Hodge, 2012). Since hemicelluloses are the essential precursors for PA formation, the effect of bark AAE pretreatment on the pesticidal activity of PAs was analyzed in this study.

The hypothesis of this study is that several valuable products can be separated from hybrid aspen biomass without losing all the potential of PAs to be suitable for herbicide and fungicide applications. The herbicidal activity of PAs produced from wood, bark, and pre-extracted bark was tested using *Brassica rapa* as the model plant and the fungicidal activity tested using *Fusarium culmorum*. The activity tests examined how well the bio-based pesticides compete with the efficacy of commercial products and whether the biomass can be utilized in the production of biopesticides according to the cascade principle.

MATERIALS AND METHODS

Chemical Analysis of Wood and Bark Biomass Samples

Six sample trees of hybrid aspen clones (*P. tremula* L. × *P. tremuloides* Michx.) were randomly selected from a designed field trial of the Natural Resources Institute Finland (Luke) near Lohja, Southern Finland (60°12' N, 23°55' E). For chemical analyses of hybrid aspen biomass, a sample disc was cut from each tree at breast height (1.3 m). Bark mass, including both inner and outer layers, was peeled from the wood, after which both separated sample fractions were freeze dried. Dried bark and wood samples were ground with a 0.75 mm milling blade (rotor mill PULVERISETTE; FRITSCH, Idar-Oberstein, Germany) and stored at -20°C until analysis. Chemical assays made from wood and bark were used to characterize the wood chemical composition of hybrid aspen biomass and to examine the differences between the separated biomass fractions. Chemical characterizations were determined by performing similar chemical analyses for both sample fractions, except for suberinic acids which were determined only from bark samples (Table 1).

For the torrefaction and the bark cascade processing experiments, wood, bark, hot water-extracted bark (HWE bark), and hot water and alkaline alcohol-extracted bark (HWE+AAE bark) samples were prepared by pooling the biomass of six sample trees into representative bulk samples of each feedstock. Feedstock samples were prepared for the torrefaction experiments freshly after collection. For the pesticide (i.e., herbicide and fungicide) experiments, one PA sample was produced from each of the feedstocks. The collected PA samples were used for pesticide experiments and for acid strength analysis shortly after the conversion. Information on the hybrid aspen tree, sampling data, and the list of chemical analyses are shown in Table 1.

Lipophilic and Hydrophilic Extractive Contents

Lipophilic and hydrophilic extractives of wood (*n* = 6) and bark (*n* = 6) were determined from freeze-dried and finely ground samples using the accelerated solvent extraction (ASE-350, Dionex, Sunnyvale, CA, USA) method. Lipophilic compounds were extracted with hexane at 90°C three times for 15 min, followed by extraction of the hydrophilic compounds with 95% acetone (aq) at 100°C three times for 15 min. Each separated lipophilic and hydrophilic extractive solution was adjusted to a final volume of 50 ml with used extractants, after which samples of each solution were dried in a nitrogen evaporator at 40°C to a dry matter residue to determine the extractive yields. Extract-free wood and bark samples were used for the determination of hemicellulose, cellulose, lignin, and suberinic acid contents of the bark. The method was modified from Willför et al. (2003).

Determination of Bark Suberinic Acid

The suberinic acid content of the bark was determined from extractive-free samples (*n* = 6) with a modified method adapted from Krogell et al. (2012). Bark samples were weighed into seal

TABLE 1 | Basic information on hybrid aspen tree samples, chemical composition analysis for the wood and bark biomass fractions, number of biomass samples prepared for torrefaction, and chemical characterization of pyroligneous acids

Hybrid aspen clone sample tree information	
<i>Populus tremula</i> L. × <i>Populus tremuloides</i> Michx.	<i>n</i> = 6
Planting year	1998
National Register ID ^a	C05-99-14
Log volume (m ³)	0.571 ± 0.068
Height (dm)	278 ± 10
Diameter 1.3 (mm)	236 ± 22
Diameter 5.0 (mm)	216 ± 19
Bark yield, fresh weight (wt%)	6.5 ± 0.4
Chemical analyses of the hybrid aspen wood and bark samples	
Tree trunk sampling height	1.3 m
No. of bark and wood samples	<i>n</i> = 6
Hydrophilic extractives: <i>wood and bark</i>	Gravimetric analysis
Lipophilic extractives: <i>wood and bark</i>	Gravimetric analysis
Suberin-derived fatty acid: <i>bark</i>	GC-MS
Lignin: <i>wood and bark</i>	Soluble and insoluble lignin
Cellulose: <i>wood and bark</i>	Acid hydrolysis, GC-FID
Hemicellulose: <i>wood and bark</i>	Acid methanolysis, GC-FID
Hybrid aspen feedstock samples for torrefaction	
Wood	<i>n</i> = 1
Bark	<i>n</i> = 1
HWE bark	Hot water extracted, <i>n</i> = 1
HWE+AAE bark	Hot water and alkaline alcohol extracted, <i>n</i> = 1
Chemical analyses of pyroligneous acids	
Acid content	Titrimetric determination
Water content	Karl Fischer titration
Organic matter	Calculated based on acid and water contents
Compositional analysis of organic matter	FT-ICR characterization

HWE, *hot water extraction*; AAE, *alkaline alcohol extraction*; GC-FID, *gas chromatography with a flame ionization detector*; FT-ICR, *Fourier transform ion cyclotron resonance*

^aThe national list of approved basic forest reproductive material, kept by the Finnish Food Authority (Finnish Food Authority, 2021).

tight test tubes, followed by the addition of 3% potassium hydroxide–ethanol solution (KOH, *w/v*). The bark samples were extracted for 2 h at 70°C. The solution containing suberinic acids was separated and collected by vacuum filtration. The bark residue was dried overnight at 105°C and saved for lignin assays. Suberinic acid solution samples were measured into sample tubes and diluted with water. Bromocresol green was added to the samples as a pH indicator, after which the sample solutions were acidified with 0.25 M aqueous sulfuric acid. After pH adjustment, an internal standard mix of C21:0 and betulinol in *tert*-butyl methyl ether (MTBE) was added to the samples. Suberinic acids, including the internal standard, were separated from aqueous solution using liquid–liquid extraction with the MTBE solvent. The liquid–liquid extraction was repeated a total of three times. Finally, the collected suberinic acid and the internal standard containing the MTBE solution was washed with water before drying in a nitrogen evaporator at 40°C. The dry residues of the samples were silylated by adding a reagent mix of pyridine–BSTFA–TMCS in a 1:4:1 ratio and allowed to react at 70°C for 45 min. The clear phase of the silylated samples was collected and the content of suberinic acids was quantitated against the internal standard of C21:0 using gas chromatography–mass spectrometry (GC-MS).

Determination of Lignin Content

The lignin content of the hybrid aspen samples was determined for wood from the extractive-free samples (*n* = 6) and for the bark from samples previously prepared for the determination of suberinic acids (*n* = 6). The total lignin content of the samples was determined as the sum of acid-soluble and insoluble (Klason) lignin. The prepared bark and wood samples were dried at 105°C overnight and weighed in duplicate for analysis. Of sulfuric acid, 72% was added to the sample vessels and mixed thoroughly, after which the samples were incubated for 1 h at 30°C. After incubation, the acid content of the samples was diluted to 4% with water, and the solution was transferred into a glass vessel with a screw cap. The samples were then placed in an autoclave at 120–125°C for 1 h, after which they were removed from the autoclave and allowed to cool to room temperature. Acid-insoluble lignin was separated from the samples using a vacuum filter and finally dried overnight at 105°C for weighing. The acid-soluble lignin separated by vacuum filtration was analyzed spectrophotometrically at 240 nm. The lignin content was analyzed and calculated according to the laboratory analytical procedure (LAP) (Sluiter et al., 2012).

Determination of Cellulose Content

The cellulose content of bark ($n = 6$) and wood ($n = 6$) was determined from the extract-free samples with the acid hydrolysis method adapted from Krogell et al. (2012). Samples and cellulose standards were weighed into sealable glass tubes, followed by the addition of 72% aqueous sulfuric acid. The strong acid solution was allowed to take effect for 2 h, after which it was diluted with water and allowed to react for the next 4 h. The acid content of the samples was further reduced by the addition of water and the samples left to stand overnight at room temperature. The following day, the samples were placed in an autoclave for 1 h at 120–125°C. Bromocresol green was added as a pH indicator, and the acidity of the solutions was neutralized with barium carbonate. D-Sorbitol was added into the wood, bark, and standard samples as an internal standard, after which the samples were mixed thoroughly and centrifuged. The separated clear phase was collected and evaporated to dryness in a nitrogen evaporator at 40°C, and finally in a vacuum oven at 40°C. Samples were silylated by the addition of pyridine, hexamethyldisilazane (HMDS), and trimethylchlorosilane (TMCS) and left to react overnight. The next day, the samples were analyzed by gas chromatography with a flame ionization detector (GC-FID). The cellulose contents of the samples were calculated by means of an inner standard.

Determination of Hemicelluloses Content

The acid methanolysis method for the determination of bark ($n = 6$) and wood ($n = 6$) hemicelluloses content was adapted from Sundberg et al. (1996). Extract free bark and wood samples, as well as standard samples (monosaccharide mix of arabinose (Ara), glucose (Glc), glucuronic acid (GlcA), galactose (Gal), galacturonic acid (GalA), mannose (Man), rhamnose (Rha), 4-*O*-methylglucuronic acid (4-*O*-Me-GlcA), and xylose (Xyl); 1.0 mg/ml of each) were measured in sealable pressure-resistant glass containers. Methanolysis reagent (2 M HCl in anhydrous methanol) was added to the samples and placed in a 100°C oven for 5 h. After cooling the samples, the acid content of the samples was neutralized with pyridine, and a mixture of sorbitol and resorcinol in methanol was added to the samples as an internal standard. The separated clear phase was collected from the samples and dried in a nitrogen evaporator at 40°C to dryness. Samples were silylated by the addition of pyridine, HMDS, and TMCS and left to react overnight at room temperature. The samples were then analyzed with GC-FID to identify hemicellulose sugar units and to calculate the concentrations by using internal standards to determine the hemicellulose content.

Biomass Pre-Extraction and Torrefaction Process to Produce Plant Protection Chemicals

Preparation of a Hot Water-Extracted Bark Sample for Torrefaction

To prepare the HWE bark feedstock sample ($n = 1$), 2 kg of bark mass was pooled from six sample trees. For the extraction, the water-to-dry matter ratio was adjusted to

6.1:1 (v/m) by checking the dry matter (d.m.) content of the bark sample with a moisture analyzer (MLB 50-3N, KERN & Sohn GmbH, Balingen, Germany) before adding the required amount of water. Bark mass was extracted in a steel boiler at normal atmospheric pressure at 90°C for 2 h. After extraction, the HWE bark sample was divided into two: one half was saved for torrefaction and the other half saved for the following alkaline alcohol extraction (Figure 1).

Preparation of the Alkaline Alcohol-Extracted Bark Sample for Torrefaction

The hot water and alkaline alcohol-extracted bark (HWE+AAE bark, $n = 1$) was prepared from the previously prepared HWE bark mass. The AAE method was adapted from Ržíkovs et al. (2014) and Korpinen et al. (2019). The AAE extractant mixture was prepared from crystalline sodium hydroxide (NaOH), water, and IPA (2-propanol) (Merck KGaA, Darmstadt, Germany) in a ratio of 1,200 ml IPA:300 ml H₂O:20 g NaOH:100 g HWE bark d.m. The amounts of NaOH, water, and IPA required for the extractant mixture were calculated based on the d.m. content of the HWE bark sample, which was checked with a moisture analyzer (MLB 50-3N, KERN & Sohn GmbH, Balingen, Germany). The extraction solvent was prepared by dissolving NaOH in water before mixing with IPA and finally adding with HWE bark into a glass laboratory flask. The sample was extracted at normal atmospheric pressure by heating the extraction vessel in a hot water bath at 85°C for 3 h. After extraction, the HWE+AAE bark sample was rinsed with water until the pH of the rinsing water decreased.

Torrefaction of Wood, Bark, and Pre-Extracted Bark Biomass

The biomass conversion process was carried out in a bench-scale slow pyrolysis batch reactor under anaerobic conditions. The oxygen in the system was removed by purging the pyrolysis vessel with nitrogen gas before heating. The pyrolysis equipment consisted of a temperature control unit, an indirectly heating furnace, a gas-tight pyrolysis vessel with an internal thermometer (TCC-K250-6.0-KY), a water-cooled condenser with a condensate collection vessel, and a gas flow meter (drum-type gas meter, TG1/5, RITTER, Bochum, Germany). Hybrid aspen wood, bark, HWE bark, and HWE+AAE bark feedstocks were dried at 37°C before being placed into the pyrolysis apparatus. The sample sizes and d.m. contents (in weight percent), respectively, of dried biomass were 440.1 g, 97.7 wt.% for wood; 440.0 g, 96.2 wt.% for bark; 440.0 g, 96.0 wt.% for HWE bark; and 231.0 g, 96.2 wt.% for HWE+AAE bark. The torrefaction heating steps were programmed to ramp up from the pre-drying phase to the target temperature of 280°C. The actual measured heating rate of the pyrolysis vessel was 1.7°C/min from an initial temperature range of 30–250°C, after which the heating rate was decreased before reaching the temperature of 279 ± 2°C. The level of the target temperature was maintained for 40–50 min. The yields of solids and PAs formed during torrefaction were weighed and the total mass of gas formed calculated by subtracting the total mass of the solid and PA products from the weights of the feedstock samples loaded. All

product yields were determined as mass percentages (weight percent) of the amount of samples loaded into the pyrolysis vessel.

Chemical Analysis of Conversion Distillates Pyroligneous Acid Titratable Acidity

The titratable acid strength of the PAs was determined by titrating the solutions with 1 M aqueous NaOH solution and calculating the result as acetic acid equivalent. Titration pH change was measured with a pH meter (SevenExcellence, Mettler-Toledo, Columbus, OH, USA) and electrode (Mettler-Toledo InLab Expert Pro-2m-ISM). The acetic acid equivalence of the condensates was determined by plotting the change in pH with the consumption of NaOH, verifying the titration equivalence point with the first ($\Delta\text{pH}/\Delta V$) and second ($\Delta\text{pH}^2/\Delta^2 V$) derivatives, and finally calculating the titratable acid content of the solutions as acetic acid CH_3COOH (% *m/v*) equivalence.

Water and Organic Matter Contents of Condensates

The water contents of the condensed liquids were determined with Karl Fisher titration using the volumetric ASTM E203-08 method. The measurements were made with the Metrohm 870KF Titrino Plus titrator equipped with double Pt-wire electrode (Metrohm AG, Herisau, Switzerland). The titrant was the commercial Hydranal Composite 5K reagent (Sigma-Aldrich, St. Louis, MO, USA). A mixture of chloroform and methanol (3:1, *v/v*) was used as the solvent. The result of each sample was reported as the average of three parallel measurements. The proportion of organic matter in pyroligneous acids was determined by subtracting the water and the titratable acid contents from the total mass of the liquid.

Compositional Analysis of Organic Matter

A further compositional analysis of the organic matter in the conversion distillates was performed using ultrahigh-resolution direct-infusion mass spectrometry, which allows a non-targeted complex mixture characterization without chromatographic separation. All the measurements were performed on a 12-T solarix XR Fourier transform ion cyclotron resonance (FT-ICR) mass spectrometer (Bruker Daltonics GmbH, Bremen, Germany) using negative-ion electrospray ionization (ESI). This instrument has been described in detail elsewhere (Zhao et al., 2020). The distillates were diluted with methanol at a ratio of 1:1,000 (*v/v*) and directly infused into the ion source with a syringe pump, operating at a flow rate of 2 $\mu\text{L}/\text{min}$. Dry nitrogen was used as the drying (200°C, flow rate of 4 L/min) and nebulizing gas (1 bar). The calibration of the mass spectra was done externally using sodium trifluoroacetate clusters. The ions were detected within a mass range of *m/z* 98–1,000. Three hundred time-domain transients were co-added for each spectrum with a data size of 4 MWord. Bruker Compass fmsControl 2.1 software was used for the instrument control and data acquisition, and Bruker DataAnalysis 5.1 software was used for data post-processing. To improve mass accuracy, the mass spectra were further internally recalibrated with selected analyte ions. The signal-to-noise ratio was set at 5.0 for the peak picking, and the

relative intensity threshold was 0.01%. The following parameters were used for the molecular formula assignment: elemental formula, $^{12}\text{C}_{1-100}$ $^1\text{H}_{1-2000}$ $^{14}\text{N}_{0-2}$ $^{16}\text{O}_{0-25}$ $^{32}\text{S}_{0-1}$; double bond equivalent (DBE), 0–80; and mass error, ≤ 0.8 ppm. Microsoft Excel (Microsoft Corporation, Redmond, WA, USA) and CERES viewer 1.82 were used for the data sorting and visualization.

Pesticidal Tests

Herbicidal Activity Test

In the herbicide tests, turnip rape (*B. rapa*; Apollo, Boreal Plant Breeding Ltd.) was used as the test species due to its recommended use in phytotoxicity assessments (OECD, 2006). The herbicidal effect of the PAs was assessed according to Hagner et al. (2020) using a Jacobsen germinator (Rubart Apparate GmbH, Laatzen, Germany) that consists of a germination plate being temperature-conditioned by means of a water basin below. Germination spirals (filter papers, $\varnothing = 6$ cm) equipped with a paper wick were placed on the germination plate. The wick was led through slots in the germination plate into the water basin below, thus supplying the required humidity and temperature (20°C) to the germination spiral. Turnip rape seeds (20 pieces) were placed on the germination spirals, which were covered with a transparent glass dome to provide the air humidity required for germination. A little hole in the dome ensured minimum evaporation. Seeds achieved 16-h light a day. After 7 days, the covers were removed, the germinated seedlings were counted, and the germination spirals with seedlings were gently transferred into Petri dishes for herbicide treatments. An even deposit of the test liquid over the seedlings was achieved using a Potter precision laboratory spray tower spraying 1.0 ml of the selected liquid per filter paper. Tap water was used as an inert control and BioNeko (120 g/L acetic acid) as the active control. The concentrations of the PAs tested were 50%, 25%, 12.5%, and 5% (*v/v*), each with four replicates. The treated germination spirals were returned into the Jacobsen germinator and the cover domes were set on their places. The number of living seedlings was counted after 7 days.

Fungicidal Activity Test

The fungicidal properties of the tested PAs were estimated using *F. culmorum* as the test species. The utilized *F. culmorum* was separated in 2005 from barley (*Hordeum vulgare* strain: Presitge) grown in Sotkamo, Finland, and stored in liquid nitrogen (−190°C) since then. Each test liquid was examined in the concentrations of 100%, 50%, 25%, 10%, and 5% (*v/v*). Tap water was used as an inert control and 1.5 g/L Switch (active substances: 375 g/kg cyprodinil and 250 g/kg fludioxonil) as an active control. Each treatment had three replicates. The test was conducted in Petri dishes containing 25 ml of potato dextrose agar (PDA) as growth media for fungus. Four filter papers (6 mm diameter) treated with 100 μm of the test liquid were placed on the growth medium of each Petri dish. The fungus was inoculated in the middle of the Petri dish and the lids closed. The dishes were incubated at 20°C. After 2, 4, and 7 days of incubation, the fungal-covered area was measured.

Statistical Analysis

All dependent variables (percentage of dead *B. rapa*, the *F. culmorum*-covered area, and the development of fungal coverage) were analyzed using generalized linear models (GLMs) with treatment (BioNeko/Switch, wood, bark, HWE bark, HWE+AAE bark, and water control), concentration (from 5% to 50%), and their interaction as fixed effects. The concentrations of the first model were 5%, 12.5%, and 20%, and those of the second were 5%, 10%, 25%, and 50%. In the latter model, a concentration of 25% was chosen and the measurement day (2, 4, and 7 days) was used as a fixed effect instead of concentration. Four replicates were used without randomization.

The assumption of beta distribution with a logit link was used for percentages (model 1), and for coverage areas, the assumptions of log-normal distribution with an identity link (model 2) and gamma distribution with a log link (model 3) were used because the distributions of areas were highly skewed. The restricted maximum likelihood (REML) estimation method was used for the second model, maximum likelihood (ML) for the first model, and residual pseudo-likelihood (REPL) for the third model.

Heterogeneous variances for treatments were allowed in the second model. In the third model, correlations between measurement days within the same experimental unit were taken into account using the unstructured covariance structure, which estimates unique correlations for each pair of time points. Both solutions were based on lower values of the information criterion (corrected Akaike information criterion, AICc), although a likelihood test was also used for the decision of heterogeneous variances for treatments.

All treatments were compared within each concentration (models 1 and 2) or measurement days (model 3). The step-down method of Westfall, which is known to be one of the most effective when the design is balanced, was used for the pairwise comparisons of means with a significance level of 0.05 (Westfall, 1997). The method of Kenward and Roger was used for calculating the degrees of freedom for models 2 and 3 and the residual method used for the first model (Kenward and Roger, 2009).

TABLE 2 | Basic wood chemical composition of the wood and bark biomass fractions (mean \pm SD, $n = 6$) of *Populus tremula* L. \times *Populus tremuloides* Michx.

Basic composition	Wood	Bark
Lipophilic extractives (mg/g)	7.7 \pm 2.6	27.3 \pm 7.1
Hydrophilic extractives (mg/g)	20.9 \pm 3.3	168.0 \pm 66.5
Suberin-derived fatty acids (mg/g)	NA	23.7 \pm 1.6
Cellulose (mg/g)	501.1 \pm 19.9	200.2 \pm 5.8
Hemicellulose (mg/g)	223.3 \pm 8.2	300.4 \pm 18.9
Lignin total ^a (mg/g)	229.9 \pm 5.4	266.4 \pm 15.5
Acid-insoluble lignin (mg/g)	166.6 \pm 3.8	223.6 \pm 14.3
Acid-soluble lignin (mg/g)	63.6 \pm 4.5	42.8 \pm 2.8

^aTotal lignin content is the sum of acid-insoluble and acid-soluble lignin.

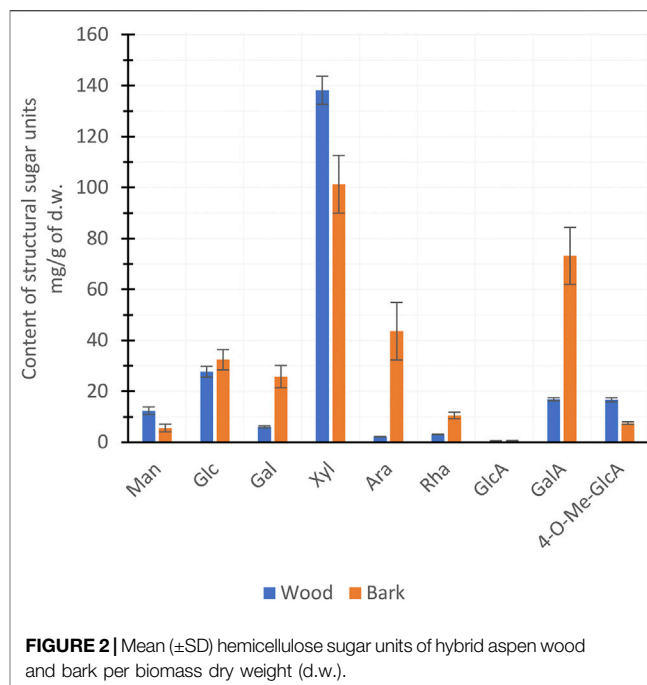


FIGURE 2 | Mean (\pm SD) hemicellulose sugar units of hybrid aspen wood and bark per biomass dry weight (d.w.).

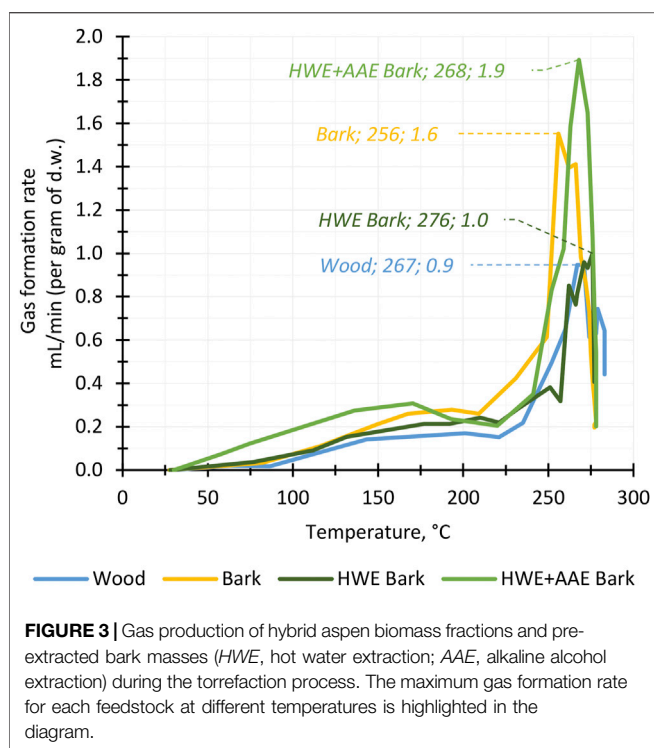
The analyses were performed using the GLIMMIX procedure of the SAS Enterprise Guide 7.15 (SAS Institute Inc., Cary, NC, USA).

RESULTS AND DISCUSSION

We hypothesized that several valuable products can be separated from hybrid aspen biomass without losing all the potential of PAs suitable for herbicide and fungicide applications. To prove this, the herbicidal and fungicidal activities of PAs produced from 1) wood, 2) untreated bark, 3) HWE-treated bark, and 4) HWE+AAE-treated bark were examined. The activity tests showed that aspen wood and bark can be used as raw materials for bio-based pesticides as the herbicidal and fungicidal activities of undiluted PA were comparable to those of commercial products. In addition, the bark biomass can be utilized in the production of biopesticides according to the cascade principle as HWE pretreatment even improved the herbicidal activity of bark PA.

Basic Composition of Hybrid Aspen Biomass Fractions

The chemical characterization of the bark and wood of hybrid aspen trees was used to evaluate the potential of the raw material in terms of cascade processing and to consider the composition of the biomass in relation to the yield of PAs. In the chemical compositions of wood and bark (Table 2), the most significant difference in terms of cascade use can be found in the extractive contents. The bark was found to have a significantly higher content of hydrophilic extractives than



wood, bark biomass thus having more potential as feedstock for cascade utilization. Due to its low hydrophilic extractive content, wood is best suited for direct conversion to PAs without pre-extractions. The content of lipophilic extractives in both biomass fractions was low. Thus, the separation of lipophilic compounds from wood or bark before conversion to PAs does not seem a promising way to increase the value of biomass. Variations in the cellulose and lignin contents were also found between wood and bark, but the differences were not considered essential as pesticidal active PAs are converted at $\leq 280^{\circ}\text{C}$, i.e., below the temperature where cellulose and lignin are thermally degraded (Collard and Blin, 2014).

In the torrefaction of lignocellulosic biomass at $\leq 280^{\circ}\text{C}$, hemicelluloses are the most important precursors in PA production (Collard and Blin, 2014). The hemicelluloses of hardwood species consist mainly of xylan and, to a lesser extent, glucomannan and pectin (Sjöström, 1993; Willför et al., 2005). The chain structure of xylan consists of xylose (Xyl) units with an *O*-acetyl group attached to 7 units out of 10 and 4-*O*-Me-GlcA to 1 unit out of 10 in ratios (Sjöström, 1993). The *O*-acetyl groups of xylans are precursors of the acetic acid formed in thermochemical conversion; therefore, a proportion of xylan is the most decisive hemicellulose characteristic of biomass (Chen et al., 2019). The xylan content of the wood and bark of hybrid aspen was estimated from the concentrations of the Xyl and 4-*O*-Me-GlcA sugar units (Figure 2). The bark was found to have a higher total amount of hemicellulose (Table 2), but a lower xylan content compared to the wood fraction (Figure 2). Due

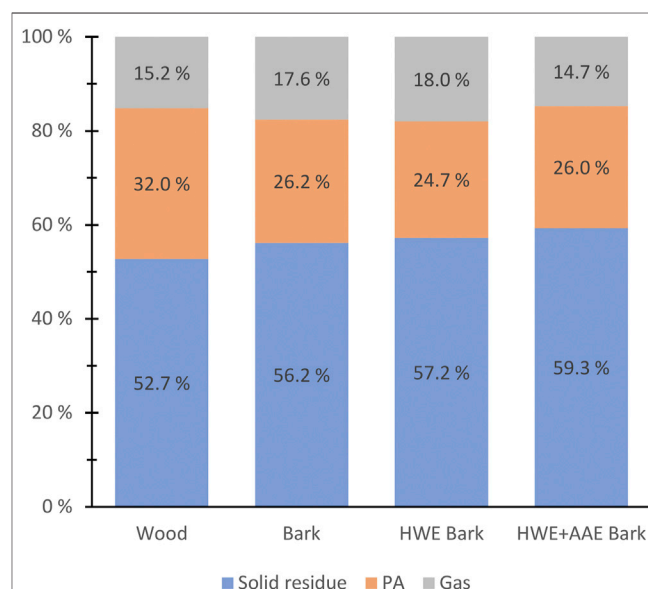
to its higher xylan content, wood can be considered as a more promising feedstock for the production of PAs with a stronger acid concentration.

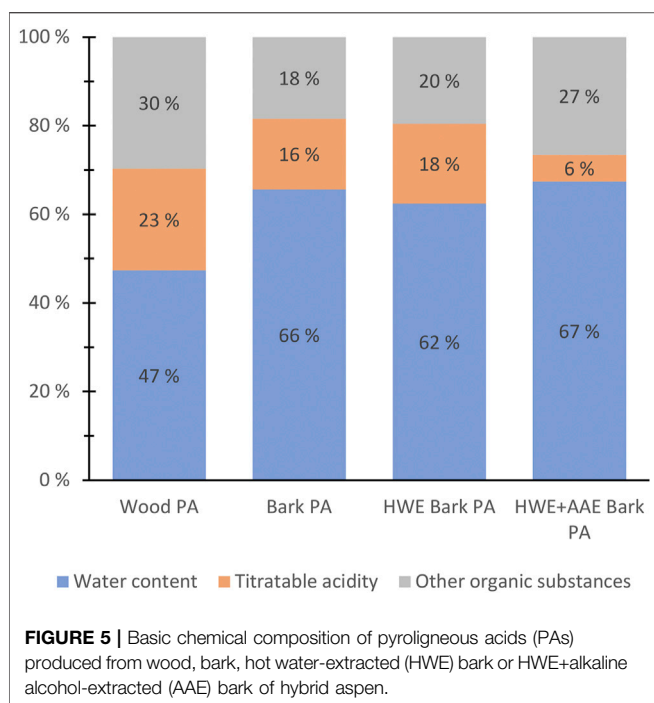
Torrefaction Process and Pyrolygneous Acid Formation

Torrefaction Product Yields

The formation of torrefaction products was used to examine the behavior of wood, bark, and pre-extracted bark during the conversion process. In torrefaction, the reactive temperature range for lignocellulosic biomass conversion begins at $150\text{--}175^{\circ}\text{C}$, and the actual conversion of hemicellulose occurs between 200°C and 300°C (Basu, 2013; Collard and Blin, 2014). The graph of the biomass gas formation rate during conversion showed that the reactive phase of hybrid aspen bark, wood, and pre-extracted bark biomasses began above 220°C and was at its most active phase above 250°C (Figure 3). Bark pre-extractions did not appear to have a significant effect on the reactive temperature range as all biomasses produced gas over the same temperature range. Although there were differences in the gas formation rates between the different biomasses, the total amounts of gases produced were only a few percentage points apart and did not appear to follow a clear trend relative to bark cascading pretreatments. For all feedstocks, gas formation ceased during the temperature maintenance phase at 280°C . Thus, it can be assumed that the biomass conversion reactions reached their end point and that the maximum yields of solid, liquid, and gas products were achieved.

Figure 4 shows the weight percent (wt.%) yields of the conversion products produced from wood, bark, and pre-extracted bark biomasses. The wood raw material was found to form the highest amount of PAs relative to the dry matter mass,





although the total content of hemicelluloses was found to be lower than that in the bark. The higher wood PA yield can be expected as due to the higher xylan ratio of wood hemicelluloses (Prins et al., 2006). Pre-extractions of bark did not appear to have a notable effect on the total yields of PAs.

Wood biomass had the highest mass loss compared to bark and pre-treated bark biomasses during conversion (Figure 4). In bark torrefaction, HWE and HWE+AAE pretreatments appeared to decrease mass loss, although the differences were small (Figure 4). The effect of AAE treatment on bark mass loss was not expected, as various studies have found that alkali metals bound to organic sites in lignocellulosic biomass can significantly increase mass loss during torrefaction (Shoulaifar et al., 2016a; Shoulaifar et al., 2016b; Macedo et al., 2018; Zhang et al., 2018). The observed opposite result is interesting since bark AAE pretreatment is likely to cause Na residues in the biomass and would be expected to cause accelerated mass loss.

Pyroligneous Acid Composition

PAs contain precipitate (tar) and liquid phases, both of which were summed to give the total yield of PAs. Tar was separated from the solutions by centrifugation, and only the separated liquids were included in the subsequent herbicide and fungicide experiments to avoid the polyaromatic hydrocarbons (PAHs) in the tar fraction (Fagnäs et al., 2012). PAs obtained from HWE-treated bark contained the highest amount of tar (8.75 wt.%), followed by bark PA (4.09 wt.%), wood PA (1.85 wt.%), and HWE+AAE bark PA (1.29 wt.%).

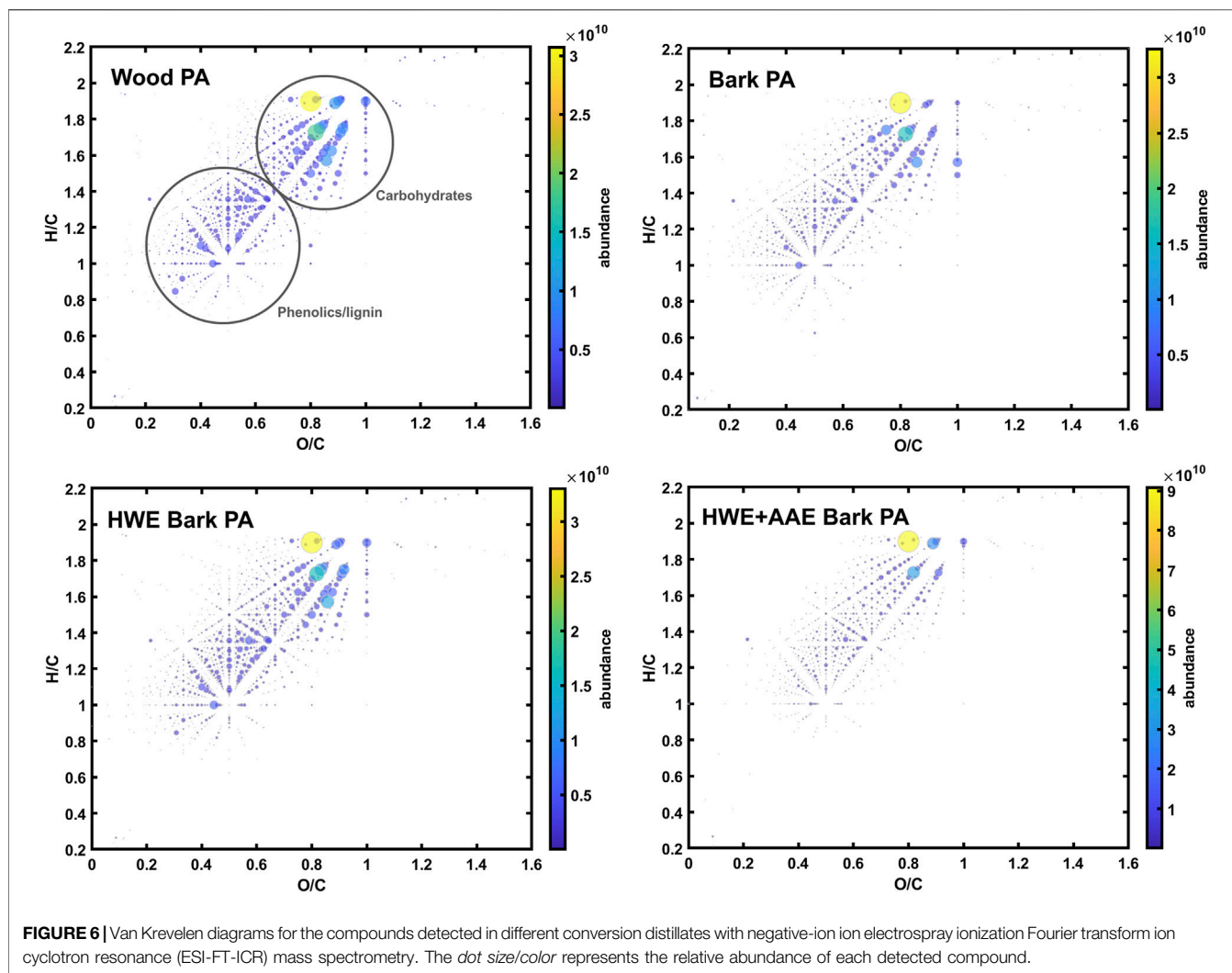
Tar-free samples of bark PA were found to differ significantly from wood PA in their basic chemical composition (Figure 5). Bark pre-extractions also had a notable effect on the basic composition of PAs (bark PA vs. HWE bark PA vs.

HWE+AAE bark PA) (Figure 5). The basic chemical composition of the PAs was determined by dividing the chemical fractions into groups of water content, acid content (CH_3COOH w/v percent equivalent), and other contents of organic matter (Figure 5). Wood PA was found to contain a higher amount of acid, as well as organic matter, compared to the bark PA product. The higher acid content is explained by the higher xylan content of the wood (Prins et al., 2006). In terms of the bark feedstock pre-extraction processing, the most interesting finding emerged from the effect of HWE on the chemical composition of the produced PAs. The acid strength of PAs, as well as the proportion of organic matter, appeared to have increased because of HWE of the bark (bark PA vs. HWE bark PA) (Figure 5). However, following AAE, a significant negative effect on the acid content of PAs was shown, but the proportions of other soluble organic substances were clearly increased (HWE bark PA vs. HWE+AAE bark PA) (Figure 5). The decreased acid content of PAs can be explained by the alkaline extraction conditions that likely affected the hemicellulose xylan (Borrega et al., 2013).

The composition of the organic matter in the PA samples was further analyzed with negative-ion ESI-FT-ICR mass spectrometry, which specifically targets less volatile organic compounds present in thermochemical wood distillates (Zhao et al., 2020; Zhao et al., 2021), such as organic acids, phenolic compounds, and carbohydrates (sugars and anhydro sugars). Zhao et al. have previously shown that extractives, some phenolics, and hydrocarbons are enriched in the tar (i.e., water-insoluble) fractions, while the more polar oxygenates are enriched in the PA (i.e., water-soluble) fractions (Zhao et al., 2021). The van Krevelen diagrams for all the detected compounds in each sample are presented in Figure 6, which allow the overall chemical compositions to be compared. The compositions of the tar-free PA samples were similar, mainly comprising different phenolic compounds and carbohydrates (mainly hemicellulose-derived mono- and disaccharides) (Figure 6), consistent with the previous work of Zhao et al. (2021). However, the HWE+AAE bark PA had clearly lower amounts of phenolics and monosaccharides than the other samples. Due to the complex chemical nature of the samples, individual compounds were not further identified in this work. The smallest organic acids, alcohols, or furanic compounds were not efficiently ionized by ESI and needed to be analyzed by other means, e.g., GC-MS or photoionization combined with FT-ICR MS. These further analyses remain as a topic for future studies. The negative-ion ESI-FT-ICR mass spectra of the PAs are shown in the Supplementary Material (Supplementary Figure S1).

Herbicidal Activity

The herbicidal activity of the PAs produced from hybrid aspen fractions and pretreated bark masses was compared with that of the acetic acid-based commercial herbicide (BioNeko) and that of water. Seven days after the spraying, all PA solutions with 20% or higher concentrations eliminated 100% of the *B. rapa* seedlings, being as effective as the commercial herbicide (BioNeko), but each differing significantly from water ($p < 0.05$). At lower dilutions, differences between the PAs produced from various



feedstocks were revealed (**Figure 7**): as 12.5% solutions, wood PA, bark PA, and HWE bark PA were as herbicidal active as BioNeko, but HWE+AAE bark PA was found to have a significantly reduced activity (HWE+AAE bark PA vs. all others, $p < 0.05$). At 5% dilutions (**Figure 7**), wood PA still retained its herbicidal activity, being as effective as the commercial herbicide (wood PA vs. BioNeko, $p = 0.847$). However, the herbicidal activity of bark PA was significantly lower than that of wood PA (5% bark PA vs. 5% wood PA, $p < 0.001$). HWE of the bark had a significant positive effect on the herbicidal activity of the PAs produced from the bark, as the performance of HWE bark PA was not statistically different from that of wood PA (HWE bark PA vs. wood PA, $p = 0.919$) or that of BioNeko (HWE bark PA vs. BioNeko, $p = 0.274$).

Fungicidal Activity

To investigate the fungicidal (*F. culmorum*) activity of PAs produced from hybrid aspen biomasses, we compared the antifungal efficiency of 50%, 25%, 10%, and 5% PA dilutions (**Figure 8**). In addition, the antifungal effect of 25% dilution of

PAs produced from different biomasses was monitored for 7 days (**Figure 9**). Wood PA, bark PA, HWE bark PA, and HWE+AAE bark PA corresponded in 50% solutions to the commercial product Switch during the 7-day observation period, preventing *F. culmorum* from spreading almost completely (**Figure 8**). Dilutions of 25% of bark PA and pre-extracted bark PA showed a reduced antifungal effect, but wood PA still corresponded to Switch (wood PA vs. Switch, $p = 0.866$). It can be seen from the 25% dilutions in **Figure 8** that the bark pre-extractions were found to have a negative effect on the fungicidal performance of the PAs produced. The growth area of *F. culmorum* was shown to be increased when comparing the growth inhibition performance of bark PA to that of HWE bark PA ($p = 0.006$). Comparison of the fungicidal performance between HWE bark PA vs. HWE+AAE bark PA showed that the effect appeared to have decreased further, although statistical difference was not found ($p = 0.167$). All PA solutions significantly lost their fungicidal activity against *F. culmorum* at 10% dilutions, and the activities no longer differed from water at 5% dilutions (all 5% PAs vs. water, $p > 0.05$).

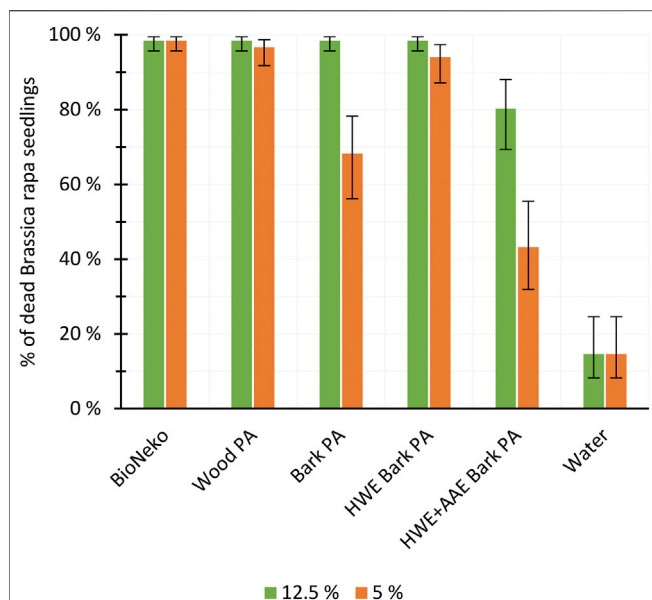


FIGURE 7 | Herbicidal effectivity of pyrolygneous acids (PAs) produced from wood and variously treated (HWE, hot water extracted; AAE, alkaline alcohol extraction) bark products (mean \pm SD, $n = 4$) against *Brassica rapa* seedlings 7 days after the spraying compared to that of a commercial product (BioNeko) and water controls.

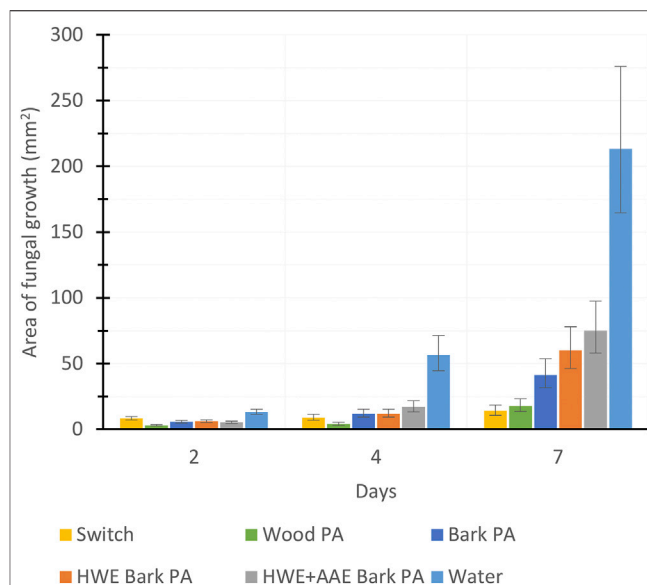


FIGURE 9 | Fungal coverage area (in square millimeters) at 2, 4, and 7 days after treating the growth media with pyrolysis acids produced from wood, bark, hot water-extracted (HWE) bark, or HWE+alkaline alcohol-extracted (AAE) bark (mean \pm SD, $n = 4$).

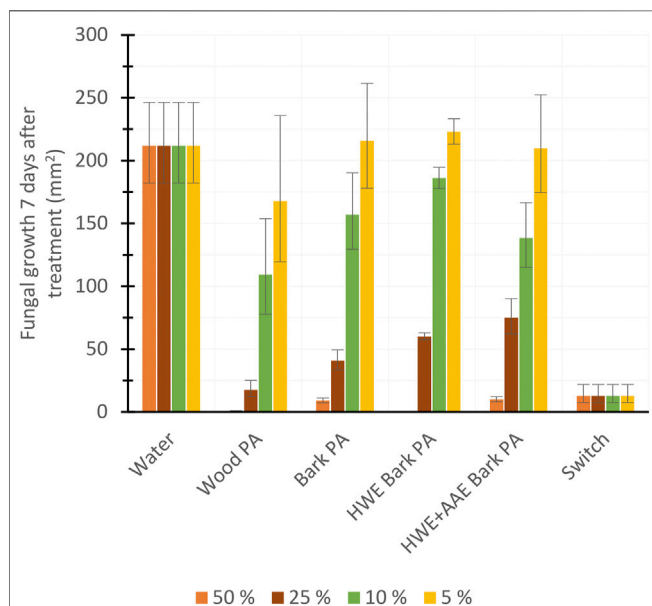


FIGURE 8 | Fungicide potency of pyrolygneous acids (PAs) produced from aspen tree wood, bark, or variously extracted bark (HWE, hot water extraction; AAE, alkaline alcohol extraction), commercial herbicide (Switch), or water measured via the inhibition of fungal (*Fusarium culmorum*) growth 7 days after the treatments (mean \pm SD), $n = 4$.

Figure 9 shows the *F. culmorum* growth inhibitory ability of 25% PAs over a 7-day follow-up period. After 4 days from treatments, differences in the fungicidal activity of PAs slightly appeared, but

on day 7, only wood PA corresponded to the Switch product. Ascending growth trends suggest that the fungicidal performance of all tested treatment agents appeared to have decreased over the follow-up period, but this should be verified by extending the observation period.

Current State of Pyrolygneous Biopesticide Usage and Research

The use of PAs as herbicides, insecticides, and fungicides has a long tradition in many Asian countries (Yatagai et al., 2002; Tiilikkala et al., 2010; Hossain et al., 2015). PAs produced by slow pyrolysis have been proven to be effective against a wide number of pests (Yatagai et al., 2002; Lindqvist et al., 2010; Hossain et al., 2015), to have antifungal activity against pathogenic fungi and yeasts (Ibrahim et al., 2013; Oramahi and Yoshimura, 2013; Mashuni et al., 2020), and to induce systemic resistance to fungal diseases in plants (Kärlund et al., 2014). The results of our study agree with those of previous studies and extend the results to also concern PAs produced by torrefaction. However, we are not aware of any studies concerning the utilization of biomasses according to the cascade principle, which allows the separation of specific soluble and insoluble compounds before pyrolysis and biopesticide production. As HWE pretreatment even improved the herbicidal activity of bark PA, the cascading use, i.e., the separation and utilization of hot water-extractable chemicals before the production of PAs for herbicidal purposes, is possible. However, the pretreatments used decreased the fungicidal properties of the PAs. Consequently, it is the target organism that determines the usability of various

pretreatments to produce biopesticides from wood biomass by torrefaction.

CONCLUSION

The results of the study showed that both wood and bark biomasses of hybrid aspen (*Populus tremula* L. × *P. tremuloides* Michx.) are promising raw materials for the production of pesticide-active PAs on weeds and fungal diseases. PAs converted from wood, bark, HWE bark, and HWE+AAE bark were equally herbicidal active solutions at >20% and fungicidal active solutions at >50% with commercial products. The results are novel, as we showed for the first time that, along with the production of biopesticides, several other valuable products can also be separated from the bark, if the solution strengths of the herbicides and fungicides used are at least as described above. We further observed that HWE pretreatment improved the herbicidal activity of bark PA, which also supports the cascade utilization potential of the bark. No similar benefit was observed with alkaline alcohol extraction, but despite pretreatment, the PA did not completely lose its biopesticide potency. The results also showed that the fungicidal activity of PAs produced from hybrid aspen biomasses was lower compared to its herbicidal activity. This is evident in the differences of the activity of the PA dilution ratios tested. It can be summarized that utilization according to the cascade principle is possible by separating the tree biomass fractions into their own raw material sources and by using different separation extractions to form value side streams. Still, further research is needed to determine the market value and market entry potential of the products. Also, more detailed characterization of the chemical products produced from hybrid aspen biomasses awaits further research.

DATA AVAILABILITY STATEMENT

The raw data supporting the conclusions of this article will be made available by the authors, without undue reservation.

AUTHOR CONTRIBUTIONS

PK conceptualized the study, helped with the methodology, performed formal analysis and investigation, wrote the original

draft, reviewed and edited the manuscript, and contributed to visualization. MH conceptualized the study, helped with the methodology, performed formal analysis and investigation, and reviewed and edited the manuscript. JJ contributed to resources and visualization, performed investigation, and reviewed and edited the manuscript. MM performed investigation, reviewed and edited the paper, and helped with visualization. JK conducted formal analysis and reviewed and edited the manuscript. UL supervised the study. KR contributed to conceptualization, reviewed and edited the paper, and supervised the study. TJ acquired funds, administered the project, helped with resources, reviewed and edited the paper, and supervised the study. All authors contributed to the article and approved the submitted version.

FUNDING

This research was supported by the Finnish Natural Resources Research Foundation (grant no. 20210080) and the Ministry of Education and Culture (diary no. OKM/66/523/2018).

ACKNOWLEDGMENTS

This work is part of the projects of Boosting the use of fast-growing Aspen: green source of high-added value chemicals and energy (BoostA), and Bioproduct and Clean Bioeconomy—RDI FlagShip in Xamk. Kalle Kaipainen, Pauli Karppinen, Piia Grandell, Johanna Nikama, Tytti Sarjala, Egbert Beuker, Riikka Keskinen, Risto Korpinen, Jussi Tiainen, Jari Ilomäki, and Veli Suihkonen are thanked for their knowledge on wood materials and chemistry and their skillful expertise in the laboratory and in the field. Martti Venäläinen (Luke) and the Xamk collaboration team are thanked for the opportunity to participate in the Bioproduct and Clean Bioeconomy—RDI FlagShip in Xamk project, which, alongside the BoostA project, largely enabled the research to be conducted.

SUPPLEMENTARY MATERIAL

The Supplementary Material for this article can be found online at: <https://www.frontiersin.org/articles/10.3389/fchem.2021.821806/full#supplementary-material>

REFERENCES

- Azapagic, A. (2014). Sustainability Considerations for Integrated Biorefineries. *Trends Biotechnol.* 32 (1), 1–4. doi:10.1016/j.tibtech.2013.10.009
- Basu, P. (2013). *Biomass Gasification, Pyrolysis and Torrefaction – Practical Design and Theory*. 2nd edition. USA: Academic Press.
- Beuker, E., Viherä-Aarnio, A., and Hynynen, J. (2016). “Growth Potential of First Generation Hybrid Aspen Plantations in Southern Finland. Poplars and Other Fast-Growing Trees—Renewable Resources for Future Green Economies.”. Working Paper IPC 14 in Proceedings of the International Poplar Commission, 25th Session, Berlin, Germany, 13–16 September 2016 (Rome, Italy: FAO), 118.
- Borrega, M., Tolonen, L. K., Bardot, F., Testova, L., and Sixta, H. (2013). Potential of Hot Water Extraction of Birch wood to Produce High-Purity Dissolving Pulp after Alkaline Pulp. *Bioresour. Technol.* 135, 665–671. doi:10.1016/j.biortech.2012.11.107
- Cahyanti, M. N., Doddapaneni, T. R. K. C., and Kikas, T. (2020). Biomass Torrefaction: An Overview on Process Parameters, Economic and Environmental Aspects and Recent Advancements. *Bioresour. Technol.* 301, 122737. doi:10.1016/j.biortech.2020.122737

- Cambero, C., and Sowlati, T. (2014). Assessment and Optimization of forest Biomass Supply Chains from Economic, Social and Environmental Perspectives - A Review of Literature. *Renew. Sustain. Energy Rev.* 36, 62–73. doi:10.1016/j.rser.2014.04.041
- Chen, W.-H., Wang, C.-W., Ong, H. C., Show, P. L., and Hsieh, T.-H. (2019). Torrefaction, Pyrolysis and Two-Stage Thermodegradation of Hemicellulose, Cellulose and Lignin. *Fuel* 258, 116168. doi:10.1016/j.fuel.2019.116168
- Cherubini, F. (2010). The Biorefinery Concept: Using Biomass Instead of Oil for Producing Energy and Chemicals. *Energ. Convers. Manage.* 51, 1412–1421. doi:10.1016/j.enconman.2010.01.015
- Collard, F.-X., and Blin, J. (2014). A Review on Pyrolysis of Biomass Constituents: Mechanisms and Composition of the Products Obtained from the Conversion of Cellulose, Hemicelluloses and Lignin. *Renew. Sustain. Energy Rev.* 38, 594–608. doi:10.1016/j.rser.2014.06.013
- Fagernäs, L., Kuoppala, E., and Simell, P. (2012). Polycyclic Aromatic Hydrocarbons in Birch Wood Slow Pyrolysis Products. *Energy Fuels* 26 (11), 6960–6970. doi:10.1021/ef3010515
- Fagernäs, L., Kuoppala, E., and Arpiainen, V. (2015). Composition, Utilization and Economic Assessment of Torrefaction Condensates. *Energy Fuels* 29 (5), 3134–3142. doi:10.1021/acs.energyfuels.5b00004
- Finnish Food Authority (2021). *National List of Basic Material Approved in Finland*. Available at: <https://www.ruokavirasto.fi/en/farmers/plant-production/forest-tree-seed-and-seedling-production/basic-material/approved-basic-material/> (Accessed November 17, 2021).
- Grewal, A., Abbey, L., and Gunupuru, L. R. (2018). Production, Prospects and Potential Application of Pyrolygneous Acid in Agriculture. *J. Anal. Appl. Pyrolysis* 135, 152–159. doi:10.1016/j.jaap.2018.09.008
- Hagner, M., Tiilikkala, K., Lindqvist, I., Niemelä, K., Wikberg, H., Källi, A., et al. (2020). Performance of Liquids from Slow Pyrolysis and Hydrothermal Carbonization in Plant protection. *Waste Biomass Valor.* 11, 1005–1016. doi:10.1007/s12649-018-00545-1
- Hassan, S. S., Williams, G. A., and Jaiswal, A. K. (2019). Lignocellulosic Biorefineries in Europe: Current State and Prospects. *Trends Biotechnol.* 37 (3), 231–234. doi:10.1016/j.tibtech.2018.07.002
- Hossain, M. M., Scott, I. M., McGarvey, B. D., Conn, K., Ferrante, L., Berruti, F., et al. (2015). Insecticidal and Anti-microbial Activity of Bio-Oil Derived from Fast Pyrolysis of Lignin, Cellulose, and Hemicellulose. *J. Pest Sci.* 88, 171–179. doi:10.1007/s10340-014-0568-4
- Ibrahim, D., Kassim, J., Sheh-Hong, L., and Rusli, W. (2013). Efficacy of Pyrolygneous Acid from Rhizophora Apiculate on Pathogenic Candida Albicans. *J. Appl. Pharm. Sci.* 3, 7–13. doi:10.7324/JAPS.2013.3702
- Kärlund, A., Salminen, J. P., Koskinen, P., Ahern, J. R., Karonen, M., Tiilikkala, K., et al. (2014). Polyphenols in Strawberry (*Fragaria* × *Ananassa*) Leaves Induced by Plant Activators. *J. Agric. Food Chem.* 62, 4592–4600. doi:10.1021/jf405589f
- Keegan, D., Kretschmer, B., Elbersen, B., and Panoutsou, C. (2013). Cascading Use: a Systematic Approach to Biomass beyond the Energy Sector. *Biofuels, Bioprod. Bioref.* 7, 193–206. doi:10.1002/bbb.1351
- Kenward, M. G., and Roger, J. H. (2009). An Improved Approximation to the Precision of Fixed Effects from Restricted Maximum Likelihood. *Comput. Stat. Data Anal.* 53, 2583–2595. doi:10.1016/j.csda.2008.12.013
- Korkalo, P., Korpinen, R., Beuker, E., Sarjala, T., Hellström, J., Kaseva, J., et al. (2020). Clonal Variation in the Bark Chemical Properties of Hybrid Aspen: Potential for Added Value Chemicals. *Molecules* 25 (19), 4403. doi:10.3390/molecules25194403
- Korpinen, R. I., Kilpeläinen, P., Sarjala, T., Nurmi, M., Saloranta, P., Holmbom, T., et al. (2019). The Hydrophobicity of Lignocellulosic Fiber Network Can Be Enhanced with Suberin Fatty Acids. *Molecules* 24, 4391. doi:10.3390/molecules24234391
- Krogell, J., Holmbom, B., Pranovich, A., Hemming, J., and Willför, S. (2012). Extraction and Chemical Characterization of Norway spruce Inner and Outer Bark. *Nord. Pulp Pap. Res. J.* 27, 6–17. doi:10.3183/npprj-2012-27-01-p006-017
- Lindqvist, I., Lindqvist, B., Tiilikkala, K., Hagner, M., Penttinen, O.-P., Pasanen, T., et al. (2010). Birch Tar Oil Is an Effective Mollusc Repellent: Field and Laboratory Experiments Using *Arianta arbustorum* (Gastropoda, Helicidae) and *Arion lusitanicus* (Gastropoda, Arionidae). *Agric. Food Sci.* 19, 1–12. doi:10.2137/145960610791015050
- Macedo, L. A. d., Commandré, J.-M., Rousset, P., Valette, J., and Pétrissans, M. (2018). Influence of Potassium Carbonate Addition on the Condensable Species Released during wood Torrefaction. *Fuel Process. Technol.* 169, 248–257. doi:10.1016/j.fuproc.2017.10.012
- Mashuni, Y. N. A., Yanti, N. A., Jahiding, M., Kadidae, L. O., Djaila, R., and Hamid, F. H. (2020). Analysis of Liquid Volatile Matters from Coconut Shell Pyrolysis by GC-MS and its Potential as Antifungal Agent. *Asian J. Chem.* 32, 1728–1732. doi:10.14233/ajchem.2020.21657
- OECD (2006). *OECD Guidelines for the Testing of Chemicals, Section 2 Test No. 227: Terrestrial Plant Test: Vegetative Vigour Test*. (Paris: OECD Publishing). doi:10.1787/9789264067295-en
- Oramahi, H. A., and Yoshimura, T. (2013). Antifungal and Antitermitic Activities of wood Vinegar from *Vitex Pubescens* Vahl. *J. Wood Sci.* 59, 344–350. doi:10.1007/s10086-013-1340-8
- Oramahi, H. A., Yoshimura, T., Diba, F., Setyawati, D., and Nurhaida, N. (2018). Antifungal and Antitermitic Activities of wood Vinegar from Oil palm Trunk. *J. Wood Sci.* 64, 311–317. doi:10.1007/s10086-018-1703-2
- Prins, M. J., Ptasiński, K. J., and Janssen, F. J. G. (2006). Torrefaction of wood: Part 2. Analysis of products. *J. Anal. Appl. Pyrolysis* 77 (1), 35–40. doi:10.1016/j.jaap.2006.01.001
- Rasi, S., Kilpeläinen, P., Rasa, K., Korpinen, R., Raitanen, J.-E., Vainio, M., et al. (2019). Cascade Processing of Softwood Bark with Hot Water Extraction, Pyrolysis and Anaerobic Digestion. *Bioresour. Technol.* 292, 121893. doi:10.1016/j.biortech.2019.121893
- Reuter, J., Merfort, I., and Schempp, C. M. (2010). Botanicals in Dermatology. *Am. J. Clin. Dermatol.* 11, 1–267. doi:10.2165/11533220-000000000-00000
- Rizikovs, J., Zandersons, J., Paže, A., Tardenaka, A., and Spince, B. (2014). Isolation of Suberinic Acids from Extracted Outer Birch Bark Depending on the Application Purposes. *Balt. For.* 20, 98–105.
- Khazraie Shoulafar, T., DeMartini, N., Karlström, O., and Hupa, M. (2016a). Impact of Organically Bonded Potassium on Torrefaction: Part 1. Experimental. *Fuel* 165, 544–552. doi:10.1016/j.fuel.2015.06.024
- Khazraie Shoulafar, T., DeMartini, N., Karlström, O., Hemming, J., and Hupa, M. (2016b). Impact of Organically Bonded Potassium on Torrefaction: Part 2. Modeling. *Fuel* 168, 107–115. doi:10.1016/j.fuel.2015.11.084
- Sjöström, E. (1993). *Wood Chemistry—Fundamentals and Applications*. London: Academic.
- Sluiter, A., Hames, B., Ruiz, R., Scarlata, C., Sluiter, J., Templeton, D., et al. (2012). “Determination of Structural Carbohydrates and Lignin in Biomass,” in *Laboratory Analytical Procedure (LAP)* (Denver, CO, USA: NREL), 1–15.
- Sokka, L., Koponen, K., and Keränen, J. T. (2015). *Cascading Use of Wood in Finland: With Comparison to Selected EU Countries*. VTT Technical Research Centre of Finland. VTT Research Report Vol. VTT-R-03979-15. <http://www.vtt.fi/inf/julkaisut/muut/2015/VTT-R-03979-15.pdf>, 1–25.
- Stoklosa, R. J., and Hodge, D. B. (2012). Extraction, Recovery, and Characterization of Hardwood and Grass Hemicelluloses for Integration into Biorefining Processes. *Ind. Eng. Chem. Res.* 51, 11045–11053. doi:10.1021/ie301260w
- Sundheq, A., Sundberg, K., Lillandt, C., and Holmhö, B. (1996). Determination of Hemicelluloses and Pectins in wood and Pulp Fibres by Acid Methanolysis and Gas Chromatography. *Res. J.* 11, 216–219. doi:10.3183/npprj-1996-11-04-p216-219
- Theapparath, Y., Chandumpai, A., Leelasuphakul, W., and Laemsak, N. (2015). Pyrolygneous Acids from Carbonisation of wood and Bamboo: Their Components and Antifungal Activity. *J. Trop. For. Sci.* 27, 517–526.
- Tiilikkala, K., Fagernäs, L., and Tiilikkala, J. (2010). History and Use of Wood Pyrolysis Liquids as Biocide and Plant Protection Product. *Toasj* 4, 111–118. doi:10.2174/1874331501004010111
- Toivanen, T., Vaden, T., Majava, A., Järvensivu, P., Lähde, V., and Eronen, J. T. (2021). Teollinen Murros Ekohyvinvointivaltiossa. *A&Y* 50 (2), 8–27. doi:10.30663/ay.109701
- Tondi, G., and Pizzi, A. (2009). Tannin-based Rigid Foams: Characterization and Modification. *Ind. Crops Prod.* 29, 356–363. doi:10.1016/j.indcrop.2008.07.003
- Van der Stelt, M. J. C., Gerhauser, H., Kiel, J. H. A., and Ptasiński, K. J. (2011). Biomass Upgrading by Torrefaction for the Production of Biofuels: A Review. *Biomass Bioenergy* 35, 3748–3762. doi:10.1016/j.biombioe.2011.06.023

- Varila, T., Brännström, H., Kilpeläinen, P., Hellström, J., Romar, H., Nurmi, J., et al. (2020). From Norway spruce Bark to Carbon Foams: Characterization and Applications. *BioRes* 15, 3651–3666. doi:10.15376/biores.15.2.3651-3666
- Westfall, P. H. (1997). Multiple Testing of General Contrasts Using Logical Constraints and Correlations. *J. Am. Stat. Assoc.* 92, 299–306. doi:10.2307/229147410.1080/01621459.1997.10473627
- Willför, S., Hemming, J., Reunanen, M., Eckerman, C., and Holmbom, B. (2003). Lignans and Lipophilic Extractives in Norway spruce Knots and Stemwood. *Holzforschung* 57, 27–36. doi:10.1515/HF.2003.005
- Willför, S., Sundberg, A., Pranovich, A., and Holmbom, B. (2005). Polysaccharides in Some Industrially Important Hardwood Species. *Wood Sci. Technol.* 39, 601–617. doi:10.1007/s00226-005-0039-4
- Yatagai, M., Nishimoto, M., Hori, K., Ohira, T., and Shibata, A. (2002). Termiticidal Activity of wood Vinegar, its Components and Their Homologues. *J. Wood Sci.* 48, 338–342. doi:10.1007/bf00831357
- Zhang, S., Su, Y., Ding, K., Zhu, S., Zhang, H., Liu, X., et al. (2018). Effect of Inorganic Species on Torrefaction Process and Product Properties of rice Husk. *Bioresour. Technol.* 265, 450–455. doi:10.1016/j.biortech.2018.06.042
- Zhao, Q., Mäkinen, M., Haapala, A., and Jänis, J. (2020). Thermochemical Conversion of Birch Bark by Temperature-Programmed Slow Pyrolysis with Fractional Condensation. *J. Anal. Appl. Pyrolysis* 150, 104843. doi:10.1016/j.jaap.2020.104843
- Zhao, Q., Mäkinen, M., Haapala, A., and Jänis, J. (2021). Valorization of Bark from Short Rotation Trees by Temperature-Programmed Slow Pyrolysis. *ACS Omega* 6 (14), 9771–9779. doi:10.1021/acsomega.1c00434
- Conflict of Interest:** The authors declare that the research was conducted in the absence of any commercial or financial relationships that could be construed as a potential conflict of interest.
- Publisher's Note:** All claims expressed in this article are solely those of the authors and do not necessarily represent those of their affiliated organizations, or those of the publisher, the editors and the reviewers. Any product that may be evaluated in this article, or claim that may be made by its manufacturer, is not guaranteed or endorsed by the publisher.
- Copyright © 2022 Korkalo, Hagner, Jänis, Mäkinen, Kaseva, Lassi, Rasa and Jyske. This is an open-access article distributed under the terms of the Creative Commons Attribution License (CC BY). The use, distribution or reproduction in other forums is permitted, provided the original author(s) and the copyright owner(s) are credited and that the original publication in this journal is cited, in accordance with accepted academic practice. No use, distribution or reproduction is permitted which does not comply with these terms.



Production of Hydroxymethylfurfural Derivatives From Furfural Derivatives via Hydroxymethylation

Xianqing Lv^{1†}, Xiaolin Luo^{1†}, Xin Cheng¹, Jing Liu¹, Changzhi Li^{2*} and Li Shuai^{1*}

¹College of Materials Engineering, Fujian Agriculture and Forestry University, Fuzhou, China, ²CAS Key Laboratory of Science and Technology on Applied Catalysis, Dalian Institute of Chemical Physics, Chinese Academy of Sciences, Dalian, China

OPEN ACCESS

Edited by:

Caoxing Huang,
Nanjing Forestry University, China

Reviewed by:

Sibao Liu,
Tianjin University, China
Zhiwen Wang,
University of Groningen, Netherlands

*Correspondence:

Changzhi Li
licz@dicp.ac.cn
Li Shuai
lishuai@fafu.edu.cn

[†]These authors have contributed
equally to this work

Specialty section:

This article was submitted to
Bioprocess Engineering,
a section of the journal
Frontiers in Bioengineering and
Biotechnology

Received: 10 January 2022

Accepted: 24 January 2022

Published: 15 February 2022

Citation:

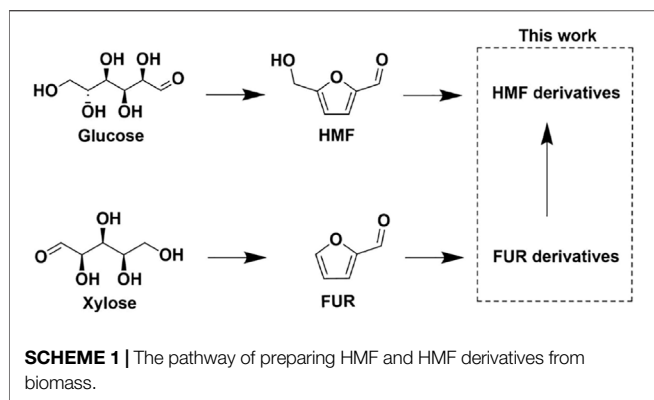
Lv X, Luo X, Cheng X, Liu J, Li C and
Shuai L (2022) Production of
Hydroxymethylfurfural Derivatives
From Furfural Derivatives
via Hydroxymethylation.
Front. Bioeng. Biotechnol. 10:851668.
doi: 10.3389/fbioe.2022.851668

Hydroxymethylfurfural (HMF) derivatives such as 2,5-bis(hydroxymethyl)furan (BHMF) and furandicarboxylic acid (FDCA) are promising alternative of fossil-based diols and dicarboxylic acids for synthesis of polyesters such as polyethylene terephthalate (PET). However, high cost for preparing HMF from biomass discourages the commercialization of HMF-derived polyesters. Since producing furfural (FUR) from five-carbon sugars (e.g., xylose) via dehydration is an inexpensive and commercialized process, we herein reported a method to synthesize BHMF derivatives (5-(ethoxymethyl)furan-2-methanol (EMFM), 2,5-bis(hydroxymethyl)furan monoacetate (BHMFM) and 2,5-bis(hydroxymethyl)furan diacetate (BHMFD) from furfural derivatives, i.e., (2-(ethoxymethyl)furan (EMF) and furfuryl acetate (FA)). To avoid strong acid-induced side reactions (e.g., furan ring opening, condensation and carbonization), two reaction systems, i.e., a low-concentration HCl aqueous solution combined with formaldehyde and anhydrous acetic acid combined with paraformaldehyde, were found to be suitable for such a hydroxymethylation reaction and could lead to decent product yields. In order to improve the carbon utilization, condensed furanic byproducts were further converted into hydrocarbon fuels via a reported two-step hydrodeoxygenation (HDO) process. This study not only validates the possibility of synthesizing functional HMF derivatives (EMFM, BHMFM, and BHMFD) from commercially-available FUR derivatives (EMF and FA), but also provide a new way to transform condensed furanics to value-added hydrocarbon fuels.

Keywords: furfural derivatives, hydroxymethylfurfural derivatives, hydroxymethylation, hydrocarbon fuel, hydrodeoxygenation

INTRODUCTION

Synthetic polymers are important material basis for promoting the development of industry and human society. Most of the commercialized polymers [e.g., polyethylene terephthalate (PET)] are synthesized based on fossil-based chemicals (e.g., terephthalic acid). However, the extensive use of fossil-based chemicals brings about severe environmental problems such as the greenhouse effect and the shortage of nonrenewable resources. Developing alternatives of fossil-based chemicals and materials from renewable biomass is a promising way to overcome or at least alleviate these problems. For example, 2, 5-furandicarboxylic acid (FDCA) can be used to substitute terephthalic acid for synthesis of polyesters such as polyethylene furandicarboxylate (PEF), which showed better performance (e.g., thermostability and elasticity modulus) than that of PET (Guan et al., 2021; Yang and Mu, 2021). Polyesters could also be synthesized by using 2,5-bis(hydroxymethyl)furan (BHMF)



as an alternative of fossil-based diols (e.g., ethylene glycol). As a result, hydroxymethylfurfural (HMF) derivatives such as FDCA and BHMF have been considered as important platform chemicals for synthesizing bio-based polymers, which thereby stimulate intensive studies in preparing the two chemicals from renewable biomass (Scheme 1).

At present, FDCA is synthesized from 5-hydroxymethylfurfural (HMF) through hydrothermal (Gao et al., 2017; Cheng et al., 2021; Kandasamy et al., 2021; Yu et al., 2021) or electrochemical oxidation (Hu et al., 2021; Zhang et al., 2021). During the hydrothermal oxidation process, HMF is initially oxidized to 2, 5-diformylfuran (DFF) and/or 5-hydroxymethyl-2-furanoic acid (HMFA), which is further converted to 5-formyl-2-furanoic acid (FFCA) and FDCA under aerobic conditions (Kandasamy et al., 2021). The reaction pathway of converting HMF to FDCA via electrochemical oxidation is similar to that of hydrothermal oxidation, but such a method showed good selectivity only at low substrate concentrations. In addition to FDCA, HMF can be also reductively converted to BHMF, which is a furanic diol for synthesis of polyesters. With the input of H_2 , different catalysts such as Ru/Co₃O₄ (Chen et al., 2021), Cu-Al₂O₃ (Rao et al., 2021), Ni-Cu/HT (Gupta et al., 2020), and CuO-Fe₃O₄/AC (Elsayed et al., 2020), had been developed for reducing HMF to BHMF. These studies indicate that HMF and its derivatives are important bio-based small molecules for synthesizing FDCA, BHMF and many other value-added derivatives. However, a critical issue related to HMF and its derivatives is the high cost for preparing them from biomass. HMF is generally produced via the dehydration of six-carbon carbohydrates (e.g. glucose and fructose) while the dehydration process is either inefficient due to low selectivity of HMF or costly due to energy-intensive solvent recovery and separation (Sajid et al., 2018). In contrast, dehydration of five-carbon sugars (e.g. xylose) to produce furfural (FUR) is a commercialized process and furfural has been successfully used to synthesize furan resin (Ye et al., 2021).

As the production of FUR from five-carbon sugars such as xylose is easy and inexpensive, we believe that synthesis of HMF or HMF derivatives (e.g. BHMF ethers and esters) from inexpensive FUR or its derivatives (e.g., furfuryl acetate and 2-(ethoxymethyl)furan) would be an interesting and potential way for further investigation. Such a pathway requires incorporation

of one carbon to the C-5 position of furfural via hydroxymethylation, which was rarely reported. Therefore, in this article we proposed new reaction pathways for synthesizing BHMF derivatives (2,5-bis(hydroxymethyl)furan diacetate and 5-(ethoxymethyl)furan-2-methanol) via hydroxymethylation of furfuryl alcohol derivatives (furfuryl acetate and 2-(ethoxymethyl)furan) with formaldehyde or paraformaldehyde (Figures 1A, 2A). The reason we chose etherified or esterified furfural derivatives as starting materials was that these derivatives were more stable than FUR and furfuryl alcohol under acidic conditions. During these reactions, we found that acid could lead to the opening of furan rings, which produced carbonyl compounds that would further condense to form humins-like products. To improve the utilization efficiency of bio-based carbon resources, the oxygen-containing condensed products were converted to hydrocarbon fuels via hydrodeoxygenation. These results validate not only a new way to synthesize HMF derivatives but also a new method for utilizing condensed furan products for hydrocarbon fuels production.

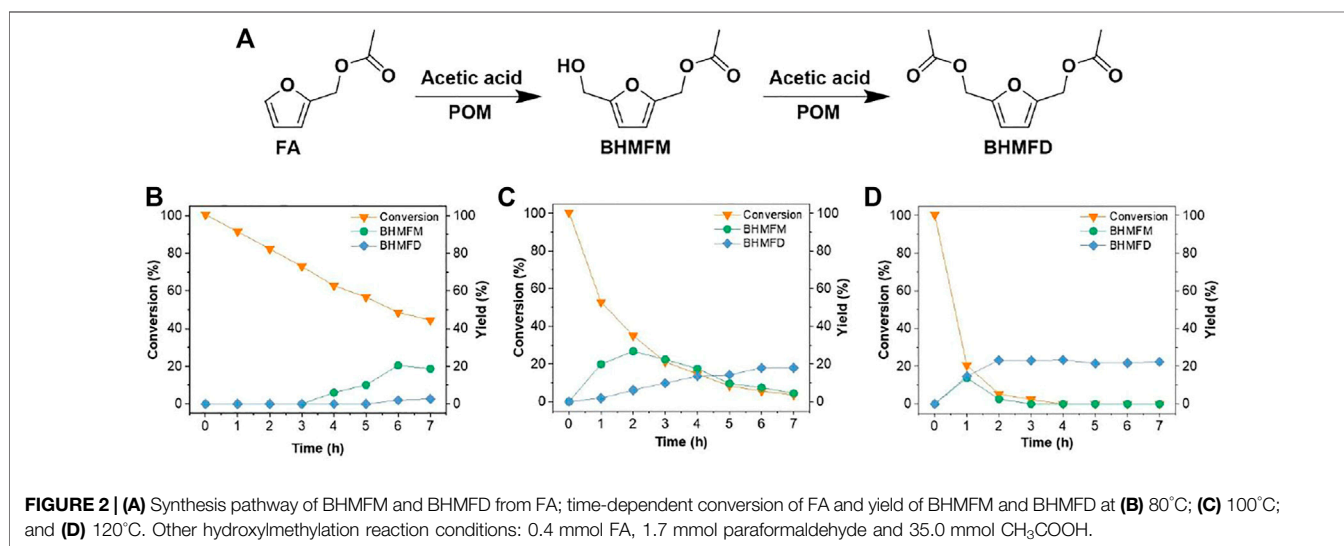
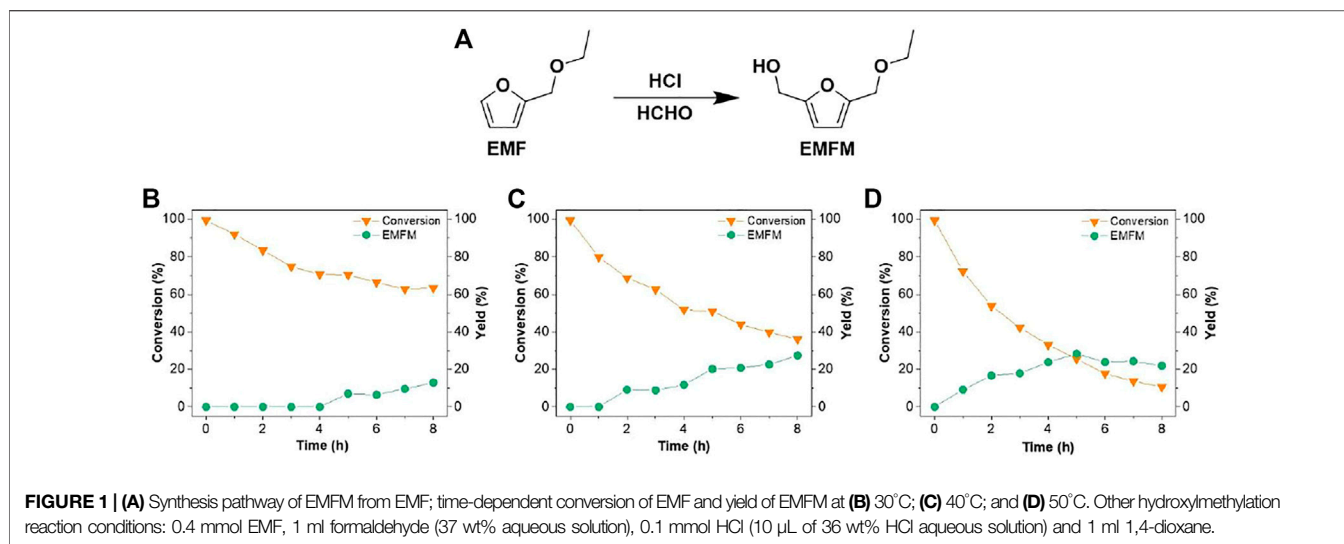
MATERIALS AND METHODS

Materials

Furfuryl acetate (99%) and 2-(ethoxymethyl)furan (98%) were purchased from Rhawn Chemical Technology Co., Ltd. (Shanghai, China). Paraformaldehyde (98%), Na₂HPO₄·H₂O (98%) and NaH₂PO₄ (98%) were purchased from Maclin Biochemical Co., Ltd. (Shanghai, China). Pt on carbon (Pt 5 wt %), n-hexane (98%), n-hexadecane (99.5%, GC), chloroform-d (99.8%), formic acid (99%), trifluoromethanesulfonic acid (98%) and MgSO₄ (AR) were ordered from Aladdin® Biochemical Technology Co., Ltd. (Shanghai, China). Phosphotungstic acid anhydride (99%) was purchased from Titan Scientific Co., Ltd. (Shanghai, China). Anhydrous acetic acid (99.5%), formaldehyde (37 wt%), chloroform, concentrated sulfuric acid (98 wt%) and concentrated hydrochloric acid (36 wt%) were all obtained from XiLong Scientific Co., Ltd. (Shantou, China). All reagents were used as received without further purification.

Synthesis of 5-(ethoxymethyl)furan-2-methanol

Initially, 0.4 mmol of 2-(ethoxymethyl)furan (EMF) was mixed with 10 mmol of formaldehyde (37 wt%), 1 ml of 1,4-dioxane and 10 μ L of concentrated hydrochloric acid (36 wt%) in a 15-ml vial. The vial was placed in oil bath, magnetically stirred and heated to a desired temperature (30–50 °C) for 1–8 h. After the reaction, the vial was immediately taken out from the oil bath and cooled by tap water to room temperature. Around 0.25 mg n-hexadecane was added into the reaction liquor as an internal standard and 50 μ L of the liquid was sampled and extracted by 1 ml of chloroform. The extract was dehydrated by around 200 mg anhydrous MgSO₄. The resulting solution was analyzed by a gas chromatograph-mass spectrometer (GC-MS, SCION 436GC-SQ, Techcomp group, Shanghai, China) to identify products and the identified products were further quantitatively analyzed by a



gas chromatograph (GC, SCION 436C, Techcomp group, Shanghai, China).

quantitatively analyzed by a GC (SCION 436C, Techcomp group, Shanghai, China).

Synthesis of 2,5-bis(Hydroxymethyl)Furan Monoacetate (BHMFM) and 2,5-bis(Hydroxymethyl)Furan Diacetate (BHMFD)

A mixture of furfuryl acetate (FA, 0.4 mmol), paraformaldehyde (50 mg) and anhydrous acetic acid (2 ml) was loaded into a 15-ml vial. The vial was magnetically stirred and heated at 100–120°C in an oil bath for 1–7 h. After the reaction, the vial was immediately taken out from the oil bath and cooled by tap water to room temperature. Around 0.25 mg n-hexadecane was added into the reaction liquor as an internal standard. 50 μ L of the liquid was sampled and analyzed by a GC-MS (SCION 436GC-SQ, Techcomp group, Shanghai, China) to identify products and the identified products were further

Separation of Monomeric Furanic Products From Condensed Furanics

The solvent in the final product mixture was carefully removed with a rotary evaporator under vacuum. The monomeric furanic products in the residual mixture were extracted with 10 ml hexane three times and the residual was considered as condensed furanics and used for oil production *via* hydrodeoxygenation.

Hydrodeoxygenation of Condensed Furanics to Hydrocarbon Fuels

The condensed furanics separated in last section was used as raw materials for production of hydrocarbon fuels (also termed as oil) through the following hydrodeoxygenation reactions.

About 300 mg of the residual product was re-dissolved with methanol (25 ml) in a 50-ml stainless steel reactor (WZD-50, Wuzhou Dingchuang Technology Co., Ltd., Beijing, China) followed by the addition of Pt/C catalyst (200 mg). The reactor was flushed three times with hydrogen gas, and then pressurized with hydrogen gas to 3 MPa. The mixture was mechanically stirred, and then heated to 250°C and kept at this temperature for 4 h. After the reaction, the reactor was cooled to room temperature and depressurized carefully. The catalyst was separated by filtration, and the reaction liquor was collected. Methanol in the reaction liquor was removed by a vacuum rotary evaporator. The residual organics was further mixed with Pt/C catalyst (200 mg), phosphotungstic acid (Li et al., 2021) (200 mg) and n-hexane (25 ml) in the reactor (WZD-50, Wuzhou Dingchuang Technology Co., Ltd., Beijing, China). The reactor was also flushed and pressurized with hydrogen gas to 3 MPa. The mixture was mechanically stirred at 300 rpm, and then heated to 250°C and reacted at the temperature for 4 h. The reactor was cooled to room temperature and depressurized carefully after the reaction. After the catalyst was separated via filtration, n-hexane in the resultant filtrate was removed by a vacuum rotary evaporator. The resultant viscous oil was used for further characterization.

Monomeric Furanics Purification and Characterization

Purification of Monomeric Furanics

Products obtained in the sections of “Synthesis of EMFM” and “Synthesis of BHMFM and BHMFD” were separated by a preparative liquid chromatograph (Sepabean machine2, Santai Technologies, Changzhou, China), which was equipped with a DAD detector and a Spherical C18 column (SW025, 20–45 µm). The following separation conditions were used: 100% phosphate buffer (pH 6.5, 10 mM) at 5 ml/min for 2 min, increasing volumetric ratio of acetonitrile from 20 to 100% with 35 min and keeping flow rate of eluent at 5 ml/min, 100% acetonitrile at 5 ml/min for 10 min (McKenna et al., 2015). UV wavelengths at 225 nm for EMFM and at 230 nm for BHMFM and BHMFD collections were selected, respectively. Once a UV signal was detected, the fraction containing the targeted products was automatically collected. The structure of the collected fraction was identified by GC-MS, and then further analyzed by NMR.

Identification of Monomeric Furanics

Products separated by the preparative liquid chromatograph were initially identified by a GC-MS (SCION 436GC-SQ, Techcomp group, Shanghai, China) that was installed with a SCION-5 MS column (30 m × 0.32 mm × 0.25 µm). The following temperature program was used for GC-MS analysis: the column temperature was initially set at 50°C and held at the temperature for 5 min, heated at a rate of 10°C/min to 300°C and held at 300°C for 5 min.

After the solvent was removed from the fraction collected from the preparative liquid chromatograph, about 5–10 mg of the purified product was dissolved in 0.5 ml chloroform-d for nuclear magnetic resonance (NMR) spectrum analysis. All

¹H-NMR spectra were acquired on a Bruker Ascend™ 600 NMR Spectrum with an operating frequency of 600 MHz.

Quantitation of Monomeric Furanics

The products in the prepared samples (Sections of “Synthesis of EMFM” and “Synthesis of BHMFM and BHMFD”) were quantitatively analyzed by GC (SCION 436C, Techcomp group, Shanghai, China). The following temperature program was used for GC analysis: the column temperature was initially set at 50°C and held at 50°C for 5 min, then heated at a rate of 10°C/min to 300°C and held at 300°C for 5 min.

The concentrations of reactants and products in chloroform solutions were quantified by a well-known effective carbon number method (Shuai et al., 2016). The conversion of reactants and the yield of products were thereby calculated as follows:

$$\text{Reactant conversion (\%)} = \frac{\text{mol of reacted reactant}}{\text{Initial mol of reactant}} \times 100$$

$$\text{Product yield (\%)} = \frac{\text{mol of product}}{\text{Initial mol of reactant}} \times 100$$

Elemental Analysis of Condensed Furanics Before and After Hydrodeoxygenation

To evaluate the efficiency of hydrodeoxygenation reactions and the quality of hydrocarbon fuels, the contents (wt%) of C and H elements in the prepared oil samples were analyzed by an element analyzer (Vario EL Cube, Elementar, Germany). Prior to the elemental analysis, solvent-free viscous oils obtained in the Section of “Hydrodeoxygenation of condensed furanics to hydrocarbon fuels” were further dried in a vacuum drying oven at 80°C for 48 h and then ground to powder in an agate mortar. The contents of O element in the samples was calculated by assuming that the total content of C, H and O elements for each sample was 100%.

RESULTS AND DISCUSSION

This study intends to introduce a hydroxymethyl group (-CH₂OH) at the C-5 position of furan derivatives (2-(ethoxymethyl)furan (EMF) and furfuryl acetate (FA)) via electrophilic addition of formaldehyde for synthesizing 2,5-bis(hydroxymethyl)furan (BHMFM) derivatives (5-(ethoxymethyl)furan-2-methanol (EMFM), 2,5-bis(hydroxymethyl)furan monoacetate (BHMFM) and 2,5-bis(hydroxymethyl)furan diacetate (BHMFD)) (Figure 1A, Figure 2A). Because furanics are unstable under acidic conditions, the effects of different acids such as hydrochloric acid, sulfuric acid, formic acid, acetic acid and trifluoromethanesulfonic acid on the hydroxymethylations of EMF and FA were initially investigated.

Synthesis of EMFM From EMF

The results show that the strength of the acid in the reaction system has a great influence on the reaction. When the acidity used in the reaction medium was too high, the substrate was easily carbonized due to the acid-catalyzed ring opening of furan rings

and severe condensation of the ring-opening products such as aldehydes or ketones. As such, strong acidity-induced carbonization reactions (e.g., entries 7,8,10, and 11 in **Supplementary Table S1**; entries 3,4,6,8,9, and 10 in **Supplementary Table S2**) resulted in dark colored reaction liquors and no hydroxymethylated product was detected in these reactions (**Supplementary Table S1**, **Supplementary Table S2**). Low-concentration hydrochloric or and anhydrous acetic acid exhibited better balance between acid-catalyzed hydroxymethylation and carbonization reactions, resulting in decent product yields. Therefore, these two catalytic systems were further studied for hydroxymethylation of furfuryl alcohol derivatives.

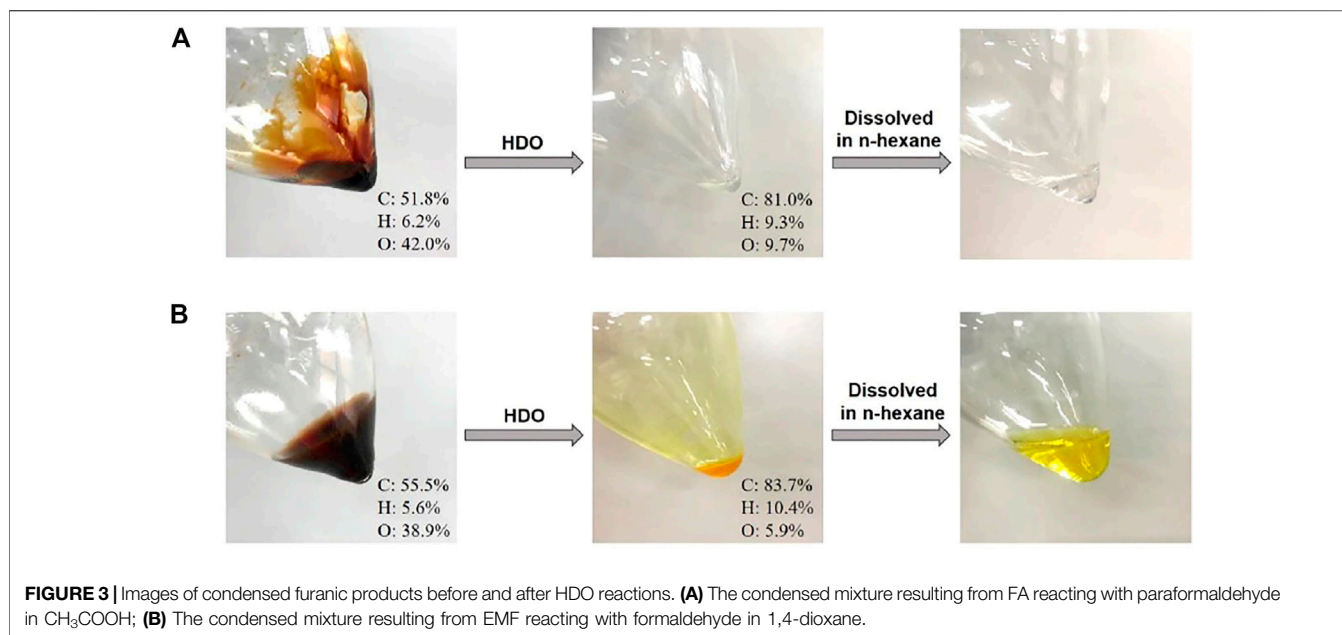
The results above demonstrated that low-concentration HCl aqueous solution was more beneficial than other reaction systems to facilitate the hydroxymethylation reaction of EMF with formaldehyde. Since the acidity would be an important factor affecting the hydroxymethylation reaction efficiency, the effect of HCl aqueous solution loading was thereby further investigated. 5-(ethoxymethyl)furan-2-methanol (EMFM), a hydroxymethylated product of EMF, was identified by MS (**Supplementary Figure S1**) and $^1\text{H-NMR}$ (**Supplementary Figure S2**) and quantified by GC (**Supplementary Figure S3**), when the reaction between EMF (0.4 mmol) and formaldehyde (1 ml of 37 wt% aqueous solution, 10 mmol) was catalyzed by 10 μL of 36 wt% HCl aqueous solution (0.1 mmol H^+) in 1 ml of 1,4-dioxane at 50°C for 7 h. However, without the change of other reaction conditions, increasing the loading of 36 wt% HCl aqueous solution to 20 μL (0.2 mmol H^+) resulted in a dark reaction solution and reduced hydroxymethylated product. This could be mainly caused by the increased concentration of H^+ in water and 1, 4-dioxane mixture, which could accelerate the ring opening reactions of furanics (EMF and/or EMFM) and the condensation (e.g., aldol condensation) of corresponding ring-opening products (Nakagawa and Tomishige, 2012). Meanwhile, we did not observe any hydroxymethylated product with a decreased acid loading of 1 μL (0.01 mmol H^+) and a reaction time of 4 h at 60°C, further indicating that acid-catalyzed ring opening and condensation reactions was kinetically faster than the hydroxymethylation reaction of EMF. With an appropriate loading (10 μL , 0.1 mmol H^+) of HCl aqueous solution, the effects of reaction temperature and time on the hydroxymethylation efficiency of EMF were further investigated. Overall, increasing the reaction temperature and time facilitated the EMF conversion and the formation of hydroxymethylated product (EMFM). When the reaction temperature was 30°C, no desired product was detected in the early stage of the reaction (<4 h) (**Figure 1B**); when the reaction temperature was increased to 40°C, the EMFM yield gradually increased with the increase of the reaction time (**Figure 1C**). At an elevated reaction temperature of 50°C, the maximum yield (28.3 mol%) of EMFM was achieved at 5 h (**Figure 1D**) but the EMFM yield slightly decreased at an extended reaction time (6–8 h) likely due to the condensation of furanics. With the same loading (10 μL , 0.1 mmol H^+) of HCl aqueous solution, severe condensation or carbonization was observed when a higher temperature of 60°C was used. High-molecular-weight products (300–1,000 Da) (Entry 1 in

Supplementary Table S1) observed in the GPC results (**Supplementary Figure S9**) confirmed the occurrence of condensation during the reaction. In the reaction system of HCl and formaldehyde aqueous solution, these results indicated that a high reaction temperature could significantly increase the rate of side reactions (furan ring opening and condensation), resulting in a serious decrease in the yield of the hydroxymethylated product.

Synthesis of BHMFM and BHMFD From FA

Under the similar conditions, above results promoted us to conduct the hydroxymethylation reaction of FA (entry 1 in **Supplementary Table S1**) with formaldehyde and HCl aqueous solutions in 1,4-dioxane at 50 °C for 1 and 5 h. However, no hydroxymethylated products were detected after replacing the EMF with FA (entry 11 in **Supplementary Table S2**). In addition to the furan ring opening (Liang et al., 2017) and aldol condensation of ring opening products, we infer that in the presence of water, acid could also catalyze the hydrolysis of the ester linkage of FA to form furfuryl alcohol, which could easily condense. Such side reactions could occur for the newly formed hydroxymethylated products of FA. The hydroxyl groups could be protonated to form a carbonium ion, which could attack the electron-rich furan ring to form condensed products (He et al., 2021).

To avoid the hydrolysis of the ester linkages of FA and condensation reactions caused by strong acid in the aqueous solution, we therefore explored the hydroxymethylation reaction of FA using a weak anhydrous acid (i.e., anhydrous acetic acid) and paraformaldehyde (Entry 1 in **Supplementary Table S2**) instead of formaldehyde and HCl aqueous solutions. In an anhydrous reaction medium, a hydroxymethylated product of FA (2,5-bis(hydroxymethyl)furan monoacetate (BHMFM)) was identified by MS (**Supplementary Figure S4**) and $^1\text{H-NMR}$ (**Supplementary Figure S5**) under an elevated temperature from 80 to 120°C. With acetic acid in the reaction system, BHMFM was further esterified by acetic acid to produce another derivative, 2,5-bis(hydroxymethyl)furan diacetate (BHMFD), which was also confirmed by MS (**Supplementary Figure S6**) and $^1\text{H-NMR}$ (**Supplementary Figure S7**). The results indicated that anhydrous acidic environment was favorable to the hydroxymethylation of FA while the aqueous reaction system (e.g., formaldehyde and HCl aqueous solution) was indeed not favorable to the hydroxymethylation of FA under acidic conditions. At a mild reaction temperature of 80°C, no BHMFM was detected within 3 h. After that, BHMFM yield gradually increased with the extension of the reaction time (**Figure 2B**). When the reaction temperature was elevated to 100 °C, BHMFM was quickly formed within 2 h. Further increasing the reaction time resulted in decreased BHMFM yields (**Figure 2C**). This was mainly caused by the esterification of BHMFM to form BHMFD (**Figure 2A**). The acetylation of BHMFM to form BHMFD was more evident at 120°C than those at 100°C (**Figure 2D**). At a reaction time of 3 h at 120°C, BHMFM was almost completely esterified to form BHMFD while the total yield of BHMFM and BHMFD was not improved at elevated reaction temperatures (>120 °C).



In-situ esterification could be considered as a protection strategy to prevent the condensation of BHMFM in acidic reaction system. However, the yield of BHMFM or BHMFD was not beyond 30 mol% under the investigated conditions. Similar to the hydroxymethylation reaction of EMF, this would be mainly caused by different reaction rates of target (hydroxymethylation and esterification) and side reactions (dehydration, furan ring opening and condensation). First, it is difficult to improve the yields of BHMFM and BHMFD if the ring-opening rate of furan rings is faster than the hydroxymethylation rate of FA. Second, even the reaction rate of hydroxymethylation is faster than that of furan ring opening, newly formed hydroxymethyl group could be immediately protonated by hydrogen proton and dehydrated to produce carbonium ions in an acidic medium. Carbonium ions are active components that would initiate methylene-bridging condensation products, making the esterification of BHMFM difficult and also resulting in low yields of BHMFM and BHMFD.

Synthesis of Hydrocarbon Fuels From Condensed Furanic Products

From the perspective of kinetics, it can be seen that no matter how to optimize the reaction conditions, part of the furanics would condense to form higher-molecular-weight products (Supplementary Figure S9). Such an issue is also associated with many other studies involving HMF, furfural and their derivatives (Randolph et al., 2018; Chang et al., 2020; Modugno and Titirici, 2021). In addition to the synthesis of hydroxymethylated products, we tentatively hydrogenated the condensed furanic products into hydrocarbon fuels in order to improve carbon utilization. Oligomerization of furanics followed

by hydrodeoxygenation (HDO) reactions to produce hydrocarbon fuels and lubricants have been intensively studied (Li et al., 2021). Herein, we investigated the possibility of hydrogenating the condensed furanics into hydrocarbon fuels.

The residue after the removal of furanic monomers via hexane extraction was considered as condensed mixture and used to produce hydrocarbon fuels *via* hydrodeoxygenation. According to a previously reported procedure (Huber et al., 2005), we used two-step HDO reactions to remove oxygen-containing functional groups from the condensed furanics. The first step was to partially hydrogenate the oxygenated furanic products to increase its solubility in the hydrophobic solvents that was used in the second step; the second step was to near completely remove oxygen from the oxygenated furanic products to obtain hydrocarbon fuels. After these HDO reactions, the color of EMF- and FA-derived oily products changed from dark to colorless and light yellow (Figure 3), respectively. Moreover, the oily products produced by HDO reactions could be well dissolved in n-hexane to form homogeneous and transparent solutions (Figure 3), indicating that these condensed furanics were successfully hydrodeoxygenated and the resultant oily products can be possibly used as drop-in hydrocarbon fuels or additives in gasoline or diesel.

The element contents of the condensed furanics before and after HDO reactions were further analyzed to confirm the occurrence of hydrodeoxygenation. It can be seen from Figure 3 that, the oxygen content of EMF-derived oily products was significantly decreased from 38.9 to 5.9% after HDO reactions, at which the contents of C and H in HDO products were increased from initial 55.5 and 5.6%–83.7 and 10.4% (Supplementary Table S3), respectively. Similar results were also obtained for that of FA-derived oily products (Supplementary Table S3), where O content decreased from

42.0 to 9.7% and C and H contents increased from 51.8 to 6.2%–81.0 and 9.3%, respectively. These results indicate that oxygen was efficiently removed from EMF- and FA-derived condensates to form hydrophobic hydrocarbon fuels with good solubility in n-hexane. As it was known, HMF-involved reactions generally lead to many condensed products, this preliminary study opened up a new way to produce hydrocarbon fuels from condensed furanics products which has been considered as waste, improving the carbon utilization efficiency.

CONCLUSION

In this study, HMF derivatives, i.e., EMFM, BHMFM and BHMFD were synthesized using FA and EMF as raw materials through acid-catalyzed hydroxymethylation, proving the possibility of making six-carbon HMF derivatives from five-carbon furfural derivatives. Although such pathway is feasible, achieving high yields of hydroxymethylated products in these reactions seems challenging due to the paralleled ring-opening reaction of furanics and condensation of the resulting ring-opening products. Therefore, future research would be development of more efficient catalysts or reaction systems to suppress these side reactions to improve the selectivity of the targeted products. Alternatively, the by-products of these reactions were successfully converted into oil through hydrodeoxygenation reactions in order to improve the carbon utilization of furanics. This study provides a new route to synthesize the intermediate products of BHMFM and FDCA from easily available raw materials and also prove the feasibility of converting condensed furanic by-products into drop-in hydrocarbon fuels.

REFERENCES

- Chang, H., Bajaj, I., Huber, G. W., Maravelias, C. T., and Dumesic, J. A. (2020). Catalytic Strategy for Conversion of Fructose to Organic Dyes, Polymers, and Liquid Fuels. *Green. Chem.* 22 (16), 5285–5295. doi:10.1039/d0gc01576h
- Chen, D., Cang, R., Zhang, Z.-D., Huang, H., Zhang, Z.-G., and Ji, X.-J. (2021). Efficient Reduction of 5-hydroxymethylfurfural to 2, 5-bis (Hydroxymethyl) Furan by a Fungal Whole-Cell Biocatalyst. *Mol. Catal.* 500 (3), 111341–111347. doi:10.1016/j.mcat.2020.111341
- Cheng, F., Guo, D., Lai, J., Long, M., Zhao, W., Liu, X., et al. (2021). Efficient Base-free Oxidation of 5-hydroxymethylfurfural to 2,5-furandicarboxylic Acid over Copper-Doped Manganese Oxide Nanorods with Tert-Butanol as Solvent. *Front. Chem. Sci. Eng.* 15 (4), 960–968. doi:10.1007/s11705-020-1999-5
- Elsayed, I., Jackson, M. A., and Hassan, E. B. (2020). Hydrogen-Free Catalytic Reduction of Biomass-Derived 5-Hydroxymethylfurfural into 2,5-Bis(hydroxymethyl)furan Using Copper-Iron Oxides Bimetallic Nanocatalyst. *ACS Sustain. Chem. Eng.* 8 (4), 1774–1785. doi:10.1021/acsschemeng.9b05575
- Gao, T., Gao, T., Fang, W., and Cao, Q. (2017). Base-free Aerobic Oxidation of 5-hydroxymethylfurfural to 2,5-furandicarboxylic Acid in Water by Hydrotalcite-Activated Carbon Composite Supported Gold Catalyst. *Mol. Catal.* 439, 171–179. doi:10.1016/j.mcat.2017.06.034
- Guan, W., Zhang, Y., Chen, Y., Wu, J., Cao, Y., Wei, Y., et al. (2021). Hierarchical Porous Bowl-like Nitrogen-Doped Carbon Supported Bimetallic AuPd Nanoparticles as Nanoreactors for High Efficient Catalytic Oxidation of HMF to FDCA. *J. Catal.* 396, 40–53. doi:10.1016/j.jcat.2021.02.012
- Gupta, D., Kumar, R., and Pant, K. K. (2020). Hydrotalcite Supported Bimetallic (Ni-Cu) Catalyst: A Smart Choice for One-Pot Conversion of Biomass-Derived

DATA AVAILABILITY STATEMENT

The original contributions presented in the study are included in the article/**Supplementary Material**, further inquiries can be directed to the corresponding authors.

AUTHOR CONTRIBUTIONS

LS and CL developed the concept; XLV conducted the synthesis and GC analysis of the products; XC conducted the separation of products; JL conducted the elemental analysis; XLU conducted the NMR analysis and wrote the manuscript. LS and CL modified the concept and proofread the manuscript for language and technicalities.

FUNDING

This work was supported by National Natural Science Foundation of China (31870559, 31901262 and 32071716), Fujian Provincial Department of Science and Technology (2018J01590 and 2019J01387), Outstanding Youth Funding (xjq201923) of Fujian Agriculture and Forestry University.

SUPPLEMENTARY MATERIAL

The Supplementary Material for this article can be found online at: <https://www.frontiersin.org/articles/10.3389/fbioe.2022.851668/full#supplementary-material>

- Platform Chemicals to Hydrogenated Biofuels. *Fuel* 277, 118111–118121. doi:10.1016/j.fuel.2020.118111
- He, J., Qiang, Q., Liu, S., Song, K., Zhou, X., Guo, J., et al. (2021). Upgrading of Biomass-Derived Furanic Compounds into High-Quality Fuels Involving Aldol Condensation Strategy. *Fuel* 306, 121765–121789. doi:10.1016/j.fuel.2021.121765
- Hu, K., Zhang, M., Liu, B., Yang, Z., Li, R., and Yan, K. (2021). Efficient Electrochemical Oxidation of 5-hydroxymethylfurfural to 2,5-furandicarboxylic Acid Using the Facilely Synthesized 3D Porous WO₃/Ni Electrode. *Mol. Catal.* 504, 111459–111467. doi:10.1016/j.mcat.2021.111459
- Huber, G. W., Chheda, J. N., Barrett, C. J., and Dumesic, J. A. (2005). Production of Liquid Alkanes by Aqueous-phase Processing of Biomass-Derived Carbohydrates. *Science* 308 (5727), 1446–1450. doi:10.1126/science.1111166
- Kandasamy, P., Gogoi, P., Venugopalan, A. T., and Raja, T. (2021). A Highly Efficient and Reusable Ru-NaY Catalyst for the Base Free Oxidation of 5-Hydroxymethylfurfural to 2,5-Furandicarboxylic Acid. *Catal. Today* 375, 145–154. doi:10.1016/j.cattod.2020.05.009
- Li, S., Ma, Q., Zhong, W., Zhao, X., Wei, X., Zhang, X., et al. (2021). One-pot Hydrodeoxygenation of Bioderived Furans into Octane at Low Temperatures via an Octanediol Route. *Green. Chem.* 23 (13), 4741–4752. doi:10.1039/d1gc00916h
- Liang, X., Haynes, B. S., and Montoya, A. (2017). Acid-Catalyzed Ring Opening of Furan in Aqueous Solution. *Energy Fuels* 32 (4), 4139–4148. doi:10.1021/acs.energyfuels.7b03239
- McKenna, S. M., Leimkühler, S., Herter, S., Turner, N. J., and Carnell, A. J. (2015). Enzyme cascade Reactions: Synthesis of Furandicarboxylic Acid (FDCA) and Carboxylic Acids Using Oxidases in Tandem. *Green. Chem.* 17 (6), 3271–3275. doi:10.1039/c5gc00707k

- Modugno, P., and Titirici, M. M. (2021). Influence of Reaction Conditions on Hydrothermal Carbonization of Fructose. *ChemSusChem* 14 (23), 5271–5282. doi:10.1002/cssc.202101348
- Nakagawa, Y., and Tomishige, K. (2012). Production of 1,5-pentanediol from Biomass via Furfural and Tetrahydrofurfuryl Alcohol. *Catal. Today* 195 (1), 136–143. doi:10.1016/j.cattod.2012.04.048
- Randolph, C., Lahive, C. W., Sami, S., Havenith, R. W. A., Heeres, H. J., and Deuss, P. J. (2018). Biobased Chemicals: 1,2,4-Benzenetriol, Selective Deuteration and Dimerization to Bifunctional Aromatic Compounds. *Org. Process. Res. Dev.* 22 (12), 1663–1671. doi:10.1021/acs.oprd.8b00303
- Rao, K. T. V., Hu, Y., Yuan, Z., Zhang, Y., and Xu, C. C. (2021). Green Synthesis of Heterogeneous Copper-Alumina Catalyst for Selective Hydrogenation of Pure and Biomass-Derived 5-hydroxymethylfurfural to 2,5-bis(hydroxymethyl)furan. *Appl. Catal. A: Gen.* 609, 117892–117936. doi:10.1016/j.apcata.2020.117892
- Sajid, M., Zhao, X., and Liu, D. (2018). Production of 2,5-furandicarboxylic Acid (FDCA) from 5-hydroxymethylfurfural (HMF): Recent Progress Focusing on the Chemical-Catalytic Routes. *Green. Chem.* 20 (24), 5427–5453. doi:10.1039/c8gc02680g
- Shuai, L., Amiri, M. T., Questell-Santiago, Y. M., Héroguel, F., Li, Y., Kim, H., et al. (2016). Formaldehyde Stabilization Facilitates Lignin Monomer Production during Biomass Depolymerization. *Science* 354 (6310), 329–333. doi:10.1126/science.aaf7810
- Yang, Y., and Mu, T. (2021). Electrochemical Oxidation of Biomass Derived 5-hydroxymethylfurfural (HMF): Pathway, Mechanism, Catalysts and Coupling Reactions. *Green. Chem.* 23 (12), 4228–4254. doi:10.1039/d1gc00914a
- Ye, L., Han, Y., Wang, X., Lu, X., Qi, X., and Yu, H. (2021). Recent Progress in Furfural Production from Hemicellulose and its Derivatives: Conversion Mechanism, Catalytic System, Solvent Selection. *Mol. Catal.* 515, 111899–111910. doi:10.1016/j.mcat.2021.111899
- Yu, L., Chen, H., Wen, Z., Jin, M., Ma, X., Li, Y., et al. (2021). Efficient Aerobic Oxidation of 5-Hydroxymethylfurfural to 2, 5-Furandicarboxylic Acid over a Nanofiber Globule La-MnO₂ Catalyst. *Ind. Eng. Chem. Res.* 60 (4), 1624–1632. doi:10.1021/acs.iecr.0c05561
- Zhang, J., Gong, W., Yin, H., Wang, D., Zhang, Y., Zhang, H., et al. (2021). *In Situ* Growth of Ultrathin Ni(OH)₂ Nanosheets as Catalyst for Electrocatalytic Oxidation Reactions. *ChemSusChem* 14 (14), 2935–2942. doi:10.1002/cssc.202100811

Conflict of Interest: The authors declare that the research was conducted in the absence of any commercial or financial relationships that could be construed as a potential conflict of interest.

Publisher's Note: All claims expressed in this article are solely those of the authors and do not necessarily represent those of their affiliated organizations, or those of the publisher, the editors and the reviewers. Any product that may be evaluated in this article, or claim that may be made by its manufacturer, is not guaranteed or endorsed by the publisher.

Copyright © 2022 Lv, Luo, Cheng, Liu, Li and Shuai. This is an open-access article distributed under the terms of the Creative Commons Attribution License (CC BY). The use, distribution or reproduction in other forums is permitted, provided the original author(s) and the copyright owner(s) are credited and that the original publication in this journal is cited, in accordance with accepted academic practice. No use, distribution or reproduction is permitted which does not comply with these terms.



Hydrothermal Pretreatment of Lignocellulosic Feedstocks to Facilitate Biochemical Conversion

Carlos Martín^{1,2}, Pooja Dixit¹, Forough Momayez¹ and Leif J. Jönsson^{1*}

¹Department of Chemistry, Umeå University, Umeå, Sweden, ²Department of Biotechnology, Inland Norway University of Applied Sciences, Hamar, Norway

OPEN ACCESS

Edited by:

Zhongqing Ma,
Zhejiang Agriculture and Forestry
University, China

Reviewed by:

Nur Izyan Wan Azelee,
University of Technology Malaysia,
Malaysia

Feng Peng,
Beijing Forestry University, China
Zhichao Deng,
Chongqing University, China

*Correspondence:

Leif J. Jönsson
leif.jonsson@umu.se

Specialty section:

This article was submitted to
Bioprocess Engineering,
a section of the journal
Frontiers in Bioengineering and
Biotechnology

Received: 31 December 2021

Accepted: 24 January 2022

Published: 16 February 2022

Citation:

Martín C, Dixit P, Momayez F and
Jönsson LJ (2022) Hydrothermal
Pretreatment of Lignocellulosic
Feedstocks to Facilitate
Biochemical Conversion.
Front. Bioeng. Biotechnol. 10:846592.
doi: 10.3389/fbioe.2022.846592

Biochemical conversion of lignocellulosic feedstocks to advanced biofuels and other bio-based commodities typically includes physical diminution, hydrothermal pretreatment, enzymatic saccharification, and valorization of sugars and hydrolysis lignin. This approach is also known as a sugar-platform process. The goal of the pretreatment is to facilitate the ensuing enzymatic saccharification of cellulose, which is otherwise impractical due to the recalcitrance of lignocellulosic feedstocks. This review focuses on hydrothermal pretreatment in comparison to alternative pretreatment methods, biomass properties and recalcitrance, reaction conditions and chemistry of hydrothermal pretreatment, methodology for characterization of pretreatment processes and pretreated materials, and how pretreatment affects subsequent process steps, such as enzymatic saccharification and microbial fermentation. Biochemical conversion based on hydrothermal pretreatment of lignocellulosic feedstocks has emerged as a technology of high industrial relevance and as an area where advances in modern industrial biotechnology become useful for reducing environmental problems and the dependence on fossil resources.

Keywords: hydrothermal pretreatment, lignocellulose, enzymatic saccharification, biochemical conversion, sugar-platform process

INTRODUCTION

The negative environmental impact of the extensive use of fossil fuels and problems associated with the dependency on fossil resources to produce energy, chemicals, and materials have strengthened efforts devoted to increased utilization of renewable feedstocks (Weinberg and Kaltschmitt, 2013). Lignocellulosic biomass is formed at a high rate ($\sim 200 \times 10^9$ tons per year), is relatively inexpensive, and has large potential as feedstock for sustainable production of biofuels, platform chemicals, and value-added products (Bhowmick et al., 2018).

Lignocellulosic biomass includes agricultural and agro-industrial residues, forest and wood-processing residues, herbaceous energy crops and short-rotation trees, and a part of municipal solid waste. An overview of the composition of different lignocellulosic materials, including softwood (pine), hardwood (eucalyptus), an agro-industrial by-product (sugarcane bagasse), and two agricultural residues (wheat straw and corn stover), is given in **Table 1**. The main organic constituents of lignocellulosic biomass are cellulose, hemicelluloses, and lignin, which are closely associated in lignin-carbohydrate complexes (LCC) in the secondary cell walls of vascular plants (Fengel and Wegener, 1989). The cellulose content is comparable in most lignocellulosic materials, while the contents of hemicelluloses and lignin differ greatly in different types of biomass. Besides

TABLE 1 | Summary of the composition of different types of lignocellulosic biomass (mass fraction in percent dry weight).

Biomass	Cellulose	Hemi-celluloses	Lignin	Extractives	Minerals	References
Maritime pine (<i>Pinus pinaster</i>)	45.0	22.2 ^a	26.8 ^b	2.9	0.2	López et al. (2020)
Eucalyptus (<i>Eucalyptus nitens</i>)	42.0	22.2 ^c	22.9	4.7	0.3	Penín et al. (2019)
Sugarcane (<i>Saccharum officinarum</i>) bagasse	36.9	24.5	22.0	4.7	4.5	Neves et al. (2016)
Wheat (<i>Triticum aestivum</i>) straw	34.0	22.9 ^c	15.0	14.8	4.3	Cornejo et al. (2019)
Corn (<i>Zea mays</i>) stover	38.2	25.8 ^c	17.4	13.3	5.3	Li and Kim, (2011)

^aMainly hexosans.^bKlason lignin.^cMainly pentosans.

water, other constituents include extractives and minerals. The distribution of extractives and minerals varies greatly depending on the type of biomass (Table 1).

Plant cellulose is a linear polysaccharide composed of glucose units linked by β -1,4-glycosidic bonds. The degree of polymerization (DP) reaches as high as 15,000 (Fengel and Wegener, 1989). Cellulose chains are packed in a compact crystalline structure stabilized by hydrogen bonds and hydrophobic interactions (Lindman et al., 2021). Crystallinity contributes to giving cellulose a low reactivity towards chemicals and enzymes. There are also amorphous regions, which are more prone to chemical and enzymatic reactions, but they are a minor part of the macromolecule.

Hemicelluloses are branched heteropolysaccharides composed of units of pentoses, hexoses, and uronic acids. They have relatively low DP (Fengel and Wegener, 1989). Softwood hemicelluloses are rich in hexose units, while pentose units are prevalent in hardwood hemicelluloses. O-Acetyl-galactoglucomannan and O-acetyl-4-O-methylglucurono-D-xylan are the main hemicelluloses in softwood and hardwood, respectively. In gramineous plants, which are the main source of agricultural and agro-industrial residues, hemicelluloses are predominantly pentosans. Hemicelluloses are amorphous and have higher reactivity than cellulose. They can undergo hydrolysis under relatively mild conditions, which is of crucial importance in lignocellulose biorefining.

Lignin is a polymer consisting of phenylpropane units, which are linked by ether and carbon-carbon bonds and which form a three-dimensional network (Fengel and Wegener, 1989; Ralph et al., 2019). The β -O-4 ether linkage is the most common intermonomeric linkage in lignin. The lignin content is typically higher in wood than in gramineous biomass, and is especially high in softwood (Table 1). Lignin is primarily composed of three types of phenylpropanoid units, i.e., guaiacyl (G), syringyl (S), and *p*-hydroxyphenyl (H). These units are derived from three different monolignols: G units from coniferyl alcohol, S units from sinapyl alcohol, and H units from *p*-coumaryl alcohol. Softwood lignin consists almost exclusively of G units, while hardwood lignin is a mixture of G and S units. In gramineous lignin, H units are also important constituents, besides G and S. Although less prominent than G, S, and H units, other types of units sometimes occur, such as cinnamyl alcohol end groups, and *p*-hydroxybenzoate and *p*-coumarate conjugates (Ralph et al., 2019). Since the association of lignin with

polysaccharides in LCC makes enzymatic access to cellulose difficult, removal of lignin is beneficial for enzymatic saccharification.

In a lignocellulose biorefinery, hemicelluloses, lignin, and cellulose are fractionated into streams that are then valorized to fuels, chemicals, and materials. Carbohydrates can be processed to biofuels (such as ethanol and butanol) and to platform chemicals (such as furans and organic acids). Lignin can be converted to phenols, polymers, composites and different added-value specialty chemicals and fuels. Lignocellulose biorefining can be based on different fractionation sequences. One approach is to first separate hemicelluloses, and then submit the resulting cellulignin to further fractionation by either lignin solubilization or cellulose saccharification. Another approach is to target the lignin, which is an approach that has been used for a long time in chemical pulping processes (the Kraft process, the sulfite process, the soda process, and the organosolv process). More recently, this fractionation approach has become known as the lignin-first approach (Matsakas et al., 2019).

Although the first mention of the word “biorefinery” dates from the early 1990s (Wyman and Goodman, 1993), industrial biorefining has preceded the usage of the term. The fundamentals of biorefining were set by the pulp and paper industry for more than one century ago (Alén, 2015), and since then it has for a long time produced a variety of bio-based commodities beyond pulp and paper. Cane sugar mills serve as another example of proto-biorefineries. Sugarcane bagasse, molasses, and filter cakes have for a long time been used for energy generation, ethanol production, and wax extraction, respectively. Modern pulp mills performing green manufacturing of several end-products from one feedstock are sophisticated biorefineries (Alén, 2015). The same applies to state-of-the-art sugarcane-processing complexes, where production of food, biofuel, chemicals, electricity, and heat is integrated at the same production plant (Vaz, 2019).

The term “pretreatment” is used in different areas for referring to operations that are performed prior to certain major processes in order to improve their performance. In this paper, pretreatment refers to processing of lignocellulosic biomass to facilitate enzymatic saccharification of cellulose. Pretreatment and enzymatic saccharification, followed by microbial fermentation or chemical conversion of sugars and valorization of lignin, are parts of the sugar-platform route, which aims at producing advanced biofuels and other bio-based products from lignocellulose (Wyman and Dale, 2015).

TABLE 2 | Examples of hydrothermal pretreatment approaches and other commercially relevant methods.

Method	Effects on lignocellulose constituents	Upscaling examples
Auto-catalyzed hydrothermal pretreatment	Partial solubilization of hemicelluloses, slight effects on cellulose and lignin	Inbicon, RE Energy (Denmark), Clariant (Switzerland)
Hydrothermal pretreatment with dilute acid	Extensive hydrolysis of hemicelluloses, hydrolysis of amorphous cellulose, minor fragmentation of lignin	logen Corporation (Canada), POET-DSM (United States), Raízen Energia (Brazil)
Hydrothermal pretreatment with steam explosion	Partial to complete solubilization of hemicelluloses, fragmentation of cellulose, minor fragmentation of lignin	Sekab (Sweden), Abengoa Bioenergy (United States)
Mild alkaline methods	Significant removal of lignin, partial solubilization of hemicelluloses, deacetylation	DuPont (United States)
Chemical pulping- processes (including sulfite and organosolv)	Extensive removal of lignin, variable removal of hemicelluloses, decrease of degree of polymerization and crystallinity of cellulose	Borregaard (BALI process) (Norway), Chempolis (Finland)

Enzymatic saccharification of raw lignocellulose would result in low rates and yields due to feedstock recalcitrance, a set of properties that obstruct the access of enzymes to cellulose. Pretreatment is required to reduce the recalcitrance and thereby facilitate enzymatic saccharification. Pretreatment would typically affect both the structure and the chemistry of the biomass (Zhao et al., 2012a). An effective pretreatment should result in greatly enhanced enzymatic digestibility of cellulose and in high recovery of hemicellulosic saccharides (Jönsson and Martín, 2016). Many pretreatment approaches have been developed as a result of intense research in the area, and some of the most effective methods have been validated at demonstration scale (Galbe and Wallberg, 2019). Research on different raw materials has shown that the effectiveness of pretreatment is feedstock-dependent, and that the effects of a given method can diverge for different types of lignocellulosic biomass (Martín, 2021). Low capital expenditures (capex) and operational expenditures (opex) are key criteria for industrially viable pretreatment methods. In that sense, methods allowing operation at high-solids loadings and with low use of expensive chemical additives are relevant for upscaling. Demonstration-scale operations have allowed the gathering of engineering information needed for full-scale design, and some technically relevant methods have been upscaled to commercial plants (Table 2).

Different varieties of hydrothermal pretreatment (HTP) and some processes originating from the pulping industry are among the methods of higher technical relevance (Table 2). In HTP, moist feedstocks, either alone or in the presence of chemical additives, are subjected to high temperature for a certain period of time. HTP is generally performed at acidic pH, which is caused either by organic acids released from the biomass or by added acids. In HTP, especially when a low initial pH is applied, hemicelluloses are hydrolyzed, while most of the cellulose and lignin will remain in the pretreated solid biomass. Removal of hemicelluloses increases biomass surface area, and results in an improvement of the enzymatic digestibility of cellulose.

The sulfite-based BALI (short for “Borregaard Advanced Lignin”) process of Borregaard (Table 2) (Rødsrud et al., 2012) and organosolv pretreatment are technically-relevant methods that emerged from the pulping industry. In contrast

to HTP under acidic conditions, chemical-pulping-based methods follow the lignin-first philosophy, i.e., lignin is the main target. Hemicelluloses are also solubilized and can potentially be separated from lignin before upgrading. Cellulose remains in the solid fraction, and its susceptibility to enzymatic saccharification is greatly enhanced. Other pretreatment methods than HTP are, however, beyond the scope of this review, and more detailed information about them can be found elsewhere (Jönsson and Martín, 2016; Galbe and Wallberg, 2019).

In hydrothermal processing biomass is treated in the presence of water at temperatures in the order ~200–400°C and at high pressure. Although hydrothermal processing includes hydrothermal (HT) liquefaction, HT gasification, and HT carbonization (Tekin et al., 2014), this review focuses on hydrothermal pretreatment (HTP) of lignocellulosic biomass prior to enzymatic saccharification of cellulose.

HTP is one of the most technologically-mature pretreatment methods for lignocellulosic feedstocks (Ruiz et al., 2020), and it is used in many biorefinery upscaling attempts. The simplest HTP procedure is auto-catalyzed hydrothermal pretreatment (A-HTP), which includes only disintegrated biomass, water, and heating to temperatures typically in the range ~150–230°C. A major strength of A-HTP is that neither chemical additives (except water and alkali for subsequent pH adjustments), nor expensive anticorrosion materials are required, which lowers capex. Furthermore, A-HTP can be performed continuously and with high-solids loading, which is convenient for industrial operation. An A-HTP process was validated for wheat straw at the Inbicon demonstration plant in Kalundborg, Denmark (Larsen et al., 2012). Commercial-scale initiatives based on A-HTP include, e.g., the plant of Clariant in Podari, Romania (Hortsch and Corvo, 2020) and RE Energy (BEST, 2021).

In HTP, temperature and residence time can be modified to modulate the severity of the pretreatment. HTP severity can be estimated by using the severity factor (SF), an equation combining time and temperature into a single variable (Chornet and Overend, 2017). The severity concept can also cover acidity, which is included in the combined severity factor (CSF). HTP effectiveness for different biomass materials can be optimized by tuning SF or CSF.

The effects of HTP can be potentiated by either including an explosion at the end of the holding period or running the process at starting pH values far from neutrality. In hydrothermal pretreatment with steam explosion (HTP-SE), a sudden decompression is applied after steaming the biomass in a closed chamber. This results in mechanical disruption of the material. Low starting pH, achieved by adding an acid, is typical for dilute-acid-catalyzed hydrothermal pretreatment (DA-HTP), commonly known as dilute-acid pretreatment. DA-HTP is also often combined with steam explosion. Treatment at higher pH (Kim et al., 2016), such as mild alkaline conditions, can be considered as another type of HTP approach.

Depending on the pH of the pretreatment, the composition of the lignocellulose will change dramatically (Galbe and Wallberg, 2019). At acidic pH, the main effect is hydrolysis of hemicelluloses, often all the way to monosaccharides. Alkaline pH promotes the dissolution of lignin, whereas cellulose and a part of the hemicelluloses remain in the solid fraction (**Table 2**). In A-HTP, where the pH becomes acidic after a short while, hemicelluloses are hydrolyzed to a lesser extent than in DA-HTP, but to a greater extent than under mild alkaline conditions. Lignin is fragmented by cleavage of some of the β -O-4 linkages, but most of it is not dissolved as under strong alkaline conditions. A reason for that is that alkaline conditions cause deprotonation of phenolic hydroxyl groups in lignin to phenolate ions, which facilitate dissolution of lignin in aqueous medium. Compared to hydrothermal pretreatment under mild alkaline conditions, DA-HTP requires higher temperatures, and compared to A-HTP, it requires corrosion-resistant alloys and typically leads to more by-product formation. Nevertheless, due to its effectiveness and ease of implementation, DA-HTP is the option of choice in many upscaling initiatives (Solarte-Toro et al., 2019) (**Table 2**). HTP-SE requires energy for reaching the required temperatures and pressures and also sophisticated equipment, but that is counterbalanced by its effectiveness towards different feedstocks, and, therefore, it is also attractive for commercial applications (BEST, 2021).

HTP can be discussed in a narrow sense and, as in this review, in a broad sense. In a more narrow sense, it is restricted to pretreatment of biomass in hot water or steam, as in A-HTP. However, due to auto-catalysis and formation of carboxylic acids that acidify the reaction mixture, A-HTP is an acidic pretreatment process and final pH values in the range 2-3 are commonly observed. In a broader sense, HTP also includes pretreatment techniques in which small amounts of acid or alkali are added to the reaction mixture, and certain variations that can be used to enhance the effect of hydrothermal pretreatment, such as HTP-SE and HTP with addition of gas (Ilanidis et al., 2021a). As higher temperature and/or longer residence time leads to formation of more carboxylic acids and results in lower pH, the differences between A-HTP under harsh conditions and DA-HTP under mild conditions become small. Furthermore, the same equipment is typically used for both A-HTP and DA-HTP, and the choice between them is governed mainly by which type of biomass that is pretreated (as wood, and particularly softwood, typically requires harsher conditions than gramineous plants). These aspects motivate a discussion of HTP in the broader sense.

HYDROTHERMAL PRETREATMENT FOR BIOCHEMICAL CONVERSION

Hydrothermal Pretreatment

Hydrolysis of hemicelluloses, a crucial aspect of HTP, follows the classical mechanism of acid hydrolysis of polysaccharides, i.e., splitting of glycosidic linkages is catalyzed by a proton transferred from an acid catalyst to the glycosidic oxygen atom, followed by water addition to the anomeric carbon (Loerbroeks et al., 2015). The simplest catalysis approach in HTP is auto-catalysis, typical for A-HTP, which is also known as auto-hydrolysis. In A-HTP, heating of moist biomass causes water auto-ionization, and the formed hydronium ions catalyze xylan deacetylation. Dissociation of resulting acetic acid provides protons that push partial hydrolysis of hemicelluloses (Ruiz et al., 2020). Uronic acids released from hemicelluloses also contribute to the catalysis. Hydrolysis proceeds deeper in DA-HTP, where the catalysis is reinforced by inclusion of an acid in the reaction mixture. The acid catalyst is typically a mineral acid, e.g., sulfuric acid, but organic acids or reagents like sulfur dioxide can also be used. The low pH drives the hydrolysis of hemicelluloses until near completion resulting in a massive release of sugar. The acid catalysis can also lead to sugar degradation, especially if the pretreatment is long and the temperature high (Fengel and Wegener, 1989). Degradation reactions result in formation of furans, such as furfural and 5-hydroxymethylfurfural (HMF), and carboxylic acids, such as formic acid and levulinic acid, which represent a loss in sugar yield and which are also inhibitory to fermenting microorganisms (Jönsson and Martín, 2016).

Some mild alkaline treatments, mostly with strong bases, are performed in water-biomass systems under temperatures within the typical HTP range. They represent an HTP variation that is sometimes referred to as alkaline hydrothermal pretreatment (Zakaria et al., 2014). In alkaline hydrothermal pretreatment, hydroxide anions resulting from dissociation of the base effectively attack linkages between hemicelluloses and lignin, and they can also promote some cellulose peeling reactions (Kim et al., 2016). The removal of lignin and hemicelluloses results in enhanced enzymatic digestibility of cellulose. Treatments with lime or ammonia are performed at lower temperature and lie outside the HTP classification used here.

Hydrothermal pretreatment with steam explosion (HTP-SE), commonly known as steam explosion, is an extensively investigated method that is used for different raw materials (Galbe and Wallberg, 2019). It can be performed either as an auto-catalytic process or assisted by acidic or alkaline catalysts. HTP-SE can be operated in both batch and continuous modes. Batch mode consists in placing the required amount of biomass in a reactor chamber, and treating it with saturated steam. After a certain time period, from seconds to a few minutes, the reactor is depressurized, and its content is shot into a cyclone, where the pretreated slurry is separated from the stream of steam and volatiles. In continuous systems, which are of special interest for industrial operations, moisturized biomass is screw-conveyed to a plug feeder and forced into the reactor, where steam is applied. Ensuring a controlled time at the work temperature, the material is ejected into a flash tank, where the vent stream flows

upwards to a condenser, and the slurry is collected from the bottom (Wang et al., 2015).

HTP-SE is a texturing-hydrolysis process disrupting biomass structure and increasing its porosity. It also causes partial hydrolysis of hemicelluloses, and some fragmentation of cellulose and lignin. Those effects lead to improved susceptibility of cellulose to enzymatic saccharification. There has been controversy on the role of the explosion (Galbe and Wallberg, 2019), which was initially believed to be the main cause of the changes during pretreatment. It has recently been shown that the driving force is the synergy of different actions, including the explosion itself, but also other physical events and chemical reactions (Muzamal et al., 2015). Recent studies comparing steam pretreatment of softwood with and without explosion bring back the attention to the importance of the explosion for enhancing enzymatic digestibility of cellulose (Pielhop et al., 2016).

Conditions for Hydrothermal Pretreatment

In HTP, biomass and water is heated to from around 150°C to around 220°C for a period ranging from a few minutes to around 1 hour (Ruiz et al., 2020). Pressure of up to around 25 bar is applied, which forces the water to remain in liquid state. Time and temperature are set so that the severity is suitable for achieving effective solubilization of hemicelluloses, activation of cellulose, and minimal formation of by-products. Based on detailed studies on the kinetics of lignocellulosics fractionation by steam-aqueous pretreatments (Overend and Chornet, 1987), a severity factor (SF) has been established. The SF is calculated as the logarithm of the reaction ordinate R_0 :

$$R_0 = t \times \exp\left(\frac{T_i - 100}{14.75}\right) \quad (1)$$

where t is time in minutes, and T_i is temperature in °C (Eq. 1). SF calculations are often restricted to the isothermal period, and exclude the heating and the cooling period. It is more rational to calculate the SF based on temperature profiles built by measurements along the whole process using the equation:

$$R_0 = \int_0^t \exp\left(\frac{T_i - 100}{14.75}\right) dt, \text{ or} \quad (2)$$

$$SF = \log \sum_{i=1}^n \left[t \times \exp\left(\frac{T_i - 100}{14.75}\right) \right]$$

The required severity depends on the type of raw material. For example, lower severity is typically needed for gramineous biomass than for wood. A-HTP at SF 3.8 resulted in good enzymatic convertibility for sugarcane bagasse (Ilanidis et al., 2021b) and wheat straw (Ilanidis et al., 2021c). An SF below 3.0 was not effective, and a value above 4.3 resulted in excessive sugar degradation. A similar trend was reported for sugarcane straw, where SF 3.2 was not enough and 4.1 was optimal (Batista et al., 2019). For poplar, an SF between 4.2 and 4.6 resulted in substantial solubilization of hemicelluloses and positively affected other factors associated with reduced recalcitrance (Li et al., 2017).

In DA-HTP, the combined severity factor (CSF = SF – pH) is an important indicator, but the determination of the pH value is a

complication. A common approach is to measure the pH of the liquid after pretreatment (Kellock et al., 2019). Other options are to measure it in the beginning, which might be physically difficult if the solids loading is high, or to calculate it based on the definition of pH.

Other key operational conditions are the solids loading and the amount of added acid or alkali. Solids loading is commonly reported as weight percentage of dry matter in the suspension or as liquid-to-solid ratio (LSR). The percentage approach is rather clear for comparison of reported results, and typical values for A-HTP are ~5–20% (w/w) depending on the experimental setup. Although the LSR procedure is accurate with regard to inclusion of biomass moisture as part of the liquid fraction, it is often ambiguous considering that the liquid fraction can be given in either weight or volume units.

It is often difficult to compare dosages of acid or alkali in descriptions of DA-HTP or mild alkaline pretreatment, respectively. Dosages can be given in different ways, e.g., as concentration in solutions added to reaction mixtures, as weight percentage based on the whole reaction mixture, or as weight percentage based on dry weight of biomass. For example, a dosage of “1% H₂SO₄” might refer to 1) 1% H₂SO₄ solution used for preparing a reaction mixture, 2) 1 g H₂SO₄ per 100 g suspension, or 3) 1 g H₂SO₄ per 100 g dry biomass. Explicit descriptions of the used procedures are required for facilitating interpretation of research efforts in the area.

In some HTP methods, oxygen or air are used for stimulating delignification through wet oxidation. Typically, those oxidative pretreatments are applied to herbaceous biomass, and are assisted by alkaline additives, such as sodium carbonate (Martín et al., 2007) or ammonium hydroxide (An et al., 2019). In a recent study, an oxidative approach was applied to softwood and sugarcane bagasse under acidic conditions, and it was shown that oxygen addition can modulate the severity of hydrothermal pretreatment also under acidic conditions (Ilanidis et al., 2021a).

Enzymatic Saccharification

Enzymatic saccharification aims at breaking down cellulose and potential residual hemicelluloses into monomeric sugars. It is a synergistic multi-step process that is carried out with heterogeneous enzyme cocktails containing both cellulose-active glycoside hydrolases (GHs) and accessory enzymes (Van Dyk and Pletschke, 2012). These enzymes can be derived from lignocellolytic fungi or bacteria. However, the most extensively studied cellulase preparations are derived from *Trichoderma reesei* (Kubicek, 2013).

Cellulose depolymerization is a complex process, in which enzymes adsorb on the surface of cellulose, get access to the cellulose chains, and catalyze deconstruction of cellulose to glucose (Figure 1). The first two steps are related to cellulose accessibility and amorphogenesis (Arantes and Saddler, 2010; Arantes and Saddler, 2011). Hydrolysis of cellulose to glucose is catalyzed mainly by three enzymes: endoglucanase (EG), cellobiohydrolase (CBH) (or exoglucanase), and β-glucosidase (BGL) (Van Dyk and Pletschke, 2012). EG catalyzes the hydrolysis of interior glycosidic bonds of cellulose chains to oligomeric cellulose chains. CBH attacks the ends of cellulose

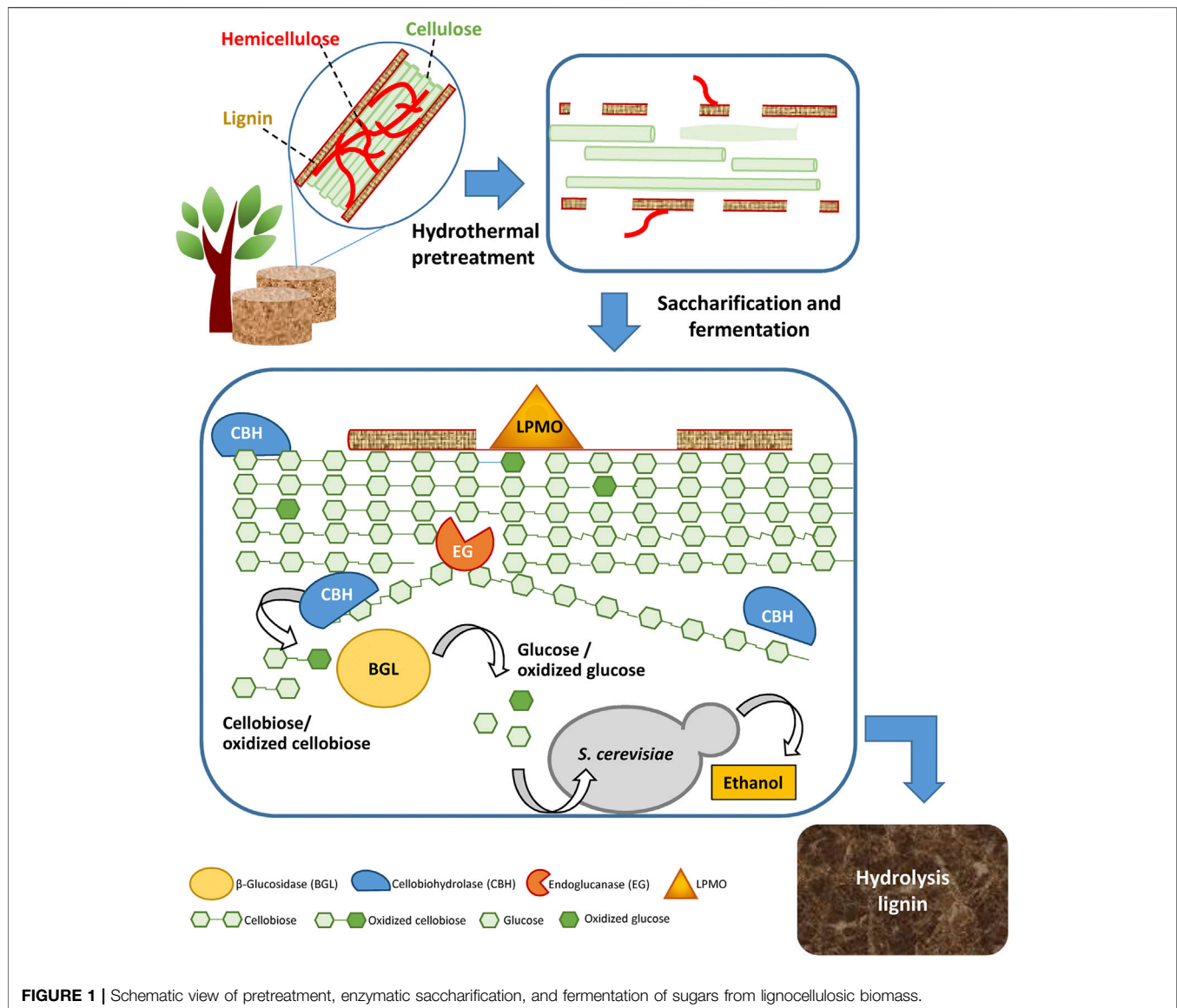


FIGURE 1 | Schematic view of pretreatment, enzymatic saccharification, and fermentation of sugars from lignocellulosic biomass.

chains, either at reducing ends (as CBH I) or at the non-reducing ends (as CBH II), thereby incrementally shortening the chains by splitting off the disaccharide cellobiose. BGL catalyzes the hydrolysis of cellobiose to glucose (**Figure 1**).

Cellulase cocktails are often supplemented with accessory enzymes, such as lytic polysaccharide mono-oxygenase (LPMO) belonging to Auxiliary Activity Family 9 (AA9), formerly GH61. LPMO, which is an oxidoreductase rather than a hydrolase, splits cellulose chains by catalyzing formation of oxidative nicks (**Figure 1**). By creating shorter glucan chains, LPMO acts synergistically with hydrolases and accelerates the saccharification of lignocellulosic biomass (Horn et al., 2012). Thus, the catalytic action of LPMO is covered by the term saccharification, whereas the term hydrolysis covers most, but not all, reactions occurring during enzymatic saccharification. Other important accessory enzymes include various hemicellulases, such as xylanase, xylosidase, mannanase,

mannosidase, α -glucuronidase, α -arabinosidase, acetyl xylan esterase, and others. They act in concert to remove residual hemicelluloses and thereby further improve cellulose accessibility in pretreated biomass (Hu et al., 2011).

Slurries recovered after hydrothermal pretreatment have acidic pH (often around pH 2), and hence the pH needs to be adjusted (typically to around 5). Incubation of reaction mixtures is typically performed with agitation at 45–50 °C for 24–72 h. Enzyme dosages are based on enzyme activity units, enzyme protein, volume or mass fractions of enzyme preparations (in which enzyme protein may account for only a minor fraction), or even molarity. Common examples include filter paper units (FPU), carboxymethyl cellulose units (CMCase units), enzyme protein per dry weight of biomass or glucan, and enzyme preparation per dry weight of biomass or glucan.

Preparative enzymatic saccharification typically aims at obtaining as high sugar yield as possible in an economically

sound way. In contrast, analytical enzymatic saccharification aims at comparison of the susceptibility of different biomass preparations to enzymatic saccharification, comparison of different pretreatment methods or other experimental conditions, or comparison of different enzyme preparations (Gandla et al., 2018). Therefore, analytical enzymatic saccharification is typically not exhaustive, as that would blur the result of the comparisons.

In an industrial context it would be desirable to have a high product titers, and, therefore, enzymatic saccharification of lignocellulosic biomass at high solids loading (such as a content of water-insoluble solids above 15%) would be preferable (Kristensen et al., 2009). However, the use of high solids loadings is often associated with operational challenges and sugar yields are typically comparatively low.

Microbial Fermentation

‘Fermentation’ can be used in a broad and a narrow sense. In a broad sense, ‘fermentation’ unspecifically refers to a cultivation of a microorganism. In a narrow sense, it is an anaerobic energy-yielding metabolic activity in which organic substances serve as both electron donor and electron acceptor. Typical electron acceptors are pyruvate or a derivative of pyruvate, and common products include lactic acid and ethanol.

Sugars derived from pretreatment and enzymatic saccharification of lignocellulosic biomass are typically fermented to cellulosic ethanol using yeast (such as *Saccharomyces cerevisiae*) or bacteria (such as *Zymomonas mobilis*). As 2 mol of ethanol (46.1 g/mol) can be obtained from 1 mol of glucose (180 g/mol) (Eq. 3), the maximum theoretical yield is $(2 \times 46.1)/180 = 0.51$ g ethanol per g glucose.



As cellulose consists of glucose units (on average 162 g/mol) and as a consequence of water (18 g/mol) addition to glycosidic linkages during hydrolysis of cellulose to glucose, the maximum theoretical yield from 1.00 g cellulose is $180/162 = 1.11$ g glucose. Thus, the maximum theoretical yield from 1.00 g cellulose is $1.11 \times 0.51 = 0.57$ g ethanol. Common alternative fermentation products include biobutanol and lactic acid, which can be produced via ABE (acetone-butanol-ethanol) and LAB (lactic acid bacteria) fermentation, respectively (Sivanarutselvi et al., 2017; Tu et al., 2019).

Saccharification and fermentation can be carried out using various configurations, such as Separate Hydrolysis and Fermentation (SHF) (Galbe and Zacchi, 2002), Simultaneous Saccharification and Fermentation (SSF) (Galbe and Zacchi, 2002), Hybrid Hydrolysis and Fermentation (HHF) (Teter et al., 2014), and Consolidated Bio-Processing (CBP) (Lynd et al., 2017). SHF is a two-step process where enzymatic saccharification of pretreated biomass and microbial fermentation of sugars are carried out sequentially. Advantages include that optimal conditions can be used for both enzymatic saccharification and microbial fermentation, and that the residual solids, the hydrolysis lignin, can be separated from the liquid phase, the hydrolysate, before microbes are added. However,

sugars will accumulate during the process and cause end-product inhibition of cellulolytic enzymes. In SSF, enzymatic saccharification and microbial fermentation are carried out in parallel as a one-step process. Since optimal temperatures for enzymatic saccharification (typically around 50°C) and fermentation (typically around 30°C) differ, and since optimal pH and aeration conditions may also differ, the conditions used for SSF are a compromise and are thus suboptimal for at least some of the biocatalysts involved. At least to some extent, end-product inhibition by sugars is avoided, but it is more challenging to recycle the microorganism as it will be mixed with hydrolysis lignin. HHF is a two-step process, in which the first step only includes enzymatic saccharification and the second step includes both enzymatic saccharification and microbial fermentation. In the first step, enzymatic saccharification can be carried out under optimal conditions, but the second step suffers from the same drawbacks as SSF. In CBP, production of enzymes, saccharification of pretreated biomass, and fermentation of sugars are carried out as a one-pot process. Thermophilic anaerobic bacteria, such as *Clostridium thermocellum* (Olson et al., 2015), and *S. cerevisiae* engineered to produce cellulases (Kroukamp et al., 2018) are two options that have been considered.

Microbial fermentation processes can also be carried out in batch, fed-batch, and continuous mode. In batch mode, all medium is added directly to the reactor in the beginning of the process and the final culture volume is similar to the initial volume. In fed-batch mode, the fermentation is initiated using a minor portion of the medium, and then more medium is gradually fed into the bioreactor until it is full or all medium has been consumed. In a continuous fermentation process, the medium is fed into the bioreactor reactor continuously, but is also continuously removed. In Brazil, 83% of distilleries that produce first generation bioethanol rely on fed-batch processes, while continuous processes account for only 17% (Godoy et al., 2008).

Factors Affecting Biomass Recalcitrance

The resistance to biochemical processing of lignocellulosic feedstocks is known as “recalcitrance”. Recalcitrance refers to barriers to access of enzymatic and microbial biocatalysts to carbohydrates in the biomass. There are multiple interrelated factors that contribute to recalcitrance (Table 3), and they include both factors related to the physical structure of the biomass and factors related to the chemical composition (Wang et al., 2018a). Structural features that affect biomass recalcitrance include the highly organized architecture of secondary cell walls, the particle size, the porosity, and the accessible surface area of cellulose. Chemical features include hemicelluloses and lignin, substances that create physical barriers that limit the accessibility of enzymes to cellulose (Zhao et al., 2012b). Higher fractions of hemicelluloses and lignin in the material obviously contribute to recalcitrance, but some investigations indicate that also certain chemical features of hemicelluloses and lignin affect the recalcitrance. Examples of that include the prevalence of different types of building blocks (i.e., the chemical composition of hemicelluloses and lignin), and the acetylation of hemicelluloses (Chen et al., 2012; Herbaut et al., 2018). The DP

TABLE 3 | Factors affecting recalcitrance of lignocellulosic feedstocks, and common detection methods with references^a.

Recalcitrance factor	Common detection methods	References
Cellulose accessibility	Simons' staining	Chandra et al. (2008)
Cellulose crystallinity	XRD	Kumar et al. (2009)
Cellulose DP	GPC	Kumar et al. (2009)
Cell wall architecture	Fluorescence microscopy, SEM	Wang et al. (2018a)
Hemicellulose acetylation	HPAEC, NMR, OLIMP	Wang et al. (2020)
Hemicellulose and lignin content	Analytical acid hydrolysis combined with HPLC or HPAEC	Ilanidis et al. (2021b)
Particle size	Sieving	Ilanidis et al. (2021d)
Porosity	BET analysis	Wang et al. (2018b)
S:G ratio	Py-GC/MS	Wang et al. (2020)
		Ilanidis et al. (2021b)
		Ilanidis et al. (2021d)

^aBET, Brunauer–Emmett–Teller; DP, degree of polymerization; FTIR, Fourier-transform infrared spectroscopy; GC, gas chromatography; GPC, gel permeation chromatography; HPLC, High-pressure liquid chromatography; NMR, nuclear magnetic resonance; OLIMP, oligosaccharide mass profiling, Py-GC/MS, Pyrolysis-gas chromatography/mass spectrometry; SEM, scanning electron microscopy; S:G ratio, ratio of syringyl units and guaiacyl units in lignin; XRD, X-ray diffraction.

and the crystallinity of the cellulose may also affect recalcitrance (Kumar et al., 2009).

Hydrothermal pretreatment removes hemicelluloses, modifies cellulose and lignin, creates cell-wall disorder, and increases biomass porosity and cellulose accessibility (Wang et al., 2018a). It is noteworthy that hydrothermal pretreatment under acidic conditions increases the fraction of lignin and the cellulose crystallinity, but still improves biomass digestibility (Foston and Ragauskas, 2010). Although an increased fraction of lignin and an increase in cellulose crystallinity should theoretically increase the recalcitrance, the positive effects of the pretreatment, such as disruption of cell wall architecture and a decreased fraction of hemicelluloses, are evidently much more important for recalcitrance, and overshadow the negative effects and lead to greatly improved enzymatic digestibility. In line with that, a recent study on *Eucalyptus* wood indicated that, on the one hand, pretreatment effects such as partial removal of lignin, increased S/G ratio in lignin, and lowered cellulose crystallinity exhibited no significant positive effects (Thoresen et al., 2021). On the other hand, effects such as disruption of cell wall architecture, exposure of fibres and increased cellulose accessibility, and substantial removal of hemicelluloses had a positive impact on enzymatic digestibility. Evidently, the impact of different recalcitrance factors varies greatly. Consequently, the impact of recalcitrance factors of relatively low importance, such as cellulose crystallinity, may not be easily observed in complex systems, where recalcitrance factors of high importance, such as preserved cell wall architecture and high hemicellulose content, are predominant.

BY-PRODUCTS OF HYDROTHERMAL PRETREATMENT

Pretreatment Liquid

After hydrothermal pretreatment, typically under acidic conditions, the liquid phase will contain organic substances such as aliphatic aldehydes, aliphatic carboxylic acids, benzoquinones, disaccharides, furans (such as furan aldehydes and furoic acids), monosaccharides, oligosaccharides, phenolic

substances (phenolic as well as non-phenolic aromatics), and uronic acids (Jönsson and Martín, 2016). These are summarized in **Table 4**, which also indicates their main precursor(s) and contains examples of references that address occurrence, formation, and analysis. Whereas glucose is a product that fermenting microorganisms can utilize under anaerobic or oxygen-limited conditions, this is not always the case for other lignocellulose-derived monosaccharides, disaccharides, and oligosaccharides. Disaccharides and oligosaccharides can tentatively be converted to monosaccharides using post-hydrolysis (Shevchenko et al., 2000), an approach that is also used for analytical purposes, or by using enzyme cocktails that not only degrade cellulose but also assist degradation of dimeric and oligomeric saccharides and make them available to microorganisms. Inhibitory effects of by-products and conditioning of lignocellulosic hydrolysates was recently reviewed (Jönsson and Martín, 2016), and this subsection will therefore be restricted to recently discovered inhibitors and novel findings about enzyme inhibition.

Benzoquinones, such as *p*-benzoquinone and 2,6-dimethoxybenzoquinone, were found to be ubiquitous in pretreated biomass, albeit in very low concentrations (for *p*-benzoquinone up to around 6 mg/L or 60 µM) (Stagge et al., 2015). However, as *p*-benzoquinone exhibited an inhibitory effect on *S. cerevisiae* already at around 20 µM, its high molecular toxicity nevertheless makes it relevant as an inhibitor. Furthermore, benzoquinones are oxidation products of benzenediols, such as hydroquinone. The presence of oxidants and reductants, and the handling and storage of pretreated biomass may therefore affect formation and occurrence (Martín et al., 2018).

Formaldehyde and acetaldehyde were found to be prevalent in pretreated biomass in concentrations up to ~4 and ~2 mM, respectively (Cavka et al., 2015). Although lignin is probably the main precursor for formaldehyde, other lignocellulosic constituents, including extractives and polysaccharides, could be other sources. Acetyl groups in hemicelluloses are a tentative precursor for acetaldehyde, although this has to be investigated in more detail. Unsurprisingly considering its central role in the metabolic pathway of ethanolic

TABLE 4 | Groups of products and by-products solubilized by hydrothermal pretreatment.

Group	Description/Examples	Main precursors	References
Aliphatic aldehydes	Acetaldehyde, formaldehyde	Probably lignin (formaldehyde) and hemicelluloses (acetaldehyde)	Cavka et al. (2015)
Aliphatic carboxylic acids	Acetic acid, formic acid, levulinic acid	Hemicelluloses, cellulose; acetic acid from acetyl groups; sugar degradation	Du et al. (2010)
Benzoquinones	<i>p</i> -Benzoquinone, 2,6-dimethoxybenzoquinone	Lignin, phenolic extractives	Stagge et al. (2015)
Disaccharides	Cellobiose, xylobiose	Hemicelluloses, cellulose	Xu et al. (2013)
Furans	Heteroaromatics such as furfural, HMF, 2-furoic acid	Hemicelluloses, cellulose; sugar degradation	Du et al. (2010)
Monosaccharides	Arabinose, galactose, glucose, mannose, xylose	Hemicelluloses, cellulose	Shevchenko et al. (2000)
Oligosaccharides	Glucooligosaccharides, xylooligosaccharides	Hemicelluloses, cellulose	Xu et al. (2013)
Phenolic compounds	Phenolic and non-phenolic aromatic compounds	Lignin, phenolic extractives	Du et al. (2010)
Uronic acids	Galacturonic acid, glucuronic acid, 4-O-methyl-glucuronic acid	Hemicelluloses	Wang et al. (2018a)

fermentation, acetaldehyde was much less toxic to yeast than formaldehyde (Cavka et al., 2015). Formaldehyde was found to be the single most important inhibitor of yeast in hydrothermally pretreated softwood (Martín et al., 2018). Although phenolic inhibitors and synergistic effects of different groups of inhibitors also play a role, the discovery of previously unknown inhibitors, such as formaldehyde and *p*-benzoquinone, can help explaining toxic effects of lignocellulosic hydrolysates containing non-toxic levels of furan aldehydes and aliphatic acids.

Inhibition of cellulose-degrading enzymes by pretreatment by-products differs from inhibition of microorganisms. Monomeric sugars causing end-product inhibition of cellulolytic enzymes and phenolic substances have been found to be major contributors to enzyme inhibition in the liquid fraction of steam-pretreated biomass (Zhai et al., 2016). Oligosaccharides produced during pretreatment could also contribute to enzyme inhibition (Kumar and Wyman, 2014). There are several direct studies of the inhibitory effects of phenols on enzymes (e.g., Ximenes et al., 2011; Zhai et al., 2018). Phenols may exert several effects on enzymes. Conditioning of lignocellulosic hydrolysates using sulfur oxyanions, such as sodium sulfite or sodium dithionite, alleviated inhibition of both yeast and enzymes, whereas conditioning using sodium borohydride only alleviated inhibition of yeast (Cavka and Jönsson, 2013). A difference between sulfur oxyanions, on the one hand, and sodium borohydride, on the other hand, is the capacity of the former to strongly hydrophilize inhibitors by sulfonation (Cavka and Jönsson, 2013; Jönsson and Martín, 2016). This suggests that hydrophobic interactions is one cause of inhibition of enzymes, whereas inhibition of microorganisms is more related to reactivity and interference of metabolism. In line with that, studies of steam-pretreated woody biomass have indicated that hydrophobic phenolics are the major inhibitory compounds for enzymes (Zhai et al., 2018).

Solid Phase

Pseudo-lignin is an aromatic Klason-lignin-positive substance derived from carbohydrates during thermal treatment of biomass,

including hydrothermal pretreatment (Shinde et al., 2018). Pseudo-lignin is typically derived mostly from hemicelluloses, such as xylan, which are more heat labile than cellulose and decompose to form pseudo-lignin at lower temperatures (Normark et al., 2016). In contrast, real lignin is a polymeric substance consisting of phenylpropane units, and it is formed by combinatorial cross-linking of radicals created by oxidation of monolignols (Ralph et al., 2019). The monolignols are formed via the shikimate pathway, which is also involved in the biosynthesis of aromatic amino acids. Thus, although pseudo-lignin and real lignin share some common features, such as aromaticity, insolubility in water under neutral conditions, and acid-resistance (i.e., being Klason-lignin-positive substances), their basic chemical structure and their origin are fundamentally different.

Pseudo-lignin formation represents a yield loss, as the fraction of carbohydrates that form pseudo-lignin is not converted to fermentable sugars. Pseudo-lignin also has a negative impact on enzymatic saccharification of cellulose. This negative impact is caused by reduced cellulose accessibility and by catalytically non-productive binding of enzymes to pseudo-lignin (Kumar et al., 2013; Wang and Jönsson, 2018).

Gas Phase

Some volatile substances originating from the biomass and from the pretreatment reactions have been captured from pretreatment vapor and analyzed using mass spectrometry. Condensate from steam-explosion of corn stalks contained furans, phenols, and carboxylic acids (Yang et al., 2017). Main constituents, as judged from peak areas, were furfural, phenol, and 4-hydroxy-butanoic acid. Phenol was the predominant analyte in non-condensable gas collected using dichloromethane (Yang et al., 2017). Analysis of a set of condensates from pretreatment of sugarcane bagasse showed that furfural accumulated in the condensates and that the levels were related to sugar degradation and furan aldehyde formation during pretreatment (Ilanidis et al., 2021b). Further investigations are needed to characterize volatile substances formed during hydrothermal pretreatment of biomass and to understand their potential contribution to the mass balance of hydrothermal pretreatment.

CHARACTERIZATION OF PRETREATED LIGNOCELLULOSE

Pretreatment of lignocellulosic materials results in a slurry of variable consistency depending on the pretreatment method and the initial solids loading. Based on the downstream strategy, the slurry can either be separated into a solid fraction (i.e., pretreated solids) and a liquid fraction (i.e., pretreatment liquid or hemicellulose hydrolysate) to be processed separately, or be used directly as it is for conditioning and biocatalytic conversion. Regardless of the processing strategy, a thorough characterization of the pretreated material is required in order to assess the efficiency of the pretreatment. That includes determination of the gravimetric yield of solids, the chemical composition of the solid and liquid phases, evaluation of the recovery of the main organic components of biomass, and assessment of enzymatic digestibility and fermentability. An overview of methodology useful for characterization of pretreated biomass is provided below.

Slurry Characteristics

The characteristics of slurries produced during the pretreatment step have a critical effect on subsequent processing steps. The dry-matter (DM) content of a slurry is comprised of insoluble solids, often referred to as water-insoluble solids (WIS), and soluble solids (SS). Main components of SS include organic degradation products derived from hemicelluloses (such as sugars), some degradation products from cellulose and lignin, hydrophilic extractives, and salts. WIS is composed mainly of cellulose and lignin, and typically some residual hemicelluloses.

The DM of the slurry can be measured by using an oven or an automatic infrared moisture analyzer. In both cases, a certain amount of slurry, usually 2–5 g, is heated at 105 °C until a constant mass is reached (Sluiter et al., 2008a). To determine the fractions of WIS and SS, the first step is separation of the solid and the liquid phase (Sluiter et al., 2008b). Vacuum filtration is commonly used for separation. However, if clogging of filters is a problem, centrifugation may serve as an alternative. To determine the SS content, the liquid fraction is passed through a 0.2 µm filter. After that, about 10 mL of the filtrate is dried, typically using an oven, and the residual solids are analyzed gravimetrically. To determine the WIS content, the solid fraction obtained after filtration or centrifugation could be washed several times with deionized water to remove residual liquor. The wash is finished when the glucose concentration in the wash water is < 0.05 g/L. The washed solids are then dried at 105°C using one of the previously mentioned methods. Alternatively, the determination can also be performed without washing (Weiss et al., 2010).

Analysis of Liquid Phase

Hydrothermal pretreatment fractionates biomass by solubilizing hemicelluloses into monomeric, dimeric, or oligomeric products in the liquid fraction of a biomass slurry, while keeping cellulose and lignin relatively intact in the solid fraction (Galbe and Wallberg, 2019). Characterization of pretreatment liquids to determine the content of sugars as well as by-products helps

in evaluating hydrothermal pretreatments aiming at maximal conversion of polysaccharides into sugars. Mild hydrothermal pretreatment would typically result in the formation of substantial amounts of disaccharides and oligosaccharides. Hence, a mild post-hydrolysis of the pretreatment liquid can be done by sulfuric acid at a concentration of 4% (w/w) at 121°C for 60 min, to completely hydrolyze dimeric and oligomeric saccharides to monomers. Monosaccharides generated after hydrothermal pretreatment and post-processing of liquids, such as arabinose, galactose, glucose, mannose, xylose, are generally detected either through high-performance liquid chromatography (HPLC) combined with refractive-index detection (RID) or through high-performance anion-exchange chromatography (HPAEC) combined with pulsed-amperometric detection (PAD). The latter approach typically offers superior resolution and higher sensitivity (Gandla et al., 2018).

Heteroaromatic degradation by-products, such as furfural and HMF, are typically determined using HPLC with UV detection or DAD (diode-array detection). Aliphatic acids, such as acetic acid, levulinic acid, and formic acid, are typically analyzed using HPLC or using HPAEC with conductivity detection (Du et al., 2010; Gandla et al., 2018). Splitting of β -O-4 ether bonds of lignin during hydrothermal pretreatment generates phenolic substances, many of which are phenolic. Mononuclear aromatic substances are typically detected using mass spectrometry (Du et al., 2010; Martín et al., 2018).

Apart from determination of individual substances, group analyses are also useful. Determination of total phenolics in pretreatment liquid is often carried out using the Folin-Ciocalteu colorimetric assay with vanillin as a calibration standard (Persson et al., 2002). The total aromatic content (TAC) of pretreatment liquids is analyzed using UV absorbance at 280 nm (Wang et al., 2018b). TAC analysis covers both heteroaromatics, such as furans, and aromatics, such as phenolic and non-phenolic substances. The total carboxylic acid content (TCAC), which covers both aliphatic and aromatic carboxylic acids, is determined by titration (Wang et al., 2018b).

Analysis of Solid Phase

Determination of the composition of biomass by hydrolysis of the polysaccharides using sulfuric acid has been used for more than a hundred years. The method was further developed by the introduction of two-step treatment with sulfuric acid (TSSA), in which the second step is performed with more diluted acid but at higher temperature. Today, NREL/TP-510-42618 (Sluiter et al., 2012) is a commonly used protocol for performing TSSA. The biomass needs to be extracted prior to TSSA. The solvent could be, for example, ethanol, acetone, a mixture of petroleum ether and acetone, or a mixture of cyclohexane and acetone. A less polar solvent or mix of solvents is useful for efficient extraction of resin from softwood. Biomass extractives are typically measured gravimetrically after solvent evaporation, whereas individual extractives are analyzed using mass spectrometry.

The dried solid residue obtained after extraction is fractionated using 72% (w/w) sulfuric acid for 1 h at 30°C. The

mixture is then diluted to 4% (w/w) sulfuric acid with deionized water and is autoclaved at 121°C for 1 hour. Vacuum filtration is applied for separation. The solid fraction is composed of Klason lignin (acid-insoluble lignin) and ash, while sugars and acid-soluble lignin (ASL) are found in the liquid fraction. The monosaccharides are often analyzed using HPAEC-PAD, which offers better resolution and higher sensitivity than HPLC-RID. Klason lignin is determined gravimetrically and ASL is estimated using UV/Vis spectrophotometry. The recommended wavelength and absorptivity used for ASL determination vary depending on the type of biomass investigated (Sluiter et al., 2012). Wavelengths used for ASL determination are in no way specific for lignin, but are subject to interference, e.g., by the presence of furans. The conditions used in TSSA for hydrolysis of the carbohydrates are important for the accuracy of the method. Too low severity will result in residual cellulose in the solid fraction leading to underestimation of the carbohydrate content and overestimation of the Klason lignin content. Too high severity will result in degradation of sugars to furans and carboxylic acids leading to underestimation of the carbohydrate content and, if sugar degradation products are not analyzed and accounted for, poor mass balance (Wang et al., 2017). Although the hydrolysis conditions mentioned above are suitable in many cases, they are not optimal for all sorts of biomass and processed biomass samples.

Ash or mineral content is typically determined gravimetrically after heating at 550–600°C. Ash content may refer to the total ash in non-extracted biomass or to acid-insoluble ash, i.e., the fraction of ash left in the residue after hydrolysis of carbohydrates using the TSSA method. The ash content varies greatly depending on plant species but also depending on the type of tissue. A review of data from 144 species of lignocellulosic biomass (Tao et al., 2012) indicated that the ash content of dry biomass varied between 0.1 and 26.2% (with a mean of 3.5%). The ash content of woody biomass (0.1–6.4% with a mean of 1.9%) was typically lower than that of non-woody biomass (1.0–26.2%, with a mean of 7.0%) (Tao et al., 2012).

Pyrolysis-gas chromatography/mass spectrometry (Py-GC/MS) is another way to compare the contents of carbohydrates and lignin in biomass samples, although the method provides no detailed information on the carbohydrate composition. Initially, the biomass is pyrolyzed at around 500°C in the presence of a gas stream consisting of helium, nitrogen, or argon gas. The fragments are separated by GC and identified by mass spectrometry (Gerber et al., 2012). The method is useful for determination of the ratio of lignin subunits, i.e., the S:G or S:G:H ratio.

Analysis using solution-state and solid-state nuclear magnetic resonance (NMR) is useful for obtaining information about the effects of pretreatment on biomass (Lu and Ralph, 2011; Bryant et al., 2020). Solid-state NMR offers relatively low resolution and sensitivity, but has the advantage that the original structure of the biomass sample is maintained. Methods such as solid-state cross-polarization/magic angle spinning (CP/MAS) ^{13}C NMR are therefore useful for studies of the crystallinity and ultrastructure of cellulose. Solution-state NMR offers higher resolution and sensitivity, and can provide detailed

information on lignin and hemicelluloses. Two dimensional heteronuclear single quantum coherence (2D HSQC) NMR offers detailed information on the composition and linkages of lignin and biomass polysaccharides. However, dissolution typically causes some degradation of the sample, and information on cellulose crystallinity is lost.

Infrared light is applied in Fourier-transform infrared (FTIR) spectroscopy to scan lignocellulosic materials and study structural features before and after pretreatment. FTIR is a simple and fast analytical technique with easy sample preparation that identifies functional groups in a semi-quantitative manner. It has sometimes been used to estimate changes in CrI (crystallinity index). Absorption bands between 800 and 1800 cm^{-1} are assigned to the main components of lignocellulosic materials (Faix and Böttcher, 1992).

X-ray diffraction (XRD) is commonly used to estimate the crystallinity of cellulose in biomass. However, CrI values might be affected both by the methodology and by factors such as moisture content (Agarwal et al., 2017).

Pseudo-lignin might be difficult to distinguish from real lignin as both substances end up as Klason lignin in compositional analysis using TSSA. Several different methods can be used to get an indication of the occurrence of pseudo-lignin (Shinde et al., 2018). An approach to estimate the pseudo-lignin content is to combine compositional analysis using TSSA with Py-GC/MS. The Klason lignin determined using TSSA will include both real lignin and pseudo-lignin, but in analysis using Py-GC/MS pseudo-lignin will be included in the carbohydrate fraction rather than in the lignin fraction. Hence, a relative value for the pseudo-lignin content can be estimated by subtracting the peak area fraction assigned to lignin in the Py-GC/MS analysis from the mass fraction of lignin determined using compositional analysis with TSSA (Normark et al., 2016; Ilanidis et al., 2021a).

The Simons' staining method gives a relative estimate of cellulose accessibility based on dye adsorption using Direct Blue (DB) and Direct Orange (DO). The larger DO dye (>100 kDa) has affinity for cellulose and a size that is as large or even larger than that of many enzymes. The DB dye, which is smaller than the enzymes, populates only small pores and is less relevant with regard to determination of cellulose accessibility. The difference between final and initial concentrations of each dye indicates the amounts of adsorbed dyes (Chandra et al., 2008).

The Brunauer–Emmett–Teller (BET) method is useful for investigating the specific surface area and the pore-size distribution of biomass before and after pretreatment (Wang et al., 2020). The BET method is typically based on monitoring adsorption of nitrogen gas on the sample surface.

Surface modifications, fragmentation of biomass, and changes in cell wall integrity as a result of pretreatment can be investigated using microscopy, including light microscopy, electron microscopy, atomic force microscopy, and fluorescence microscopy. Staining with dyes such as phloroglucinol-HCl, which causes purple staining of cinnamaldehydes in lignin, is a way to use light microscopy for qualitative assessment of changes in cell wall architecture during pretreatment

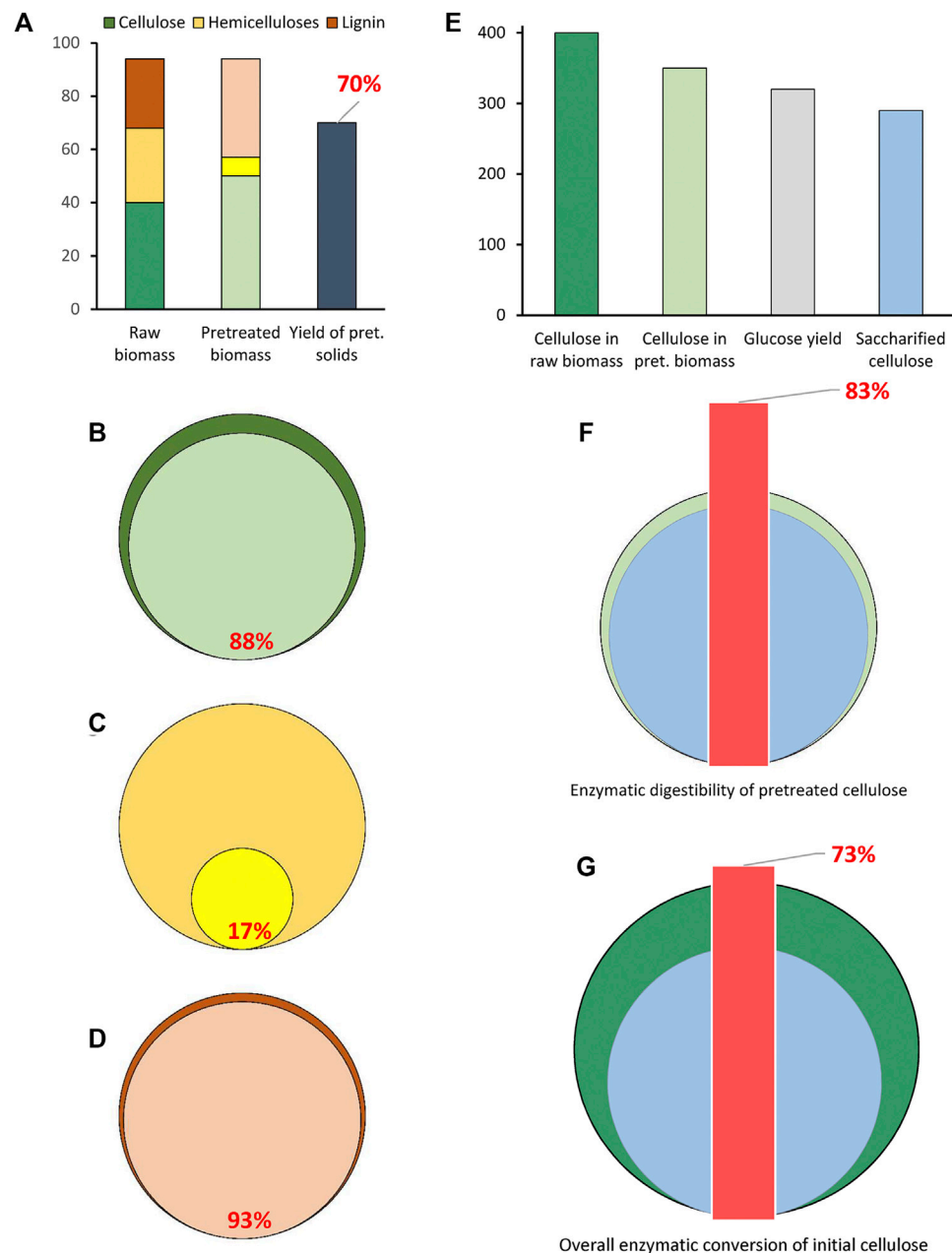


FIGURE 2 | Graphical representation of recovery of the main components in pretreated solids (A–D) and enzymatic saccharification indicators (E–G). Input parameters (A) for recovery calculations (%) for cellulose (B), hemicelluloses (C), and lignin (D) in pretreated solid biomass. Input parameters (E) for calculation of enzymatic saccharification indicators (kg/ton initial biomass); enzymatic digestibility of pretreated cellulose (%) (F); overall enzymatic conversion of initial cellulose (%) (G). In (B), (C) and (D), internal circles represent the recovery of each component in pretreated biomass and external circles represent the initial amount (100%) of the component in raw biomass. In (F) and (G), the internal circles represent saccharified cellulose, and the external ones represent cellulose in pretreated (F) or raw (G) biomass.

(Thoresen et al., 2021). Electron microscopy results in two-dimensional images, while atomic force microscopy provides three-dimensional images with high resolution (Karimi and Taherzadeh, 2016). Due to the autofluorescence of lignin (Donaldson, 2020), fluorescence microscopy is useful for studying the effects of pretreatment on cell wall architecture and the distribution of lignin (e.g., Wang et al., 2018a).

Fragmentation of biomass during pretreatment can be analyzed using sieving or image analysis. Using a series of sieves in the range 50–800 μm , pretreated softwood was fractionated into four size ranges (dust, 50–100 μm ; fine particles, 100–500 μm ; small particles, 500–800 μm ; large particles, >800 μm) and quantitated (Wang et al., 2018b). The particle size distribution was found to be correlated ($R^2 \geq 0.96$) to

the ASL content of pretreated softwood, the glucose content in the pretreatment liquid, and to the enzymatic digestibility.

Recoveries

The compositional analysis is not enough for having a full picture of the fate of lignocellulose constituents during pretreatment (**Figure 2A**). In an example with a hypothetical lignocellulosic material processed through HTP, the composition of raw biomass (**Figure 2A**, left column) and pretreated solids (**Figure 2A**, middle column) points at an apparent increase of the contents of cellulose and lignin, from 40 to 50% and from 26 to 38%, respectively, while the content of hemicelluloses drops from 28 to 7%. A better representation is provided by mass balances, which disclose the recoveries of biomass constituents after pretreatment. Considering an input of 100 kg raw biomass with an output of 70 kg of pretreated solids (**Figure 2A**, right column), the recovered cellulose (**Eq. 4**) would be:

$$\begin{aligned} \text{Cellulose recovery (\%)} &= \frac{\text{Cellulose in pret. solids} \times \text{Pret. solids weight}}{\text{Cellulose in raw biomass} \times \text{Raw biomass weight}} \times 100 \\ &= \frac{50 \times 70}{40 \times 100} \times 100 = 88\% \end{aligned} \quad (4)$$

...which is graphically shown in **Figure 2B**. This reveals that 12% of initial cellulose was not recovered in the pretreated solids. Non-recovered cellulose corresponds to a minor fraction that is susceptible to hydrolysis during pretreatment, primarily amorphous cellulose, and it ends up in the liquid stream as, for example, glucose or degradation products such as HMF, formic acid, and levulinic acid. The same calculations reveal recoveries of 17% (**Figure 2C**) and 93% (**Figure 2D**), respectively, for hemicelluloses and lignin. The actual carbohydrate availability for bioconversion and the amount of sugar lost during pretreatment can be elucidated if the liquid fraction is included in the mass balances. It should be noted that apparent lignin recovery over 100% can be achieved in some experiments. That happens when pseudo-lignin formation occurs in combination with low solubilization of real lignin. This is typical for DA-HTP, but it happens also for A-HTP under severe conditions.

Enzymatic Digestibility and Enzyme Inhibition

Quantification of changes in the susceptibility of cellulose to enzymatic saccharification after pretreatment is crucial for assessing the efficiency of the applied method. The enzymatic digestibility (or convertibility) based on cellulose contained in the sample subjected to saccharification is often reported. Although that indicator shows how susceptible to saccharification the cellulose that remained in the solids after pretreatment is, it fails to capture the fact that a fraction of the cellulose was lost during pretreatment. A more rational approach is the overall conversion, which is based on the cellulose contained in the raw biomass.

Below, a calculation example based on the parameters given in **Figure 2E** is provided. One ton of a biomass material containing

400 kg cellulose is subjected to pretreatment. A cellulose recovery of 88%, i.e., 350 kg, results from the pretreatment. An aliquot of pretreated solids suspended in a buffer solution and submitted to enzymatic saccharification results in 320 kg glucose, which corresponds to 290 kg of saccharified cellulose. The amount of glucose is higher than that of cellulose because, due to water addition to glycosidic linkages, the mass of sugars resulting from hydrolysis of hexosans is increased by a factor of 1.11 compared to the polysaccharide mass. The enzymatic digestibility (ED), calculated as indicated in **Eq. 5**,

$$\begin{aligned} \text{ED (\%)} &= \frac{\text{Saccharified cellulose}}{\text{Cellulose submitted to saccharification}} \times 100 \\ &= \frac{290}{350} \times 100 = 83\% \end{aligned} \quad (5)$$

indicates that 83% (w/w) of the cellulose contained in the pretreated solids is susceptible to conversion to glucose under the conditions applied (**Figure 2F**). The overall conversion (OC), can be calculated as indicated in **Eq. 6**, and it shows that 73% (w/w) of cellulose contained in the raw material is saccharified upon pretreatment and enzymatic saccharification (**Figure 2G**).

$$\begin{aligned} \text{OC (\%)} &= \frac{\text{Saccharified cellulose}}{\text{Cellulose in raw biomass}} \times 100, \text{ or as} \\ \text{OC (\%)} &= \frac{\text{ED} \times \text{Cell. recovery in pret.}}{100} = \frac{83 \times 88}{100} = 73\% \end{aligned} \quad (6)$$

Since pretreatment liquids contain substances that inhibit enzyme activity, it is important to assess the level of the inhibitory effect. For doing that, analytical enzymatic saccharification is run in parallel for microcrystalline cellulose suspended in either pretreatment liquid or a buffer solution. A parameter showing the degree of inhibition (DI) (**Eq. 7**) can be calculated by comparing the enzymatic digestibility of both reactions:

$$\text{DI (\%)} = \frac{\text{ED}_{\text{Buffer}} - \text{ED}_{\text{Pret liq}}}{\text{ED}_{\text{Buffer}}} \times 100 \quad (7)$$

This calculation procedure can also be applied if it is necessary to assess feedback inhibition by sugars released during pretreatment and contained in the pretreatment liquid. In such a case (Wang et al., 2018b), references with the relevant sugars are included in the enzymatic saccharification experiment.

Fermentability

Hydrothermal pretreatment of lignocelluloses generates by-products that are inhibitory to fermenting microbes such as yeasts or bacteria. The toxic effects of inhibitory by-products on fermenting microbes (most commonly *S. cerevisiae*) are evaluated through the fermentability of pretreatment liquids. Fermentability is analyzed by carrying out microbial fermentation in the pretreatment liquids (PL) fortified with sugar and nutrient mixtures, and a control fermentation medium devoid of PL can be used as the reference (Martín et al., 2002). Using ethanolic fermentation as an example,

important indicators include: the ethanol yield on consumed sugar (Y_{con}), the ethanol yield on initial sugar (Y_{ini}), the volumetric ethanol productivity (Q), and the specific ethanol productivity (q). Y_{con} is calculated as the amount of ethanol formed per gram of consumed sugar, and Y_{ini} is calculated as amount of ethanol formed per gram of initial sugar content. Q is calculated as the amount of ethanol produced per liter of culture medium and hour during the fermentation [$\text{g}/(\text{L}/\text{h}^{-1})$]. Q is dependent on the inoculum size and it can be enhanced by increasing the inoculum size and by performing fermentations at high cell density. The specific ethanol productivity, q , is indicative of the performance of a microbial strain. It is often calculated as the volumetric productivity divided by the initial cell concentration [$\text{g}/(\text{g}/\text{h}^{-1})$].

CONCLUSION

Technologies for biochemical conversion of biomass through a sugar-platform approach including hydrothermal pretreatment and enzymatic saccharification have developed rapidly during recent decades and reached industrial implementation. Despite this, intensive research efforts continue and further technology improvements can be expected in the near future. These will likely include innovative technologies addressing aspects such as

conditioning to improve biocatalytic performance, enzyme properties and enzyme recycling, microbial strain development, carbon capture and storage with regard to both heat and power generation and carbon dioxide from fermentation processes, lignin valorization, and characterization and management of residual streams, such as pretreatment vapors and stillage constituents.

AUTHOR CONTRIBUTIONS

Conceptualization, CM and LJ; resources, CM and LJ; writing—original draft preparation, CM, PD, FM, and LJ; writing—review and editing, CM and LJ; visualization, CM, PD, and FM; supervision, CM and LJ; project administration, CM and LJ; funding acquisition, CM and LJ. All authors read and approved the manuscript.

FUNDING

This work was supported by the Swedish Energy Agency (P47516-1), the Kempe Foundations (SMK-1853 and SMK-1969.6), and the strategic research environment Bio4Energy (www.bio4energy.se).

REFERENCES

- Agarwal, U. P., Ralph, S. A., Baez, C., Reiner, R. S., and Verrill, S. P. (2017). Effect of Sample Moisture Content on XRD-Estimated Cellulose Crystallinity Index and Crystallite Size. *Cellulose* 24, 1971–1984. doi:10.1007/s10570-017-1259-0
- Alén, R. (2015). "Pulp Mills and Wood-Based Biorefineries," in *Industrial Biorefineries & White Biotechnology*. Editors A. Pandey, R. Höfer, M. Taherzadeh, K. M. Nampoothiri, and C. Larroche (Amsterdam: Elsevier), 91–126.
- An, S., Li, W., Liu, Q., Xia, Y., Zhang, T., Huang, F., et al. (2019). Combined Dilute Hydrochloric Acid and Alkaline Wet Oxidation Pretreatment to Improve Sugar Recovery of Corn Stover. *Bioresour. Technology* 271, 283–288. doi:10.1016/j.biortech.2018.09.126
- Arantes, V., and Saddler, J. N. (2010). Access to Cellulose Limits the Efficiency of Enzymatic Hydrolysis: the Role of Amorphogenesis. *Biotechnol. Biofuels* 3, 4. doi:10.1186/1754-6834-3-4
- Arantes, V., and Saddler, J. N. (2011). Cellulose Accessibility Limits the Effectiveness of Minimum Cellulase Loading on the Efficient Hydrolysis of Pretreated Lignocellulosic Substrates. *Biotechnol. Biofuels* 4, 3–17. doi:10.1186/1754-6834-4-3
- Batista, G., Souza, R. B. A., Pratto, B., dos Santos-Rocha, M. S. R., and Cruz, A. J. G. (2019). Effect of Severity Factor on the Hydrothermal Pretreatment of Sugarcane Straw. *Bioresour. Technology* 275, 321–327. doi:10.1016/j.biortech.2018.12.073
- Best (2021). *BEST – Bioenergy and Sustainable Technologies*. Austria: Graz. Available at: <https://best-research.eu> (Accessed on December 28, 2021).
- Bryant, N., G. Yoo, C., Pu, Y., and Ragauskas, A. J. (2020). 2D HSQC Chemical Shifts of Impurities from Biomass Pretreatment. *ChemistrySelect* 5, 3359–3364. doi:10.1002/slct.202000406
- Cavka, A., and Jönsson, L. J. (2013). Detoxification of Lignocellulosic Hydrolysates Using Sodium Borohydride. *Bioresour. Technology* 136, 368–376. doi:10.1016/j.biortech.2013.03.014
- Cavka, A., Stagge, S., and Jönsson, L. J. (2015). Identification of Small Aliphatic Aldehydes in Pretreated Lignocellulosic Feedstocks and Evaluation of Their Inhibitory Effects on Yeast. *J. Agric. Food Chem.* 63, 9747–9754. doi:10.1021/acs.jafc.5b04803
- Chandra, R., Ewanick, S., Hsieh, C., and Saddler, J. N. (2008). The Characterization of Pretreated Lignocellulosic Substrates Prior to Enzymatic Hydrolysis, Part 1: A Modified Simons' Staining Technique. *Biotechnol. Prog.* 24, 1178–1185. doi:10.1002/btpr.33
- Chen, X., Shekiri, J., Franden, M. A., Wang, W., Zhang, M., Kuhn, E., et al. (2012). The Impacts of Deacetylation Prior to Dilute Acid Pretreatment on the Bioethanol Process. *Biotechnol. Biofuels* 5, 8–14. doi:10.1186/1754-6834-5-8
- Chornet, E., and Overend, R. P. (2017). "How the Severity Factor in Biomass Hydrolysis Came about," in *Hydrothermal Processing in Biorefineries: Production of Bioethanol and High Added-Value Compounds of Second and Third Generation Biomass*. Editors H. A. Ruiz, M. H. Thomsen, and H. L. Trajano (Cham: Springer International Publishing), 1–3. doi:10.1007/978-3-319-56457-9_1
- Cornejo, A., Alegria-Dallo, I., García-Yoldi, Í., Sarobe, Í., Sánchez, D., Otazu, E., et al. (2019). Pretreatment and Enzymatic Hydrolysis for the Efficient Production of Glucose and Furfural from Wheat Straw, Pine and Poplar Chips. *Bioresour. Technology* 288, 121583. doi:10.1016/j.biortech.2019.121583
- De Bhowmick, G., Sarmah, A. K., and Sen, R. (2018). Lignocellulosic Biorefinery as a Model for Sustainable Development of Biofuels and Value Added Products. *Bioresour. Technology* 247, 1144–1154. doi:10.1016/j.biortech.2017.09.163
- Donaldson, L. (2020). Autofluorescence in Plants. *Molecules* 25, 2393. doi:10.3390/molecules25102393
- Du, B., Sharma, L. N., Becker, C., Chen, S.-F., Mowery, R. A., van Walsum, G. P., et al. (2010). Effect of Varying Feedstock-Pretreatment Chemistry Combinations on the Formation and Accumulation of Potentially Inhibitory Degradation Products in Biomass Hydrolysates. *Biotechnol. Bioeng.* 107, 430–440. doi:10.1002/bit.22829
- Faix, O., and Böttcher, J. H. (1992). The Influence of Particle Size and Concentration in Transmission and Diffuse Reflectance Spectroscopy of wood. *Holz als Roh- und Werkstoff* 50, 221–226. doi:10.1007/bf02650312
- Fengel, D., and Wegener, G. (1989). *Wood – Chemistry, Ultrastructure, Reactions*. Berlin, Germany: De Gruyter.

- Foston, M., and Ragauskas, A. J. (2010). Changes in Lignocellulosic Supramolecular and Ultrastructure during Dilute Acid Pretreatment of *Populus* and Switchgrass. *Biomass and Bioenergy* 34, 1885–1895. doi:10.1016/j.biombioe.2010.07.023
- Galbe, M., and Wallberg, O. (2019). Pretreatment for Biorefineries: A Review of Common Methods for Efficient Utilisation of Lignocellulosic Materials. *Biotechnol. Biofuels* 12, 294. doi:10.1186/s13068-019-1634-1
- Galbe, M., and Zacchi, G. (2002). A Review of the Production of Ethanol from Softwood. *Appl. Microbiol. Biotechnol.* 59, 618–628. doi:10.1007/s00253-002-1058-9
- Gandla, M., Martín, C., and Jönsson, L. (2018). Analytical Enzymatic Saccharification of Lignocellulosic Biomass for Conversion to Biofuels and Bio-Based Chemicals. *Energies* 11, 2936. doi:10.3390/en1112936
- Gerber, L., Eliasson, M., Trygg, J., Moritz, T., and Sundberg, B. (2012). Multivariate Curve Resolution Provides a High-Throughput Data Processing Pipeline for Pyrolysis-Gas Chromatography/Mass Spectrometry. *J. Anal. Appl. Pyrolysis* 95, 95–100. doi:10.1016/j.jaap.2012.01.011
- Godoy, A., Amorim, H. V., Lopes, M. L., and Oliveira, A. J. (2008). Continuous and Batch Fermentation Processes: Advantages and Disadvantages of These Processes in the Brazilian Ethanol Production. *Int. Sugar J.* 110, 175–181.
- Herbaut, M., Zoghalmi, A., Habrant, A., Falourd, X., Foucat, L., Chabbert, B., et al. (2018). Multimodal Analysis of Pretreated Biomass Species Highlights Generic Markers of Lignocellulose Recalcitrance. *Biotechnol. Biofuels* 11, 52. doi:10.1186/s13068-018-1053-8
- Horn, S. J., Vaaje-Kolstad, G., Westereng, B., and Eijsink, V. (2012). Novel Enzymes for the Degradation of Cellulose. *Biotechnol. Biofuels* 5, 45. doi:10.1186/1754-6834-5-45
- Hortsch, R., and Corvo, P. (2020). The Biorefinery Concept: Producing Cellulosic Ethanol from Agricultural Residues. *Chem. Ingenieur Technik* 92, 1803–1809. doi:10.1002/cite.202000203
- Hu, J., Arantes, V., and Saddler, J. N. (2011). The Enhancement of Enzymatic Hydrolysis of Lignocellulosic Substrates by the Addition of Accessory Enzymes Such as Xylanase: Is it an Additive or Synergistic Effect? *Biotechnol. Biofuels* 4, 36. doi:10.1186/1754-6834-4-36
- Ilanidis, D., Stagge, S., Alriksson, B., and Jönsson, L. J. (2021d). Factors Affecting Detoxification of Softwood Enzymatic Hydrolysates Using Sodium Dithionite. *Processes* 9, 887. doi:10.3390/pr9050887
- Ilanidis, D., Stagge, S., Jönsson, L. J., and Martín, C. (2021b). Effects of Operational Conditions on Auto-Catalyzed and Sulfuric-Acid-Catalyzed Hydrothermal Pretreatment of Sugarcane Bagasse at Different Severity Factor. *Ind. Crops Prod.* 159, 113077. doi:10.1016/j.indcrop.2020.113077
- Ilanidis, D., Stagge, S., Jönsson, L. J., and Martín, C. (2021c). Hydrothermal Pretreatment of Wheat Straw: Effects of Temperature and Acidity on Byproduct Formation and Inhibition of Enzymatic Hydrolysis and Ethanol Fermentation. *Agronomy* 11, 487. doi:10.3390/agronomy11030487
- Ilanidis, D., Wu, G., Stagge, S., Martín, C., and Jönsson, L. J. (2021a). Effects of Redox Environment on Hydrothermal Pretreatment of Lignocellulosic Biomass under Acidic Conditions. *Bioresour. Technology* 319, 124211. doi:10.1016/j.biortech.2020.124211
- Jönsson, L. J., and Martín, C. (2016). Pretreatment of Lignocellulose: Formation of Inhibitory By-Products and Strategies for Minimizing Their Effects. *Bioresour. Technol.* 199, 103–112. doi:10.1016/j.biortech.2015.10.009
- Karimi, K., and Taherzadeh, M. J. (2016). A Critical Review of Analytical Methods in Pretreatment of Lignocelluloses: Composition, Imaging, and Crystallinity. *Bioresour. Technology* 200, 1008–1018. doi:10.1016/j.biortech.2015.11.022
- Kellock, M., Maaheimo, H., Marjamaa, K., Rahikainen, J., Zhang, H., Holopainen-Mantila, U., et al. (2019). Effect of Hydrothermal Pretreatment Severity on Lignin Inhibition in Enzymatic Hydrolysis. *Bioresour. Technology* 280, 303–312. doi:10.1016/j.biortech.2019.02.051
- Kim, J. S., Lee, Y. Y., and Kim, T. H. (2016). A Review on Alkaline Pretreatment Technology for Bioconversion of Lignocellulosic Biomass. *Bioresour. Technology* 199, 42–48. doi:10.1016/j.biortech.2015.08.085
- Kristensen, J. B., Felby, C., and Jørgensen, H. (2009). Determining Yields in High Solids Enzymatic Hydrolysis of Biomass. *Appl. Biochem. Biotechnol.* 156, 127–132. doi:10.1007/s12010-008-8375-0
- Kroukamp, H., den Haan, R., van Zyl, J. H., and van Zyl, W. H. (2018). Rational Strain Engineering Interventions to Enhance Cellulase Secretion by *Saccharomyces cerevisiae*. *Biofuels, Bioprod. Biorefin. Biofuel. Bioprod. Biorefin.* 12, 108–124. doi:10.1002/bbb.1824
- Kubicek, C. P. (2013). Systems Biological Approaches towards Understanding Cellulase Production by *Trichoderma reesei*. *J. Biotechnol.* 163, 133–142. doi:10.1016/j.jbiotec.2012.05.020
- Kumar, R., Hu, F., Sannigrahi, P., Jung, S., Ragauskas, A. J., and Wyman, C. E. (2013). Carbohydrate Derived-Pseudo-Lignin Can Retard Cellulose Biological Conversion. *Biotechnol. Bioeng.* 110, 737–753. doi:10.1002/bit.24744
- Kumar, R., Mago, G., Balan, V., and Wyman, C. E. (2009). Physical and Chemical Characterizations of Corn Stover and Poplar Solids Resulting from Leading Pretreatment Technologies. *Bioresour. Technology* 100, 3948–3962. doi:10.1016/j.biortech.2009.01.075
- Kumar, R., and Wyman, C. E. (2014). Strong Cellulase Inhibition by Mannan Polysaccharides in Cellulose Conversion to Sugars. *Biotechnol. Bioeng.* 111, 1341–1353. doi:10.1002/bit.25218
- Larsen, J., Haven, M. Ø., and Thirup, L. (2012). Inbicon Makes Lignocellulosic Ethanol a Commercial Reality. *Biomass Bioenerg.* 46, 36–45. doi:10.1016/j.biombioe.2012.03.033
- Li, M., Cao, S., Meng, X., Studer, M., Wyman, C. E., Ragauskas, A. J., et al. (2017). The Effect of Liquid Hot Water Pretreatment on the Chemical-Structural Alteration and the Reduced Recalcitrance in Poplar. *Biotechnol. Biofuels* 10, 237–248. doi:10.1186/s13068-017-0926-6
- Li, X., and Kim, T. H. (2011). Low-liquid Pretreatment of Corn Stover with Aqueous Ammonia. *Bioresour. Technology* 102, 4779–4786. doi:10.1016/j.biortech.2011.01.008
- Lindman, B., Medronho, B., Alves, L., Norgren, M., and Nordenskiöld, L. (2021). Hydrophobic Interactions Control the Self-Assembly of DNA and Cellulose. *Quart. Rev. Biophys.* 54, e3. doi:10.1017/s0033583521000019
- Loerbroeks, C., Heimermann, A., and Thiel, W. (2015). Solvents Effects on the Mechanism of Cellulose Hydrolysis: A QM/MM Study. *J. Comput. Chem.* 36, 1114–1123. doi:10.1002/jcc.23898
- López, M., Vila, C., Santos, V., and Parajó, J. C. (2020). Manufacture of Platform Chemicals from Pine Wood Polysaccharides in Media Containing Acidic Ionic Liquids. *Polymers* 12, 1215.
- Lu, F., and Ralph, J. (2011). Solution-state NMR of Lignocellulosic Biomass. *J. Biobased Mat Bioenergy* 5, 169–180. doi:10.1166/jbmb.2011.1131
- Lynd, L. R., Liang, X., Biddy, M. J., Allee, A., Cai, H., Foust, T., et al. (2017). Cellulosic Ethanol: Status and Innovation. *Curr. Opin. Biotechnol.* 45, 202–211. doi:10.1016/j.copbio.2017.03.008
- Martín, C. (2021). Pretreatment of Crop Residues for Bioconversion. *Agronomy* 11, 924. doi:10.3390/agronomy11050924
- Martín, C., Galbe, M., Nilvebrant, N.-O., and Jönsson, L. J. (2002). Comparison of the Fermentability of Enzymatic Hydrolysates of Sugarcane Bagasse Pretreated by Steam Explosion Using Different Impregnating Agents. *Appl. Biochem. Biotechnol.* 98, 699–716. doi:10.1385/ABAB:98-100:1-9:699
- Martín, C., Klink, H. B., and Thomsen, A. B. (2007). Wet Oxidation as a Pretreatment Method for Enhancing the Enzymatic Convertibility of Sugarcane Bagasse. *Enzyme Microb. Technol.* 40, 426–432. doi:10.1016/j.enzmictec.2006.07.015
- Martín, C., Wu, G., Wang, Z., Stagge, S., and Jönsson, L. J. (2018). Formation of Microbial Inhibitors in Steam-Explosion Pretreatment of Softwood Impregnated with Sulfuric Acid and Sulfur Dioxide. *Bioresour. Technol.* 262, 242–250. doi:10.1016/j.biortech.2018.04.074
- Matsakas, L., Raghavendran, V., Yakimenko, O., Persson, G., Olsson, E., Rova, U., et al. (2019). Lignin-first Biomass Fractionation Using a Hybrid Organosolv - Steam Explosion Pretreatment Technology Improves the Saccharification and Fermentability of Spruce Biomass. *Bioresour. Technology* 273, 521–528. doi:10.1016/j.biortech.2018.11.055
- Muzamal, M., Jedvert, K., Theliander, H., and Rasmuson, A. (2015). Structural Changes in Spruce Wood During Different Steps of Steam Explosion Pretreatment. *Holzforschung* 69, 61–66. doi:10.1515/hf-2013-0234
- Neves, P. V., Pitarello, A. P., and Ramos, L. P. (2016). Production of Cellulosic Ethanol from Sugarcane Bagasse by Steam Explosion: Effect of Extractives Content, Acid Catalysis and Different Fermentation Technologies. *Bioresour. Technology* 208, 184–194. doi:10.1016/j.biortech.2016.02.085

- Normark, M., Pommer, L., Gräsvik, J., Hedenström, M., Gorzsás, A., Winstrand, S., et al. (2016). Biochemical Conversion of Torrefied Norway Spruce after Pretreatment with Acid or Ionic Liquid. *Bioenerg. Res.* 9, 355–368. doi:10.1007/s12155-015-9698-7
- Olson, D. G., Sparling, R., and Lynd, L. R. (2015). Ethanol Production by Engineered Thermophiles. *Curr. Opin. Biotechnol.* 33, 130–141. doi:10.1016/j.copbio.2015.02.006
- Overend, R. P., and Chornet, E. (1987). Fractionation of Lignocellulosics by Steam-Aqueous Pretreatments. *Philos. Trans. R. Soc. Lond. A.* 321, 523–536. doi:10.1098/rsta.1987.0029
- Penín, L., Peleteiro, S., Santos, V., Alonso, J. L., and Parajó, J. C. (2019). Selective Fractionation and Enzymatic Hydrolysis of *Eucalyptus nitens* wood. *Cellulose* 26, 1125–1139. doi:10.1007/s10570-018-2109-4
- Persson, P., Larsson, S., Jönsson, L. J., Nilvebrant, N.-O., Sivik, B., Munteanu, F., et al. (2002). Supercritical Fluid Extraction of a Lignocellulosic Hydrolysate of Spruce for Detoxification and to Facilitate Analysis of Inhibitors. *Biotechnol. Bioeng.* 79, 694–700. doi:10.1002/bit.10324
- Pielhop, T., Amgarten, J., von Rohr, P. R., and Studer, M. H. (2016). Steam Explosion Pretreatment of Softwood: the Effect of the Explosive Decompression on Enzymatic Digestibility. *Biotechnol. Biofuels* 9, 152. doi:10.1186/s13068-016-0567-1
- Ralph, J., Lapierre, C., and Boerjan, W. (2019). Lignin Structure and its Engineering. *Curr. Opin. Biotechnol.* 56, 240–249. doi:10.1016/j.copbio.2019.02.019
- Rødsrud, G., Lersch, M., and Sjöde, A. (2012). History and Future of World's Most Advanced Biorefinery in Operation. *Biomass Bioenerg.* 46, 46–59. doi:10.1016/j.biombioe.2012.03.028
- Ruiz, H. A., Conrad, M., Sun, S.-N., Sanchez, A., Rocha, G. J. M., Romani, A., et al. (2020). Engineering Aspects of Hydrothermal Pretreatment: From Batch to Continuous Operation, Scale-Up and Pilot Reactor under Biorefinery Concept. *Bioresour. Technology* 299, 122685. doi:10.1016/j.biortech.2019.122685
- Shevchenko, S. M., Chang, K., Robinson, J., and Saddler, J. N. (2000). Optimization of Monosaccharide Recovery by Post-hydrolysis of the Water-Soluble Hemicellulose Component after Steam Explosion of Softwood Chips. *Bioresour. Technology* 72, 207–211. doi:10.1016/s0960-8524(99)00125-x
- Shinde, S. D., Meng, X., Kumar, R., and Ragauskas, A. J. (2018). Recent Advances in Understanding the Pseudo-lignin Formation in a Lignocellulosic Biorefinery. *Green. Chem.* 20, 2192–2205. doi:10.1039/c8gc00353j
- Sivanarutselvi, S., Muthukumar, K., and Velan, M. (2017). Studies on the Effect of Hydrothermal Pretreatment of Sugarcane Bagasse for Biobutanol Production. *Energy Sour. A: Recovery, Utilization, Environ. Effects* 39, 1771–1777. doi:10.1080/15567036.2017.1359705
- Sluiter, A., Hames, B., Hyman, D., Payne, C., Ruiz, R., Scarlata, C., et al. (2008a). *Determination of Total Solids in Biomass and Total Dissolved Solids in Liquid Process samples Laboratory Analytical Procedure (LAP)*. Golden, CO, USA: National Renewable Energy Laboratory NREL.
- Sluiter, A., Hames, B., Ruiz, R., Scarlata, C., Sluiter, J., Templeton, D., et al. (2012). *Determination of Structural Carbohydrates and Lignin in Biomass. Laboratory Analytical Procedure (LAP). Version 08-03-12*. Golden, CO, USA: National Renewable Energy Laboratory NREL.
- Sluiter, A., Hyman, D., Payne, C., and Wolfe, J. (2008b). *Determination of Insoluble Solids in Pretreated Biomass Material. Laboratory Analytical Procedure (LAP)*. Golden, CO, USA: National Renewable Energy Laboratory NREL.
- Solarte-Toro, J. C., Romero-García, J. M., Martínez-Patiño, J. C., Ruiz-Ramos, E., Castro-Galiano, E., and Cardona-Alzate, C. A. (2019). Acid Pretreatment of Lignocellulosic Biomass for Energy Vectors Production: A Review Focused on Operational Conditions and Techno-Economic Assessment for Bioethanol Production. *Renew. Sustainable Energ. Rev.* 107, 587–601. doi:10.1016/j.rser.2019.02.024
- Stagge, S., Cavka, A., and Jönsson, L. J. (2015). Identification of Benzoquinones in Pretreated Lignocellulosic Feedstocks and Inhibitory Effects on Yeast. *AMB Expr.* 5, 62. doi:10.1186/s13568-015-0149-9
- Tao, G., Lestander, T. A., Geladi, P., and Xiong, S. (2012). Biomass Properties in Association with Plant Species and Assortments I: A Synthesis Based on Literature Data of Energy Properties. *Renew. Sustainable Energ. Rev.* 16, 3481–3506. doi:10.1016/j.rser.2012.02.039
- Tekin, K., Karagöz, S., and Bektaş, S. (2014). A Review of Hydrothermal Biomass Processing. *Renew. Sustainable Energ. Rev.* 40, 673–687. doi:10.1016/j.rser.2014.07.216
- Teter, S. A., Sutton, K. B., and Emme, B. (2014). “Enzymatic Processes and Enzyme Development in Biorefining,” in *Advances in Biorefineries*. Editor K. W. Waldron (Amsterdam: Woodhead Publishing Series in Energy), 199–233. doi:10.1533/9780857097385.1.199
- Thoresen, M., Malgas, S., Gandla, M. L., Jönsson, L. J., Sithole, B., and Pletschke, B. I. (2021). The Effects of Chemical and Structural Factors on the Enzymatic Saccharification of *Eucalyptus* Sp. Samples Pre-treated by Various Technologies. *Ind. Crops Prod.* 166, 113449. doi:10.1016/j.indcrop.2021.113449
- Tu, W.-L., Hsu, T.-C., Wang, C.-A., Guo, G.-L., and Chao, Y. (2019). Using Novel *Lactobacillus Plantarum* to Produce Lactic Acid from Lignocellulosic Biomass in an Integrated Simultaneous Saccharification and Fermentation Process. *BioResources* 14, 3873–3885.
- Van Dyk, J. S., and Pletschke, B. I. (2012). A Review of Lignocellulose Bioconversion Using Enzymatic Hydrolysis and Synergistic Cooperation between Enzymes-Factors Affecting Enzymes, Conversion and Synergy. *Biotechnol. Adv.* 30, 1458–1480. doi:10.1016/j.biotechadv.2012.03.002
- Vaz, S., Jr. (2019). Sugarcane-biorefinery. *Adv. Biochem. Eng. Biotechnol.* 166, 125–136. doi:10.1007/10_2016_70
- Wang, K., Chen, J., Sun, S.-N., and Sun, R.-C. (2015). “Steam Explosion,” in *Pretreatment of Biomass*. Editors A. Pandey, S. Negi, P. Binod, and C. Larroche (Amsterdam: Elsevier), 75–104. doi:10.1016/b978-0-12-800080-9.00006-2
- Wang, Z., Gräsvik, J., Jönsson, L. J., and Winstrand, S. (2017). Comparison of $[\text{HSO}_4]^-$, $[\text{Cl}]^-$ and $[\text{MeCO}_2]^-$ as Anions in Pretreatment of Aspen and Spruce with Imidazolium-Based Ionic Liquids. *BMC Biotechnol.* 17, 82. doi:10.1186/s12896-017-0403-0
- Wang, Z., and Jönsson, L. J. (2018). Comparison of Catalytically Non-productive Adsorption of Fungal Proteins to Lignins and Pseudo-lignin Using Isobaric Mass Tagging. *Bioresour. Technology* 268, 393–401. doi:10.1016/j.biortech.2018.07.149
- Wang, Z., Pawar, P. M.-A., Derba-Maceluch, M., Hedenström, M., Chong, S.-L., Tenkanen, M., et al. (2020). Hybrid aspen Expressing a Carbohydrate Esterase Family 5 Acetyl Xylan Esterase under Control of a Wood-specific Promoter Shows Improved Saccharification. *Front. Plant Sci.* 11, 380. doi:10.3389/fpls.2020.00380
- Wang, Z., Winstrand, S., Gillgren, T., and Jönsson, L. J. (2018a). Chemical and Structural Factors Influencing Enzymatic Saccharification of Wood from Aspen, Birch and Spruce. *Biomass and Bioenergy* 109, 125–134. doi:10.1016/j.biombioe.2017.12.020
- Wang, Z., Wu, G., and Jönsson, L. J. (2018b). Effects of Impregnation of Softwood with Sulfuric Acid and Sulfur Dioxide on Chemical and Physical Characteristics, Enzymatic Digestibility, and Fermentability. *Bioresour. Technology* 247, 200–208. doi:10.1016/j.biortech.2017.09.081
- Weinberg, J., and Kaltschmitt, M. (2013). Life Cycle Assessment of Mobility Options Using Wood Based Fuels - Comparison of Selected Environmental Effects and Costs. *Bioresour. Technology* 150, 420–428. doi:10.1016/j.biortech.2013.08.093
- Weiss, N. D., Stickel, J. J., Wolfe, J. L., and Nguyen, Q. A. (2010). A Simplified Method for the Measurement of Insoluble Solids in Pretreated Biomass Slurries. *Appl. Biochem. Biotechnol.* 162, 975–987. doi:10.1007/s12010-009-8806-6
- Wyman, C. E., and Dale, B. E. (2015). Producing Biofuels via the Sugar Platform. *Chem. Eng. Prog.* 111, 45–51.
- Wyman, C. E., and Goodman, B. J. (1993). Biotechnology for Production of Fuels, Chemicals, and Materials from Biomass. *Appl. Biochem. Biotechnol.* 39–40, 41–59. doi:10.1007/bf02918976
- Ximenes, E., Kim, Y., Mosier, N., Dien, B., and Ladisch, M. (2011). Deactivation of Cellulases by Phenols. *Enzyme Microb. Technology* 48, 54–60. doi:10.1016/j.enzmtec.2010.09.006
- Xu, Y., Fan, L., Wang, X., Yong, Q., and Yu, S.-Y. (2013). Simultaneous Separation and Quantification of Linear Xylo- and Cello-Oligosaccharides Mixtures in Lignocellulosics Processing Products on High-Performance Anion-Exchange Chromatography Coupled with Pulsed Amperometric Detection. *BioResources* 8, 3247–3259. doi:10.15376/biores.8.3.3247-3259
- Yang, H., Li, J., Mo, L., and Xu, J. (2017). Gas-trap Capturing of Enzyme Inhibitors in Explosion Gas from the Pretreatment of Corn Stalk with Dilute-

- Sulfuric Acid Steam. *BioResources* 12, 1136–1149. doi:10.15376/biores.12.1.1136-1149
- Zakaria, M. R., Hirata, S., and Hassan, M. A. (2014). Combined Pretreatment Using Alkaline Hydrothermal and Ball Milling to Enhance Enzymatic Hydrolysis of Oil palm Mesocarp Fiber. *Bioresour. Technology* 169, 236–243. doi:10.1016/j.biortech.2014.06.095
- Zhai, R., Hu, J., and Saddler, J. N. (2018). Understanding the Slowdown of Whole Slurry Hydrolysis of Steam Pretreated Lignocellulosic Woody Biomass Catalyzed by an Up-To-Date Enzyme Cocktail. *Sustainable Energ. Fuels* 2, 1048–1056. doi:10.1039/c7se00569e
- Zhai, R., Hu, J., and Saddler, J. N. (2016). What Are the Major Components in Steam Pretreated Lignocellulosic Biomass that Inhibit the Efficacy of Cellulase Enzyme Mixtures? *ACS Sustainable Chem. Eng.* 4, 3429–3436. doi:10.1021/acssuschemeng.6b00481
- Zhao, X., Zhang, L., and Liu, D. (2012b). Biomass Recalcitrance. Part I: the Chemical Compositions and Physical Structures Affecting the Enzymatic Hydrolysis of Lignocellulose. *Biofuels, Bioprod. Bioref.* 6, 465–482. doi:10.1002/bbb.1331
- Zhao, X., Zhang, L., and Liu, D. (2012a). Biomass Recalcitrance. Part II: Fundamentals of Different Pre-treatments to Increase the Enzymatic Digestibility of Lignocellulose. *Biofuels, Bioprod. Bioref.* 6, 561–579. doi:10.1002/bbb.1350

Conflict of Interest: One of the authors LJ is co-inventor of patents/patent applications in the area biomass processing.

The remaining authors declare that the research was conducted in the absence of any commercial or financial relationships that could be construed as a potential conflict of interest.

Publisher's Note: All claims expressed in this article are solely those of the authors and do not necessarily represent those of their affiliated organizations, or those of the publisher, the editors, and the reviewers. Any product that may be evaluated in this article, or claim that may be made by its manufacturer, is not guaranteed or endorsed by the publisher.

Copyright © 2022 Martín, Dixit, Momayez and Jönsson. This is an open-access article distributed under the terms of the Creative Commons Attribution License (CC BY). The use, distribution or reproduction in other forums is permitted, provided the original author(s) and the copyright owner(s) are credited and that the original publication in this journal is cited, in accordance with accepted academic practice. No use, distribution or reproduction is permitted which does not comply with these terms.



Expression, Purification, and Preliminary Protection Study of Dehydrin PicW1 From the Biomass of *Picea wilsonii*

Junhua Liu¹, Mei Dai¹, Jiangtao Li¹, Yitong Zhang¹, Yangjie Ren¹, Jichen Xu², Wei Gao^{1*} and Sujuan Guo^{3*}

¹Biological Physics Laboratory, College of Science, Beijing Forestry University, Beijing, China, ²National Engineering Laboratory of Tree Breeding, Beijing Forestry University, Beijing, China, ³Key Laboratory of Forest Cultivation and Conservation, Ministry of Education, Beijing Forestry University, Beijing, China

OPEN ACCESS

Edited by:

Caixing Huang,
Nanjing Forestry University, China

Reviewed by:

Chuan-Ling Si,
Tianjin University of Science and
Technology, China
Shaoyang Ji,
Institute of Process Engineering (CAS),
China

*Correspondence:

Wei Gao
w_gao@bjfu.edu.cn
Sujuan Guo
gwangzs@263.net

Specialty section:

This article was submitted to
Bioprocess Engineering,
a section of the journal
Frontiers in Bioengineering and
Biotechnology

Received: 07 February 2022

Accepted: 07 March 2022

Published: 05 April 2022

Citation:

Liu J, Dai M, Li J, Zhang Y, Ren Y, Xu J,
Gao W and Guo S (2022) Expression,
Purification, and Preliminary Protection
Study of Dehydrin PicW1 From the
Biomass of *Picea wilsonii*.
Front. Bioeng. Biotechnol. 10:870672.
doi: 10.3389/fbioe.2022.870672

Dehydrins (DHNs) belong to group II of late embryogenesis-abundant (LEA) proteins, which are up-regulated in most plants during cold, drought, heat, or salinity stress. Despite the importance of dehydrins for the plants to resist abiotic stresses, it is necessary to obtain plant-derived dehydrins from different biomass. Generally, dehydrin PicW1 from *Picea wilsonii* is involved in Kn-type dehydrin with five K-segments, which has a variety of biological activities. In this work, *Picea wilsonii* dehydrin PicW1 was expressed in *Escherichia coli* and purified by chitin-affinity chromatography and size-exclusion chromatography, which showed as a single band by SDS-PAGE. A cold-sensitive enzyme of lactate dehydrogenase (LDH) is used to explore the protective activities of other proteins. Temperature stress assays showed that PicW1 had an effective protective effect on LDH activity, which was better than that of bovine serum albumin (BSA). This study provides insights into the purification and protective activity of K5 DHNs for the advancement of dehydrin structure and function from biomass.

Keywords: dehydrin, expression, purification, lactate dehydrogenase, protective effects

INTRODUCTION

Biomass refers to the organic matter produced by all organisms and growth. Generally, biomass is the abundant renewable resource that can not only be transformed into many high value-added products of chemicals, biofuels, and advanced materials (Dong et al., 2020; Liu et al., 2021; Wang et al., 2021; Xu et al., 2021; Hu et al., 2022) but also contains highly abundant stress-resistant gene resources (Ning et al., 2021). Obtaining proteins from biomass tissues requires extracting genomic DNA and RNA, reverse transcription to obtain cDNA, and then designing specific primers to amplify a specific segment of genomic DNA according to the known similar biomass genes. PCR primers were designed with the recombinant plasmid containing the target gene as the template. The amplified products were recovered and connected to the cloning vector, transformed into *E. coli* and extracted the plasmid, and then the appropriate expression vector was selected. The target protein was successfully obtained through a variety of separation and purification techniques (Zhou et al., 2006). An area of considerable research interest is the plant's ability to resist a variety of abiotic stresses such as drought, cold, high temperature, and high salinity (Hara et al., 2003; Saavedra et al., 2006; Hundertmark and Hinch, 2008; Hirayama and Shinozaki, 2010). All of these result in cell

dehydration (Galau et al., 1986). One family of proteins that is expressed during cell dehydration has been named dehydration proteins (dehydrins, or DHNs) (Close, 1996; Graether and Boddington, 2014). DHNs are highly hydrophilic, and their structural analysis implies that they are intrinsically disordered proteins (IDPs), which provide a flexible property to interact with metal ions and biomolecules (Dunker et al., 2001; Halder et al., 2018; Lv et al., 2018; Gupta et al., 2019). DHNs belong to LEA-DII (late embryogenesis-abundant proteins) family and their types have been classified using the segments K, Y, and S. The K-segment is an approximately 15-amino-acid-long conserved lysine-rich motif, and it tends to adopt an amphipathic α -helix structure according to computational prediction (Lv et al., 2018). The Y-segment is a relatively short segment which is named for the conserved tyrosine residues (Hara et al., 2010). The S-segment is a serine-rich region that can be phosphorylated, and it may play a role in the protein delivery to the nucleus (Goday, 1994). In addition to these segments, Φ -segments (G- and polar amino acid-rich sequences) (Close, 1997), F-segments (Strimbeck, 2017; Wei et al., 2019; Ohkubo et al., 2020), and ChP-segments (Graether and Boddington, 2014) have also been described.

In previous studies, four different proteins from various Spruce species, namely, PicW1, PicW2, PicM, and PicK, were identified and expressed in *E. coli*. It had been proved that PicW genes were an effective antifreeze resource by thermal hysteresis activity and *E. coli* antifreeze tests (Zhao et al., 2017; Zhang et al., 2018). In this study, we report the purification of a protective protein PicW1 from *Picea wilsonii*. PicW1 belongs to the K₅DHN family, because the protein has five highly conservative QKA segments, and each segment contains 2–5 Lys amino acids. PicW1 was cloned from *Picea wilsonii* and expressed in *E. coli*, and the protein was separated and purified by chitin-affinity chromatography and gel filtration chromatography. In addition, the activity of LDH is commonly used as a marker for the ability of dehydrins to rescue protein function during stress. We found that PicW1 can protect the enzyme activity of LDH which is better than BSA (a known protective protein) under freeze-thaw stress. However, in the high-temperature tests, the protective effect of PicW1 is similar to that of BSA and better than the negative control lysozyme (LZM).

MATERIALS AND METHODS

Materials and Instruments

The chitin column (New England Biolabs, United States) and AKTA protein purification system were used for two-step protein purification. An ultrafiltration tube (Amicon ultra, United States) of 10 kDa millipore was used for protein concentration in the purification process. Liquid nitrogen was purchased from the Institute of Semiconductors, Chinese Academy of Sciences. The DU730 ultraviolet spectrophotometer (BECKMAN COULTER, United States) was used to measure the absorbance in the enzyme activity reaction. The protein concentration was measured using NanoDrop 2000c (Thermo Fisher Scientific, United States).

Plasmid and Bacterial Strains

The *Picea wilsonii* dehydrin gene pTWIN1-PicW1 was given by Professor Jichen Xu (National Engineering Laboratory of Tree Breeding, Beijing Forestry University), and the recombinant plasmid, pRSF-Duet-LDH5, was given by Professor Fei Xiao (Peking University Fifth Clinical College of Geriatrics Key Laboratory). Both *E. coli* DH5 α strain and *E. coli* BL21 (DE3) were purchased from TaKaRa Company.

Protein Expression

E. coli BL21 (DE3) competent cells were transformed with the recombinant construct (Figure 1A). Ten milliliters of LB medium pH 7.0 containing ampicillin (100 μ g/ml) were inoculated with a positive BL21 colony and then incubated for 12 h at 37°C with shaking at 220 rpm. One liter fresh LB medium containing ampicillin (100 μ g/ml) was inoculated with the aforementioned cells and grown until the OD_{600 nm} reached 0.6–0.8 absorbance units (mid-log phase). Upon reaching the mid-log phase, protein expression was induced with isopropyl β -D-thiogalactoside (IPTG) at a concentration of 0.5 mM for 20 h at 16°C and 180 rpm. Then, the cells were harvested by centrifugation at 4,000 rpm for 30 min at 4°C. The pellet was saved and the supernatant was discarded.

Protein Separation and Purification

The pellet was collected from 300 ml culture, lysed in 25 ml lysis buffer A containing 20 mM Tris-HCl pH 8.0, 500 mM NaCl, 1 mM EDTA, and 1 mM phenylmethylsulfonylmethyl fluoride (PMSF). The cells were sonicated on ice for 4 s 70–100 times spaced by about 6 s time interval to disrupt cell membranes. Then, the lysates were centrifuged for 30 min at 13,000 rpm at 4°C to separate soluble proteins from other cellular components. The clarified lysate was used for further purification.

Chitin-affinity chromatography was equilibrated with buffer A1 (20 mM Tris-HCl pH 8.0, 500 mM NaCl, and 1 mM EDTA). The clarified lysate (supernatant) was run onto a 3 ml chitin column which was followed by washing with 20-bed volumes of washing buffer B (20 mM Tris-HCl pH 8.0, 500 mM NaCl, 1 mM EDTA, 0.1% Triton-X100) to thoroughly remove non-specific proteins (O'Shea et al., 2015). The column was supplemented with three column volumes of cleavage buffer C (20 mM Tris-HCl pH 8.0, 500 mM NaCl, 1 mM EDTA, and 120 mM DTT) and placed on a rotary mixer. Then, the flow was stopped and the column was placed on a rotary mixer at 4°C for 48 h for the on-column cleavage of PicW1 protein. DTT was added every 6 h. The samples were collected in 6, 12, 18, 24, 30, 36, and 48 h and analyzed by 15% polyacrylamide gel electrophoresis on sodium dodecyl sulfate (SDS-PAGE). When the cutting was completed, the chitin matrix naturally settled through gravity sedimentation. The protein that flowed down was concentrated to within 2 ml in a 10 kDa concentration tube at 4,000 rpm, filtered through a 0.22 ultrafiltration membrane to remove impurities, and then prepared for the next purification operation.

The preliminarily purified protein solution was applied onto a Superdex 200 pg 10/300 GL column which was equilibrated with buffer D (20 mM Tris-HCl pH 8.0, 100 mM NaCl, 5 mM DTT) (O'Shea et al., 2015). Size exclusion was performed at 0.4 ml/min.

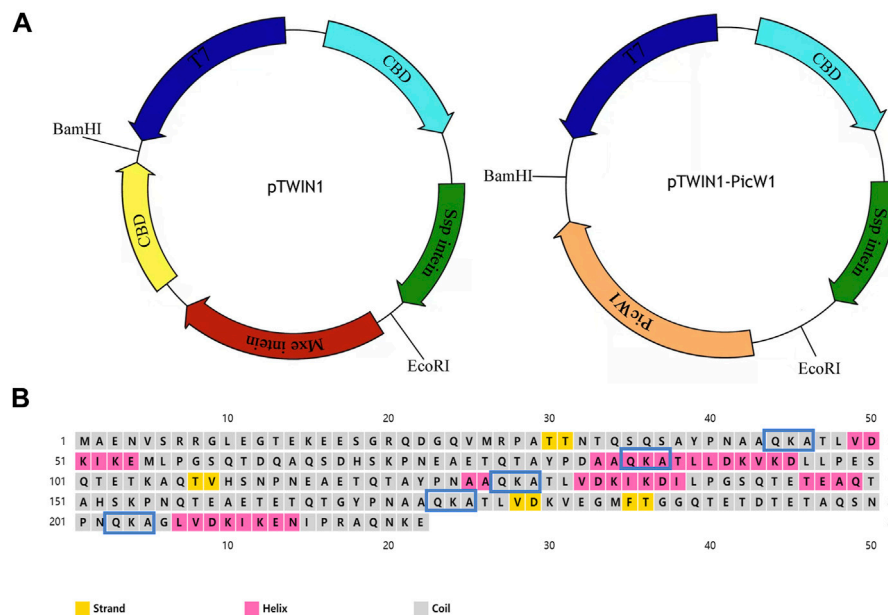


FIGURE 1 | Prokaryotic expression vector pTWIN1 and secondary structures of PicW1. **(A)** CBD, chitin-binding domain; Mxe intein, *Mycobacterium xenopi* GyrA intein; Ssp intein, *Synechocystis* sp. DnaB intein gene; PicW1, the coding region of PicW1 gene; T7, T7promoter. **(B)** PicW1 has 222 amino acids, of which 5 K-segments start from the amino acid sequence QKA. Yellow squares represent the strand, pink squares represent the helix, and gray squares represent the coil.

The peaks of the target proteins were collected and concentrated to 10 mg/ml. The purified proteins were collected and tested through 18% SDS-PAGE. The LDH5 was prepared as previously described (Liu et al., 2017). The purified PicW1 and LDH5 were temporarily stored at 4°C. If long-term storage is required, 50% glycerol can be added to the protein and stored at -80°C.

Lactate Dehydrogenase Protection Assay

The LDH protection assay was carried out in order to determine the protective role of the PicW1 protein. The activity of LDH was measured using the modified technique of Lin and Thomashow (1992). The negative control was LZM and the positive control was bovine serum albumin (BSA). All the proteins and reagents were dissolved in buffer E (10 mM phosphate buffer, pH 7.5). Different protein samples and LDH were mixed at the molar ratio of 0:1, 5:1, 10:1, and 20:1 into a 60 µl solution; the final concentration of LDH was 0.13 µM. The enzyme solution was divided equally into six tubes. For the cryoprotective assay, three tubes were subjected to freeze-thaw stress treatment and the other three tubes were left untreated. Freezing stress was imparted on the enzyme by five cycles of freezing in liquid nitrogen for 1 min and subsequent thawing in a water bath at 25°C for 5 min in the presence and absence of the PicW1 protein.

For the high-temperature stress assay, we set four temperatures which were 43, 49, 55, and 61°C, respectively, and prepared 60 µl enzyme solutions with the molar ratio (5:1) of different protein samples and LDH. The protein mixture solution was equally divided into six tubes; three copies were not processed, and the others were treated in the specific temperature water bath for 2 min, and then it was placed in the 25°C water bath for 5 min renaturation; the process was repeated three times.

Then, 5 µl enzyme solution was added to 2 ml of substrate (10 mM phosphate buffer pH 7.5, 0.1 mM NADH, and 7.5 mM pyruvate). The reduction of A₃₄₀ in the reaction system was determined using a DU730 ultraviolet spectrophotometer within 3 min. The results were expressed as the LDH5 residual enzyme activity (%) relative to the activity prior to treatment. The untreated LDH activity was considered to be 100% at 25°C.

$$\text{LDH}_5 \text{ residual enzyme activity (\%)} = \Delta A_{340b} / \Delta A_{340a} \times 100\%$$

Here, ΔA_{340a} is the difference of A_{340} before the test sample is processed and ΔA_{340b} is the difference of A_{340} after the test sample is processed.

Three independent assays were performed, and SE was included. Values were the mean \pm SD ($n = 3$). Student's *t*-test analysis was performed between each sample of enzyme solution low-temperature protection experiment and 61°C high-temperature stress experiment.

RESULTS AND DISCUSSION

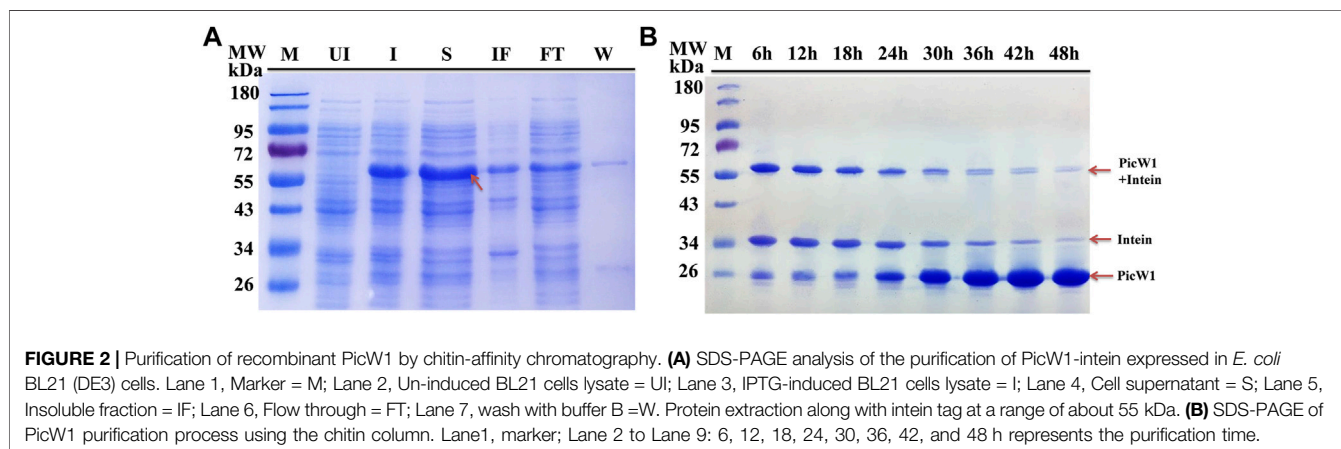
Amino Acid Composition and Segment Characteristics of PicW1

In previous research, the full-length DHN gene PicW1 was isolated from *P. wilsonii* (Liu et al., 2014). Protein sequence analysis shows that PicW1 has a total length of 669 bp and encodes 222 amino acids. It is mainly composed of hydrophilic amino acids without cysteine (C) and tryptophan (W), with a high proportion of charged and polar amino acids and a low proportion of non-polar and hydrophobic residues (Table 1).

TABLE 1 | Protein and amino acid properties analysis.

Pro	Analysis			Amino acids (% by frequency)				
	L	MW	pI	Polar	Charged	Hydrophobic	Basic	Acidic
PicW1	222	24.1	4.9	35.43	29.60	23.77	11.21	15.25

L = length; MW = molecular weight; pI = isoelectric point; polar = NCQSTY; charged = RKHYCDE; hydrophobic = AILFWV; basic = KR; acidic = DE.



According to **Figure 1B**, PicW1 is mainly composed of coil, which is normal for an IDP. DHNs contain at least one K-segment and as many as eleven (Jean-Marie et al., 2008), while PicW1 has five K-segments. Four K-segments are in the helical region predicted by the secondary structure, but only the second K-segment and the fourth K-segment form a relatively complete helical structure. The K-segment could form α -helices under abiotic stress to help stabilize membranes and proteins (Eriksson et al., 2011; Matthew et al., 2015; Mouillon et al., 2008). Some studies showed that the K-segment played a major role in the protection of enzymes at low temperatures, and prevented harmful changes in the secondary and tertiary structure of proteins (Yang et al., 2015). The truncated K-segment experiment showed that ERD10, RcdHN 5, and TaDHN -5 decreased the low-temperature protection of LDH (Peng et al., 2010; Cedeno et al., 2017). In addition, the lipid vesicle binding analysis of the three K-segments deletion derivatives of maize DHN1 proved that the α -helical conformation of the K-segment was essential for the binding of DHN to anionic phospholipid vesicles (Hara et al., 2011). The K-segment of wheat DHN-5 (YSK2) protected *E. coli* exposed to various stresses by preventing protein aggregation (Clarke et al., 2015).

Protein Expression and On-Column Purification by Affinity Chromatography

The constructs used in the study are shown in **Figure 1A**. We selected *E. coli* as the heterologous expression system of Picea dehydrin gene, and the expressed protein can play its protective function (Yin et al., 2007). Some studies have shown that wheat dehydrin DHN-5, *Ammopiptanthus mongolicus* dehydrin

AmCIP, and *Arabidopsis thaliana* dehydrins RAB18, LTI29, LTI30, and COR47 were heterologously expressed in the prokaryotic expression system, and the protein size and activity are correct (Svensson et al., 2000; Brini et al., 2010; Shi et al., 2016). The presence of the expressed protein in the supernatant of lysates from the transformant cells was examined by SDS-PAGE gel electrophoresis. **Figure 2A** indicated that induced cells produced a band with a predicted molecular weight of CBD-intein-PicW1 at around 55 kDa. The recombinant protein mainly existed in the supernatant after cell disruption and a small amount in insoluble components. We purified the PicW1 protein by affinity chromatography via intein-mediated purification using an affinity chitin-binding tag system; a novel protein purification system which utilizes the inducible self-cleavage activity of protein splicing elements (termed inteins) to separate the target protein from the affinity tag. PicW1-intein-CBD can specifically bind to chitin beads. Intein could self-cleave in the presence of the reducing agent DTT, so that the target protein PicW1 and intein-CBD will be separated. Intein-CBD was adsorbed on the chitin beads, and the target protein PicW1 existed in the cutting buffer and was finally eluted by the gravity flow. As shown in **Figure 2B**, most of the target proteins were completely cleaved at 48 h.

PicW1 was further purified using the AKTA protein purification system of the Superdex 200 pg 10/300 GL column, with a major and symmetrical peak at 17 ml. The gel filtration curve of the Superdex 200 preparative column showed that PicW1 was a monomer that matched with the molecular weight value calculated from its primary sequence (**Figure 3A**). The PicW1 components were collected from the AKTA system for crystallization and subsequent functional tests. As shown in

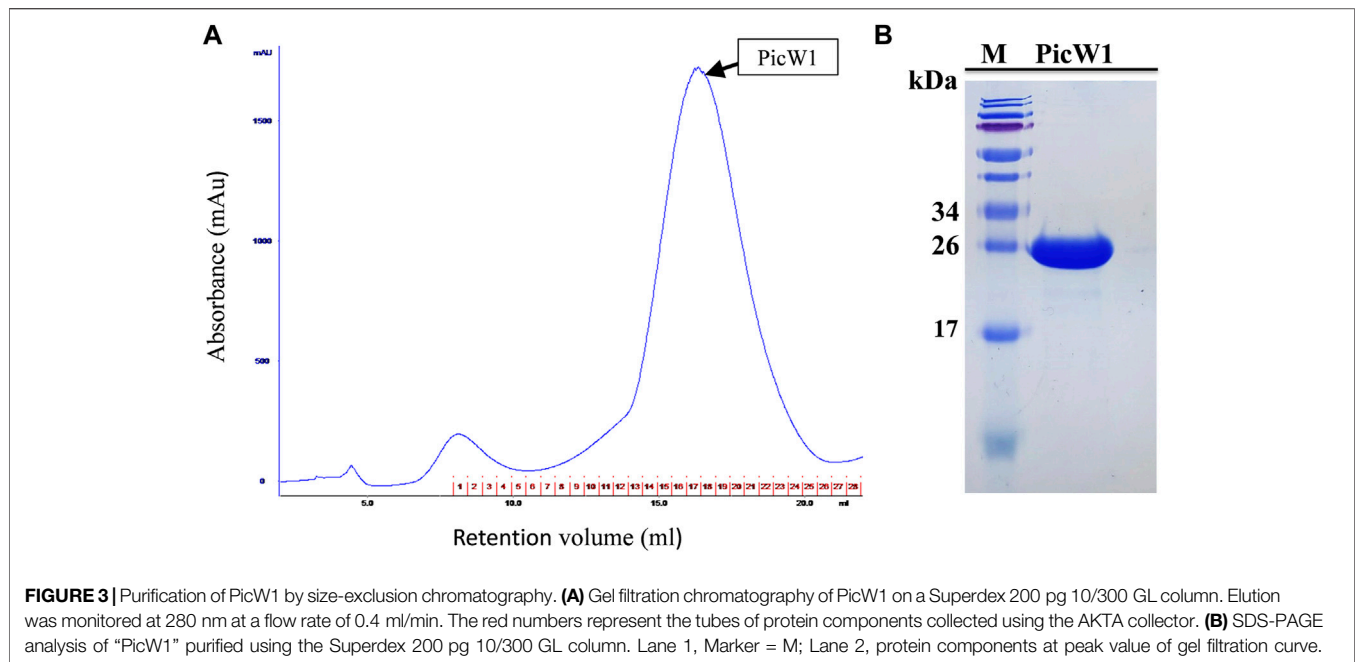


Figure 3B, the target protein at the peak of the curve was identified using 18% SDS-PAGE, with a molecular weight of about 24 kDa. The final yield was ~20 mg PicW1 per liter of culture medium.

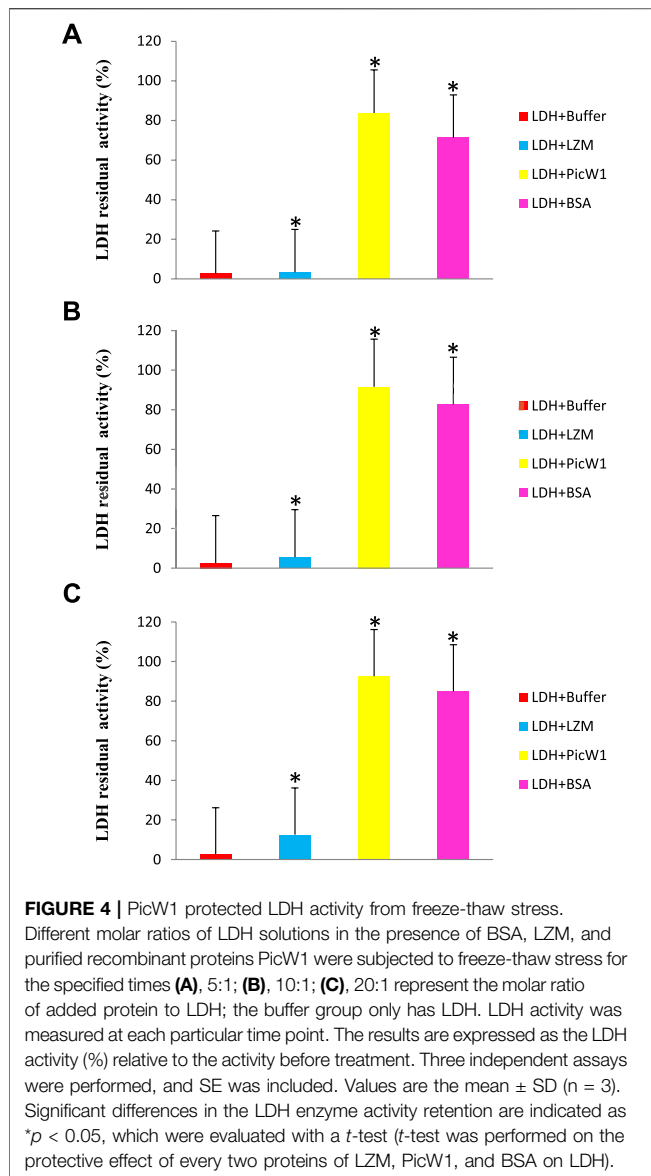
PicW1 Protect the Enzyme Lactate Dehydrogenase Under Freezing Stress and High Temperature

Because LDH loses its activity during freezing and high-temperature stress, we select this enzyme to evaluate the protective effect of PicW1. The activity of LDH before the experiment was considered as 100%. The enzyme LDH lost its activity completely upon repeated 1 min freezing and 5 min thawing at -196°C for five times (**Figure 4A**). In contrast, LDH activity retained to nearly 84% in the presence of $0.65\ \mu\text{M}$ (5:1) PicW1, which was higher than that with BSA (71%; **Figure 4A**). We also found approximately 92% LDH activity was retained when $1.30\ \mu\text{M}$ (10:1) and $2.6\ \mu\text{M}$ (20:1) PicW1 were added, which was higher than that with BSA (84%; **Figure 4B**, **Figure 4C**). The increased concentration of purified PicW1 increased the percentage of LDH activity retained after freeze-thaw assay (**Figure 4**).

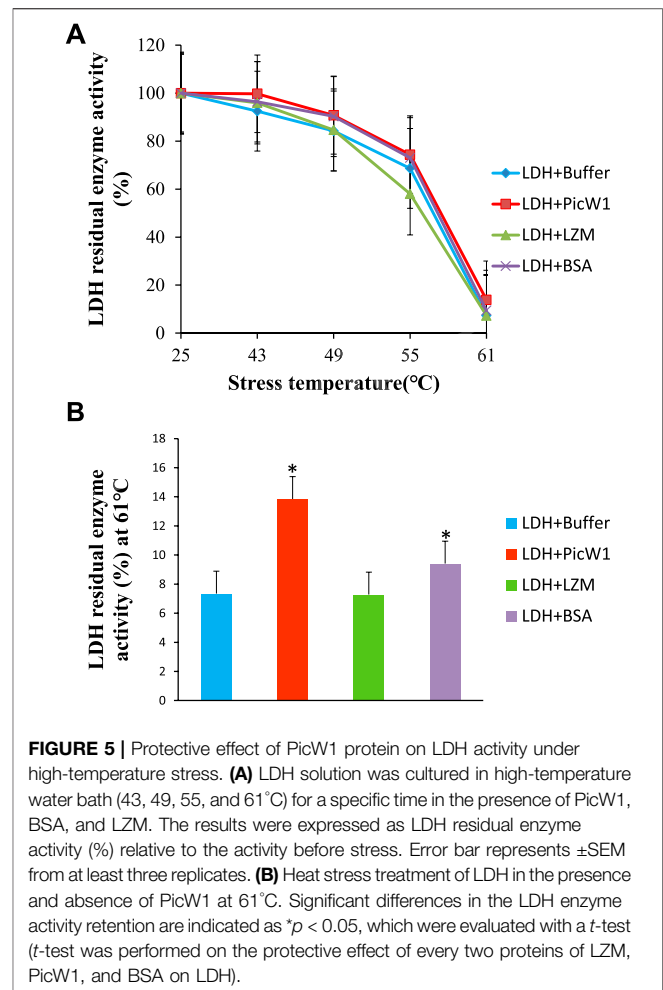
Many cold sensitive enzymes are oligomers, including LDH, β -glucosidase (bglG), and catalase. Low-temperature stress makes subunit denaturation unable to combine correctly, and then irreversibly reduces the enzyme activity (Goyal et al., 2005). Brini et al. showed that wheat DHN-5 increased the activity and thermal stability of fungal bglG and glucose oxidase (GOD/POD) (Brini et al., 2010). However, PicW1 contains five K-segments and is different from the typical K-segment sequence. It has been reported that the deletion of K-segment of wheat dehydrin WZY2 leads to the reduction of low-

temperature protection, indicating that these segments are involved in low-temperature protection (Yang et al., 2015). It is speculated that the hydrophobic side of picw1 may interact with the lipid components of the biofilm or combine with the hydrophobic region of the denatured part of the protein to form a protective layer to prevent the denatured macromolecular substances from further denaturation and polymerization (Rahman et al., 2010). Cor15 may form a random curl in the low-temperature protection experiment, which means that except for the K-segment, the irregular curl improves the structural flexibility and may play an important role in the low-temperature protection of cold-sensitive enzymes (Ingram and Bartels, 1996). Picw1 protein contains a large number of irregular curls, which may play a positive role in freeze-thaw stress. In conclusion, PicW1 has cryoprotective activity on LDH and has a more significant protective effect than BSA (a known protective protein) from the deleterious effects of freeze-thaw treatment. These findings serve to not only further define the molecular characteristics and possible functions of PicW1, but also add to the pool of evidence that supports a role for DHN proteins in cold tolerance.

The effect of PicW1 in protecting LDH activity during high-temperature stress was also evaluated. Similarly, BSA was selected as a positive control, and LZM was used as a negative control. As shown in **Figure 5A**, the enzyme activity of LDH decreased with the increase of stress treatment temperature. The LDH enzyme activity in the presence of PicW1 was higher than that in the LZM experimental group and blank control group at each temperature, but it was only slightly better than that in the BSA group at 43 – 55°C . The LDH enzyme almost completely lost its activity after three heat stress cycles at 61°C , only 7%. A minimum concentration of $0.65\ \mu\text{M}$ PicW1 was found to be

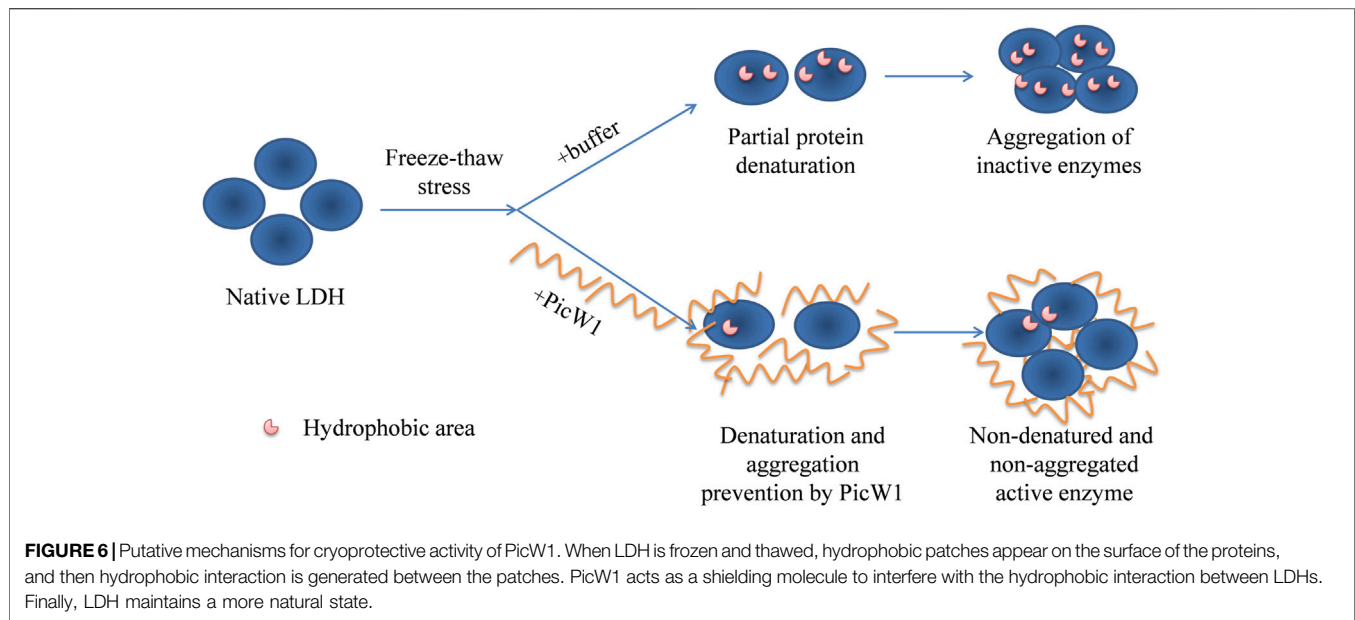


sufficient to retain 14% of the enzymatic activity under high-temperature stress (61°C) than the 9% of 0.65 μ M BSA. The student t -test of 61°C data (Figure 5B) showed that the protective effect of PicW1 on LDH was better than that of other experimental groups, including the BSA group. The cryoprotection of dehydrin on LDH has been widely studied. The dehydrated protein is more effective than small molecules (such as sucrose) or other proteins (such as BSA) in protecting LDH activity from freeze-thaw damage (Hughes and Graether, 2011). The protective effect of BSA is generally considered as non-specific ones of high protein concentrations (Abriata et al., 2016; Huang et al., 2022). Although the protective effect of dehydrins on other proteins is mainly observed at low temperature, there are relatively few studies on high-temperature stress. Previously, LEA protein COR15 could protect the activity of LDH, but the temperature study was limited to 43°C (Nakayama et al., 2008). In addition,



DHN-5 could significantly improve the activity and thermal stability of bglG at 50 and 70°C (Brini et al., 2010). Here, we propose a heat stress assay at 43–61°C, which shows that PicW1 can effectively protect LDH under high-temperature treatment up to 61°C.

Dehydrin interacts with the lipid components of biofilm or combines with the hydrophobic region of protein denatured part to form a protective layer, prevent the further denaturation and polymerization of denatured macromolecules, and help plants stabilize cell membrane and proteins under stress. Immunolocalization studies showed that dehydrin accumulated more in the plasma membrane or areas rich in the membrane structure, around lipids and proteins. For example, the dehydrin lti29 gene was overexpressed in Arabidopsis. During cold acclimation, the LTI29 of transgenic plants was transferred from cytoplasm to near membrane, and the survival rate of plants under freezing stress was improved (Puhakainen et al., 2004). DHN can act as a partner for other proteins to help them fold correctly and prevent them from aggregating under heat or cold stress (Hara et al., 2001). However, the chaperone activity of traditional proteins can also form specific complexes with target proteins through the interaction of hydrophobic plaques (Ellis, 2004). Therefore, DHN is more like a barrier between molecules,



preventing the aggregation of denatured proteins. We have compared the activity of the PicW1 protein with another known protectant like BSA. The results showed that PicW1 protein could protect the LDH activity better than BSA under freeze-thaw stress. In addition, the higher the concentration of PicW1, the greater the protective effect on LDH. It may be imagined that PicW1 is like a “wall” that prevents the denaturation and aggregation of LDH. The more the “walls”, the more LDH activity is retained (**Figure 6**).

SUMMARY

Among the group of LEA proteins, dehydrins play a major role in protection during abiotic stress. DHNs are known as stress-responsive proteins that are up-regulated in plants during stress such as drought, cold, and salinity (Hara et al., 2005). In this work, we have highly expressed cold acclimation protein PicW1 from *Picea wilsonii* in *E. coli*. We also proved that PicW1 has superior low-temperature protection on LDH. These approaches should be applicable to other plant dehydrins. The success in PicW1 expression and purification will facilitate future structural studies to understand how it works in stress resistance. In the future, we will explore the mechanism of PicW1 in depth.

REFERENCES

- Abriata, L. A., Spiga, E., and Peraro, M. D. (2016). Molecular Effects of Concentrated Solutes on Protein Hydration, Dynamics, and Electrostatics. *Biophysical J.* 111 (4), 743–755. doi:10.1016/j.bpj.2016.07.011
- Brini, F., Saibi, W., Amara, I., Gargouri, A., Masmoudi, K., and Hanin, M. (2010). Wheat Dehydrin DHN-5 Exerts a Heat-Protective Effect on β -Glucosidase and

DATA AVAILABILITY STATEMENT

The original contributions presented in the study are included in the article/Supplementary Material; further inquiries can be directed to the corresponding authors.

AUTHOR CONTRIBUTIONS

JuL performed the experiment of dehydrin protein expression and purification and the experiment of enzyme activity protection under temperature stress, and wrote the manuscript. MD did the expression and purification of LDH protein. JiL, YZ, and YR carried out image processing. JX provides the dehydrin gene. WG and SG proposed this idea and revised the manuscript.

FUNDING

We greatly acknowledge the National Key R&D Program of China (2019YFD1001604); the Fundamental Research Funds for the Central Universities (grant number 2018ZY18); and the National Natural Science Foundation of China (grant number 31070651).

- Glucose Oxidase Activities. *Biosci. Biotechnol. Biochem.* 74 (5), 1050–1054. doi:10.1271/bbb.90949
- Cedeño, C., Žerko, S., Tompa, P., and Koźmiński, W. (2017). ^1H , ^{15}N , ^{13}C Resonance Assignment of Plant Dehydrin Early Response to Dehydration 10 (ERD10). *Biomol. NMR Assign* 11 (2), 127–131. doi:10.1007/s12104-017-9732-0
- Clarke, M. W., Boddington, K. F., Warnica, J. M., Atkinson, J., McKenna, S., Madge, J., et al. (2015). Structural and Functional Insights into the

- Cryoprotection of Membranes by the Intrinsically Disordered Dehydrins. *J. Biol. Chem.* 290 (45), 26900–26913. doi:10.1074/jbc.M115.678219
- Close, T. J. (1997). Dehydrins: A Commonality in the Response of Plants to Dehydration and Low Temperature. *Physiol. Plant* 100 (2), 291–296. doi:10.1111/j.1399-3054.1997.tb04785.x
- Close, T. J. (1996). Dehydrins: Emergence of a Biochemical Role of a Family of Plant Dehydration Proteins. *Physiol. Plant* 97 (4), 795–803. doi:10.1111/j.1399-3054.1996.tb00546.x
- Dong, H., Zheng, L., Yu, P., Jiang, Q., Wu, Y., Huang, C., et al. (2020). Characterization and Application of Lignin-Carbohydrate Complexes from Lignocellulosic Materials as Antioxidants for Scavenging *In Vitro* and *In Vivo* Reactive Oxygen Species. *ACS Sust. Chem. Eng.* 8 (1), 256–266. doi:10.1021/acsschemeng.9b05290
- Dunker, A. K., Lawson, J. D., Brown, C. J., Williams, R. M., Romero, P., Oh, J. S., et al. (2001). Intrinsically Disordered Protein. *J. Mol. Graphics Model.* 19 (1), 26–59. doi:10.1016/s1093-3263(00)00138-8
- Eriksson, S. K., Kutzer, M., Procek, J., Gröbner, G., and Harryson, P. (2011). Tunable Membrane Binding of the Intrinsically Disordered Dehydrin Lti30, a Cold-Induced Plant Stress Protein. *Plant Cell* 23, 2391–2404. doi:10.1105/tpc.111.085183
- Galau, G. A., Hughes, D. W., and Dure, L., 3rd (1986). Absciscic Acid Induction of Cloned Cotton Late Embryogenesis-Abundant (Lea) mRNAs. *Plant Mol. Biol.* 7 (3), 155–170. doi:10.1007/bf00021327
- Goday, A., Jensen, A. B., Culiñez-Macià, F. A., Mar Albà, M., Figueras, M., Serratos, J., et al. (1994). The maize Absciscic Acid-Responsive Protein Rab17 Is Located in the Nucleus and Interacts with Nuclear Localization Signals. *Plant Cell* 6, 351–360. doi:10.1105/tpc.6.3.351
- Goyal, K., Walton, L. J., and Tunnaclyffe, A. (2005). LEA Proteins Prevent Protein Aggregation Due to Water Stress. *Biochem. J.* 388 (Pt 1), 151–157. doi:10.1042/BJ20041931
- Graether, S. P., and Boddington, K. F. (2014). Disorder and Function: A Review of the Dehydrin Protein Family. *Front. Plant Sci.* 5, 576. doi:10.3389/fpls.2014.00576
- Gupta, A., Marzinek, J. K., Jefferies, D., Bond, P. J., Harryson, P., and Wohland, T. (2019). The Disordered Plant Dehydrin Lti30 Protects the Membrane during Water-Related Stress by Cross-Linking Lipids. *J. Biol. Chem.* 294 (29416), 6468–6482. doi:10.1074/jbc.RA118.007163
- Halder, T., Upadhyaya, G., Basak, C., Das, A., Chakraborty, C., and Ray, S. (2018). Dehydrins Impart Protection against Oxidative Stress in Transgenic Tobacco Plants. *Front. Plant Sci.* 9 (9), 136. doi:10.3389/fpls.2018.00136
- Hara, M., Shinoda, Y., Tanaka, Y., and Kuboi, T. (2010). DNA Binding of Citrus Dehydrin Promoted by Zinc Ion. *Plant Cell Environ.* 32 (5), 532–541. doi:10.1111/j.1365-3040.2009.01947.x
- Hara, M., Fujinaga, M., and Kuboi, T. (2005). Metal Binding by Citrus Dehydrin with Histidine-Rich Domains. *J. Exp. Bot.* 56 (420), 2695–2703. doi:10.1093/jxb/eri262
- Hara, M., Shinoda, Y., Kubo, M., Kashima, D., Takahashi, I., Kato, T., et al. (2011). Biochemical Characterization of the Arabidopsis KS-type Dehydrin Protein, Whose Gene Expression Is Constitutively Abundant rather Than Stress Dependent. *Acta Physiol. Plant* 33 (6), 2103–2116. doi:10.1007/s11738-011-0749-1
- Hara, M., Terashima, S., Fukaya, T., and Kuboi, T. (2003). Enhancement of Cold Tolerance and Inhibition of Lipid Peroxidation by Citrus Dehydrin in Transgenic Tobacco. *Planta* 217 (2), 290–298. doi:10.1007/s00425-003-0986-7
- Hara, M., Terashima, S., and Kuboi, T. (2001). Characterization and Cryoprotective Activity of Cold-Responsive Dehydrin from Citrus Unshiu. *J. Plant Physiol.* 158 (10), 1333–1339. doi:10.1078/0176-1617-00600
- Hirayama, T., and Shinozaki, K. (2010). Research on Plant Abiotic Stress Responses in the post-genome Era: Past, Present and Future. *Plant J.* 61 (6), 1041–1052. doi:10.1111/j.1365-3113.2010.04124.x
- Hu, Y., Yan, B., Stephen Chen, Z., Wang, L., and Tang and Caixing Huang, W. (2022). Recent Technologies for the Extraction and Separation of Polyphenols in Different Plants: A Review. *J. Renew. Mater.* 10 (6), 1471–1490. doi:10.32604/jrm.2022.018811
- Huang, C., Jiang, X., Shen, X., Hu, J., Tang, W., Wu, X., et al. (2022). Lignin-enzyme Interaction: A Roadblock for Efficient Enzymatic Hydrolysis of Lignocellulosics. *Renew. Sust. Energ. Rev.* 154, 111822. doi:10.1016/j.rser.2021.111822
- Hughes, S., and Graether, S. P. (2011). Cryoprotective Mechanism of a Small Intrinsically Disordered Dehydrin Protein. *Protein Sci.* 20 (1), 42–50. doi:10.1002/pro.534
- Hundertmark, M., and Hinch, D. K. (2008). LEA (Late Embryogenesis Abundant) Proteins and Their Encoding Genes in *Arabidopsis thaliana*. *Bmc Genomics* 9 (1), 118. doi:10.1186/1471-2164-9-118
- Ingram, J., and Bartels, D. (1996). The Molecular Basis of Dehydration Tolerance in Plants. *Annu. Rev. Plant Physiol. Plant Mol. Biol.* 47 (1), 377–403. doi:10.1146/annurev.arplant.47.1.377
- John Ellis, R. (2004). From Chloroplasts to Chaperones: How One Thing Led to Another. *Photosynth Res.* 80 (1–3), 333–343. doi:10.1023/B:PRES.0000030439.62331.d0
- Lin, C., and Thomashow, M. F. (1992). A Cold-Regulated Arabidopsis Gene Encodes A Polypeptide Having Potent Cryoprotective Activity. *Biochem. Biophysical Res. Commun.* 183 (3), 1103–1108. doi:10.1016/s0006-291x(05)80304-3
- Liu, C., Wang, Y., Wei, H., Meng, W., Zhang, E., and Jian, G. (2017). Expression and Purification of Recombinant Human LDH5 in *Escherichia coli*. *Biotechnology* 27 (2), 174–179.
- Liu, H., Du, H., Zheng, T., Liu, K., Ji, X., Xu, T., et al. (2021). Cellulose Based Composite Foams and Aerogels for Advanced Energy Storage Devices. *Chem. Eng. J.* 426, 130817. doi:10.1016/j.cej.2021.130817
- Liu, J., Xu, X., Xu, Q., Wang, S., and Xu, J. (2014). Transgenic Tobacco Plants Expressing PicW Gene from *Picea wilsonii* Exhibit Enhanced Freezing Tolerance. *Plant Cell Tissue Organ. Cult.* 118 (3), 391–400. doi:10.1007/s11240-014-0491-7
- Lv, A., Su, L., Liu, X., Xing, Q., Huang, B., An, Y., et al. (2018). Characterization of Dehydrin Protein, CdDHN4-L and CdDHN4-S, and Their Differential Protective Roles against Abiotic Stress *In Vitro*. *BMC Plant Biol.* 18 (18), 299. doi:10.1186/s12870-018-1511-2
- Matthew, W., Clarkeand Kelly, F. (2015). Structural and Functional Insights into the Cryoprotection of Membranes by the Intrinsically Disordered Dehydrins. *The Journal of biological chemistry* 290 (45), 26900–26913.
- Mouillon, J.-M., Eriksson, S. K., and Harryson, P. (2008). Mimicking the Plant Cell Interior under Water Stress by Macromolecular Crowding: Disordered Dehydrin Proteins Are Highly Resistant to Structural Collapse. *Plant Physiol.* 148 (4), 1925–1937. doi:10.1104/pp.108.124099
- Nakayama, K., Okawa, K., Kakizaki, T., and Inaba, T. (2008). Evaluation of the Protective Activities of a Late Embryogenesis Abundant (LEA) Related Protein, Cor15am, during Various Stresses *In Vitro*. *Biosci. Biotechnol. Biochem.* 72 (6), 1642–1645. doi:10.1271/bbb.80214
- Ning, P., Yang, G., Hu, L., Sun, J., Shi, L., Zhou, Y., et al. (2021). Recent Advances in the Valorization of Plant Biomass. *Biotechnol. Biofuels* 14 (1), 102. doi:10.1186/s13068-021-01949-3
- O'Shea, C., Kryger, M., Stender, E. G., Kragelund, B. B., Willemoes, M., and Skriver, K. (2015). Protein Intrinsic Disorder in Arabidopsis NAC Transcription Factors: Transcriptional Activation by ANAC013 and ANAC046 and Their Interactions with RCD1. *Biochem. J.* 465 (465), 281–294. doi:10.1042/BJ20141045
- Ohkubo, T., Kameyama, A., Kamiya, K., Kondo, M., and Hara, M. (2020). F-segments of Arabidopsis Dehydrins Show Cryoprotective Activities for Lactate Dehydrogenase Depending on the Hydrophobic Residues. *Phytochemistry* 173, 112300. doi:10.1016/j.phytochem.2020.112300
- Peng, Y., Reyes, J. L., Wei, H., Yang, Y., Karlson, D., Covarrubias, A. A., et al. (2010). RcDhn5, a Cold Acclimation-Responsive Dehydrin from *Rhododendron Catawbiense* Rescues Enzyme Activity from Dehydration Effects *In Vitro* and Enhances Freezing Tolerance in RcDhn5-Overexpressing Arabidopsis Plants. *Physiol. Plant* 134, 583–597. doi:10.1111/j.1399-3054.2008.01164.x
- Puhakainen, T., Hess, M. W., Mäkelä, P., Svensson, J., Heino, P., and Palva, E. T. (2004). Overexpression of Multiple Dehydrin Genes Enhances Tolerance to Freezing Stress in Arabidopsis. *Plant Mol. Biol.* 54 (5), 743–753. doi:10.1023/b:plan.0000040903.66496.a4
- Rahman, L. N., Chen, L., Nazim, S., Bamm, V. V., Yaish, M. W., Moffatt, B. A., et al. (2010). Interactions of Intrinsically Disordered Thellungiella Salsuginea Dehydrins TsDHN-1 and TsDHN-2 with Membranes - Synergistic Effects of Lipid Composition and Temperature on Secondary Structure. *Biochem. Cel Biol.* 88 (5), 791–807. doi:10.1139/o10-026

- Richard Strimbeck, G. (2017). Hiding in plain Sight: the F Segment and Other Conserved Features of Seed Plant SKn Dehydrins. *Planta* 245 (5), 1061–1066. doi:10.1007/s00425-017-2679-7
- Saavedra, L., Svensson, J., Carballo, V., Izmendi, D., Welin, B., and Vidal, S. (2006). A Dehydrin Gene in *Physcomitrella Patensis* Required for Salt and Osmotic Stress Tolerance. *Plant J.* 45 (2), 237–249. doi:10.1111/j.1365-3113x.2005.02603.x
- Shi, J., Liu, M., Chen, Y., Wang, J., and Lu, C. (2016). Heterologous Expression of the Dehydrin-like Protein Gene AmCIP from *Ammopiptanthus Mongolicus* Enhances Viability of *Escherichia coli* and Tobacco under Cold Stress. *Plant Growth Regul.* 79 (1), 71–80. doi:10.1007/s10725-015-0112-4
- Svensson, J., Palva, E. T., and Welin, B. (2000). Purification of Recombinant *Arabidopsis thaliana* Dehydrins by Metal Ion Affinity Chromatography. *Protein Expr. Purif.* 20 (2), 169–178. doi:10.1006/prep.2000.1297
- Wang, X., Tang, S., Chai, S., Wang, P., Qin, J., Pei, W., et al. (2021). Preparing Printable Bacterial Cellulose Based Gelatin Gel to Promote *In Vivo* Bone Regeneration. *Carbohydr. Polym.* 270 (11), 118342. doi:10.1016/j.carbpol.2021.118342
- Wei, H., Yang, Y., Himmel, M. E., Tucker, M. P., Ding, S.-Y., Yang, S., et al. (2019). Identification and Characterization of Five Cold Stress-Related Rhododendron Dehydrin Genes: Spotlight on a FSK-type Dehydrin with Multiple F-Segments. *Front. Bioeng. Biotechnol.* 7, 30. doi:10.3389/fbioe.2019.00030
- Xu, T., Du, H., Liu, H., Liu, W., Zhang, X., Si, C., et al. (2021). Advanced Nanocellulose-Based Composites for Flexible Functional Energy Storage Devices. *Adv. Mater.* 33 (48), 2101368. doi:10.1002/adma.202101368
- Yang, W., Zhang, L., Lv, H., Li, H., Zhang, Y., Xu, Y., et al. (2015). The K-Segments of Wheat Dehydrin WZY2 Are Essential for its Protective Functions under Temperature Stress. *Front. Plant Sci.* 6, 406. doi:10.3389/fpls.2015.00406
- Yin, J., Li, G., Ren, X., and Herrler, G. (2007). Select what You Need: a Comparative Evaluation of the Advantages and Limitations of Frequently Used Expression Systems for Foreign Genes. *J. Biotechnol.* 127 (3), 335–347. doi:10.1016/j.jbiotec.2006.07.012
- Zhang, B., Guo, G., Lu, F., Song, Y., Liu, Y., Xu, J., et al. (2018). PicW2 from *Picea wilsonii*: Preparation, Purification, Crystallization and X-ray Diffraction Analysis. *Acta Crystallogr. F Struct. Biol. Commun.* 74 (Pt 6), 363–366. doi:10.1107/S2053230X18007537
- Zhao, Q. H., Liu, J., Xu, X., Xu, Q., Gao, W., Xu, J. C., et al. (2017). PicW Orthologs from spruce with Differential Freezing Tolerance Expressed in *Escherichia coli*. *Int. J. Biol. Macromolecules* 101, 595–602.
- Zou, C. J., Zhang, C., Ma, Y. L., and Xu, W. D. (2006). Comparison of Different Methods for Extraction of Gross DNA of Three Ecotype *Picea mongolia*. *J. Inn Mon Sci. Tech.* 32 (3), 35–38.

Conflict of Interest: The authors declare that the research was conducted in the absence of any commercial or financial relationships that could be construed as a potential conflict of interest.

Publisher's Note: All claims expressed in this article are solely those of the authors and do not necessarily represent those of their affiliated organizations, or those of the publisher, the editors, and the reviewers. Any product that may be evaluated in this article, or claim that may be made by its manufacturer, is not guaranteed or endorsed by the publisher.

Copyright © 2022 Liu, Dai, Li, Zhang, Ren, Xu, Gao and Guo. This is an open-access article distributed under the terms of the Creative Commons Attribution License (CC BY). The use, distribution or reproduction in other forums is permitted, provided the original author(s) and the copyright owner(s) are credited and that the original publication in this journal is cited, in accordance with accepted academic practice. No use, distribution or reproduction is permitted which does not comply with these terms.



Multifunctional Cellulose and Cellulose-Based (Nano) Composite Adsorbents

Ru-Jie Shi^{1*}, Tian Wang¹, Jia-Qi Lang¹, Nong Zhou¹ and Ming-Guo Ma^{1,2*}

¹Chongqing Engineering Laboratory of Green Planting and Deep Processing of Famous-Region Drug in the Three Gorges Reservoir Region, College of Biology and Food Engineering, Chongqing Three Gorges University, Chongqing, China,

²Engineering Research Center of Forestry Biomass Materials and Bioenergy, Beijing Key Laboratory of Lignocellulosic Chemistry, Research Center of Biomass Clean Utilization, College of Materials Science and Technology, Beijing Forestry University, Beijing, China

OPEN ACCESS

Edited by:

Caixing Huang,
Nanjing Forestry University,
China

Reviewed by:

Jiefang Zhu,
Uppsala University, Sweden
Baoliang Xue,
Shaanxi University of Technology,
China

*Correspondence:

Ru-Jie Shi
20050020@sanxiao.edu.cn
Ming-Guo Ma
mg_ma@bjfu.edu.cn

Specialty section:

This article was submitted to
Bioprocess Engineering,
a section of the journal
Frontiers in Bioengineering and
Biotechnology

Received: 07 March 2022

Accepted: 21 March 2022

Published: 14 April 2022

Citation:

Shi R-J, Wang T, Lang J-Q, Zhou N
and Ma M-G (2022) Multifunctional
Cellulose and Cellulose-Based (Nano)
Composite Adsorbents.
Front. Bioeng. Biotechnol. 10:891034.
doi: 10.3389/fbioe.2022.891034

In recent years, faced with the improvement of environmental quality problems, cellulose and cellulose-based (nano) composites have attracted great attention as adsorbents. In this review article, we first report the recent progress of modification and functionalization of cellulose adsorbents. In addition, the adsorbents produced by the modification and functionalization of carboxymethyl cellulose are also introduced. Moreover, the cellulose-based (nano) composites as adsorbents are reviewed in detail. Finally, the development prospect of cellulose and cellulose-based (nano) composites is studied in the field of the environment. In this review article, a critical comment is given based on our knowledge. It is believed that these biomass adsorbents will play an increasingly important role in the field of the environment.

Keywords: adsorbents, cellulose, (nano) composites, heavy metals ions, organic pollutants

INTRODUCTION

In recent years, many environmental problems have attracted more and more attention because they are related to human survival and development (Jarup and Akesson, 2009). Heavy metals ions and organic pollutants play an important role in human health, disturbing the normal growth of plants and damaging the ecological balance (Heppner et al., 2009). Some heavy metals ions and organic pollutants are teratogenic, mutagenic, and carcinogenic substances. There is no doubt that heavy metals ions and organic pollutants accumulate in the environment and biological energy is enriched through the food chain. Therefore, it is very important to remove these pollutants using adsorbents from wastewater (Chen et al., 2015).

It is believed that lignocellulose is an important renewable biomass, consisting of cellulose, hemicelluloses, and lignin, which is used as feedstock to fabricate bio-based fuels, chemicals, and materials (Menon and Rao, 2012; Huang et al., 2018; Dong H. et al., 2020; Huang et al., 2021b). Cellulose is a polysaccharide composed of glucose molecules and the most abundant renewable biomass in the world. Cellulose is the main component of the plant cell wall. It is expected that the conversion of bio-ethanol from cellulose will be a clean energy technology, replacing the traditional grain ethanol technology to meet global energy demand (Asgher et al., 2013). However, it is still difficult to achieve large-scale industrialization due to the pretreatment of raw materials and the high cost of cellulose (Mansfield et al., 1999). Therefore, bio-based chemicals and materials produced from cellulose are expected to be beneficial to the application of cellulose (Nzediegwu and Dumont, 2021). It is believed that bio-based materials produced from cellulose have become the main research focus

of academia (Klemm et al., 2005; Li et al., 2011; Liu et al., 2017; Cao et al., 2018). In addition, carboxymethyl cellulose is an organic substance, a carboxymethylated derivative of cellulose, which is easy to disperse in water to form a transparent colloidal solution.

It is well known that adsorption is considered to be an economic route to remove heavy metals ions and organic pollutants from wastewater (Yagub et al., 2014). In addition, the adsorbent could be reused through an appropriate desorption and regeneration process. Activated carbon adsorbents are widely used to remove heavy metal pollutants due to their large pore volume and high surface area (Mohan and Pittman, 2006; Liu et al., 2018; Liu et al., 2019). To date, hundreds of adsorbents have been reported in the literature (Babel and Kurniawan, 2003; Crini, 2006). The cellulose and cellulose-based (nano) composites have different compositions, structures, and properties, compared with activated carbon adsorbent. It is believed that bio-sorption of agricultural wastes, by-products, and natural substances is a promising and emerging adsorbent method for the treatment of heavy metals ions and organic pollutants due to its high efficiency and wide sources (Volesky and Holan, 1995; O'Connell et al., 2008).

Herein, this review article introduces the application of cellulose and cellulose-based (nano) composites in the removal of heavy metals ions and organic pollutants from wastewater. The adsorbents produced by modification and functionalization of cellulose, carboxymethyl cellulose, and cellulose-based (nano) composites are reviewed. In addition, the adsorption mechanism is briefly discussed. Finally, we try to put forward the possible future development of cellulose and cellulose-based materials in the field of the environment.

ADSORBENTS PRODUCED BY MODIFICATION AND FUNCTIONALIZATION OF CELLULOSE

Heavy metals ions and organic pollutants are the main factors causing wastewater pollution. The modification and functionalization of cellulose are usually utilized to create adsorbents to remove heavy metals ions. In early 2001, Liu's group did pioneering work (Liu et al., 2001). They developed spherical cellulose as an adsorbent to remove and recover Cr^{3+} with a recovery rate of approximately 85.2%, following the predominant complex adsorption mechanism. It is reported that the adsorption of Cr^{3+} ions by an adsorbent depends on time, concentration, pH, and temperature. Then, Xu et al. (2002) also reported the removal of Cd^{2+} by immobilized cellulose-binding domains synthetic phytochelatin bio-adsorbents at the level of per million. Shukla and Pai (2005) assessed the cellulose-containing biomass for Pb^{2+} removal. The results showed the maximum cation uptake value of $0.127 \text{ mmol g}^{-1}$ for coir, $0.087 \text{ mmol g}^{-1}$ for sawdust, $0.090 \text{ mmol g}^{-1}$ for jute, and $0.106 \text{ mmol g}^{-1}$ for groundnut shell. Acrylonitrile-grafted cyanoethyl cellulose was also formed from cyanoethyl cellulose by the ionic-xanthate method to graft the acrylonitrile (Kamel et al., 2006). Undoubtedly, these early works showed that the

modification and functionalization of cellulose is a promising bio-adsorbent method to remove heavy metals ions. After that, more and more research groups have paid more attention to the synthesis, properties, and application potential of bio-adsorbents.

O'Connell et al. (2006b) produced a regenerated cellulose adsorbent. It was found that glycidyl methacrylate-modified cellulose could remove 72 mg g^{-1} of Pb^{2+} ions from aqueous solution at 23°C . In addition, the adsorbent was also applied to remove Ni^{2+} ions from an aqueous solution with approximately 48 mg g^{-1} removed (O'Connell et al., 2006a). It should be pointed out, however, that there are still some debates about the function of cellulose. Garcia-Reyes and Rangel-Mendez (2009) demonstrated that hemicellulose and lignin were the main contributors for the removal of Cr^{3+} in aqueous solution, while cellulose did not seem to be involved. Recently, a microcrystalline cellulose (MCC) adsorbent was used to remove Pb^{2+} ions from aqueous solution with 1,2,3,4-butanetetracarboxylic acid (Hashem et al., 2020). According to the Langmuir theory, the maximum adsorption capacity was $1,155 \text{ mg g}^{-1}$ at pH 5 and 30°C . The pseudo-second order kinetic model indicated the chemisorption in the adsorption process due to the high density of active sites. It observed the endothermic and nonspontaneous adsorption of Pb^{2+} ions by MCC.

Cadmium, a typical heavy metal, has the characteristics of high fat solubility, bioaccumulation, and toxicity, contributing to wastewater pollution. Belhaffaoui and co-workers chemically modified cellulose with succinic anhydride in toluene to obtain succinylated cellulose (Belhaffaoui et al., 2009). Sodium succinylated cellulose displayed high sorption efficiency and high selectivity to remove Cd^{2+} with a maximum uptake of 185.2 mg g^{-1} for distilled water and 178.6 mg g^{-1} for spiked groundwater solutions. It suggested that active functional groups played a major role in metal sorption. It followed an ion-exchange mechanism in the removal process. We would like to point out that this work provided a very valuable example for the research of adsorption mechanisms. In Lu's work, the different adsorption capacities from Langmuir-Freundlich were carried out using lawn grass modified by citric acid as an adsorbent to remove Cd^{2+} from aqueous solution (Lu et al., 2010).

In the literature, the modification and functionalization of cellulose were also applied to absorb toxic and radioactive elements such as Hg^{2+} , UO_2^{2+} , Th^{4+} , and arsenate anions. It also reported that 95.5% alpha-cellulose grafting with acrylamide was utilized as an adsorbent to remove Hg^{2+} ions with an adsorption capacity of 625 mg g^{-1} (Hashem et al., 2006). Takagai et al. (2011) investigated different thio-modified cellulose resins to remove Hg^{2+} ions in acidic solutions. Furthermore, three silylcellulosic derivatives of cellulose, trimethylsilyl-cellulose, and triphenylsilyl-cellulose with different substitution degrees were examined as sorbents for uranyl ions in wastewaters. The results revealed that the complexation of cellulose and trimethylsilyl-cellulose with UO_2^{2+} improved the thermal stability (Bontea et al., 2006). Anirudhan and Rejeena (2011) synthesized a tannin-modified poly (glycidylmethacrylate)-grafted zirconium oxide-densified cellulose adsorbent. The procedure adopted for the preparation of the adsorbent is

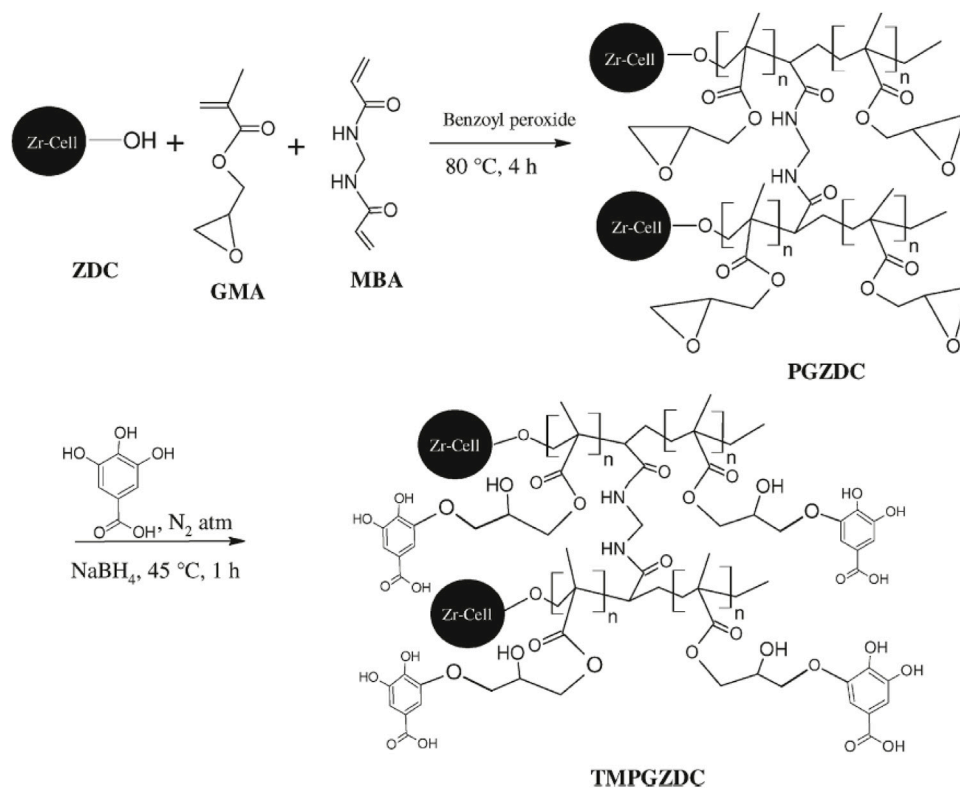


FIGURE 1 | Proposed reaction mechanism for the synthesis of tannin-modified poly (glycidylmethacrylate)-grafted zirconium oxide densified cellulose (TMPGZDC): zirconium oxide densified cellulose (ZDC) grafted with glycidylmethacrylate (GMA), N,N'-methylenebisacrylamide (MBA), and poly (glycidylmethacrylate)-grafted zirconium oxide densified cellulose (PGZDC) (Anirudhan and Rejeena, 2011).

presented in **Figure 1**. The authors indicated that the pH was found to be 5.5 with the adsorption rate of 99.2% for Th⁴⁺. Moreover, an Fe³⁺-loaded ligand exchange cotton cellulose macroporous bead adsorbent was applied for selective adsorption of arsenate anions by Zhao et al. (2009). The cellulose nanofibrils (CNFs) were reported to have various applications (Cao et al., 2019; Cao et al., 2020; Huang et al., 2020; Wang P. et al., 2020). More recently, CNFs were used to adsorb Hg²⁺ ions in an aqueous solution (Bisla et al., 2020). Modified CNFs had an adsorption capacity of 131.86 mg g⁻¹ for Hg²⁺ ions. The pseudo-second order kinetic model implied chemisorption during the removal of Hg²⁺ ions from simulated wastewater. The diethylenetriaminepentaacetic acid-modified cellulose was obtained by a pre-grafting technique (Li et al., 2021). The adsorbent showed an ultrahigh adsorption capacity of 443.8 mg g⁻¹ for Hg²⁺ in aqueous solution. A total of 88.13% of the original adsorption capacity was maintained after five cycles of the regeneration process. Aminotriazole isomer-modified cellulose microspheres with high nitrogen content showed potential affinity for U⁶⁺ (Wen et al., 2021). The microspheres possessed good adsorption capacity, selectivity, and reusability for U⁶⁺. It removed 99.45% from uranium contaminated water, 21.68% from contaminated groundwater, and 75.97% from simulated seawater.

Generally, the modification and functionalization of cellulose can remove all kinds of heavy metals ions simultaneously. In fact,

wastewater contains a variety of heavy metals ions. There are some reports about this type of research. For example, Guclu et al. (2003) found four types of cellulose graft copolymers that removed Pb²⁺, Cu²⁺, and Cd²⁺ ions from aqueous solution. Cellulosic materials containing grafted polyacrylonitrile and poly (acrylic acid) molecules were also reported to remove Cd²⁺ and Cu²⁺ ions from aqueous solutions (Okieimen et al., 2005). Norkus et al. (2006) applied an oxygen delignified alkaline cellulose pulp slurry to remove Fe, Mn, and Cu. The maximum adsorption capacities of Ni²⁺, Co²⁺, Zn²⁺, and Cd²⁺ were 1.28, 1.23, 1.21, and 1.13 mol kg⁻¹ by using chemically modified orange peel cellulose adsorbents, which increased by 95, 178, 60, and 130%, respectively, compared with that of raw orange peel (Li et al., 2008). The modified sugarcane bagasse and chemically modified cellulose displayed adsorption capacities for Ca²⁺ from 15.6 to 54.1 mg g⁻¹ and Mg²⁺ from 13.5 to 42.6 mg g⁻¹ (Karnitz et al., 2010). Recently, modified cellulose hydrogels were reported for the adsorption of heavy metals ions by the ion-exchange mechanism (Zhao et al., 2019). The maximum absorption capacity of 157.51, 393.28, and 289.97 mg g⁻¹ for Cu²⁺, Pb²⁺, and Cd²⁺ ions was found in modified cellulose hydrogels, respectively. The thiol-functionalized cellulose nanofiber membrane was reported to adsorb heavy metals ions by chemisorption (Choi et al., 2020). It achieved adsorption capacities of 49.0 mg g⁻¹ for Cu²⁺, 45.9 mg g⁻¹ for Cd²⁺, and

22.0 mg g⁻¹ for Pb²⁺ in the Langmuir isotherm. The microwave-functionalized cellulose derived from rice husk was reported to eliminate Pb²⁺, Cd²⁺, and Ni²⁺ (Qu et al., 2020). It achieved adsorption capacities of 295.20 mg g⁻¹ for Pb²⁺, 151.51 mg g⁻¹ for Cd²⁺, and 72.80 mg g⁻¹ for Ni²⁺. The functionalized cellulose was found to have good recoverability and adsorption efficiency after five cycles.

Besides the removal of heavy metals ions, the modification and functionalization of cellulose are also applied to the removal of inorganic pollutants. Inukai et al. (2004) firstly used *N*-methylglucamine-type cellulose derivatives to remove B³⁺. Then, Fe³⁺-loaded ligand exchange cotton cellulose as a bead adsorbent was reported to remove fluoride from drinking water by Zhao et al. (2008). Anirudhan et al. (2009) synthesized a cellulose-based anion exchanger bearing the -N⁺HR₂Cl⁻ functional group with the adsorption capacity of 197.75 mg g⁻¹ for V⁵⁺ at 30°C. After that, they demonstrated that about 99.6% of phosphate was adsorbed in 180 min of contact at 100 mg L⁻¹ by using a cellulose-grafted epichlorohydrin functionalized polyethylenimine graft copolymer as an adsorbent (Anirudhan et al., 2012). Besides the removal of heavy metals ions, it is also important for the modification and functionalization of cellulose to remove organic pollutants. For example, Fang et al. (2004) prepared a lysine-cellulose bead adsorbent for removing bacterial endotoxins. The adsorbent had the characteristics of mechanical strength, blood compatibility, and cytotoxicity. Alila and Boufi (2009) constructed a modified cellulose fiber adsorbent to remove several aromatic organic compounds and three herbicides of Alachlor, Linuron, and Atrazine. More recently, a cellulose acetate fiber membrane was reported to remove methylene blue (MB) and Congo red (CR) dyes (Chen et al., 2020). It was observed that the adsorption capacities were 69.89 mg g⁻¹ for MB and 67.31 mg g⁻¹ for CR. An anionic cellulose foam was obtained by grafting and chemical crosslinking (Feng et al., 2020). It exhibited an adsorption capacity of 364.22 mg g⁻¹ for anionic dye Eosin Y and a removal efficiency of 99.58%. The chemical and monolayer action anionic dyes were suggested during the adsorption procedure.

There have been many reports about the removal of lipoprotein by modification and functionalization of cellulose. As early as 1988, Franceschini et al. (1988) comparatively tested a dextran sulfate cellulose column and double membrane filtration for the extracorporeal removal of low density lipoproteins. Schulzeck et al. (1992) further discovered five patients with familial hypercholesterolemia and diet- and drug-resistant low-density lipoprotein cholesterol greater than 230 mg dl⁻¹ using dextran sulfate cellulose adsorption. Olbricht (1996) indicated the extracorporeal removal of low-density lipoprotein cholesterol by dextran sulfate cellulose adsorption. It reported that the reduction in cholesterol per treatment was 65–75% and in most patients one treatment per week was sufficient to reduce cholesterol to 100–150 mg dl⁻¹. In Wang's work, a cellulose adsorbent with amphiphilic ligands was applied to adsorb low-density lipoprotein with a better selectivity and adsorption capacity for the removal of low density lipoprotein (LDL), total cholesterol (TC), total proteins (TP) at 0.857, 1.317, and 1.002 mg ml⁻¹, respectively

(Wang et al., 2002). The adsorbent showed quite good adsorption performance for selective removal of LDL from human plasma (Yu et al., 2006). Wang et al. (2006) synthesized a carboxyl modified polyethylene glycol (PEG) spacer and linked it covalently to cellulose beads. Both the adsorption capacity and adsorption efficiency of the ligand was increased for adsorption of LDL-cholesterol and the average adsorption capacity of LDL-cholesterol was increased to 0.903 mg ml⁻¹.

Beutler and Gelbart (1986) reported that cellulose columns efficiently removed leukocytes from whole blood, and the leukocyte removal activity of cellulose columns was due to mechanical filtration. Weber et al. (1995) produced regenerated cellulose (RC) of 1–8 μm modified with polyethylenimine or diethylaminoethyl groups. RC had high adsorption capacity for endotoxins in human plasma. Butnaru et al. (2003) discussed the treatment of wastewater from cellulose dyeing with direct dyes by electro-coagulation. A cellulose microporous hollow fiber membrane was applied for the dispersion-free reactive extraction of thiol compounds (Yang et al., 2007). Greben et al. (2007) demonstrated that salinity (sulphate) could be removed using the fermentation products of grass-cellulose. The polycation-immobilized pore cellulose spherical particles were also reported to remove the endotoxin by Sakata et al. (2007).

Zhang and Akbulut (2011) investigated the adsorption, desorption, and removal behavior of polymeric nanoparticulate drug delivery systems (PNDDS). **Figure 2A** shows the unimodal and relatively narrow intensity-weighted particle size distribution of PNDDS. It obtained six different particle size distributions of 46 ± 1, 81 ± 2, 159 ± 1, 197 ± 4, 238 ± 7, and 271 ± 2 nm. Based on TEM images, they observed core-shell spherical PNDDS (**Figures 2B,C**). The size had an effect on the adsorption, desorption, and removal of polymeric nanomedicine. Experimental results indicated that the removal rate of the particles increased with the increased particle size. More recently, a cross-linked cellulose aerogel from rice straw with a density of 2.2–24 mg cm⁻³ and porosity of 98.4–99.8% was achieved by a freeze-drying process (Dilamian and Noroozi, 2021). Different shapes of two types of dilute cellulose suspensions were found. The aerogels had a specific area of 178.8 m² g⁻¹ and mesopore volume of 0.8 cm³ g⁻¹. It achieved adsorption capacities up to 170 g g⁻¹ for the super-hydrophobic and oleophilic cellulose aerogels. A cellulose-rich modified rice husk was also reported for the removal of MB and Al³⁺ (You et al., 2021). It carried out the uptake for MB of 50.15 mg g⁻¹ and the uptake for Al³⁺ of 2.87 mg g⁻¹. Authors suggested this was due to the adsorption mechanisms of MB including pore filling, π-π interaction, and electrostatic attraction, as well as the adsorption mechanisms of Al³⁺, such as surface complexation, n-π interaction, and ion exchange. The functionalization of cellulose with hyperbranched polyamide was prepared for adsorption of orange II (OT) and Cu²⁺ ions (Yu et al., 2019). It achieved maximum sorption capacities of 976 mg g⁻¹ for OT and 138 mg g⁻¹ for Cu²⁺ ions. Authors indicated an electrostatic interaction for OT adsorption and the complexation/chelation of Cu²⁺ adsorption.

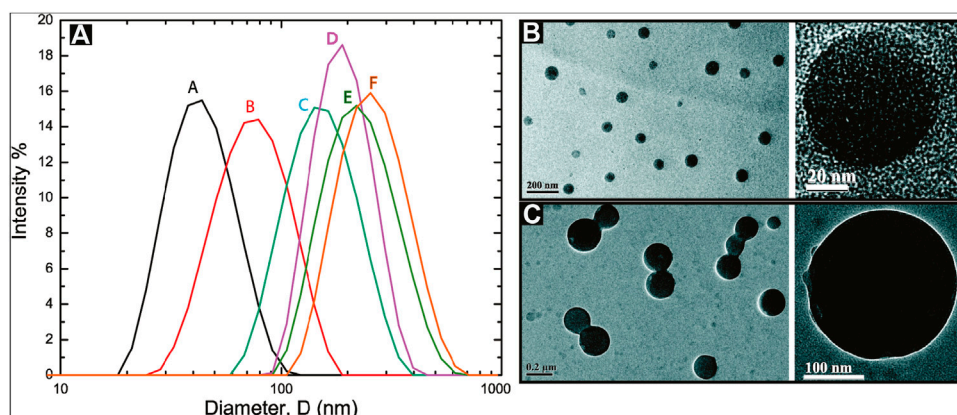


FIGURE 2 | (A) Intensity-weighted particle size distributions for polymeric nanoparticulate drug delivery systems (PNDDS). The mean values of Z-average sizes of different batches of PNDDS were 46 ± 1 nm (black, A), 81 ± 2 nm (red, B), 159 ± 1 nm (cyan, C), 197 ± 4 nm (magenta, D), 238 ± 7 nm (dark yellow, E), and 271 ± 2 nm (orange, F). TEM micrographs for **(B)** 46 nm PNDDS and **(C)** 271 nm PNDDS described in a dynamic light scattering (DLS) study (Zhang and Akbulut, 2011).

ADSORBENTS PRODUCED BY MODIFICATION AND FUNCTIONALIZATION OF CARBOXYMETHYL CELLULOSE

Carboxymethyl cellulose (CMC) is the carboxymethyl group-substituted product of cellulose. CMC has the characteristics of high viscosity, adhesion, acid resistance, and physiological harm, which is widely used in food, medicine, papermaking, and textiles. According to the reports in the literature, it should be pointed out that the modification and functionalization of CMC are widely applied to remove heavy metals ions and organic pollutants. Bacterial cellulose (BC) was found to have important application potential (Ma et al., 2021; Mai et al., 2021; Wang X. et al., 2021; Guo et al., 2022). The early work had been done by Cavus et al. (2006). They developed a crosslinked hydroxyethyl cellulose-g-poly (acrylic acid) graft copolymer to remove Pb^{2+} , Cu^{2+} , and Cd^{2+} . In Chen's work, it was reported that carboxymethylated-BC performed better adsorption with values of 12.63 mg g^{-1} (copper) and 60.42 mg g^{-1} (lead) (Chen et al., 2009), compared with the values of 9.67 mg g^{-1} (copper) and 22.56 mg g^{-1} (lead) of BC. Obviously, carboxymethylated-BC had better adsorption performance. They demonstrated the pseudo-second-order kinetic model and the Langmuir model. Yang et al. (2011) applied CMC hydrogel beads with the maximum adsorption capacity of 6.49, 4.06, and 5.15 mmol g^{-1} for Cu^{2+} , Ni^{2+} , and Pb^{2+} , respectively. Ali (2012) discovered that the CMC and 2-acrylamido-2-methyl propane sulfonic acid hydrogels showed a great capability and were reused at least five times to recover toxic metal ions such as Mn^{2+} , Co^{2+} , Cu^{2+} , and Fe^{3+} from their aqueous solutions. Undoubtedly, the modification and functionalization of CMC displayed amazing absorption capacity for various heavy metals ions. The cellulose acetate/sulfonated poly (ether ketone) blend

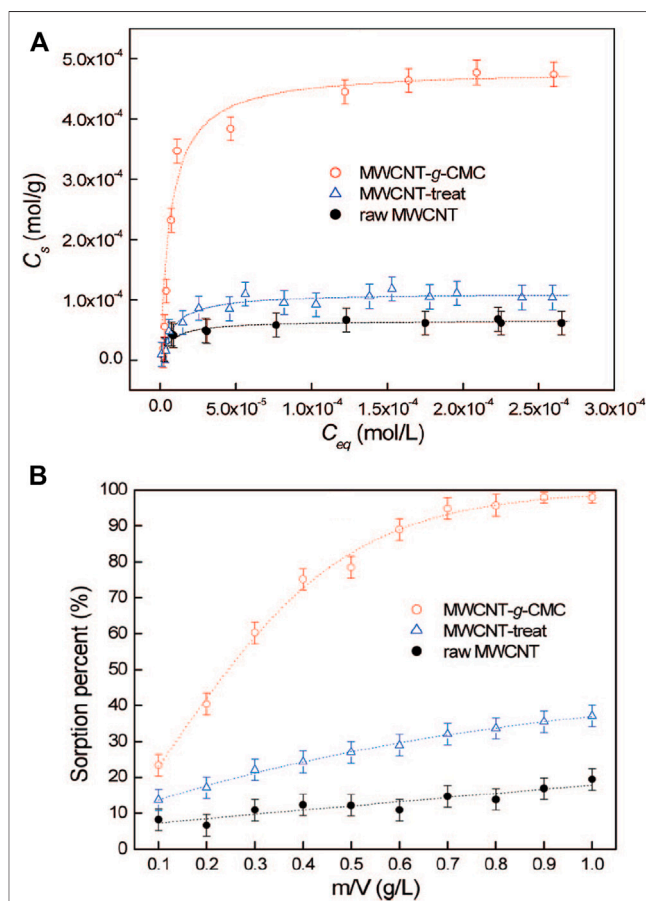


FIGURE 3 | Sorption isotherms **(A)** and effect of sorbent content **(B)** on the removal of UO_2^{2+} from solution on raw MWCNT, on MWCNT-treat, and on MWCNT-g-CMC. $T = 25 \pm 2^\circ\text{C}$, equilibrium time 24 h, $\text{pH} = 5.0 \pm 0.1$, $C[\text{NaClO}_4] = 1.0 \times 10^{-2} \text{ mol/L}$ **(A)** $m/V = 0.4 \text{ g/L}$, **(B)** $C[\text{UO}_2^{2+}]_{\text{initial}} = 2.00 \times 10^{-4} \text{ mol/L}$ (Shao et al., 2009).

ultrafiltration membranes were applied for the separation of Cr^{3+} ions from aqueous streams by ultrafiltration processes (Arthanareeswaran et al., 2007a). Dewangan et al. (2011) also developed the removal of Cr^{6+} by adsorption beads of sodium alginate and CMC.

There are also some reports on the removal of individual metal ions. For example, the removal of arsenic ions was reported using a crosslinked sodium alginate/CMC adsorbent (Tiwari et al., 2008). Shao et al. (2009) developed the application of CMC grafted multiwalled carbon nanotubes (MWCNT-g-CMC) by using plasma techniques in the removal of UO_2^{2+} from the aqueous solution, which had much higher sorption capacity than raw MWCNT. It obtained the sorption capacity of 6.0×10^{-5} mol/g for raw MWCNT, 1.1×10^{-4} mol/g for MWCNT-treat, and 4.7×10^{-4} mol/g for MWCNT-g-CMC (Figure 3A). MWCNT-g-CMC displayed a sorption percentage of UO_2^{2+} from ~23% to ~98% with the increasing MWCNT-g-CMC content from 0.10 to 1.0 g/L (Figure 3B). Zhang et al. (2010) demonstrated that the carboxylate-functionalized cellulose possessed excellent adsorption capacity of 84.4% for Pb^{2+} , which was significantly higher than that of unmodified cellulose. These examples further implied that modification and functionalization improved the adsorption performance. The ethylenediaminetetraacetic acid-functionalized magnetic Fe_3O_4 chitosan oligosaccharide and CMC nanocomposite adsorbent was fabricated for Pb^{2+} adsorption (Lian et al., 2020). The adsorption capacity for monolayer chemical adsorption was 432.34 mg g^{-1} . The nanocomposite exhibited a Pb^{2+} removal rate of ~100% using metal ion solutions of 100 and 200 mg L^{-1} .

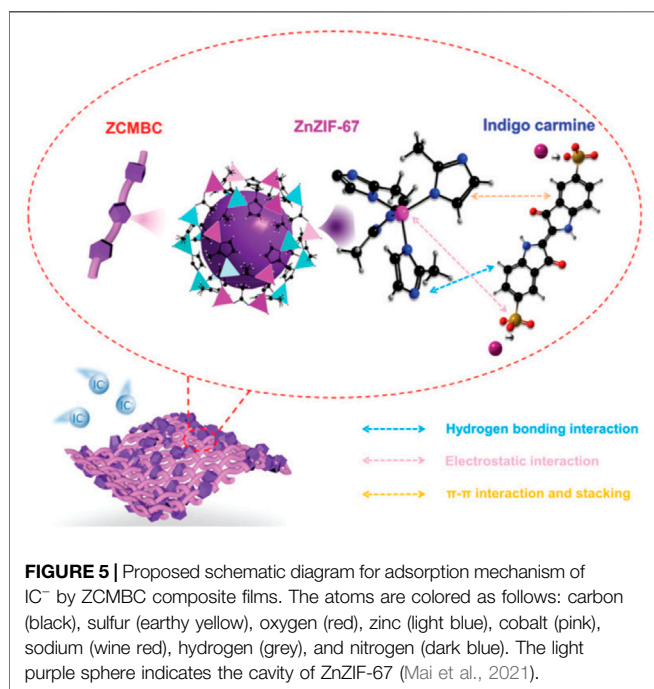
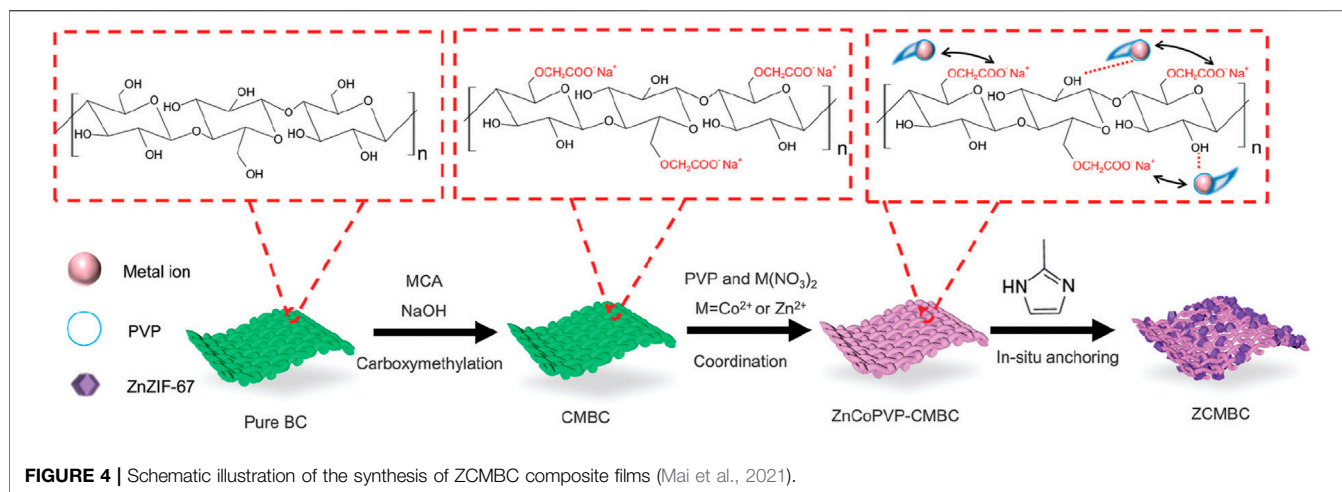
As mentioned above, it is very important to remove organic pollutants from wastewater. Ghanta et al. (2005) applied cellulose acetate blend and aromatic polyamide hydrazide reverse osmosis membranes for their separation behavior of phenol from phenol-water mixtures. Then, Eberhardt et al. (2006) reported the removal of (ortho) phosphate by refined aspen wood fiber treated with CMC and ferrous chloride. After that, De Smet's group developed a super-flux cellulose triacetate dialyzer membrane to remove non-protein-bound and protein-bound uremic solutes (De Smet et al., 2007). The application of a microporous cationic hydrogel of hydroxypropyl cellulose in the removal of anionic dye was carried out by Yan et al. (2009). It was found that the adsorbent displayed an adsorption capacity of $2,478 \text{ g kg}^{-1}$ for anionic dye AO7 at pH 3.96. Bodalo et al. (2005) reported the behavior of cellulose acetate membranes by reverse osmosis of ammonium aqueous solutions. The modification and functionalization of CMC also had the ability to remove protein. Metal ion separation and protein removal were also investigated using modified cellulose acetate membranes by Arthanareeswaran et al. (2007b). The millimeter-sized chitosan/CMC hollow capsules were prepared to remove three typical dyes such as MB, methyl orange (MO), and acid blue-113 (AB) by mixing and stirring positively charged chitosan and negatively charged CMC solutions under an electrostatic interaction (Kong et al., 2020). They achieved removal capacities of 64.6 mg g^{-1} for MB, 334.8 mg g^{-1} for MO, and 526.8 mg g^{-1} for

AB. CMC/carboxylated graphene oxide composite microbeads were achieved to remove cationic MB dye (Eltaweil et al., 2020). They had an adsorption capacity of 180.32 mg g^{-1} . The adsorbent had better reusability for nine cycles with improved adsorption properties. More recently, Mai et al. (2021) applied an *in situ* anchoring method to prepare zeolitic imidazolate frameworks (ZIFs)@carboxymethylated bacterial cellulose (ZCMBC) composite films (Figure 4). The ZCMBC composite films were reported to have a high ZIFs loading rate and satisfactory selective indigo carmine removal efficiency (98.7%). The authors suggested the adsorption mechanism of IC^- by ZCMBC composite films (Figure 5).

Millimeter hollow CMC microspheres/poly (ethyleneimine) (PEI) microspheres were fabricated for dye adsorption (Yang et al., 2021). The hollow microspheres had an adsorption capacity of 452 mg g^{-1} for MB. CMC and genipin crosslinked carboxyalkyl-chitosan combined with a sulfonated graphene oxide sponge with multiple active sites was fabricated for adsorbing sulfonamide antibiotics (Liu Y. et al., 2021). The composite showed high sulfamethoxazole and sulfapyridine. It obtained an adsorption capacity of 312.28 mg g^{-1} for sulfamethoxazole and 161.89 mg g^{-1} for sulfapyridine at 298 K. CTAB-modified CMC/bagasse cryogels were reported to remove bisphenol A (BPA), MB, and Cr^{6+} ions in binary or ternary aqueous mixtures (Meneses et al., 2022). They exhibited a removal rate of 100% for MB, 70% for Cr^{6+} , and 95% for BPA. They observed an increased adsorption capacity of Cr^{6+} ions in the binary mixture or ternary mixture due to the synergistic effect.

ADSORBENTS PRODUCED BY CELLULOSE-BASED (NANO) COMPOSITES

It is known that (nano) composites are composed of two or more kinds of materials, which have synergistic effects and new properties, compared with an individual component. It means that cellulose-based (nano) composites were fabricated by using cellulose as the matrix and using inorganic or organic materials as reinforcement. In the literature, there are reports about the applications of cellulose-based (nano) composites. It is of great importance for cellulose-based (nano) composites adsorbents to remove heavy metals ions and organic pollutants. In early 2005, Guo and Chen (2005) completed pioneering work to remove heavy metals ions by using cellulose-based composites as adsorbents. They firstly applied cellulose/iron oxyhydroxide to remove arsenate and arsenite from groundwater. It was reported that the adsorbents displayed high removal efficiency of arsenite (99.6 mg g^{-1}) and arsenate (33.2 mg g^{-1}) at pH 7.0. They also summarized three reasons for and five advantages of cellulose/iron oxyhydroxide, such as cheap resources, recycled materials, excellent mechanical strength, high adsorption capacity, and high regeneration efficiency. Then, they used EXAFS to investigate the removal mechanism of cellulose/iron oxyhydroxide for arsenic (Guo et al., 2007). From then on, many groups explored the applications of cellulose-based (nano) composites in the



removal of heavy metals ions and organic pollutants. For example, Maliyekkal et al. (2010) reported the applications for Pb^{2+} removal from aqueous solutions by using cellulose/manganese oxide nanocomposites. The physic-sorption played a dominant role in the adsorption of Pb^{2+} . Nata et al. (2011) made amine-rich magnetite/BC nanocomposites by the solvothermal reaction. It was found that these nanocomposites displayed an adsorption capacity towards As^{5+} ions. Kumar et al. (2012) reported a cellulose-montmorillonite composite with an adsorption capacity of 22.2 mg g^{-1} for the detoxification of Cr^{6+} ions from industrial wastewater by a column methodology. It should be noted that the composite was reused for 10 adsorption-desorption cycles.

It is worth noting that hydroxyapatite has an excellent ion-exchangeability. In 2008, Choi and Jeong (2008) applied a

hydroxyapatite/cellulose composite to remove heavy metals in aqueous solution. Islam et al. (2011) evaluated the feasibility of cellulose/carbonated hydroxyapatite nanocomposites for As^{5+} removal with the adsorption capacity of 12.72 mg g^{-1} . Authors found the chemical process in the adsorption process. In the research of water treatment using adsorbents, it is very important to judge the chemisorption and/or physisorption process on the absorption mechanism. The above results indicated that cellulose/carbonated hydroxyapatite (nano) composites are promising adsorbents in the removal of heavy metals ions.

Similarly, cellulose-based (nano) composites including organic polymers are also applied in the removal of heavy metals ions. For example, Lima et al. (2005) developed chitosan/cellulose acetate film with an affinity for adsorbing copper. Highly porous adsorptive chitosan/cellulose acetate blend hollow fiber membranes were applied for copper ion removal in a batch adsorption mode (Liu and Bai, 2006). Cifci and Kaya (2010) used a poly (vinyl alcohol) (PVA)/cellulose membranes composite for metal removal from aqueous solutions.

There are a few reports about cellulose-based (nano) composites as adsorbents in the removal of organic pollutants. Cellulose acetate-supported Ni/Fe nanoparticles were first carried out to remove trichloroethylene from water by Wu and Ritchie (2006). Dridi-Dhaouadi et al. (2011) researched the sorption behavior of Pb^{2+} and C.I. acid yellow 44 on posidonia oceanica. Zhu et al. (2011) also applied magnetic cellulose/ Fe_3O_4 /activated carbon composites to remove CR. The nanocellulose hybrid containing polyhedral oligomeric silsesquioxane was also investigated to remove reactive dyes (Xie et al., 2011b). More recently, iron-based metal-organic framework@cellulose aerogels were obtained for CR dye adsorption by the *in situ* growing method (Huang et al., 2021a). It achieved an adsorption capacity of 280.3 mg g^{-1} . Lemon peel/MCC hydrogels with porous structure and surface roughness were obtained for MB adsorption by direct co-dissolving in 1-butyl-3-methylimidazolium chloride (BmimCl) (Dai et al., 2021). The introduction of lemon peel increased the porosity and improved the thermal stability of the hydrogels. It

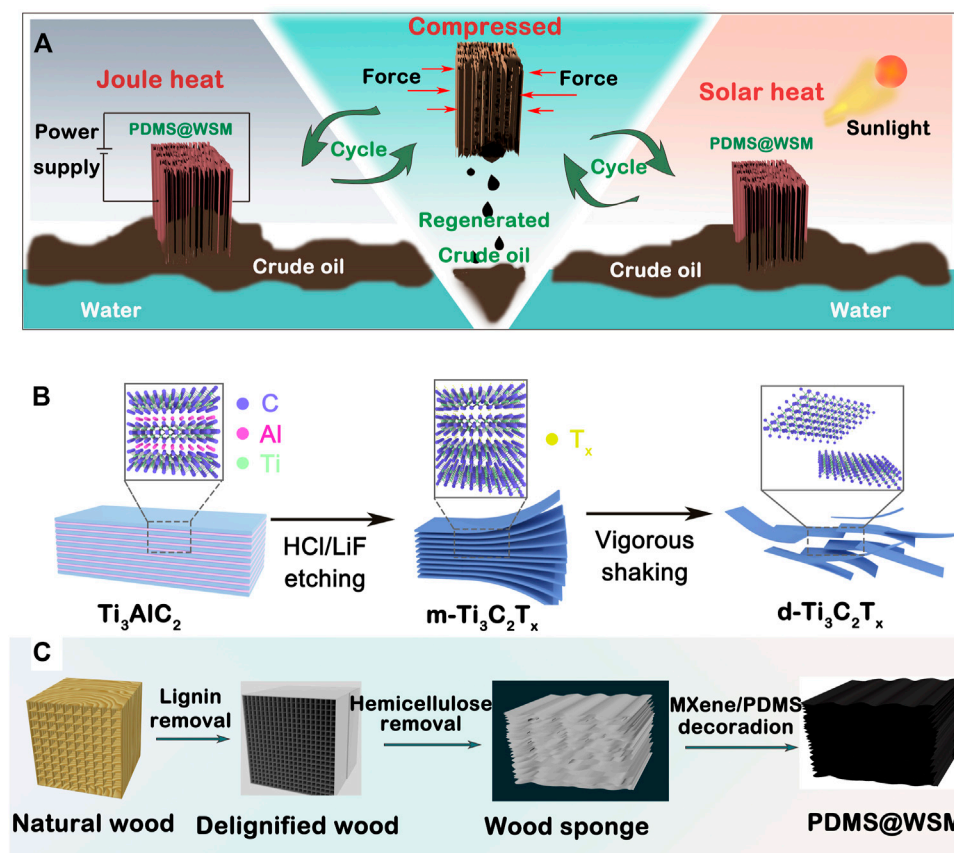


FIGURE 6 | (A) Schematic illustration of Joule-heating and solar-heating PDMS@WSM to clean up and recover a viscous crude oil spill. **(B)** Schematic showing the synthesis process of the MXene nanosheet. **(C)** Schematic illustration of the fabrication of the wood sponge and PDMS@WSM (Wang et al., 2022).

obtained the maximum adsorption capacity of 57.54 mg g^{-1} for hydrogels.

The hollow cellulose/carbon nanotubes composite beads with aligned porous structure were fabricated by ice template and freeze-drying technology (Ding et al., 2021). All cellulose concentrations, pre-freeze temperatures, and voltages affected the hollow structure and diameter of the beads. Authors discovered the enhanced diameter of the beads with the increase of cellulose concentration, the different structure of beads at different pre-freeze temperatures, and the decreased diameter of beads with increased voltage. The composite showed good reusability, biodegradability, and an adsorption capacity of 285.71 mg g^{-1} . A polyaniline/dicarboxyl acid cellulose@graphene oxide (GO) composite was synthesized to remove the reactive brilliant red K-2G (Liu T. et al., 2021). It obtained an adsorption capacity of 447.0 mg g^{-1} for the first scenario, and 729.0 mg g^{-1} during the subsequent photocatalysis process. A graphene oxide/cellulose nanocrystals nanocomposite was obtained to remove MB (Zaman et al., 2020). It removed around 98% of MB in 135 min and the maximum adsorption capacity was 751.88 mg g^{-1} Wang et al. (2022) also reported porous polydimethylsiloxane@wood sponge/MXene (PDMS@WSM) with outstanding compressibility and hydrophobic/lipophilic

ability as a crude oil absorbent (Figure 6). The wood sponge consisted of cellulose by the removal of lignin and hemicellulose from natural wood. The PDMS@WSM had a maximum adsorption capacity of $11.2 \times 10^5 \text{ g m}^{-3}$ due to the excellent Joule heating and photothermal conversion effect.

In fact, organic solvent can also improve the adsorption capacity of cellulose. Musyoka et al. (2011) reported ethylenediamine-modified cellulose with adsorption capacities of $0.0136 \text{ mmol g}^{-1}$ for Cd^{2+} and $0.0179 \text{ mmol g}^{-1}$ for Pb^{2+} ions. Xie et al. (2011a) synthesized nanocellulose hybrid biosorbents for adsorbing copper and nickel ions in aqueous solution. Hierarchical pore UiO-66/nanocellulose aerogels were prepared by a self-crosslinking method (Wang et al., 2019). The composite aerogels had adsorption capacities of 71.7 mg g^{-1} for anionic methyl orange and 51.8 mg g^{-1} for cationic MB. TEMPO-CNC MWCN/GO composite films were reported with a partition coefficient of $872.266 \text{ ml g}^{-1}$ (Zheng et al., 2020). Porous cellulose/chitosan spheres were prepared to adsorb Cu^{2+} (Wittmar et al., 2020). They obtained a maximum adsorption capacity of 52.5 mg g^{-1} due to the amino group in the chitosan unit. Park et al. (2020) prepared poly (acryloyl hydrazide)-grafted CNC particles for adsorption of Cr^{6+} by strong electrostatic, hydrogen bonding, and chelating interactions. The adsorbents

exhibited a high Cr^{6+} adsorption capacity of $\sim 457.6 \text{ mg g}^{-1}$ by intra-particle diffusion resistance. CNC/iron oxide composites were prepared to remove arsenic (Dong F. et al., 2020). They obtained the maximal amount of 13.866 mg g^{-1} for As^{3+} and 15.712 mg g^{-1} for As^{5+} . They exhibited chemical adsorption of monolayers. A TEMPO-oxidized CNF/magnetite was prepared to adsorb lead ions with a removal rate of 80% (Abou-Zeid et al., 2021). An MCC/magnesium sulfate hexahydrate (MCC/MH) composite adsorbent was used to adsorb heavy metal Co^{2+} ions (Wang R. et al., 2021). It obtained a removal rate of 97.67% and adsorption capacity of 153.84 mg g^{-1} . Dialdehyde cellulose/GO composites adsorbents with high carboxyl groups density, high surface area, and low crystallinity index were obtained in both heterogeneous and homogeneous systems (Wang Z. et al., 2020). The adsorbents showed the adsorption capacities of 74.2 mg g^{-1} for Cu^{2+} and 91.7 mg g^{-1} for Pb^{2+} . CNF/PVA composite gel spheres with 1–3 mm were prepared for organic pollutants and heavy metals ions (Yi et al., 2022). The spheres showed adsorption properties for simulated pollutants, including Cu^{2+} , phenol, and aniline in water. They achieved a maximum absorption capacity of 17.22 mg g^{-1} for As^{3+} and 15.712 mg g^{-1} for As^{5+} , 176.72 mg g^{-1} for phenol, and 341.93 mg g^{-1} for aniline. The composite spheres also had good absorption properties for petroleum ether, ethyl acetate, and toluene. A liquid nitrogen directional freezing method was used to prepare CNF/chitosan/montmorillonite aerogels for wastewater treatment (Rong et al., 2021). The aerogels had a homogeneous three-dimensional directional pore structure, good mechanical properties, good adsorption performance, and reusability. They exhibited an adsorption capacity of 181.92 mg g^{-1} for Cu^{2+} , 170.19 mg g^{-1} for Pb^{2+} , and 163.85 mg g^{-1} for Cd^{2+} .

MECHANISM OF ADSORPTION

As mentioned above, it seems that the mechanism of adsorption can be simply divided into physisorption and chemisorption. In fact, it is believed that there exists simultaneous physisorption and chemisorption. In the adsorption process of adsorbents, the main mechanism still needs to be determined. As described in the literature, the physical forces include Van der Waals forces, hydrophobicity, hydrogen bonds, polarity and steric interaction, dipole induced dipole interaction, and pep interaction. Generally, it is reported that physisorption has the characteristics of low adsorption heat, does not require activation energy, single or multi molecular layer adsorption, no structure change of adsorbed molecules, no form of new chemical bonds, and is reversible. For the chemisorption process, it is considered that the adsorption heat is approximately equal to the reaction heat. The adsorption force is similar to the chemical bond and much stronger than Van der Waals forces. Chemisorption, as a single molecular layer adsorption, is selective and can be described by the Langmuir isotherm. In addition, chemisorption displays irreversibility to temperature and pressure, which requires activation energy. At present, the adsorption mechanisms are researched by adsorption kinetics,

adsorption isotherms (Langmuir isotherm and Freundlich isotherm), and thermodynamics, which could explain the problems of physisorption and chemisorption, monolayer and multilayer adsorption. Therefore, it is very important to determine the type of adsorption. First, it can be judged according to the value of adsorption heat. The value of chemisorption heat is similar to that of the chemical reaction. In general, the value of chemisorption heat ranges from $83,740$ to $418,680 \text{ J mol}^{-1}$, while the value of physisorption heat is approximately $20,000 \text{ J mol}^{-1}$. Secondly, the effect of temperature on the adsorption rate should be explored in the near future. During the chemisorption process, the adsorption rate is an activated process, which increases with the increase of temperature. However, physisorption is not an activated process, which has a high adsorption rate even at low temperatures. One can judge the type of adsorption by different adsorption processes at different temperatures. In the research of adsorption, adsorption capacities, regeneration efficiency, and selectivity are important factors. Moreover, in view of the above mentioned physisorption and chemisorption, one can conclude that chemisorption may have a high adsorption capacity and good selectivity due to chemical properties. However, physisorption has poor selectivity, which depends on the characteristics of the adsorbents.

Although most groups have investigated the mechanism of the adsorption process, we still have to say that it is not enough. For example, the famous Langmuir isotherm is based on the following assumptions of the uniformity of adsorbent surface, monolayer adsorption, dynamic adsorption, without force between the adsorbate molecules, etc., The Langmuir adsorption isotherm can be used in the low pressure range. When the gas pressure is higher in the adsorbate, close to the saturation vapor pressure, the equation produces a deviation due to the condensation of the adsorbate in the micro capillary and no single molecule layer adsorption. As for the Freundlich isotherm, it is an empirical formula in a narrow pressure range. In the low pressure or high pressure region, it cannot obtain satisfactory experimental results. Therefore, it is necessary to combine the new measurement method with molecular dynamics simulation to explore the adsorption mechanism. In fact, we believe that the adsorption is a very complex process, and some adsorption processes also include a chemical reaction and ion-exchange. Understanding the adsorption mechanism is of great significance for the synthesis and application of adsorbents.

FUTURE PERSPECTIVES

We believe that there is an increasing demand for environmentally friendly and economically friendly adsorbents in the field of water treatment. As discussed in this review article, cellulose is one of the polysaccharides composed of glucose molecules and the most abundant natural renewable biomass in the world. Undoubtedly, the modification and functionalization of cellulose and cellulose-based (nano) composites meet these requirements. Although there is a long road ahead for these applications, cellulose has a very bright

future as an amazing and promising bio-adsorbent for wastewater treatment. More importantly, we expect that low-cost and greener bio-adsorbents will open a new window for the high value-added applications of cellulose, compared with other adsorbents. Besides heavy metals ions and organic pollutants, the modification and functionalization of cellulose and cellulose-based (nano) composites were also reported for protein adsorption (Zhao et al., 2021), drugs adsorption and release (Zhang et al., 2019), bilirubin (Wang Y. et al., 2021), carbon dioxide (CO₂) adsorption (Sepahvand et al., 2020), and lysozymes (Rahmatika et al., 2020).

As described by Ali et al. (2012), there are many issues that need to be solved in the next step, such as adsorption mechanism, industrial scales preparation, regeneration, specific surface area, the management of removed pollutants, dispersion, etc., We would like to point out that there are many requirements for adsorbents in wastewater treatment, such as inexpensive, eco-friendly, environmentally friendly, good selectivity, high adsorption capacities, good regeneration efficiency, broad spectrum, etc., As we all know, it is difficult to obtain perfect adsorbents. Therefore, finding a balance among all factors is very important for practical applications.

The adsorbents are expected to have practical applications, which is the first and only standard to measure the quality of adsorbents. It is necessary to investigate the mechanism and eliminate interference at lab-scale batch studies. Obviously, unlike lab-scale batch studies, industrial waste water containing various heavy metals ions and organic pollutants is more complex. Sometimes, it was found that the adsorbents displayed good performance at lab studies and poor performance in industrial wastewater. At least, the adsorbent with good performance at lab studies should be characterized and tested with industrial wastewater. So, the design of adsorbents should be based on realistic industrial applications, not the opposite. As described above, hundreds of cellulose-based bio-adsorbents were reported in the literature. However, few types of bio-adsorbents can be used in practical applications. The modification and functionalization of cellulose, CMC, and cellulose-based (nano) composites could be used to create bio-adsorbents to remove heavy metals ions and organic pollutants. The future development direction is put forward from the aspects of adsorption mechanism, theoretical simulation, and experimental verification. Although there is no common standard to judge these bio-adsorbents, it is necessary to narrow the scope.

In addition, it is worth noting that the main components of biomass are polysaccharides (cellulose and hemicellulose) and lignin. Cellulose is obtained by pretreatment of biomass. It seems that the development of pretreatment methods on biomass is of great importance to broaden its industrial applications.

REFERENCES

- Abou-Zeid, R. E., Kamal, K. H., Abd El-Aziz, M. E., Morsi, S. M., and Kamel, S. (2021). Grafted TEMPO-Oxidized Cellulose Nanofiber Embedded with
- Obviously, the pretreatment methods determine whether cellulose and cellulose-based (nano) composites are economically friendly adsorbents. In general, cellulose can be used as a raw material to produce bio-based fuels, chemicals, and materials. Therefore, cellulose-based bio-adsorbents should have high value-added and low price capabilities, compared with other applications such as bio-based fuels, chemicals, and materials. Of course, the high regeneration efficiency of bio-adsorbents would contribute to reduce the cost.
- Moreover, science and technology are like brothers. The problems of the adsorption mechanism, preparation, property, etc., may belong to the scientific field. However, the application in the wastewater field may belong to the technical field. It is found that the problems of technology always determine the quality and price of bio-adsorbents in the industrial process. So, there is still a long way to go from lab-scale batch studies to large-scale industrial applications of bio-adsorbents. We would like to point out that the research in the lab should meet industrial applications and resolve industrial problems, not the opposite.
- ## CONCLUSION
- In this review article, we summarized the recent progress of adsorbents produced by modification and functionalization of cellulose and cellulose-based (nano) composites to remove heavy metals ions and organic pollutants. We believe that the modification and functionalization of cellulose, carboxymethyl cellulose, and cellulose-based (nano) composites are amazing and promising methods to create bio-adsorbents in the field of water treatment. It is expected that cellulose and cellulose-based (nano) composites will have promising applications in the field of wastewater treatment.
- ## AUTHOR CONTRIBUTIONS
- R-JS, TW, J-QL, NZ and M-GM: investigation. R-JS, NZ, and M-GM: supervision. R-JS, TW, J-QL, NZ and M-GM: writing-original draft. R-JS, NZ and M-GM: writing-review and editing. All authors contributed to the article and approved the submitted version.
- ## FUNDING
- The financial support from the National Key R & D Program of China (2019YFC1905901) and the Key Production Innovative Development Plan of the Southern Bingtuan (2019DB007) is gratefully acknowledged.
- Modified Magnetite for Effective Adsorption of lead Ions. *Int. J. Biol. Macromolecules* 167, 1091–1101. doi:10.1016/j.ijbiomac.2020.11.063
- Ali, A. E. H. (2012). Removal of Heavy Metals from Model Wastewater by Using Carboxymethyl Cellulose/2-Acrylamido-2-Methyl Propane Sulfonic Acid Hydrogels. *J. Appl. Polym. Sci.* 123, 763–769. doi:10.1002/app.34470

- Ali, I., Asim, M., and Khan, T. A. (2012). Low Cost Adsorbents for the Removal of Organic Pollutants from Wastewater. *J. Environ. Manage.* 113, 170–183. doi:10.1016/j.jenvman.2012.08.028
- Alila, S., and Boufi, S. (2009). Removal of Organic Pollutants from Water by Modified Cellulose Fibres. *Ind. Crops Prod.* 30, 93–104. doi:10.1016/j.indcrop.2009.02.005
- Anirudhan, T. S., Jalajamony, S., and Divya, L. (2009). Efficiency of Amine-Modified Poly(glycidyl Methacrylate)-Grafted Cellulose in the Removal and Recovery of Vanadium(V) from Aqueous Solutions. *Ind. Eng. Chem. Res.* 48, 2118–2124. doi:10.1021/ie8000869
- Anirudhan, T. S., Rauf, T. A., and Rejeena, S. R. (2012). Removal and Recovery of Phosphate Ions from Aqueous Solutions by Amine Functionalized Epichlorohydrin-Grafted Cellulose. *Desalination* 285, 277–284. doi:10.1016/j.desal.2011.10.014
- Anirudhan, T. S., and Rejeena, S. R. (2011). Thorium(IV) Removal and Recovery from Aqueous Solutions Using Tannin-Modified Poly(glycidylmethacrylate)-Grafted Zirconium Oxide Densified Cellulose. *Ind. Eng. Chem. Res.* 50, 13288–13298. doi:10.1021/ie2015679
- Arthanareeswaran, G., Thanikaivelan, P., Jaya, N., Mohan, D., and Raajenthiren, M. (2007a). Removal of Chromium from Aqueous Solution Using Cellulose Acetate and Sulfonated Poly(Ether Ether Ketone) Blend Ultrafiltration Membranes. *J. Hazard. Mater.* 139, 44–49. doi:10.1016/j.jhazmat.2006.06.006
- Arthanareeswaran, G., Thanikaivelan, P., Raghuime, J. A., Raajenthiren, M., and Mohan, D. (2007b). Metal Ion Separation and Protein Removal from Aqueous Solutions Using Modified Cellulose Acetate Membranes: Role of Polymeric Additives. *Separat. Purif. Technol.* 55, 8–15. doi:10.1016/j.seppur.2006.10.014
- Asgher, M., Ahmad, Z., and Iqbal, H. M. N. (2013). Alkali and Enzymatic Delignification of Sugarcane Bagasse to Expose Cellulose Polymers for Saccharification and Bio-Ethanol Production. *Ind. Crops Prod.* 44, 488–495. doi:10.1016/j.indcrop.2012.10.005
- Babel, S., and Kurniawan, T. A. (2003). Low-Cost Adsorbents for Heavy Metals Uptake from Contaminated Water: A Review. *J. Hazard. Mater.* 97 (1–3), 219–243. doi:10.1016/s0304-3894(02)00263-7
- Belhallaoui, B., Aziz, A., Elandaloussi, E. H., Ouali, M. S., and De Ménorval, L. C. (2009). Succinate-Bonded Cellulose: A Regenerable and Powerful Sorbent for Cadmium-Removal from Spiked High-Hardness Groundwater. *J. Hazard. Mater.* 169, 831–837. doi:10.1016/j.jhazmat.2009.04.021
- Beutler, E., and Gelbart, T. (1986). The Mechanism of Removal of Leukocytes by Cellulose Columns. *Blood cells* 12, 57–64.
- Bisla, V., Rattan, G., Singhal, S., and Kaushik, A. (2020). Green and Novel Adsorbent from Rice Straw Extracted Cellulose for Efficient Adsorption of Hg (II) Ions in an Aqueous Medium. *Int. J. Biol. Macromolecules* 161, 194–203. doi:10.1016/j.ijbiomac.2020.06.035
- Bódalo, A., Gómez, J.-L., Gómez, E., León, G., and Tejera, M. (2005). Ammonium Removal from Aqueous Solutions by Reverse Osmosis Using Cellulose Acetate Membranes. *Desalination* 184, 149–155. doi:10.1016/j.desal.2005.03.062
- Bontea, D., Mita, C., and Humelnicu, D. (2006). Removal of Uranyl Ions from Wastewaters Using Cellulose and Modified Cellulose Materials. *J. Radioanal. Nucl. Chem.* 268, 305–311. doi:10.1007/s10967-006-0167-9
- Butnaru, R., Berteau, A., and Dobrescu, L. (2003). Colour Removal of Wastewaters from Cellulose Fibers' Dyeing with Direct Dyes by Electrocoagulation. *Cellul. Chem. Technol.* 37, 477–486.
- Cao, W.-T., Chen, F.-F., Zhu, Y.-J., Zhang, Y.-G., Jiang, Y.-Y., Ma, M.-G., et al. (2018). Binary Strengthening and Toughening of MXene/Cellulose Nanofiber Composite Paper with Nacre-Inspired Structure and Superior Electromagnetic Interference Shielding Properties. *ACS Nano* 12, 4583–4593. doi:10.1021/acsnano.8b00997
- Cao, W., Ma, C., Tan, S., Ma, M., Wan, P., and Chen, F. (2019). Ultrathin and Flexible CNTs/MXene/Cellulose Nanofibrils Composite Paper for Electromagnetic Interference Shielding. *Nano-Micro Lett.* 11, 72. doi:10.1007/s40820-019-0304-y
- Cao, W. T., Ouyang, H., Xin, W., Chao, S., Ma, C., Li, Z., et al. (2020). A Stretchable Highoutput Triboelectric Nanogenerator Improved by MXene Liquid Electrode with High Electronegativity. *Adv. Funct. Mater.* 30, 2004181. doi:10.1002/adfm.202004181
- Cavus, S., Gurdag, G., Yasar, M., Guclu, K., and Gurdag, M. A. (2006). The Competitive Heavy Metal Removal by Hydroxyethyl Cellulose-G-Poly(acrylic Acid) Copolymer and its Sodium Salt: The Effect of Copper Content on the Adsorption Capacity. *Polym. Bull.* 57, 445–456. doi:10.1007/s00289-006-0583-6
- Chen, H., Wang, X., Li, J., and Wang, X. (2015). Cotton Derived Carbonaceous Aerogels for the Efficient Removal of Organic Pollutants and Heavy Metal Ions. *J. Mater. Chem. A.* 3, 6073–6081. doi:10.1039/c5ta00299k
- Chen, S., Zou, Y., Yan, Z., Shen, W., Shi, S., Zhang, X., et al. (2009). Carboxymethylated-Bacterial Cellulose for Copper and lead Ion Removal. *J. Hazard. Mater.* 161, 1355–1359. doi:10.1016/j.jhazmat.2008.04.098
- Chen, W., Ma, H., and Xing, B. (2020). Electrospinning of Multifunctional Cellulose Acetate Membrane and its Adsorption Properties for Ionic Dyes. *Int. J. Biol. Macromolecules* 158, 1342–1351. doi:10.1016/j.ijbiomac.2020.04.249
- Choi, H. Y., Bae, J. H., Hasegawa, Y., An, S., Kim, I. S., Lee, H., et al. (2020). Thiol-Functionalized Cellulose Nanofiber Membranes for the Effective Adsorption of Heavy Metal Ions in Water. *Carbohydr. Polym.* 234, 115881. doi:10.1016/j.carbpol.2020.115881
- Choi, S., and Jeong, Y. (2008). The Removal of Heavy Metals in Aqueous Solution by Hydroxyapatite/Cellulose Composite. *Fibers Polym.* 9, 267–270. doi:10.1007/s12221-008-0042-0
- Cıfci, C., and Kaya, A. (2010). Preparation of Poly(Vinyl Alcohol)/Cellulose Composite Membranes for Metal Removal from Aqueous Solutions. *Desalination* 253, 175–179. doi:10.1016/j.desal.2009.11.010
- Crini, G. (2006). Non-Conventional Low-Cost Adsorbents for Dye Removal: A Review. *Bioresour. Technol.* 97 (9), 1061–1085. doi:10.1016/j.biortech.2005.05.001
- Dai, H., Chen, Y., Ma, L., Zhang, Y., and Cui, B. (2021). Direct Regeneration of Hydrogels Based on Lemon Peel and its Isolated Microcrystalline Cellulose: Characterization and Application for Methylene Blue Adsorption. *Int. J. Biol. Macromolecules* 191, 129–138. doi:10.1016/j.ijbiomac.2021.09.063
- De Smet, R., Dhondt, A., Eloit, S., Galli, F., Waterloos, M. A., and Vanholder, R. (2007). Effect of the Super-Flux Cellulose Triacetate Dialyser Membrane on the Removal of Non-Protein-Bound and Protein-Bound Uraemic Solutes. *Nephrol. Dial. Transplant.* 22, 2006–2012. doi:10.1093/ndt/gfm065
- Dewangan, T., Tiwari, A., and Bajpai, A. K. (2011). Removal of Chromium(VI) Ions by Adsorption onto Binary Biopolymeric Beads of Sodium Alginate and Carboxymethyl Cellulose. *J. Dispersion Sci. Technol.* 32, 1075–1082. doi:10.1080/01932691003659403
- Dilamian, M., and Noroozi, B. (2021). Rice Straw Agri-Waste for Water Pollutant Adsorption: Relevant Mesoporous Super Hydrophobic Cellulose Aerogel. *Carbohydr. Polym.* 251, 117016. doi:10.1016/j.carbpol.2020.117016
- Ding, F., Ren, P., Wang, G., Wu, S., Du, Y., and Zou, X. (2021). Hollow Cellulose-Carbon Nanotubes Composite Beads with Aligned Porous Structure for Fast Methylene Blue Adsorption. *Int. J. Biol. Macromolecules* 182, 750–759. doi:10.1016/j.ijbiomac.2021.03.194
- Dong, F., Xu, X., Shaghaleh, H., Guo, J., Guo, L., Qian, Y., et al. (2020a). Factors Influencing the Morphology and Adsorption Performance of Cellulose Nanocrystal/iron Oxide Nanorod Composites for the Removal of Arsenic during Water Treatment. *Int. J. Biol. Macromol.* 156, 1418–1424. doi:10.1016/j.ijbiomac.2019.11.182
- Dong, H., Zheng, L., Yu, P., Jiang, Q., Wu, Y., Huang, C., et al. (2020b). Characterization and Application of Lignin-Carbohydrate Complexes from Lignocellulosic Materials as Antioxidants for Scavenging *In Vitro* and *In Vivo* Reactive Oxygen Species. *ACS Sustain. Chem. Eng.* 8 (1), 256–266. doi:10.1021/acssuschemeng.9b05290
- Dridi-Dhaouadi, S., Ben Douissa-Lazreg, N., and M'Henni, M. F. (2011). Removal of lead and Yellow 44 Acid Dye in Single and Binary Component Systems by Raw Posidonia Oceanica and the Cellulose Extracted from the Raw Biomass. *Environ. Technol.* 32 (3), 325–340. doi:10.1080/09593330.2010.499545
- Eberhardt, T. L., Min, S.-H., and Han, J. S. (2006). Phosphate Removal by Refined aspen Wood Fiber Treated with Carboxymethyl Cellulose and Ferrous Chloride. *Bioresour. Technol.* 97, 2371–2376. doi:10.1016/j.biortech.2005.10.040
- Eltaweil, A. S., Elgarhy, G. S., El-Subriti, G. M., and Omer, A. M. (2020). Carboxymethyl Cellulose/Carboxylated Graphene Oxide Composite Microbeads for Efficient Adsorption of Cationic Methylene Blue Dye. *Int. J. Biol. Macromolecules* 154, 307–318. doi:10.1016/j.ijbiomac.2020.03.122
- Fang, H., Wei, J., and Yu, Y. (2004). *In Vivo* Studies of Endotoxin Removal by Lysine-Cellulose Adsorbents. *Biomaterials* 25, 5433–5440. doi:10.1016/j.biomaterials.2003.12.035

- Feng, C., Ren, P., Huo, M., Dai, Z., Liang, D., Jin, Y., et al. (2020). Facile Synthesis of Trimethylammonium Grafted Cellulose Foams with High Capacity for Selective Adsorption of Anionic Dyes from Water. *Carbohydr. Polym.* 241, 116369. doi:10.1016/j.carbpol.2020.116369
- Franceschini, G., Busnach, G., Vaccarino, V., Calabresi, L., Gianfranceschi, G., and Sirtori, C. R. (1988). Apheretic Treatment of Severe Familial Hypercholesterolemia: Comparison of Dextran Sulfate Cellulose and Double Membrane Filtration Methods for Low Density Lipoprotein Removal. *Atherosclerosis* 73, 197–202. doi:10.1016/0021-9150(88)90042-1
- Garcia-Reyes, R. B., and Rangel-Mendez, J. R. (2009). Contribution of Agro-Waste Material Main Components (Hemicelluloses, Cellulose, and Lignin) to the Removal of Chromium (III) from Aqueous Solution. *J. Chem. Technol. Biotechnol.* 84, 1533–1538. doi:10.1002/jctb.2215
- Ghanta, K. C., Ghosh, A. K., and Ramachandran, V. (2005). Separation Characteristics of Cellulose Acetate Blend (CAB) and Aromatic Polyamide Hydrazide (PAH) Reverse Osmosis (RO) Membranes for Removal of Phenol from Phenol Water-Mixtures. *J. Polym. Mater.* 22, 313–319.
- Greben, H. A., Baloyi, L. J., and Venter, S. N. (2007). Grass Cellulose as Cost-Effective Energy Source for Biological Sulphate Removal. *Water SA* 33, 729–733. doi:10.4314/wsa.v33i5.184095
- Guo, W.-Y., Yuan, Q., Huang, L.-Z., Zhang, W., Li, D.-D., Yao, C., et al. (2022). Multifunctional Bacterial Cellulose-Based Organohydrogels with Long-Term Environmental Stability. *J. Colloid Interf. Sci.* 608, 820–829. doi:10.1016/j.jcis.2021.10.057
- Guo, X., and Chen, F. (2005). Removal of Arsenic by Bead Cellulose Loaded with Iron Oxyhydroxide from Groundwater. *Environ. Sci. Technol.* 39, 6808–6818. doi:10.1021/es048080k
- Guo, X., Du, Y., Chen, F., Park, H.-S., and Xie, Y. (2007). Mechanism of Removal of Arsenic by Bead Cellulose Loaded with Iron Oxyhydroxide (β -FeOOH): EXAFS Study. *J. Coll. Interf. Sci.* 314, 427–433. doi:10.1016/j.jcis.2007.05.071
- Güçlü, G., Gürdağ, G., and Özgümüş, S. (2003). Competitive Removal of Heavy Metal Ions by Cellulose Graft Copolymers. *J. Appl. Polym. Sci.* 90, 2034–2039. doi:10.1002/app.12728
- Hashem, A., Abou-Okeil, A., El-Shafie, A., and El-Sakhawy, M. (2006). Grafting of High α -Cellulose Pulp Extracted from Sunflower Stalks for Removal of Hg (II) from Aqueous Solution. *Polymer-Plastics Technol. Eng.* 45, 135–141. doi:10.1080/03602550500373790
- Hashem, A., Fletcher, A. J., Younis, H., Mauof, H., and Abou-Okeil, A. (2020). Adsorption of Pb(II) Ions from Contaminated Water by 1,2,3,4-butanetetracarboxylic Acid-Modified Microcrystalline Cellulose: Isotherms, Kinetics, and Thermodynamic Studies. *Int. J. Biol. Macromolecules* 164, 3193–3203. doi:10.1016/j.ijbiomac.2020.08.159
- Heppner, C., Åkesson, A., Amzal, B., Di Domenico, A., Dorne, J. L. C. M., Cristoph, E. H., et al. (2009). Risk Assessment of Cadmium in Food: Implications for Human Health. *Toxicol. Lett.* 189, S233. doi:10.1016/j.toxlet.2009.06.500
- Huang, C., Cai, B., Zhang, L., Zhang, C., and Pan, H. (2021a). Preparation of Iron-Based Metal-Organic Framework @cellulose Aerogel by *In Situ* Growth Method and its Application to Dye Adsorption. *J. Solid State. Chem.* 297, 122030. doi:10.1016/j.jssc.2021.122030
- Huang, C., Dong, H., Zhang, Z., Bian, H., and Yong, Q. (2020). Procuring the Nano-Scale Lignin in Prehydrolyzate as Ingredient to Prepare Cellulose Nanofibril Composite Film with Multiple Functions. *Cellulose* 27 (16), 9355–9370. doi:10.1007/s10570-020-03427-9
- Huang, C., Dong, J., Zhang, Y., Chai, S., Wang, X., Kang, S., et al. (2021b). Gold Nanoparticles-Loaded Polyvinylpyrrolidone/Ethylcellulose Coaxial Electrospun Nanofibers with Enhanced Osteogenic Capability for Bone Tissue Regeneration. *Mater. Des.* 212, 110240. doi:10.1016/j.matdes.2021.110240
- Huang, C., Tang, S., Zhang, W., Tao, Y., Lai, C., Li, X., et al. (2018). Unveiling the Structural Properties of Lignin-Carbohydrate Complexes in Bamboo Residues and its Functionality as Antioxidants and Immunostimulants. *ACS Sustain. Chem. Eng.* 6 (9), 12522–12531. doi:10.1021/acssuschemeng.8b03262
- Inukai, Y., Tanaka, Y., Matsuda, T., Mihara, N., Yamada, K., Nambu, N., et al. (2004). Removal of Boron(III) by N-Methylglucamine-Type Cellulose Derivatives with Higher Adsorption Rate. *Analytica Chim. Acta* 511, 261–265. doi:10.1016/j.aca.2004.01.054
- Islam, M., Mishra, P. C., and Patel, R. (2011). Arsenate Removal from Aqueous Solution by Cellulose-Carbonated Hydroxyapatite Nanocomposites. *J. Hazard. Mater.* 189, 755–763. doi:10.1016/j.jhazmat.2011.03.051
- Jarup, L., and Åkesson, A. (2009). Current Status of Cadmium as an Environmental Health Problem. *Toxicol. Appl. Pharmacol.* 238 (3), 201–208. doi:10.1016/j.taap.2009.04.020
- Kamel, S., Hassan, E. M., and El-Sakhawy, M. (2006). Preparation and Application of Acrylonitrile-Grafted Cyanoethyl Cellulose for the Removal of Copper (II) Ions. *J. Appl. Polym. Sci.* 100, 329–334. doi:10.1002/app.23317
- Karnitz, O., Gurgel, L. V. A., and Gil, L. F. (2010). Removal of Ca(II) and Mg(II) from Aqueous Single Metal Solutions by Mercerized Cellulose and Mercerized Sugarcane Bagasse Grafted with EDTA Dianhydride (EDTAD). *Carbohydr. Polym.* 79, 184–191. doi:10.1016/j.carbpol.2009.07.048
- Klemm, D., Heublein, B., Fink, H.-P., and Bohn, A. (2005). Cellulose: Fascinating Biopolymer and Sustainable Raw Material. *Angew. Chem. Int. Ed.* 44, 3358–3393. doi:10.1002/anie.200460587
- Kong, Q., Wang, X., and Lou, T. (2020). Preparation of Millimeter-Sized Chitosan/Carboxymethyl Cellulose Hollow Capsule and its Dye Adsorption Properties. *Carbohydr. Polym.* 244, 116481. doi:10.1016/j.carbpol.2020.116481
- Kumar, A. S. K., Kalidhasan, S., Rajesh, V., and Rajesh, N. (2012). Application of Cellulose-Clay Composite Biosorbent toward the Effective Adsorption and Removal of Chromium from Industrial Wastewater. *Ind. Eng. Chem. Res.* 51, 58–69. doi:10.1021/ie201349h
- Li, M., Zhang, S., Cui, S., Qin, K., Zhang, Y., Li, P., et al. (2021). Pre-Grafting Effect on Improving Adsorption Efficiency of Cellulose Based Biosorbent for Hg (II) Removal from Aqueous Solution. *Separat. Purif. Technol.* 277, 119493. doi:10.1016/j.seppur.2021.119493
- Li, S.-M., Jia, N., Ma, M.-G., Zhang, Z., Liu, Q.-H., and Sun, R.-C. (2011). Cellulose-Silver Nanocomposites: Microwave-Assisted Synthesis, Characterization, Their Thermal Stability, and Antimicrobial Property. *Carbohydr. Polym.* 86, 441–447. doi:10.1016/j.carbpol.2011.04.060
- Li, X., Tang, Y., Cao, X., Lu, D., Luo, F., and Shao, W. (2008). Preparation and Evaluation of Orange Peel Cellulose Adsorbents for Effective Removal of Cadmium, Zinc, Cobalt and Nickel. *Colloids Surf. A: Physicochemical Eng. Aspects* 317, 512–521. doi:10.1016/j.colsurfa.2007.11.031
- Lian, Z., Li, Y., Xian, H., Ouyang, X.-k., Lu, Y., Peng, X., et al. (2020). EDTA-Functionalized Magnetic Chitosan Oligosaccharide and Carboxymethyl Cellulose Nanocomposite: Synthesis, Characterization, and Pb(II) Adsorption Performance. *Int. J. Biol. Macromolecules* 165, 591–600. doi:10.1016/j.ijbiomac.2020.09.156
- Lima, I. S., Lazarin, A. M., and Airoidi, C. (2005). Favorable Chitosan/Cellulose Film Combinations for Copper Removal from Aqueous Solutions. *Int. J. Biol. Macromolecules* 36, 79–83. doi:10.1016/j.ijbiomac.2005.04.001
- Liu, C., and Bai, R. (2006). Adsorptive Removal of Copper Ions with Highly Porous Chitosan/Cellulose Acetate Blend Hollow Fiber Membranes. *J. Membr. Sci.* 284, 313–322. doi:10.1016/j.memsci.2006.07.045
- Liu, M., Zhang, H., Zhang, X., Deng, Y., Liu, W., and Zhan, H. (2001). Removal and Recovery of Chromium (III) from Aqueous Solutions by a Spheroidal Cellulose Adsorbent. *Water Environm. Res.* 73, 322–328. doi:10.2175/106143001x139344
- Liu, S., Du, X.-L., Ma, C., Ji, X.-X., Ma, M.-G., and Li, J.-F. (2019). Synthesis of Magnetic Carbon/Iron Oxide Nanocomposites in Ethylene Glycol/water Mixed Solvents and Their Highly Adsorption Performance. *Sci. Adv. Mater.* 11, 33–40. doi:10.1166/sam.2019.3349
- Liu, T., Wang, Z., Wang, X., Yang, G., and Liu, Y. (2021a). Adsorption-Photocatalysis Performance of Polyaniline/Dicarboxyl Acid Cellulose@graphene Oxide for Dye Removal. *Int. J. Biolog. Macromol.* 182, 492–501. doi:10.1016/j.ijbiomac.2021.04.038
- Liu, Y.-J., Cao, W.-T., Ma, M.-G., and Wan, P. (2017). Ultrasensitive Wearable Soft Strain Sensors of Conductive, Self-Healing, and Elastic Hydrogels with Synergistic "Soft and Hard" Hybrid Networks. *ACS Appl. Mater. Inter.* 9, 25559–25570. doi:10.1021/acsaami.7b07639
- Liu, Y.-J., Liu, S., Li, Z.-W., Ma, M.-G., and Wang, B. (2018). Microwave Synthetic Mesoporous Carbon Sponge as an Efficient Adsorbent for Cr(VI) Removal. *RSC Adv.* 8, 7892–7898. doi:10.1039/c8ra00012c
- Liu, Y., Nie, P., and Yu, F. (2021b). Enhanced Adsorption of Sulfonamides by a Novel Carboxymethyl Cellulose and Chitosan-Based Composite with

- Sulfonated Graphene Oxide. *Bioresour. Technol.* 320, 124373. doi:10.1016/j.biortech.2020.124373
- Lü, L., Lu, D., Chen, L., and Luo, F. (2010). Removal of Cd (II) by Modified Lawn Grass Cellulose Adsorbent. *Desalination* 259, 120–130. doi:10.1016/j.desal.2010.04.022
- Ma, C., Cao, W. T., Zhang, W., Ma, M. G., Sun, W. M., Zhang, J., et al. (2021). Wearable, Ultrathin and Transparent Bacterial Celluloses/MXene Film with Janus Structure and Excellent Mechanical Property for Electromagnetic Interference Shielding. *Chem. Eng. J.* 403, 126438. doi:10.1016/j.cej.2020.126438
- Mai, T., Wang, P.-L., Yuan, Q., Ma, C., and Ma, M.-G. (2021). *In Situ* Anchoring Zn-Doped ZIF-67 on Carboxymethylated Bacterial Cellulose for Effective Indigo Carmine Capture. *Nanoscale* 13, 18210–18217. doi:10.1039/d1nr05388d
- Maliyekkal, S. M., Lisha, K. P., and Pradeep, T. (2010). A Novel Cellulose-Manganese Oxide Hybrid Material by *In Situ* Soft Chemical Synthesis and its Application for the Removal of Pb(II) from Water. *J. Hazard. Mater.* 181, 986–995. doi:10.1016/j.jhazmat.2010.05.112
- Mansfield, S. D., Mooney, C., and Saddler, J. N. (1999). Substrate and Enzyme Characteristics that Limit Cellulose Hydrolysis. *Biotechnol. Prog.* 15, 804–816. doi:10.1021/bp9900864
- Meneses, I. P., Novaes, S. D., Dezotti, R. S., Oliveira, P. V., and Petri, D. F. S. (2022). CTAB-Modified Carboxymethyl Cellulose/Bagasse Cryogels for the Efficient Removal of Bisphenol A, Methylene Blue and Cr(VI) Ions: Batch and Column Adsorption Studies. *J. Hazard. Mater.* 421, 126804. doi:10.1016/j.jhazmat.2021.126804
- Menon, V., and Rao, M. (2012). Trends in Bioconversion of Lignocellulose: Biofuels, Platform Chemicals & Biorefinery Concept. *Prog. Energ. Combustion Sci.* 38 (4), 522–550. doi:10.1016/j.pecs.2012.02.002
- Mohan, D., and Pittman, C. U. (2006). Activated Carbons and Low Cost Adsorbents for Remediation of Tri- and Hexavalent Chromium from Water. *J. Hazard. Mater.* 137 (2), 762–811. doi:10.1016/j.jhazmat.2006.06.060
- Musyoka, S. M., Ngila, J. C., Moodley, B., Petrik, L., and Kindness, A. (2011). Synthesis, Characterization, and Adsorption Kinetic Studies of Ethylenediamine Modified Cellulose for Removal of Cd and Pb. *Anal. Lett.* 44, 1925–1936. doi:10.1080/00032719.2010.539736
- Nata, I. F., Sureshkumar, M., and Lee, C.-K. (2011). One-pot Preparation of Amine-Rich Magnetite/Bacterial Cellulose Nanocomposite and its Application for Arsenate Removal. *RSC Adv.* 1, 625–631. doi:10.1039/c1ra00153a
- Norkus, E., Vaičiūnienė, J., and Vuorinen, T. (2006). Removal of Transition Metals from Alkaline Suspensions of Cellulose Pulp Using CDTA as Chelating Agent. *Carbohydr. Polym.* 66, 316–320. doi:10.1016/j.carbpol.2006.03.018
- Nzediegwu, E., and Dumont, M.-J. (2021). Chemo-Catalytic Transformation of Cellulose and Cellulosic-Derived Waste Materials into Platform Chemicals. *Waste Biomass Valor.* 12 (6), 2825–2851. doi:10.1007/s12649-020-01179-y
- O'Connell, D. W., Birkinshaw, C., and O'Dwyer, T. F. (2008). Heavy Metal Adsorbents Prepared from the Modification of Cellulose: A Review. *Bioresour. Technol.* 99, 6709–6724. doi:10.1016/j.biortech.2008.01.036
- O'Connell, D. W., Birkinshaw, C., and O'Dwyer, T. F. (2006a). A Modified Cellulose Adsorbent for the Removal of Nickel (II) from Aqueous Solutions. *J. Chem. Technol. Biotechnol.* 81, 1820–1828. doi:10.1002/jctb.1609
- O'Connell, D. W., Birkinshaw, C., and O'Dwyer, T. F. (2006b). Removal of Lead (II) Ions from Aqueous Solutions Using a Modified Cellulose Adsorbent. *Adsorpt. Sci. Technol.* 24, 337–348. doi:10.1260/026361706779319670
- Okieimen, F. E., Sogbaike, C. E., and Ebhoaye, J. E. (2005). Removal of Cadmium and Copper Ions from Aqueous Solution with Cellulose Graft Copolymers. *Separat. Purif. Technol.* 44, 85–89. doi:10.1016/j.seppur.2004.11.003
- Olbricht, C. J. (1996). Extracorporeal Removal of Lipids by Dextran Sulfate Cellulose Adsorption. *Artif. Organs* 20 (4), 332–335. doi:10.1111/j.1525-1594.1996.tb04454.x
- Park, S.-H., Shin, S. S., Park, C. H., Jeon, S., Gwon, J., Lee, S.-Y., et al. (2020). Poly(acryloyl Hydrazide)-Grafted Cellulose Nanocrystal Adsorbents with an Excellent Cr(VI) Adsorption Capacity. *J. Hazard. Mater.* 394, 122512. doi:10.1016/j.jhazmat.2020.122512
- Qu, J., Tian, X., Jiang, Z., Cao, B., Akindolie, M. S., Hu, Q., et al. (2020). Multi-Component Adsorption of Pb(II), Cd(II) and Ni(II) onto Microwavefunctionalized Cellulose: Kinetics, Isotherms, Thermodynamics, Mechanisms and Application for Electroprecipitating Wastewater Purification. *J. Hazard. Mater.* 387, 121718. doi:10.1016/j.jhazmat.2019.121718
- Rahmatika, A. M., Goi, Y., Kitamura, T., Morita, Y., Iskandar, F., and Ogi, T. (2020). Silica-Supported Carboxylated Cellulose Nanofibers for Effective Lysozyme Adsorption: Effect of Macropore Size. *Adv. Powder Technol.* 31, 2932–2941. doi:10.1016/j.apt.2020.05.021
- Rong, N., Chen, C., Ouyang, K., Zhang, K., Wang, X., and Xu, Z. (2021). Adsorption Characteristics of Directional Cellulose Nanofiber/Chitosan/Montmorillonite Aerogel as Adsorbent for Wastewater Treatment. *Separat. Purif. Technol.* 274, 119120. doi:10.1016/j.seppur.2021.119120
- Sakata, M., Todokoro, M., and Kunitake, M. (2007). Pore-Size Controlled and Polycation-Immobilized Cellulose Spherical Particles for Removal of Endotoxin. *Kobunshi Ronbunshu* 64, 821–829. doi:10.1295/koron.64.821
- Schulzeck, P., Olbricht, C. J., and Koch, K. M. (1992). Long-Term Experience with Extracorporeal Low-Density Lipoprotein Cholesterol Removal by Dextran Sulfate Cellulose Adsorption. *Clin. Investig.* 70, 99–104. doi:10.1007/BF00227348
- Sepehvand, S., Jonoobi, M., Ashori, A., Gauvin, F., Brouwers, H. J. H., Oksman, K., et al. (2020). A Promising Process to Modify Cellulose Nanofibers for Carbon Dioxide (CO₂) Adsorption. *Carbohydr. Polym.* 230, 115571. doi:10.1016/j.carbpol.2019.115571
- Shao, D., Jiang, Z., Wang, X., Li, J., and Meng, Y. (2009). Plasma Induced Grafting Carboxymethyl Cellulose on Multiwalled Carbon Nanotubes for the Removal of UO₂²⁺ from Aqueous Solution. *J. Phys. Chem. B* 113, 860–864. doi:10.1021/jp8091094
- Shukla, S., and Pai, R. S. (2005). Removal of Pb(II) from Solution Using Cellulose-Containing Materials. *J. Chem. Technol. Biotechnol.* 80, 176–183. doi:10.1002/jctb.1176
- Takagai, Y., Shibata, A., Kiyokawa, S., and Takase, T. (2011). Synthesis and Evaluation of Different Thio-Modified Cellulose Resins for the Removal of Mercury (II) Ion from Highly Acidic Aqueous Solutions. *J. Colloid Interf. Sci.* 353, 593–597. doi:10.1016/j.jcis.2010.09.070
- Tiwari, A., Dewangan, T., and Bajpai, A. K. (2008). Removal of Toxic as (V) Ions by Adsorption onto Alginate and Carboxymethyl Cellulose Beads. *Jnl Chin. Chem. Soc.* 55, 952–961. doi:10.1002/jccs.200800142
- Volesky, B., and Holan, Z. R. (1995). Biosorption of Heavy Metals. *Biotechnol. Prog.* 11 (3), 235–250. doi:10.1021/bp00033a001
- Wang, P.-L., Ma, C., Yuan, Q., Mai, T., and Ma, M.-G. (2022). Novel Ti₃C₂T_x MXene Wrapped Wood Sponges for Fast Cleanup of Crude Oil Spills by Outstanding Joule Heating and Photothermal Effect. *J. Coll. Interf. Sci.* 606, 971–982. doi:10.1016/j.jcis.2021.08.092
- Wang, P., Yin, B., Dong, H., Zhang, Y., Zhang, Y., Chen, R., et al. (2020a). Coupling Biocompatible Au Nanoclusters and Cellulose Nanofibrils to Prepare the Antibacterial Nanocomposite Films. *Front. Bioeng. Biotechnol.* 8, 986. doi:10.3389/fbioe.2020.00986
- Wang, R., Deng, L., Fan, X., Li, K., Lu, H., and Li, W. (2021a). Removal of Heavy Metal Ion Co²⁺ from Wastewater via Adsorption Method Using Microcrystalline Cellulose-Magnesium Hydroxide. *Int. J. Biol. Macromol.* 189, 607–617. doi:10.1016/j.ijbiomac.2021.08.156
- Wang, S., Guo, X., Wang, L., Wang, W., and Yu, Y. (2006). Effect of PEG Spacer on Cellulose Adsorbent for the Removal of Low Density Lipoprotein-Cholesterol. *Artif. Cell Blood Substitutes, Biotechnol.* 34, 101–112. doi:10.1080/10731190500430222
- Wang, S. Q., Yu, Y. T., Cui, T., and Cheng, Y. (2002). Cellulose Amphiphilic Adsorbent for the Removal of Low Density Lipoprotein. Artificial Cells, Blood Substitutes. *Immobilization Biotechnol.* 30, 285–292. doi:10.1081/BIO-120006119
- Wang, X., Tang, S., Chai, S., Wang, P., Qin, J., Pei, W., et al. (2021b). Preparing Printable Bacterial Cellulose Based Gelatin Gel to Promote *In Vivo* Bone Regeneration. *Carbohydr. Polym.* 270, 118342. doi:10.1016/j.carbpol.2021.118342
- Wang, Y., Li, C., Zheng, Y., Xie, Y., Qiao, K., He, W., et al. (2021c). Plant Protein Modified Natural Cellulose with Multiple Adsorption Effects Used for Bilirubin Removal. *Int. J. Biol. Macromolecules* 166, 179–189. doi:10.1016/j.ijbiomac.2020.10.131
- Wang, Z., Song, L., Wang, Y., Zhang, X.-F., Hao, D., Feng, Y., et al. (2019). Lightweight UiO-66/Cellulose Aerogels Constructed through Self-Crosslinking Strategy for Adsorption Applications. *Chem. Eng. J.* 371, 138–144. doi:10.1016/j.cej.2019.04.022

- Wang, Z., Yao, M., Wang, X., Li, S., Liu, Y., and Yang, G. (2020b). Influence of Reaction media on Synthesis of Dialdehyde Cellulose/GO Composites and Their Adsorption Performances on Heavy Metals. *Carbohydr. Polym.* 232, 115781. doi:10.1016/j.carbpol.2019.115781
- Weber, C., Henne, B., Loth, F., Schoenhofen, M., and Falkenhagen, D. (1995). Development of Cationically Modified Cellulose Adsorbents for the Removal of Endotoxins. *ASAIO J.* 41, M430–M434. doi:10.1097/00002480-199507000-00046
- Wen, D., Dong, Z., Ao, Y., Xie, K., Zhai, M., and Zhao, L. (2021). Aminotriazole Isomers Modified Cellulose Microspheres for Selective Adsorption of U(VI): Performance and Mechanism Investigation. *Carbohydr. Polym.* 257, 117666. doi:10.1016/j.carbpol.2021.117666
- Wittmar, A. S. M., Klug, J., and Ulbricht, M. (2020). Cellulose/Chitosan Porous Spheres Prepared from 1-Butyl-3-Methylimidazolium Acetate/Dimethylformamide Solutions for Cu²⁺ Adsorption. *Carbohydr. Polym.* 237, 116135. doi:10.1016/j.carbpol.2020.116135
- Wu, L., and Ritchie, S. M. C. (2006). Removal of Trichloroethylene from Water by Cellulose Acetate Supported Bimetallic Ni/Fe Nanoparticles. *Chemosphere* 63, 285–292. doi:10.1016/j.chemosphere.2005.07.021
- Xie, K., Jing, L., Zhao, W., and Zhang, Y. (2011a). Adsorption Removal of Cu²⁺ and Ni²⁺ from Waste Water Using Nano-Cellulose Hybrids Containing Reactive Polyhedral Oligomeric Silsesquioxanes. *J. Appl. Polym. Sci.* 122, 2864–2868. doi:10.1002/app.34411
- Xie, K., Zhao, W., and He, X. (2011b). Adsorption Properties of Nano-Cellulose Hybrid Containing Polyhedral Oligomeric Silsesquioxane and Removal of Reactive Dyes from Aqueous Solution. *Carbohydr. Polym.* 83, 1516–1520. doi:10.1016/j.carbpol.2010.09.064
- Xu, Z., Bae, W., Mulchandani, A., Mehra, R. K., and Chen, W. (2002). Heavy Metal Removal by Novel CBD-EC20 Sorbents Immobilized on Cellulose. *Biomacromolecules* 3, 462–465. doi:10.1021/bm015631f
- Yagub, M. T., Sen, T. K., Afroze, S., and Ang, H. M. (2014). Dye and its Removal from Aqueous Solution by Adsorption: A Review. *Adv. Colloid Interf. Sci.* 209, 172–184. doi:10.1016/j.cis.2014.04.002
- Yan, L., Shuai, Q., Gong, X., Gu, Q., and Yu, H. (2009). Synthesis of Microporous Cationic Hydrogel of Hydroxypropyl Cellulose (HPC) and its Application on Anionic Dye Removal. *Clean. Soil Air Water* 37, 392–398. doi:10.1002/clen.200900006
- Yang, H.-R., Li, S.-S., An, Q.-D., Zhai, S.-R., Xiao, Z.-Y., and Zhang, L.-P. (2021). Facile Transformation of Carboxymethyl Cellulose Beads into Hollow Composites for Dye Adsorption. *Int. J. Biol. Macromolecules* 190, 919–926. doi:10.1016/j.ijbiomac.2021.08.229
- Yang, S., Fu, S., Liu, H., Zhou, Y., and Li, X. (2011). Hydrogel Beads Based on Carboxymethyl Cellulose for Removal Heavy Metal Ions. *J. Appl. Polym. Sci.* 119, 1204–1210. doi:10.1002/app.32822
- Yang, X., Cao, Y.-M., Wang, R., and Yuan, Q. (2007). Study on Highly Hydrophilic Cellulose Hollow Fiber Membrane Contactors for Thiol Sulfur Removal. *J. Membr. Sci.* 305, 247–256. doi:10.1016/j.memsci.2007.08.020
- Yi, Q., Lu, S., Fan, Y., Cheng, D., Wang, X., Cheng, S., et al. (2022). Preparation and Adsorption Performance of Cellulose Nanofibrils/polyvinyl Alcohol Composite Gel Spheres with Millimeter Size. *Carbohydr. Polym.* 277, 118850. doi:10.1016/j.carbpol.2021.118850
- You, X., Wang, R., Zhu, Y., Sui, W., and Cheng, D. (2021). Comparison of Adsorption Properties of a Cellulose-Rich Modified rice Husk for the Removal of Methylene Blue and Aluminum (III) from Their Aqueous Solution. *Ind. Crops Prod.* 170, 113687. doi:10.1016/j.indcrop.2021.113687
- Yu, D., Wang, Y., Wu, M., Zhang, L., Wang, L., and Ni, H. (2019). Surface Functionalization of Cellulose with Hyperbranched Polyamide for Efficient Adsorption of Organic Dyes and Heavy Metals. *J. Clean. Prod.* 232, 774–783. doi:10.1016/j.jclepro.2019.06.024
- Yu, H. F., Fu, G. Q., Liu, L., and He, B. L. (2006). Facile Synthesis and Adsorption Properties of Phosphonated Cellulose Beads for Selective Removal of Low-Density Lipoprotein. *Chin. Chem. Lett.* 17, 1193–1196.
- Zaman, A., Orasugh, J. T., Banerjee, P., Dutta, S., Ali, M. S., Das, D., et al. (2020). Facile One-Pot *In-Situ* Synthesis of Novel Graphene Oxide-Cellulose Nanocomposite for Enhanced Azo Dye Adsorption at Optimized Conditions. *Carbohydr. Polym.* 246, 116661. doi:10.1016/j.carbpol.2020.116661
- Zhang, M., and Akbulut, M. (2011). Adsorption, Desorption, and Removal of Polymeric Nanomedicine on and from Cellulose Surfaces: Effect of Size. *Langmuir* 27, 12550–12559. doi:10.1021/la202287k
- Zhang, W., Li, C., Liang, M., Geng, Y., and Lu, C. (2010). Preparation of Carboxylate-Functionalized Cellulose via Solvent-Free Mechanochemistry and its Characterization as a Biosorbent for Removal of Pb²⁺ from Aqueous Solution. *J. Hazard. Mater.* 181, 468–473. doi:10.1016/j.jhazmat.2010.05.036
- Zhang, W., Wang, X.-c., Wang, J.-j., and Zhang, L.-l. (2019). Drugs Adsorption and Release Behavior of Collagen/Bacterial Cellulose Porous Microspheres. *Int. J. Biol. Macromolecules* 140, 196–205. doi:10.1016/j.ijbiomac.2019.08.139
- Zhao, B., Jiang, H., Lin, Z., Xu, S., Xie, J., and Zhang, A. (2019). Preparation of Acrylamide/Acrylic Acid Cellulose Hydrogels for the Adsorption of Heavy Metal Ions. *Carbohydr. Polym.* 224, 115022. doi:10.1016/j.carbpol.2019.115022
- Zhao, L., Li, S., Liang, C., Qiao, L., and Du, K. (2021). High-Strength and Low-Crystallinity Cellulose/Agarose Composite Microspheres: Fabrication, Characterization and Protein Adsorption. *Biochem. Eng. J.* 166, 107826. doi:10.1016/j.bej.2020.107826
- Zhao, Y., Huang, M., Wu, W., and Jin, W. (2009). Synthesis of the Cotton Cellulose Based Fe(III)-Loaded Adsorbent for Arsenic(V) Removal from Drinking Water. *Desalination* 249, 1006–1011. doi:10.1016/j.desal.2009.09.015
- Zhao, Y., Li, X., Liu, L., and Chen, F. (2008). Fluoride Removal by Fe(III)-Loaded Ligand Exchange Cotton Cellulose Adsorbent from Drinking Water. *Carbohydr. Polym.* 72, 144–150. doi:10.1016/j.carbpol.2007.07.038
- Zheng, X., Zhang, Y., Bian, T., Zhang, Y., Li, Z., and Pan, J. (2020). Oxidized Carbon Materials Cooperative Construct Ionic Imprinted Cellulose Nanocrystals Films for Efficient Adsorption of Dy(III). *Chem. Eng. J.* 381, 122669. doi:10.1016/j.cej.2019.122669
- Zhu, H.-Y., Fu, Y.-Q., Jiang, R., Jiang, J.-H., Xiao, L., Zeng, G.-M., et al. (2011). Adsorption Removal of Congo Red onto Magnetic cellulose/Fe₃O₄/activated Carbon Composite: Equilibrium, Kinetic and Thermodynamic Studies. *Chem. Eng. J.* 173, 494–502. doi:10.1016/j.cej.2011.08.020

Conflict of Interest: The authors declare that the research was conducted in the absence of any commercial or financial relationships that could be construed as a potential conflict of interest.

Publisher's Note: All claims expressed in this article are solely those of the authors and do not necessarily represent those of their affiliated organizations, or those of the publisher, the editors and the reviewers. Any product that may be evaluated in this article, or claim that may be made by its manufacturer, is not guaranteed or endorsed by the publisher.

Copyright © 2022 Shi, Wang, Lang, Zhou and Ma. This is an open-access article distributed under the terms of the Creative Commons Attribution License (CC BY). The use, distribution or reproduction in other forums is permitted, provided the original author(s) and the copyright owner(s) are credited and that the original publication in this journal is cited, in accordance with accepted academic practice. No use, distribution or reproduction is permitted which does not comply with these terms.



Sustainable Production of Bioethanol Using Levulinic Acid Pretreated Sawdust

Ali Nawaz^{1,2*}, Rong Huang^{1†}, Farah Junaid^{2†}, Yiwei Feng³, Ikram Ul Haq², Hamid Mukhtar² and Kankan Jiang^{1*}

¹School of Basic Medical Sciences and Forensic Medicine, Hangzhou Medical College, Hangzhou, China, ²Institute of Industrial Biotechnology, Government College University, Lahore, Pakistan, ³School of Clinical Medicine, Hangzhou Medical College, Hangzhou, China

OPEN ACCESS

Edited by:

Caoxing Huang,
Nanjing Forestry University, China

Reviewed by:

Xiaojun Shen,
Dalian Institute of Chemical Physics
(CAS), China
Mahwish Aftab,
Lahore College for Women University,
Pakistan

*Correspondence:

Ali Nawaz
ali.nawaz@gcu.edu.pk
Kankan Jiang
jiangkankan@126.com

[†]These authors have contributed
equally to this work

Specialty section:

This article was submitted to
Bioprocess Engineering,
a section of the journal
Frontiers in Bioengineering and
Biotechnology

Received: 06 May 2022

Accepted: 20 May 2022

Published: 30 June 2022

Citation:

Nawaz A, Huang R, Junaid F, Feng Y,
Haq IU, Mukhtar H and Jiang K (2022)
Sustainable Production of Bioethanol
Using Levulinic Acid
Pretreated Sawdust.
Front. Bioeng. Biotechnol. 10:937838.
doi: 10.3389/fbioe.2022.937838

The sustainability and economic viability of the bioethanol production process from lignocellulosic biomass depend on efficient and effective pretreatment of biomass. Traditional pretreatment strategies implicating the use of mineral acids, alkalis, and organic solvents release toxic effluents and the formation of inhibitory compounds posing detrimental effects on the environment and interfering with the enzymatic saccharification process, respectively. Ionic liquids (ILs) as green solvents were used to overcome this issue, but the deep eutectic solvent as an emerging class of ionic liquids performed better in terms of making the process environmentally and economically viable. The green solvent-based pretreatment strategy applied in the current research was levulinic, acid-based natural deep eutectic solvent (NADES). Three different hydrogen bond acceptors (HBAs)—acetamide, betaine, and choline chloride—in combination with levulinic acid as hydrogen bond donor (HBD) in (HBD: HBA) molar ratio 2:1, were screened for biomass pretreatment. The best deep eutectic solvent was levulinic acid: choline chloride in an optimized molar ratio of 1:0.5, resulting in 91% delignification. The physicochemical parametric optimization of saccharification exhibited maximum enzymatic hydrolysis of 25.87% with 125 mg of pretreated sawdust *via* simultaneous addition of three thermostable cellulases [i.e., endo-1,4- β -D-glucanase (240 U), exo-1,4- β -D-glucanase (180 U), and β -glucosidase (320 U)] for 5 h of incubation at 75°C. The reducing sugar slurry obtained from the saccharified biomass was then added to a fermentation medium for bioethanol production, and a maximum of 11.82% of production was obtained at 30°C, 72 h, and 180 rpm using a 2.5% 24 h old *Saccharomyces cerevisiae* seed culture. The current study revealed that the levulinic-based deep eutectic solvent exhibited remarkable delignification, which led to the efficient enzymatic hydrolysis of sawdust and hence bioethanol production. Furthermore, it will prospect new avenues in bioethanol production using a deep eutectic solvent. Deep eutectic solvent overcame the issues posed by ionic liquids: toxicity, expensive and complex preparation, and non-biodegradability.

Keywords: deep eutectic solvent, enzymatic saccharification, green biorefinery, levulinic acid, ionic liquids, bioethanol

1 INTRODUCTION

Depletion of fossil fuel reserves and increased emission of greenhouse gases leading to climatic changes and global warming have necessitated the notion of alternative bio-based fuel to be practically implemented in the near future. The key step in shifting from a non-renewable to a renewable energy source, which is a shift from petroleum-based to bio-based fuels, is the driving phenomena of biorefineries (Cunha et al., 2020). Biorefinery is defined as the equivalent renewable of a petroleum refinery, the difference being in the starting raw material. Biorefinery converts the raw material into a wide variety of chemicals and energy carriers, which can lead to the development of the circular economy. The biorefinery concept is based on lignocellulosic materials, which produce bio-based products that are recoverable (to a certain degree) and recyclable. Biorefineries have made a fine amalgam of green chemistry, keeping in view the environmental impact of fuel. This amalgam aims to limit or minimize the use and generation of hazardous chemicals (Capolupo and Faraco, 2016). Therefore, sustainable bioethanol production can be achieved using green solvents that are deep eutectic solvents, so the end product of green biorefineries is environmentally benign and recyclable and produces minimum waste.

Lignocellulosic biomass is an inexhaustible biomaterial, mainly composed of lignin, hemicellulose, cellulose, and extractives in different proportions (Huang et al., 2022a). Sawdust from the sawmill industry is a potential, cost-efficient raw material to produce bioethanol. The use of sawdust for biofuel production promotes the local valorization of wood waste, establishing the concept of forest biorefinery (Alio et al., 2021). From the bioethanol production perspective, lignin is a barrier to enzymatic hydrolysis because it irreversibly binds to the cellulases rendering enzyme adsorption on cellulose (Takada et al., 2020; Huang et al., 2022b). Pretreatment is employed to disintegrate the cross-linked biomass fractions, enhancing the biodegradability and ease of access of hemicellulose and cellulose for enzymatic hydrolysis (Robak and Balcerek, 2020).

The choice of an appropriate pretreatment method is critical in terms of determining the sustenance and the economic viability of a project. It is evident from the literature that the previous pretreatment techniques were more concentrated on the techno-economic viability than on the sustenance of the environment (Vieira et al., 2020). The green solvent used in this research is deep eutectic solvent (DES), acknowledged as a class of ionic liquids (ILs). Deep eutectic solvents are defined as a group of large, non-symmetrical ions with low lattice energy and hence low melting points (Smith et al., 2014). They are prepared *via* complexation or a combination of hydrogen bond donors (HBDs) (alcohols, amides, amines, or carboxylic acids) and quaternary ammonium salts as hydrogen bond acceptors (HBA) at a moderate temperature of 60°C–80°C in a certain ratio to form a eutectic mixture (Satlewal et al., 2018).

Deep eutectic solvents and ionic liquids are alike in their physical properties but have varying chemical properties. Both exhibits low or negligible vapor pressure, non-flammability, and a wide liquid range. Ionic liquids have wide electrochemical

windows and high dissolution ability, used in biomass dissolution and conversion as a solvent and a catalyst (Smith et al., 2014; Chen and Mu, 2019). The drawbacks that hold back ILs as a green solvent are their complex, expensive preparation, toxicity, and non-biodegradability. On the contrary, these deep eutectic solvents are cost-effective, easily prepared, potentially biodegradable, innocuous, and safe (Zhang et al., 2020). Deep eutectic solvents fulfill the twelve principles of green chemistry, which entails their use in the sustainable pretreatment of biomass. They have high air stability, thermal stability, low volatility, non-inflammability, and high purity (Xu et al., 2020).

The molar ratio of HBD and HBA is closely related in the context of their potential to remove lignin and hemicellulose or their dissolution ability of chemical components, that is, lignin and cellulose, subsequently influencing the saccharification process/enzymatic hydrolysis of the pretreated substrate (Xu et al., 2020). Saccharification of pretreated lignocellulosic biomass is another crucial step in the bioconversion of substrate into the desired end product, ethanol, *via* releasing fermentable sugars from crystalline cellulose and hemicellulose (Kucharska et al., 2020). Enzymatic saccharification/hydrolysis is usually carried out *via* cellulases and hemicellulases. Cellulases are commonly used to refer to the three enzymes that convert cellulose into glucose (fermentable monosaccharide): endocellulase, exocellulase, and glucosidase (Zhao et al., 2019). Different physicochemical parameters affect hydrolysis efficiency, such as incubation temperature, pH, agitation speed/rpm, incubation time, enzyme/substrate ratio, and particle size (Chavan and Gaikwad, 2021; Faizal et al., 2021).

Separate hydrolysis and fermentation (SHF) is the most studied technique in the bioethanol production process. This process enables independent optimization of the saccharification step for maximal sugar release and the fermentation step for ethanol production (Moodley and Gueguim Kana, 2019). Limitations of this strategy are inhibition of cellulases by cellobiose and glucose and the potential risk of contamination due to the prolonged duration of saccharification (Keshav et al., 2021).

Maugeri and Domı (2012) first prepared choline chloride: levulinic acid DES in equimolar concentration, but exploitation of DES for biomass pretreatment was first reported by Gunny et al. (2014). Several reports were available with choline chloride-based DES pretreatment of lignocellulosic biomass (Wang et al., 2020). However, reports regarding levulinic acid-based DES are infrequent (Ling et al., 2020). By considering the research gap, the current research work focuses on selecting HBA for levulinic acid-based DES pretreatment, optimization of the molar ratio (HBD:HBA), and physicochemical parametric optimization of saccharification and bioethanol production.

2 MATERIALS AND METHODS

2.1 Thermophilic Cellulases

The thermophilic cellulases, endo-1,4- β -glucanase (E.C. 3.2.1.4) of *Thermotoga naphthophila*, and exo-1,4- β -glucanase (E.C. 3.2.1.91) and β -1,4-glucosidase (E.C. 3.2.1.21) of *Thermotoga*

petrophila cloned in *Escherichia coli* were obtained from the project entitled “Production of Bioenergy From Plant Biomass” at the Institute of Industrial Biotechnology, GC University Lahore, Pakistan.

2.2 Substrate

Sawdust was acquired from the local furniture market of Lahore, Punjab, Pakistan. The biomass was washed, dried, and sieved with mesh size 400 to attain homogeneously sized particles.

2.3 DES Preparation and Pretreatment

Levulinic acid-based DES with three variable HBAs (i.e., acetamide, betaine, and choline chloride) was prepared at an initial molar ratio of 2:1 (HBD: HBA) in screw-capped reagent bottles and kept in a shaking water bath, 80°C, 120 rpm for 1–2 h till complete dissolution and appearance of clear solution (Ling et al., 2020). After selecting the appropriate HBA for DES, molar ratios of both HBA and HBD varied from 0.1 to 2.5 M.

Pretreatment was conducted for 1 g/100 ml of DES in a screw-capped reagent bottle at 121°C, 15 psi for 30 min. Upon pretreatment, the pretreated sample was separated from DES by filtration. The filtered pretreated biomass was washed to neutral pH to remove all the residual DES.

2.4 Lignocellulosic Content Estimation

The lignin content of untreated and pretreated biomass was estimated using the following equation (Irfan et al., 2011):

$$\text{Lignin (\%)} = \frac{\text{Lignin weight (g)}}{\text{Biomass (g)}} \times 100.$$

The percentage delignification was calculated using the following formula:

$$\text{Delignification (\%)} = \frac{L1 - L2}{L1} \times 100,$$

L1 = lignin content of control (untreated substrate).

L2 = lignin content of the pretreated substrate.

Cellulosic content on a dry matter basis was estimated using the method of Gopal and Ranjhan (1980) using the following equation:

$$\text{Cellulose (DM basis)} = \frac{\text{Weight of digested material} - \text{Weight of ash}}{\text{Weight of substrate (DM basis)}} \times 100.$$

The hemicellulosic content of the pretreated and untreated substrate was determined by NDF and ADF treatment (Van Soest and Roberston, 1979):

$$\% \text{ Hemicellulose} = \text{NDF} - \text{ADF}.$$

2.5 Enzymatic Saccharification

The saccharification of pretreated sawdust was conducted by taking 100 mg of the pretreated substrate in a screw-capped reagent bottle. Cellulases, endo-1,4-β-glucanase (90 U), exo-1,4-β-glucanase (80 U), and β-1,4-glucosidase (220 U) were taken in experimental and control (lacking substrate) reagent bottles, incubated at 85 in shaking water 50 rpm. After 2 h of

regular intervals, each cellulase was added. The samples were withdrawn at a regular interval of 1 h to estimate the release of reducing sugar *via* the DNS method of Miller (1959). The percentage saccharification was determined using the proposed equation of Vallander and Erikson (1987):

$$\% \text{ Saccharification} = \frac{R.S \times V \times F1}{M \times F2} \times 100.$$

2.6 Effect of Physicochemical Parameters on Saccharification

The physicochemical parameters optimized for saccharification were sequential/simultaneous addition of cellulases, incubation time (1–7 h), incubation temperature (70 °C –90°C), substrate concentration (50–200 mg), concentration of endo-1,4-β-glucanase (40–290 U), exo-1,4-β-glucanase (30–230 U), and β-glucosidase (120–370 U).

2.7 Preparation of Seed Inoculum for Ethanol Fermentation

The vegetative seed inoculum of *Saccharomyces cerevisiae* (IIB-56) acquired from the culture bank of the Institute of Industrial Biotechnology, GC University Lahore, Pakistan, was prepared by aseptically transferring dry (granulated) baker's yeast into a 50 ml medium containing 10 g glucose, 0.25 g yeast extract, and 0.15 g ammonium sulfate. The flask was incubated at 30 °C, 180 rpm for 24 h.

2.8 Submerged Fermentation for Ethanol Production

The submerged fermentation for ethanol production was carried out in a fermentation medium using the reducing sugar slurry (in place of glucose) obtained after optimization. The fermentation medium was inoculated with 2.5% of 24 h seed inoculum of *S. cerevisiae* aseptically, incubated at 30°C, 180 rpm for 72 h. The samples were harvested at regular intervals to estimate the ethanol content during fermentation (Yuan et al., 2011).

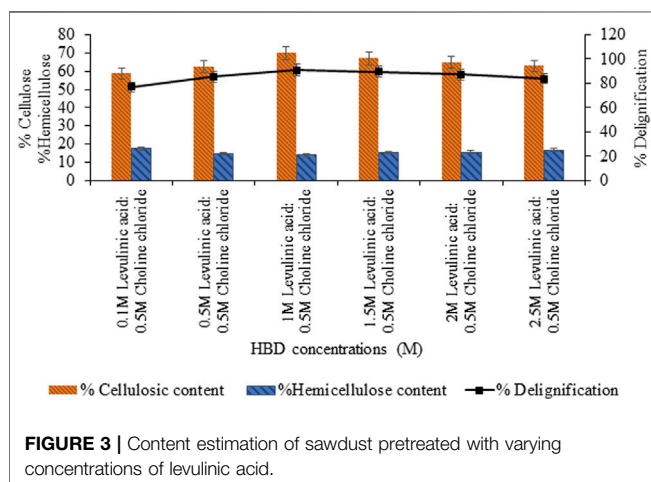
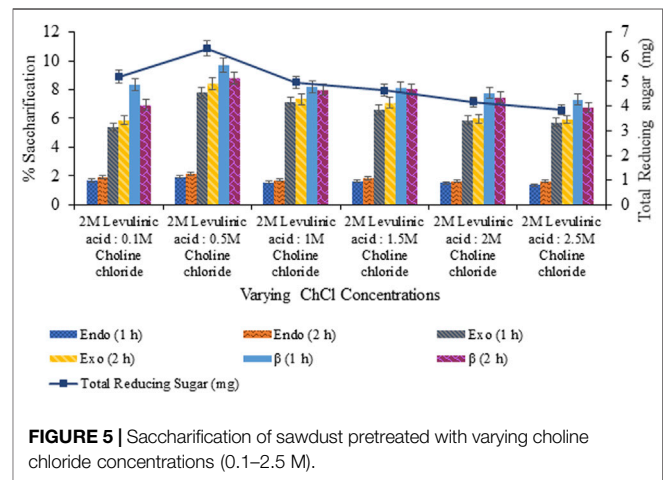
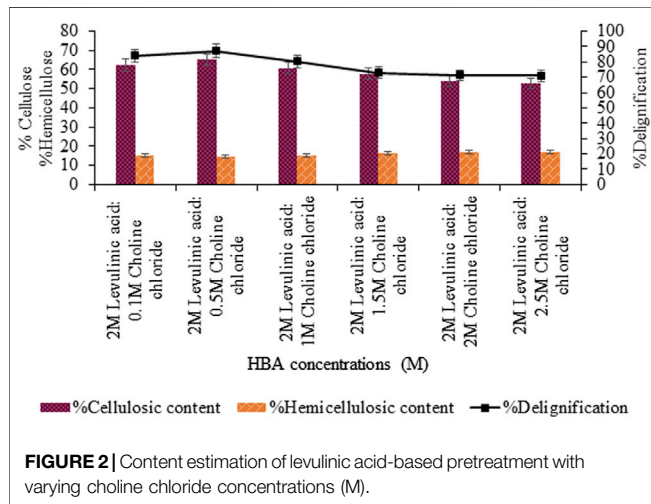
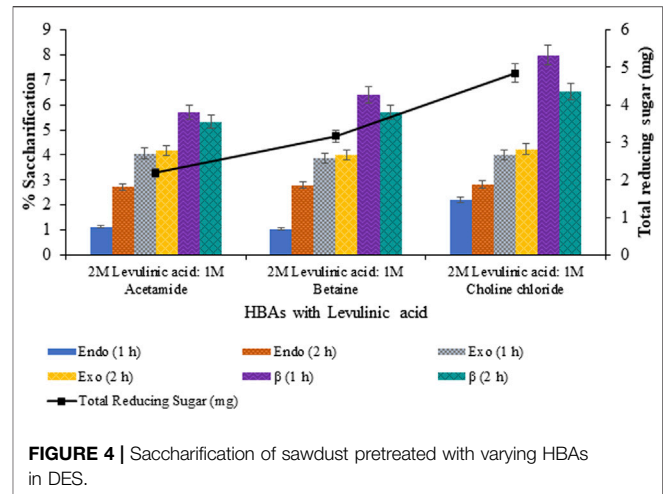
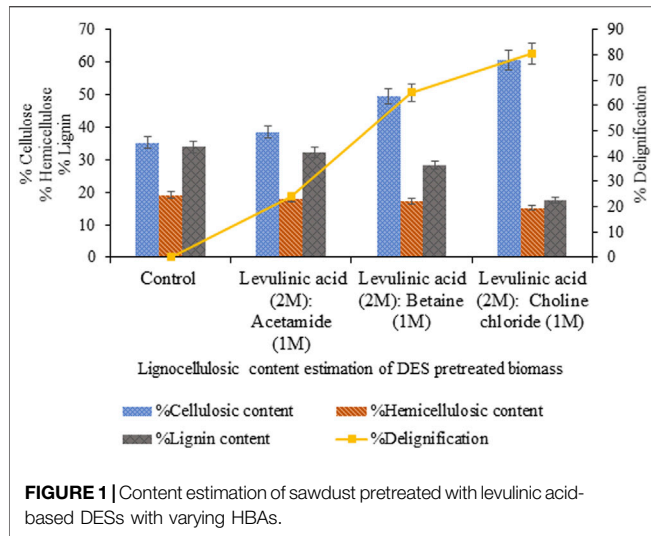
2.9 Statistical Analysis

The experiment was run in triplicate. Statistical analysis was done using SPSS version 16.00 (IBM Analytics, New York, United States). One-way ANOVA was applied on replicates to observe the significant difference with the probability (*p*) value. Error bars in the figures of the Results section indicated standard deviation (± SD) among the replicates run, varying significantly at *p* < 0.05.

3 RESULTS

3.1 Pretreatment of Lignocellulosic Biomass (Sawdust)

The pretreatment of sawdust with levulinic acid-based DES prepared with three variable HBAs exhibited maximum delignification

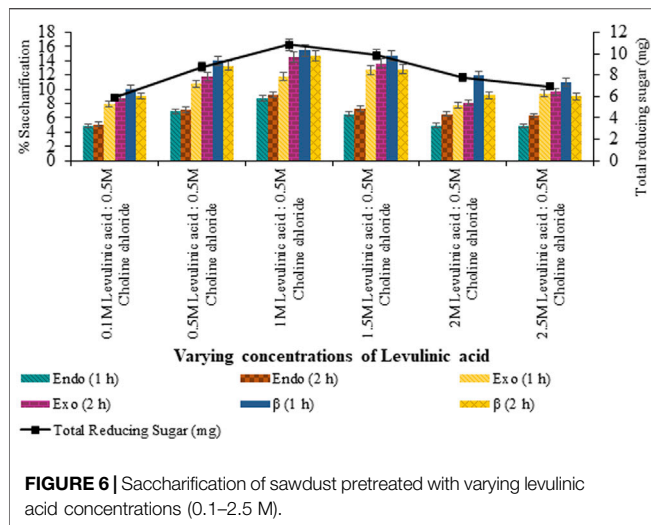


(80.5%, $p < 0.05$) and cellulosic content (60.7%, $p < 0.05$) for levulinic acid: choline chloride DES (2:1) compared to levulinic acid: betaine, levulinic acid: acetamide DES exhibiting 65% ($p < 0.05$) and 24% ($p < 0.05$) delignification, as shown in **Figure 1**.

Further optimization of the molar ratio of HBA, that is, choline chloride varying from 0.1 to 2.5 M, showed maximum delignification (87.1%, $p < 0.05$) for 0.5 M choline chloride: 2 M levulinic acid based-DES shown in **Figure 2**. However, upon varying concentration of levulinic acid (0.1–2.5 M), maximum delignification (90.1%, $p < 0.05$) and cellulosic content (70.16%, $p < 0.05$) was recorded for the 1:0.5 M concentration of levulinic acid and choline chloride DES (**Figure 3**).

3.2 Enzymatic Saccharification of Pretreated Sawdust

Saccharification of pretreated sawdust with variable HBAs and molar ratios of DES constituents resulted in maximum saccharification (7.99%; $p < 0.05$) for levulinic acid: choline chloride (2:1) pretreated sawdust (**Figure 4**). However, upon the varying concentration of HBA of selected DES, maximum

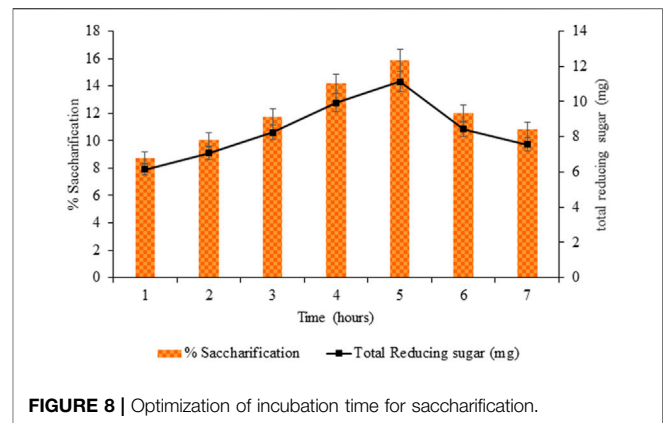
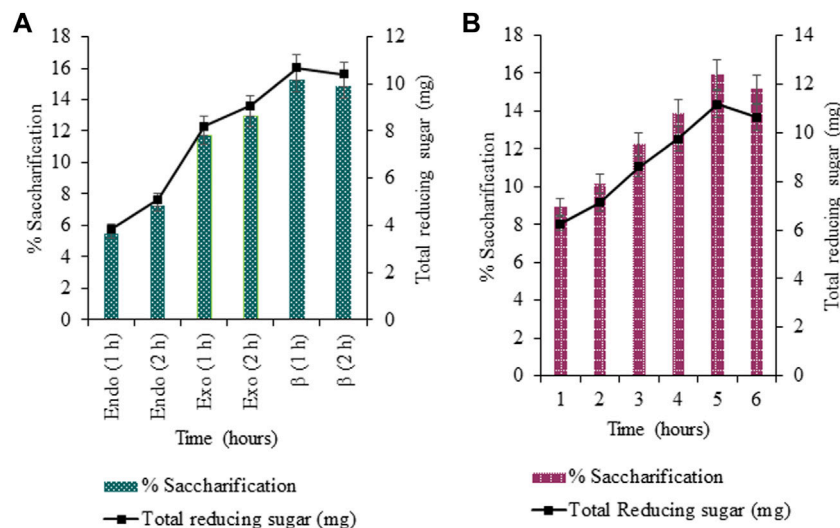


saccharification of 9.73% ($p < 0.05$) was recorded for levulinic acid: choline chloride (2:0.5) and 15.44% ($p < 0.05$) for levulinic acid: choline chloride (1:0.5), upon the varying concentration of HBD as evident from **Figures 5, 6** respectively.

3.3 Effects of Physicochemical Parameters on Enzymatic Saccharification

3.3.1 Effect of Cellulase Addition on Saccharification

The effect of cellulase addition was evaluated by adding cellulases simultaneously (all at once) and sequentially (after a regular interval of 2 h) for 6 h; at 85°C; 50 rpm. Maximum saccharification for simultaneous and sequential addition of cellulases was 15.93% ($p < 0.05$) and 15.23% ($p < 0.05$) respectively, as exhibited in **Figure 7** (**Figures 7A,B**). Thus, the simultaneous addition of cellulases exhibited better hydrolysis than the sequential one.



3.3.2 Optimization of Incubation Time for Saccharification

The incubation time of the simultaneously added cellulase mixture for saccharification was 5 h, exhibiting maximum saccharification and total reducing sugar of 15.88% ($p < 0.05$) and 11.44 mg ($p < 0.05$), respectively (**Figure 8**).

3.3.3 Effect of Incubation Temperature on Saccharification

For thermophilic cellulases, temperature regimes (70°C–90°C) with a regular increment of 5°C were used to evaluate the optimum saccharification of biomass. Maximum saccharification (16.62%, $p < 0.05$) and total reducing sugar (11.66 mg, $p < 0.05$) was estimated at 75°C, 5 h, 50 rpm, using 100 mg of pretreated sawdust, evident from **Figure 9**.

3.3.4 Optimization of Substrate Concentration for Saccharification

By increasing substrate concentration from 50 to 125 mg, saccharification also increased from 11.31% ($p < 0.05$) to

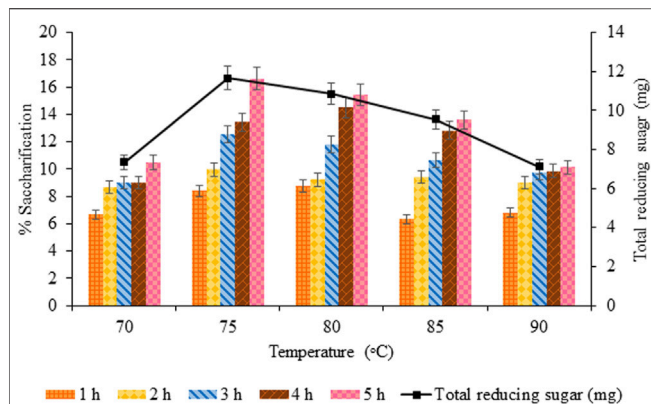


FIGURE 9 | Effect of incubation temperature on saccharification.

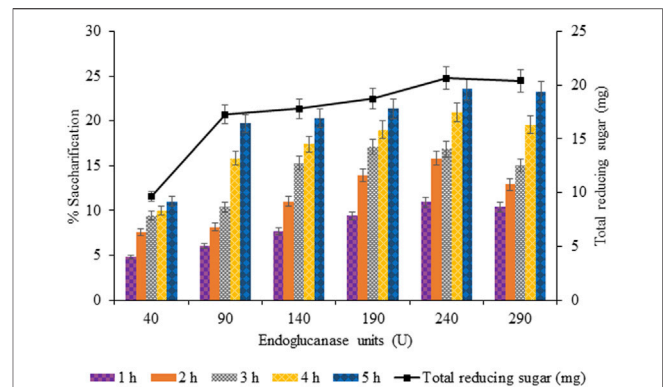


FIGURE 11 | Effect of endo-1,4- β -glucanase (40–290 U) on enzymatic saccharification.

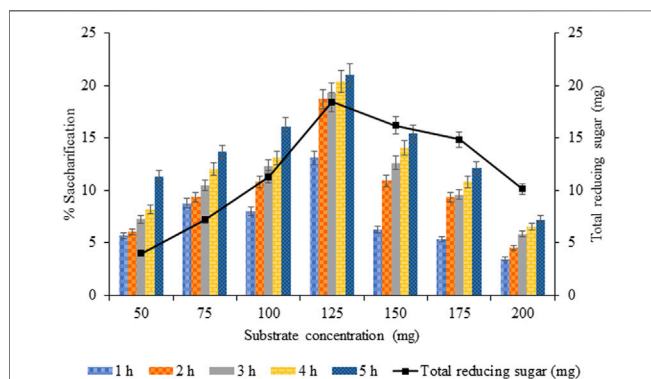


FIGURE 10 | Optimization of substrate concentration for saccharification.

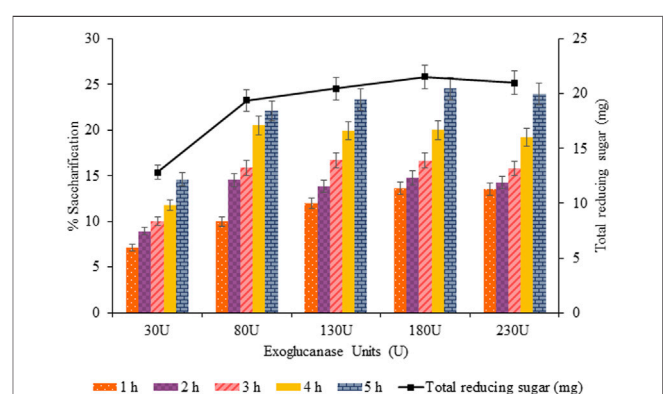


FIGURE 12 | Effect of exo-1,4- β -glucanase (30–230 U) on saccharification.

20.99% ($p < 0.05$). However, a further increase in biomass concentration decreased saccharification to 7.22%, but the total reducing sugar did not follow the same trend (Figure 10). Thus, substrate concentration of 125 mg was optimum with maximum saccharification (20.99%, $p < 0.05$) and release of total reducing sugar (18.41 mg, $p < 0.05$).

3.3.5 Effect of Endo-1,4- β -Glucanase on Enzymatic Saccharification

The units of endoglucanase varied from 40 to 290 U with a regular increment of 50 U to analyze the concentration required for optimal saccharification while keeping the units of the remaining two cellulases constant. Endoglucanase (240 U) gave maximum saccharification of 23.55% ($p < 0.05$), upon 5 h of incubation at 75°C using 125 mg of pretreated sawdust (Figure 11).

3.3.6 Effect of Exo-1,4- β -Glucanase on Saccharification

The units of exoglucanase varied from 30 to 230 U with a regular increment of 50 U to evaluate the optimum enzyme units for enzymatic hydrolysis. The maximum saccharification and total

reducing sugar was 24.54% ($p < 0.05$) and 21.52 mg ($p < 0.05$) for 180 U of exoglucanase with 240 U of endoglucanase and 220 U of β -glucosidase, as shown in Figure 12.

3.3.7 Effect of β -Glucosidase on Enzymatic Hydrolysis

β -Glucosidase is responsible for producing fermentable sugar (i.e., glucose) to be used to produce ethanol. β -Glucosidase (320 U) was estimated for maximum saccharification (25.87%, $p < 0.05$) and the highest release of total reducing sugar (22.69 mg, $p < 0.05$) with optimized units of endoglucanase (240 U) and exoglucanase (180 U). Upon increasing the concentration, saccharification dropped (25.62%, $p < 0.05$), evident from Figure 13.

3.4 Fermentation of Saccharides Into Ethanol

The released reducing sugars obtained after optimized saccharification of pretreated sawdust were subjected to the final step of ethanol production by *S. cerevisiae*. The ethanol production was estimated by potassium dichromate reagent, which turned green from orange, indicating the presence of

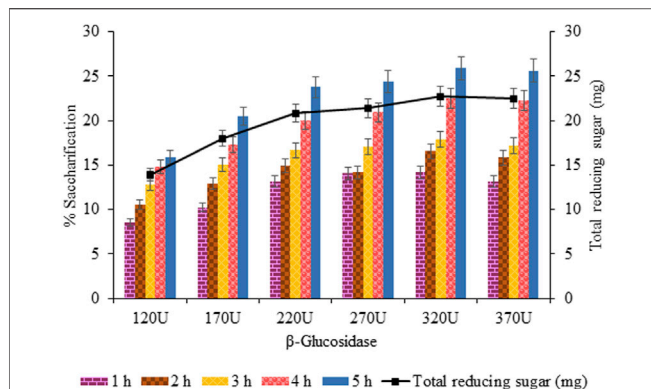


FIGURE 13 | Effect of β -glucosidase (120–370 U) on enzymatic hydrolysis.

ethanol in the supernatant. Maximum ethanol production (11.82%, $p < 0.05$) was obtained after 72 h of incubation at 30°C, 180 rpm. Initially, ethanol production estimated after 24 h was not appreciable (0.647%, $p < 0.05$), but after 48 h, a noticeable increase in ethanol production was estimated. Upon 96 h of incubation, ethanol production (11.23%, $p < 0.05$) was observed to decline (Figure 14).

4 DISCUSSION

The sustainability and the economic viability of bioethanol production were achieved *via* lignocellulosic biomass (sawdust) and novel levulinic acid-based pretreatment applied in current research. Pretreatment is the key bottleneck and the costliest step in the sustenance of such projects. DES pretreatment resolved the issue. The DES used in the current research were natural deep eutectic solvents belonging to Class III, reported to be used in biomass valorization (Scelsi et al., 2021). Levulinic acid as HBD was used because it had a single carboxyl group; the second functional group was a ketonic group that interacted with lignin rather than the carboxyl group, which was responsible for the reduction in lignin solubility (Soares et al., 2017; Magalhães et al., 2021). Three hydrogen bond acceptors—acetamide, betaine, and choline chloride—were of natural origin to prepare natural deep eutectic solvent (NADES) to out rule the potential environmental hazards posed by ILs and other organic solvents used for pretreatment (Scelsi et al., 2021).

The efficient removal of lignin and hemicellulose depends on the cleavage of a covalent bond between lignin and hemicellulose containing phenyl glucoside, benzyl ester/ether groups, and cross-linking hydrogen bonds. The strong hydrogen bond in lignocellulosic biomass might be weakened by a competing hydrogen bond formed between the chloride ions from choline chloride constituting DES and the hydroxyl group of lignin and carbohydrate. Thus, breaking the lignin carbohydrate complexes and removing lignin and hemicellulose in DES during

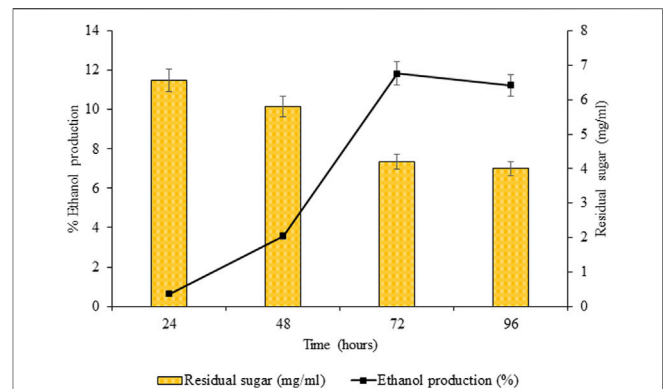


FIGURE 14 | Fermentation of saccharides into ethanol.

pretreatment (Liu et al., 2017; Smink et al., 2019). On this basis, levulinic acid: choline chloride DES exhibited better potential to remove lignin and hemicellulose than levulinic acid: betaine and levulinic acid: acetamide DESs. Similarly, in the literature, a few articles reported the exploitation of levulinic acid and keto-organic acid in DES preparation used for biomass valorization.

The molar ratio of HBD (i.e., levulinic acid) and selected hydrogen bond acceptor (HBA) (i.e., choline chloride) was optimized to be 1:0.5 whereas, the reported molar ratio for this combination was 2:1 by Ling et al. (2020) and 1:1 by Alvarez-Vasco et al. (2016). The molar ratio of levulinic acid (HBD) to choline chloride (HBA) was responsible for affecting the strength of the hydrogen bond in the resulting DES. The strength of the DES hydrogen bond, as a result, affects their mobility as well as the degradation potential of biomass in pretreatment (Xu et al., 2021). Therefore, maybe the molar ratio of 1:0.5 exhibited strong hydrogen bonding compared to the other variable ratios of HBD to HBA. Thus, pretreatment intensity was best at this molar ratio of HBD to HBA forming DES, that is, 91% of delignification and cellulosic content of 70.16%.

After the pretreatment process, enzymatic hydrolysis/saccharification of lignocellulosic biomass was recognized as the techno-economic bottleneck in converting lignocellulosic biomass into ethanol (Alio et al., 2020). The type of pretreatment given to the substrate was among the factors influencing saccharification (Vasić et al., 2021). This was evident from the result of saccharification for DES pretreatment with variable HBAs and varying concentrations of HBA and HBD. Chourasia et al. (2021) reported efficient saccharification of choline chloride-based DES pretreated biomass. Ling et al. (2020) also reported maximum enzymatic hydrolysis for the pretreated biomass exhibiting maximum delignification with levulinic acid: choline chloride DES. The maximum saccharification of 15.44% for the optimized levulinic acid and choline chloride molar ratio of 1:0.5 from the initial pretreatment molar ratio of 2:1 was 7.99%. Thus, the adsorption of cellulases to exposed cellulose after efficient delignification

increased saccharification. The decrease in percentage saccharification might be due to the deposition of lignin and pseudo lignin droplets on the surface of pretreated biomass, due to which enzymes adsorb unproductively on the substrate (Lin et al., 2021).

The addition of cellulases played a critical role in saccharification; three basic cellulases (endoglucanases, exoglucanases, and β -glucosidases) were employed to deconstruct cellulose into reducing sugars. In the current research, the simultaneous addition of cellulases (i.e., a blend of three cellulases) gave higher saccharification compared to the sequential addition of cellulases for 90 U of endoglucanase, 80 U of exoglucanase, and 220 U of β -glucosidase. Obeng et al. (2018) and Malgas et al. (2020) also reported cellulase synergism for a cocktail of cellulases in enzymatic hydrolysis of biomass. However, the blend ratio and enzyme source were different, which might be responsible for the variation in results. However, a commercial preparation of cellulases also supports the simultaneous addition of cellulases for their synergistic action in saccharification compared to their sequential addition.

Incubation time for enzymatic hydrolysis determines the extent of contact between enzyme (i.e., cellulase) and pretreated substrate (sawdust) molecules involved in the reaction, affecting the rate of product formation (i.e., reducing sugar). After 5 h of incubation, saccharification decreased due to the exhaustion of amorphous cellulose by cellulases attack in the initial stages and the deferred hydrolysis rate of crystalline cellulose (Sridevi et al., 2015).

In the current research, the thermostable cellulase sourced from *Thermotoga petrophila* cloned in *Escherichia coli* exhibited maximum enzymatic hydrolysis of 16.62% at 75°C. According to Arrhenius's theory, the rate of enzyme-catalyzed reaction rises with increasing temperature but up to a certain limit. The kinetic energy of reacting molecules increases with the temperature rise, resulting in a higher collision rate and subsequent substrate conversion into a product. However, at elevated temperature, water that critically affects protein folding and structure are lost, due to which enzyme activity is compromised (Chavan and Gaikwad, 2021). The deviations were possibly due to the difference in the substrate used in enzyme assay and saccharification, as cellulases exhibit differential specificity and affinity for soluble and insoluble substrates (Sidar et al., 2020). Most of the thermophilic microbes did not have the potential to degrade crystalline cellulose due to the lack of cellulose-binding modules (CBMs) (Maki et al., 2009). The half-life of cellulases has been reported to be 8 h at 80°C (with optimum pH) by Wang et al. (2011), so upon increasing temperature, the half-life decreases. That is why the saccharification dropped at elevated temperatures.

The maximum substrate concentration of 125 mg exhibited the highest saccharification yield (20.99%), and a further increase in the substrate was not supportive in increasing saccharification percentage and release of reducing sugar. A similar effect of increasing substrate concentration resulting

in deferred conversion rate/enzymatic hydrolysis was justifiable for the factors limiting the substrate conversion into the product as inadequate stirring for higher substrate loadings, increased viscosity, deferred seepage of cellulases to cellulose, and mass transfer limitations (Althuri and Banerjee, 2019; Ailo et al., 2020).

The saccharification process of pretreated sawdust was influenced by substrate-related factors and other physical conditions, and enzyme-related factors were also responsible for affecting the hydrolysis rate positively and negatively. In the current findings, the optimized concentration of crude cellulases (i.e., endoglucanase, exoglucanase, and β -glucosidase) was 240, 180, and 320 U for increasing the saccharification percentage from 20.99 to 25.87 (4.88%). Upon further increasing the concentration of each cellulase, no further increase was observed, although a slight decrease in percentage saccharification was recorded.

The long-chain oligosaccharides (cello-oligosaccharides) are the end product of endoglucanases, which are then processed by exoglucanases, and the resulting disaccharides (cellodextrins/cellobiose) are then cleaved by β -glucosidases. Thus, endoglucanase and exoglucanase activity is the rate-limiting step in this substrate processivity and channeling *via* cellulases interactions. Therefore, the optimal amount of exoglucanase was required for a higher endoglucanase titer to prevent feedback inhibition. Similarly, a higher titer of glucosidase was required to prevent the feedback inhibition of endoglucanases and exoglucanases by cellobiose accumulation (Obeng et al., 2018).

The jamming effect was created by the overcrowding of cellobiohydrolases (CBH) in the crystalline cellulose due to the orientation of cellulose fiber and restricted movement of enzymes over it in one direction (i.e., along with the fiber). That is why upon increasing the concentration of cellulases, several molecules bound adjacent to each other over the exposed cellulosic content tend to impede each other. As a result, not all enzymes were able to move at the same pace, causing a reduction in cellulose to glucose conversion rate (Bommarius et al., 2008).

However, further increase in enzyme concentration was not supportive in increasing percentage saccharification probably due to the following reasons: source of cellulases, product inhibition, synergism among cellulases, non-specific binding, and specific activity of enzymes, as well as their processivity and compatibility with the substrate to be saccharified (Yang et al., 2011). However, other reasons were the increased rate of transglycosylation reactions, inadequate mixing, hydrodynamic instability, and slurry suspension (Alrumman, 2016).

The bioethanol production of 11.82% using *S. cerevisiae*, with a maximum consumption of reducing sugar slurry, was obtained within 72 h. After 72 h, a slight decrease in glucose consumption and its subsequent conversion into ethanol was observed. The decrease might be due to the depletion of essential nutrients supporting yeast growth and the

accumulation of toxic metabolites. Alio et al. (2020) reported ethanol production of 16 g/L from saccharified biomass with substrate (sawmill mixed feedstock) loading of 7.5% using *S. cerevisiae*. However, with DES pretreated sorghum straw, Wu et al. (2021) reported 0.45 g ethanol/g glucose using *S. cerevisiae*. Thus, variation in results was due to the difference in the substrate, using saccharified biomass slurry of reducing sugar instead of saccharified biomass.

DATA AVAILABILITY STATEMENT

The raw data supporting the conclusion of this article will be made available by the authors without undue reservation.

REFERENCES

- Abdou Alio, M., Marcati, A., Pons, A., and Vial, C. (2021). Modeling and Simulation of a Sawdust Mixture-Based Integrated Biorefinery Plant Producing Bioethanol. *Bioresour. Technol.* 325, 124650. doi:10.1016/j.biortech.2020.124650
- Alio, M. A., Tugui, O.-C., Rusu, L., Pons, A., and Vial, C. (2020). Hydrolysis and Fermentation Steps of a Pretreated Sawmill Mixed Feedstock for Bioethanol Production in a Wood Biorefinery. *Bioresour. Technol.* 310, 123412. doi:10.1016/j.biortech.2020.123412
- Alrumman, S. A. (2016). Enzymatic Saccharification and Fermentation of Cellulosic Date Palm Wastes to Glucose and Lactic Acid. *Braz. J. Microbiol.* 47 (1), 110–119. doi:10.1016/j.bjm.2015.11.015
- Althuri, A., and Banerjee, R. (2019). Separate and Simultaneous Saccharification and Fermentation of a Pretreated Mixture of Lignocellulosic Biomass for Ethanol Production. *Biofuels* 10 (1), 61–72. doi:10.1080/17597269.2017.1409059
- Alvarez-Vasco, C., Ma, R., Quintero, M., Guo, M., Geleynse, S., Ramasamy, K. K., et al. (2016). Unique Low-Molecular-Weight Lignin with High Purity Extracted from Wood by Deep Eutectic Solvents (DES): A Source of Lignin for Valorization. *Green Chem.* 18, 5133–5141. doi:10.1039/C6GC01007E
- Bommarius, A. S., Katona, A., Cheben, S. E., Patel, A. S., Ragauskas, A. J., Knudson, K., et al. (2008). Cellulase Kinetics as a Function of Cellulose Pretreatment. *Metab. Eng.* 10 (6), 370–381. doi:10.1016/j.ymben.2008.06.008
- Capolupo, L., and Faraco, V. (2016). Green Methods of Lignocellulose Pretreatment for Biorefinery Development. *Appl. Microbiol. Biotechnol.* 100 (22), 9451–9467. doi:10.1007/s00253-016-7884-y
- Chavan, S., and Gaikwad, A. (2021). Optimization of Enzymatic Hydrolysis of Bamboo Biomass for Enhanced Saccharification of Cellulose through Taguchi Orthogonal Design. *J. Environ. Chem. Eng.* 9 (1), 104807. doi:10.1016/j.jece.2020.104807
- Chen, Y., and Mu, T. (2019). Application of Deep Eutectic Solvents in Biomass Pretreatment and Conversion. *Green Energy & Environ.* 4 (2), 95–115. doi:10.1016/j.gee.2019.01.012
- Chourasia, V. R., Pandey, A., Pant, K. K., and Henry, R. J. (2021). Improving Enzymatic Digestibility of Sugarcane Bagasse from Different Varieties of Sugarcane Using Deep Eutectic Solvent Pretreatment. *Bioresour. Technol.* 337, 125480. doi:10.1016/j.biortech.2021.125480
- Cunha, J. T., Soares, P. O., Baptista, S. L., Costa, C. E., and Domingues, L. (2020). Engineered *Saccharomyces cerevisiae* for Lignocellulosic Valorization: a Review and Perspectives on Bioethanol Production. *Bioengineered* 11 (1), 883–903. doi:10.1080/21655979.2020.1801178
- Faizal, A., Sembada, A. A., and Priharto, N. (2021). Production of Bioethanol from Four Species of Duckweeds (*Landoltia Punctata*, *Lemna Aequinoctialis*, *Spirodela Polyrhiza*, and *Wolffia Arrhiza*) through Optimization of Saccharification Process and Fermentation with *Saccharomyces cerevisiae*. *Saudi J. Biol. Sci.* 28 (1), 294–301. doi:10.1016/j.sjbs.2020.10.002

AUTHOR CONTRIBUTIONS

AN, FJ, RH, and YF conceptualized the study and developed and conducted the research idea. IH and KJ helped in manuscript preparation. AN, FJ, HM, and YF helped in manuscript proofreading and statistical analysis.

FUNDING

The authors acknowledge the financial support of National Innovation and Entrepreneurship Training program for College Students (202213023009) and the Doctoral Scientific Research Foundation of Hangzhou Medical College (0004F1RCYJ1905).

- Gopal, K., and Ranjhan, S. K. (1980). *Laboratory Manual for Nutrition Research*. India: Roland Press (India) Private Ltd, 56–60.
- Gunny, A. A. N., Arbain, D., Daud, M. Z. M., and Jamel, P. (2014). A Synergistic Action of Deep Eutectic Solvents and Cellulases for Lignocellulosic Biomass Hydrolysis. *Mat. Res. Innovat.* 18 sup6, S6-65-S6-67. doi:10.1179/1432891714Z.000000000933
- Huang, C., Jiang, X., Shen, X., Hu, J., Tang, W., Wu, X., et al. (2022b). Lignin-enzyme Interaction: A Roadblock for Efficient Enzymatic Hydrolysis of Lignocellulosics. *Renew. Sustain. Energy Rev.* 154, 111822. doi:10.1016/j.rser.2021.111822
- Huang, C., Xu, C., Meng, X., Wang, L., and Zhou, X. (2022a). Editorial: Isolation, Modification, and Characterization of the Constituents (Cellulose, Hemicellulose, Lignin, et al.) in Biomass and Their Bio-Based Applications. *Front. Bioeng. Biotechnol.* 10, 866531. doi:10.3389/fbioe.2022.866531
- Irfan, M., Gulsher, M., Abbas, S., Syed, Q., Nadeem, M., and Baig, S. (2011). Effect of Various Pretreatment Conditions on Enzymatic Saccharification. *Songklanakarin J. Sci. Technol.* 33 (4), 397–404.
- Keshav, P. K., Banoth, C., Kethavath, S. N., and Bhukya, B. (2021). Lignocellulosic Ethanol Production from Cotton Stalk: an Overview on Pretreatment, Saccharification and Fermentation Methods for Improved Bioconversion Process. *Biomass Convers. biorefin.* doi:10.1007/s13399-021-01468-z
- Kucharska, K., Słupek, E., Cieśliński, H., and Kamiński, M. (2020). Advantageous Conditions of Saccharification of Lignocellulosic Biomass for Biofuels Generation via Fermentation Processes. *Chem. Pap.* 74, 1199–1209. doi:10.1007/s11696-019-00960-1
- Lin, W., Yang, J., Zheng, Y., Huang, C., and Yong, Q. (2021). Understanding the Effects of Different Residual Lignin Fractions in Acid-Pretreated Bamboo Residues on its Enzymatic Digestibility. *Biotechnol. Biofuels* 14, 143. doi:10.1186/s13068-021-01994-y
- Ling, Z., Guo, Z., Huang, C., Yao, L., and Xu, F. (2020). Deconstruction of Oriented Crystalline Cellulose by Novel Levulinic Acid Based Deep Eutectic Solvents Pretreatment for Improved Enzymatic Accessibility. *Bioresour. Technol.* 305, 123025. doi:10.1016/j.biortech.2020.123025
- Liu, Y., Chen, W., Xia, Q., Guo, B., Wang, Q., Liu, S., et al. (2017). Efficient Cleavage of Lignin-Carbohydrate Complexes and Ultrafast Extraction of Lignin Oligomers from Wood Biomass by Microwave-Assisted Treatment with Deep Eutectic Solvent. *ChemSusChem* 10 (8), 1692–1700. doi:10.1002/cssc.201601795
- Magalhães, S., Filipe, A., Melro, E., Fernandes, C., Vitorino, C., Alves, L., et al. (2021). Lignin Extraction from Waste Pine Sawdust Using a Biomass Derived Binary Solvent System. *Polymers* 13 (7), 1090. doi:10.3390/polym13071090
- Maki, M., Leung, K. T., and Qin, W. (2009). The Prospects of Cellulase-Producing Bacteria for the Bioconversion of Lignocellulosic Biomass. *Int. J. Biol. Sci.* 5 (5), 500–516. doi:10.7150/ijbs.5.500
- Malgas, S., Rose, S. H., van Zyl, W. H., and Pletschke, B. I. (2020). Enzymatic Hydrolysis of Softwood Derived Paper Sludge by an *In Vitro* Recombinant Cellulase Cocktail for the Production of Fermentable Sugars. *Catalysts* 10 (7), 775. doi:10.3390/catal10070775

- Maugeri, Z., and Domi, P. (2012). RSC Advances Novel Choline-Chloride-Based Deep-Eutectic-Solvents with Renewable Hydrogen Bond Donors: Levulinic Acid and Sugar-Based Polyols. *RSC Advanc.* 421, C425. doi:10.1039/C1RA00630D
- Miller, G. L. (1959). Use of Dinitrosalicylic Acid Reagent for Determination of Reducing Sugar. *Anal. Chem.* 31 (3), 426–428. doi:10.1021/ac60147a030
- Moodley, P., and Gueguim Kana, E. B. (2019). Bioethanol Production from Sugarcane Leaf Waste: Effect of Various Optimized Pretreatments and Fermentation Conditions on Process Kinetics. *Biotechnol. Rep.* 22, e00329. doi:10.1016/j.btre.2019.e00329
- Obeng, E. M., Ongkudon, C. M., Budiman, C., Maas, R., and Jose, J. (2018). An Optimal Blend of Single Autodisplayed Cellulases for Cellulose Saccharification - a Proof of Concept. *J. Chem. Technol. Biotechnol.* 93 (9), 2719–2728. doi:10.1002/jctb.5628
- Robak, K., and Balcerek, M. (2020). Current State-Of-The-Art in Ethanol Production from Lignocellulosic Feedstocks. *Microbiol. Res.* 240, 126534. doi:10.1016/j.micres.2020.126534
- Satlewal, A., Agrawal, R., Bhagia, S., Sangoro, J., and Ragauskas, A. J. (2018). Natural Deep Eutectic Solvents for Lignocellulosic Biomass Pretreatment: Recent Developments, Challenges and Novel Opportunities. *Biotechnol. Adv.* 36 (8), 2032–2050. doi:10.1016/j.biotechadv.2018.08.009
- Scelsi, E., Angelini, A., and Pastore, C. (2021). Deep Eutectic Solvents for the Valorisation of Lignocellulosic Biomasses towards Fine Chemicals. *Biomass* 1, 29–59. doi:10.3390/biomass1010003
- Sidar, A., Albuquerque, E. D., Voshol, G. P., Ram, A. F. J., Vijgenboom, E., and Punt, P. J. (2020). Carbohydrate Binding Modules: Diversity of Domain Architecture in Amylases and Cellulases from Filamentous Microorganisms. *Front. Bioeng. Biotechnol.* 8, 871–871. doi:10.3389/fbioe.2020.00871
- Smink, D., Juan, A., Schuur, B., and Kersten, S. R. A. (2019). Understanding the Role of Choline Chloride in Deep Eutectic Solvents Used for Biomass Delignification. *Ind. Eng. Chem. Res.* 58 (36), 16348–16357. doi:10.1021/acs.iecr.9b03588
- Smith, E. L., Abbott, A. P., and Ryder, K. S. (2014). Deep Eutectic Solvents (DESs) and Their Applications. *Chem. Rev.* 114 (21), 11060–11082. doi:10.1021/cr300162p
- Soares, B., Tavares, D. J. P., Amaral, J. L., Silvestre, A. J. D., Freire, C. S. R., and Coutinho, J. A. P. (2017). Enhanced Solubility of Lignin Monomeric Model Compounds and Technical Lignins in Aqueous Solutions of Deep Eutectic Solvents. *ACS Sustain. Chem. Eng.* 5 (5), 4056–4065. doi:10.1021/acssuschemeng.7b00053
- Sridevi, A., Narasimha, G., Ramanjaneyulu, G., Dileepkumar, K., Reddy, B. R., and Devi, P. S. (2015). Saccharification of Pretreated Sawdust by *Aspergillus niger* Cellulase. *3 Biotech.* 5 (6), 883–892. doi:10.1007/s13205-015-0284-7
- Takada, M., Chandra, R., Wu, J., and Saddler, J. N. (2020). The Influence of Lignin on the Effectiveness of Using a Chemithermomechanical Pulping Based Process to Pretreat Softwood Chips and Pellets Prior to Enzymatic Hydrolysis. *Bioresour. Technol.* 302, 122895. doi:10.1016/j.biortech.2020.122895
- Vallander, L., and Eriksson, K.-E. (1987). Enzyme Recirculation in Saccharification of Lignocellulosic Materials. *Enzyme Microb. Technol.* 9 (12), 714–720. doi:10.1016/0141-0229(87)90030-5
- Van Soest, P., and Robertson, J. (1979). "Systems of Analysis for Evaluating Fibrous Feeds in Standardization of Analytical Methodology for Feeds," in Proceedings IDRC, Ottawa, ON, Canada, March 12–14, 1979 (IDRC).
- Vasić, K., Knez, Ž., and Leitgeb, M. (2021). Bioethanol Production by Enzymatic Hydrolysis from Different Lignocellulosic Sources. *Molecules* 26 (3), 753. doi:10.3390/molecules26030753
- Vieira, S., Barros, M. V., Sydney, A. C. N., Piekarski, C. M., de Francisco, A. C., Vandenberghe, L. P. D. S., et al. (2020). Sustainability of Sugarcane Lignocellulosic Biomass Pretreatment for the Production of Bioethanol. *Bioresour. Technol.* 299, 122635. doi:10.1016/j.biortech.2019.122635
- Wang, H., Squina, F., Segato, F., Mort, A., Lee, D., Pappan, K., et al. (2011). High-Temperature Enzymatic Breakdown of Cellulose. *Appl. Environ. Microbiol.* 77 (15), 5199–5206. doi:10.1128/AEM.00199-11
- Wang, Z. H., Li, X., Lin, T., Tang, J., Chen, J., Mo, R., et al. (2020). Bioresource Technology Novel Recyclable Deep Eutectic Solvent Boost Biomass Pretreatment for Enzymatic Hydrolysis. *Bioresour. Technol.* 307, 123237. doi:10.1016/j.biortech.2020.123237
- Wu, M., Gong, L., Ma, C., and He, Y.-C. (2021). Enhanced Enzymatic Saccharification of Sorghum Straw by Effective Delignification via Combined Pretreatment with Alkali Extraction and Deep Eutectic Solvent Soaking. *Bioresour. Technol.* 340, 125695. doi:10.1016/j.biortech.2021.125695
- Xu, H., Kong, Y., Peng, J., Song, X., Liu, Y., Su, Z., et al. (2021). Comprehensive Analysis of Important Parameters of Choline Chloride-Based Deep Eutectic Solvent Pretreatment of Lignocellulosic Biomass. *Bioresour. Technol.* 319, 124209. doi:10.1016/j.biortech.2020.124209
- Xu, H., Peng, J., Kong, Y., Liu, Y., Su, Z., Li, B., et al. (2020). Key Process Parameters for Deep Eutectic Solvents Pretreatment of Lignocellulosic Biomass Materials: A Review. *Bioresour. Technol.* 310, 123416. doi:10.1016/j.biortech.2020.123416
- Yang, B., Dai, Z., Ding, S.-Y., and Wyman, C. E. (2011). Enzymatic Hydrolysis of Cellulosic Biomass. *Biofuels* 2 (4), 421–449. doi:10.4155/bfs.11.116
- Yuan, D., Rao, K., Relue, P., and Varanasi, S. (2011). Fermentation of Biomass Sugars to Ethanol Using Native Industrial Yeast Strains. *Bioresour. Technol.* 102 (3), 3246–3253. doi:10.1016/j.biortech.2010.11.034
- Zhang, H., Lang, J., Lan, P., Yang, H., Lu, J., and Wang, Z. (2020). Study on the Dissolution Mechanism of Cellulose by ChCl-Based Deep Eutectic Solvents. *Materials* 13 (2), 278. doi:10.3390/ma13020278
- Zhao, W., Zhao, F., Zhang, S., Gong, Q., and Chen, G. (2019). Ethanol Production by Simultaneous Saccharification and Cofermentation of Pretreated Corn Stalk. *J. Basic Microbiol.* 59 (7), 744–753. doi:10.1002/jobm.201900117

Conflict of Interest: The authors declare that the research was conducted in the absence of any commercial or financial relationships that could be construed as a potential conflict of interest.

Publisher's Note: All claims expressed in this article are solely those of the authors and do not necessarily represent those of their affiliated organizations or those of the publisher, the editors, and the reviewers. Any product that may be evaluated in this article, or claim that may be made by its manufacturer, is not guaranteed or endorsed by the publisher.

Copyright © 2022 Nawaz, Huang, Junaid, Feng, Haq, Mukhtar and Jiang. This is an open-access article distributed under the terms of the Creative Commons Attribution License (CC BY). The use, distribution or reproduction in other forums is permitted, provided the original author(s) and the copyright owner(s) are credited and that the original publication in this journal is cited, in accordance with accepted academic practice. No use, distribution or reproduction is permitted which does not comply with these terms.

Advantages of publishing in Frontiers



OPEN ACCESS

Articles are free to read
for greatest visibility
and readership



FAST PUBLICATION

Around 90 days
from submission
to decision



HIGH QUALITY PEER-REVIEW

Rigorous, collaborative,
and constructive
peer-review



TRANSPARENT PEER-REVIEW

Editors and reviewers
acknowledged by name
on published articles

Frontiers

Avenue du Tribunal-Fédéral 34
1005 Lausanne | Switzerland

Visit us: www.frontiersin.org

Contact us: frontiersin.org/about/contact



REPRODUCIBILITY OF RESEARCH

Support open data
and methods to enhance
research reproducibility



DIGITAL PUBLISHING

Articles designed
for optimal readership
across devices



FOLLOW US

@frontiersin



IMPACT METRICS

Advanced article metrics
track visibility across
digital media



EXTENSIVE PROMOTION

Marketing
and promotion
of impactful research



LOOP RESEARCH NETWORK

Our network
increases your
article's readership